

The Geothermal Features of Erzurum and Surroundings (Turkey)

Oya Pamukcu¹, Cagatay Pamukcu¹

Abstract

Geothermal fluids have a wide spectrum of utilization areas ranging from district heating to balneology, greenhouses and fish farming. Turkey happens to be a rich country from the aspect geothermal fluids. Some part of the geothermal fields in Turkey are located in the region covering the vicinities of Bayburt, Erzincan and Erzurum corresponding to the junction point of North Anatolian and East Anatolian fault zones. For this reason, this region has a high potential for geothermal resources. However, due to the lack of drilling studies and insufficiency of the existing thermal facilities, the region is not capable of benefiting from this potential significantly. Among these cities located in Eastern Europe, especially Erzurum has an advantageous and remarkable standing because of the adequate number of drilling studies, high fluid temperature associated with high flow rate and also facility allocations. In this scope, by benefiting from the aeromagnetic data of Eastern Anatolia, Curie point depths were calculated. First of all, spectrum analysis was applied to the aeromagnetic data and Curie depths were computed. Then, by using these depths the heat flow of the region was calculated. Finally, the obtained findings were evaluated together with the previous studies conducted for the region. Benefiting from the geophysical findings of Erzurum and surroundings were analyzed.

Keywords: *Erzurum, geothermal, gravity, magnetic, Turkey.*

1. INTRODUCTION

The city of Erzurum is located in Eastern Anatolian accretionary complex between Pontide-Anatolide tectonic structures and within a significant metallogenic belt, which extends from the Balkans to Eastern Turkey and from Eastern Turkey to Iran (Figure 1). Additionally, Erzurum city sits on the junction point of North Anatolian and East Anatolian Fault zones. The region has a rich potential in terms of geothermal resources but it utilizes a small amount of this potential due to the lack of drills and existing facilities. Erzurum has more advantages than other cities located in the same region in terms of thermal tourism owing to the existence of high water temperature, greater number of drilling and facilities. Erzurum has the more than 10 identified geothermal regions according to the geothermal inventory of General Directorate of Mineral Research and Exploration [1].

In the scope of this study, the heat flow changes and geothermal potential of Erzurum city and its surroundings were examined with the Curie depths calculated by using magnetic data. If ferromagnetic materials are heated up to the

Curie point temperature, the atoms of the materials vibrate at greater frequency and amplitude than the normal temperature. During these movements of the atoms, the spin moments take random directions. The ferromagnetic materials present paramagnetic behaviour above the Curie point temperature. In a region, the Curie depths, which are obtained by magnetic anomalies, are the initial limits of paramagnetic behaviours. The heat flow values are determined by calculating the changing of Curie temperature within this depth, in the other words, by using the gradients.

The high valued heat flow regions are related with the areas which consist of faulting, geothermal basins, thin crustal structures and thermal mechanism formed by thrusts [2].

surroundings, they were found as relatively high in the regions of geothermal sources.

¹ *Dokuz eylul university, engineering faculty department of geophysical engineering, tinaztepe campus, 35160, Buca/Izmir, Turkey.
oya.pamukcu@deu.edu.tr

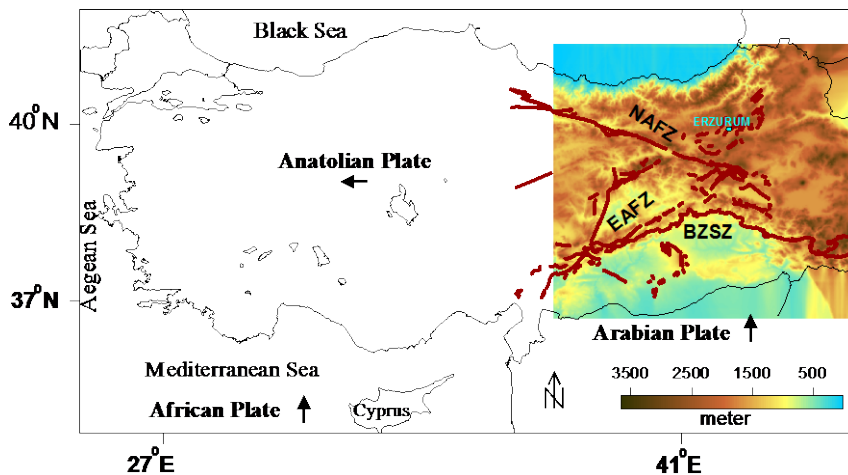


Figure 1. Topographic changes in Eastern Anatolia, main tectonic structures and the location of Erzurum city.

2. HYPOTHETICAL STUDY AND ANALYSIS

Generally, in the studies conducted in Eastern Anatolian Region, it was pointed out that the lithosphere was thin and the asthenosphere was close to the surface in that region [3], [4], [5], [6], [7], [8], [9], [10], [11], [12]. In that scope, and also in the Curie depth calculations [2], shallow Curie depths and high heat flow values were obtained in the region (Figure 2). Additionally, the gravity gradient tensor analyses [13] were performed for that region. In stratigraphic sequence of Erzurum and its surroundings, the hydrocarbon outcomes has not been founded widely due to the existence of thick sediment thickness. In the study of 3D gravity inversions carried out in Erzurum and its surroundings, it was found that the basement represented increasing and descending values and additionally, there were major faults in the direction NE–SW and E–W fracture systems of the basement. Therefore, it was pointed out that these properties may be attributed to the potential of new oil and gas reservoirs in the study area of the Erzurum [13].

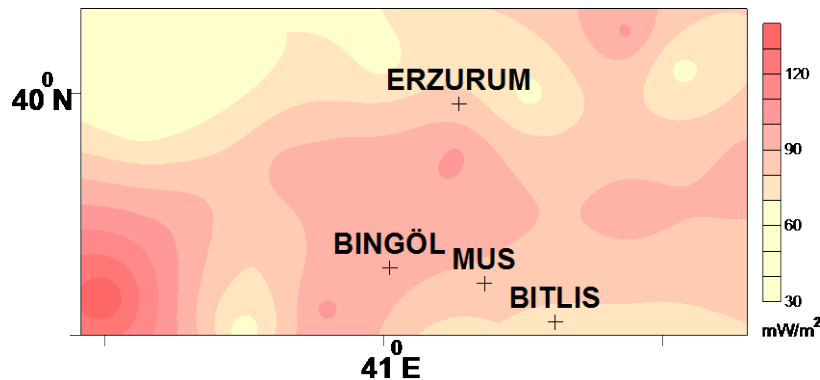


Figure 2. The changes in heat flow values calculated from the Curie Depths in Erzurum and its surroundings (modified from [2])

The temperatures of geothermal sources in Erzurum vary between 250°C and 570°C and the significant geothermal areas are determined as; Uzunahmet, Pasinler, Pasinler-Asboğa, Köprüköy, Ilıca, Dumlu-Akdağ, Tekman-Gökoğlan, Tekman-Meman, Tekman-Hamzan, Horosan-Çermik, Çat-Hölenk, Olur [1], (Figure 3). In the chemical analyses of hot water obtained from geothermal sources and drillings, it was found that the pH was above 6 and the amount of total boron varies between 4-30 mg/l (B total) [1]. When the changing of heat flow values (Figure 2) and the distribution of identified geothermal sources in the region (Figure 3) are compared together, it is observed that there are the geothermal sources wherein the high heat flow values exist.



Figure 3 The distributions of geothermal sources in Erzurum city centre and its districts.

3. RESULTS

As the results of the analysis, the distributions of geothermal potential of Erzurum and its surroundingS were consistent with the changes of heat flow values obtained by using Curie depths, which were calculated with magnetic anomalies of the region. Besides, the increasing values within the wide area in the heat flux map represent that Erzurum and it surroundings may have more geothermal potential than identified. In regards to the overall chemical analyses; moderate heavy metal content and considerably high boron amounts were encountered in occasional parts of the geothermal fluids of Erzurum and its surroundings. Therefore, the utilized geothermal fluid should neither be discharged to nearby streams nor be used directly for irrigation of crops. Instead, a well-organized reinjection procedure should be implemented at the geothermal sites to prevent environmental toxification and subsidence on the surface.

REFERENCES

- [1]. I. Akkus, H. Akilli, S. Ceyhan, A. Dilemre, Z. Tekin, *Geothermal Inventory of Turkey, M.T.A. Inventory Series-201*, Ankara (in Turkish), 2005.
- [2]. O. Pamukçu, Z. Akçığ, M. Hisarlı, and S. Tosun, *Curie Point Depths and Heat Flow of Eastern Anatolia (Turkey)*. Energy Sources, Part A: Recovery, Utilization, and Environmental Effects, 36(24), 2699-2706, 2014.
- [3]. A.I. Al-Lazki, D. Seber, E. Sandvol, N. Turkelli, R. Mohamad and M. Barazangi, *Tomographic Pn velocity and anisotropy structure beneath the Anatolian plateau (eastern Turkey) and the surrounding regions*. Geophysical Research Letters, 30(24), 2003.
- [4]. R. Gök, E. Sandvol, N. Türkelli, D. Seber and M. Barazangi, *Sn attenuation in the Anatolian and Iranian plateau and surrounding regions*, Geophysical Research Letters, 30(24), 2003.
- [5]. N. Turkelli, E. Sandvol, E. Zor, R. Gok, T. Bekler, A. Al-Lazki and S. Bayraktutan, *Seismogenic zones in eastern Turkey*, Geophysical Research Letters, 30(24), 2003.
- [6]. E. Sandvol, N. Turkelli, E. Zor, R. Gok, T. Bekler, C. Gurbuz and M. Barazangi, *Shear wave splitting in a young continent-continent collision: An example from eastern Turkey*, Geophysical Research Letters, 30(24), 2003.
- [7]. E. Zor, E. Sandvol, C. Gürbüz, N. Türkelli, D. Seber and M. Barazangi, *The crustal structure of the East Anatolian plateau (Turkey) from receiver functions*, Geophysical Research Letters, 30(24), 2003.
- [8]. A.M.C. Şengör, S. Özeren, T. Genç and E. Zor, *East Anatolian high plateau as a mantle-supported, north-south shortened domal structure*, Geophysical Research Letters, 30, 24, 8045, 2003.
- [9]. M. Keskin, *Magma generation by slab steepening and breakoff beneath a subduction-accretion complex: An alternative model for collision-related volcanism in Eastern Anatolia, Turkey*, Geophysical Research Letters, 30, 24, 8046, 2003.
- [10]. O.A. Pamukçu, Z. Akçığ, Ş. Demirbaş and E. Zor, *Investigation of crustal thickness in Eastern Anatolia using gravity, magnetic and topographic data*, Pure and Applied Geophysics, 164(11), 2345-2358, 2007.
- [11]. O.A. Pamukçu, Z. Akçığ, *Isostasy of the Eastern Anatolia (Turkey) and discontinuities of its crust*, Pure Applied Geophysics, 168/901-917, 2011.
- [12]. O. Pamukçu, T. Gönenç, A.Y. Çirmik, Ş. Demirbaş and S. Tosun, *Vertical and horizontal analysis of crustal structure in Eastern Anatolia Region*. Bulletin of the Mineral Research and Exploration, (151), 2015.
- [13]. B. Oruç, I. Sertçelik, Ö. Kafadar, and H. H. Selim, *Structural interpretation of the Erzurum Basin, eastern Turkey, using curvature gravity gradient tensor and gravity inversion of basement relief*. Journal of Applied Geophysics, 88, 105-113, 2013.

Second Record of *Autogneta (Rhaphigneta) numidiana* (Grandjean, 1960) (Acari, Oribatida) from Turkey

*Sule Baran*¹

Abstract

The species A. (R.) numidiana was previously recorded in Turkey only from the Artvin province. In this study a new distributional record belonging to this species from Sakarya province is given and redescription of A. (R.) numidiana by SEM investigation is also provided. Morphological features of our specimens are in accordance with those of previously studied specimens.

Keywords: Acari, Oribatida, Autogneta, Rhaphigneta Turkey

1. INTRODUCTION

Oribatid mites are mainly soil living decomposer microarthropods and consist of more than 10,000 described species [1]. Among the soil fauna, oribatid mites have an important role in mineralization and decomposition of plant residues especially in acidic soils [2].

In general, oribatid mites distinguished from other mite suborders by subdivided body into the prodorsum (anterior prosoma) and notogaster (posterior opisthosoma), having chelate-dentate chelicera, simple palpi, bothridial sensilla and being well sclerotized [3].

The subgenus *Autogneta (Rhaphigneta)* Grandjean, 1960 contains three species and distributed in Southern Palearctic region [1]. The main characteristics of this subgenus are the presence of an incision in the rostral apex, narrow costulae and granular sculpturing on the lateral sides of prodorsum [4].

Hitherto 237 species included in 115 genus and 57 families belonging to oribatid mites were recorded from Turkey [5]. The species *Autogneta (Rhaphigneta) numidiana* was previously recorded in Turkey only from the Artvin province [6]. In this study a new locality record belonging to this species from Sakarya province is given and redescription of *Autogneta (Rhaphigneta) numidiana* by SEM investigation is also provided. Morphological features of our specimens are in accordance with those of previously studied specimens.

2. MATERIALS AND METHODS

Mites were extracted by a Tullgren funnel apparatus from the soil samples collected from Sakarya province. They were fixed and stored in 70% ethanol. Mites were sorted from the samples under a stereomicroscope (Olympus SZX51) and mounted on slides in modified Hoyer's medium or 35% lactic acid.

The terminology used in this paper follows Balogh and Balogh (1992). Examined materials are deposited in the Acarological Collection of the second author, Sakarya University, Sakarya, Turkey.

3. RESULTS

3.1 Redescription

Material Examined. The examined material collected from grassy soil, Sakarya province, 31.07.2009 (2 specimens). **Measurements.** Mean body length 433 µm, width 246 µm. *Autogneta (Rhaphigneta) numidiana* (Grandjean, 1960) (Figures 1-4). Prodorsum - Rostrum divided in two by a deep incision. Rostral setae 33 µm and lamellar one 36 µm in length. Costulae long, reaching from interlamellar setae to bothridia. Interlamellar setae 27 µm in length, thicker than other prodorsal setae except sensillus and nearly as long as exobothridial setae. Each lateral side of prodorsum with granula. Bothridia well developed. Sensilli fusiform with long stalk and short protrusions at the apex and 67 in length.

¹

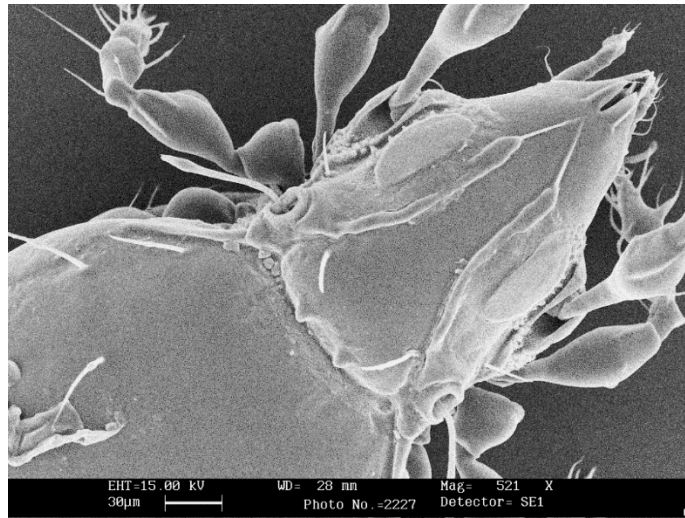


Figure 1. *Autogneta (Rhaphigneta) numidiana* SEM image of prodorsum

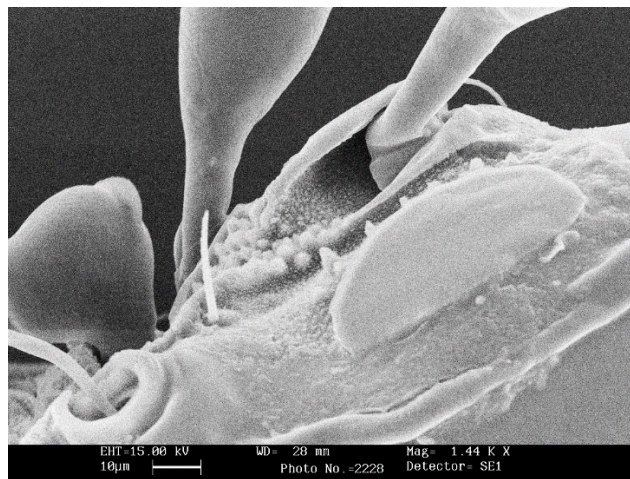


Figure 2. *Autogneta (Rhaphigneta) numidiana* SEM image of prodorsal granula

Notogaster - Notogaster oval, straight anteriorly, with a pair of median humeral processes. Ten pairs of notogastral setae present.

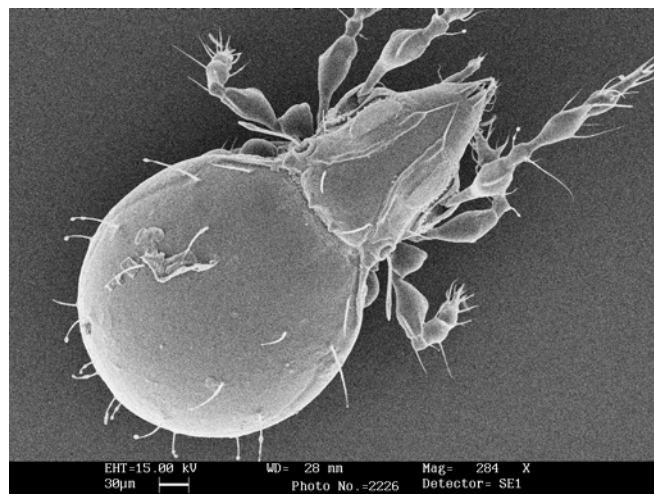


Figure 3. *Autogneta (Rhaphigneta) numidiana* SEM image of dorsal view of adult

Ventral side – Genital plate $58 \times 60 \mu\text{m}$ in size; anal plate 75×75 in size. Six pairs of genital setae; 1 pair of aggenital; 2 pairs of anal; 3 pairs of adanal setae present. Lyrifissures iad in paraanal position. The adanal setae ad1 postanal, ad2 paraanal and ad3 preanal.

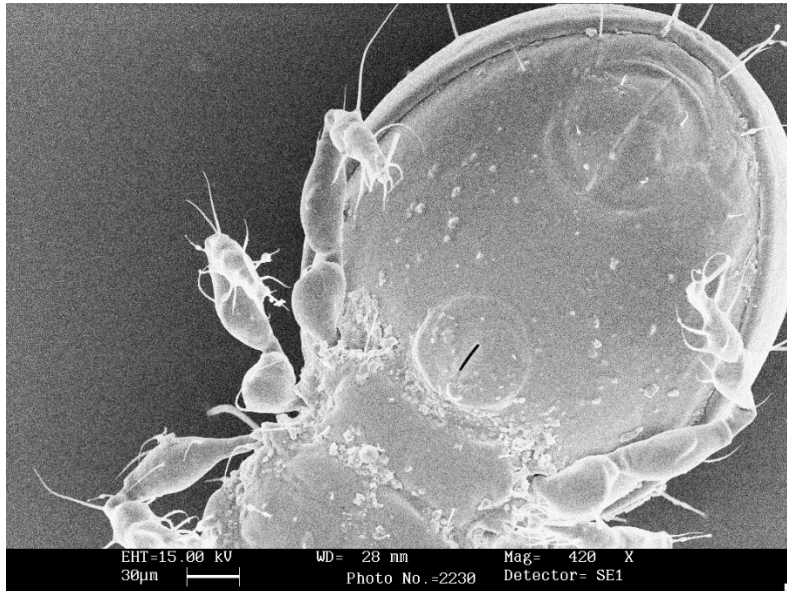


Figure 4. *Autogneta (Rhaphigneta) numidiana* SEM image of ventral view of adult

Distribution - This is the second record of this species from Turkey. This species is known from the southern palearctic region (Subías 2004, updated 2016).

3.2 Discussion

Perviously the body length of the species were given as $440\text{--}445 \mu\text{m}$ by Grandjean [7] and $360\text{--}388 \mu\text{m}$ by Toluk and Ayyıldız [6]. In this regard, the body length of our samples are in the range of previously studied specimens. Other morphological features of our specimens are consistent with those of previously studied specimens except the length of interlamellar setae which is nearly as long as exobothridial setae.

This species can easily distinguished from the related species by divided rostrum, granula laterally of prodorsum, and the shape of sensilli and costulae.

ACKNOWLEDGEMENT

We wish to thank Metallurgical and Materials Engineering Department of Sakarya University for Scanning Electron Microscopy investigations. This work was supported by the Sakarya University Scientific Research Projects Commission. Project no:2016-02-20-004

REFERENCES

- [1]. L. S. Subías, Listado sistemático, sinonímico y biogeográfico de los ácaros oribátidos (Acariformes: Oribatida) del mundo (excepto fósiles). Graellsia, 60 (número extraordinario), pp. 3–305. Online version; http://escalera.bio.ucm.es/usuarios/bba/cont/docs/RO_1.pdf (15 Feb 2016), 2004.
- [2]. T. Culliney, Role of arthropods in maintaining soil fertility. Agriculture 3:629–659, 2013.
- [3]. F. Crotty and M. Shepherd, <http://tombio.myspecies.info/files/MitesKeyTest-2014-03-07.pdf>, 2014
- [4]. J. Balogh and P. Balogh, The Oribatid Mites Genera of the World. Vol. 1. Hung. Nat. Mus. Press, Budapest, 263 pp., 1992.
- [5]. T. Bezci and Ş. Baran, First record of genus Lucoppia (Acari: Oribatida) from Turkey. Turk. J. Zool. (accepted) 2016.
- [6]. A. Toluk and N. Ayyıldız, New records of the oppioid mites (Acari: Oribatida) for the Turkish fauna from Artvin Province. Turk. J. Zool. 33: 13-21. Grandjean, F. 1960. Les Autognetidae n. fam. (Oribates). Acarologia 2: 575-609, 2009.
- [7]. F. Grandjean, Les Autognetidae n. fam. (Oribates). Acarologia 2:575-609, 1960.

Application of Aquifer Tests to Determine Hydraulic Conductivity of Aquifers in Bursa, Turkey

*Serdar Korkmaz*¹ Gokcen Eryilmaz Turkkan¹*

Abstract

The aim of this study is to determine the hydraulic conductivity of certain aquifers in Bursa region of Turkey using slug tests. Slug tests were performed by pouring instantaneously a specified amount of water into a groundwater well and observing the drawdown in the well by time. Two analytical methods namely, Bouwer-Rice and Dagan methods were applied to drawdown time-series data. In addition, the tests were modeled using the numerical model MODFLOW that solves 3-dimensional groundwater flow equations using method of finite differences. A good correspondence was obtained between the results of analytical and numerical solutions.

Keywords: *hydraulic conductivity, slug test, numerical model*

1. INTRODUCTION

Hydraulic conductivity is an important parameter in groundwater hydraulics and represents the ability of an aquifer to transmit water. There are many methods for determining hydraulic conductivity. They consist of in-situ measurements, laboratory tests and empirical approach. In this study, slug tests were performed to determine the hydraulic conductivity of several aquifers around Bursa region. The test is performed by instantaneously submerging a slug into a well or removing a previously submerged slug and measuring the drawdown in the well by time. The slug test can also be performed by pouring a definite volume of water instead of a slug which is the case in the current study. Both analytical methods and numerical modeling were used to determine hydraulic conductivity.

2. FIELD STUDY

The wells in which the slug tests were performed are summarized in Table 1. All of the wells were drilled using mud rotary drilling method. The depth of wells vary from 70 m to 284 m. Slug tests were performed by pouring 10 L of water into the wells and transient water level was measured using a level meter. The measurement continued until water level became stationary. This time period depends on the hydraulic conductivity of the aquifer.

Two analytical methods, namely, Bouwer-Rice Method ([1], [2]) and Dagan Method [3] were applied to the measured drawdown values. In addition to analytical methods, numerical models of the tests were developed using the widely known MODFLOW [4] software. Afterwards, the solutions were compared.

Table 1. Information about wells in which slug tests were performed

Place of well	Well diameter (mm)	Well depth (m)	Date of slug test
Karacabey Şahinköy	140	120	08.03.2015
Harmancık Kılavuzlar	200	132	03.03.2016
Büyükorhan Gedikler	200	70	03.03.2016
Akçalar	140	120	06.03.2016
Uludağ Üniversitesi	200	284	07.03.2016
Doğu atıksu tesisi	250	212	14.03.2016

¹ *Uludağ University, Department of Civil Engineering, 16059 Bursa, Turkey.
geryilmaz@uludag.edu.tr

3. SLUG TEST

Slug tests are relatively faster to apply and economical. One single well is needed to perform the test and there is no need for pumping. The test does not take long time, however, the hydraulic conductivity obtained through this method represents a small area around the well. Basically, slug test is performed either by dropping a slug with a definite volume into the well or by sudden removal of a previously inserted slug from the well and the change in water level is observed. A definite amount of water can also be used instead of a slug. In this study, the test is carried out by pouring water instantaneously into the well (Figure 1). Water level is recorded right from the beginning. Water level begins to decrease immediately and it is measured with time until it becomes stable. This time period can vary from several minutes to days according to the type of soil [5].

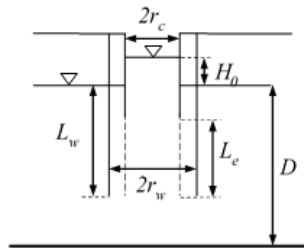


Figure 1. Condition following a sudden pouring of a definite volume of water into the well in an unconfined aquifer.

3.1 Bouwer and Rice Method

The following formulas are defined for the analytical solution using Bouwer and Rice Method.

$$H_0 = \frac{V}{\pi r_c^2} \quad (1)$$

H_0 = Change in water level right after pouring water

V = Volume of water poured

r_c = Radius of the well casing

$$K = \frac{r_c^2 \ln\left(\frac{R_e}{r_w}\right)}{2L_e} \frac{1}{t} \ln\left(\frac{H_0}{H(t)}\right) \quad (2)$$

K = Hydraulic conductivity

r_w = Radius of gravel envelope

R_e = Effective radial distance over which head is dissipated

L_e = Length of the screen

t = Time

$H(t)$ = Drawdown as a function of time

R_e is also the characteristic distance from the well over which the average value of K is measured. However, R_e can not be known for a specific well. $\ln\left(\frac{R_e}{r_w}\right)$ is calculated as follows ([1], [2]);

- a) If the distance between water table and base of well (L_w) is smaller than the saturated thickness of aquifer (D) (well partially penetrating the aquifer);

$$\ln\left(\frac{R_s}{r_w}\right) = \left[\frac{1,1}{\ln\left(\frac{L_w}{r_w}\right)} + \frac{X+Y \ln\left(\frac{D-L_w}{r_w}\right)}{\frac{L_s}{r_w}} \right]^{-1} \quad (3)$$

- b) $L_w=D$;

$$\ln\left(\frac{R_s}{r_w}\right) = \left[\frac{1,1}{\ln\left(\frac{L_w}{r_w}\right)} + \frac{Z}{\frac{L_s}{r_w}} \right]^{-1} \quad (4)$$

Dimensionless X, Y, Z parameters depend on L_e/r_w values and obtained from the curves in Figure 2. The greater the values of r_w and L_e , the greater the area of aquifer over which the hydraulic conductivity is determined [6].

Computation steps are as follows;

1. Mark $H(t)/H_0$ values on a logarithmic vertical axis and time (t) values on arithmetic horizontal axis. Draw a straight line through marked points.
2. X, Y, Z values corresponding to L_e/r_w values are read from Figure. 2.
3. Choose and apply the appropriate formula from case (a) or (b).
4. $H(t)=0.368H_0$ is chosen and the value of $\ln\left(\frac{R_s}{H(t)}\right)$ in Eq. (2) becomes 1. In order to read the necessary t value in the same formula, a correction is made to overcome the early time effect. The straight line is extended backwards till it intersects the y-axis ($[H(t)/H_0]$ axis). The point of intersection gives the $(H_0)_{new}/H_0$ ratio. This ratio is multiplied by $H(t)/H_0=0.368$ and a revised $[H(t)/H_0]_{new}$ value is obtained and the corresponding t_{new} value is read from the x-axis.
5. Finally, hydraulic conductivity is calculated from Eq. (5).

$$K = \frac{r_c^2 \ln\left(\frac{R_s}{r_w}\right)}{2L_s} \frac{1}{t_{new}} \quad (5)$$

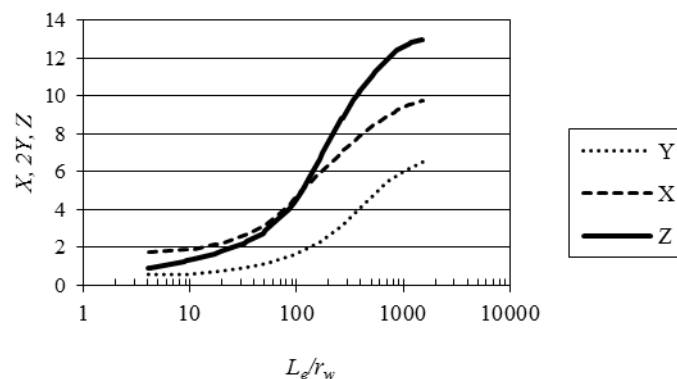


Figure 2. Dimensionless parameters X, Y, Z plotted as a function of L_e/r_w [1]

3.2 Dagan Method

Computation steps are as follows for Dagan method;

1. Mark $H(t)/H_0$ values on a logarithmic vertical axis and time (t) values on arithmetic horizontal axis. Draw a straight line through marked points.
2. The straight line is extended backwards till it intersects the y -axis ($[H(t)/H_0]$ axis). The value on the y -axis is multiplied by $H(t)/H_0=0.368$ and a revised $[H(t)/H_0]_{new}$ value is obtained. The corresponding t_{new} value is read.
3. Using the value of anisotropy ratio K_z/K_r , the parameter ψ is calculated from the following equation (in general, $K_z/K_r=1$).

$$\psi = \frac{\sqrt{\frac{K_z}{K_r}}}{L_e/r_w} \quad (6)$$

4. Using the ψ value, the dimensionless flow parameter, P , for unconfined aquifers is obtained from related tables [7].
5. Finally, hydraulic conductivity is calculated from Eq. (7).

$$K_r = \frac{r_c^2 \left(\frac{1}{P}\right)}{2L_e t_{new}} \quad (7)$$

4. NUMERICAL MODELLING

All of the well tests performed in the field were modeled using the MODFLOW software [4]. MODFLOW is U.S. Geological Survey's modular 3-dimensional numerical groundwater model with a widespread user network. MODFLOW solves the governing partial differential equations of groundwater flow using method of finite differences.

In this study, 40 m x 40 m grids were generated for modeling of slug tests. Variable cell size was used. The smallest cell was at the center of the grid and cell size gradually increased with a coefficient of 1.2. The area of the smallest cell was equal to the area of the well in which the slug test was performed. In order to represent the void in the well and to generate an equivalent water level rise as in the field, the specific yield was specified as 1 in the smallest cell. In other cells of the aquifer, specific yield was defined according to soil type. An impervious boundary condition was specified at the outer boundary of the grid. As the grid size was chosen sufficiently large considering the duration of slug tests, the outer boundary did not affect the model results. MODFLOW-2005 [8] with preconditioned conjugate-gradient (PCG2) solver was used. 2 stress periods were defined. In the first one, the water was injected in the well within a short time period and in the second one injection rate was set to zero. The measured piezometric head variations were specified as observation data and the Parameter Estimation (PEST) model was used to find the hydraulic conductivity of the aquifer through automatic calibration. PEST model performs successive runs each time changing the hydraulic conductivity value and calculating the error between observed and simulated piezometric heads. The hydraulic conductivity giving the smallest error is the final value.

5. RESULTS

The results of both analytical and numerical methods are presented in Table 2. A sample piezometric head hydrograph of both observed and simulated values is presented in Figure 3. According to the results, the two analytical methods yielded very close results, and in some of the wells MODFLOW gave similar results but in others MODFLOW results deviated from those of analytical solutions. There are severals for this deviation related to the conditions of the test and application of methods. In some wells the quality of the test was not very good due to too low a water table from the surface and difficulty to measure the drawdown using a manual level meter. In application of analytical methods, graphical techniques such as line fitting were used which is slightly user dependent. In MODFLOW, selection of specific yield values and grid size might have also affected the results.

Table 2. Hydraulic conductivity (m/s) of aquifers computed by analytical and numerical methods

	Bouwer-Rice method	Dagan method	MODFLOW
Karacabey Şahinköy	2.14E-06	2.34E-06	1.29E-05
Akçalar	2.16E-06	2.12E-06	2.47E-06
Doğu atıksu tesisi	9.50E-06	9.30E-06	4.45E-06
Harmancık Kılavuzlar	1.27E-05	1.31E-05	4.19E-05
Büyükorhan Gedikler	8.00E-06	8.78E-06	7.23E-05
Uludağ Üniversitesi	1.41E-06	1.41E-06	2.74E-06

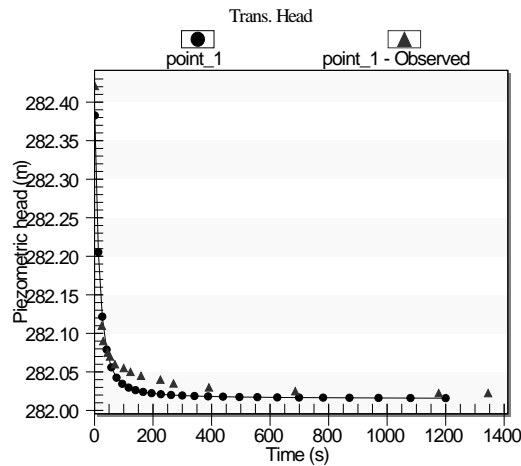


Figure 3. Piezometric head hydrograph for the slug test at Uludağ Üniversitesi; simulated and observed values

CONCLUSION

Slug tests were performed in 6 different wells around Bursa region. The depth of wells varied from 70 m to 284 m. The tests were performed by pouring 10 L of water instantaneously into the well and observing the change in water level. Two analytical methods, namely, Bouwer-Rice method and Dagan method were applied to the data to obtain the hydraulic conductivity values. In addition to these, the widely-used groundwater model MODFLOW was used for numerical modeling of the tests. A 40 m x 40 m grid was generated with a variable cell size. The cell at the center of the grid had an area equal to the area of the well and a specific yield of 1 is assigned to this cell in order to represent the actual condition. The cell size gradually increased with a coefficient of 1.2. Hydraulic conductivity was solved by PEST model which performs successive runs by trying different values and each time computing the residual between observed and simulated piezometric heads. It was observed that PEST model strongly facilitates the calibration process. According to the results, in wells in which a proper measurement was performed, such as Uludağ Üniversitesi and Akçalar, analytical results were in close agreement with those of MODFLOW. In some wells, however, discrepancy occurred between analytical and MODFLOW results. This is partly due to difficulties in doing the measurements in wells where the water table was very low. Also the user-dependent graphical technique in analytical methods as well as selection of grid size and value of specific yield in the numerical model are some reasons for differences in results.

REFERENCES

- [1] Bouwer, H., Rice R.C., "A slug test method for determining hydraulic conductivity of unconfined aquifers with completely or partially penetrating wells", *Water Resources Research*, vol. 12, no. 3, pp. 423-428, 1976.
- [2] Bouwer, H., "Estimating and enhancing groundwater recharge", In: Sharma ML (ed) *Groundwater Recharge*. Balkema, Rotterdam, pp 1-10, 1989.
- [3] Dagan, G., "A note on packer, slug, and recovery tests in unconfined aquifers", *Water Resources Research*, vol. 14, no. 5, pp. 929-934, 1978.
- [4] McDonald, M.G., Harbaugh, A.W., *A modular three-dimensional finite-difference ground-water flow model: Techniques of Water-Resources Investigations of the United States Geological Survey*, Book 6, Chapter A1, 586 p., 1988.
- [5] Eryılmaz, G., "Kuyu Testlerine Dayalı Analitik ve Sayısal Yöntemlerle Akifer Hidrolik İletkenliğinin Belirlenmesi", MSc Thesis, Department of Civil Engineering, Uludağ University, Bursa, 2013. [In Turkish]
- [6] Mays, L.W., *Ground and Surface Water Hydrology*. Wiley, 617p, 2011.
- [7] Butler, J.J., Jr., *The Design, Performance, and Analysis of Slug Tests*. Lewis Publishers, New York, 252p, 1998.
- [8] Harbaugh, A.W., MODFLOW-2005, *The U.S. Geological Survey modular ground-water model—the Ground-Water Flow Process: U.S. Geological Survey Techniques and Methods*, 6-A16, 2005.

Heat Transfer Enhancement with a Free Pulsating Turbulent Impinging Jet

Unal Akdag¹, Selma Akcay, M. Levent Karabayir, Dogan Demiral

Abstract

This study is presented convective heat transfer characteristics to a circular heated surface by impinging pulsating jet under turbulent flow conditions. In investigations, the effects of the jet Reynolds number, pulsating frequency and pulsating amplitude on heat transfer are analyzed. A numerical study was performed on the two-dimensional air jet impingement with a circular flat target surface by computational fluid dynamics method. The local-instantaneous Nusselt numbers and average Nusselt numbers are obtained along the impingement wall. The heat transfer performance of the impinging pulsating jet is compared with the conventional steady jets for the same geometry. The pulsating jet impingement leads to the periodic disruption of the boundary layer. It is observed that the heat transfer enhancement is effected the pulsating frequency and pulsating amplitude. The results demonstrated that both pulsating amplitude and pulsating frequency must be sufficiently high to influence heat transfer conditions. The obtained results are given as a function of dimensionless parameters.

Keywords: Pulsating jet, Turbulence, Heat transfer enhancement

1. INTRODUCTION

Jet impingement is used to achieve high heat and mass transfer rates in many industrial and technological fields such as annealing of metals, tempering of glass, drying of textiles and cooling of electronic components, gas turbine blades, aircraft wings. With jet impingement is obtained thin hydrodynamic and thermal boundary layer in the impingement surface thereby it causes the heat transfer enhancement. The heat transfer varies according to flow and geometric parameters such as jet Reynolds number, nozzle shape, jet array assembly, nozzle-to-plate spacing, angle of impingement etc. Several experimental and numerical studies have been carried out for improvement to the heat transfer performance of steady impinging jets on surface [1-5]. Lee and Lee [6], investigated experimentally the heat transfer characteristics of an elliptic impinging jet on a heated flat plate for different nozzle aspect ratios at constant Reynolds number. They reported that for nozzle-to-plate distance $L/D=4$, nozzle aspect ratio $AR=3$ was obtained the maximum heat transfer rate.

Recently, experimental and numerical investigations are focused on heat transfer enhancement by periodic jets. Pulsating jets disrupt the boundary layer by periodically thus the higher heat transfer improvement on surface cause. Many investigations have been performed to understand the heat transfer characteristics of the pulsating jet impingement [7-11]. Sailor et.al. [12], investigated experimentally effects of impinging pulsed air jet on heat transfer enhancement upon a heated surface with different parameters. The results shown that heat transfer enhanced exceeding 50%. Poh et.al. [13], examined numerically the heat transfer performance of a confined pulsed laminar impinging jet. They reported that the local Nusselt number at the wall jet separation region remains constant during the oscillation cycle. An experimental study was carried out on pulsating impinging jets by Hofmann et.al. [14]. The results indicated that the flow and heat transfer were affected by the pulsating parameters such as Reynolds number, nozzle-to-plate distance, frequency and amplitudes and the heat transfer decreased in the stagnation point of up to 50%. Liewkongsataporn et al. [15] investigated the effect of pulsating impinging jet on the heat transfer enhancement on a flat surface. The results demonstrated that with the increase of velocity amplitude, the time-averaged heat transfer improved on the surface. Hewakandamby [16], investigated the heat transfer enhancement on impingement surface by an array of oscillating jets using finite element methods. Numerical results shown that the oscillatory flow jets improved heat transfer efficiency approximately 100% when compared with steady flow jets.

Xu et.al. [17], investigated numerically effect of pulsations on the heat and mass transfer rate of multiple impinging jets and reported that the pulsations increased significantly heat transfer enhancement. Mohammadpour et.al. [18] examined numerically the effects of square waveform and sinusoidal waveform pulsation on the heat transfer rate from a slot jet impinging to a concave surface. Numerical results shown that the heat transfer increased from the impingement surface as the nozzle-to-surface distance reduced in the pulsed jets. Mohammadpour,et.al. [19], in another numerical studies performed to research an optimized arrangement of steady and pulsating impinging multiple submerged slot jets and denoted that the combination of pulsed jets with steady jets enhanced the Nusselt number. Bovo and Davidson [20], investigated the thermal

¹Corresponding author: Aksaray University, Department of Mechanical Engineering, 68100,Aksaray, Turkey.
uakdag@gmail.com

effects of a single-pulse jet impinging on the impingement surface using LES technique. They found high levels of agreement between the LES and the experimental results. Geng et.al. [21], investigated experimentally the enhancing heat transfer of different wavy forms designed periodic air jets on a heated surface. They reported that the heat transfer improved as Strouhal number increased from 0.004 to 0.068 for impinging jet with different waveforms.

Because of the complexity of flow structure and non-linear dynamics in the boundary layer induced by pulsation, pulsating jet impingement flow and associated heat transfer has been a challenging problem. The related physics for the pulsed jet impingement is not yet well-understood. Therefore, a numerical study is performed on a free pulsating impinging jet under large frequencies and amplitudes by using computational fluid dynamics approach. The effects of jet Reynolds number, frequency and amplitude of pulsation on the local and average Nusselt number on the target surface are discussed.

2. PHYSICAL DEFINITION OF PROBLEM

The focus of this study is the investigation of the flow and heat transfer characteristics of two-dimensional, unconfined turbulent pulsating impinging jet. Figure 1 illustrates the schematic diagram of the pulsating impinging jet, computational domain and boundary conditions simulated in this work. Because of symmetric geometry and boundary conditions, only half of the domain is considered for computations. In order to reach a pulsating flow, a sinusoidal velocity profile changing over time with various frequencies and amplitudes is used for the jet inlet.

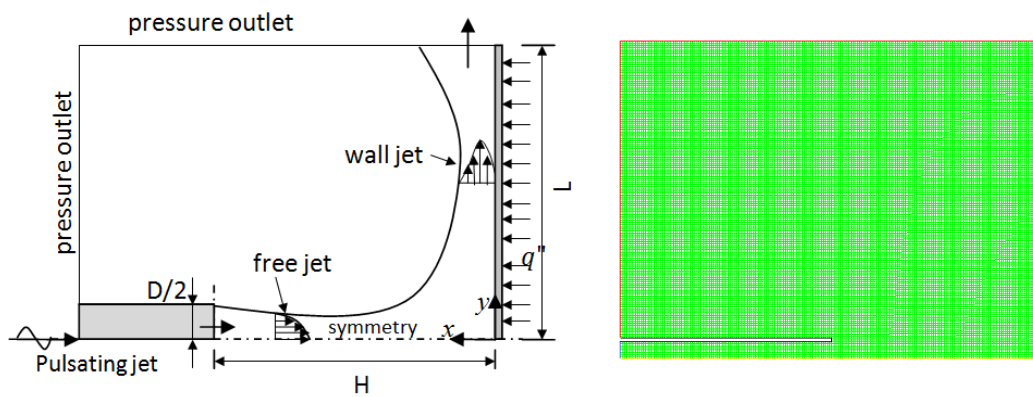


Figure 1. The schematic view of pulsating impinging jet and computational domain

2.1 Governing Equations

The fluid (air) is assumed to be incompressible and Newtonian. Gravity and radiation heat transfer are negligible. Therefore the unsteady 2-D governing equations based on these assumptions are as follows [22, 23]:

$$\frac{\partial u_i}{\partial x_i} = 0 \quad (1)$$

$$\frac{\partial u_i}{\partial t} + \rho \frac{\partial (u_i u_j)}{\partial x_j} = -\frac{\partial p}{\partial x_i} + \frac{\partial}{\partial x_j} \left[\mu \left(\frac{\partial u_i}{\partial x_j} + \frac{\partial u_j}{\partial x_i} \right) - \rho \overline{u'_i u'_j} \right] \quad (2)$$

$$\rho c_p \left[\frac{\partial T}{\partial t} + \frac{\partial (u_i T)}{\partial x_i} \right] = \frac{\partial}{\partial x_i} \left(k \frac{\partial T}{\partial x_i} - \rho c_p \overline{u'_i T'} \right) \quad (3)$$

2.2 Numerical Method and Grid Testing

The flow and thermal fields are computed with the finite volume method by using CFD code FLUENT [24]. In pulsating turbulent impingement jet, turbulence components are highly anisotropic due to strong compression of turbulence, chaotic mixing and non-linear dynamic response of boundary layers. In this study *RNG k-ε* turbulent model is used to model the turbulent behavior of the flow in the pulsating impinging jet. Because of the *RNG k-ε* model is numerically robust and fast, and has been proven to be effective in modeling this type of complex flows in impinging jets. A second order upwind

discretization scheme is used and the SIMPLE algorithm is employed for the pressure-velocity coupling. The convergence criterion for energy equation is determined to 10^{-6} , for other variables are determined to 10^{-3} .

The geometry modeling and grid generation are performed using commercial software, Gambit 2.3. A grid sensitivity analysis is performed to evaluate the effects of grid sizes on the results. A uniform structured mesh of 10.000, 20.000, 30.000 and 40000 nodes are considered. Typically, a grid density of 30.000 provides satisfactory solution for the example shown. Therefore, a domain with approximately 30.000 nodes is chosen for all cases to reduce the computing time.

2.3 Boundary and Initial Conditions

The working fluid air is blowing from the jet with uniform temperature $T_0=300$ K. At the jet inlet, the velocity profile is found by adding the uniform velocity profile with a sinusoidal pulsation. The sinusoidal pulsating velocity profile is given by

$$u_{in} = U_0 [1 + A_0 \sin(\omega t)] \quad (4)$$

where A_0 is the non-dimensional amplitude ($A_0=x_m/D$), ω is the angular frequency and the non-dimensional frequency is defined as the Womersley number, where $\frac{H}{2\sqrt{\frac{\mu}{\rho}}}$ $Wo = D/2\sqrt{\omega/\nu}$, and ν is the kinematic viscosity of the impinging jet flow.

The target surface was specified as constant heat flux and no-slip condition was imposed the impingement wall. A constant heat flux of 1000 W/m^2 is applied to the target surface. The uniform velocity, temperature, turbulent-kinetic energy and energy dissipation rate profiles were assumed at the nozzle inlet, and pressure outlet boundary condition was taken at outlet planes as showed in Fig.1. The symmetry boundary conditions were taken at symmetry planes. The initial conditions throughout the computational domain can be described as: $u=v=0, p=p_\infty, T=T_\infty$. The numerical solution parameters are given in Table.1.

Table 1 Numerical solution parameters

<i>Jet Reynolds number:</i> Re_j	<i>Amplitude:</i> A_0	<i>Frequency:</i> Wo
5000	0.5	3.71, 5.25, 7.42, 10.5
	1	3.71, 5.25, 7.42, 10.5
	2	3.71, 5.25, 7.42, 10.5

3. RESULTS AND DISCUSSION

The present study is validated by comparing the results obtained for pulsating jet flow in a confined jet condition with the numerical results of Xu et al. [22] and experimental results of Mladin and Zumbrennen [23]. Similar geometric details and boundary conditions are used to validate the this study. The comparisons are shown in Fig.2. There is significant agreement between the experimental and calculated local-averaged Nusselt Number.

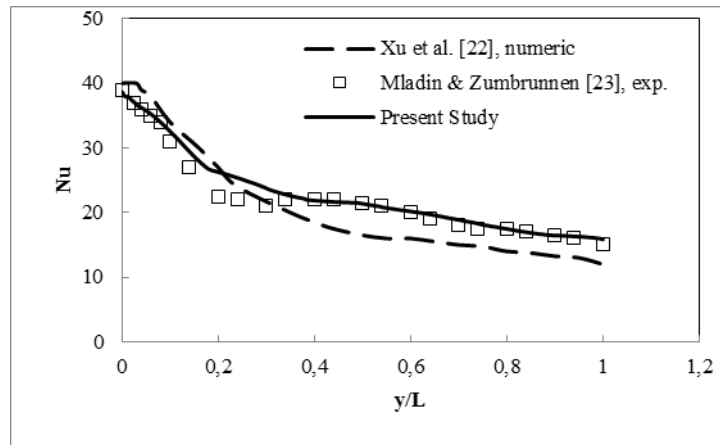
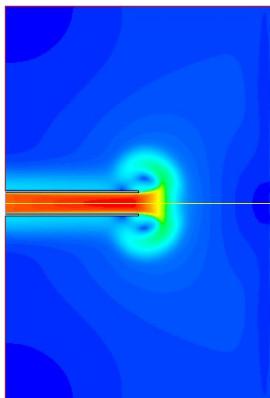
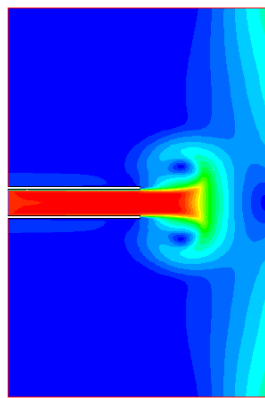


Figure 2. Verification of present study with ref [22] and [23]. ($Re_j=5000$, $H/D=5$, $A_o=0.5$, $Wo=10.5$)

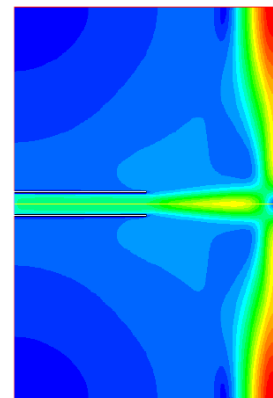
In present study, the heat transfer mechanism is discussed for cooling of a heated circular target surface using the pulsating impinging jet by examining the effects of various parameters. Geometric parameters are kept constant for all cases. The three main parameters affecting the heat transfer characteristics of jet impingement are amplitude (A_o), frequency (Wo) and jet Reynolds number (Re_j). These parameters are more important parameters for cooling of target surface with pulsating jet. Because of the computational cost, the jet Reynolds number is fixed at $Re_j=5000$. The simulations are focused on the behavior of the unsteadiness affecting the heat transfer mechanism. In this situation, owing to the pulsating component, a periodic flow field was observed on the target surface, and heat transfer was achieved periodically. Therefore, the heat transfer calculations are performed according to the amount of heat transfer achieved in one period of pulsation. To explain how the mechanisms behave during a pulsating cycle, phase angles have been used and are presented by " $\tau=\omega t$ ". The results are evaluated after the system achieved full periodic state. To explain the heat transfer mechanism instantaneous velocity and temperature distributions are obtained.



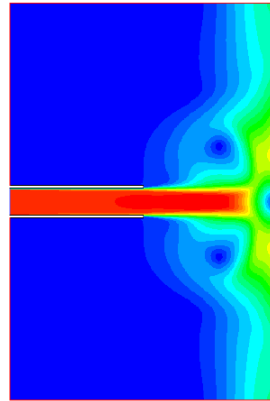
Steady flow ($H/D=10$, $A_o=0$,
 $Wo=0$)



$H/D=10$, $A_o=2$, $Wo=3.71$ $\omega t=180^\circ$



$H/D=10$, $A_o=2$, $Wo=5.25$ $\omega t=180^\circ$

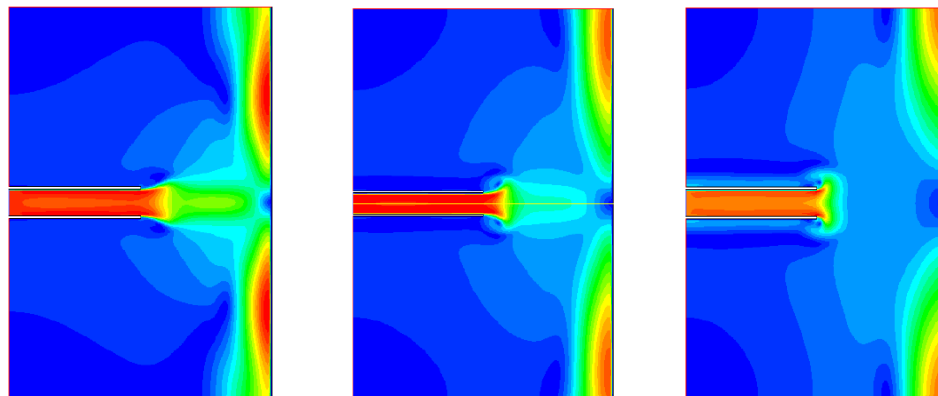


$H/D=10, A_0=2, \underline{Wo}=7.42$
 $\omega t=180^\circ$

$H/D=10, A_0=2, \underline{Wo}=10.5 \quad \omega t=180^\circ$

Figure 3. Velocity contours variations with frequency for fixed amplitude and phase angle.

The velocity contours for different frequencies at a constant amplitude ($A_0=2$) and phase angle ($\omega t=180^\circ$) are shown in Fig.3 together with steady jet conditions. It is observed that the velocity contours are symmetric about the axial direction for all cases. The velocity fields and flow structure are changed along the target wall by pulsating jet effect and varying with the frequency. As shown in the figures, the flow structure of pulsating conditions are different than steady case. Because of the unsteadiness of the pulsed jet flow, the boundary layer on the target surface is different than steady conditions. The pulsation frequency effected flow structure, and increasing the frequency is increased the unsteady effect. Thus, the renewal of boundary layer is accelerated. By comparing the steady flow with all other cases, it can be concluded that the pulsating jet significantly affected to the flow field, and contributed the heat transfer improving..



$H/D=10, \underline{A_0}=0.5, Wo=7.42 \quad \omega t=270^\circ$ $H/D=10, \underline{A_0}=1, Wo=7.42 \quad \omega t=270^\circ$ $H/D=10, \underline{A_0}=2, Wo=7.42 \quad \omega t=270^\circ$

Figure 4. Velocity contours variations with amplitude for fixed frequency and phase angle.

The velocity contours for different amplitudes at a constant frequency ($Wo=7.42$) and phase angle ($\omega t=270^\circ$) are shown in Fig.4. The velocity field is changed along the plate by pulsations of flow with increasing the amplitude compared with steady jet. The pulsating jet is changed the flow dynamics on the target surface by means of the momentum transfer. Therefore, the velocity field is changed very fast and thermal boundary layer is destroyed very fast. Because of the periodicity a new boundary layer is formed with fresh bulk fluid, and the fluid in the boundary layer is away from the wall for each cycle. Thus, this phenomenon provides an effective heat transfer rate from cooling surface during a pulsating cycle. The cooling effect of jet increases with increasing the amplitude as shown in figures.

3.1 Heat Transfer Calculation

To calculate the heat transfer for a continuously (steady) impinging jet, conventional local Nu number is defined as;

$$Nu = \frac{q''}{T_w - T_j} \frac{D}{k} \quad (5)$$

where, k is the thermal conductivity of the fluid, D is jet diameter (characteristic length), T_w is target surface temperature and T_j is the jet fluid temperature. The Nusselt number varies with time and position. Therefore, the time-averaged and space-averaged Nusselt number can be calculated by;

$$Nu_t = \frac{1}{\tau} \int_0^{\tau} Nu_{x,t} dt \quad (6)$$

$$Nu_x = \frac{1}{L} \int_0^L Nu_{x,t} dx \quad (7)$$

The overall heat transfer coefficient is obtained by an integration of the local and instantaneous Nusselt number over a cycle for a heated target surface. For this purpose, the time-averaged Nusselt and space-averaged Nusselt numbers are combined with each other, and the total or cycle-averaged Nusselt number is defined as:

$$Nu_p = \frac{1}{\tau L} \int_0^L \int_0^{\tau} Nu(x, t) dt dx \quad (8)$$

where, the enhancement factor of heat transfer is obtained by the relative heat transfer rate, which is defined by Eq. (9):

$$\frac{Nu_p}{Nu_s} \quad (9)$$

where Nu_p is the cycle-averaged Nusselt number (Eq.8), Nu_s is the Nusselt number for steady jet flow (no pulsating jet flow). Thus, a value of relative heat transfer rate greater than 1.0 denotes enhanced heat transfer.

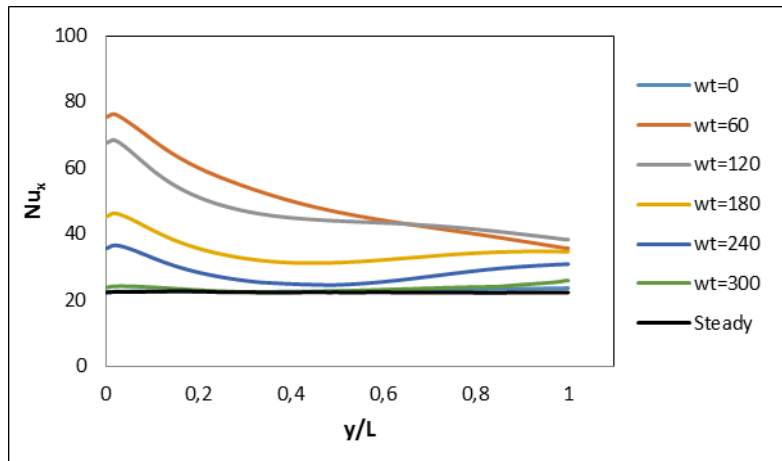


Figure 5. Local Nu number variations with phase angles. ($Re_j=5000$, $H/D=10$, $A_o=2$, $Wo=10.5$)

The distribution of local instantaneous Nusselt number on the hot surface is depicted in Fig.5, depend on phase angle for a cycle together with steady jet flow. The local Nu number along the heated wall is plotted during a pulsating cycle. The value of Nu number is changed with phase angle. Pulsation is changed the flow structure on the boundary layer and changed the thermal behaviors of the hot surface. The maximum Nu number is occurred at around the stagnation point. It is obviously shown that the pulsating jet have a significant effect on the heat transfer.

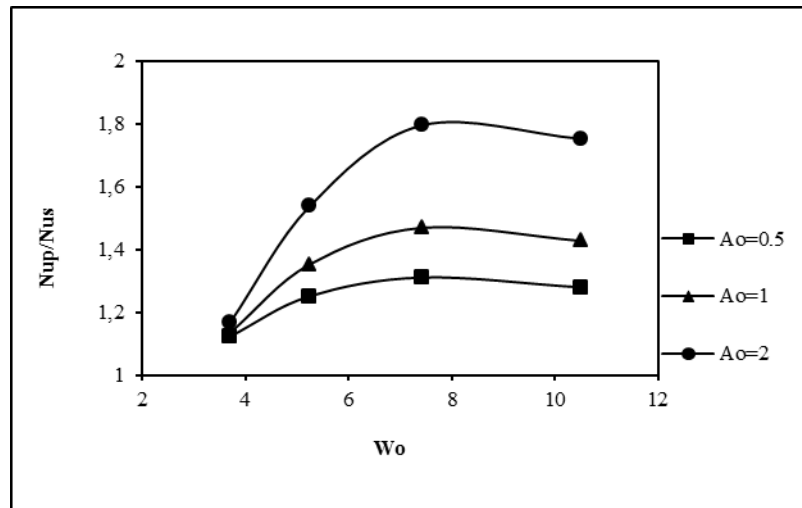


Figure 6. The variation of heat transfer enhancement factor with pulsating parameters

The heat transfer enhancement factor (Nu_p/Nu_s) at different pulsating frequencies and amplitudes is shown in Fig.6. It is found that the heat transfer enhancement factor of pulsating impinging jet can be several times as large as that steady (or continuous) jet conditions. It can be concluded that there is an optimum Womersley number at which heat transfer enhancement is maximized. Large heat transfer enhancement is obtained (up to %80) in pulsating jet with a specific pulsating frequency ($Wo=7.42$) and high amplitude ($A_o=2$) for fixed Reynolds number. It was observed that the heat transfer enhancement factor increases with frequency, but when the pulsating frequency is above the critical frequency the heat transfer is decreased. The flow characteristics of a pulsating jet are a strong function of the pulsating frequency. This behavior has been explained by corresponding change in the thickness of hydrodynamic boundary layer. However, it is relevant to note that the increase in the heat transfer is more sensitive to amplitude than to frequency, because high amplitude increases the convective effect in the flow, and very high heat transfer is achieved. The amplitude have a strong effect on the hydrodynamic and thermal boundary layer development with time.

CONCLUSIONS

In this study, the cooling characteristics of a circular target surface under the turbulent pulsating impinging jet conditions is investigated numerically by using a control volume based CFD solver. For a specific Reynolds number ($Re=5000$) the effects of pulsating jet frequency and amplitude on the average Nusselt number are presented. The results show that the heat transfer performance remarkably increased with increasing pulsating amplitude at a specific frequency compared with that in steady jet flow. Generally, increasing the frequency and amplitude leads to heat transfer enhancements and the best performance may be obtained in critical frequencies. The best heat transfer performance is obtained at $Wo=7.42$ and $A_o=2$. As a result, the pulsating jet velocity plays a noticeable role on flow structure and thermal fields on the target surface, which may lead to heat transfer enhancement. Therefore, these conditions can be proposed to achieve higher performance and design more compact thermal devices.

REFERENCES

- [1] A.H. Beitelmal, M.A. Saad, and C.D. Patel, The effect of inclination on the heat transfer between a flat surface and an impinging two-dimensional air jet, *Int. J. Heat Fluid Flow*, vol. 21, pp. 156-163, 2000.
- [2] V.A. Chiriach and A. Ortega, A numerical study of the unsteady flow and heat transfer in a transitional confined slot jet impinging on an isothermal surface, *Int. J. Heat Mass Trans*, vol. 45 (6), pp.1237-1248, 2002.
- [3] R. Dutta, A. Dewan and B. Srinivasan, Comparison of various integration to wall (ITW) RANS models for predicting turbulent slot jet impingement heat transfer, *Int. J. Heat Mass Trans*, vol. 65, pp. 750-764, 2013.
- [4] E. Oztekin, O. Aydin and M. Avcı, Heat transfer in a turbulent slot jet flow impinging on concave surfaces, *Int. Commun. Heat Mass Trans*, vol. 44, pp. 77-82, 2013.
- [5] M.V. Jensen and J.H. Walthera, Numerical Analysis of Jet Impingement Heat Transfer at High Jet Reynolds Number and Large Temperature Difference, *Heat Trans Engn.*, vol. 34, issue 10, pp. 801-809, 2013.
- [6] J. Lee and S. Lee, The effect of nozzle aspect ratio on stagnation region heat transfer characteristics of elliptic impinging jet, *Int. J. Heat Mass Trans*, vol. 43, pp. 555-575, 2000.
- [7] F. Schwertfirm, J. Gradl, H. C. Schwarzer, W. Peukert and M. Manhart, The low Reynolds number turbulent flow and mixing in a confined impinging jet reactor, *Int. J. Heat Fluid Flow*, vol. 28, pp.1429, 442, 2007.
- [8] X. Peng, Y. Boming, Q. Shuxia, J.P. Hee and S.M. Arun, Turbulent impinging jet heat transfer enhancement due to intermittent pulsation, *Int. J. Therm. Sci.*, vol. 49, pp. 1247-1252, 2010.
- [9] F. Selimefendigil and H.F. Oztop, Pulsating nanofluids jet impingement cooling of a heated horizontal Surface, *Int. J. Heat Mass Transfer*, vol. 69 pp. 54-65, 2014.

- [10] S. Alimohammadi, D.B. Murray and T. Persoons, On the numerical-experimental analysis and scaling of convective heat transfer to pulsating impinging jets, *Int. J. Therm. Sci.*, vol. 98, pp.296-31, 2015.
- [11] Z. Travnic̆ek and T. Vit, Impingement heat/mass transfer to hybrid synthetic jets and other reversible pulsating jets, *Int. J. Heat Mass Trans*, vol. 85, pp. 473–487, 2015.
- [12] D.J. Sailor, D.J. Rohli and Q. Fu, Effect of variable duty cycle flow pulsations on heat transfer enhancement for an impinging air jet, *International Journal of Heat and Fluid Flow*, vol. 20, pp. 574-580, 1999.
- [13] H.J. Poh, K. Kumar and A.S. Mujumdar, Heat transfer from a pulsed laminar impinging jet, *Int. Commun. Heat Mass Trans*, vol.32, issue10, pp. 1317–1324, 2005.
- [14] H. M. Hofmann, D. L. Movileanu, M. Kind and H. Martin, Influence of a pulsation on heat transfer and flow structure in submerged impinging jets, *Int. J. Heat Mass Trans*, vol. 50, pp. 3638–3648, 2007.
- [15] W. Liewkongsatoporn, and T. Patterson and F. Ahrens, Pulsating jet impingement heat transfer enhancement, *J. Dry. Technol.* Vol. 26 pp. 433-442, 2008.
- [16] B. N. Hewakandamby, A numerical study of heat transfer performance of oscillatory impinging jets, *Int. J. Heat Mass Trans*, vol.52, pp. 396–406 2009.
- [17] P. Xu, S. Qiu, M. Yu, X. Qiao and A. S. Mujumdar, A study on the heat and mass transfer properties of multiple pulsating impinging jets, *Int. Commun. Heat Mass Trans*, vol. 39, pp 378–382, 2012.
- [18] J. Mohammadpour, M. Rajabi-Zargarabadi, A.S. Mujumdar and H. Ahmadi, Effect of intermittent and sinusoidal pulsed flows on impingement heat transfer from a concave surface, *Int. J. Therm. Sci.*, vol. 76, pp. 118-127, 2014.
- [19] J. Mohammadpour, M. M. Zolfagharian, A. S. Mujumdar, M. R. Zargarabadi and M. Abdulhazadeh, Heat transfer under composite arrangement of pulsed and steady turbulent submerged multiple jets impinging on a flat surface, *Int. J. Therm. Sci.*, vol. 86, pp.139-147, 2014.
- [20] M. Bovo and L. Davidson, Direct comparison of LES and experiment of a single-pulse impinging jet, *Int. J. Heat Mass Trans*, vol. 88, pp. 102–110, 2015.
- [21] L. Geng, C. Zheng, and J. Zhou, Heat transfer characteristics of impinging jets: The influence of unsteadiness with different waveforms, *Int. Commun. Heat Mass Trans*, vol. 66, pp. 105–113. 2015.
- [22] P. Xu, Mujumdar A.S. Poh, H.J. and Yu B., "Heat transfer under a pulsed slot turbulent impinging jet at large temperature differences." *Thermal Science* 14(1): 271-281, 2010.
- [23] E.C. Mladin and D.A. Zumbrennen, Local convective heat transfer to submerged pulsating jets *Int. Commun. Heat Mass Trans*. 40(14): (1997) 3305-3321.
- [24] Fluent 6.3. FLUENT user's guide. Fluent, Inc., Lebanon, NH. 03766, USA, 2006.

Applications For Turkish Text Summarization

*Ozlem Evrim Gundogdu*¹, Nevcihan Duru¹*

Abstract

Computer engineering is one of the most visible departments of the human - machine interaction. The systems like making translation, classification being studied for a long time. Digital technology progresses , different needs that bring the work in this environment have occurred. The number of documents worth noting that in the digital environment, it may seem that facilitate access to resources has revealed a problem as the separation of this document which is required in. In this study, natural language processing (NLP) is one of the interest topic of human - machine interactions will be referred to the document summarizing. Common aim of this subject is to develop a system that can remove the nearest summary to man-made summary. Document summarizing studies have started with choosing the best sentence that can be entered in the summary from the document (Statistical methods); nowadays developments on semantic summarization are improved (as creating new sentences for summary according o document's main subject and sub_topics). Although the document summarizing has worked since the 1950s is an issue that can be considered new for Turkish Studies. Turkish, considered a difficult language for summarization because of morphology and synonyms due to abundance of document. Therefore requirements for summarization systems like libraries, natural language processing applications as separating words, finding word's root, noun classification are needed. With this study an entry is made for Turkish document summarization and the literature and the results of our research will be evaluated.

***Keywords:** Natural Language Processing, Text Summarization, Text Summarization on Turkish*

1. INTRODUCTION

NLP is a subject that computer science has been studying the languages that can exist with their grammar rules and structure. Cooperation of computer scientists and linguists started through transferring data or audio recording to digital environment. As a result of this process, there is a need to extract data which is increasing rapidly on our computers and on the internet.

In this study, text summarization which is one of the subtopics of NLP is studied. It is suggested that system which helps users to examine the text via summaries instead of reading all the text is more helpful. Text summarization can be found in literature because it is a subject worked on since 1959. However, a significant portion of studies focuses on English and Chinese and problem solution strategies were developed considering these languages. Turkish is a member Ural-Altaic language family and it is agglutinative. For this reason, some difficulties emerged during NLP process to produce too many words by adding suffixes in Turkish.” Osmanlılaştıramadıklarımızdanmışımızcasına” is a typical exaggerated example of this kind of production [1].

Natural language processing work as main and intermediate application can be divided into two groups. Main applications study on recovery of the information such as machine translation, automatic summarization, information extraction. The intermediate applications, separating the sentence element analysis, morphological analysis (word finding additional and roots), perform the necessary steps to clarify the meaning of the word for the main application [2] .

In the second part of the study , studies on text summarization will be examined, problems will be demonstrated, and obtained results and success rates will be discussed. Effective methods in text summarization will be explained in detail.

This study aims to be a useful source for Turkish text summarization studies and contribute to the progress on studies on this subject.

2. AUTOMATIC TEXT SUMMARIZATION

Since the main part of the subject is language, the study is located in a wider framework. Therefore, NLP can be separated to many sub_topics.

- The development of tools that help in spelling.
- Spelling correction of wrong.
- Find and replace.
- Read a printed text (optically text-to-speech) and read errors correction.
- A summary of the text.

¹Corresponding author: Kocaeli University, Department of Electronics and Communication Engineering, 41380, Izmit/Kocaeli, Turkey.
ozlemevrim@yahoo.com

- Removing the information that is contained in the text.
- Access to information.
- Understanding the text.
- Computer voice interaction.
- Computer talk (text to voice).
- Understanding speech (speech to text conversion).
- Question response strings.
- Foreign language reading helper tools.
- Writing help tools in foreign languages.
- Natural language cross translation.

There are many usages of the same language and necessity of grounding on these usages to rules causes some problems:

- Ungrammatical and unintelligible speeches.
- Ungrammatical and foul writings.
- Slicing the conversation.
- The text of the slicing.
- Word attributes.
- The meaning of uncertainties.
- Elimination of chronological promised uncertainties.
- The speech plan [3].

Text summarization which is examined in this study is a sub_topic of NLP. Automatic text summarization systems can be useful in multidocument scanning. Moreover, automatic text summarization systems can summarize one or more documents.

There are two ways in automatic text summarization:

1. Selecting a sentence summarizing: The aim of this method is to score sentences with using statistical methods, intuitive approach.
2. Semantic hashing: This type is intended to summarize the objective of shortening the sentence within the text. For example, “ Ahmet hates apple, orange and banana. ” sentence is shortened as “Ahmet hates fruits. ”. This method can be used in a table of a rich symbolic words are needed [4].

According to Lin and Hovy text summarizing consist of these steps :

- Identification of the topic: Here are the most important issues searches within the text. To generate this process; the word frequency, the position of text in sentences, sentences in the important words (as a result, most importantly, in a nutshell, etc.), common words (prepositions, and token are not required), stating the date and specific name expressions such as method are used.
- Interpretation: This process create sentences again using with general expressions. For example " Elif weared school uniform, took her bag and got in the bus " interpreted " Elif went to school".
- Generation: In the process of producing text is intended to receive the final version of the summary. At this stage, the methods used are usually obtained from the above process takes as input the words and phrases they reinterpreted the results text creates a summary of the final version [5].

During text summarization, some inputs may be requested from the user (the length of the abstract, keywords, etc.), or no restriction should be used.

When text summarization studies examined, the method that sentences are scored inside the text is more widely used, scoring is made according to a defined criteria. For this process, the text should be seperated in to paragraphs, sentences and words. Then, sentences are scored by using the following criteria.

- The entity of words used in the title of the text are checked in sentence.
- The date information is checked in sentence.
- The special names are checked in sentence.
- The words that are defined as Positive/negative word are checked in sentence. Positive words; like in summary, as a result, ultimately that are wrap up the text. Negative words; like because, however, sentences that used negative words give us detailed information about text.
- Keywords are checked. The user enters when searching on words or articles keyword are evaluated in this last criteria.

- It is important to place within the text of the sentence.
- The text of the first and last sentences in the paragraph are treated as a priority.
- The frequency of each word within the Text is calculated. When calculating the frequency the frequency rate of the transition within the text of the word is used. The most common are made by starting a sort of last word and usually %10 of list are processed. The most frequent words in sentences containing the plus points is added.
- Collocated that reinforce the meaning of the sentence are checked.
- The sentence end-marking is checked. If the sentence includes an exclamation or question mark contains, any punctuation marks that adds importance sentence, extra points are given to sentence.
- The average sentence lengths are calculated within the text. Above average ± 1 on the sentences awarded points.
- The named entity recognition method is used in a sentence, scored according to results. This method was used at first as [6].
- Text summarization shouldn't be seen as text mining. The aim of text mining is to obtain meaningful statistical data from the text. During text mining studies, attribute extraction can be made by using NLP [7].

The Studies Were Made On The Turkish Texts

Zemberek is one of the studies on Turkish and it is a source that everybody make use of during their NLP studies. Zemberek is an open source Turkish natural language processing library. It can be used to find word roots, proper names in the text during NLP studies. Its second version "Zemberek2" is online now and can be used for all Turkish languages [7].

Another study on Turkish words is done by Balkanet Group. This Project is similar to Wordnet; the group that work together for Turkish, Bulgarian, Czech language, Greek, Romanian Language and Serbian Languages. Turkish part of project is performed by K.Oflazer and study team. The aim of the this project is to classify synonymous words and to develop a database [8].

The studies were made on the Turkish texts are exhibited with two tables according to kind of text, methods and achieved results. When the tables are looked in to it seems that commonly the statistical methods are used for this subject. As a result studies on semantic summarization should be done and kind of text (in that number and diversity) should be increased.

Within the scope of this study table 1 and table 2 are generated with these questions:

- What is the distribution by years of presented studies ?
- What are the methods used by the presented studies ?
- What is the document type used in the presented studies ?
- How evaluated are provided the results and success rate of the studies ?

Table 1. The articles about Turkish text summarization

Articles About Turkish Text Summarization and Years	Methods and Algorithms	Input Documents	Flow Chart	System's Success
Altan Z., "A Turkish Automatic Text Summarization System", International Conference Artificial Intelligence and Applications, 2004, [9].	Statistical methods are used.	50 different articles on web.	Statistical methods are used and weighting factors are predetermined. Also before the process, system asks to user entry for which document will be summarized, summary length and adding to database system.	The purpose of the developed system in this study is to constitute such a summary that reflects the subject perfectly, underlying the contextual and locational relations of the sentences very carefully. The system generally utilizes statistical approximations. Key words which were previously defined by the system, most frequent words in the text, and the constituted corpus have important influence on summarization process.
Uzundere E., Dedja E., Diri B., Amasyali M. F., "Türkçe haber metinleri için otomatik özetleme ", , 2008, [10]	Sentence scored methods are used.	10 text	Sentences are scored according to feature score table.	10 texts are summarized by 15 people. When the results compared, system success rate is %55.
Kutlu M., Cıgır C., Cicekli I., "Generic Text Summarization for Turkish ", Published by Oxford University Press on behalf of The British Computer Society, 2010, [11].	Sentence scored methods are used.. Also Also key phrase method is used.	Two data sets are used, Turkish newspaper and journal articles	First of all, features are trained and correct features combination is used for sentence score process.	Performance evaluation is conducted by comparing summarization outputs with manual summaries generated by 25 independent human evaluators.
M.V. Sami, B. Diri, "Web Tabanlı Otomatik Özet	Sentence scored methods	Web pages	Every sentences are scored and according to summary	

Çıkarma Sistemi", Akıllı Sistemlerde Yenilikler ve Uygulamaları Sempozyumu, Kayseri, 2010, [12],	are used.		rate high scored sentences are chosen for system summary.	System's summaries are reached %59 success rate
Güran A., Bekar E., Akyokuş S., "A Comprasion Of Feature and Semantic-Based Summarization Algorithms For Turkish", International Symposium on Innovations in Intelligent Systems and Applicaitons, Kayseri, (21-24June 2010, [13]	Sentence scored methods , SVD algorithm and matrix methods are used.	50 documents collected from the online Turkish newspapers and some news portals	Matrixes are generated with sentences and words. SVD algorithm works and sentences are scored. In this part of study, low scored sentences that are taken to summary , a second matrix is generated and sentences are scored again. So that negativity of first methods are eliminated.	Statistical and semantic based methods are used and compared. As a result semantic methods gives more similar results according to summaries that made by people.
Özsoy M.G., Alpaslan F.N., "Text summarization using Latent Semantic Analysis", Journal of Information Science 1-13, 2011, [14].	Sentence scored methods, LSA, tf-idf, cross and topic method are used.	Four different sets of Turkish documents are used for the evaluation of summarization approaches.	In this study LSA based algorithms are used for Turkish and English documents.	Cross and topic methods have good results therefore the system that they generate could be used another languages.
Çakır M., Çelebi E., "Kapsama Katsayısı Tabanlı Kümeleme İle Belge Özetleme", IEEE 19th Signal Processing and Communications Applications Conference, SIU 2011, [15],	C3M (Cover Coefficient-Based Clustering Methodology) algorithm is used.	10 Turkish documents	C3M algorithm is used for to choose sentence with similarity feature that are could be used in summary.	System performance is evaluated by Precision, Re-call and ROUGE evaluation algorithms. Researchers exhibit that their recommended system gives better results.
Güran A., Güler Bayazıt N., Gürbüz M. Z., "Efficient feature integration with Wikipedia-based semantic feature extraction for Turkish text summarization", 2013, [16]	Structural and semantic features.	110 newspaper documents.	In this study they represent a hybrid Turkish text summarization system that combines structural and semantic features.	The summaries' success that are done by system is analyzed with summaries that are done by 3 people.
Güran A., Arslan S. N., Kılıç E., Diri B., " Sentence selection methods for text summarization", 2014, [17]	Sentence scored methods are used. In this study "name entity recognition " feature is used first time in Turkish text summarization studies.	20 newspaper documents.	Sentence scored features are evaluated with different combinations and most successful combinations are listed.	The summaries' success that are done by system is analyzed with summaries that are done by a group of people (15 female, 15 male).

Table 2. Thesis about Turkish text summarization

Thesis About Turkish Text Summarization and Years	Methods and Algorithms	Input Documents	Sentence Scored Method	System's Success
A.Güran, 2013, Phd [18]	A hybrid method (structural and semantic) is used for sentenced election. A new Weighting value based LSA is recommended	Single document summarizing / newspaper articles	Sentenced scored method used.	F-measurement score and ROUGE packets used. Also in the system document's sentences are chosen by the users for summaries and system's summary is compared with this manuell summary.
F.C.Pembe, 2010, Phd [19]	Query and structural based summarizing is presented for Web search.	Single document summarizing / Web articles / Turkish and English	Sentenced scored method used.	Researcher explained that system summaries have better performance according to Google summaries.
Ş. B. Bilgin, 2014, Master	Two different	Multi document	Sentenced scored	This system's results gives better

[20]	dependency tree based methods for finding similarities between sentences are used first time for relation extraction.	summarizing / English	method used. And new features used.	results according to statistical and semantic methods.
M.Berker, 2011, Master [21]	11 sentence features are used. In these features, lexical relations there are. Features are combined with genetic algorithms.	Single document summarizing / Newspaper articles / English	Sentenced scored method used.	System feature gives better summaries than single feature used summaries.
M.Y. Nuzumlalı, 2010, Master [22]	In different levels, root detection and sentence purification methods effects are investigated in multi-document summarization.	Multi document summarizing / Turkish		System performance is tested by Rouge.
S. Karakaynak, 2009, Master [23]	LSA based virtual centre method used for multi-documents.	Multi document summarizing / Articles are presented in DUC 2004 Conference	Sentenced scored method used.	When the results are inspected , LSA method is effective . The system results are taken with using ROUGE.
M. Tülek , 2007, Master [24]	Stemming method and some of statistical methods are used	Single document summarizing / Turkish	Sentenced scored method used.	System's results are compared with people's summaries for same documents. Development system gives good results with documents like e-mails, science articles and news paper articles; but with irregular documents like advertisements, chatting documents success is lower.
E. Gönenç, 2006, Master [25]	Key phrase are eliminated by lexical chains method and documents summarized.	Single document summarizing / English		System works with English documents.

CONCLUSIONS & FUTURE WORK

While there are numerous studies on text summarization it is still popular and developing area. It is clear that text summarization makes scanning documents on digital environment easier and decreases time and labour loss. It can also be a good source commercial software. Text summarization is a wide study area for Turkish and difficulties occurred due to Turkish grammatical structure can be through studies.

By this time statistical methods are preferred mostly for these studies. This situation may be occur because of synonym words and Turkish is an agglutinating language. So that summaries that produced by computer systems success measuring maybe difficult in that semantic context.

It is observed that both structural and semantic Turkish text summarization studies give significant results. The aim of this study is to provide a source for text summarization on Turkish documents. It is introduction to Turkish text summarization study. The next step will be developing a different system on Turkish text summarization and obtained data in different areas. Also we study about to develop Turkish natural language processing libraries and become prevalent intermediate applications for NLP.

REFERENCES

- [1] G. Eryiğit: Dependency Parsing Of Turkish, Phd Thesis, İTÜ, 2006.
- [2] Z. Altan, Z. Orhan: Anlam Belirsizliği İçeren Türkçe Sözcüklerin Hesaplamalı Dilbilim Uygulamalarıyla Belirginleştirilmesi, http://turkoloji.cu.edu.tr/DILBILIM/anlam_belirsizligi.pdf, 2015.
- [3] E. Adalı : Doğal Dil İşlemenin Temelleri, http://www.ozadalı.net/?page_id=1695, 2015.
- [4] E. Uzundere, E. Dedja, B. Diri, M. F. Amasyalı: Türkçe haber metinleri için otomatik özetleme, Akıllı Sistemlerde Yenilikler ve Uygulamaları Sempozyumu, 2008.
- [5] E. Hovy, C. Y. Lin: Automated text summarization in summarist, Annual Meeting of the ACL Proceeding of a Workshop, 1998.
- [6] A. Güran, S. N. Arslan, E. Kılıç, B. Diri : Sentence selection methods for text summarization, IEEE 22nd Signal Processing and Communications Applications Conference (SIU 2014), 2014.
- [7] www.wikipedia.com, 2015.

- [8] <https://en.wikipedia.org/wiki/WordNet>, 2015.
- [9] Z. Altan : A Turkish Automatic Text Summarization System, International Conference Artificial Intelligence and Applications, 2004.
- [10] E. Uzundere, E. Dedja, B. Diri, M. F. Amasyalı: Türkçe haber metinleri için otomatik özetleme, Akıllı Sistemlerde Yenilikler ve Uygulamaları Sempozyumu, 2008.
- [11] M. Kutlu, C. Cığır, I. Cicekli : Generic Text Summarization for Turkish, Published by Oxford University Press on behalf of The British Computer Society, 2010.
- [12] M.V. Sami, B. Diri: Web Tabanlı Otomatik Özet Çıkarma Sistemi , Akıllı Sistemlerde Yenilikler ve Uygulamaları Sempozyumu, Kayseri, 2010.
- [13] A. Güran , E. Bekar, S. Akyokuş : A Comparison Of Feature and Semantic-Based Summarization Algorithms For Turkish, International Symposium on Innovations in Intelligent Systems and Applications, Kayseri, 21-24June 2010.
- [14] M.G. Özsoy, F.N. Alpaslan: Text summarization using Latent Semantic Analysis, Journal of Information Science 1–13, 2011.
- [15] M. Çakır, E. Çelebi : Kapsama Katsayısı Tabanlı Kümeleme İle Belge Özetleme, IEEE 19th Signal Processing and Communications Applications Conference (SIU 2011), 186-189, Berlin, 2011.
- [16] A. Güran, N. Güler Bayazıt, M. Z. Gürbüz: Efficient feature integration with Wikipedia-based semantic feature extraction for Turkish text summarization, Turkish Journal of Electrical Engineering & Computer Sciences, 2013.
- [17] A. Güran, S. N. Arslan, E. Kılıç, B. Diri : Sentence selection methods for text summarization, IEEE 22nd Signal Processing and Communications Applications Conference (SIU 2014), 2014.
- [18] A. Güran :, Otomatik Metin Özetleme Sistemi, Phd Thesis, Yıldız Technical University, 2013.
- [19] F. C. Pembe: Automated Query-Biased And Structure-Preserving Document Summarization For Web Search Tasks, Phd Thesis, Boğaziçi University, 2010.
- [20] S. B. Bilgin: Multi-Document Summarization Using Dependency Grammars, Master Thesis, Boğaziçi University, 2014.
- [21] M. Berker : Using Genetic Algorithms With Lexical Chains For Automatic Text Summarization, Master Thesis, Boğaziçi University, 2011.
- [22] M. Y. Nuzumlalı: Analyzing Stemming And Sentence Simplification Methodologies For Turkish Multi-Document Text Summarization, Master Thesis, Boğaziçi University, 2010.
- [23] S. Karakaynak: Development Of Tool For Managing Semantic Text Content, Master Thesis, Çankaya University, 2009.
- [24] M. Tülek: Text Summarization For Turkish, Master Thesis, İTÜ 2007.
- [25] E. Gönenc: Automated Text Summarization And Key Phrase Extraction, Master Thesis, Çankaya University, 2006.

Determining the Relationship between Predominant Frequency and Damping Ratio by Using Single Station Microtremor Recordings

Ozgenç Akin¹, Ali Erden Babacan¹

Abstract

Microtremor measurements have been widely used to understand seismic behavior of buildings over the last decades. Predominant frequency and damping ratio obtained by Nakamura Method shows how to respond buildings during earthquakes. In this study, 10 single station microtremor recordings (SSMR) have been taken in the Karadeniz Technical University Department of Geophysical Engineering Building and 2 SSMR have been taken near the building to compare with the inside measurements. The predominant frequencies obtained by using Nakamura Method. The predominant frequency of the inside measurements are between 4.7-7.0 Hz and mean inside frequency is 5.6 Hz while the outside measurements are 3.7 Hz, 4.0 Hz and the mean outside frequency is 3.85 Hz. The inside and outside measurements show that they are not equal to each other. For this reason, the resonance risk is very low. The damping ratios of the building obtained by Half Power Bandwidth Method and change 5.32 to 17.86 percent. According these results the predominant frequency and the damping ratios correlated with each other and it was determined that there is a meaningful relation between them. The increasing predominant frequencies lead to increasing damping ratios.

Keywords: *Microtremor, Predominant Frequency, Damping Ratio*

¹ Corresponding author: Karadeniz Technical University, Department of Geophysical Engineering, 61080, Trabzon, Turkey.
ozgencakin@ktu.edu.tr

1. INTRODUCTION

Determination of ground and building characteristics is very important to provide against earthquakes. That's why the best approach for understanding these conditions is through direct observation of seismic ground motions. The fastest and the cheapest method is using Single Station Microtremor Recordings (SSMR) to detect predominant frequency and H/V ratio of the ground or building. Microtremor is a very convenient tool to estimate the effect of surface geology on seismic motion without needing other geological information [1]. The method is based on recording of ground or building vibrations which caused by natural or artificial events, such as wind, waves or vibrations of a vehicle. H/V ratio and frequency contents of the vibration of the ground or building are influenced by the factors as lithology and characteristics of building. So, ground can be classed according these vibrations by using recordings taken on ground. Also, microtremor recordings recorded in buildings are useful to detect resonance risk and damping ratio during an earthquake. Taking into account all of these, information about how secure and stable the buildings can be obtained to take precautions against earthquakes. The aim of this study is determination of the characteristics of microtremor signals of high floors building to detect damping ratio, H/V ratio and predominant frequency. Also, relationship between predominant frequency and damping ratio has been investigated to obtain a correlation among them.

2. METHODS and DATA

In this study, Karadeniz Technical University Department of Geophysical Engineering building was investigated by using SSMR. The building is located approximately 150 km distance from to The North Anatolian Fault which is the most dangerous fault system in Turkey. SSMR were taken at 10 points in the building and 2 points near the building (Figure 1). The all measurements were evaluated by using Nakamura Method [2] with *Geopsy* program [2]. A sample of data processing was given in Figure 2. The signals were Butterworth band-pass filtered (0.05-20 Hz) to remove intensive artificial disturbance. Then, they were divided into 25 seconds long windows and tapered individually by using Konno-Ohmachi window [3]. For each window, the amplitude spectra of the three components were computed using a Fast Fourier Transform (FFT) algorithm. In this way, spectra of the three components were obtained from the data (Figure 2a, b, c). Then, Nakamura Method was used and the pick of the predominant frequency was selected by taking into consideration the spectra (Figure 2d).

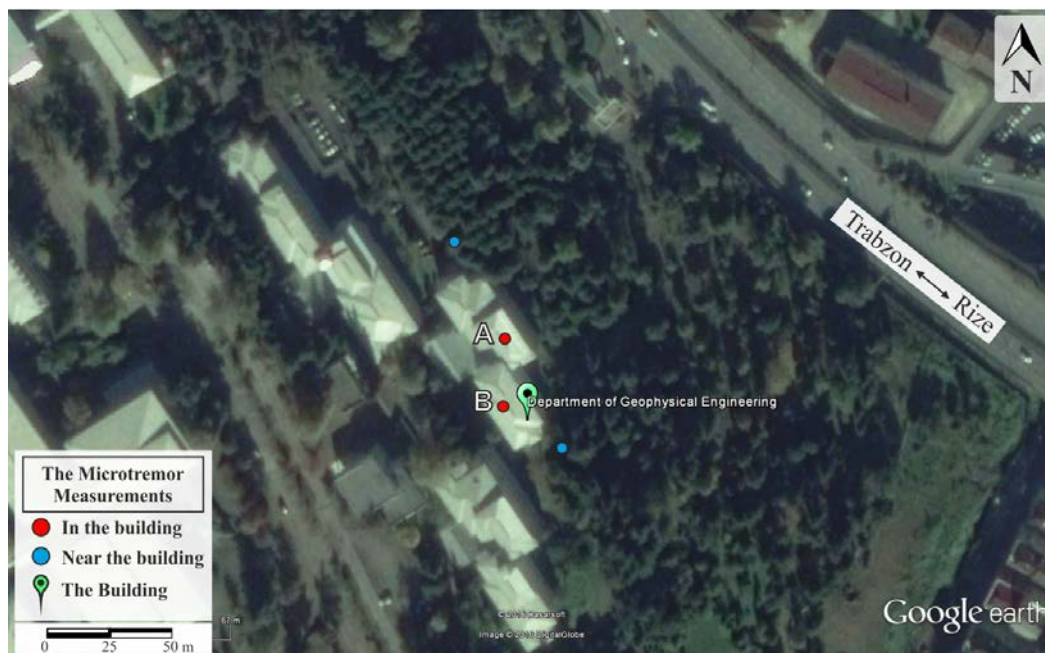


Figure 1. Location of the building and the measurements.

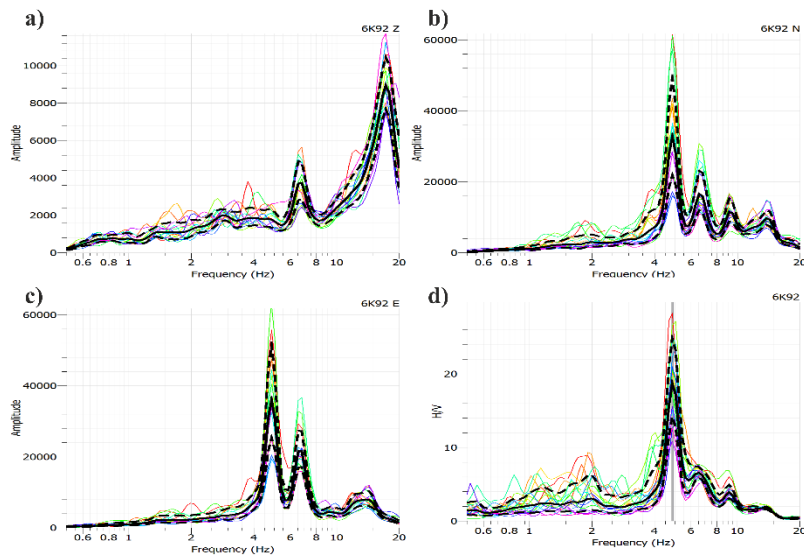
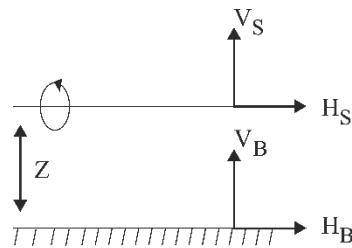


Figure 2. a) The vertical spectrum, b) and c) horizontal spectra of the measurement, d) the result of Nakamura Method according to the spectra at the 5th floor.

According to Nakamura (1989), vertical components of noise vibrations are not influenced from the ground layers. However, the horizontal components are acquired to major amplifications depending on ground layers with low velocity and density. Consequently, the ground transfer functions were obtained by divided of the horizontal components spectrum to vertical components spectrum (Figure 3 and Equation 1). By using parameters obtained from Nakamura Method, damping ratios have been calculated with Half Power (Bandwidth) Method [5] to understand vibration characteristic of the building (Figure 4).



$$S_M(\omega) = \frac{H_S(\omega)}{V_S(\omega)} \quad (1)$$

Figure 3. Simple model assumed by Nakamura (1989) to interpret microtremor measurements. V_S and H_S are vertical and horizontal components on the surface, V_B and H_B are vertical and horizontal components in depth of Z .

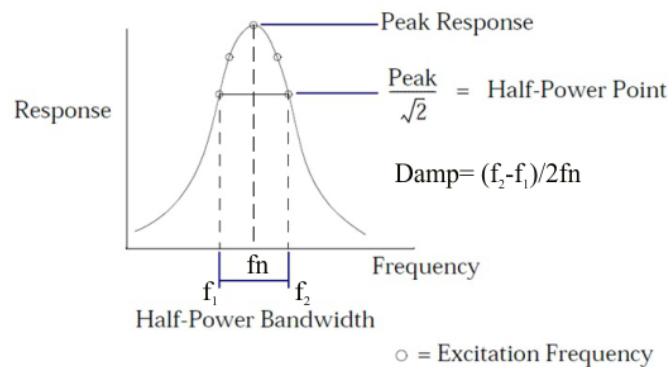


Figure 4. Frequency-response experiment to determine damping ratio.

CONCLUSIONS

The SSMR were taken in the building and at the garden, totally 12 points and compared with each other. The all recordings were evaluated by using Nakamura Method with *Geopsy* program. The predominant frequencies are slightly decreasing the basement to the top floor. This decreasing is expected because of the increasing number of the floors. The predominant frequency of the inside measurements are between 4.7-7.0 Hz and inside mean frequency is 5.6 Hz while the outside measurements are 3.7 Hz, 4.0 Hz and the outside mean frequency is 3.85 Hz. When compare the inside and outside predominant frequencies, it can be said that the resonance risk is low because the predominant frequencies are not close to each other. The H/V ratios show nearly same trend and change between 1.49-25.0 in the building and 1.5-1.6 at the outside. The damping ratios are in a harmony with the predominant frequencies shown as Table 1. When they correlated with each other it is seen that there is a meaningful relation between them ($R^2=0.70$). The increasing predominant frequencies cause to increasing damping ratios (Figure 5).

Table 3. The results of the study.

SSMR Points	Predominant Frequency (Hz)	H/V Ratio	Damping (%)
A (-1). Floor	6,30	1,49	9,92
A Basement Floor a	7,00	2,50	17,86
A Basement Floor b	6,25	2,50	11,20
A Basement Floor c	7,00	2,50	13,57
B Basement Floor	5,20	2,50	9,62
A 1. Floor	5,00	5,00	10,00
B 1. Floor	4,90	7,00	9,18
A 2. Floor a	4,80	11,00	6,77
A 2. Floor b	5,30	5,00	6,13
B 2. Floor	4,70	25,00	5,32
Ave. (A) Building	5,95	4,28	10,78
Ave. (B) Building	4,93	11,50	8,04
Ave. of the Building	5,65	6,45	9,96
A Outside	3,70	1,50	***
B Outside	4,00	1,60	***
Average of the Outside	3,85	1,55	***

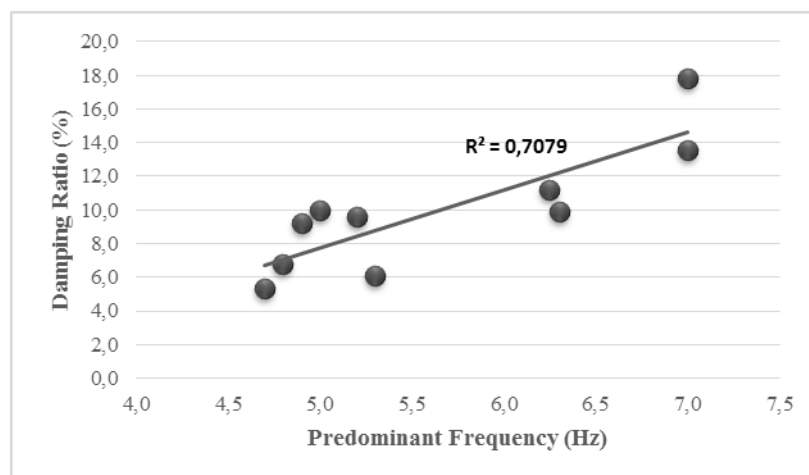


Figure 5. The correlation of the predominant frequencies and the damping ratios.

REFERENCES

- [1] Nakamura, Y., Clear Identification of Fundamental Idea of Nakamura's Technique and Its Applications, *12th WCEE*, 2000.
- [32] Nakamura, Y., A method for dynamic characteristics estimation of subsurface using microtremor on the ground surface. *QR of RTRI*, 30(1), 25-33, 1989.

- 1 SESAME, 2004. Guidelines for the implementation of the H/V spectral ratio technique on ambient vibrations: measurements, processing and interpretation, Available: http://sesame-fp5.obs.ujfgrenoble.fr/Delivrables/Del-D23HVUser_Guidelines.pdf. Zhang, C. Zhu, J. K. O. Sin, and P. K. T. Mok, "A novel ultrathin elevated channel low-temperature poly-Si TFT," *IEEE Electron Device Lett.*, vol. 20, pp. 569–571, Nov. 1999.
- 2 Konno, K. and Ohmachi, T., Ground motion characteristics estimated from spectral ratio between horizontal and vertical components of microtremors. *Bull. seism. Soc. Am.*, 88(1), 228-241, 1998.
- 3 Clough, R. W. and Penzien, J., *Dynamics of Structures, 2nd edition, McGraw-Hill, Inc. 54-56*, 1993.

An Investigation of the Usability of Yavuzeli Basalt Aggregates in Hot Mix Asphalt

Ahmet Ozbek¹, Yusuf Uras¹, Murat Gul², Huseyin Semerci¹, Samime Sener¹

Abstract

Recently, crushed stone aggregate demand is increasing around the world. This demand is going to increase due to consuming of reserves of quarry established in riverbeds. In addition, extracting materials from river beds is significantly harmful to the environment. Thus, usage field of crushed stone aggregate are quite rising. The rocks used as aggregates in Kahramanmaraş are mostly obtained from Yavuzeli basalt in Karatas town (Gaziantep, SE Turkey). These rocks are mainly used as aggregate in asphalt and road construction. Aim of this study is to determine the availability of Yavuzeli basalt for hot asphalt mix aggregates with examining the geochemistry and the physico-mechanical properties of it. For this purpose, basalt aggregate samples collected in the field, geochemical properties of them including major elements contents were determined with using ICP-MS method. Petrographic properties of aggregates were revealed by thin sections of samples. In order to determine the physico-mechanical properties of the aggregates, specific gravity, Los Angeles abrasion test, water absorption by weight, flatness and shape index, MgSO₄ frost loss, the amount of organic matter, sieve analysis and Marshall Experiments were done. According to the test results, Marshall Flow value was providing required standards, while water absorption, asphalt filled void ratio and filling/bitumen ratio were not supplying the desired standards. If all of this parameter is taken into consideration, it is thought that the basalt samples can be used as asphalt aggregates after determination of Marshall Parameters that captured the required standards by trial and error.

Keywords: *Basalt, Bitumen, Hot Mix Asphalt, Marshall Stability*

1. INTRODUCTION

The use of aggregates in concrete production and road construction materials are developed as a separate industry in the world. This industry is playing active role in the development of country via designing of flexible road and supplying a significant contribution to the economy by way of contribution to transport sector and construction industry. In Turkey, the asphalt industry shows a parallel development to the improvement in the quantity and quality of the road network. With development of the automotive industry in Turkey, freight and passenger transport rate by road has been increasing day by day and as a result of this, building of solid and durable way with high geometric standards has become inevitable.

Bituminous hot mix is a pavement obtained after initially mixing of coarse and fine aggregate filler and bitumen plant at 140-160 °C and then laying uniform layer and compressing [1]. The aggregates contain various sized mineral and form the 90-95% bituminous hot mix and skeleton of asphalt. They can use as a component of a new material by combining with other agents in asphalt production. Coarse aggregate creates a skeleton in a mixture of in the bituminous mixtures and plays an important role in resistance of mixture to flow [2]. Granulometry of aggregate affects the physical properties of asphalt concrete and have an impact on the optimum bitumen ratio. Save up to 1% of optimum bitumen is providing significant benefit to the cost of asphalt concrete pavement [3].

Several studies have been made by many researchers on the availability of basalt aggregate in bituminous hot mix asphalt. [1] investigated effects of aggregate types used in hot mix asphalt on physical properties of asphalt pavement. [4] examined the geochemical and physico-mechanical properties of dolomitic limestone, clayey limestone, micritic limestone and Yavuzeli basalt in and around Gaziantep and Kahramanmaraş in terms of availability for the asphalt aggregates. Similarly, [5] studied on the void ratio of crushed stone formed from limestone, granite and basalt and void ratio between the aggregates. [6] investigated the usability fibers in order to bear the stresses occurring at the surface layer of pavement. [7] studied performance index of basalt fiber strengthen SBS modified asphalt mixture by using two kinds of gradation. [8] researched the availability of coarse and dust waste of basalt aggregates for stone mastic asphalt production.

The aim of this study is investigating the availability of crushed stone of basalt aggregates from Karatas quarry for hot mix asphalt aggregate. For this purpose, in addition to the petrographic and chemical properties of aggregate, specific unit weight, Los Angeles abrasion, water absorption by weight, flatness and shape index, freeze loss, amount of organic material, sieve analysis and Marshall Experiments were done.

¹ Department of Geological Engineering, Kahramanmaraş Sutcu Imam University, Kahramanmaraş, Turkey
ozbekaderen@gmail.com

² Department of Geological Engineering, Mugla Sıtkı Kocman University, Mugla, Turkey

2. SAMPLE PREPARATION AND GEOLOGICAL SETTING

The age of Yavuzeli basalts located in Karataş (Gaziantep) was determined as a Middle Miocene [9] and Upper Miocene [10.] This unit is composed of generally reddish-dark brown-dark gray-black colored, massive or very thick bedded, porous, calcite-filled pores lava flows (Figure 1). Agglomerates and tuffs are locally exposed below this lava flow [11]. The thickness of basalt range between 0-50 meters. It unconformably overlies older units especially the Şelmo Formation. The crushed aggregate samples in size of 0-5 mm, 5-10mm, and 10-20 mm were picked from quarries in Karataş region (Figure 2).



Figure 1. General field view of the Yavuzeli basalts in Karataş region.



Figure 2. Crushed basalt aggregates samples in size of 0-5 mm, 5-10 mm and 10-20 mm.

3. LABORATORY INVESTIGATION

3.1. Petrographic analysis and chemical composition

The petrographic analysis of basalt sample was performed on a thin section. Yavuzeli Basalt is in ophitic texture and has an abundant iron structure. Iddingsitized olivine was determined, while unaltered olivine was not fixed. It was found that the basalt contains abundant anorthite, and iron oxides that evolved depend on alternation of orthopyroxene and clinopyroxene (Figure 3a). Anorthite 57%, augite 14%, 9.5% pigeonite, 7% montmorillonite, goethite 6.75% and chloride 5.75% were fixed (Figure 3.b).

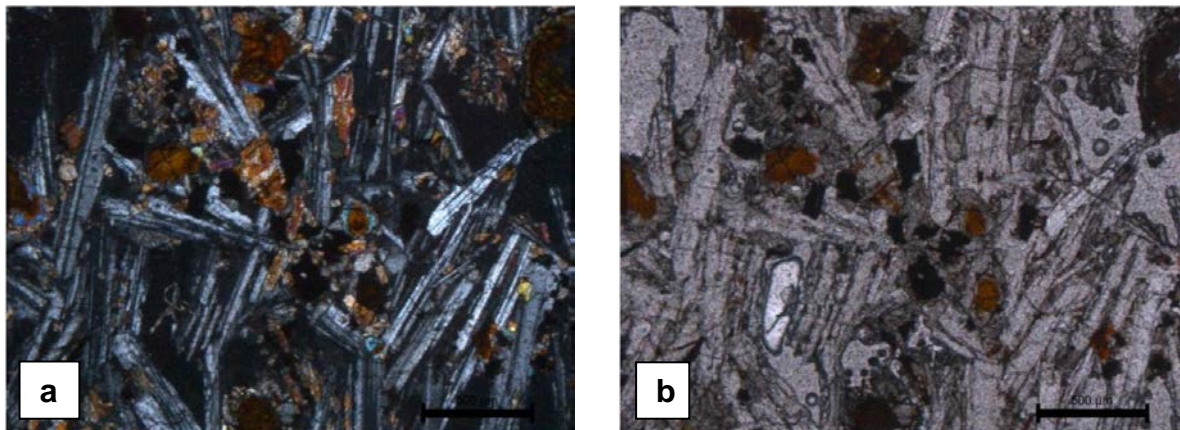


Figure 3. a. photomicrograph of basalt under cross polarized light. b. photomicrograph of basalt under normal polarized light

The geochemical characteristics of basalt aggregates obtained from quarry around Karataş were done in Acme Analytical Laboratories in Canada with using ICP-ES (Electron Spectrometer). According to results of the analysis, average major oxides of the basalt aggregates are SiO₂ 46.66 %, Al₂O₃ 14.99 %, Fe₂O₃ 13.32 %, CaO 8.90%, and MgO 8.20%, average amount of the following other components are Na₂O 3.01%, TiO₂ 1.98%, K₂O 1.15%, P₂O₅ 0.54%, and MnO 0.19% (Table 1).

3.2. Physical and mechanical properties

Determination of engineering properties specific gravity, water absorption by weight, Los Angeles abrasion loss value, elongation index, flakiness index and soundness by MgSO₄ of the basalt aggregates were performed according to the [12] and the [13]. standards. The average physical and mechanical properties of the basalt aggregates are given in Table 2.

Table 1. Chemical compositions of the basalt aggregates [4].

Sample no	SiO ₂ (%)	Al ₂ O ₃ (%)	Fe ₂ O ₃ (%)	MgO (%)	CaO (%)	Na ₂ O (%)	K ₂ O (%)	TiO ₂ (%)	P ₂ O ₅ (%)	MnO (%)	LOI (%)
B1	46.65	14.97	13.3	8.18	8.87	2.99	1.11	1.94	0.52	0.19	0.9
B2	46.61	14.92	13.25	8.2	8.9	3.01	1.15	1.96	0.53	0.19	0.9
B3	46.62	14.95	13.32	8.21	8.89	3.01	1.11	1.94	0.52	0.19	0.9
B4	46.65	14.97	13.25	8.22	8.85	2.99	1.14	1.95	0.54	0.17	0.9
B5	46.66	14.98	13.35	8.24	8.85	2.98	1.11	1.94	0.52	0.19	0.9
B6	46.62	14.97	13.25	8.21	8.87	2.99	1.13	1.97	0.52	0.19	0.9
B7	46.65	14.99	13.21	8.2	8.89	3	1.12	1.98	0.54	0.18	0.9
B8	46.61	14.91	13.22	8.17	8.88	2.99	1.15	1.96	0.52	0.19	0.9
B9	46.62	14.93	13.25	8.17	8.89	3.05	1.11	1.96	0.53	0.19	0.9
B10	46.61	14.97	13.24	8.18	8.87	2.99	1.14	1.95	0.52	0.19	0.9

According to the laboratory results assessment, Los Angeles abrasion loss, elongation index, flakiness index soundness by MgSO₄ of the basalt aggregates have supplied the [14] specification requirements. However, water absorption by weight values are providing standards for coarse aggregates, not providing required standards for fine aggregate. Fine materials ratio were determined according to the [15] standard, and according to [14] specification, the proportion of fine material in coarse aggregates is stated to be a maximum of 0.5%. However, the fine material is powder of these aggregates, thus it will not create a problem. Organic substance experiment was carried out according to [16] and no organic substance was found in basalt aggregates.

Table 2. Mean values of some physic-mechanical properties basalt aggregates and limit values [4].

Properties	Fine Aggregate (0-5 mm)	Coarse Aggregate (5-10 mm)	Coarse Aggregate (10-20 mm)	Coarse Aggregate Limit (THS, 2006)	Standarts
Specific Gravity	2,862	2,889	2,909		ASTM C -127 [17]
Water Absorption by Weight (%)	4,07	2,173	0,998	≤ 2.5	ASTM C -127 [17]
Los Angeles Abrasion Loss Value (%)	-	23,53	12,26	≤ 35	ASTM C -131 [19]
Elongation Index (%)	-	15,45	11,92	≤ 35	BS -812105 [20]
Flakiness Index (%)	-	19,78	13,6	≤ 25	BS -812 105 [20]
Soundness of Aggregates by MgSO ₄	-	-	4,72	≤ 12	ASTM C -88 [18]

The sieve analysis of crushed aggregate specimens taken from Karataş quarry was performed based on [21] standards. Maximum, minimum grain size and experimental aggregate gradation are given in Figure 4. Basalt aggregate mixing percentages that used in binder layer was designated as 57.4% for 25-4.75mm, 38.8% for 4.75-0.075 mm and 3.8% for filler.

Bitumen was defined as a material mixture of natural origin hydrocarbon or a mixture of pyrogenic origin (natural heat generated) hydrocarbon, or combination of both of them, mostly in form gas, liquid, semisolid or solid, that can be located in conjunction with a non-metallic derivatives, and material with adhesive properties and completely soluble in carbon disulfide [3]. Bitumen binders provide adhesion between the road surface and the aggregates. All physical properties of bitumen that used as binder in experimental studies are given in Table 4.

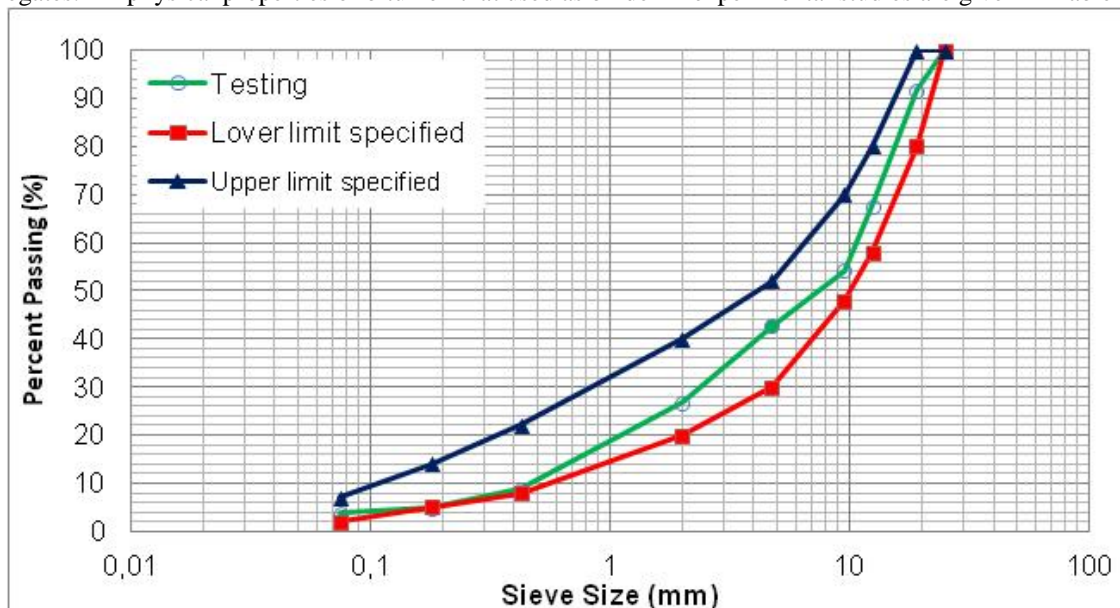


Figure 4. Grading curves of aggregate

Table 4. Basic physical characteristics of the bitumen

Properties	Values	Standard
Specific gravity	1.036	ASTM D70[22]
Penetration	63	ASTM D5[223]
Flash point	180	ASTM D92[24]
Fire point	230	ASTM D92[24]
Softening point	52	ASTM D36[25]
Ductility (5 cm/min)	>100	ASTMD113[26]
Viscosity at 135 °C	0.411 Pas	ASTM D4402[27]
Viscosity at 165 °C	0.121 Pas	ASTM D4402

4. RESULTS AND DISCUSSION

In order to determine aggregate types used in bituminous hot mix effects on physical properties of coatings, the Marshall Tests were done on 12 samples prepared for the binder layer according to specified mixing ratio in [14] specification. Briquettes be used in the experimental stage were prepared, 75 impacts were applied to briquettes. Six samples with different bitumen percentage (4.0, 4.5, 5.0, 5.5, 6.0, and 6.5%) were prepared for Marshall Tests. For each bitumen percentages, Marshall Experiment was conducted to two samples for each percentage to determine the optimum bitumen ratio. The test results of bulk specific gravity, void filled with bitumen ratio, void ratio in mineral aggregate, void ratio, Marshall Flow, and Marshall Stability for samples with different bitumen are given in Table 5.

Table 5. Marshall Test Results [4]

Bitumen Contents	Bulk Specific Gravity (g/cm ³)	Void Filled With Bitumen (%)	Void in Mineral Aggregate (%)	Void (%)	Marshall Flow (mm)	Marshall Stability (kg)
4	2.68	62.80	16.03	5.98	2.10	963
4.5	2.71	76.60	14.23	3.80	2.90	1525
5	2.72	91.00	13.80	2.56	3.30	1500
5.5	2.68	94.10	14.70	1.84	4.00	1324
6	2.66	95.80	15.30	0.90	5.58	1063
6.5	2.65	96.45	16.95	0.55	4.72	942

The method used for determining the optimum percentage of bitumen of bituminous hot mix is graphical method drawn depending on test results. According to the Marshall Test results, graphics belong to different mixture were drawn. Optimum percentage of bitumen were determined as 4.7 % that is arithmetic average percentages of bitumen of bituminous hot mix, prepared based on [14] specification in Table 6.

Table 6. Optimum bitumen specified criteria based on [14]

Properties of Mixture	THS Limits
Specific weight	Bitumen content corresponding to maximum stability
Stability	Bitumen content corresponding to maximum bulk specific gravity
Asphalt Filling Void	Bitumen content corresponding to the median of designed limits of percentage voids filled with bitumen in the total mix (i.e. 80%).
Void	Bitumen content corresponding to the median of designed limits of percentage air voids in the total mix (i.e. 4%).

Suits of them to technical requirement and changes of bulk specific gravity, void filled with bitumen ratio, void ratio, Marshall Flow, and Marshall Stability according to optimum bitumen ratio were assessed (Figure 5-9). Figure 5 shows increase in specific gravity due to increase rate of bitumen. However, it has been decreasing after bitumen optimum ratio was 4.70. The Marshall stability of asphalt mixture is rising with increasing of bitumen, however it is decreasing after the optimum bitumen ratio exceeds the 4.70 (Figure 6). This drop shows that, after the bitumen ratio increasing reach to maximum level, increasing lubricity between aggregates reduces strength. Depending upon the mixture ratio, Marshall Flow values also increase with increasing percentage of bitumen (Figure 7). After reaching the maximum point of the Marshall Flow with increasing amount of asphalt, film layer among aggregates form a slippery environment and reduces the strength. Therefore, the Marshall Flow value reach to constant value after a significant period. Void filled with bitumen as a binder percentages of mixtures is increasing with percentage of bitumen increasing (Figure 8). Void ratio in compressed mixture has been decreasing significantly due to increase of bitumen rate (Figure 9).

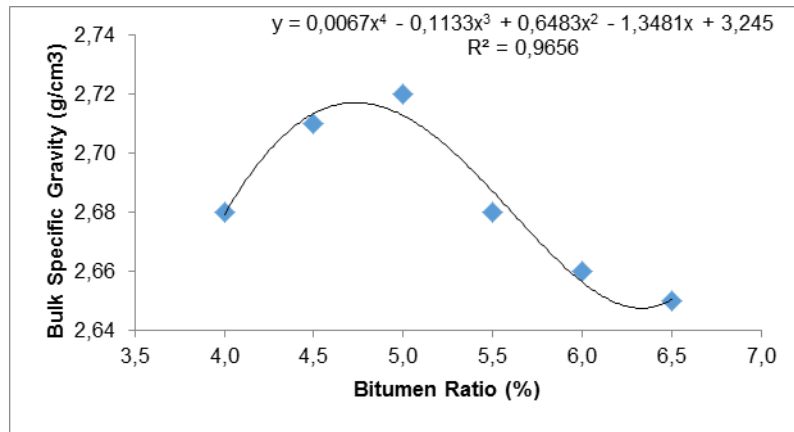


Figure 5. Bulk Specific Gravity versus bitumen content

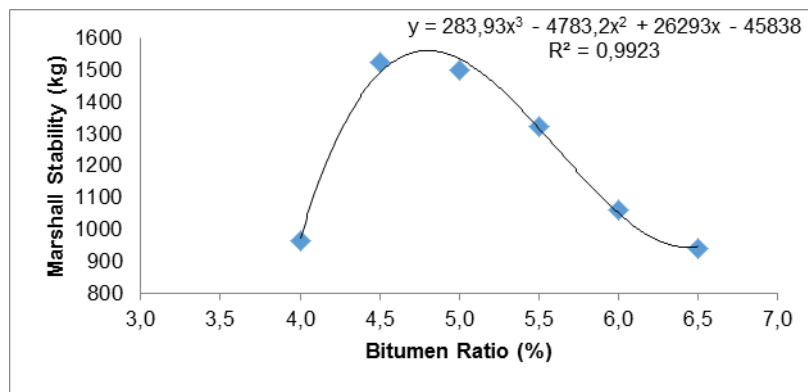


Figure 6. Marshall Stability versus bitumen content

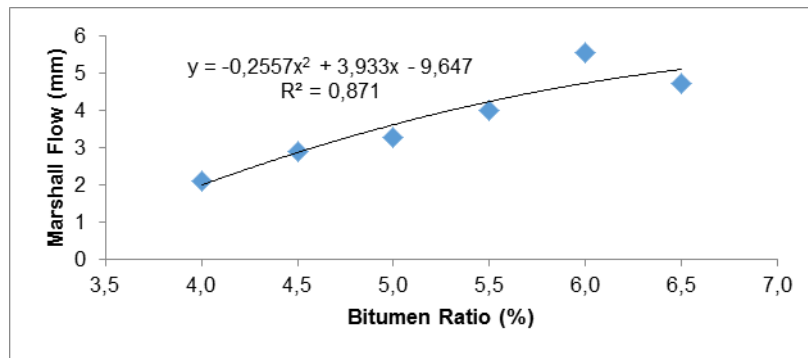


Figure 7. Marshall Flow versus bitumen content

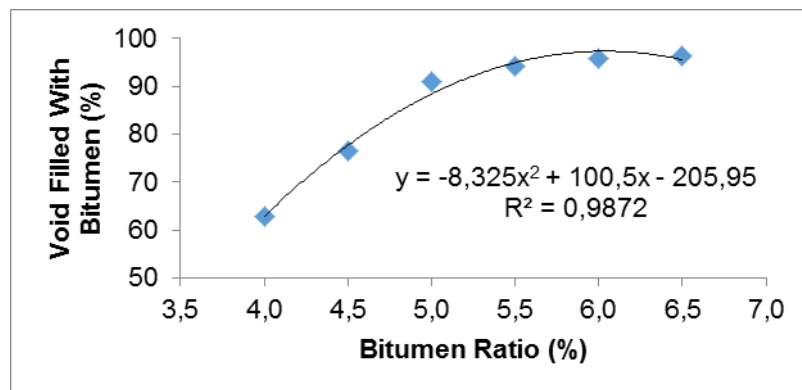


Figure 8. Void filled with bitumen versus bitumen content

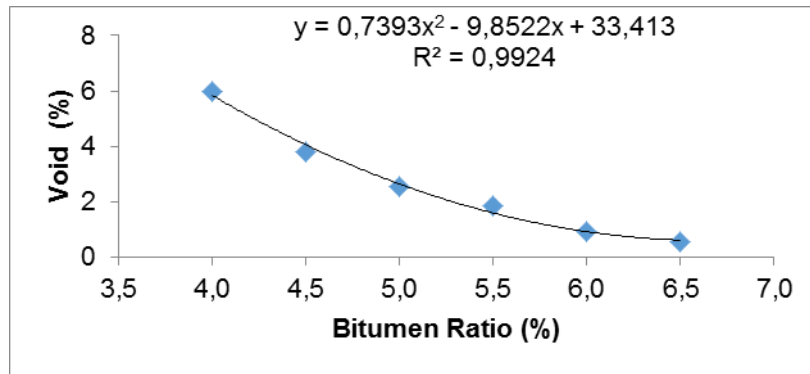


Figure 9. Percentage of void in the total mix versus bitumen content

From figures 5-9, based on optimum bitumen ratio as 4.7, the Marshall Stability value was determined as 1560 kg, bulk specific gravity 2.72 g / cm³, Marshall Flow 3.2 mm, void filled with bitumen 82 %, and void ratio 3.4%. This materials do not provide the desired values of [14] specification for asphalt filled porous basalt aggregate. The filler/bitumen ratio of basalt sample is outside the desired values, it must be fixing via the making changes in Marshall Parameters.

5. CONCLUSIONS

Within this study, the geochemical and physico-mechanical properties of aggregates of the Yavuzeli basalt were examined to determine the availability of it for a hot asphalt mixture of aggregates. Los Angeles Abrasion Loss, elongation index, flakiness index and soundness of aggregates by MgSO₄ of basalt aggregates is to stay within the limits of the desired standards of specification. Only water absorption by weight does not show the appropriate property in terms of standards. Bulk specific gravity, void filled with bitumen ratio, void ratio, Marshall Flow, and Marshall Stability were assessed according to optimum bitumen ratio with Marshall Test. The Marshall Stability value was determined as 1560 kg, bulk specific gravity 2.72 g / cm³, Marshall Flow 3.2 mm, void filled with bitumen 82 %, and void ratio 3.4%, based on optimum bitumen ratio as 4.7. This aggregates do not provide the desired values of asphalt filled porous basalt aggregate. Although the basalt aggregates are not meeting the standards of asphalt filled void ratio, desired standard values can be obtain via making some changes by trial and error method in the Marshall parameters.

ACKNOWLEDGEMENTS

The support of the Research Fund of Kahramanmaraş Sutcu Imam University (Grant FBE2010/7-4 YLS) is gratefully acknowledged.

REFERENCES

- [1] T. Alataş, P. Ahmedzade and Y. Doğan. The effect of aggregate type used in the bitumen hot mix to the physical properties of pavement. Science and Eng. J. Of Firat Univ. 18.1. pp. 81-89. 2006.
- [2] S. Serin, E. Özgan, S. Bektaş and M.M. Uzunoğlu. Investigation the usability of Duzce Region's crushed Stone aggregates in production of asphalt concrete. 6. International Advanced Technologies Symposium (IATS'11). 16-18 May. Elazığ-Turkey. 2011.
- [3] K. Yıldız. Marshall dizayn metodu ile optimum bitüm muhtevasının belirlenmesinde deney parametrelerinin sonuca etkisi. Yüksek lisans tezi. Gazi Üniversitesi Fen Bilimleri Enstitüsü. Ankara. s. 119. 2003
- [4] H. Semerci. Farklı jeokimyasal özellikteki agregaların asfalt kalitesi üzerine etkisi. Kahramanmaraş Sütçü İmam Üniversitesi Fen Bilimleri Enstitüsü. Yüksek lisans tezi. Kahramanmaraş. 2013.
- [5] W. S. Abdullah, M. T. Obaidat, and M. N. Abu-Sada. Influence of Aggregate Type and Gradation On Voids of Asphalt Concrete Pavements. Journal of Materials In Civil Engineering. pp.76-85. 1998.
- [6] N. Morova Investigation of usability of basalt fibers in hot mix asphalt concrete. Construction and Building Materials. 47. pp 175-180. 2013.
- [7] Z. Liu, C. Chen, R. Qin, X. Zou. Research to performance of basalt fibre strengthen SBS modified asphalt mixture. Adv Mater Res.. 191. 5. pp. 446-449 2012.
- [8] A. Karakuş. Investigation on possible use of Diyarbakır basalt waste in stone mastic asphalt. Construction and Building Materials 25. pp. 3502-3507. 2011.
- [9] O. Yoldemir. Suvarlı-Haydarlı-Narlı Gaziantep arasında kalan alanın jeolojisi. yapısal durumu ve petrol olaraları: TPAO Rap. no. 2257. 60s. Ankara. 1987. (yayınlanmamış).
- [10] Ü.Ulu, Ş. Genç, S. Giray, Y. Metin, E. Çörekçioğlu, S. Örcen, T. Ercan, T. Yaşa, M. Karabyıkoğlu. Belveren-Araban-Yavuzeli-Nizip-Birecik dolayının jeolojisi. Senozoyik yaşlı ve volkanik kayaların petrolojisi ve bölgesel yayılımı: MTA Rap. no.9226. Ankara 1991. (yayınlanmamış).
- [11] D. Usta and H. Beyazççek. Adana ilinin jeolojisi. M. T. A. Doğu Akdeniz Bölge Müdürlüğü. Adana 2006. (yayınlanmamış).
- [12] ASTM Standart Specification for Concrete Aggregates. Annual Book of ASTM Standards. (2001).
- [13] BS 812 Testing aggregates. British Standard Institute; 1990.
- [14] General Directorate of Highways. State Highways Technical Specifications (HTS). Ankara; 2006.
- [15] ASTM C-117. Standard Test Method for Materials Finer than 75-µm (No. 200) Sieve in Mineral Aggregates by Washing. USA. Annual Book of ASTM Standards. 1995.

- [16] AASHTO T-194. Standard method of test for determination of organic matter in soils by wet combustion. American Association of State Highway and Transportation Officials; 1997.
- [17]- [18] ASTM C-127-88. Test method for specific gravity and adsorption of coarse aggregate. USA. Annual Book of ASTM Standards; 2001.
- [19] ASTM C 131. Standard test method for resistance to abrasion of small size coarse aggregate by use of the Los Angeles machine. Annual Book of ASTM Standards; 1996.
- [20] BS-812-105 1.2. Flakiness index and Elongation index of coars aggregate 1990.
- [21] ASTM C136-06. Standard test method for sieve analysis of fine and coarse aggregates. Annual Book of ASTM Standards; 2006.
- [22] ASTM D70 Standard test method for density of semi-solid bituminous materials (pycnometer method). Annual Book of ASTM Standards USA; 1992
- [23] ASTM D5. Standard test method for penetration of bituminous materials. Annual Book of ASTM Standards USA; 1992.
- [24] ASTM D 92. Standard test method for flash and fire points by cleveland open cup tester. Annual Book of ASTM Standards USA; 1992.
- [25] ASTM D36. Standard test method for softening point of bitumen (ring-and-ball apparatus). Annual Book of ASTM Standards USA; 1992.
- [26] ASTM D113. Standard test method for ductility of bituminous materials. Annual Book of ASTM Standards USA; 1992.
- [27] ASTM D4402 Standard Test Method for Viscosity Determination of Asphalt at Elevated Temperatures Using a Rotational Viscometer. Annual Book of ASTM Standards USA; 2001.

Haploidy Role and Importance of Plant Biotechnology

Tansu Uskutoglu¹, Cüneyt Cesur², Belgin Cosge Senkal², Cennet Yaman²

Abstract

Agricultural activities are the basis of life throughout the history of mankind. People have spent their time hunting and gathering before they entered to settled life. After they entered to settled life, agricultural production has started to resume their lives. They grown plants which is located around after that they made observation based on some criteria such as some of the plant grows better or animals prefer to grazing with some of them so the most basic step of plant breeding emerge which is defined to selection. It is a fact that the human population is constantly increasing. This increase parallel with the increase in urbanization and industrialization occurring on the agricultural field as a result of these activities fertile lands reduction occurs. Therefore, it is insufficient to feed people with declining fertile land. Even today, while malnutrition and hunger is a serious matter if these condition continue it will show effect much more serious. For that reasons agriculture should focus on increasing plant yield. Plant biotechnology has emerged in the light of these objectives. In addition to conventional breeding methods, in the 1920s first haploid plant was discovered and then realized that the importance of this plants and it can used on breeding program. Due to decrease in the frequency of their occurrence in the nature of these plants has prevented their use in practice and has encouraged scientists to create plants which is haploid. The foundation of plant biotechnology was created with this studies. Especially cross-pollinated species, obtaining pure lines takes 8-12 years. If that species have self-incompatibility it will take more. One of the biotechnology technique which name is haploidy %100 homozygote line can obtain within 1-2 years. This study provide information about haploid technique and in recent years saved stages of haploid technique will be investigated.

Keywords: Haploidy, Plant Breeding, Androgenesis, Gynogenesis,

1. INTRODUCTION

The history of humanity is in a continuous development. By a large period of hunting and gathering to date adopted in early human that sustain life he has identified many plants and animals due to this mode of life and chose to carnivorous or herbivorous diet type, with the effect of environmental conditions. In later times people managed to taming some animals, not only need to feeding animals but also feed to themselves, they started paying closer attention to plants. Some plants lovingly by grazing of animals, and some plants have harmful, some of them are more productive such reasons like that human have gone too intentionally or unknowingly a plant selection[1].

On the basis of the selection made in the early period, the female genotype is based on selections and was done fertile or quality plants. This selection lead to wild forms with the choice of efficient and high-quality plants that have transformed the cultural form. Weeds form together with the selection of efficient and high quality variety that plants were transformed into culture form. A nomadic hunter-gatherer lifestyle by changing the lifestyle of people adopting more stable horticulture or the doors of a lifestyle based on agriculture has also been opened [2].

The most fundamental of human food has created a higher plant in settled life. Historical evidence show that humankind allow the development of crops which they grown and people since the early sedentary lifestyles, not only did the cultivation of crops such as grains and legumes but also improve through selection of these plants. At the end of this process they produce more efficient and high-quality plants. Plant breeding is continuity until today, starting from the first period of settled life and is constantly more and a science focused on producing high quality [3].

Mendel's laws of inheritance with the discovery of the 19th century began a new era in plant breeding and a new methods has been introduced to the breeding programs. The process that began with heterosis breeding in maize in 1909, 1920s the discovery of conventional breeding methods, mutation breeding in the 1930s and the use of statistical methods, genetic improvement of quantitative characters of the 1940s, In the 1950s plant physiology, developments in the field of biochemistry in 1960 and in the 1970s tissue culture techniques started a new era. These developments followed by molecular biology in the 1980s, continued with transfer of genes in 1990s and the foundations laid in the present plant biology [4].

It is known that there is a steady increase in the world population and that if it continue in this way in 2050, world population is expected to reach 9,7 billion people[5]-[6]. The world won't increase existing agricultural areas, unlike the existing field of agriculture expected to be further reduced by opening to human settlement development and industrialization therefore, yield

¹ Corresponding author: Bozok University, Department of Agriculture and Natural Science, 66900, Yozgat, Turkey.
tansu.uskutoglu@bozok.edu.tr

² Bozok University, Department of Agriculture and Natural Science

will be obtained from existing fields becomes even more important. Basic way to achieve that goals, the desired yield increases in shorter time passes from the breeding of better varieties.

In particular, cross-pollinated plants heterozygous rate is very high, considering obtaining pure lines of these plants take up to 10-12 years, in addition to that if species have inbreeding depression this period is further increase. Even self-pollinating plants in obtaining pure lines takes 5-7 years. 100% homozygous lines in a short period such as 1-2 years, can be obtained by haploid technique [7]-[10]. In the 1920s, the presence of first haploid plants which are found in nature and understanding the importance of haploid plants has led to trying produce of new ones. After 40 years in the result of this attempt, first haploid plant is obtained. Methods of obtaining haploid plants are based on two main methods. Normal development of male or female gamete is gametophytic, but some stimulus can change the development of gamete from gametophytic pathway to sporophytic. Haploidy is the art of routing development pathway of the plant.

2. THE FIRST DISCOVERY AND DEVELOPMENT OF HAPLOID PLANTS

Haploid plants have same number of chromosomes in somatic cell which is equal to chromosome number of gametes, in other words its containing just one set of chromosome. Spontaneously or application of some chemical can doubled chromosome of haploid plant and new plant is called Doubled Haploid (DH) [11].

The first natural haploid plant was observed in 1921 by Bergner in a weed species *Datura stramonium* which belong to solanaceae family [12]. In efforts may be other plant species have haploids in nature, in fact its seen some species such as *Nicotiana tabacum* [13], *Triticum compactum* [14] and many other species have been found natural haploids. In 1974, Kasha reported that 100 different angiosperm plant have naturally occurring haploid plant. Although spontaneous haploid plants found in nature, the frequency of use in practice, breeding and genetic studies, has been the limiting factor. Therefore, these limitations are the way scientists produce similar plants that already exist in nature in this regard has been an important factor in the search [15]. Indeed, the first haploid plants can be obtained in *Datura stramonium* via anther culture after 40 years from the first haploid plants had been discovered in nature [16]. Today, around 170 plants androgenesis being implemented [17]-[18], some species cannot be obtained any development of the male gamete. In such plant, female gamete cultured in vitro and haploid plants can be obtained. Today, around 30 plant species gynogenesis method uses for haploid plant induction [19]-[20].

As can be understood from the studies, most preferred methods are in vitro anther and microspore culture, some species cannot give good success and result in implementation of androgenesis and other methods can give good response such as ovarium and ovary culture which name is known as gynogenesis [21]. The relatively less frequently used in cross-species hybridization, in this application formation of haploid plants as a result of the loss of one chromosome set (mostly pollinator varieties chromosome disappear) from the parental. In addition to these applications without carrying male inheritance cells from eggs as a result of parthenogenesis haploid plant may occur.

3. IMPORTANCE OF HAPLOID PLANTS

After understanding genetics, theoretical and practical uses of haploid plants, it has attracted the attention of plant breeder and geneticist. Because of the advantages such as acquisition of DH line and shortening the breeding period scientist want to benefit from this technology [22]. The development of DH line, in the diploid or allopolyploid species it shorten the breeding time till 2-3 generation and in hybrid breeding developed homozygote lines are used as parents [23]. Homozygote in self-pollinating plant takes 6-7 years. When it comes to cross-pollinated species breeding time takes 10-12 years. Especially if only one generation harvested a year such as winter wheat, it takes more than 12 years and additionally sometimes cross-pollinated species observed inbreeding depression. DH lines are used in the breeding which is requested particularly high purity.

Germana (2011) report that 50% of barley grown in Europe have been derived from double haploid line [24]. FAO (2013) data, Canada is the second after the US in wheat exports. Canadian wheat is divided into nine different classes. Canadian Western Red Spring which is largest 3rd grade class has produced with doubled haploid technique. In addition, "AC Andrew" variety grows in all place where Canada Western Soft White Spring (CWSWS) has grown. The main feature of this variety is developed through anther culture [25].

Maize (*Zea mays* L.) obtaining DH line through anther culture, and it is possible to take seed of them in seven months [26]. The method of winter varieties Florin's development is one of the best examples of double haploid methodology. The process began with first crossing in 1978 and anthers were cultured in 1979. In 1982, seeds of winter varieties reproducing in the nursery and repeated yield trials began. Varieties registered after the 2-year yield trials and it started to sell in 1985. If this work had been done with conventional breeding methods it would take at least four more years and plant breeder has gained 4 years [27].

Homozygote diploid lines is very important due to the monitoring of good yield line. In perennial trees, it is very difficult to obtain a homozygote line by conventional breeding methods. When the juvenile period considered breeding process starting from 20-30 years and it takes over 100 years [28]. On the other hand haploid plant can be obtained in a single generation and doubled with colchicine application it offers the chance to obtain homozygous lines.

In plant breeding for many years the unilateral selection breeding methods are quite narrow the plant gene pool so breeders have applied to mutation breeding to create variations. Mutation breeding occur mostly in recessive character and usually not seen in the first generation. Haploid mutant can give opportunity to screening not only dominant character but also recessive characters. In addition, the desired character can be selected directly. Barley and rice DH technique is applied with success through mutation breeding. In a study performed in barley mutant pure lines obtained at a rate of 25%. The obtained line dwarfs than normal plants, but more efficient and adaptation to altitudes has been found to be better than normal lines [29]. In

the study performed in rice, pure mutant lines obtained and this line is the same yield with other varieties but it comes to harvest 19 days earlier than standard varieties [30]. Today protocols have been established for the implementation of doubled haploid technique in approximately 200 plants.

4. IN VITRO METHODOLOGY OF HAPLOID PRODUCTION IN HIGHER PLANT

4.1 Anther and microspore Culture (Androgenesis)

First Androgenic origin haploid plant were reported in 1922 by Kostoff. Because the character of one offspring among 1000 in a hybrid family between *Nicotiana tabacum* var. *macrophylla* ($2n = 6x = 72$) and *N. langsdorffii* ($2n = 2x = 18$) was totally dissimilar to the *N. tabacum* female parent, but resembled the *N. langsdorffii* male parent, it was considered to have developed through androgenesis [31]. First female gamete cell is mainly used to obtain haploid plants by parthenogenesis but it couldn't be achieved very good results for that period. Androgenic origin haploid plants obtained by Kostof, bring the question wheather male gamet can used for haploid or not. In subsequent years, Guha and Maheshwari have taken *Datura* anther in vitro culture and observed that the formation of embryo-like structures in one of the growing plants [32]. The obtained embryo-like structures is diploid but the cells origin is microspore and discovery of the cell origin is groundbreaking in the world of science. Haploid plants obtained from anther culture began to be achieved in the coming years.

Today anther culture technique can be applied in many plants and it is widely used in crop plants [33]. Procedures applied in anther culture generally similar (Fig.1) and can applied to a large group of plants [34]. There are many internal and external factors affecting the success of anther culture [35]-[36]. The most important of them; a high rate of genotype dependent, donor plant's growing conditions, development stages of microspore, culture conditions and pre-treatments. All conditions as a result of interaction with each other to give the anther response is also changing.

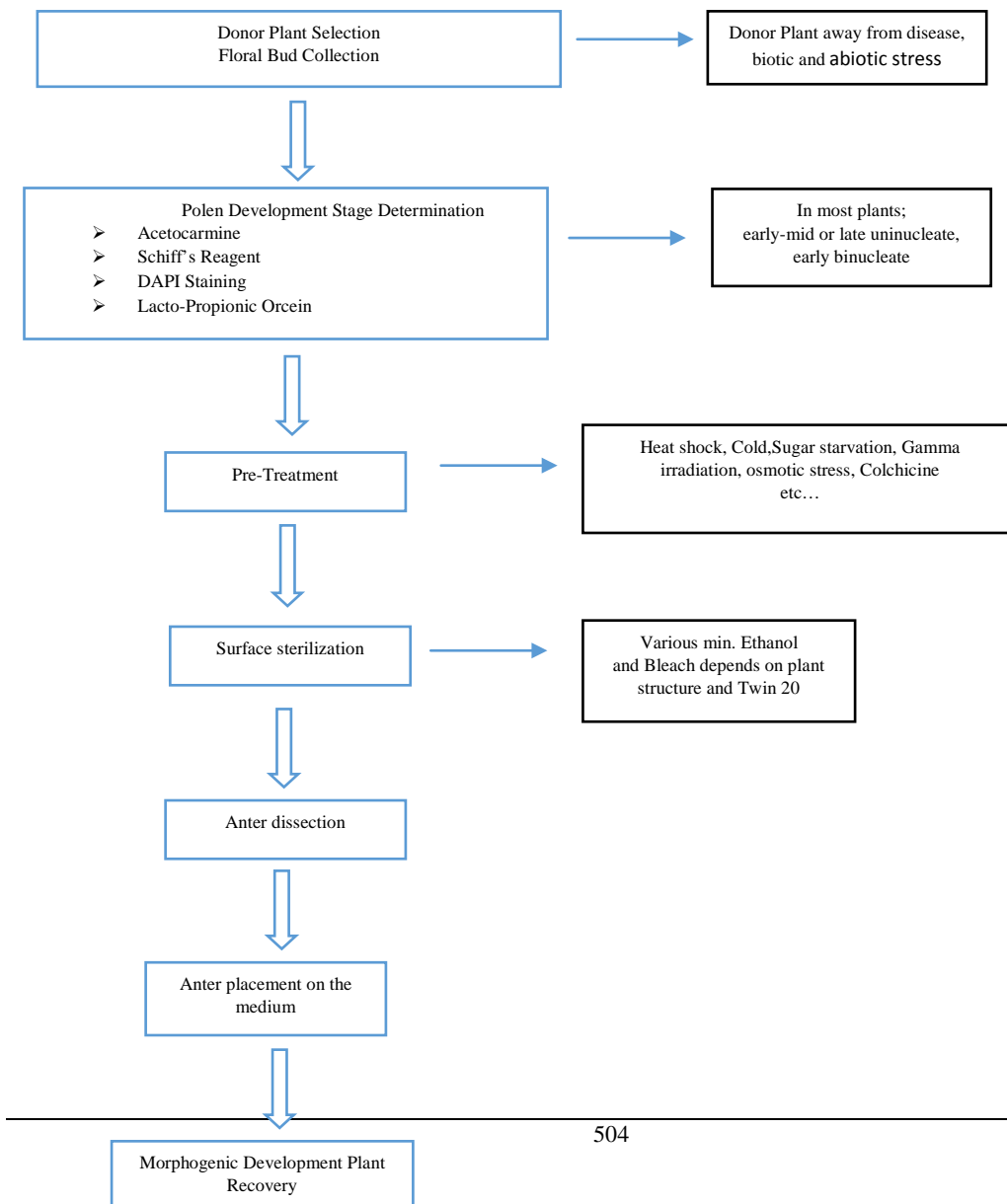




Fig 1. Common guidelines and some key points of the anther culture technique

Some problems are also encountered in anther culture. The most important problem of obtained callus is the development from the anther wall. The biggest problem is the formation of callus from anther wall. The characters of populations which is obtained via anther culture is sometimes heterozygote character. The presence of microspore in different developmental stages in the same culture creates a toxic effect on each other [37]. In such case a negative impact on the success of the case, the second way to get haploid microspore culture comes in. In microspore culture, anther walls are removed and only in the appropriate stage of microspores are cultured. The advantages of the microspore culture to anther culture can be summarized as follows;

- 1-) Anther culture can give rise to diploid plantlets from anther wall along with haploids, whereas in microspore culture plantlets always originate from microspores and that have haploid number of chromosomes.
- 2-) In case of anther culture, anther tissues other than the microspores could have a destructive influence on the growth and development of microspore.
- 3-) Isolated microspore culture provides an opportunity to better track the pathway of microspore and to better understand the most important factors contributing towards microspore embryogenesis.
- 4-) The embryogenic units are ten times greater in microspore culture as compared to anther culture.
- 5-) Transgenic plants can be identified at a very early stage of their life cycle in microspore culture [38]-[39].

4.2 Ovary and Ovules Culture (Gynogenesis)

Gynogenesis is an alternative method of obtaining haploid plant. Such methods as anther, microspore or interspecific hybridization cannot be successful or less successful [40]. Tuleck was first scientist who discovered that it can be used in the production of haploid plants from female gametes but at the same time, due to popular culture studies of anther, haploid callus derived from female gametes not noticed [41]. In anther culture some genotypes does not respond to the treatment and cannot obtaining haploid plant. Results of unsuccessful works scientists are looking for other ways. In 1971, Uchimiya has obtained callus using unfertilized ovules of *Solanum melongena* (eggplant). After the cytological examination of the developing callus, it has proved to be a haploid structure [42]. In 1976, San Noem has achieved first haploid plant which is Barley (*Hordeum Vulgare*) via gynogenesis [43].

Ovaryum culture such as anther culture is highly dependent on genotype. Gynogenesis the biggest drawback is the lack of a protocol developed for many species. Besides, generally have low productivity, it limited the use of gynogenesis factors such as there are diploid or mixoploid growing plants. Gynogenesis biggest advantage is contrast to anther culture of cereal, it does not exist albino plant consists of plantlets. Gynogenesis compared to androgenesis is slightly grueling and less common.

5. CONCLUSION

Haploid plants is vital importance for breeding and genetic studies. Plant breeding studies, shorten the breeding period and will be used as parents in hybrid breeding to offer numerous advantages to breeders. Species are considered to be grown once a year, breeding of this kind offers significant benefits in terms of the time. Especially in cross-pollinated plant breeding long period and high rate of population is heterozygous thought the necessity of the use of the haploid technology is clearly

understood. The genetically contain one set of each chromosome, recessive and dominant features allowing it to be directly observed. Mutation breeding, mutation usually occurs in recessive character and these characters are not observed in the first generation. These mutations can be identified in the first generation by obtaining haploid plants and also it allows users to select the desired character directly. Playing a major role in genetic research and provide facilities for the creation of plant genetic map but a high rate of haploid technique is genotype-dependent and only one of the problems is the lack of a common protocol for all plants. In the same variety, one genotype getting successful results, while the other genotypes may be unsuccessful results and its show us to importance of genotype. The woody plant species are known to be reluctant to haploidy. The inability fully known underlying causes, because of under influence of numerous factors, haploid stimulation constitutes a handicap. Future studies in the field of haploidy, fully understanding the underlying factors and the discovery of methods that can work on all plants by preventing dependency to genotype will no doubt be a revolution.

REFERENCES

- [1]. Murphy, D. (2007). Plant breeding and biotechnology: societal context and the future of agriculture. *Plant breeding and biotechnology: societal context and the future of agriculture*.
- [2]. Sykes, B. (2001). *The Seven Daughters of Eve*. W.W. Norton and Company. London.
- [3]. Barz, W.H. (2002). *Plant Biotechnology and Transgenic Plant* sp.20.
- [4]. Borém, A., Miranda, G.V., 2013. *Melhoramento de plantas*, sixth ed. Editora UFV, Viçosa. P.523
- [5]. (2016) Online Available: <http://www.apolo11.com/populacao.php>
- [6]. (2015) United Nations Department of Economic and Social Affairs 2015 Report Available: <http://www.un.org/en/development/desa/news/population/2015-report.html>.
- [7]. Harland, S.C. (1955) *Plant Breeding: Present Position and Future Perspective*. Third Bateson Lecture. 15 pp. Cambridge: University Press.
- [8]. Nei, M. (1963) The efficiency of haploid methods of plant breeding. *Heredity*, 18, 95–100.
- [9]. Melchers, G. (1972) Haploid higher plants for plant breeding. *Zeit. Pflanzenzücht.* 67, 19–32.
- [10]. Kihara, H. (1979) Artificially raised haploids and their uses in plant breeding. *Seiken Zihō*, 27–28, 14–29.
- [11]. Kasha KJ, Maluszynsky M (2003) Production of doubled haploids in crop plants. An introduction. In: Maluszynsky M, Kasha KJ, Forster BP, Szaejko I (eds) *Doubled haploid production in crop plants. A manual*. Kluwer/FAO-IAEA, Dordrecht/Vienna, pp 1–4.
- [12]. Blakeslee AF, Belling J, Farnham ME Bergner AD (1922) A haploid mutant in the Jimson weed, *Datura stramonium*. *Science* 55:646–647.
- [13]. Clausen RE, Mann MC (1924) Inheritance in *Nicotiana tabacum*. V. The occurrence of haploid plant in interspecific progenies. *PNAS* 10:121–124.
- [14]. Gains EF, Aase HC (1926) A haploid wheat plant. *Am J Bot* 13:373–385.
- [15]. Kimber G, Riley R (1963) Haploid angiosperms. *Botanical Rev* 29:480–531.
- [16]. Guha S, Maheshwari SC (1964) In vitro production of embryos from anthers of *Datura*. *Nature* 204:497.
- [17]. Heberle-Bors, E. 1985. In vitro haploid formation from pollen: A critical review. *Theor. Appl. Genet.* 71:361–374.
- [18]. Dunwell, J.M. (1996). Microspore culture. In: *In Vitro Haploid Production in Higher Plants, Vol. 1: Fundamental Aspects and Methods*. Ed. S.M. Jain, S.K. Sopory, and R.E. Veilleux. Kluwer Academic Publishers, Dordrecht, the Netherlands. 205–216.
- [19]. Keller, E.R.J. and L. Korzun. 1996. Ovary and ovule culture for haploid production. In: *In Vitro Haploid Production in Higher Plants, Vol. 1: Fundamental Aspects and Methods*. Ed. S.M. Jain, S.K. Sopory, and R.E. Veilleux. Kluwer Academic Publishers, Dordrecht, the Netherlands. 217–235.
- [20]. Lakshmi Sita, G. 1997. Gynogenic haploids in vitro. In: *In Vitro Haploid Production in Higher Plants, Vol.5: Oil, Ornamental and Miscellaneous Plants*. Ed. S.M. Jain, S.K. Sopory, and R.E. Veilleux. Kluwer Academic Publishers, Dordrecht, the Netherlands. 175–193.
- [21]. Hazarika, R.R., Mishra, V.K. and Chaturvedi, R. (2013) In Vitro Haploid Production—A Fast and Reliable Approach for Crop Improvement. In: Tuteja N. and Gill S. S. (eds.) *Crop improvement under adverse conditions*. Springer, Heidelberg.
- [22]. Forster BP, Thomas WTB (2005) Doubled haploids in genetics and plant breeding. *Plant Breed Rev* 25:57–88.
- [23]. Veilleux RE (1994) Development of new cultivars via anther culture. *Hortscience* 29(11):1238–1241.
- [24]. Germana MA (2011) Gametic embryogenesis and haploid technology as valuable support to plant breeding. *Plant Cell Rep* 30(5):839–857.
- [25]. Dunwell JM (2010) Haploids in flowering plants: origins and exploitation. *Plant Biotechnol J* 8 (4):377–424.
- [26]. Murigneux, A., D. Barloy, P. Leroy and M. Beckert, 1993. Molecular and morphological evaluation of doubled haploid lines in maize. I. Homogeneity within DH lines. *Theor. Appl. Genet.* 86: 837–842.
- [27]. De Buyser, J., Y. Henry, P. Lonnet, R. Hertzog and A. Hespel, 1987. "Florin": a doubled haploid wheat variety developed by the anther culture method. *Plant Breed.* 98: 53–56.
- [28]. Chen, Z. (1986) Induction of androgenesis in woody plants. In: Han H. & Hongyuan (Eds) *Haploids in Higher Plants in vitro*. China Academic Publishers, Springer-Verlag, pp. 42–66.
- [29]. Szarejko, I., J. Guzy, J. Jimenez Davalos, A. Roland Chavez and M. Maluszynski, 1995. Production of mutants using barley DH systems. In: *Induced Mutations and Molecular Techniques for Crop Improvement*. IAEA, Vienna, pp.517–530.
- [30]. Khan, A.J., S. Hassan, M. Tariq and T. Khan, 2001. Haploidy breeding and mutagenesis for drought tolerance in wheat. *Euphytica*, 120: 409–414.
- [31]. Kostoff, D., 1929. An androgenic *Nicotiana* haploid. *Zeit. Zellforschg.* 9: 640–642.
- [32]. Guha, S. and S.C. Maheshwari, 1964. In vitro production of embryos from anthers of *Datura*. *Nature* 204: 497.

- [33]. Sopory, S. and Munshi, M. (1996) Anther culture. In *In vitro Haploid Production in Higher Plants* (Vol. 1) (Mohan Jain, M. et al., Eds), pp.145–176, Kluwer Academic Publishers.
- [34]. Maluszynski, M. et al. (2003) Published protocols for other crop plant species. In *Doubled Haploid Production in Crop Plants: A Manual* (Maluszynski, M. et al., Eds), pp. 309–336.
- [35]. Atanassov A, Zagorska N, Boyadjiev P, Djilianov D (1995) *In vitro* production of haploid plants. *World J Microbiol Biotechnol* 11:400–408.
- [36]. Datta SK (2005) Androgenic haploids: factors controlling development and its application in crop improvement. *Curr Sci* 89:1870–1878.
- [37]. Bhojwani, S.S and Razdan, M.K. (1996) *Plant Tissue Culture: Theory and practice*, a revised edition. Elsevier. *Studies in Plant Science*. 5: 167-214.
- [38]. Kieffer M, Fuller MP, Chauvin JE, Schlessler A (1993) Anther culture of kale (*Brassica oleracea* L convar acephala (dc) alef). *Plant Cell Tissue Organ Culture* 33(3):303–313.
- [39]. Arnison PG, Keller WA (1990) A survey of anther culture response of *B. oleracea* L. cultivars grown under field conditions. *Plant Breed* 104:125–133
- [40]. Forster BP, Heberle-Bors E, Kasha KJ, Touraev A (2007) The resurgence of haploids in higher plants. *Trends Plant Sci* 12(8):368–375.
- [41]. Tulecke, W., 1964. A haploid tissue culture from the female gametophyte of *Ginkgo bi/oba*. *Nature* 203: 94-95.
- [42]. Uchimiya, H., T. Kameya and N. Takahashi, 1971. *In vitro* culture of unfertilized ovules in *Solanum melongena* and ovaries in *Zea mays*. *Jpn. J. Breed.* 21: 247-250.
- [43]. San Noeum, L.H., 1979. *In vitro* induction of gynogenesis in higher plants. In: A.M. van Harten and A.C Zeven (Eds.), *Proc. Conf. Broadening the Genetic Base of Crops*, Wageningen, July 3-7, 1978, pp. 327-329.

Forecasting Stock Prices by using The Fuzzy Sets: A Real Case Application in Borsa Istanbul

*Melike Erdogan*¹, Ihsan Kaya, Cansin Yildiz*

Abstract

To being predictable of returns and prices of financial assets such as stocks, bonds, foreign currency within a certain probability can provide over-normal winnings or at least an opportunity to make up the financial loss. In this paper, one of well-known forecasting methods named Exponential Smoothing Method (ESM) has been used to forecast the variability of Borsa Istanbul-30 index (BIST-30). It is aimed to estimate the stock prices of BIST-30 Index for a month of January 2015. These estimates are conducted separately for the first and second sessions and fuzzy forecast values are calculated for each day. Then the estimated values of these fuzzy forecasts have been analyzed by using control charts. Finally, two of well-known control charts named cumulative sum control chart (CUSUM) and exponentially weighted moving average chart (EWMA) have been used to analysis of variability in BIST-30.

Keywords: BIST-30 Index, CUSUM, Defuzzification, EWMA, Forecasting, Process Variability

1. INTRODUCTION

Future inherently involves risk and uncertainty; therefore attracted the curiosity of the people and has been the subject of much research. Managing the future mostly depends on the estimates. When the future predicted, it ceases to be known and so risk turns into opportunities and opportunities turns into benefits. To being predictable of returns and prices of financial assets such as stocks, bonds, foreign currency within a certain probability can provide over-normal winnings or at least an opportunity to make up the financial loss. Estimation of stock price is an important issue in taking investment / financial decisions for individual investors, fund managers, financial analysts. Volatility in stock price due to frequent fluctuations experienced in both the Borsa Istanbul and economic area shows that investors are at risk and thereof predicting the variability of prices correctly has a great importance for investors and businesses. There have been many researches about the estimation of return/prices of financial assets in the literature. Özalp and Anagün [1] used classical estimation methods for forecasting the stock prices. They showed that the best solution is obtained with Exponential Smoothing and ARIMA models. Lewellen [2] presented whether financial ratios like dividend yield can predict aggregate stock returns. Chin and Hong [3] aimed to use the dividend yield, earning to price ratio, and capital gain to predict the Malaysia stock market return from 1995 to 2005 by using the time series regression. They utilized both the univariate and multivariate Ordinary Least Square regression analysis to test the future monthly and quarterly stock return. Elleuch [4] found a positive correlation between the future stock returns with using 12 financial ratios and accounting data for the period 1995-2001 in the scope of fundamental analysis for business and suggests the conclusion that these proportions could be used to predict future stock returns.

Kheradyar and Ibrahim [5] examined the role of financial ratios as empirical predictors of stock return in separate and combined sets for the period January 2000 to December 2009 in Bursa Malaysia. Dutta et al. [6] suggested logistic regression and various financial ratios as independent variables to investigate indicators that significantly affect the performance of stocks actively traded on the Indian stock market. Vasiliou et al. [7] analyzed the performance of various technical trading rules in the Athens Stock Market and tested two of the simplest and the most popular trading rules-Moving Averages and MACD Indicator. They also evaluated how these simple forms of technical analysis can predict stock price movements in the Athens Stock Exchange. Tokuoaka and Yamawaki [8] suggested a systematic method for predicting the trend of the price time-series at several ticks ahead of the current price by means of a genetic algorithm. Metghalchi et al. [9] proposed some moving average technical trading rules for the NASDAQ Composite Index. They showed that moving average rules indeed have predictive power and could discern recurring-price patterns for profitable trading.

Control charts, which developed in 1920 by W.A. Shewhart [10], today still continue its development by integrating new applications in different disciplines. Control charts can be successfully applied in finance sector for the statistical analysis of the variables in the process. For example, Kovářik and Sarga [11] proposed financial management approach by using statistical process control. They applied cumulative sum control chart (CUSUM) and exponentially weighted moving average chart (EWMA) due to their sensitivities and proposed two case studies. Xin et al. [12] applied CUSUM to financial markets. Gerst [13] reviewed the appropriateness of using control charts in quality of life measurements for a major urban area to customer satisfaction data, to providing a digital dashboard for a medium sized bank, to measuring switching network performance of a national cellular provider and even to finance and budgeting with a number of case studies.

This paper aimed at estimating the stock price of BIST-30 Index where high variability exists and tried to determine the variability of these estimations by using statistical process control tools. The rest of the paper has been organized as follows: Section 2 presents the forecasting methods to estimate the price of BIST -30 Index. Section 3 gives some information about the fuzzy sets. Section 4 briefly explains control charts. Section 5 includes a real case application. Finally the obtained results and future research directions have been discussed into Section 6.

2. FORECASTING AND FORECASTING METHODS

A forecast is a prediction of some future event or events. Forecasting is an important decision tool for many fields such as business and industry, government, economics, environmental sciences, medicine, social science, politics, and finance [14]. Forecasting can be used in many areas such as marketing, economics, financial asset management, financial risk management, business and government budgeting, operations planning and control, demography, and crisis management [15]. Forecasting models are basically divided as qualitative and quantitative methods. Qualitative methods are generally used in strategic planning [15]. The forecasting methods can be summarized as shown in Figure 1 [14, 15, 16, 17]:

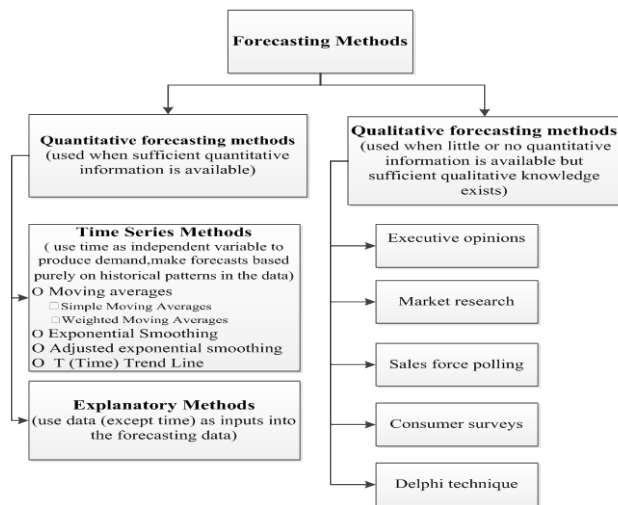


Figure 1. Forecasting Methods

2.1 Exponential Smoothing

Exponential smoothing is an averaging method that takes weighted averages of past observations. This method is applied to forecasting data that has no trend or seasonal pattern. Determining the existence of a general trend and cyclical fluctuations is extremely difficult when periodic and irregular fluctuations are too large. In such cases, using smoothing techniques provide large deviations to be avoided. This method is not recommended where general trends or the seasonal effects exist [1]. Forecasted value is calculated with using the weighted average of the available data and a predetermined estimate of the current period. Exponential smoothing is mathematically expressed as follows:

$$F_{t+1} = \alpha D_t + (1 - \alpha)F_t \tag{1}$$

where F_{t+1} : Forecasted value for next period, D_t : Actual value for current period, F_t : Forecasted value for current period, and α : Correction factor.

The correction factor, α , is the weight used for the current period and $(1 - \alpha)$ is the weight used to estimate the current period. The value of 0.01 and 0.50 is mostly used for value of α . The best value of α is the value that gives closest value to the actual demand and find by trial and error. If there is a trend in the data, it is more accurate to use adjusted exponential smoothing.

Winter model is an extended special case of basic exponential smoothing models. This method is suitable for data showing trends and seasonality. In the case of seasonal effect and trends do not exist, exponential smoothing methods works with larger error [1].

3. FUZZY SET THEORY AND DEFUZZIFICATION METHODS

The fuzzy set theory is introduced by Zadeh [18] and is suitable for dealing with the uncertainty and vagueness associated with parameters [19]. In a universal set of discourse X , a fuzzy subset \tilde{A} of X is defined by a membership function $f_{\tilde{A}}(x)$, where $f_{\tilde{A}}(x)$, $\forall x \in X$, indicates the degree of x in \tilde{A} [19]. The degree to which an element belongs to a set is defined by the value between 0 and 1. If x really belongs to, $f_{\tilde{A}}(x) = 1$, and clearly not, $f_{\tilde{A}}(x) = 0$. The higher $f_{\tilde{A}}(x)$ is the greater is the grade of membership for x in \tilde{A} [19].

3.1 Triangular Fuzzy Numbers

The fuzzy set theory uses data with boundaries that feature lower, median, and upper values that are not sharply defined [20]. Triangular fuzzy numbers (TFN) and trapezoidal fuzzy numbers (TrFN) are usually employed to capture the vagueness of the parameters [20]. TFN is expressed with boundaries instead of crisp numbers [20]. TFN is designated with reference values (a, b, c) which corresponds to median value of fuzzy number, b, the left and right side of fuzzy number, a and c [20]. The parameters a, b and c respectively denote the smallest possible value, the most promising value, and the largest possible value of a fuzzy number [21].

A TFN \tilde{A} is a fuzzy number with piecewise linear membership function $f_{\tilde{A}}(x)$ defined by [22] as follows.

$$f_{\tilde{A}}(x) = \begin{cases} 1 & x = b \\ (x-a)/(b-a) & a \leq x \leq b \\ (c-x)/(c-b) & b < x \leq c \\ 0 & \text{otherwise} \end{cases} \quad (2)$$

Where $-\infty < a \leq b \leq c < +\infty$. The TFN, \tilde{A} , can be expressed by (a, b, c) as shown in Fig. 2.

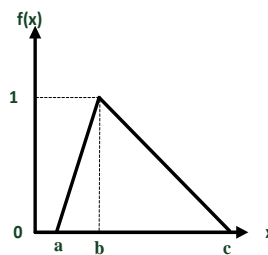


Figure 2. Triangular Fuzzy Number

There are multiple types of membership functions existing but the triangular membership function is one of the most commonly used in practice [23].

3.2 Defuzzification Methods

Defuzzification is the conversion of a fuzzy quantity to a precise quantity [24]. Information about some of the popular defuzzification methods is given below [24, 25, 26]:

Max membership principle: This method is also known as the height method, this scheme is limited to peaked output functions. This method can be explained as:

$$\mu_c(z^*) \geq \mu_c(z), \quad \text{for all } z \in Z \quad (3)$$

Centroid method: Center of area or center of gravity (shortly centroid or COA) is the most prevalent and physically appealing of all the defuzzification methods; it is given by the algebraic expression:

$$z^* = \frac{\int \mu_c(z) \cdot z \, dz}{\int \mu_c(z) \, dz}, \quad (4)$$

Weighted average method: The weighted average method is the most frequently used in fuzzy applications since it is one of the more computationally efficient methods. Unfortunately, it is usually restricted to symmetrical output membership functions. It is given by the algebraic expression where \sum denotes the algebraic sum and where \bar{z} is the centroid of each symmetric membership function:

$$z^* = \frac{\sum \mu_c(\bar{z}) \cdot \bar{z} \, d\bar{z}}{\sum \mu_c(\bar{z})}, \quad (5)$$

Mean max membership: This method (also called middle-of-maxima) is closely related to the first method, except that the locations of the maximum membership can be nonunique (i.e., the maximum membership can be a plateau rather than a single point). This method is given by the expression:

$$z^* = \frac{a+b}{2} \quad (6)$$

Center of sums: This is faster than many defuzzification methods that are currently in use, and the method is not restricted to symmetric membership functions. This process involves the algebraic sum of individual output fuzzy sets, say \tilde{C}_1 and \tilde{C}_2 , instead of their union. Two drawbacks to this method are that the intersecting areas are added twice, and the method also

involves finding the centroids of the individual membership functions. The defuzzified value z^* is given as follows where the symbol \bar{z} is the distance to the centroid of each of the respective membership functions:

$$z^* = \frac{\sum_{k=1}^n \mu_{\alpha_k}(z) \int \bar{z} dz}{\sum_{k=1}^n \mu_{\alpha_k}(z) \int dz}, \quad (7)$$

4. STATISTICAL PROCESS CONTROL

Control charts are one of the most powerful tools used in statistical process control (SPC) to monitor the process, to follow the whether the quality variables under control or not and to detect shifts in the process [27]. Coupled with classical Shewhart control charts, Cumulative sum (CUSUM) and exponential weighted moving average (EWMA) charts are used to measure drifts in the process mean, but these to control are more sensitive to the small drifts [27]. Roberts [28] firstly introduced the EWMA control chart for monitoring the process mean and Page [29] also suggested the CUSUM control chart based on sample range for monitoring the process dispersion [30]. EWMA and CUSUM charts are powerful statistical process monitoring tools because they have excellent speed in detecting small to moderate persistent process shifts [30]. These types of control charts are often used the industries such as chemical and process industries in which small disturbances cause to large financial losses [30]. The only thing missing side of these charts is that they are less sensitive to large shifts than the classical Shewhart control chart [30]. In this paper, we use CUSUM and EWMA charts to measure the variability of stock prices. The following subsections give basic information about these control charts.

4.1 CUSUM Chart

Cumulative sum and EWMA charts are designed to use the previous information along with the current to detect small to moderate shifts. Consequently, they are known as memory control charts [31]. The CUSUM chart was introduced by Page [29] and it uses the cumulative deviation from the target value. It is a favorable tool to detect small to moderate shifts. The CUSUM chart is based on the following two statistics [31]:

$$\left. \begin{aligned} C_t^+ &= \max[0, (\bar{X}_t - \mu_0) - K + C_{t-1}^+] \\ C_t^- &= \max[0, -(\bar{X}_t - \mu_0) - K + C_{t-1}^-] \end{aligned} \right\} \quad (8)$$

where t represents the time or sample number and \bar{X}_t is the mean of X for sample t , $X_t \sim N(\mu_0, \sigma_0)$, where μ_0 and σ_0 are the target mean and standard deviation, respectively. $K = k \sigma_0$ is the reference value and is mostly used half of the shift,

that is, $k = \delta / 2$, where δ is the amount of shift given as $\delta = \frac{|\mu_1 - \mu_0|}{\sigma_0 / \sqrt{n}}$, μ_1 is the out of control mean, and n is the sample size.

C_t^+ and C_t^- are the upper and lower CUSUM statistics, respectively, and are plotted against to the control limit $H = h \sigma_0$. Initially, we set $C_0^+ = C_0^- = 0$ [31].

There are two ways of representing the cumulative sum charts, the algorithmic CUSUM chart and the V-mask form of the CUSUM. The V-mask is applied to successive CUSUM statistic values [32]:

$$C_i = \sum_{j=1}^i y_j = y_i + C_{i-1} \quad (9)$$

where y_i is the standardized observation $y_i = (x_i - \mu_0) / \sigma_0$.

4.2 EWMA Chart

The EWMA control chart was introduced by Roberts [28] and it is used to detect small to moderate shifts. The EWMA statistic is defined as follows [31]:

$$Z_i = (1 - \lambda)Z_{i-1} + \lambda \bar{X}_i \quad (10)$$

where λ is the sensitivity parameter with $0 < \lambda \leq 1$. Z_0 is the starting value and is set to be equal to the target mean μ_0 . The EWMA structure has an upper control limit (UCL), lower control limit (LCL), and center line (CL) defined where L is used as width coefficient between UCL and LCL for the predefined false alarm rate as follows [31].

$$\left. \begin{aligned}
 LCL_t &= \mu_0 - L\sigma\bar{x}\sqrt{\frac{\lambda}{2-\lambda}(1-(1-\lambda)^{2t})} \\
 CL_t &= \mu_0 \\
 UCL_t &= \mu_0 + L\sigma\bar{x}\sqrt{\frac{\lambda}{2-\lambda}(1-(1-\lambda)^{2t})}
 \end{aligned} \right\} \quad (11)$$

5. A REAL CASE APPLICATION

The data that used for analyze the stock prices are composed of the data from January between the dates of 02.01.1995-02.01.2014 with the information opening, highest and closing, values of first and second sessions. Then a forecasting process has been managed for 2015 January. For this aim, the winter exponential smoothing method is used to forecast the BIST-30 Index prices by using Minitab 17 statistical software. The forecasting process is hold for all days of January separately and a sample forecast is shown in Figure 3(a), 3(b) and 3(c), respectively for January 2 and they summarized in Table 4.

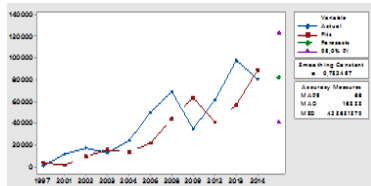


Figure 3(a) Smoothing Plot for Opening,
January 2, 2015

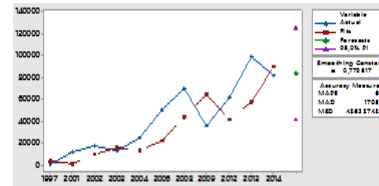


Figure 3(b) Smoothing Plot for Highest,
January 2, 2015

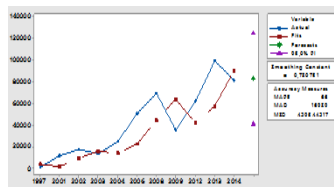


Figure 3(c) Smoothing Plot for Closing, January 2, 2015

Table 4. The forecast results for first session of January 2, 2015

2 January 2015								
Opening			Closing			Highest		
Forecast	Lower	Upper	Forecast	Lower	Upper	Forecast	Lower	Upper
82.266	41.013	123.519	83.650	41.857	125.444	82.728	41.230	124.227

The forecasting results of ISE-30 Index first and second sessions' opening, highest and closing prices for the month of January that are calculated by the Minitab with Exponential Smoothing Methods are given in Table 5.

Table 5 The Forecast Values of Stock Prices for BIST-30 Index on January 2015

First Session	Opening	Closing	Highest	Second Session	Opening	Closing	Highest
2 January 2015	82.266	82.728	83.650	2 January 2015	81.952	83.305	83.342
5 January 2015	89.578	90.002	90.315	5 January 2015	89.337	89.655	90.083
6 January 2015	75.976	76.468	76.793	6 January 2015	76.032	77.967	78.640
7 January 2015	84.458	85.449	85.988	7 January 2015	85.603	86.069	86.397
8 January 2015	84.602	84.792	85.798	8 January 2015	83.915	84.065	84.931
9 January 2015	94.605	95.541	95.545	9 January 2015	82.403	83.132	83.436
12 January 2015	94.606	95.541	95.545	12 January 2015	66.483	65.960	95.137
13 January 2015	80.850	81.111	81.574	13 January 2015	80.162	95.420	81.250
14 January 2015	84.955	85.495	85.729	14 January 2015	85.215	86.412	95.592
15 January 2015	84.860	85.090	86.034	15 January 2015	84.840	85.472	85.946
16 January 2015	83.930	84.738	84.903	16 January 2015	84.201	84.535	85.334
19 January 2015	85.305	85.606	86.139	19 January 2015	84.424	84.631	85.941
20 January 2015	76.652	77.729	77.986	20 January 2015	76.497	76.880	77.395
21 January 2015	85.069	85.741	85.950	21 January 2015	84.765	85.115	86.255
22 January 2015	83.187	84.062	84.992	22 January 2015	83.983	84.888	85.299
23 January 2015	84.684	85.100	85.569	23 January 2015	83.630	83.785	85.319
26 January 2015	83.197	83.420	85.345	26 January 2015	82.502	83.532	84.076
27 January 2015	75.331	75.786	76.690	27 January 2015	76.391	76.712	77.600
28 January 2015	82.684	82.852	83.954	28 January 2015	80.510	80.652	82.697
29 January 2015	78.339	79.110	80.843	29 January 2015	77.280	78.948	79.638
30 January 2015	78.227	78.871	79.672	30 January 2015	78.066	78.997	80.008

Then these three values which are opening closing and highest prices are forecasted for each day. These values are evaluated as lower bound, most likely value, and upper bound of a TFN. As a result, two TFNs $(X_{C_j}, X_{D_j}, X_{H_j})$ for stock price values with first and second sessions' of BIST-30 index have been obtained on January 2015. With using these two data, we would defuzzify the estimated values to obtain crisp values of price information. In this step, we used weighted average defuzzification method to obtain crisp values for the forecasted data. Finally, two control charts which are CUSUM and EWMA have been conducted to measure the variability of stock price in BIST-30 index. The obtained control charts by MINITAB shows in Figures 5, 6 and 7, respectively.

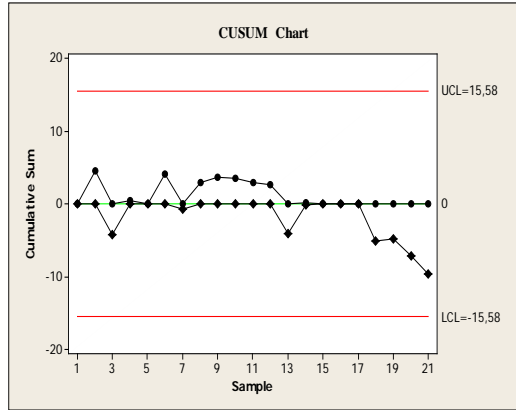


Figure 6. Cusum Chart

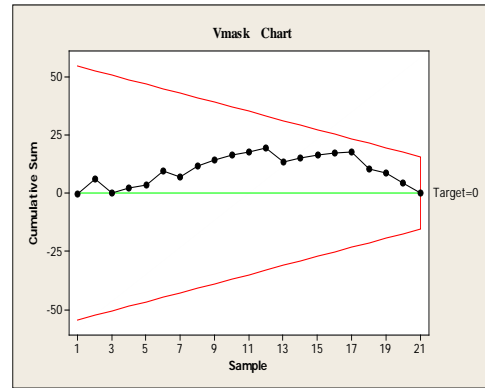


Figure 7. Cusum Chart with V Mask

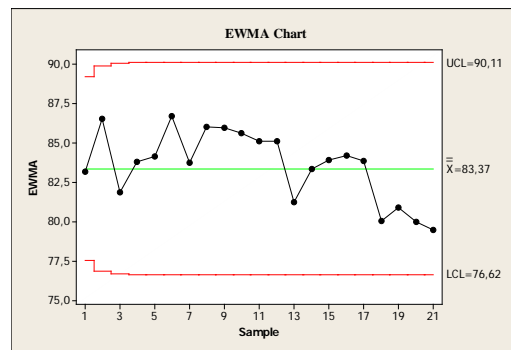


Figure 8. EWMA Chart

It is observed that all estimates are within expected range both in CUSUM and EWMA charts. CUSUM chart is plotted both of the control limits and V mask. EWMA chart is also plotted with the $\lambda=0.5$. As a result of analysis performed, it is observed that the forecasted values are under control and variability is in expected level.

CONCLUSIONS AND FUTURE SUGGESTIONS

Since the future inherently involves risk and uncertainty, it is so critical to control variability of future. Managing of the future mostly depends on the estimates. When the future has been predicted, it ceases to be known and so risk turns into opportunities, opportunities turns into benefits.

In this paper, we aim to forecast the stock prices in BIST-30 on January 2015. Two sessions estimations are obtained for opening, closing and highest values. These two separate price values with three parameters are taken into account as TFNs and a defuzzification calculation is hold to obtain crisp values to become ready for use in the control charts. CUSUM and EWMA control charts are plotted to measure the variability of estimated data whether within the control limits or not. The forecasted values are determined to be under control according to the control charts. As future directions, different defuzzification methods can be applied or different kind of control charts can be used and the obtained results can be compared.

REFERENCES

- [1] A. Özalp and S. Anagün, "Sektörel Hisse Senedi Fiyat Tahmininde Yapay Sinir Ağı Yaklaşımı ve Klasik Tahminleme Yöntemleri ile Tahminleme", *Endüstri Mühendisliği Dergisi*, vol. 12, pp. 2-17, 2001.
- [2] J. Lewellen, "Predicting Returns with Financial Ratios", *Journal of Financial Economics*, vol. 74, pp. 209-235, 2004.
- [3] L. Chin, and L. W. Hong, "Can Financial Ratios Predict The Malaysian Stock Return", *Integration & Dissemination*, vol. 2: pp. 7-8, 2008.

- [4] J. Elleuch, and L. Trabelsi, "Fundamental Analysis Strategy and the Prediction of Stock Returns", *International Research Journal of Finance and Economics*, vol. 30, pp. 95-107, 2009.
- [5] S. Kheradyar, and I. Ibrahim, "Financial Ratios as Empirical Predictors of Stock Return", *International Proceedings of Economics Development and Research*, vol. 10, pp. 318-322, 2011.
- [6] A. Dutta, G. Bandopadhyay, and S. Sengupta, "Prediction of Stock Performance in the Indian Stock Market Using Logistic Regression", *International Journal of Business and Information*, vol. 7 (1), pp. 105-136, 2012.
- [7] D. Vasiliou, N. Eriotis and Papatthanasiou, S., "How Rewarding is Technical Analysis Evidence from Athens Stock Exchange", *Operational Research. An International Journal*, vol. 6 (2), pp. 85-102, 2006.
- [8] S. Tokuoka and M. T. Yamawaki, "Trend Predictions of Tick-Wise Stock Prices by Means of Technical Indicators Selected by Genetic Algorithm", *Artificial Life and Robotics*, vol. 12 (1), pp. 180-183, 2008.
- [9] M. Metghalchi, Y. H. Chang, and J. Du, "Technical Trading Rules for NASDAQ Composite Index", *International Research Journal of Finance and Economics*, vol. 73, pp. 109-121, 2011.
- [10] W. A. Shewhart, *Economic control of quality of manufactured product*. ASQ Quality Press, 1931.
- [11] M. Kovářik, and L. Sarga, "Implementing control charts to corporate financial management", *WSEAS Transactions on Mathematics*, vol. 13, pp. 246-255, 2014.
- [12] L. Xin, P. L. Yu, and K. Lam. "An Application of CUSUM Chart on Financial Trading", 9th International Conference on Computational Intelligence and Security (CIS), IEEE, 2013, pp. 178-181.
- [13] R. Gerst, "Control Charts In The Comptrollers Office: (And Other Peculiar Places)", in *Proc. ASQ World Conference on Quality and Improvement*, 2003, vol. 57, pp. 535-546.
- [14] D. C. Montgomery, C. L. Jennings, and M. Kulahci, *Introduction to time series analysis and forecasting*, John Wiley & Sons, 2015.
- [15] F. X. Diebold, *Elements of forecasting*, 4th ed., Cengage Learning, 2006.
- [16] S. Makridakis, S. C. Wheelwright and R. J. Hyndman, *Forecasting methods and applications*, John Wiley & Sons, 2008.
- [17] P. Mendes *Demand driven supply chain: A structured and practical roadmap to increase profitability*, Springer Science & Business Media, 2011.
- [18] L. A. Zadeh, "Fuzzy sets", *Information and control*, vol. 8(3), pp. 338-353, 1965.
- [19] J. Wang, Y. Jing, C. Zhang, G. Shi and X. Zhang, "A fuzzy multi-criteria decision-making model for trigeneration system", *Energy Policy*, vol. 36, pp. 3823-3832, 2008.
- [20] S. K. Lee, G. Mogi, J. W. Kim, and B. J. Gim, "A fuzzy analytic hierarchy process approach for assessing national competitiveness in the hydrogen technology sector", *International Journal of Hydrogen Energy*, 33(23), 6840-6848, 2008.
- [21] D. Choudhary and R. Shankar, "An STEEP-fuzzy AHP-TOPSIS framework for evaluation and selection of thermal power plant location: A case study from India", *Energy*, vol. 42(1), pp. 510-521, 2012.
- [22] Y. Y. Jing, H. Bai, and J. J. Wang, "A fuzzy multi-criteria decision-making model for CCHP systems driven by different energy sources", *Energy Policy*, vol. 42, pp. 286-296, 2012.
- [23] S. L. Hsueh, "A fuzzy utility-based multi-criteria model for evaluating households' energy conservation performance: a Taiwanese Case Study", *Energies*, vol. 5(8), pp. 2818-2834, 2012.
- [24] T. J. Ross, *Fuzzy logic with engineering applications*, John Wiley & Sons, 2009.
- [25] M. Sugeno, "An introductory survey of fuzzy control", *Inf. Sci.*, vol. 36, pp. 59-83, 1985.
- [26] C. Lee, "Fuzzy logic in control systems: fuzzy logic controller - Parts I and II", *IEEE Trans. Syst. Man Cybern.*, vol. 20, pp. 404-435, 1990.
- [27] S. Singh and D. R. Prajapati, "Performance of CUSUM and EWMA charts for serial correlation", *The TQM Journal*, vol. 25(3), pp. 309-324, 2013.
- [28] S.W. Roberts. "Control chart tests based on geometric moving averages", *Technometrics*, vol 1(3), pp. 239-250, 1959.
- [29] E.S. Page, "Continuous inspection schemes", *Biometrika*, vol., 41(1/2), pp. 100-115, 1954.
- [30] A. Haq, J. Brown, and E. Moltchanova, "New synthetic EWMA and synthetic CUSUM control charts for monitoring the process mean", *Qual Reliab Eng Int*, vol. 32(1), pp. 269-290, 2014.
- [31] B. Zaman, M. Riaz, N. Abbas, and R. J. Does, "Mixed cumulative sum-exponentially weighted moving average control charts: an efficient way of monitoring process location", *Qual Reliab Eng Int*, vol. 31(8), pp. 1407-1421, 2015.
- [32] C. Vera do Carmo, L. F. D. Lopes, and A. M. Souza, "Comparative study of the performance of the CuSum and EWMA control charts", *Computers & Industrial Engineering*, vol. 46(4), pp. 707-724, 2004.

Alternatives Routes for Container Vessels Due to Bad Weather; Black Sea Region Study

Kadir Isik¹, Sibel Bayar²

Abstract

Selecting best route which permits to container vessel complete voyage rapidly, safely and also the least fuel consumption is one of main goal of shipping markets. There are many practical methods to reduce costs and speed up container vessels. And one of them is obtaining alternative routes with tracking weather forecast for maintain new legs and course in case of bad weather. Consequence of meteorological events on sailing container vessel could have both positive impacts and negative impacts. Even though positive impacts are increasing speed and decrease of fuel consumption, negative impacts are endangering ship and cargo safety and induce delaying in schedule of port of calls. Lessen adverse influence of bad weather is possible to find seasonal alternative routes for regions by using of Townsin-Kwon Speed Loss formulae (1983). In this study, we study on a container shipping line which Istanbul – Samsun - Poti in Black Sea region with real meteorological situations to shorten total voyage time between ports and also reduce total fuel consumption. As a result of this study, Townsin-Kwon Speed Loss Algorithm found very useful for west black sea area when bad weather dominant in this region and allow to ship complete her voyage 10 hours earlier and induce to decrease fuel consumption at the testing of method.

Keywords: *Townsin-Kwon Speed Loss Algorithm, Container Vessels, Route Optimization*

1. INTRODUCTION

Container ship had just 1.6 percentage of all world fleet deadweight in 1980 but it has 13 percentage in world fleet deadweight in 2015 [1]. Container transportation expanse day by day because of being practicality, safety and security in every type of transportation since beginning. In spite of having many advantages, there are several studying at container shipping in order to increase profit. For instance, decreasing wind adverse effect, port sequence optimization and etc. Especially, effect of wind is significant on container vessels; because of carrying cargoes on deck makes wind exposed area greater. Thus, route optimization to provide benefit from weather events or minimizing bad effects from rough weather is very important. Moreover, finding of optimal route for seasonal storm will help time scheduling on shipping lines.

Route optimization is generally overlooked by masters of the ship who usually use shortest way between target ports to arrive fast. However, there are many variables to choose proper route such as safety, security, weather conditions, swells, currents, ship structural design and the loaded cargo. So that, it is necessary that captains should prepare alternative routes depends on weather forecast and should consider ship stability condition before commencement of new passage.

Townsin-Kwon speed loss formulae for the meteorological events is useful and practical to calculate ship speed if one knows only the beaufort number and volumetric displacement [2]. In this method, calculate to added resistance, change in propulsion factors and propeller characteristics due to weather is non-essential [3].

2. EFFECT OF BAD WEATHER TO CONTAINER VESSELS

Container vessels are liner ships which are expected to arrive their destination on time. And there are factors effect to container ship timing which seen at figure 1. One of three main causes of ship delays were weather and mechanical problems on route in East Asia-Europe route for the fourth quarter of 2004 [14].

¹ Corresponding author: Istanbul University, Maritime Transportation Management Engineering, 34320, Avcular/Istanbul, Turkey. kadir.isik@istanbul.edu.tr

² Istanbul University, Maritime Transportation Management Engineering, sibelb@istanbul.edu.tr.

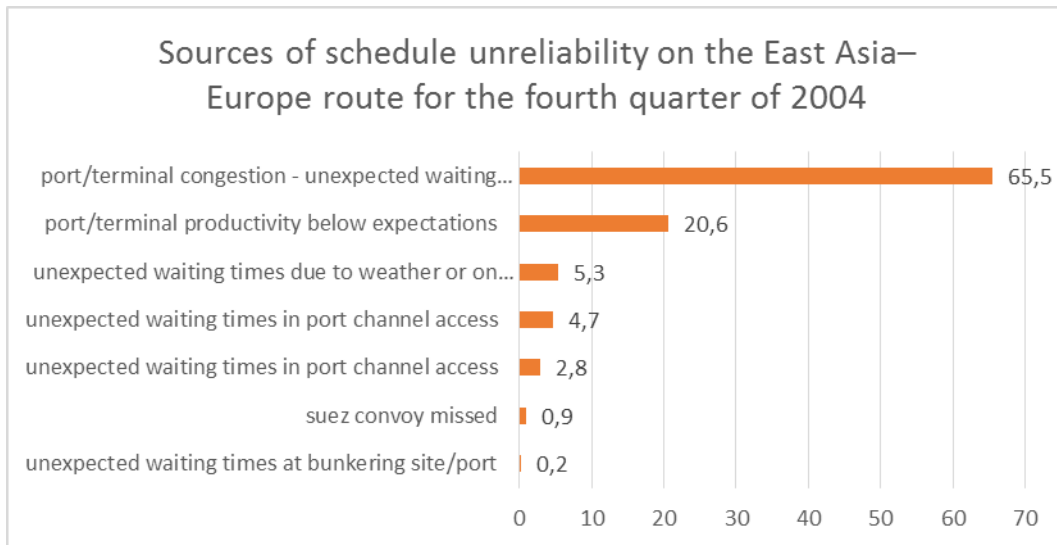


Figure 1. Sources of Schedule unreliability on the East Asia – Europe route for the fourth quarter of 2004

The wind forces generally cause increasing of propulsion resistance. While the transverse force causes yaw, drift and deviation from the course, the longitudinal force are induced resistance at the most when the yaw leads to ship listing, drift devotes to ship her course [4]. Furthermore, altering course of the ship to lead in route caused to increasing at the rudder angle which increase to propulsion resistance [5]. Besides due to propulsion resistance ship proceed slow and consume more fuel.

Moreover, effect of wind is excessively on container vessels because of their deck cargo on board. In container ships, each container on the deck increase wind effects on the ship, so the estimation of wind effect on container ship has important role for calculation of economical cost for operation. Furthermore, each container on deck raise wind effect to ship twenty percent more than not being cargo on deck[6]. Another impact of bad weather to container ships is loss of containers at sea. Study of container losses at Bay of Biscay demonstrate that 1251 containers were lost in 158 incidents and losses of %83 percent occurred between November to February when the sea is roughest. In this case crew can alter course to minimize risks [8].

3. CHARACTERISTIC FEATURE OF BLACK SEA REGION WINDS

Climate of Black Sea is sunny, hot and fine at summer season like Mediterreanean. However, it is cold and have disturbed weather occuring to mariners in winter season. Bad weather dominates the region mostly from october to mid-march. Gusts in the winter are generally caused by anticyclone which is Siberia/NW Mongolia with elongated E-W axis. When this anticyclone encounter with a transit depression from N Atlantic and N Europe induce NE and NW rough winds over the west part of Black Sea especially, in february. In may effect of siberia anticyclones finished and Azores anticyclone occasionally brings fine weather throughout summer season [9]

In winter, unless winds which are 20 miles far from coastal vary substantially due to the frequent transitting of depressions, in the W part of the region NE and NW predominate. In the South East part of the region NW winds are also frequent but winds from E are common feature for winter. As seen seasonal wind distribution chart of Black Sea, the strongest wind occurred in January [9]

Gales in the region could reached up until wind force 12 in the winter season. Generally gales are 7-8 wind force and these winds force constitute 5 percent more in the region and 10 percent more in the W part of the Black Sea. Moreover 9-10 winds force recorded up in most of area and in the W part, 12 wind force had recorded [9]. But general winds force conditions in the area are as seen figure 2 [9].

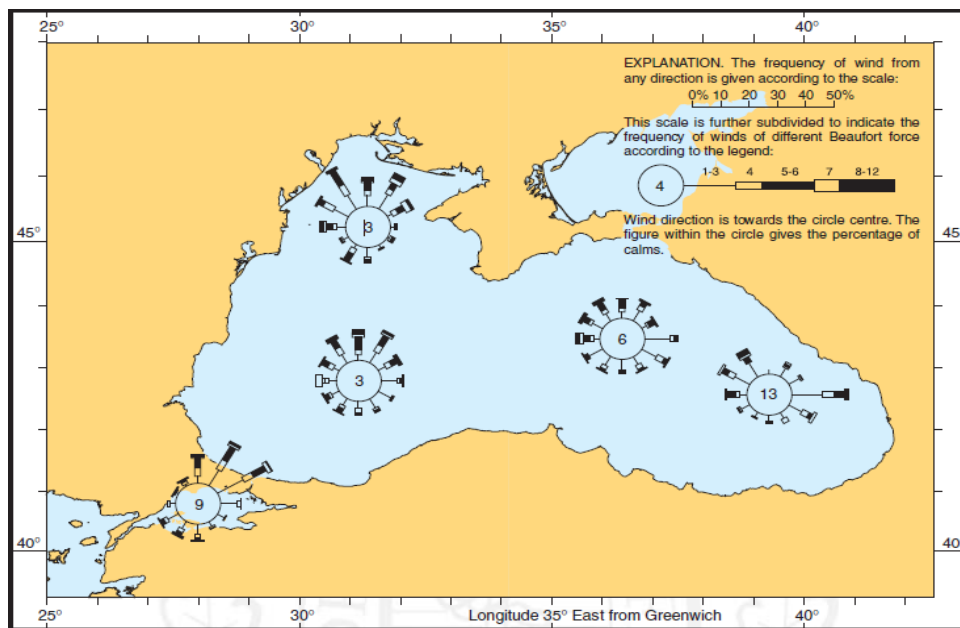


Figure 2. Wind Distribution January

4. STUDIED SHIP AND STUDIED ROUTE

The shortest route between ports are generally accepted as optimal route by captains. But in this study, alternative routes are considered to obtain sourced by weather forecast how distance between ports are evaluated by dividing legs to minimize effect of rough weather thanks to Townsin-Kwon speed loss formula. To use the method efficiently, the most severe weather period is chosen in the region which occurred in winter season. For this reason, we studied for voyage starting on 3 January of 2015 to optimize route. The weather condition on sea surface on 3 January 2016 at Figure 3. and on 14 January 2016 at figure 4 [10].

In this study, a feeder container vessel which enroute İstanbul-Samsun-Poti is chosen because ship's speed and timing schedule is very important. Furthermore, in this line vessels are exposed to high seas especially in winter season during black sea passage. At chosen line, vessel firstly departures from İstanbul to Samsun and then sails to Poti from Samsun and she returns back to İstanbul form Poti. Characteristics of the ship are displacement = 16890 m³, length over all = 182 M, CB = 0.70, Fr=0,153 and service speed of the ship is 16 knots with 32 mts ifo 380 cst daily average fuel consumption.

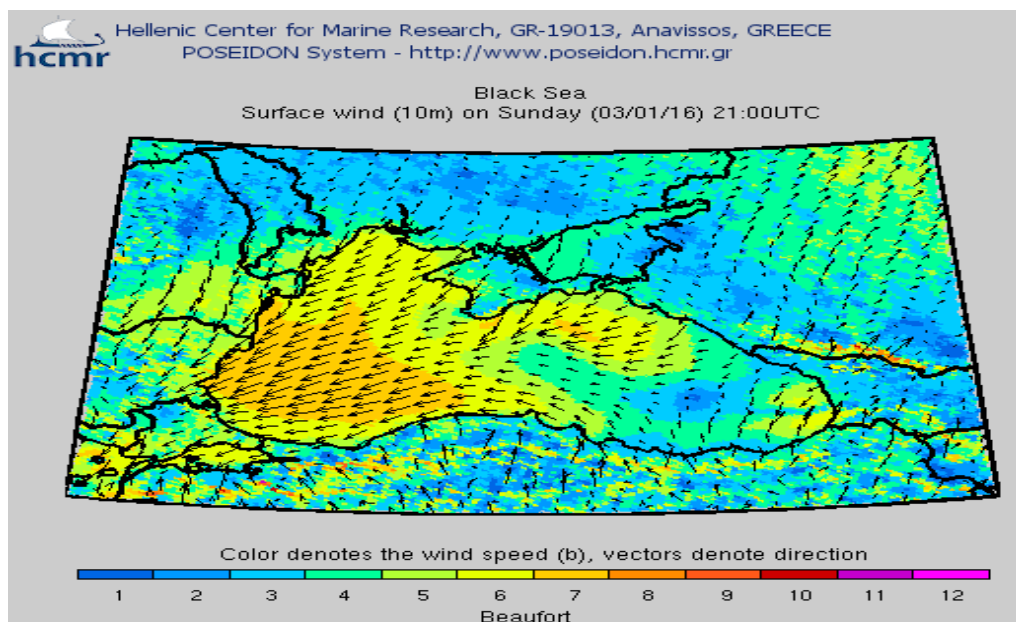


Figure 3. Surface wind (10m) on 03/01/2016 2100 UTC

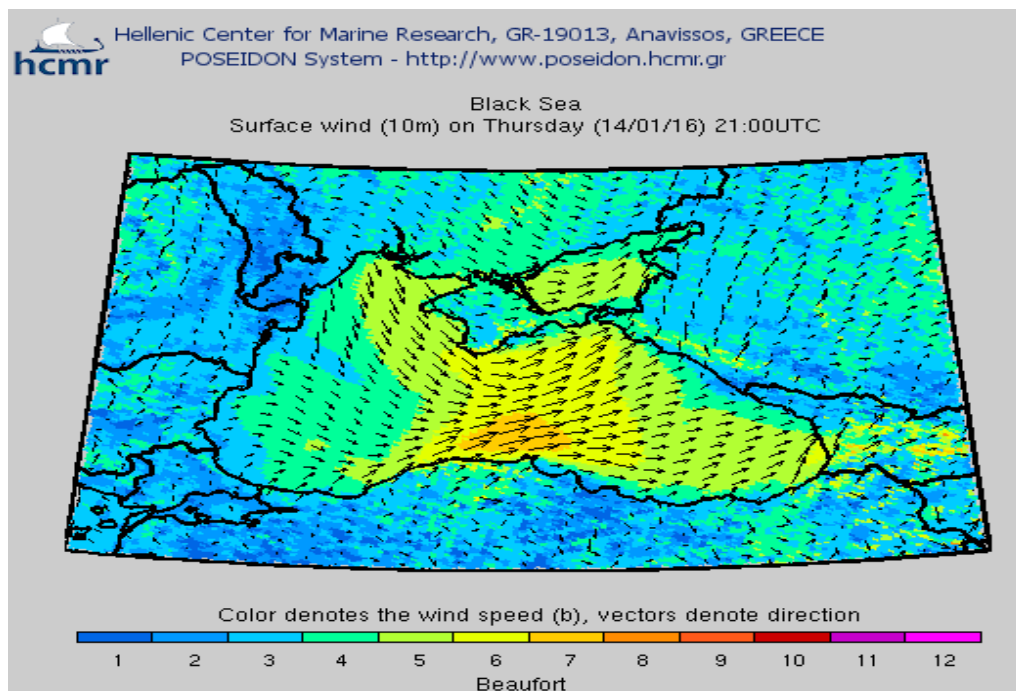


Figure 4. Surface wind (10m) on 14/01/2016 2100 UTC

5. TOWNSIN-KWON SPEED LOSS ALGORITHM

Townsin gathered data from the ships in service or measured by model tests in his studies. For this reason, his method is considered as theoretical method to investigate weather effect on ship speed performance [2]. But any other method also can't solve this problem accurately [11]. His speed loss algorithm is using for a head sea encounter situation which employed wave reflection resistance and ship motion resistance with wind resistance using Van Berlekom's algorithm (1981). Speed loss for other encounter angles are calculated by adopting a correction factor sourced on work of Aertssen (1969) [3]. Then, approximate formulas were formed by Townsin and Kwon for the speed loss in bad weather in 1983. And in 2008 Kwon brought the formula in form as seen below [12].

$$\alpha = \mu \cdot \frac{\Delta V}{V} \cdot 100\% \quad (5.1)$$

For all ships (with the exception of container ships) laden condition, $CB = 0.75, 0.80$ and 0.85 , the percentage speed loss is in head weather condition [12]

$$\frac{\Delta V}{V} \cdot 100\% = 0.5BN + \frac{BN^{4.5}}{2.7F^{0.5}} \quad (5.2)$$

For all ships (with the exception of container ships) ballast condition, $CB = 0.75, 0.80$ and 0.85 , the percentage speed loss is in head weather condition [12]

$$\frac{\Delta V}{V} \cdot 100\% = 0.7BN + \frac{BN^{4.5}}{2.7F^{0.5}} \quad (5.3)$$

For container ships, normal condition, $CB = 0.55, 0.60, 0.65$ and 0.70 , the percentage speed loss is head weather condition [12]

$$\frac{\Delta V}{V} \cdot 100\% = 0.7BN + \frac{BN^{6.5}}{22F^{2/3}} \quad (5.4)$$

ΔV is the speed loss due to head weather

V is the design speed of the ship

α is the correction factor for the block coefficient (CB) and Froude number (F_n)

BN is the Beaufort number

∇ is the volume of the displacement of ship in m^3

μ is the weather direction reduction factor calculate [12];

$$2\mu_{bow} = 1.7 - 0.03(BN - 4)^2 \quad 30^\circ-60^\circ \quad (5.5)$$

$$2\mu_{beam} = 0.9 - 0.06(BN - 6)^2 \quad 60^\circ-150^\circ \quad (5.6)$$

$$2\mu_{following} = 0.4 - 0.03(BN - 8)^2 \quad 150^\circ-180^\circ \quad (5.7)$$

Table 1. Values of correction factor α [12]

	CB	Condition	Correction factor α
0.55	Normal		$1.7 - 1.4Fr - 7.4(Fr)^2$ (5.8)
0.60	Normal		$2.2 - 2.5Fr - 9.7(Fr)^2$ (5.9)
0.65	Normal		$2.6 - 3.7Fr - 11.6(Fr)^2$ (5.10)
0.70	Normal		$3.1 - 5.3Fr - 12.4(Fr)^2$ (5.11)
0.75	Laden or normal		$2.4 - 10.6Fr - 9.5(Fr)^2$ (5.12)
0.80	Laden or normal		$2.6 - 13.1Fr - 15.1(Fr)^2$ (5.13)
0.85	Laden or normal		$3.1 - 18.7Fr + 28.0(Fr)^2$ (5.14)
0.75	Ballast		$2.6 - 12.5Fr - 13.5(Fr)^2$ (5.15)
0.80	Ballast		$3.0 - 16.3Fr - 21.6(Fr)^2$ (5.16)
0.85	Ballast		$3.4 - 20.9Fr + 31.84(Fr)^2$ (5.17)

Townsin-Kwon approximate algorithm checked by Molland (2011) with Aertssen formula for a container ship with a length of 220 m, CB = 0.60, $V = 36, 500$ mts and $Fr = 0.233$. And he found solutions for formulas approximate which is shown in table 2. [13]

Table 2. Comparison of Aertssen and Townsin-Kwon formulae

Beaufort number BN	Aertssen $\frac{2V}{V'} \%$	Townsin-Kwon $\frac{2V}{V'} \%$
5	6,1	5,4
6	11,9	9,7
7	20,5	19,4
8	34,4	39,5

6. METHOD TO FIND ALTERNATIVE ROUTES AND RESULTS OF THE TESTS

Captains of the ship often use alternative routes to decrease bad effect of the bad weather and to sail faster to his ship destination. In our study, we tested the legs of the one container line with Townsin-Kwon speed loss algorithm to suggest better route in case of heavy weather conditions. A flowchart for calculation of optimal route is set up shown in figure 3.

After testing of each leg with method, both sailing from İstanbul Boğazı to Samsun and sail Poti to İstanbul Boğazı voyages which include west part of black sea found applicable to use method. In this part of the region, despite of weather could become rough, there are free of space to maneuver for vessel. To decrease negative effect of adverse weather at the region ship altered her course at figure 6 and figure 7. as shown. Also calculated distances and calculated voyage duration time with predicted ship speed are shown at table 3. and table 4.

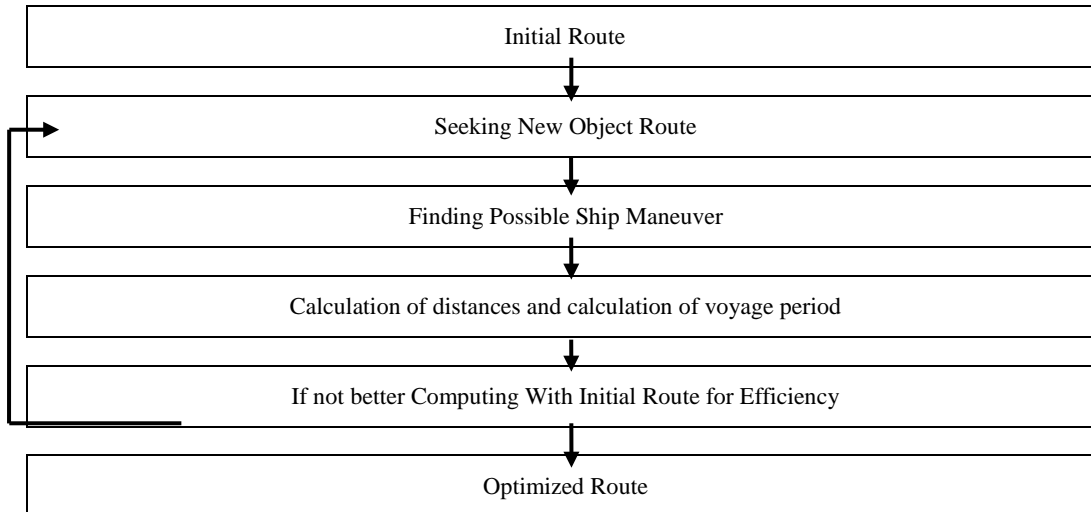


Figure 5. Alternative route for Poti to İstanbul Bogazı

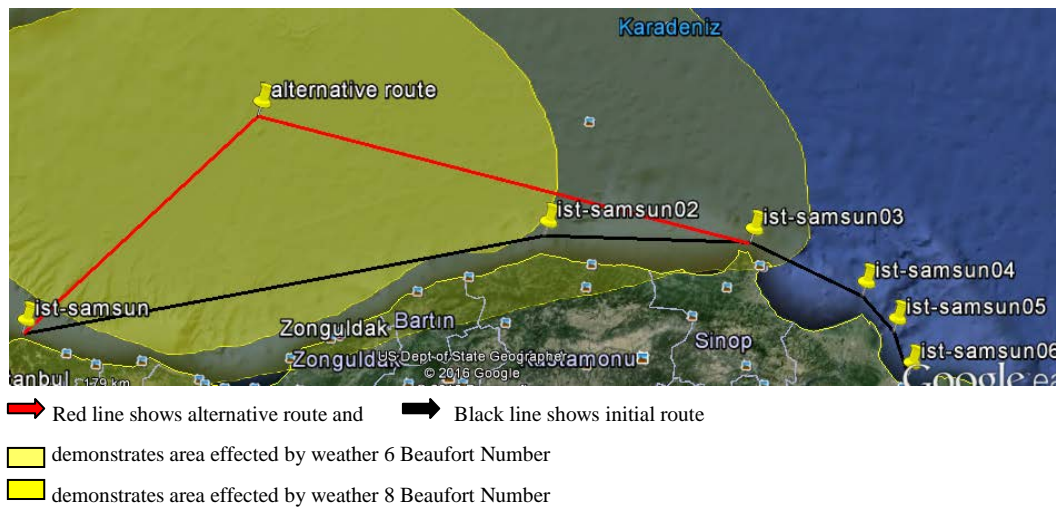


Table 3. Comparison of alternative and initial route for İstanbul Bogazı to Samsun

	Total Distance	Total Steaming Time	Approximate Fuel Consumption(ifo 380cst)
Initial Route	346,1 NM	36 Hours 50 Min	48,944 Mts
Alternative Route	407,4 NM	32 Hours 22 Min	42,998 Mts
Total Gain	- 61,3 NM	4 Hours 28 Min	5.946 Mts



- ➔ Red line shows alternative route and ➔ Black line shows initial route
- 🟡 demonstrates area effected by weather 6 Beaufort Number
- 🟠 demonstrates area effected by weather 8 Beaufort Number

Figure 6. Alternative route for Poti to İstanbul Bogazi

Table 4. Comparison of alternative and initial route for Poti to İstanbul Bogazi

	Total Distance	Total Steaming Time	Approximate Fuel Consumption (ifo 380cst)
Initial Route	558 NM	42 Hours 20 Min	56,298 Mts
Alternative Route	573 NM	38 Hours 20 Min	50,978 Mts
Total Gain	-15 NM	6 Hours 0 Min	5,32 Mts

ACKNOWLEDGEMENT

In this study, Townsin-Kwon method is employed to minimize voyage duration as advanced weather routing for a container vessel line in heavy weather condition. Sourced on real ship particular information and with real time forecasts, results of the applicability of this method for black sea region as follows:

- Results of the tests, the wind forces should be 7 beaufort number or 8 beaufort number to use method productively,
- The bad weather should continue until arrive next alternative waypoint, if not; it is necessary altering course to initial waypoint to arrive destination faster,
- The forecasts information should be accurate to shorten the time between ports,
- There are almost none island and shallow water in black sea which helps maneuver easily,
- Townsin-Kwon speed loss formula is not difficult to use, it can be used by officers widely.

REFERENCES

- [1] Review of Maritime Transport 2015, Chapter 2 Structure, Ownership And Registration Of The World Fleet, Available: http://unctad.org/en/PublicationChapters/rmt2015ch2_en.pdf
- [2] Kwon, “ The effectof the weather, particularly short sea waves, on ship speed performance” Doctorate thesis, University of Newcastle, Newcastle, Nov. 1981
- [3] Calvert, “Optimal weather routing procedures for vessels on trans-oceanic voyages”, Doctorate thesis, University of Plymouth, Plymouth, Mar.1990.
- [4] I. M. V. Andersen, “Wind-tunnel investigation of wind loads on a post-panamax container ship as a function of the container configuration on deck ” 11th International Marine Design Conference2012.Proceedings Vol.3, p. 46.
- [5] W. B. Berlekom, “ Wind Forces on Modern Ship Forms – Effects on Performance”, Transactions of the North East Institute of Engineers and Shipbuilders, Vol. 97, No. 4, 1981.
- [6] (2016) Veristar website. [Online]. Available: http://www1.veristar.com/veristar/bvrules/E_2_s2_4_2.htm
- [7] O.T. Frey, A. P. Vogelaere, “ The Containerized Shipping Industry and the Phenomenon of Containers Lost at Sea ” Marine Sanctuaries Conservation Series ONMS-14-07, U.S. Department of Commerce ,p.13, Mar. 2014,
- [8] FLEXChip Signal Processor (MC68175/D), Motorola, 1996.
- [9] The United Kingdom Hydrographic Office, “Black Sea and Sea of Azov Pilot” 4th Edition, 2013.
- [10] (2016) Poseidon website .[Online]. Available <http://www.poseidon.hcmr.gr/index.php>.
- [11] Eide, “ Calculation of service and sea margins” Master thesis, Norwegian University of Science and Technology, Trondheim, Jun. 2015
- [12] Y.J. Kwon, ” Speed loss due to added resistance in wind and waves”, The Naval Architect Mar.2008, pp. 14-16, Mar. 2008
- [13] A. F. Molland, S. R. Turnock, D.A. Hudson, Ship resistance and propulsion: practical estimation of ship propulsive power, 1st ed., Cambridge University Press, United States of America, 2011
- [14] T.E. Notteboom, “The time factor in liner shipping services”, Maritime Economics & Logistics, Vol. 8, No. 1, pp. 19–39. Mar. 2006.

Performance and Sustainability Assessment of Hydrogen Generation Step of Boron Based Thermochemical Cycle

Fatih Yilmaz¹, Mustafa Tolga Balta¹, Resat Selbas²,

Abstract

This study deals with performance analysis of hydrogen generation step of boron based thermochemical cycle. The energy, exergy analyses and sustainability index of the hydrogen generation step investigated at various reference temperatures. The energy, exergy efficiencies and sustainability index of the considered step are calculated as 11.00%, 20.34 % and 1.255 respectively.

Keywords: hydrogen, exergy, energy, sustainability index

1. INTRODUCTION

Nowadays the debate on related to energy demand increases in the world. In this regard, many researchers and groups have afforded on alternative forms of energy options during the past decades. For future generation, the development of alternative energy options and fuels are top priority to ensure a sustainability energy issue. Therefore many scientist and researchers purpose a large variety of solutions on this issue.

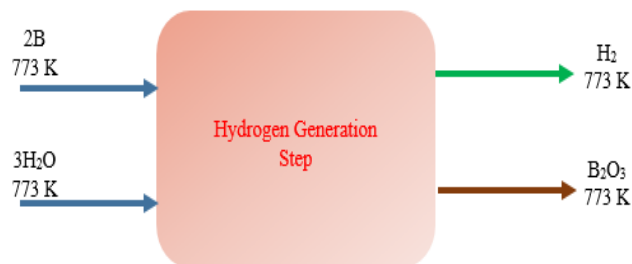
Currently fossil fuels energy sources account for more than 85% of primarily energy consumption of worldwide. Thus fossil fuels energy sources used for meeting the demands started to causes many environmental issues such as acid rain, stratospheric ozone depletion and global climate change [1, 2].

In the literature numerous studies on hydrogen generation via thermochemical cycle have been conducted. Rosen [3] studied on exergy analysis of hydrogen generation by thermochemical water decomposition via Ispra Mark-10 cycle. The use of a chemical heat pump to link a supercritical water-cooled nuclear reactor (SCWR) and a thermochemical water-splitting cycle for hydrogen generation carried out by Granovskii et al. [4]. Orhan et al. [5-9] have been examined in detail the steps of Cu-Cl cycle for hydrogen generation using exergy analysis approach. The hydrogen production from photovoltaic electricity utilization of water decomposition system have been conducted by El-Shatter et al. [10].

In this study, performance and sustainably assessment of hydrogen generation step of the boron based thermochemical cycle analyzed. Energy and exergy analyses of the considered step are investigated for various reference environment temperatures.

2. BORON BASED THERMOCHEMICAL CYCLE OF HYDROGEN GENERATION STEP

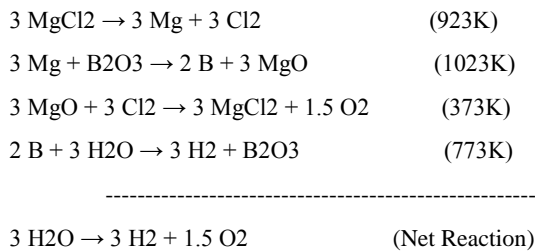
In Fig.1 the hydrogen production step of the boron based thermochemical hydrogen production cycle is given.



¹ Corresponding author: Aksaray University, Department of Technical Science of Vocational School, 68100, Aksaray, Turkey.
fatiyilmaz7@gmail.com

Figure 1 Hydrogen generation step

Mg can be generated from the first step the cycle at 923 K. In the second step, Mg reacts with B₂O₃ and then boron can be generated in this step. In the third step of the cycle, MgO and Cl₂ reacts and then MgCl₂ and O₂ are produced. In the last step of considered cycle which is hydrogen generation step, hydrogen produced from the reaction of the boron and H₂O at 773K.



3. ANALYSIS

We consider 1 mol of hydrogen produced per cycle, and hence, all quantities are provided per mol of hydrogen produced.

Before getting into energy and exergy analyses, the following assumptions are made:

- The values for the reference environment (dead state) temperature (T₀) and pressure (P₀) are 298 K and 100 kPa, respectively.
- All processes are considered steady-state
- The potential and kinetic energy are negligible

For the steady-state process, the mass, energy and exergy balance for the each control volume can be expressed as follows:

$$\sum \dot{m}_{in} = \sum \dot{m}_{out} \quad (2)$$

where \dot{m} is the mass flow rate, and the subscript in stands for inlet and out for outlet. The general energy balance can be expressed in the rate form as;

$$\dot{E}_{in} - \dot{E}_{out} = \Delta \dot{E}_s \quad (3)$$

which becomes [11];

$$\dot{Q} - \dot{W} = \sum \dot{m}_{out} h_{out} - \sum \dot{m}_{in} h_{in} \quad (4)$$

where \dot{Q} and \dot{W} denote heat and work, respectively. Eq. (4) can be written for a chemical reaction as:

$$\dot{Q} - \dot{W} = \sum n_p (\bar{h}_f + \bar{h} - \bar{h})_p - \sum n_R (\bar{h}_f + \bar{h} - \bar{h})_R \quad (5)$$

where \bar{h}_f is specific enthalpy of formation, \bar{h} is specific enthalpy at reference state and \bar{h} is specific enthalpy in kJ/kmol, n stands for number of moles, M stands for atomic mass and subscripts R and P represents reactants and products, respectively.

The exergy balance for a process can be written as;

$$\Delta \dot{E}x_{sys} = \sum \dot{E}x_{in} - \sum \dot{E}x_{out} - \dot{E}x_{dest} \quad (6)$$

where $\dot{E}x_{in}$ and $\dot{E}x_{out}$ are the rate of exergy input and output. $\dot{E}x_{dest}$ is the rate of exergy destruction.

$$\dot{E}x_Q - \dot{E}x_W + \dot{E}x_{mass,in} - \dot{E}x_{mass,out} = \dot{E}x_{dest} \quad (7)$$

The physical and chemical exergy:

$$ex = ex^{ph} + ex^{ch} \quad (8)$$

The specific exergy term can be written as:

$$ex = (h - h_0) - T_0(s - s_0) + ex^{ch} \quad (9)$$

where h is enthalpy, s is entropy, and the subscript zero indicates properties at the reference (dead) state of P_0 and T_0 . The exergy rate is calculated by [12]:

$$\dot{E}x = \dot{m} ex \quad (10)$$

After writing mass, energy and exergy balances for the system, enthalpy values of H_2 , O_2 and H_2O are evaluated with Shomate equations [13] as follows:

$$\bar{h} - \bar{h}_0 = AT + B\frac{T^2}{2} + C\frac{T^3}{3} + D\frac{T^4}{4} - E\frac{1}{T} + F - H \quad (11)$$

$$\bar{s} = A \ln(T) + B * T + C * \frac{T^2}{2} + D * \frac{T^3}{3} E * \frac{1}{2T^2} + G \quad (12)$$

where T is 1/1000 of the specified temperature (in K) of compound and A, B, C, D, E, F, G and H are constants, as given in Table 1 for boron based thermochemical hydrogen production steps chemicals. The values of the chemical exergies for the reactants and products are taken from the literature [14] as given in Table 2.

Table 1. Enthalpy of formation, reference entropy and Shomate constants for chemical compounds Ref. [13].

Compounds	\bar{h}_f^o (kJ/mol)	$\bar{h} - \bar{h}^o$ (kJ/mol)	\bar{s}_0 (J/mol*K)	A	B	C	D	E	F	G	H
H ₂ O	-241.82	16.97	188.84	3.0092	6.8325	6.7934	-2.5345	0.0821	-250.8810	223.3967	-241.8264
B	0	8.90	26.54	1.0186	2.9244	-1.8021	4.2123	-0.5509	-6.0362	7.0890	0.0000
H ₂	0	13.90	130.68	33.0662	-11.3634	11.4328	-2.7729	-0.1585	-9.98080	172.7079	0.0000
B ₂ O ₃	-1253.36	49.59	53.97	1.1157	2.3174	-1.0322	1.5332	3.5395	-1.2909	1.8808	-1.2534

Table 2. Standard chemical exergy for chemical compounds Ref. [14].

Compounds	ex^{ch} (kJ/mol)
H ₂ O	9.34
B	628.60
B ₂ O ₃	79.96
H ₂	236.10

The energy efficiency of the step can be defined by;

$$\eta_E = \frac{\dot{E}_{out}}{\dot{E}_{in}} \quad (15)$$

The exergy efficiency of the step can be defined by:

$$\psi_s = \frac{Ex_{out,s}}{Ex_{in,s}} \quad (16)$$

The relation between exergy efficiency (ψ_s) and the sustainability index (SI) is given in ref. [15].

$$SI = \frac{1}{(1-\psi_s)} \quad (17)$$

4. RESULTS AND DISCUSSION

The variation of inlet and outlet exergy rates for hydrogen production step with the various reference environment temperatures is shown in Fig. 2. As can be seen that in this figure the inlet and outlet exergy rates are nearly linear when reference environment temperature changing from 5 °C to 45 °C. Hydrogen production step of the cycle inlet and outlet exergy rates are calculated as 1653.32 kJ/mol, 336.31 kJ/mol and 317.02 kJ/mol while the reference environment temperature kept at 25 °C,

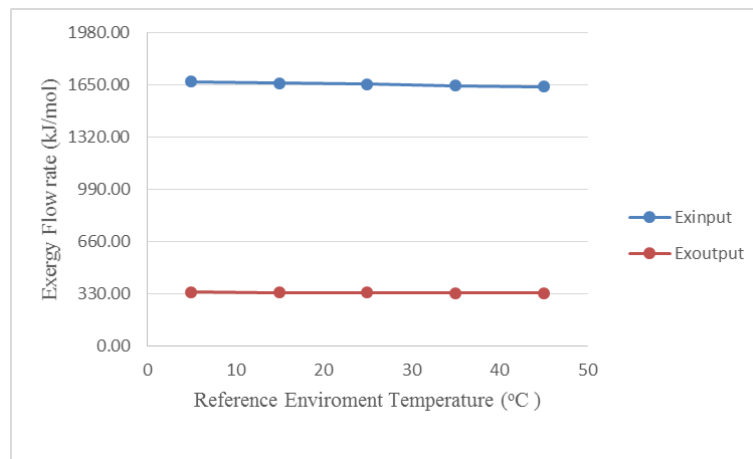


Figure 2. The effect of reference environment temperatures on inlet and outlet exergy rates of hydrogen production step

Fig.3. presented that variation of energy and exergy efficiency with different reference environment temperature. When the reference environment temperature is increasing from 5 °C to 45 °C, energy efficiency is constant, but the exergy efficiency is increases. The hydrogen production step of the boron based thermochemical hydrogen production cycle of energy and exergy analyses are calculated as 11.00% and 20.34%, reference environment temperature at 25 °C.

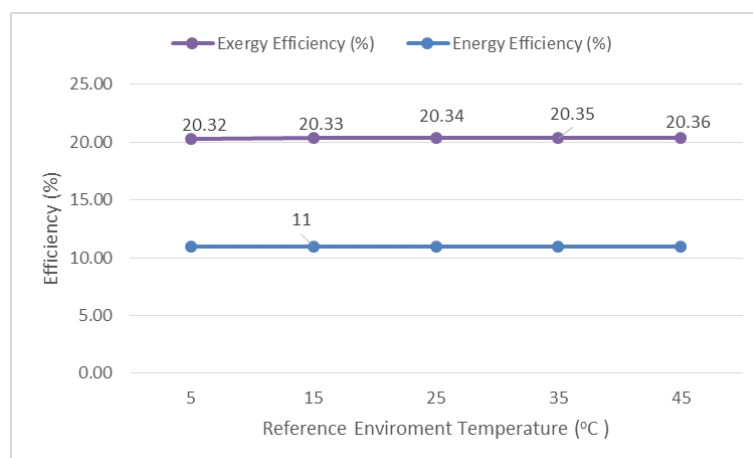


Figure 3. The effect of the reference environment temperature on energy and exergy efficiencies of the step

The variation of sustainability index rate of the hydrogen production step can be seen in Fig.4. sustainability index rate is increases with reference environment temperature is increasing from 5 °C to 45 °C. The sustainability index rate is calculated as 1.255 while the reference environment temperature kept at 25 °C.

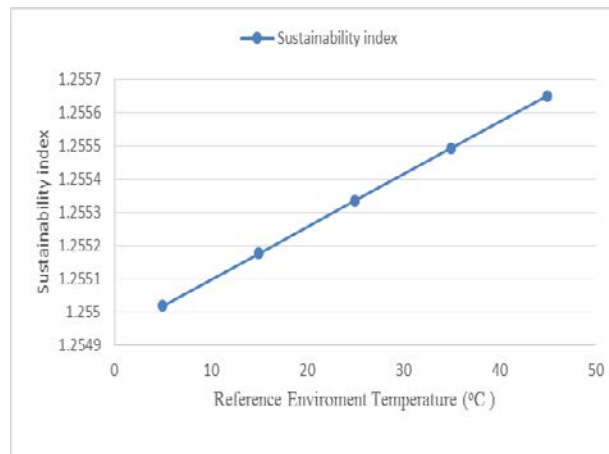


Figure.4 Variation of sustainability index with reference environment temperature.

CONCLUSION

The energy, exergy and sustainability analysis methods are applied to the hydrogen production step of boron based thermochemical cycle. In this study conducted variation energy, exergy efficiency and sustainability index rate with different reference environment temperature. The following conclusion can be drawn from this study;

- The energy, exergy efficiencies and sustainability index rate are calculated as 11.00%, 20.34% and 1.255, respectively, at 25 oC reference environment temperature.
- When the reference environment temperature is increased, the exergy efficiency and sustainability index rate are increases.
- Boron based thermochemical cycle for hydrogen production is good potential and route.

REFERENCES

- [1] Dincer I. Technical, environmental and exergetic aspects of hydrogen energy systems. *Int J Hydrogen Energy* 2002; 27:265-85.
- [2] Dincer I. Energy and environmental impacts: present and future perspectives. *Energy Sources* 1998; 20(4/5):427-53.
- [3] Rosen MA. Exergy analysis of hydrogen production by thermochemical water decomposition using the Ispra Mark-10 cycle. *International Journal of Hydrogen Energy* 2008;33:6921-33.
- [5] Granowski M, Dincer I, Rosen MA, Pioro I. Thermodynamic analysis of the use a chemical heat pump to link a supercritical water-cooled nuclear reactor and a thermochemical water-splitting cycle for hydrogen production. *Journal of Power and Energy Systems* 2008;2:756-67.
- [6] Orhan MF, Dincer I, Rosen MA. The oxygen production step of a copperechlorine thermochemical water decomposition cycle for hydrogen production: energy and exergy analyses. *Chemical Engineering Science* 2009;64:860-9.
- [7] Orhan MF, Dincer I, Rosen MA. Energy and exergy analyses of the fluidized bed of a copperechlorine cycle for nuclear-based hydrogen production via thermochemical water decomposition. *Chemical Engineering Research and Design* 2009;87:684-94.
- [8] Orhan MF, Dincer I, Rosen MA. Thermodynamic analysis of the copper production step in a copperechlorine cycle for hydrogen production. *ThermochimicaActa* 2008;480:22-9.
- [9] Orhan MF, Dincer I, Rosen MA. Energy and exergy assessments of the hydrogen production step of a copperechlorine thermochemical water splitting cycle driven by nuclear-based heat. *International Journal of Hydrogen Energy* 2008;33:6456-66.
- [10] Orhan MF, Dincer I, Rosen MA. Energy and exergy analyses of the drying step of a copperechlorine thermochemical cycle for hydrogen production. *International Journal of Exergy* 2009;6(6):793-808
- [11] El-Shatter T.F.,Eskandar M.N. and El-Hagry M.T. "Hybrid PV/Fuel Cell System Design and Simulation", *Renewable Energy*,2002,27: 479–485
- [12] Ozcan H, Dincer I. Energy and exergy analyses of a solar driven Mg-Cl hybrid thermochemical cycle for co-production of power and hydrogen. *International Journal of Hydrogen Energy* 2014; 39:15330-1534
- [13] Dincer, I. and Rosen, M. A. 2007. *EXERGY: Energy, Environment and Sustainable Development*. Elsevier Science; 1st ed., 472, Oxford, UK.
- [14] NIST, 2005. National Institute of Standards and Technology (NIST), 2009, [http://webbook.nist.gov/chemistry/\(23.02.2015\)](http://webbook.nist.gov/chemistry/(23.02.2015))
- [15] The Exergoecology Portal, 2015. <http://www.exergoecology.com/excalc/>; (22.02.2015).

- [16] Rosen, M.A., Dincer, I. and Kanoğlu, M. (2008) 'Role of exergy in increasing efficiency and sustainability and reducing environmental impact', *Energy Policy*, Vol. 36, No. 1, pp.128–137.

Dissolved Oxygen and Chlorophyll a Levels in an Urban Stream, Değirmendere, Northeast Turkey

Ugur Satilmis¹, Adem Bayram², Sinan Nacar³

Abstract

Dissolved oxygen (DO) in waterbodies is a vital indicator that determines quality of aquatic systems. The deficient or excessive DO concentration in rivers leads to adverse effects on aquatic environments, such as mortality of benthic fauna, fish kills, and habitat loss thus level of DO in natural equilibrium is very important. The aim of this study is to determine and evaluate the spatial and temporal variation of DO concentration and saturation, water temperature (T_w), pH, specific conductivity (SC), chlorophyll a (Chl-a) concentration, and air temperature (T_a) in the Değirmendere Stream, Eastern Black Sea Basin, Turkey. A yearlong field study was conducted in five monitoring stations selected on the main branch. Considering the seasonal mean values of each station in the Değirmendere Stream, the highest DO concentrations varying between 11.40 and 12.34 mg/L were monitored in the winter as a result of the lowest seasonal T_w values, while the lowest concentrations varying between 8.68 and 9.59 mg/L were determined in the summer due to the highest T_w values. T_w , pH and Chl-a showed a steadily increasing trend along the stream, and were at their highest values: 16.02°C, 8.35, and 1.67 mg/L, respectively, regarding the annual mean values. Pearson correlation analysis showed that the DO concentration was negatively but significantly correlated with T_w (up to $R = -0.985$) and T_a (up to $R = -0.919$).

Keywords: *Chlorophyll a, Değirmendere Stream, Dissolved oxygen, Water temperature.*

1 INTRODUCTION

Dissolved oxygen (DO) is a strongly indicator exhibiting health and behavior of aquatic life [1], [2]. DO concentration in surface waters depends on the water temperature (T_w), salinity and altitude. Natural waters in equilibrium with the atmosphere typically contain DO concentrations in the range from 5 to 15 mg/L [3]. Chlorophyll a (Chl-a) is a well-known indicator for the presence of phytoplankton biomass. Chl-a may be used to show environmental degradation in freshwater environments, e.g., streams [4]–[8] while DO represents quality of aquatic life. Various environmental water-quality indicators such as DO, pH, T_w , and light intensity are closely related to algal growth [9]–[11]. The pH, which is a key chemical water-quality indicator, has higher values for eutrophic waters [9], [12] so a high pH may cause an increase in phytoplankton biomass [11], [13]. T_w is a vital parameter due to its effect on chemical reactions, aquatic life, and the suitability of the water for beneficial uses. Oxygen, for instance, is less soluble in warm water than in cold water. Temperature rise and the decrease in the quantity of oxygen present in the surface water increased the rate of biochemical reactions. Especially in the summer months, serious depletions in DO concentrations occur in the water bodies [14]. Decreases of water temperature lead to enhancement of DO saturation. Fluctuation in the saturation affects the DO deficit and ultimately the reaeration driving force [15], [16].

Investigations of spatial and temporal variations of DO, T_w , Chl-a and other water-quality variables have been increased gradually in many basins and sub-basins around the world for decades [8], [17]–[24]. The aim of this study is to determine and evaluate the spatial and temporal variations of DO concentration and saturation, T_w , pH, specific conductivity (SC), Chl-a concentration, and air temperature (T_a) in the Değirmendere Stream, Eastern Black Sea Basin, Turkey. Moreover, this study reveals the relationships between these water-quality variables.

2 STUDY AREA

Turkey is hydrologically divided into 26 drainage basins in order to identify water resources, to improve and to use. One of the most important basins is the Eastern Black Sea Basin having a catchment area of 24,077 km² and a surface water potential of 15,331 billion m³ consists of 17 sub-basins [25]. With a main branch length of 55 km, a mean annual surface

¹ Corresponding author: Karadeniz Technical University, Department of Civil Engineering, 61080. Trabzon, Turkey.
ugrsatilmis@gmail.com

² Karadeniz Technical University, Faculty of Engineering, Department of Civil Engineering, 61080. Trabzon, Turkey,
adembayram@gmail.com

³ Karadeniz Technical University, Faculty of Engineering, Department of Civil Engineering, 61080. Trabzon, Turkey,
ssinannacar@gmail.com

water potential of 560 billion m³, and catchment area of 1,042 km², the Değirmendere watershed has a place in these sub-basins.

The Değirmendere Stream originates from Kalkanlı and Zigana Mountains having an elevation of 3,080 m and is formed by small streams, namely Hamsiköy, Maçka, Larhan, Sumela, Galyan, Kuştul, and Ziganoy. After it is formed, it passes through the settlements of Hamsiköy, Maçka, Esiroğlu, Çağlayan, and Değirmendere, respectively, before draining into the Southeastern Black Sea at the junction 41°00'10.9"N–39°45'26.1"E [26]. The Değirmendere watershed is prime importance for water demand of Trabzon Province having a total population of 766,782 according to the 2015 census [27].

There are settlements such as Maçka, Değirmendere, Sanayi, Çukurçayır, Dolaylı, Akoluk, Çağlayan, and Esiroğlu within the Değirmendere watershed. A lot of run-of-river hydropower plants have been constructed and operated in the upper part of the watershed. The anthropogenic activities such as construction regarding bridge, levee, and relocation of road and operation regarding drinking water treatment plants, concrete plants, crushing, screening and washing plants as well as small industrial areas, vehicle repair shops, coal yards, various factories, etc., are especially increasing towards to the mouth where Değirmendere Stream discharges into the Black Sea.

In this study, five water-quality monitoring stations were selected on the main branch of the Değirmendere Stream (Fig. 1). The location features of the monitoring stations in the stream are given Table 1.

Table 1. Location of the stations in the Değirmendere Stream

Stations	Coordinates	Altitude (m)	Distance (km) of the mount
D1	40°48'14.2"N–39°35'20.9"E	374	30.0
D2	40°49'10.3"N–39°36'46.6"E	332	25.0
D3	40°52'10.9"N–39°41'03.3"E	153	17.0
D4	40°54'01.6"N–39°42'57.6"E	97	13.7
D5	40°00'10.9"N–39°45'26.1"E	3	0.1

3 MATERIALS AND METHODS

3.1 The Surface Water Monitoring

DO concentration (mg/L), DO saturation (%), Chl-a concentration (µg/L), T_w (°C), pH and SC (µS/cm) were automatically measured and recorded in situ for 15 minutes at 10 second intervals using the Hydrolab DS5 multiparameter water-quality sonde, the final results were presented as the arithmetic mean of the ninety readings. The study was started in January 2014, conducted semimonthly, and terminated in December 2014.

The Hydrolab DS5 uses the luminescent sensor for DO, a glass bulb measuring electrode and refillable reference electrode probe for pH, the four graphite electrodes probe for SC, and integrated submersible fluorescence sensor for Chl-a measurements. The sensors were calibrated before each field study using standard solutions.

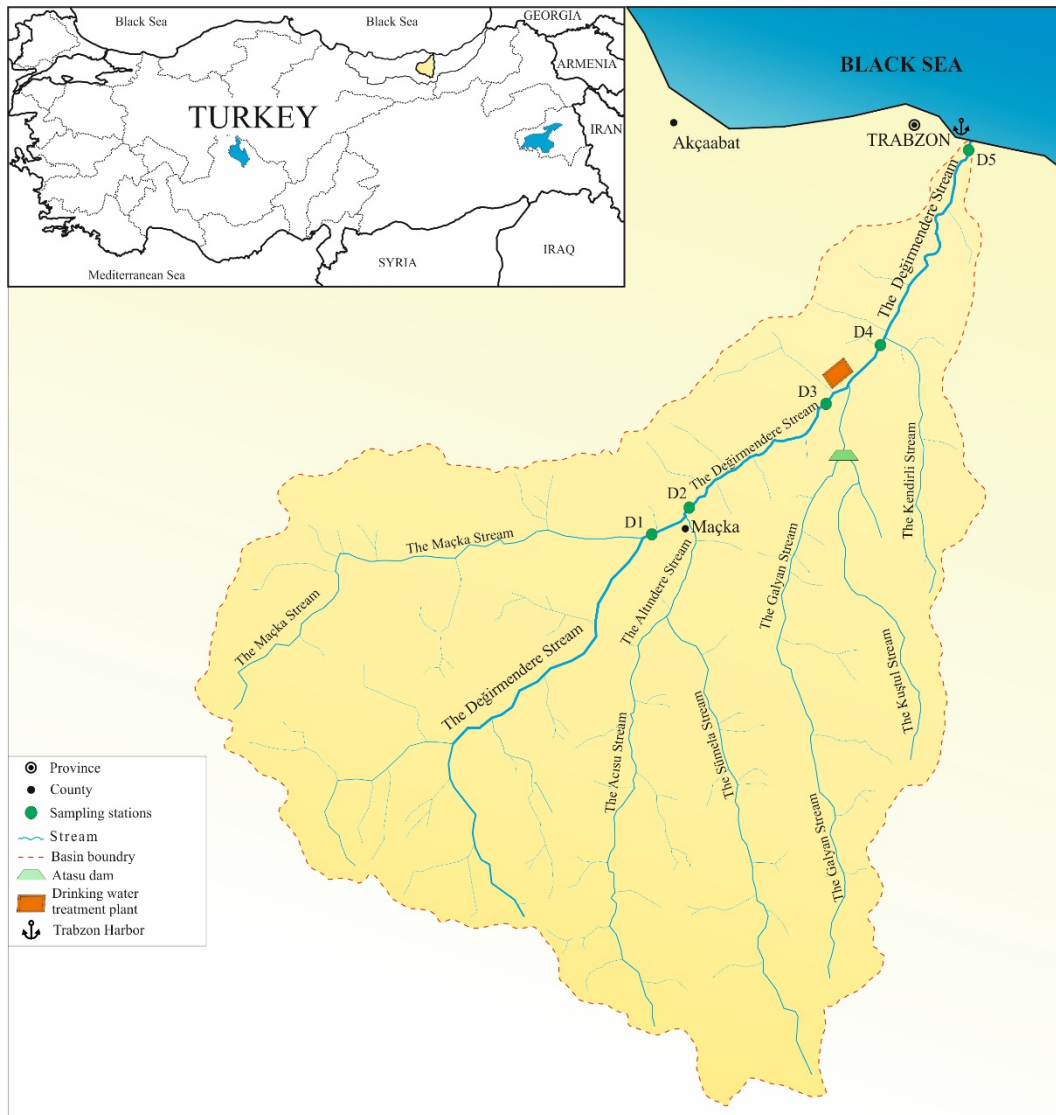


Figure 1. Locations of monitoring stations and the Değirmendere Stream watershed

3.2 The Statistical Analysis

Two statistical features, namely average and standard deviation, were calculated for each station. The water quality data were analyzed with the IBM SPSS Statistics 23 for Windows. The Pearson correlation analysis was used to determine whether there were relationships between any two indicators.

4. RESULTS AND DISCUSSION

Temporal and spatial variations of DO concentration and saturation, T_w , pH, SC, Chl-a concentration, and T_a were investigated in the five stations along the Değirmendere Stream. For all of the stations, the highest DO concentrations varying between 11.40 and 12.34 mg/L were measured in the winter as a result of the lowest seasonal T_w values while the lowest concentrations varying between 8.68 and 9.59 mg/L were determined in the summer due to the highest T_w values. Considering annual mean values of each station in the Değirmendere Stream, DO concentration decreased in the D2 station due to discharging of untreated wastewater from Maçka town having a population of 23,603 according to the 2015 census after the D1 station although Altındere Stream joins the main branch [27]. When D2 and D3 stations were compared, DO concentrations in the D3 station increased in an-eight km distance thanks to reaeration of the water despite the fact that T_w constantly rose along the Değirmendere Stream. After the D3 station, DO concentration showed an ever decreasing trend and reached to the minimum levels in the station D5 (Table 2)

Table 2. Basic statistics of the water-quality indicators monitored for the Degimenderska Stream

Water quality indicators	Stations	Winter					Spring					Summer					Autumn					
		Min.	Mean	Max.	S. D.	Min.	Mean	Max.	S. D.	Min.	Mean	Max.	S. D.	Min.	Mean	Max.	S. D.	Min.	Mean	Max.	S. D.	
DO (mg/L)	D1	11.61	12.28	13.24	0.56	10.19	11.01	12.28	0.75	8.78	9.20	9.72	0.41	9.11	10.66	11.79	1.03					
	D2	11.46	11.93	12.30	0.33	10.19	11.04	12.09	0.65	8.72	9.12	9.44	0.25	9.04	10.54	11.60	1.00					
	D3	11.59	12.34	13.10	0.60	9.95	11.00	12.21	0.75	9.33	9.54	9.96	0.26	10.46	11.11	11.82	0.55					
	D4	11.27	11.59	12.01	0.28	10.01	10.70	11.84	0.63	9.22	9.59	10.36	0.43	9.77	10.48	11.24	0.60					
	D5	11.19	11.40	11.82	0.23	9.85	10.46	11.31	0.48	7.96	8.68	9.80	0.65	8.28	10.17	11.07	1.02					
DO (%)	D1	97.80	102.05	106.51	3.60	98.14	99.40	100.37	0.86	97.95	99.50	100.74	1.14	98.89	99.91	101.64	1.04					
	D2	98.18	102.25	105.68	3.18	100.06	100.90	101.65	0.66	98.05	100.45	101.35	1.31	99.55	100.58	102.11	1.00					
	D3	98.51	103.79	109.48	5.15	100.11	101.09	102.20	0.93	100.69	105.08	110.71	3.85	98.95	105.29	126.22	10.68					
	D4	98.13	101.02	105.78	2.65	100.33	101.81	103.14	1.11	102.69	109.20	124.26	7.66	98.55	102.60	110.41	4.74					
	D5	95.68	98.87	100.69	1.96	100.25	101.85	103.92	1.49	97.52	103.41	112.17	5.24	98.91	101.56	108.91	3.78					
F _w (°C)	D1	4.67	6.09	7.30	1.11	4.77	9.31	12.82	2.96	15.03	17.15	19.44	1.79	6.32	11.19	18.48	4.60					
	D2	5.32	7.49	9.33	1.30	6.04	9.99	13.66	2.64	16.78	18.14	19.30	0.94	7.64	12.23	19.43	4.60					
	D3	5.05	7.51	8.98	1.49	6.47	10.96	14.89	2.85	17.88	19.02	20.22	0.86	7.73	12.47	20.14	4.68					
	D4	7.26	9.20	10.67	1.23	8.06	12.58	15.97	2.70	19.00	20.55	22.68	1.31	9.66	14.17	20.24	4.34					
	D5	8.64	9.60	10.80	0.99	10.40	14.24	17.12	2.28	22.20	24.21	27.37	2.05	10.84	16.03	24.10	5.14					
pH	D1	7.33	8.04	8.41	0.45	8.07	8.24	8.54	0.16	8.12	8.19	8.34	0.08	7.61	7.73	7.89	0.11					
	D2	7.33	8.16	8.52	0.50	8.05	8.15	8.31	0.09	7.99	8.17	8.32	0.13	7.60	7.71	7.93	0.12					
	D3	7.66	8.25	8.60	0.37	8.04	8.15	8.33	0.10	7.94	8.15	8.29	0.15	7.50	7.77	8.32	0.29					
	D4	7.54	8.13	8.54	0.41	8.23	8.27	8.33	0.04	8.15	8.39	8.71	0.19	7.61	7.86	8.30	0.26					
	D5	7.94	8.42	8.74	0.35	8.35	8.49	8.63	0.10	8.37	8.58	8.79	0.19	7.70	7.93	8.20	0.20					
SC (µS/cm)	D1	112.7	238.93	325.64	82.32	119.45	145.81	172.58	19.80	182.45	316.35	381.88	74.55	141.63	228.54	435.55	113.37					
	D2	127.83	228.30	256.50	49.52	91.00	126.93	158.47	23.09	140.60	236.82	286.88	54.99	158.18	207.74	322.40	62.45					
	D3	139.07	230.93	278.75	53.69	105.97	137.12	169.05	22.48	172.77	241.71	282.85	39.13	156.77	211.10	332.22	67.88					
	D4	145.57	214.45	257.50	37.77	113.70	146.08	178.43	23.49	161.90	219.67	238.25	28.84	171.67	198.02	243.82	25.12					
	D5	164.65	239.62	281.25	41.02	126.32	160.90	202.67	27.13	188.63	234.78	275.05	30.39	179.20	213.73	264.05	33.75					
Chl-a (µg/L)	D1	0.33	1.02	2.17	0.78	0.45	0.91	1.51	0.37	0.40	0.51	0.77	0.15	0.30	0.92	2.27	0.71					
	D2	0.29	1.31	2.77	0.89	0.57	1.13	2.14	0.55	0.36	0.55	1.02	0.24	0.33	0.63	0.93	0.25					
	D3	0.26	0.77	1.57	0.48	0.72	1.33	3.26	0.96	0.26	1.01	2.76	0.94	0.24	0.79	1.17	0.32					
	D4	0.41	2.10	5.21	1.75	0.58	1.13	1.55	0.38	0.46	0.95	1.95	0.56	0.51	0.94	1.74	0.43					
	D5	1.16	2.22	4.29	1.08	1.26	1.96	2.90	0.55	0.57	1.30	2.62	0.76	0.79	1.20	1.77	0.43					

n increases. However, from upstream to downstream, although the stations' altitude steadily declined so atmospheric pressure rose and joining of the stream tributaries, up to %22 (in June 2014) of DO concentrations decreased due to on the rise of T_w values as well as the effects of increase in population density especially in the near the Black Sea coastal areas and an expansion of anthropogenic activities such as coal yards, repair shops, various industrial plants etc., and also discharge from domestic and industrial wastewater.

The statistical analysis obviously showed that DO concentrations were negatively and significantly correlated with T_a having the Pearson correlation coefficient (R)= -0.919 in the D1 station and T_w having R=-0.985 in the D2 station. T_a and T_w had good relationships in the all stations with up to R=0.930 (Table 3).

For all of the stations, the lowest pH values were determined in the autumn and highest values usually were observed in the summer except D3 station. The high pH and T_w values might cause an ever increasing in Chl-a concentration along the Değirmendere Stream [9], [12] reached the maximum levels in the D5 station. It was also determined that spatially the highest values were observed in the D5, regarding the yearly mean values. While the lowest SC values were determined in the spring, the highest values were observed in the summer except D5 station.

Contrary to DO, while the lowest Chl-a values were measured in the summer and autumn, the highest values were determined in the winter and spring. Moreover the lowest Chl-a values were showed D1 station, the greatest concentrations were determined in the D5 station due to the same reasons which reduces DO. T_w , pH and Chl-a values showed a steadily increasing trend along the stream, and were at their highest values: 16.02°C, 8.35, and 1.67 mg/L, respectively, regarding the annual mean values.

Table 3. The Pearson correlation coefficient (R) and the corresponding value (P) for each station

	D1						D2					
	T_w	T_a	pH	LDO	LDO %	SC	T_w	T_a	pH	LDO	LDO %	SC
T_a	0.904						0.901					
	0.000						0.000					
pH	0.093	0.272					0.111	0.391				
	0.665	0.233					0.606	0.080				
LDO	-0.978	-0.919	-0.013				-0.985	-0.919	-0.018			
	0.000	0.000	0.952				0.000	0.000	0.935			
LDO %	-0.188	0.282	0.405	0.366			-0.061	0.268	0.567	0.212		
	0.380	0.216	0.049	0.078			0.778	0.239	0.004	0.320		
SC	0.575	0.611	0.242	-0.435	0.301		0.402	0.367	0.332	-0.309	0.200	
	0.003	0.003	0.255	0.034	0.153		0.052	0.102	0.113	0.142	0.348	
Chl-a	-0.400	-0.506	-0.219	0.328	-0.201	-0.470	-0.406	-0.314	0.280	0.428	0.236	-0.194
	0.053	0.019	0.305	0.118	0.347	0.020	0.049	0.165	0.184	0.037	0.268	0.364
	D3						D4					
	T_w	T_a	pH	LDO	LDO %	SC	T_w	T_a	pH	LDO	LDO %	SC
T_a	0.913						0.930					
	0.000						0.000					
pH	0.174	0.461					0.420	0.613				
	0.417	0.035					0.041	0.003				
LDO	-0.870	-0.852	0.100				-0.918	-0.864	-0.231			
	0.000	0.000	0.641				0.000	0.000	0.277			
LDO %	0.461	0.526	0.524	0.026			0.744	0.732	0.596	-0.428		
	0.023	0.014	0.009	0.902			0.000	0.000	0.002	0.037		
SC	0.368	0.460	0.425	0.055	0.768		0.239	0.312	0.340	-0.028	0.416	
	0.077	0.036	0.038	0.800	0.000		0.261	0.169	0.104	0.896	0.043	
Chl-a	0.134	0.150	0.089	-0.190	-0.025	-0.122	-0.354	-0.254	0.144	0.316	-0.313	0.150
	0.532	0.516	0.678	0.375	0.908	0.569	0.090	0.267	0.502	0.133	0.137	0.483
	D5											
	T_w	T_a	pH	LDO	LDO %	SC						
T_a	0.922											
	0.000											
pH	0.254	0.449										
	0.230	0.041										
LDO	-0.969	-0.894	-0.226									
	0.000	0.000	0.289									
LDO %	0.439	0.394	0.161	-0.225								
	0.032	0.077	0.452	0.290								
SC	0.137	0.162	0.224	-0.090	0.008							
	0.522	0.482	0.293	0.674	0.970							
Chl-a	-0.309	-0.086	0.311	0.234	-0.373	0.017						
	0.142	0.712	0.140	0.271	0.073	0.936						

CONCLUSIONS

Spatial and temporal variations of DO, T_w , pH, SC, Chl-a, and T_a were semimonthly determined and evaluated for a period of twelve months in the selected five monitoring stations along the main branch of Değirmendere.

DO concentrations showed an ever decreasing trend due to increasing of T_w values and discharging of domestic and industrial wastewater into the stream, considering the yearly mean values of each station in Değirmendere. However, DO concentrations in the D3 station, increased thanks to reeration mechanism and joining of small tributaries.

The results showed that the lowest DO concentrations were observed in the D5, the last station in the Değirmendere watershed, T_w , pH and Chl-a values had a steadily increasing trend along the stream and reached the maximum levels in the D5 station. The highest pH and T_w values might cause an increasing in Chl-a concentration along the stream. In contrary to T_w , the lowest DO values were determined for all stations in the summer months, while the highest DO concentrations were observed winter months.

There was a negative and important relationship between T_w and DO with up to $R = -0.985$ as well as T_w and T_a had positive and significant relationship with up to $R = 0.930$ (Table 3). So, when T_w values decreased, DO concentrations always rose.

REFERENCES

- [1]. A. C. Demetracopoulos and H. G. Stefan, "Model of Mississippi River Pool: Dissolved Oxygen," *J. Environ. Eng.*, vol. 109, no. 5, pp. 1020–1034, 1983.
- [2]. B. Rajwa, A. Bialik, R. J., Karpinski, M., Luks, "Dissolved Oxygen in Rivers: Concepts and Measuring Techniques," in *Achievements, History and Challenges in Geophysics*, R. Bialik, M. Majdanski, and M. Moskalik, Eds. London: Springer International Publishing, 2014, pp. 337–350.
- [3]. APHA, *Standard methods for the Examination of Water and Wastewater*, 20th ed. Washington, DC., 1998.
- [4]. C. Xie, J. Chang, and Y. Zhang, "A New Method for Estimating Chlorophyll-a Concentration in the Pearl River Estuary," *Opt. Int. J. Light Electron Opt.*, vol. 126, no. 23, pp. 4510–4515, 2015.
- [5]. D. Figueroa-Nieves, T. V. Royer, and M. B. David, "Controls on Chlorophyll-a in Nutrient-rich Agricultural Streams in Illinois, USA," *Hydrobiologia*, vol. 568, no. 1, pp. 287–298, 2006.
- [6]. F. M. Carneiro, J. C. Nabout, L. C. G. Vieira, F. Roland, and L. M. Bini, "Determinants of Chlorophyll-a Concentration in Tropical Reservoirs," *Hydrobiologia*, vol. 740, pp. 89–99, 2014.
- [7]. J. N. Boyer, C. R. Kelble, P. B. Ortner, and D. T. Rudnick, "Phytoplankton Bloom Status: Chlorophyll a Biomass as an Indicator of Water Quality Condition in the Southern Estuaries of Florida, USA," *Ecol. Indic.*, vol. 9, no. 6, pp. S56–S67, 2009.
- [8]. P. P. Borges, F. B. Terasa, P. T. D. A. Martins, and J. C. Nabout, "Relative Influence of Direct and Indirect Environmental Effects on Sestonic Chlorophyll-a Concentration in Cerrado Streams," *Acta Limnol. Bras.*, vol. 27, no. 3, pp. 301–310, 2015.
- [9]. M. Scholz, *Wetland Systems to Control Urban Runoff*. Elsevier, 2006.
- [10]. C. R. Lovell and A. Konopka, "Excretion of Photosynthetically Fixed Organic Carbon by Metalimnetic Phytoplankton," *Microb. Ecol.*, vol. 11, no. 1, pp. 1–9, 1985.
- [11]. C. Zang, S. Huang, M. Wu, S. Du, M. Scholz, F. Gao, C. Lin, Y. Guo, and Y. Dong, "Comparison of Relationships Between pH, Dissolved Oxygen and Chlorophyll a for Aquaculture and Non-aquaculture Waters," *Water, Air Soil Pollut.*, pp. 157–174, 2011.
- [12]. R. J. M. Howland, A. D. Tappin, R. J. Uncles, D. H. Plummer, and N. J. Bloomer, "Distributions and Seasonal Variability of pH and Alkalinity in the Tweed Estuary, UK," *Sci. Total Environ.*, vol. 251, pp. 125–138, 2000.
- [13]. T. G. Dai, "Causes and Treatment Measures of Exceedings of pH Value in Yu Dong Reservoir," *Water Resour. Res.*, vol. 30, no. 3, pp. 37–38, 2009.
- [14]. E. Metcalf, "Wastewater Engineering, Treatment and Reuse," *New York McGraw-Hill*, 2003.
- [15]. J. Colt, *Computation of Dissolved Gas Concentrations in Water as Functions of Temperature, Salinity, and Pressure*. American Fisheries Society, 1984.
- [16]. J. V. Loperfido, C. L. Just, J. L. Schnoor, and M. Asce, "High-Frequency Diel Dissolved Oxygen Stream Data Modeled for Variable Temperature and Scale," vol. 135, pp. 1250–1256, 2009.
- [17]. R. J. Williams, C. White, M. L. Harrow, and C. Neal, "Temporal and Small-scale Spatial Variations of Dissolved Oxygen in the Rivers Thames, Pang and Kennet, UK," *Sci. Total Environ.*, pp. 497–510, 2000.
- [18]. S. Muangkaew, I. D. Mckel, M. R. Grace, M. Rayanakorn, K. Grudpan, J. Jakmunee, and D. Nacapricha, "A Reverse-flow Injection Analysis Method for the Determination of Dissolved Oxygen in Fresh and Marine Waters," *Talanta*, vol. 58, pp. 1285–1291, 2002.
- [19]. R. J. Williams and D. B. Boorman, "Science of the Total Environment Modelling in-stream Temperature and Dissolved Oxygen at Sub-daily Time Steps: An Application to the River Kennet, UK," *Sci. Total Environ.*, vol. 423, pp. 104–110, 2012.
- [20]. G. Urrea-Clos, E. Garcia-Berthou, and S. Sabater, "Factors Explaining the Patterns of Benthic Chlorophyll-a Distribution in a Large Agricultural Iberian Watershed (Guadiana River)," *Ecol. Indic.*, vol. 36, pp. 463–469, Jan. 2014.
- [21]. Y. Wang, H. Jiang, J. Jin, X. Zhang, X. Lu, and Y. Wang, "Spatial-Temporal Variations of Chlorophyll-a in the Adjacent Sea Area of the Yangtze River Estuary Influenced by Yangtze River Discharge," *Int. J. Environ. Res. Public Health* pp. 5420–5438, 2015.
- [22]. A. Rajwa-Kuligiewicz, R. J. Bialik, and M. Rowi, "Dissolved Oxygen and Water Temperature Dynamics in Lowland Rivers over Various Timescales," *J. Hydrol. Hydromechanics*, pp. 353–363, 2015.
- [23]. I. V. Mosharova, V. V. Il'inskii, D. N. Matorin, S. A. Mosharov, A. Y. Akulova, and F. F. Protopopov, "Monitoring of the Moskva River Water Using Microbiological Parameters and Chlorophyll a Fluorescence," vol. 84, no. 6, pp. 811–821, 2015.
- [24]. A. Bayram, H. Onsoy, V. N. Bulut, and M. Tufekci, "Dissolved Oxygen Levels in the Stream Harşit (Turkey)," *BCCCE*, 2010, pp. 963–973.
- [25]. DSI, "Land and Water Resources" *General Directorate of State Water Works*, 2016. [Online]. Available: <http://en.dsi.gov.tr/land-water-resources>.
- [26]. U. Satılmış, "A Study on Spatial and Temporal Variation of Surface Water Quality in the Stream Değirmendere Watershed (Trabzon)," M. Eng. thesis, Karadeniz Technical University, Trabzon, Turkey (in Turkish with English abstract), 2015.
- [27]. TurkStat, "Address Based Population Registration System Results," 2015. [Online]. Available: <https://biruni.tuik.gov.tr/medas/?kn=95&locale=tr>.

Determination of Site Characteristics with Standard Spectral Ratio (SSR) Method in Akçakale (Gumushane) Province, Ne Turkey

Yasemin Beker¹, Nilgun Sayil²

Abstract

Microtremor survey method used for engineering seismology is very important for determining of dynamic ground parameters and its variations. Recently, Microtremor survey method used for engineering seismology provides the quick and economic results for estimating of dynamic ground parameters. Amplitude and frequency contents of the nature vibration of the ground are influenced by the factors as lithology and geometry of the ground. Predominant frequency and amplification values of the ground are determined by natural vibrations and regional ground classifications can be made according to these parameters. In this study, in order to determine the site characteristics of Akçakale (Gumushane) Province, NE Turkey, microtremor records taken in 53 single-station and 2 reference stations with CMG-6TD three-component broad-band velocity seismometer. The obtained microtremor records are estimated by Standard Spectral Ratio (SSR) method. The amplification and frequency maps of the study area generated to result of SSR method. The amplification and predominant frequency values obtained from SSR method are 1.1-6.23 and 1.8-5.4Hz, respectively.

Keywords: *Gumushane, Microtremor, Standard Spectral Ratio Method, Predominant Frequency, Amplification*

1. INTRODUCTION

To minimize damages and great losses caused by earthquakes, the soil dynamic characteristics must be known. Two of these characteristics are the ground amplification and the predominant frequency or period of ground. The soil parameters are generally determined with drilling and other geophysical methods. Recently, Microtremor survey method used for engineering seismology provides the quick and economic results for estimating of dynamic ground parameters. Amplitude and frequency contents of the nature vibration of the ground are influenced by the factors as lithology and geometry of the ground [1,2].

In this study, Standard Spectral Ratio Method (SSR) has been applied to microtremor records taken with CMG-6TD three component broad band velocity seismometers in 53 single-station and 2 reference stations with the aim of determining ground predominant period and amplification parameters of the Akçakale (Gumushane) Province, NE Turkey.

2. METHOD

The site effect can be considered as empirical transfer functions of the surficial layers. The standard spectral ratio can be calculated by dividing the average horizontal Fourier spectrum of the ground motions recorded on an alluvium site, Y , by that recorded on a nearby rock site, Y_R . The latter station is considered to be a reference station.

In this technique, the intense S-wave part of the strong-motion recording is commonly used for the estimation of the spectral ratio, S_T ,

$$S_T = \frac{Y}{Y_R} \quad (1)$$

where Y_R ,

$$Y_R = \frac{\left[\sum_{i=1}^n Y_{NS} + \sum_{i=1}^n Y_{EW} \right]}{n} \quad (2)$$

¹ Corresponding author: Gümüşhane University, Department of Geophysical Engineering, 29100, Bağlarbaşı/Gümüşhane, Turkey. yaseminbeker@gumushane.edu.tr

²Karadeniz Technical University, Department of Geophysical Engineering, 61080, Trabzon, Turkey.

$Y_{NS,EW}$: The amplitude spectrum of horizontal components of reference stations.

n : The number of reference stations.

In order to determine the soil amplification of KTU Campus area, microtremor records taken in 53 single-station and 2 reference stations with CMG-6TD three-component broad-band velocity seismometer (Figure 1). The duration of microtremor records are 15 minutes. The distance between microtremor measurement points is 50-100 m.

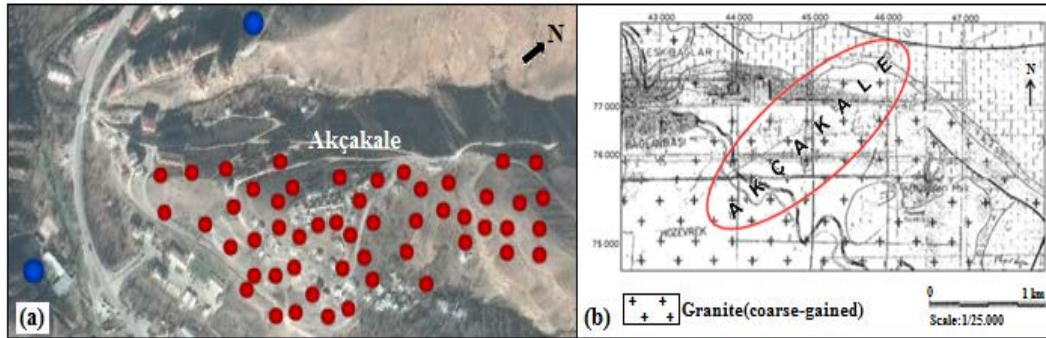


Figure 1. (a) Microtremor measurement points (red circle: single-station, blue circle: reference station); (b) The geology map of the study area [3].

The obtained microtremor records are estimated by the Standard Spectral Ratio (SSR) method (Figure 2).

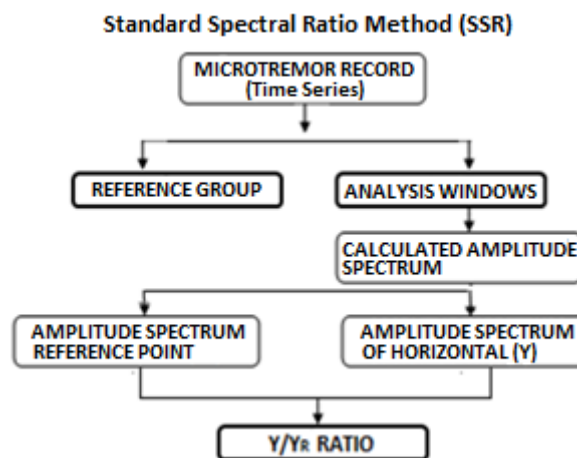


Figure 2. The flow charts of the Standard Spectral Ratio (SSR) method.

3. RESULTS

The soil-site to rock-site spectral ratio has been a popular method to provide a rough estimate on site effects due to local geology. This method establishes a plausible physical basis in terms of source effect and path effect removal. In this study, Standard Spectral Ratio (SSR) method have been applied to microtremor records taken with three component broad band velocity seismometers in 53 single-station and 2 reference stations with the aim of determining ground characteristics of the Akçakale (Gumushane) Province, NE Turkey. The obtained microtremor records are estimated by SSR method. The amplification and predominant frequency maps of the study area are generated to the results of SSR method (Figure 5 and 6). The amplification and predominant frequency obtained from SSR method are 1.1-6.23 and 1.5-8.4 Hz, respectively. These values are consistent with the geology of the study area. The results indicate that the Standard spectral ratio furnishes a reasonably adequate estimate for the predominant frequency and the approximate amplification level.

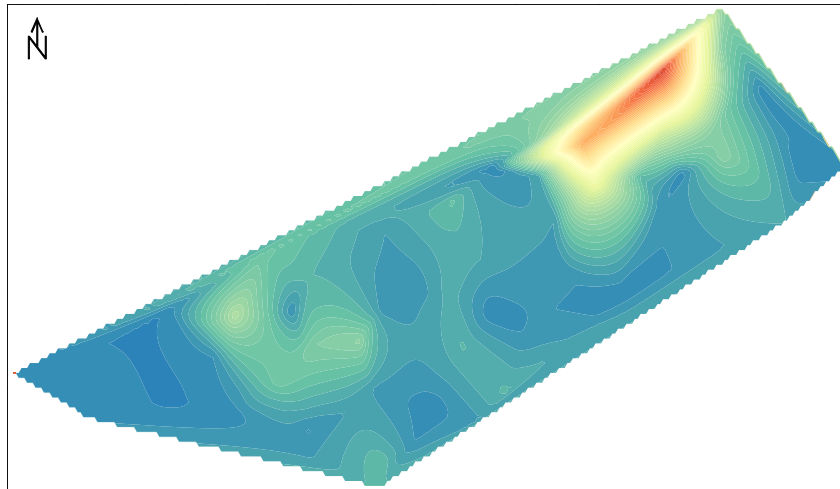


Figure 5. The amplification contour map of study area.

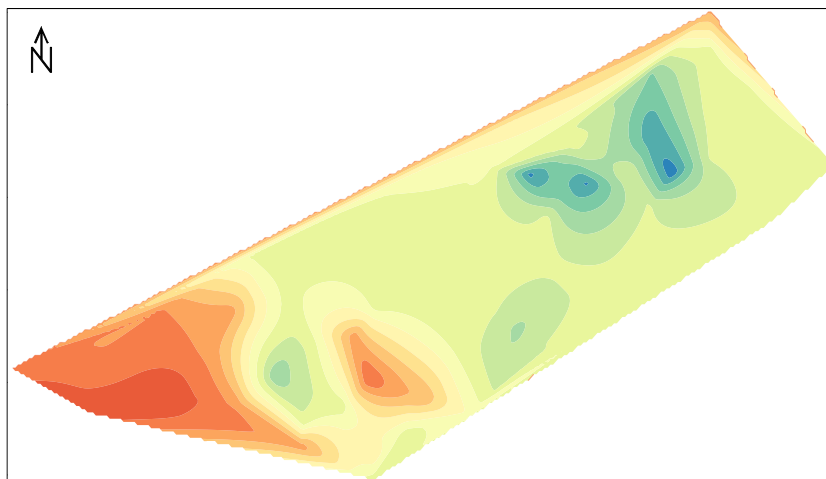


Figure 6. The predominant frequency contour map of study area

REFERENCES

- [1] Kanai, K. and Tanaka, T., Measurement of the Microtremor, *Bulletin of the Earthquake Research Institute*, University of Tokyo, 32, 192-209, 1954.
- [2] Kanai, K. and Tanaka, T., On Microtremors, VII, *Bulletin of the Earthquake Research Institute*, 39, 97-114, 1961.
- [3] Guven, I.H., *Measurement Complication with 1/25000 of Eastern Pontides*, Mining Technical Institute, Ankara, 1993.

Optimization of Ammonia Removal from Leachate by Ammonia Stripping Using Response Surface Methodology

Özlem Tepe¹, Muslun Sara Tunc²

Abstract

For the disposal of municipal solid waste, one of the most common used methods is landfill. Leachate forms in consequence of percolation of rain-water and moisture through waste disposed in landfill. Leachate formed contains high organic matter and ammonium nitrogen. For the removal of ammonium nitrogen from landfill leachate, ammonia stripping is used as a pretreatment method to maintain the ammonia concentration of the effluent in a range that is safe for subsequent biological processes. In this study, ammonia removal from landfill leachate using ammonia stripping was investigated. The operating variables such as pH and mixing rate were optimized via response surface methodology (RSM) using central composite design (CCD) to obtain the maximum removal of ammonia nitrogen. Ammonia removal efficiency increased significantly as pH and mixing rate increased. Ammonia removal efficiency of about 99% was obtained.

Keywords: Ammonia stripping, leachate, response surface methodology

1 INTRODUCTION

With population growth and new patterns of consumption, big amounts of municipal solid wastes have been producing [1]. In many regions in the world, municipal solid waste (MSW) has been considered to be one of the most serious environmental issues [2]. In order to protect the environment and public health, one of essential and fundamental service that should be provided by municipal authorities is MSW management [3]. Several techniques used for MSW management are recycling, composting, incineration, and sanitary landfill [4]. For municipal solid waste management, sanitary landfilling is the most common disposal method. In addition, it is considered as the most economical and environmentally acceptable method for municipal and industrial solid wastes disposal [5]. However, as a result of the rain water percolation through the wastes, degradation of wastes and so on for sanitary landfills, a very complex wastewater known as sanitary landfill leachate is produced [1, 6].

Quality and quantity of the leachate vary depending upon many factors such as waste composition, elapsed time, moisture content, temperature, depth of landfilling, co-disposal with specific wastes and site hydrology [7]. The leachate generated from sanitary landfill contains a large amount of organic pollutants, inorganic salts, ammonia nitrogen (NH₃-N) and many other contaminants [8]. Ammonia nitrogen acts as a nutrient for aquatic plants and algae [9]. High concentration of ammonia leads to eutrophication in rivers and lakes, and depletion of dissolved oxygen in receiving water bodies. Also, unionized ammonia is toxic to most fish species even at low concentrations (0.53-22.8 mg/L) [10]. Therefore, wastewaters containing high concentrations of ammonia such as leachate should treat before discharge in the receiving bodies.

In order to remove ammonia from wastewater, several treatment processes such as biological nitrification/denitrification, air stripping, adsorption and ion-exchange have been applied [10]. Among these processes, as the ammonia stripping method generates less extra sludge and is associated with modest reagent costs and an easy operation, this method is considered as the most applicable, especially for wastewaters containing high concentrations of ammonia such as leachate [11].

In this study, ammonia removal from landfill leachate using ammonia stripping was investigated. pH and mixing rate selected as operating variables were optimized via response surface methodology (RSM) using central composite design (CCD) to obtain the maximum removal of ammonia nitrogen.

¹Corresponding author: Firat University, Department of Environmental Engineering, 23119, Elazığ, Turkey. otepe@firat.edu.tr

²Firat University, Department of Environmental Engineering, 23119, Elazığ, Turkey. saratunc@firat.edu.tr

2. MATERIALS AND METHODS

2.1. Chemicals

Sodium hydroxide supplied from Merck Company was used for pH adjustment of wastewater samples in the study. All reagents used in COD test (potassium dichromate, sulfuric acid (98%), silver sulfate, mercury sulfate and ferrous ammonium sulfate) were supplied from Sigma-Aldrich. All chemicals used in the present study were of analytical grade.

2.2. Landfill leachate sample

Landfill leachate was supplied from sanitary landfill area in City of Elazığ, Turkey. Solid waste of 350 tons in City of Elazığ is being disposed daily at sanitary landfill area. After sampling of the leachate, the samples were preserved in dark polyethylene containers and kept in temperature of 4 °C in order to prevent reduction of organic matter and ammonia nitrogen content. The landfill leachate was characterized.

2.3. Experiments

The ammonia stripping experiments were carried out by employing a series of 6 glass beakers of 500 mL and jar test apparatuses (Wise Stir) at the different pH values and mixing rates. All tests were conducted at room temperature (20 ± 1 °C). The leachate sample of 250 mL was filled in each of the glass beakers. pH of the leachate samples was adjusted to desired values using concentrated sodium hydroxide solution. The prepared samples were mixed for 8 h at different mixing rate (rpm). Then, the samples were settled for 60 min. After the settling process, the supernatant samples were taken from the beakers to measure of ammonium concentrations.

2.4. Design of experiments

Response surface methodology (RSM) is a combination of mathematical and statistical techniques commonly used in optimization of chemical reactions and industrial processes [10]. In this study, response surface methodology (RSM) was used to evaluate the process of ammonia removal from leachate using ammonia stripping. The 'Design-Expert' software (version 7.0, Stat-Ease, Inc., Minneapolis, USA) statistical package was used for regression and graphical analyses of the data obtained. Central Composite Design (CCD) was used to optimize pH and mixing rate as main factors in ammonia stripping. The study ranges were chosen as 9.6-12.4 for pH and as 95-300 rpm for mixing rate. Thirteen experiments were carried out. The experimental values of the independent variables are presented in Table 1. Experimental result (response) is shown as percent removal of ammonia.

Ammonia removal, Y (%), was calculated using the following equation:

$$Y(\%) = \frac{C_0 - C}{C_0} \cdot 100 \quad (1)$$

where C_0 is the initial ammonia nitrogen concentration and C is the ammonia nitrogen concentration after treatment.

Table 1. Coded and actual levels of independent variables

Independent variable	Coded levels				
	-1.41	-1	0	1	+1.41
pH (A)	9.6	10.0	11.0	12.0	12.4
Mixing rate (rpm) (B)	95	125.0	197.5	270.0	300.0

2.5. Analyses

Chemical oxygen demand, total solid and total suspended solids were determined according to Standard Methods for Examination of Water and Wastewater (APHA, 1989). The nitrogen species (ammonium-nitrogen (NH₄-N), nitrite-nitrogen (NO₂-N) and nitrate-nitrogen (NO₃-N) were measured by standard test kits (Merck Spectroquant) using Nova 60 Spectroquant. pH was measured using a pH meter (Thermo Scientific Orion 3 Star).

3. RESULTS AND DISCUSSION

3.1. Leachate Characterization

The properties of leachate used in the study are given in Table 2. As shown in Table 2, COD, TS, TSS, NH₄-N concentration of the leachate varied in the range of 3240-3580 mg/L, 16170-17025 mg/L, 1140-2120 mg/L, and 840-1000 mg/L, respectively.

Table 2. The properties of the leachate used in the study

Parameters	Unit	Range
pH		7.86-7.87
COD	mg/L	3240-3580
TS	mg/L	16170-17025
TSS	mg/L	1140-2120
NH ₄ -N	mg/L	840-1000
NO ₂ -N	mg/L	0.04
NO ₃ -N	mg/L	4.4

3.2. Optimization of the ammonia stripping process based on the RSM

In this study, pH and mixing rate (rpm) were chosen as independent variables. Thirteen runs were performed for experimental set. Table 3 shows the complete design matrixes with the response values obtained from the experiment. The quadratic model were expressed by following a second-order polynomial equation in which the ammonia removal (%) (*Y*) was assessed as a function of pH (*A*) and mixing rate (rpm) (*B*).

$$\text{Ammonia removal (\%)} (Y): +98.22 + 7.21 A + 7.19 B - 2.02 AB - 3.05 A^2 - 6.92 B^2 \quad (2)$$

Table 3. Central composite design and response results

Runs	Uncoded variables		Response
	A (pH)	B (Mixing rate, rpm)	Ammonia removal (%)
1	11.0	197.5	98.2
2	10.0	125.0	76.2
3	11.0	300.0	98.8
4	10.0	270.0	86.6
5	12.0	125.0	96.8
6	9.6	197.5	82.0
7	12.0	270.0	99.1
8	11.0	95.0	67.1
9	11.0	197.5	98.0
10	11.0	197.5	98.2
11	12.4	197.5	99.4
12	11.0	197.5	98.5
13	11.0	197.5	98.2

The role of factors on the response is revealed by comparing the factor coefficients in the coded equations. Negative coefficient values indicate that factors negatively affect the response, whereas the positive coefficient values indicate that the factors increase the response in the tested range [12]. The coefficient values in Eqs. (2) reveal that the percentage of ammonia removal increase with pH (*A*) and mixing rate.

The ANOVA results given in Tables 4 and 5 confirm adequacy of the quadratic model because of value of probability (*P*) less than 0.05. The model is highly significant, as is evident from the model *F* value and low probability value (*P* value: 0.0033). The *P* value serves as a tool for checking the significance of each of the coefficients, which also indicates the interaction strength of each parameter. The low values of *P* of less than 0.05 indicate the more significant correlation of the coefficients. The smaller the *P* values are, the bigger the significance of the corresponding coefficient. It is observed that the coefficients for the linear effect of pH and mixing rate (*P*=0.0034 and *P*=0.0034, respectively) for ammonia removal are significant. The coefficient of the quadratic term of concentration of mixing rate (*P*=0.0060) appear to be significant. The interaction effect between pH and mixing rate (*P*= 0.4171) had no significance.

The *R*² coefficient gives the proportion of the total variation in the response predicted by the model, ensuring a satisfactory adjustment of the quadratic model to the experimental data. A high *R*² value close to 1 is desirable and a reasonable agreement with adjusted *R*² is necessary [12]. When expressed as a percentage, *R*² implies that the total variation of 89% for ammonia removal is attributed to the independent variables and only about 11 % of the total variation cannot be explained by the model. A model normally can be considered reproducible if coefficient of variance (*CV*) is not greater than 10%. As shown in Table 4, the value of *CV* is 5.10% confirming the reproducibility of the model.

Table 4. ANOVA for analysis of variance and adequacy of quadratic model

Source	Sum of squares	DF	Mean square	F- value	Probability (P) > F
Model	1212.30	5	242.46	10.99	0.0033 significant
Residual	154.44	7	22.06		
Lack of fit	154.31	3	51.44	1607.37	<0.0001 significant
Pure error	0.13	4	0.032		
Cor total	1366.74	12			

CV;5.10, R²; 0.89, Adj R²; 0.81, Adeq Precision; 9.560

Table 5. The least-squares fit and parameter estimates (significance of regression coefficient)

Source	Parameter estimate	F- value	Probability (P) > F
Intercept	98.22	10.99	0.0033 significant
A	7.21	18.87	0.0034
B	7.19	18.75	0.0034
AB	-2.02	0.74	0.4171
A ²	-3.05	2.93	0.1308
B ²	-6.92	15.11	0.0060

The actual versus predicted value plots of the responses illustrated in Fig. 1 showed a sufficient agreement between the actual and predicted data obtained from the model.

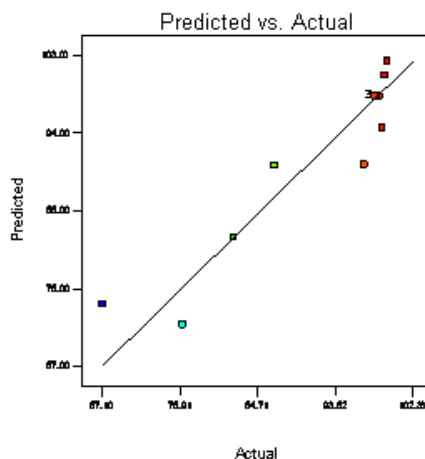


Figure 1. Design-expert plot; predicted vs. actual values plot for ammonia removal

The regression equation obtained by RSM analysis can be expressed with three-dimensional and two-dimensional contour plots. Response surface curves are drawn with a statistically appropriate model to find optimal concentrations of each component and to understand the interaction of media components [13]. All plots are presented in Fig 2. pH control is a critical step in the ammonia stripping process. A high pH (10.5–11.5) was required to achieve high ammonia removal efficiency [14]. As seen Fig 2, high pH (pH>10.5) and intermediate mixing rate led to high ammonia removal (99.4%).

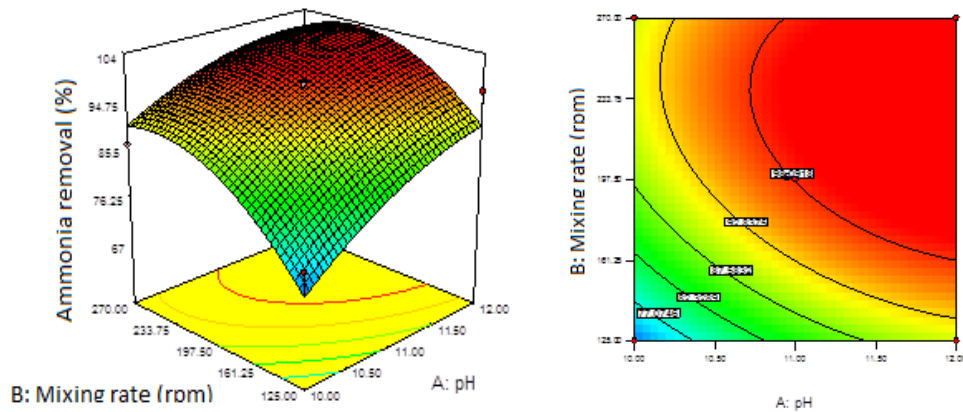


Figure 2. Three-dimensional and two-dimensional response surface plots showing the effect of pH and mixing rate on ammonia removal

4. CONCLUSION

Ammonia removal for landfill leachate was investigated by ammonia stripping process. To optimize pH and mixing rate being operational variables for the treatment process, RSM was applied. High ammonia removal was achieved on high pH (pH>10.5) and intermediate mixing rate.

REFERENCES

- [1]. A. Fernandes, M.J. Pacheco, L. Ciríaco, and A. Lopes, "Review on the electrochemical processes for the treatment of sanitary landfill leachates: Present and future," *Applied Catalysis B: Environmental*, vol. 176-177, pp. 183-200, 2015.
- [2]. A. Mojiri, L. Ziyang, R.M. Tajuddin, H. Farraji, and N. Alifar, "Co-treatment of landfill leachate and municipal wastewater using the ZELIAC/zeolite constructed wetland system," *Journal of Environmental Management*, vol. 166, pp. 124-130, 2016.
- [3]. M.A. Rasool, B. Tavakoli, N. Chaibakhsh, A.R. Pendashteh, and A.S. Mirroshandel, "Use of a plant-based coagulant in coagulation-ozonation combined treatment of leachate from a waste dumping site," *Ecological Engineering*, vol. 90, pp. 431-437, 2016.
- [4]. W. Dastyar, T. Amani, S. Elyasi, "Investigation of affecting parameters on treating high-strength compost leachate in a hybrid EGSB and fixed-bed reactor followed by electrocoagulation-flotation process," *Process Safety and Environmental Protection*, vol. 95, pp. 1-11, 2015.
- [5]. A.H. Hilles, S. S. Abu Amr, R. A. Hussein, O. D. El-Sebaie, and A. I. Arafa, "Performance of combined sodium persulfate/H₂O₂ based advanced oxidation process in stabilized landfill leachate treatment," *Journal of Environmental Management*, vol. 166, pp. 493-498, 2016.
- [6]. H. Chen, Y. Sun, X. Ruan, Y. Yu, M. Zhu, J. Zhang, J. Zhou, Y. Xu, J. Liu, and G. Qian, "Advanced treatment of stabilized landfill leachate after biochemical process with hydrocalumite chloride (Ca/Al-Cl LDH)," *Bioresource Technology*, vol. 210, pp. 131-137, 2016.
- [7]. A. Amiri, and M. R. Sabour, "Multi-response optimization of Fenton process for applicability assessment in landfill leachate treatment," *Waste Management*, vol. 34, pp. 2528-2536, 2014.
- [8]. Z. Ye, H. Zhang, X. Zhang, and D. Zhou, "Treatment of landfill leachate using electrochemically assisted UV/chlorine process: Effect of operating conditions, molecular weight distribution and fluorescence EEM-PARAFAC analysis", *Chemical Engineering Journal*, vol. 286, pp. 508-516, 2016.
- [9]. M.-H. Yuan, Y.-H. Chen, J.-Y. Tsai, and C.-Y. Chang, "Removal of ammonia from wastewater by air stripping process in laboratory and pilot scales using a rotating packed bed at ambient temperature", *Journal of the Taiwan Institute of Chemical Engineers*, vol. 60, pp. 488-495, 2016.
- [10]. Y. Ding, and M. Sartaj, "Statistical analysis and optimization of ammonia removal from aqueous solution by zeolite using factorial design and response surface methodology," *Journal of Environmental Chemical Engineering*, vol. 3, pp. 807-814, 2015.
- [11]. L. Zhang, Y.-W. Lee, and D. Jahng, "Ammonia stripping for enhanced biomethanization of piggery wastewater," *Journal of Hazardous Materials*, vol. 199-200, pp. 36-42, 2012.
- [12]. P. Ghosh, Swati and I. S. Thakur, "Enhanced removal of COD and color from landfill leachate in a sequential Bioreactor", *Bioresource Technology*, vol. 170, pp. 10-19, 2014.
- [13]. R. Kaushik, S. Saran, J. Isar and R.K. Saxena, "Statistical optimization of medium components and growth conditions by response surface methodology to enhance lipase production by *Aspergillus carneus*," *J Mol Catal B Enzym*, 40, pp. 121-126, 2006.
- [14]. L. Zhang, and D. Jahng, "Enhanced anaerobic digestion of piggery wastewater by ammonia stripping: Effects of alkali types," *Journal of Hazardous Materials*, vol. 36-42, pp. 199-200, 2012.

Performance of Nitrogen and Phosphorus Removal of Moving Bed Biofilm Reactor Operated as Sequencing Batch

Muslun Sara Tunc¹, Ayhan Unlu²

Abstract

In this study, nitrogen and phosphorus removal from municipal wastewater in moving bed biofilm reactor operated as sequencing batch was investigated. Kaldnes (K1) material as biofilm carrier media was used in the study. Operation consisted of anaerobic/aerobic/anoxic/aerobic phases with hydraulic residence times of 120 min/330 min/210 min/50 min. In the moving bed biofilm reactor with the filling ratio of 50% operated as sequencing batch, average effluent chemical oxygen demand (COD), ammonium-nitrogen (NH₄-N), nitrite-nitrogen (NO₂-N), nitrate-nitrogen (NO₃-N) and phosphate-phosphorus (PO₄-P) values after the cycle duration of 12 h were determined to be 27 mg/L, 0.7 mg/L, 0.04 mg/L, 0.6 mg/L and 0.7 mg/L, respectively. The average COD, NH₄-N and PO₄-P removal efficiencies were obtained as 92%, 97.5% and 91.3%, respectively.

Keywords: *moving bed biofilm reactor, nitrogen removal, phosphorus removal, sequencing batch biofilm reactor*

1. INTRODUCTION

Nitrogen and phosphorus are commonly present in wastewater streams such as municipal, industrial and agricultural wastewaters [1]. When untreated or insufficiently treated wastewater discharges to water bodies such as lake and river, it causes several problems such as eutrophication and the depletion of dissolved oxygen [2]. Therefore, removal of these contaminants from wastewaters for reducing their damage to the environment is of great importance [3, 4].

In order to improve the quality of treated wastewater and meet the demands of environmental regulations, advanced treatment technologies have been developed [2]. The moving bed biofilm reactor (MBBR) having advantages of both attached and suspended growth systems is one of the advanced wastewater treatment process [5]. It is filled with carrier materials, on which biomass is attached, and freely move and circulate in the reactor by aeration in aerobic process or mechanical stirring in anoxic/anaerobic process. The carrier materials are kept inside the reactor by means of a sieve placed outlet of the reactor [6]. The MBBR relies on the attachment of biomass on plastic carriers, which allows retaining a significant amount of active biomass in the reactor regardless of the hydraulic conditions. This feature is very attractive for preventing washout of slow growing microorganisms like nitrifiers from the process [7]. It is a continuously operating, non-cloggable biofilm reactor with no need for backwashing, low head-loss and a high specific biofilm surface area [5]. It has some advantages such as a shorter hydraulic retention time (HRT), higher organic loading rates, a higher nitrification rate and larger surface area for mass transfer [8]. It has been widely applied to treat both municipal and industrial wastewaters due to the advantages of the attached growth process such as compact, stable removal efficiency and simplicity of operation without its limitations such as medium channeling and clogging [3, 9]. Also, it has been used for upgrading and retrofitting existing wastewater treatment plants due to having advantages of both suspended and attached growth systems [6, 10].

Nitrogen is removed by the combination of nitrification by autotrophs under aerobic conditions and denitrification by heterotrophs under anaerobic conditions. Phosphorus removal is achieved by its uptake into biomass which can be discharged from the system as a surplus sludge. It is possible that nitrification, denitrification and phosphorus removal are achieved in one reactor when a sequencing batch reactor system (SBR) is used [11]. SBR systems have been modified to achieve nitrification and denitrification as well as COD and phosphate removal because of regulations on nutrient discharge limitations. When biological nutrient removal is desired, its cycle format can be flexibly adjusted to provide anaerobic, anoxic and aerobic phases in certain number and sequence [12]. Among various biological treatment systems, they have many advantages such as lower capital and operational costs and less bulking [1, 11, 13]. Over the years, many efforts have been made to modify the SBR system to improve the performance. Among others, the moving bed sequencing batch reactor (MBSBR) which incorporates both suspended-growth and attached-growth processes has attracted much interest among researchers in the field of wastewater treatment [1]. Nitrification and denitrification can also be successfully achieved in biofilm-based processes because nitrifiers, which are slow growing microorganisms, are retained by the biofilm [5].

¹Corresponding author: Firat University, Department of Environmental Engineering, 23119, Elazığ, Turkey. saratunc@firat.edu.tr

²Firat University, Department of Environmental Engineering, 23119, Elazığ, Turkey. aunlu@firat.edu.tr

In this study, removal of nitrogen and phosphorus from municipal wastewater was investigated in the moving bed biofilm reactor operated in the sequencing batch mode.

2. MATERIALS AND METHODS

2.1. Experimental set-up and operation

A schematic diagram of the experimental set up is depicted in Fig. 1. The reactor used in the study was made of plexiglass material and had a working volume of 1 L. The carrier elements, called K1, were used as support materials to provide a surface for biofilm growth in the moving bed biofilm reactor (MBBR). The reactor was filled with 50% carrier elements.

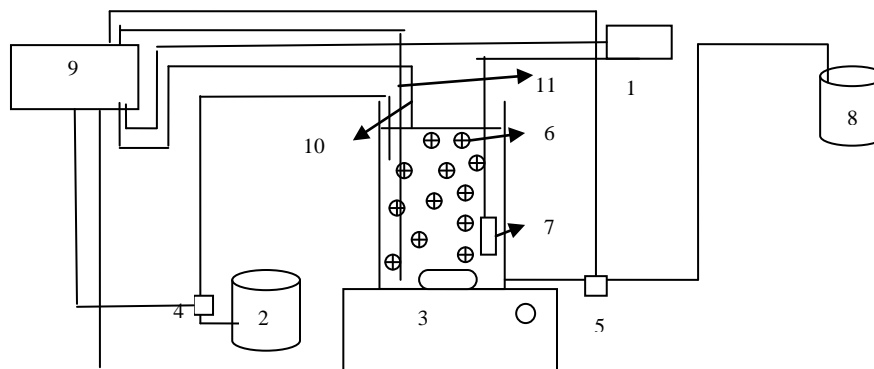


Figure 1. Schematic diagram of experimental set up. 1. air pump; 2. feed tank; 3. magnetic stirrer; 4. dosage pump; 5. drawing pump; 6. biofilm carrier materials; 7. air stone; 8. effluent tank; 9. programmable logic device; 10. filling level electrode; 11. drawing level electrode,

The reactor was inoculated with activated sludge taken from the secondary settling tank of the municipal wastewater treatment plant in Malatya, Turkey. The reactor was operated in a sequencing batch mode for COD, nitrogen and phosphorus removal. An operation cycle comprised a filling, reaction and drawing period. Reaction period consisted of anaerobic/aerobic/anoxic/aerobic phases with hydraulic residence times of 120 min/330 min/210 min/50 min. The filling plus drawing period was 10 minute. The MBBR was operated under hydraulic retention times of 12 h. The reactor was completely drained during drawing period at the end of each cycle. Aeration was supplied by air stone placed in the reactor by using an aquarium air pump. Airflow rate was controlled by rotometer. The alternation between aerobic, anoxic and anaerobic conditions was provided by the on and off control of the air pump. To make it work this way, the programmable logic device was used. The feed tank was filled periodically with the effluents collected from primary settler tank of the municipal wastewater plant in Elazığ, Turkey. Sufficient amount of ethanol solution was added in the reactor as an external carbon source at the beginning of the anoxic phase to reduce oxidized nitrogen ($\text{NO}_2\text{-N} + \text{NO}_3\text{-N}$) to nitrogen gas.

2.2. Biofilm carrier

The carrier, called K1, was used in this study. The carrier was made from polyethylene with a density of 0.96 g/cm^3 slightly lower than the density of water and had an effective surface of $500 \text{ m}^2/\text{m}^3$. It was cylindrical with internal walls and external fins that protect the biofilm from abrasion. With a filling ratio of 50%, the available surface area (referred to the reactor volume) was $250 \text{ m}^2/\text{m}^3$.

2.3. Wastewater Characteristics

The study was carried out using wastewater collected from the primary settler tank of municipal wastewater plant in Elazığ, Turkey. The wastewater had chemical oxygen demand (COD) in the range of 328-336 mg/L, ammonium-nitrogen ($\text{NH}_4\text{-N}$) in the range of 17.3-21.7 mg/L, phosphate-phosphorus in the range of 8.7-10.8. The samples were stored in a refrigerator at $4 \text{ }^\circ\text{C}$ until use.

2.4. Analytical methods

Samples were taken from the reactor at the beginning and at the end of anaerobic, aerobic and anoxic phases. To remove microorganisms from the mixed liquid medium, these samples were centrifuged at 5000 rpm for 10 min. Supernatants were analyzed for COD, ammonium-nitrogen, nitrite-nitrogen, nitrate-nitrogen and phosphate-phosphorus contents. The concentration of COD and total suspended solids (TSS) in the liquid phase was determined in accordance with Standard Methods for Examination of Water and Wastewater [14]. In order to determine the amount of the biofilm in the reactor, 10 carrier materials taken from reactor was dried at $70 \text{ }^\circ\text{C}$ for 48 h and weighed. The higher temperature was not used because of

deformation risk of the carrier materials [15]. It was subsequently cleaned to remove the attached biofilm, followed by drying and weighing again. Then, biofilm amount was calculated taking into account the number of elements per liter. The nitrogen species (ammonium-nitrogen ($\text{NH}_4\text{-N}$), nitrite-nitrogen ($\text{NO}_2\text{-N}$) and nitrate-nitrogen ($\text{NO}_3\text{-N}$)) and phosphate-phosphorus ($\text{PO}_4\text{-P}$) were measured by standard test kits (Merck Spectroquant) using Nova 60 Spectroquant. The dissolved oxygen concentration and pH in the reactor were measured using an O_2 electrode and a pH electrode by a multimeter (Hach HQ40D).

3.1 RESULTS AND DISCUSSION

3.1 COD Removal

Effluent COD concentration and COD removal efficiency obtained in the moving bed biofilm reactor operated as the sequencing batch are depicted in Fig. 1. Effluent COD concentration obtained after 12-h cycle changed in the range of 16 to 32 mg/L. Average effluent COD concentration was 27 mg/L. COD removal efficiency changed in the range of 90.5-95.2%, with average removal efficiency of 92%. Effluent TSS concentration varied in the range of 220 to 280 mg/L. The average amount of biomass attached to the carrier materials was 3.1 kg/m^3 .

3.2. Nitrogen removal

Variation of effluent $\text{NH}_4\text{-N}$, $\text{NO}_2\text{-N}$ and $\text{NO}_3\text{-N}$ concentration and $\text{NH}_4\text{-N}$ removal efficiency obtained is depicted in Fig 3. Effluent $\text{NH}_4\text{-N}$ concentration varied between 0.1 and 0.8 mg/L, with average effluent level of 0.7 mg/L. Effluent $\text{NO}_2\text{-N}$ and $\text{NO}_3\text{-N}$ concentration changed in range of 0.01-0.1 mg/L and 0.1-1.8 mg/L, respectively. Average effluent level of $\text{NO}_2\text{-N}$ and $\text{NO}_3\text{-N}$ was observed to be 0.04 mg/L and 0.6 mg/L. $\text{NH}_4\text{-N}$ removal efficiency varied between 96% and 99.5%, with average removal efficiency of 97.5%. As can be seen from the results obtained, nitrogen removal from the municipal wastewater can be removed by moving bed biofilm reactor operated in the sequencing batch mode with the cycle of 12 h.

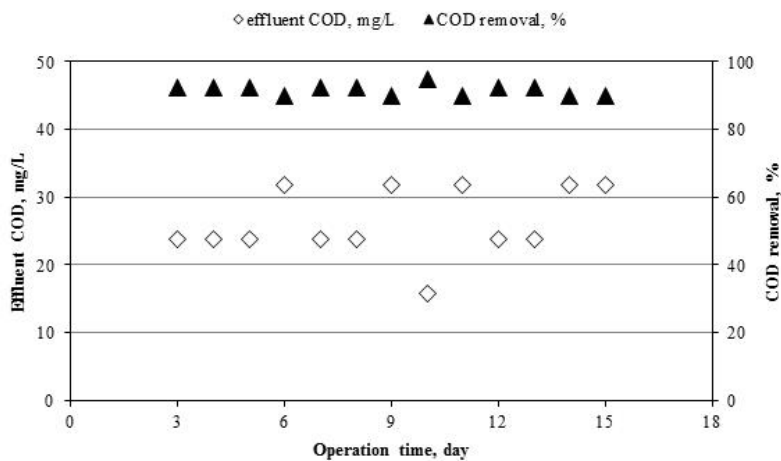


Figure 2. Effluent COD concentrations and COD removal obtained by MBBR operated as sequencing batch

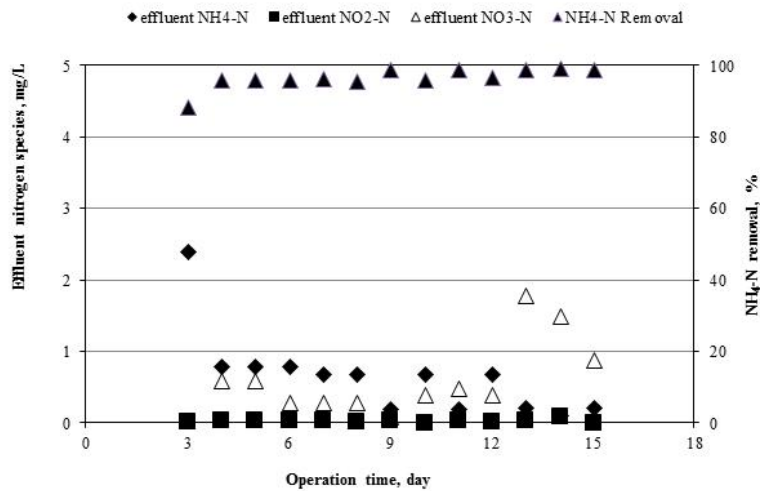


Figure 3. Concentrations of effluent nitrogen species and NH₄-N removal obtained by MBBR operated as sequencing batch

Biological nitrogen removal from wastewater is achieved by nitrification under aerobic conditions and heterotrophic denitrification under anaerobic conditions [1, 16]. Nitrification is a process consists of two steps which ammonia is converted to nitrite by ammonia-oxidizing bacteria and then nitrite is converted to nitrate by nitrite-oxidizing bacteria. Nitrite and/or nitrate are reduced to nitrogen gas by heterotrophic bacteria during denitrification process [16, 17]. In the anaerobic, first aerobic (I), anoxic and last aerobic (II) phases of the cycle, variation of NH₄-N, NO₂-N and NO₃-N concentration is shown in Fig. 4. NH₄-N, NO₂-N and NO₃-N concentration at the beginning of the cycle was 21.7 mg/L, 0.05 mg/L and 0.4 mg/L, respectively. As can be shown from Fig. 4, NH₄-N, NO₂-N and NO₃-N were nearly constant during the anaerobic phase. NH₄-N was removed by assimilation and nitrification during the first aerobic phase. NH₄-N transformed to NO₃-N as result of nitrification in the end of the first aerobic phase and NO₃-N increased to 19.2 mg/L. NO₂-N did not accumulate in the reactor since the complete nitrification happened in the aerobic phases. In the anoxic and the last aerobic (II) phase, NH₄-N concentration was almost the same as NH₄-N concentration of aerobic (I). Adequate amount of ethanol solution was added into the reactor as a carbon source at the beginning of the anoxic phase to reduce the oxidized nitrogen (NO₂-N and NO₃-N) to nitrogen. As result of assimilation and denitrification, NO₃-N decreased to 0 mg/L in the anoxic phase in the present of the external carbon source added. Complete removal of the nitrogen species was achieved due to the addition of ethanol solution at the beginning of the anoxic phase. Nitrogen gas generated in the anoxic phase as result of denitrification was removed in the last aerobic phase.

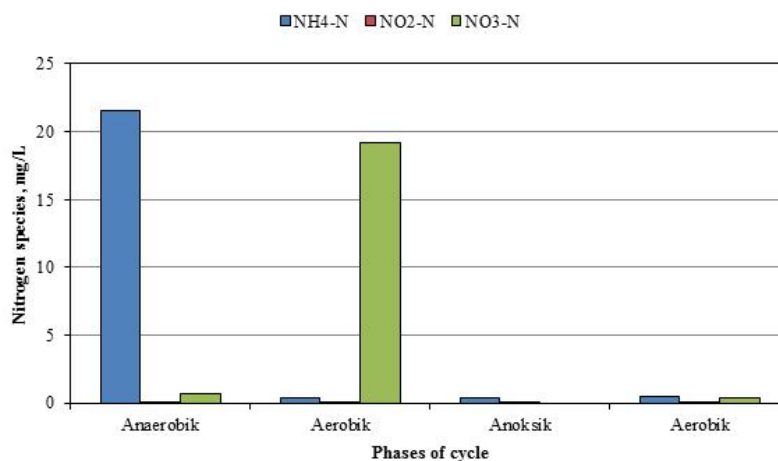


Figure 4. Concentrations of nitrogen species in phases of cycle in MBBR operated as sequencing batch

3.3. Phosphorus removal

Variation of effluent PO₄-P concentration and PO₄-P removal efficiency obtained in the moving bed biofilm reactor operated as sequencing batch with the cycle of 12 h is depicted in Fig 5. Effluent PO₄-P concentration varied between 0.3 and 0.9 mg/L, with average effluent level of 0.7 mg/L. PO₄-N removal efficiency varied between 88.6% and 95.6%, with average removal efficiency of 91.3%. As can be seen from the results obtained, phosphorus from the municipal wastewater can be removed by moving bed biofilm reactor operated in the sequencing batch mode with the cycle of 12 h.

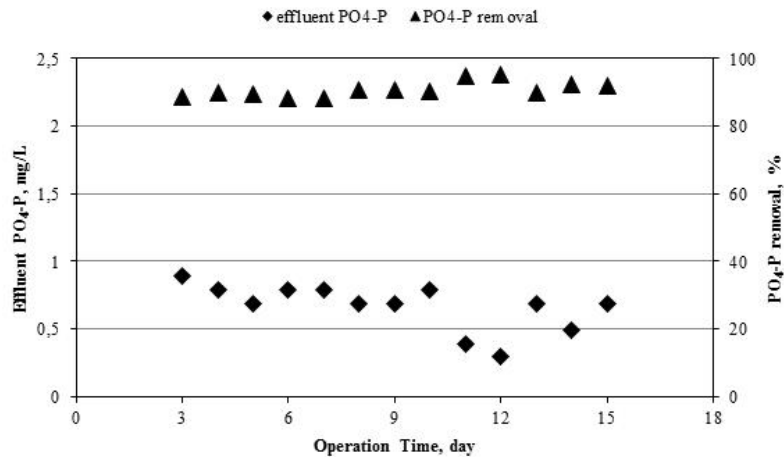


Figure 5. Effluent PO₄-P concentrations and PO₄-P removal in MBBR operated as sequencing batch

In the anaerobic, first aerobic (I), anoxic and last aerobic (II) phases of the cycle, variation of PO₄-P concentration is shown in Fig. 6. Initial PO₄-P concentration of 7.1 mg/L increased to 22.5 mg/L at the end of the anaerobic phase because of phosphate release by phosphorus accumulating organisms (PAOs). PO₄-P concentration decreased from 22.5 mg/L to 0.5 mg/L during the first aerobic phase due to phosphate uptake of PAOs. Phosphorus was significantly released by PAO during anaerobic phase while rapidly absorbed for PAOs growth and intracellular poly-P formation in aerobic phase [18, 19].

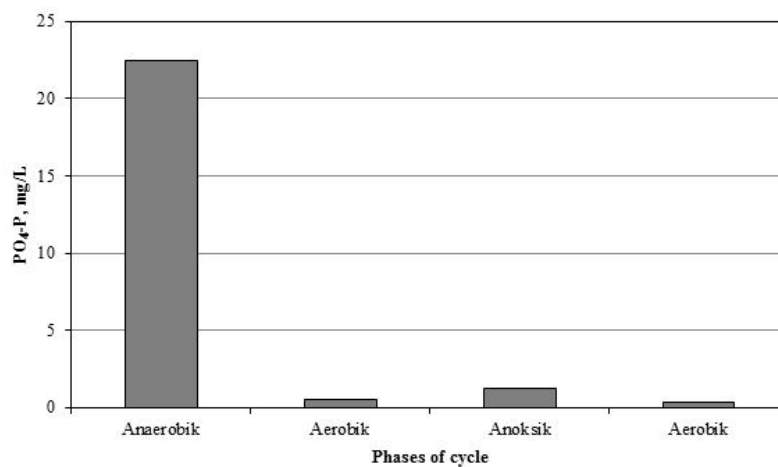


Figure 6. PO₄-P concentrations in phases of cycle in MBBR operated as sequencing batch

4. CONCLUSION

The moving bed biofilm reactor operated as sequencing batch with a cycle consist of anaerobic/aerobic/anoxic/aerobic showed good performance for removal of COD, nitrogen and phosphorus from the municipal wastewater. Effluent COD, NH₄-N, NO₂-N, NO₃-N and PO₄-P concentrations were on average 27 mg/L, 0.7 mg/L, 0.04 mg/L, 0.6 mg/L and 0.7 mg/L, respectively. When a cycle consists of anaerobic/aerobic/anoxic/aerobic with hydraulic residence times of 120 min/330 min/210 min/50 min, on average removal percentage of COD, NH₄-N and PO₄-P were obtained as 92%, 97.5% and 91.3%, respectively.

ACKNOWLEDGEMENTS

The authors wish to tank AnoxKaldnes AS for supplying the Kaldnes (K1) carrier materials.

REFERENCES

- [1]. J.-W. Lim, C.-E. Seng, P.-E. Lim, S.-L. Ng, and A.-N. A. Sujari, "Nitrogen removal in moving bed sequencing batch reactor using polyurethane foam cubes of various sizes as carrier materials," *Bioresource Technology*, vol. 102, pp. 9876-9883, 2011.
- [2]. K. Calderón, J. Martín-Pascual, J.M. Poyatos, B. Rodelas, A. González-Martínez, J. González-López, Comparative analysis of the bacterial diversity in a lab-scale moving bed biofilm reactor (MBBR) applied to treat urban wastewater under different operational conditions, *Bioresource Technology*, vol. 121, 119-126, 2012.
- [3]. X. J. Wang, S. Q. Xia, L. Chen, J. F. Zhao, N. J. Renault, and J. M. Chovelon, "Nutrients removal from municipal wastewater by chemical precipitation in a moving bed biofilm reactor," *Process Biochemistry*, vol. 41, pp. 824-828, 2006.
- [4]. A. A. L. Zinatizadeh, and E. Ghaytooli, "Simultaneous nitrogen and carbon removal from wastewater at different operating conditions in a moving bed biofilm reactor (MBBR): Process modeling and optimization," *Journal of the Taiwan Institute of Chemical Engineers*, vol. 53, pp. 98-111, 2015.
- [5]. A. Barwal, and R. Chaudhary, "To study the performance of biocarriers in moving bed biofilm reactor (MBBR) technology and kinetics of biofilm for retrofitting the existing aerobic treatment systems: a review," *Rev Environ Sci Biotechnol*, vol. 13, pp. 285-299, 2014.
- [6]. B. L. Nogueira, J. Pérez, M. C. M. van Loosdrecht, A. R. Secchi, M. Dezotti, and E. C. Biscaia Jr., "Determination of the external mass transfer coefficient and influence of mixing intensity in moving bed biofilm reactors for wastewater treatment," *Water Research*, vol. 80, 90-98, 2015.
- [7]. J. P. Bassin, B. Abbas, C. L. S. Vilela, R. Kleerebezem, G. Muyzer, A. S. Rosado, M. C. M. van Loosdrecht, and M. Dezotti, "Tracking the dynamics of heterotrophs and nitrifiers in moving-bed biofilm reactors operated at different COD/N ratios," *Bioresource Technology*, vol. 192, 131-141, 2015.
- [8]. J. C. Leyva-Díaz, J. Martín-Pascual, M. M. Muñío, J. González-López, E. Hontoriaa, and J. M. Poyatos, "Comparative kinetics of hybrid and pure moving bed reactor-membrane bioreactors," *Ecological Engineering*, vol. 70, pp. 227-234, 2014.
- [9]. Y. Zhu, Y. Zhang, H.-Q. Ren, J.-J. Geng, K. Xu, H. Huang, and L.-L. Ding, "Physicochemical characteristics and microbial community evolution of biofilms during the start-up period in a moving bed biofilm reactor," *Bioresource Technology*, vol. 180, 345-351, 2015.
- [10]. L. Chu, J. Wang, F. Quan, X.-H. Xing, L. Tang, and C. Zhang, "Modification of polyurethane foam carriers and application in a moving bed biofilm reactor," *Process Biochemistry*, vol. 49, 979-1982, 2014.
- [11]. S. Yang, F. Yang, Z. Fu, T. Wang, and R. Lei, "Simultaneous nitrogen and phosphorus removal by a novel sequencing batch moving bed membrane bioreactor for wastewater treatment," *Journal of Hazardous Material*, vol.175, pp. 551-557, 2010.
- [12]. F. Kargi, and A. Uygur, "Nutrient loading rate effects on nutrient removal in a five-step sequencing batch reactor," *Process Biochemistry*, vol. 39, pp. 507-512. 2003.
- [13]. F. Kargi, and A. Uygur, "Effect of carbon source on biological nutrient removal in a sequencing batch reactor," *Bioresource Technology*, vol. 89, 89-93, 2003.
- [14]. APHA, *Standard Methods for the Examination of Water and Wastewater*, 17th ed. APHA, AWWA, WPCF, American Public Health Association, Washington, DC, 1989.
- [15]. B. Rusten, L.J. Hem, and H. Ødegaard, Nitrogen removal from dilute wastewater in cold climate using moving-bed biofilm reactors, *Water Environmental research*, vol. 67, pp.65-74, 1995.
- [16]. P. Reboleiro-Rivas, J. Martín-Pascual, B. Juárez-Jiménez, J. M. Poyatos, R. Vílchez-Vargas, S. E. Vlaeminck, B. Rodelas, and J. González-López, "Nitrogen removal in a moving bed membrane bioreactor for municipal sewage treatment: Community differentiation in attached biofilm and suspended biomass," *Chemical Engineering Journal*, vol. 277, pp. 209-218, 2015.
- [17]. J.C. Leyva-Díaz, A. Gonzalez-Martinez, J. Gonzalez-Lopez, M. M. Munio, and J. M. Poyatos, "Kinetic modeling and microbiological study of two-step nitrification in a membrane bioreactor and hybrid moving bed biofilm reactor-membrane bioreactor for wastewater treatment," *Chemical Engineering Journal*, vol. 259, pp. 692-702, 2015.
- [18]. A. Oehmen, P.C. Lemos, G. Carvalho, Z. Yuan, J. Keller, L.L. Blackall, and M.A.M. Reis, "Review Advances in enhanced biological phosphorus removal: From micro to macro scale", *Water Research*, vol. 41, pp. 2271-2300, 2007.
- [19]. W. Cai, B. Zhang, Y. Jin, Z. Lei, C. Feng, D. Ding, W. Hua, N. Chen, and T. Suemura, "Behavior of total phosphorus removal in an intelligent controlled sequencing batch biofilm reactor for municipal wastewater treatment," *Bioresource Technology*, vol. 132, pp. 190-196, 2013.

Relationships between EC, pH and SAR with Cations and Anions Related to salinity in Groundwater: a Case Study of Amik Plain

Necat Agca¹

Abstract

In this research, relationships between electrical conductivity (EC), pH and sodium adsorption ratio (SAR) both cations (Na, K, Ca, Mg) and anions (CO₃, HCO₃, SO₄ and Cl) related to salinity in the groundwater of Amik Plain. For this purpose, EC, pH, Na, K, Ca, Mg, CO₃, HCO₃, SO₄ and Cl were determined in a total of 94 groundwater samples. Then SAR values calculated from Na, Ca and Mg values. Afterwards, the relationships between EC, pH, SAR and Na, K, Ca, Mg, CO₃, HCO₃, SO₄ and Cl values were examined by simple and multiple linear regression analyses and regression equations were developed between these data. In the most regression analyses, intercept values and coefficients of regression equations determined between the above mentioned groundwater were found to be significant at 0.01 levels. In some multiple regressions, 95-97% of variation of dependent variable results from independent variables. This has shown that those equations can be used in the application. In other words, once one of these properties is determined, the other property can be calculated using those equations. In Some multiple regressions, 15-25% of variation of dependent variable results from independent variables. These equations cannot be used in the calculations. In addition, according to Anova test results, relationships between variables were found to be statistically significant (p<0.01).

Key words: Groundwater, regression, use of regression equations, groundwater salinity

1. INTRODUCTION

Water is not only the essence of life but also the single most crucial factor determining the quality of people's life. The climate change and increasing disruptions in the rainfall patterns, temperature and soil moisture directly have an impact on water availability and its drinking quality as well as its use for livestock, agriculture and various other purposes [1].

Groundwater is the major source of freshwater in many parts of the world for meeting the demands for domestic and agricultural purposes [2]. Due to the scarcity of surface water in many regions around the world and the rapid increase in the population, there has been a sharp increase in the potable water demand. Groundwater is becoming an important source of drinking water supply. The value of groundwater depends not only on its availability but also on its consistent good quality [3]. Water quality for irrigation can vary greatly depending on the type and quantity of dissolved salts. Salts originate from dissolution or weathering of the rocks and soil, including dissolution of lime, gypsum and other slowly dissolved soil minerals. These salts are carried with the water to wherever it is used. In the case of irrigation, the salts are applied with the water and remain behind in the soil as water evaporates or is used by the crop. The suitability of water for irrigation is determined not only by the total amount of salt present, but also by the type of salt. Various soil and cropping problems develop as the total salt content increases, and special management practices may be required to maintain acceptable crop yields. Water quality or suitability for use is judged on the potential severity of problems that can be expected to develop during long-term use [4]. Linear regression will be conducted to investigate whether or not independent variable predicts dependent variable. When there is a single continuous dependent variable and a single independent variable, the analysis is called a simple linear regression analysis [5]. In this case, the following regression equation will be used:

$$y = a + bx$$

Where, y= estimated dependent variable, a= intercept value, b = regression coefficient and x= independent variable [6].

Multiple linear regression analysis is an extension of simple linear regression analysis, used to assess the association between two or more independent variables and a single continuous dependent variable. The multiple linear regression equation is as follows:

$$y = a + b_1x_1 + b_2x_2 + b_3x_3 + \dots + b_nx_n$$

Where y is the predicted or expected value of the dependent variable, a is intercept value, x₁ through x_n are n distinct independent or predictor variables, and b₁ through b_n are the estimated regression coefficients [5].

The aim of this study is to determine mathematical relationships between electrical conductivity (EC), pH and sodium adsorption ratio (SAR) both cations (Na, K, Ca, Mg) and anions (CO₃, HCO₃, SO₄ and Cl) related to salinity by using single and multiple regression analyses in the groundwater of Amik Plain were determined.

¹Corresponding author: Mustafa Kemal University, Faculty of Agriculture, Department of Soil Science and Plant Nutrition, Antakya/Hatay, Turkey. necagca@gmail.com

2. MATERIAL AND METHODS

In this research, EC, total dissolved solid (TDS) pH, Na, K, Ca, Mg, CO₃, HCO₃, SO₄ Cl and salt content (SC) were determined using routine analyzing methods [7] in a total of 94 groundwater samples taken from Amik plain. Then SAR values calculated from Na, Ca and Mg ions using $SAR = (Na / ((Ca + Mg) / 2))^{1/2}$ [8]. Amik Plain is one of the most important plain in Turkey, located in the southern parts of Turkey and near Syrian border (Figure 1). It is within Hatay province and has an area about 75000 ha.

Afterwards, the mathematical relationships between EC, pH and SAR with Na, K, Ca, Mg, CO₃, HCO₃, SO₄ and Cl values were examined by simple and multiple linear regression analyses and regression equations were developed between these data. All regression analyses were performed using SPSS 17.0. Statistical software.

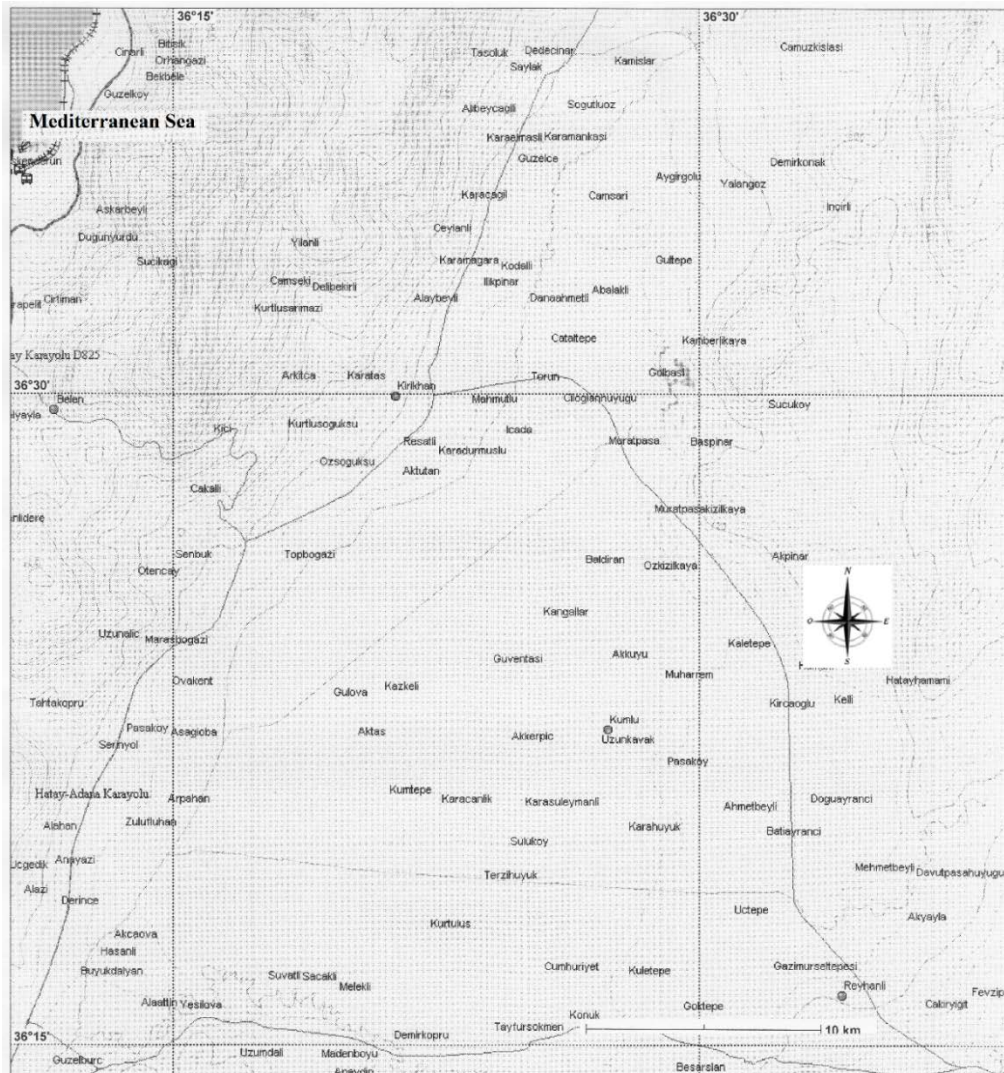


Figure 1. Geographic position of Amik Plain

3. RESULTS AND DISCUSSION

The results of single and multiple regression analyses of groundwater samples were presented in Figure 1 and 2. Linear regression is used to specify the nature of the relation between variables. The model summary part of output is most useful when you are performing regression analyses. R square values in single regression equations changed between 0.081 (relationship between EC with Cl) and 1.000 (relationship between EC with TDS) (Table 1) and changed in multiple regression analyses ranged from 0.157 to 0.976 (Table 2). R square is correlation coefficient square of single or multiple regression equations that tell us

Table 1. Single Regression Equations between EC, SAR and pH with other properties.

R ²	ANOVA		Simple Regression Equations	t	p
	F	p			
0.891	750.0	0.000	EC = 450.50 + 9.17 Na	5.45 (Cons.) 27.4 (Na)	0.000 0.000
0.799	366.80	0.000	EC = 804.15+31.0 Ca	7.86 (Cons.) 19.152 (Ca)	0.000 0.000
0.249	30.478	0.000	EC = -1946.48+48.23 Mg	-2.604 (Cons.) 5.521 (Mg)	0.011 0.000
0.960	2181.7	0.000	EC = -212.94+7.49 TCC	-3.529 (Cons.) 46.709 (TCC)	0.001 0.000
0.844	496.96	0.000	EC = 609.60+6.04 Cl	6.404(Cons.) 22.293(Cl)	0.000 0.000
0.485	86.49	0.000	EC = 492.26+5.38 SO ₄	2.321 (Cons.) 9.300 (SO ₄)	0.023 0.000
0.998	49191.23	0.000	EC = 174.66+177736.0 SC	15.307 (Cons.) 221.791(SC)	0.000 0.000
1.000	2147912	0.000	EC = 5.67+1.536 TDS	3.122 (Cons.) 1465.576 (TDS)	0.002 0.000
0.915	996.08	0.000	SAR = 0.76+0.02 Na	6.386 (Cons.) 31.561(Na)	0.000 0.000
0.343	48.05	0.000	SAR = 2.11+0.03 Ca	6.950 (Cons.) 6.932 (Ca)	0.000 0.000
0.674	190.14	0.000	SAR =0.682+0.002 TDS	2.63 (Cons.) 13.79 (TDS)	0.010 0.000
0.813	399.50	0.000	SAR =0.013+ 0.011TCC	0.061 (Cons.) 19.98 (TCC)	0.952 0.000
0.651	171.46	0.000	SAR = 1.35+0.009 Cl	5.82 (Cons.) 13.09 (Cl)	0.000 0.000
0.380	56.36	0.000	SAR = 1.166+0.008SO ₄	3.06 (Cons.) 7.51 (SO ₄)	0.003 0.000
0.074	7.40	0.008	PH = 7.87+0.00 Na	188.317 (Cons.) -2.720 (Na)	0.000 0.008
0.050	4.89	0.030	PH = 7.93+-0.04 K	112.434 (Cons.) -2.211 (K)	0.000 0.030
0.176	19.71	0.000	PH = 7.89+-0.03 Ca	219.187 (Cons.) -4.439 (Ca)	0.000 0.000

*Cons. = Constant **TCC = Total cation concentration

how strongly the single or multiple independent variable(s) are related to dependent variable. [9]. For example, in the relationship between EC and SAR, 89.1 per cent of variation in EC values results from SAR values (Table 1). On the other hand, in the relationship between pH with Na, K, Ca and Mg, only 25.1 per cent of variation in pH values results from Na, K, Ca and Mg values (Table 2). But, both regression equations, R² values were statistically important also (p<0.001) according to results of Anova tests. In results of Anova tests, F-test gives us to determine whether the model is a good fit for data according to p values [10]. In other words, Anova basically tell us whether the regression equation is explaining a statistically significant portion of the variability in dependent variable from variability in the independent variable(s).

In the single regression equations t values varied between -3.953 and 219.19 (Table 1). All single regression equations were statistically significant at 0.001 level. The t test will be used to determine the significance of constant and regression coefficients in the multi regression equations, t values ranged from -5.65 to 94.78. Regressions between EC, pH and SAR with cations statistically significant at 0.001 level.

Table 2. Multiple Regression Equations between EC, SAR and Ph with other properties.

R2	ANOVA		Multiple Regression Equations	t	p
	F	p			
0.976	1197.6	0.000	EC= -541.3+5.89Na+ 13.21Ca+12.29 Mg	-3.87 (Constant) 23.54 (Na) 14.60 (Ca) 7.05 (Mg)	0.000 0.000 0.000 0.000
0.973	1064.5	0.000	EC= -498.1+ 4.91Cl+ 2.97SO ₄ + 2.45 (CO ₃ +HCO ₃)	-5.65 (Constant) 38.55(Cl) 19.82(SO ₄) 7.01(CO ₃ +HCO ₃)	0.000 0.000 0.000 0.000
0.202	7.56	0.000	pH=8.08+0.000Na - 0.003Ca- 0.003Mg	58.19 (Constant) 0.96(Na) -3.14(Ca) -1.48(Mg)	0.000 0.339 0.002 0.142
0.157	5.57	0.001	pH=8.05+0.000Cl+ 0.000SO ₄ + 0.000 (CO ₃ +HCO ₃)	94.78 (Constant) -2.58(Cl) -0.80(SO ₄) -2.19(CO ₃ +HCO ₃)	0.000 0.012 0.424 0.031
0.974	1144.3	0.000	SAR=1.97+0.020Na -0.019Ca - 0.015Mg	8.41 (Constant) 47.16 (Na) -12.29 (Ca) -5.09 (Mg)	0.000 0.000 0.000 0.000
0.770	100.23	0.000	SAR= - 0.652+ 0.007Cl +0.004SO ₄ + (0.005CO ₃ +HCO ₃)	-1.56 (Constant) 11.52 (Cl) 6.21 (SO ₄) 3.29 (CO ₃ +HCO ₃)	0.123 0.000 0.000 0.000

4. CONCLUSIONS

While all single regression equations have very high t values, the R square values of most of them are very low. Therefore regression equation that have R square values higher than 0.95 can be used in application. In this case, regression equations of EC-TCC, EC-Salt and EC-TDS can be used in application. But, relationships between EC and Na, EC and Cl, and EC and Na may be used because R square values of them are high (>0.800).

In the multiple regression equations, Relationships between EC and SAR with Na, Ca and Mg and EC with Cl, SO₄ and (CO₃+HCO₃) have R square values are higher than 0.95. Therefore these regression equations can be used in application. Assessing only the p values suggests that these three independent variables (Na, Ca and Mg) are equally statistically significant (p<0.001). The magnitude of the t statistics provides a means to judge relative importance of independent variables. For example, in multiple regression equation between EC with Na, Ca and Mg, Na is the most significant independent variable, followed by Ca and Mg.

REFERENCES

- [1]. P. Patel, N.J Raju, B. C. Reddy, S.R.U. Suresh, W. Goss and P. Peter Wycisk, Geochemical processes and multivariate statistical analysis for the assessment of groundwater quality in the Swarnamukhi River basin, Andhra Pradesh, India. *Environ Earth Science*. 75:611. DOI 10.1007/s12665-015-5108-x. 2016.
- [2]. I. Golchin and A.M. Moghaddam, Hydro-geochemical characteristics and groundwater quality assessment in Iranshahr plain aquifer, Iran. *Environ Earth Sci* (2016) 75:317 DOI 10.1007/s12665-015-5077-0. 2016.
- [3]. B. A. Zakhem and R. Hafez, Heavy metal pollution index for groundwater quality assessment in Damascus Oasis, Syria. *Environ Earth Sci* (2015) 73:6591–6600 DOI 10.1007/s12665-014-3882-5. 2015.
- [4]. R.S. Ayers and D.W. Westcot, Water quality for agriculture. FAO irrigation and drainage paper no. 29, rev. 1, 1994.
- [5]. Anonymous 2016 a. Multiple Linear Regression Analysis http://sphweb.bumc.bu.edu/otlt/MPH-Modules/BS/BS704_Multivariable/BS704_Multivariable7.html
- [6]. Anonymous 2013. Statistics solution. Data analysis plan: Linear Regression [WWW Document]. <http://www.statisticssolution.com/academic-solutions/member-resources/member-profile/data-analysis-plan-templates/data-analysis-plan-linear-regression/>
- [7]. M.R. Carter and E.G. Gregorich, Eds, Soil Sampling and methods of analysis. Canadian Society of Soil Science. CRC Press. Taylor and Francis Group. 1224 p. 2008.
- [8]. L.A. Richards, Diagnosis and improvement of saline and alkali soils. US. Dep. Agr. Handbook. 60:147. 1954.
- [9]. Anonymous b, Doing multiple regression with SPSS. http://www.bwgriffin.com/gsu/courses/edur8131/spss/1_regression_b.pdf, 2016
- [10]. Anonymous c. Using SPSS for Linear Regression. <http://academic.udayton.edu/GregElvers/psy216/spss/reg.htm>, 2016.

**Curriculum Vitae**

I was born on April 31, 1962 in Mersin, Turkey. I graduated as Agricultural Engineer from University of Çukurova, Department of Soil Science in Adana in 1983. I obtained my M.Sc. and Ph.D. degrees in science of Soil Chemistry from University of Çukurova in 1985 and 1990, respectively. I worked for University of Çukurova, Adana and University of Harran, Şanlıurfa from 1985 to 1995. I became Assoc. Prof. in 1995 and Professor in 2000. Since 1995, I have been working for Mustafa Kemal University, Faculty of Agriculture, Department of Soil Science and Plant Nutrition in Antakya-Hatay/ Turkey. Soil salinity and alkalinity; soil pollution; water quality and pollution are my main interests' subjects. I have been married and have a daughter and a son.

ANN-based Classification of Sound Signals Using AR Parameters Methods

*Yusuf Gurbuz*¹, Yusuf Uzun¹, A. Afsin Kulaksiz², Huseyin Arikan¹*

Abstract

In this paper, one of our writers 20 "Open" and 20 "Close" the original voice data has been recorded. For classifying artificial neural network (ANN) using Matlab program, have been arranged 10 in training and 10 in testing procedure of this audio data. Have been examined difference periodogram between "Open" and "Close" signals, autoregressive parameters (AR), methods has been classified with ANN. After the classification process was investigated how the training and test data is classified. In the study, some of the data can't be classified and the classification error was seen that higher than expected. Therefore, the audio data have been checked and was seen that corrupt some data. The classification process is reconstructed by distorted audio data is replaced with robust new audio data. As a result of classification is 100% classified all of the data and the classification error has been shown to be very small.

Keywords: artificial neural network, autoregressive parameters, classification

1. INTRODUCTION

1.1 Artificial Neural Network (ANN)

ANN is an experimental method inspired by neural networks contained within the brain and a very popular method used in classification problems. In this study, the back-propagation algorithm was preferred to TANN. The architecture of ANN with one hidden layers indicated in Figure 1. ANN consists of an input, an output and at least one hidden layers that were weighted interconnected with each other. The number of nodes in the input and output layers are determined according to the problems. In this study, the ANN was trained using the binary coded vectors belonging to input features and output classes, as input and output desired dataset respectively. The training process of ANN was continued until the desired output value was reached.

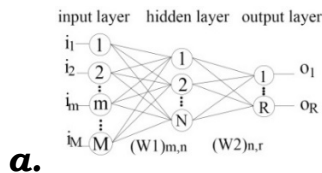


Figure 1 The ANN structure

¹ Corresponding author: Necmettin Erbakan University, Seydişehir Vocational School, Department of Electrical & Automation, 42360, Seydişehir/Konya, Turkey.

ygurbuz@konya.edu.tr

² Selçuk University, Faculty of Engineering, Department of Electrical & Electronic Engineering, Konya, Turkey.

afsin@selcuk.edu.tr

Once training process was completed, two weight vectors were obtained. $W_{1,m,n}$ is the weight vector between input and hidden layers' nodes, and $W_{2,n,r}$ is the weight vector between hidden and output layers. Also sigmoid function was preferred as activation function in hidden and output layers' nodes. Using $W_{1,m,n}$ and $W_{2,n,r}$ weight vectors, the value of the r th output node S_r was provided by;

$$S_r = \left\{ \frac{1}{1 + e^{-\left[\sum_{m=1}^N (W_{1,m,n})_{m,r} + \sum_{n=1}^M (W_{2,n,r})_{m,r} \right]}} \right\} \quad (1)$$

Where M , N and R are the number of input, hidden and output layers' nodes. The nonlinear exponential function, S_r is based on the sigmoid function. The maximum achievable value of this function is 1. Finally, it was required to achieve the input vector that maximizes the function S_r for rules extraction from TANN [1]. The encoded best values were used to obtain a rule of class _{i} ;

$$\text{Max } S_r(i_m) = \left\{ \frac{1}{1 + e^{-\left[\sum_{m=1}^N (W_{1,m,n})_{m,r} + \sum_{n=1}^M (W_{2,n,r})_{m,r} \right]}} \right\} \quad (2)$$

$i_m = 0$ or 1 .

1.2 Autoregressive Models

A time series is a sequence of measurements of the same variable(s) made over time. Usually the measurements are made at evenly spaced times, for example, monthly or yearly. Let us first consider the problem in which we have a y -variable measured as a time series. As an example, we might have y a measure of global temperature, with measurements observed each year. To emphasize that we have measured values over time, we use " t " as a subscript rather than the usual " i ," i.e., y_t means y measured in time period t . An autoregressive model is when a value from a time series is regressed on previous values from that same time series. For example, y_t on y_{t-1}

$$y_t = \beta_0 + \beta_1 y_{t-1} + \varepsilon_t \quad (3)$$

In this regression model, the response variable in the previous time period has become the predictor and the errors have our usual assumptions about errors in a simple linear regression model. The order of an autoregression is the number of immediately preceding values in the series that are used to predict the value at the present time. So, the preceding model is a first-order autoregression, written as AR(1) [2][3].

If we want to predict y this year (y_t) using measurements of global temperature in the previous two years (y_{t-1} , y_{t-2}), then the autoregressive model for doing so would be:

$$y_t = \beta_0 + \beta_1 y_{t-1} + \beta_2 y_{t-2} + \varepsilon_t \quad (4)$$

This model is a second-order autoregression, written as AR(2), since the value at time t is predicted from the values at times $t-1$ and $t-2$. More generally, a_k^{th} order autoregression, written as AR(k), is a multiple linear regression in which the value of the series at any time t is a (linear) function of the values at times $t-1, t-2, \dots, t-k$.

2 FINDINGS AND DISPUTES

2.1 Revealing/Finding/Obtaining The Open and Close Voice Data Signals of PSD With Various methods

20 "Open" and 20 "Close" voice data signals have been recorded. First and second 10 of these data are separated as training data (open_training, close_training) and test data (open_test, close_test) respectively. Sampling frequency is selected as

48KHZ and the number of data in all voice data is adjusted as 18400. One of the open and close voice signal's drawn graphics according to time are taken part in Figure.1a and Figure.1b respectively.

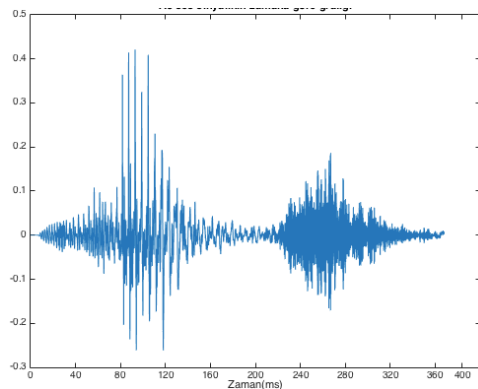
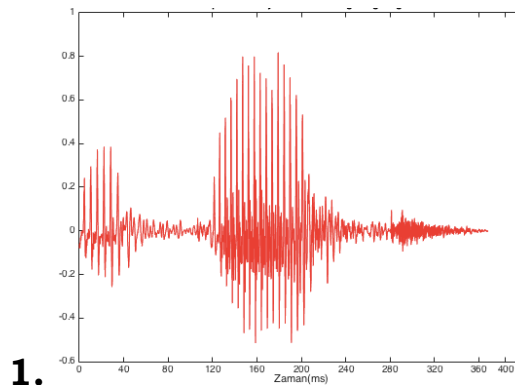


Figure 2. (a) Drawing the Open data signal according to time



1. Figure 2. (b) Drawing the Close data signal according to time

Open and Close voice data signals' graphs of PSD are given in Figure.3a and Figure.3b according to Barlett Method, Because of the fact that frame type is not specified, it is selected rectangle by default.

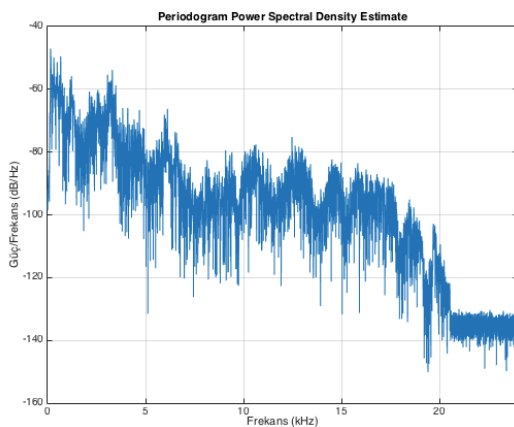


Figure 3. (a) Open Voice Signal's PSD according to Barlett Method

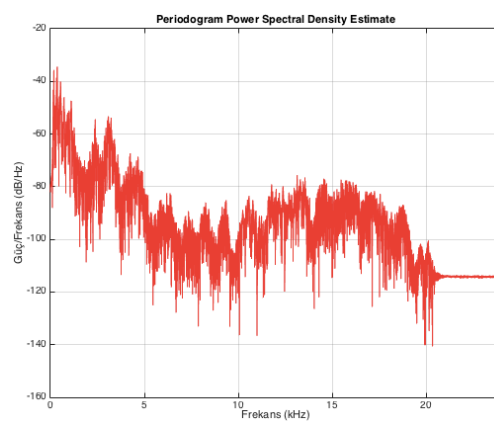


Figure 3. (b) Close Voice Signal's PSD according to Barlett Method

According to Welch method, frame type is Haming and default overlap is %50, Voice signal's PSD is given in Figure-4a and Figure-4b.

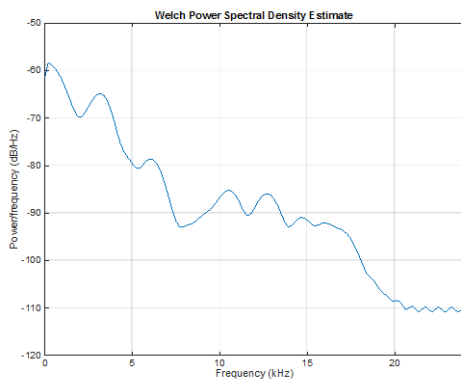


Figure 4. (a) Open Voice Signal's PSD according to Welch Method

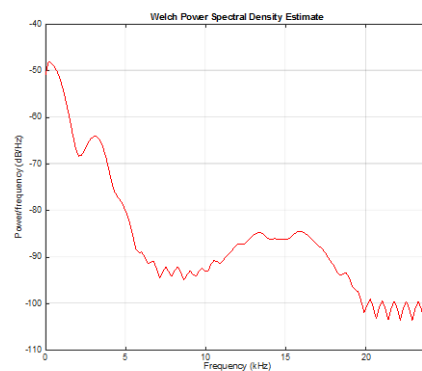


Figure 4. (b) Close Voice Signal's PSD according to Welch Method

Figure.5 shows open and close voice signals' PSD are plotted on the same graph according to Welch Method

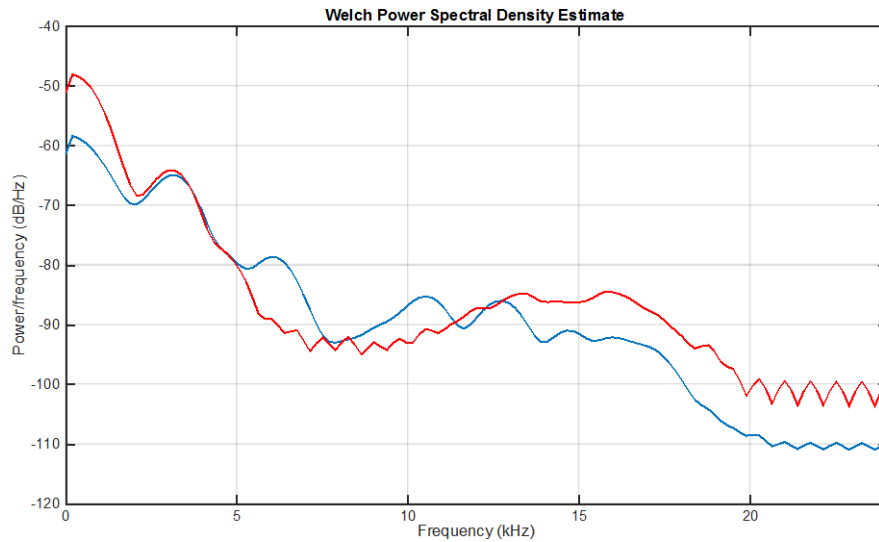


Figure 5. Plotting Open and Close Voice Signals on the same graph

2.2 Extracting Voice Signals' parameters of AR and Classifying with ANN

Firstly Voice Signals' parameters of AR are extracted and classified with ANN. Figure 6 shows voice signals' AR parameters that were found and power spectrum estimation.

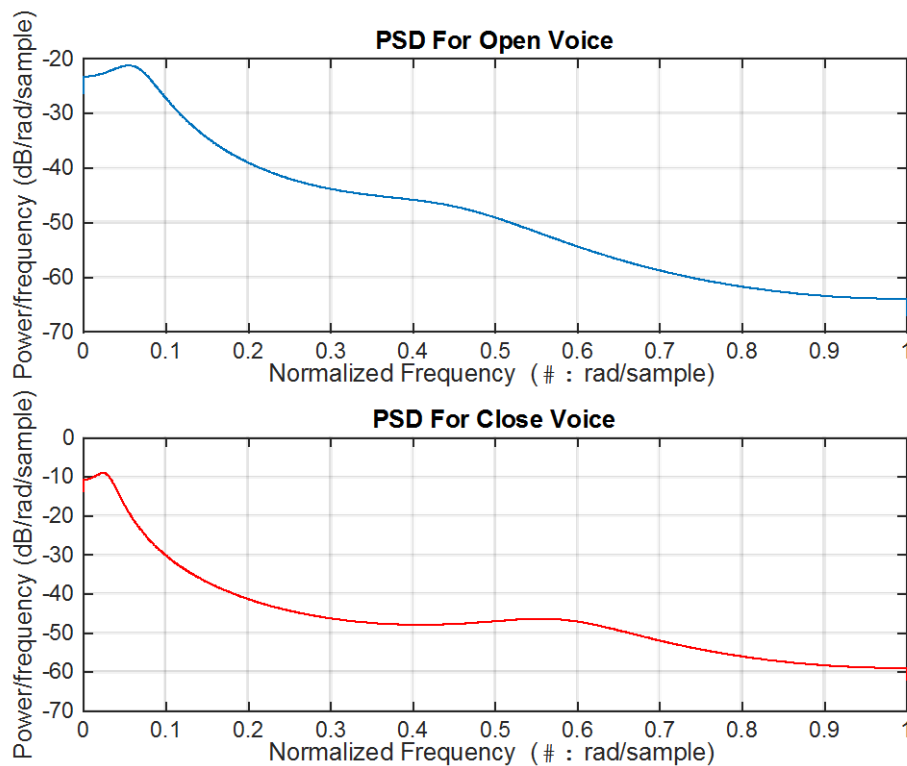


Figure 6. Voice signals' estimation according to AR Parameters

When voice signals are classified according to AR parameters, It is seen that %100 of training data are classified except two of them. The numbers of iteration have been increased from 500 to 3000 but the result has not changed. The graph, which is shown net performance, is given in Figure 7.

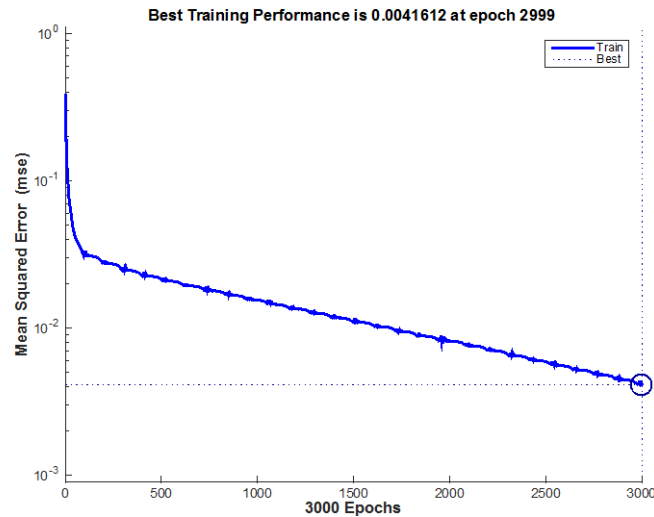


Figure 7. Performance changes, depending on the number of iteration

Whatever the fault is seen as decrease depending on the number of iteration, 10^{-2} is very high as fault value. While one person's open and close voice signals also able to recognize easily with naked eye, it is confusing situation that the signals do not recognize at the rate of %100 with ANN. Therefore, in case there is a problem in voice data, they are checked one by one as following.

```
p=audioplayer(ac_egitim(:,1), 48000);
```

```
play(p);
```

Result of the check, it is seen that second of close_training data, fourth and fifth of open_training data are be corrupt. Saving again, this data have been replaced with corruption data. Afterwards, all procedures have been repeated and realized classification at the rate of %100. Figure.8 shows net performance according to new data.

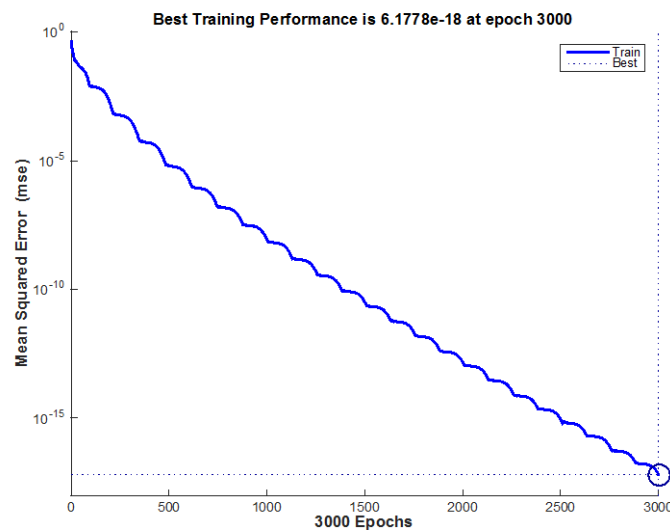


Figure 8. Net performance according to new data

As shown in the graph(Fig8), the fault value decreases depending on the number of iteration.

In previous data, as shown in Figure 7, the fault value decreases depending on the number of iteration but Figure 8 shows that the fault carries on to very small value in new data. It shows that this net's learning performance is improved.

out =(Classifying data of training)

0.0000 0.0000 0.0000 0.0000 0.0000 0.0000 0.0000 0.0000 0.0000 0.0000

1.0000 1.0000 1.0000 1.0000 1.0000 1.0000 1.0000 1.0000 1.0000 1.0000

out_test =(Classifying data of test)

0.0000 0.0000 0.0000 0.0000 0.0000 0.0000 0.0000 0.0000 0.0000 0.0000

1.0000 1.0000 1.0000 1.0000 1.0000 1.0000 1.0000 1.0000 1.0000 1.0000

3 CONCLUSIONS

In this study, have been recorded 20 "Open" and 20 "close" the original audio data. For classifying artificial neural network (ANN) using Matlab program, have been arranged 10 in training and 10 in testing procedure of this audio data. Later, have been examined difference periodogram between "Open" and "Close" signals. Different voices signals belong to same people have been classified using ANN with AR parameter over. After the classification process was investigated how the training and test data is classified. While training data can be 100% classified, no classification of two the test data and classification error was found to be higher than expected. Therefore, the audio data have been checked again and was determined to be broken three of the training data. The corrupted data is replaced by the re-recording robust audio data. Later, has been performed again classification process with the same methods and both the training data and the test data was showed to be 100% of classification process. Furthermore, the classification error is detected to be too low. As a result, in the classification process of test data have been seemed to be a problem. Disturbances in the data used in the educational process affects the whole system and cause the system to malfunction.

REFERENCES

- [1] Elalfi, E., Haque, R., Elalami, M.E., "Extracting Rules from Trained Neural Network Using GA for Managing E-business", Applied Soft Computing, 4, (2004), pp. 65-77.
- [2] (2016) The PSU website [Online] Available : <https://onlinecourses.science.psu.edu/stat501/node/358>
- [3] Haykin, S., "Neural Networks and Learning Machines", Pearson, 3, (2009), pp. 32-34.

BIOGRAPHY



Yusuf GÜRBÜZ has been working as a full-time lecturer at Seydisehir Vocational High School from Konya Necmettin Erbakan University at the Turkey. He received his MSc in Electrical and Electronic Engineer from the Selcuk University of Konya. Also, he received his Ph. D. in Electrical and Electronic Engineer from the Selcuk University of Konya. He has been involved in research and development in the areas of power electronics, electrical machines, new generation led and driver circuits.



Yusuf UZUN has been working as a full-time lecturer at Seydisehir Vocational High School from Konya Necmettin Erbakan University at the Turkey. He received his MSc in Computer Engineer from the Selcuk University of Konya. In his Master Thesis, he extracted rules with the machine learning algorithms and fuzzy logic over the medical data. Also, he received his Ph. D. in Computer Engineer from the Selcuk University of Konya. He has been involved in research and development in the areas of metaheuristic methods, data mining, fuzzy logic and machine learning systems.



Assoc. Prof. Dr. Ahmet Afşin KULAKSIZ has been working as a full-time associate professor at **faculty of engineering department of electrical-electronic engineering program of electrical machines** at the Turkey. He has been involved in research and development in the areas of electrical machines and renewable energy.



Assoc. Prof. Dr. Huseyin ARIKAN was born in KONYA, Turkey, in 1967. He received the B.E. degree in mechanical engineering from the University of Selcuk, Konya, Turkey, in 1989, and the M.S. and Ph.D. degrees in mechanical engineering from the Institute of Science and Technology of University of Selcuk in 1993 and 2002, respectively. Since 2007, he has been with the Department of Mechanical Department, Seydisehir Vocational School, where he was an Assistant Professor. he has been with the Department of Mechanical Engineering, became an Associate Professor in Seydisehir Ahmet Cengiz Engineering Faculty in 2011. His current research interests include Materials science, fracture mechanics, machine design and polymer composites, metal matrix composites and structural analysis. Since 2011, he has been with the Head of Department of Mechanical Engineering, also since 2013, he has been with the Manager of Seydisehir Vocational School.

Computational Modeling of Wave Interaction with Solid Body in a Numerical Wave Tank

Halil Ibrahim Yamac¹, Ahmet Koca²

Abstract

In this paper, computational modeling of wave interactions with solid body is given. The numerical wave tank (NWT) can be considered as the engineering research tool about sea waves that requires the least manpower and material resources. NWT can be used to simulate the motion of ocean and sea waves with modeling moving wall as wave-maker. NWT based on Navier-Stokes (N-S) equations and Volume of Fluid (VOF) method is modeled by using dynamic mesh technique (DMT) to generate regular gravity waves. A solid body is placed into computational fluid domain in the simulation. The wave dissipation induced by solid body and also the field of flow under the effect of waves are simulated. The results of fluid-solid interactions are obtained. The analysis in that study can be used in research of using energy harvesting devices to produce the electrical energy from sea waves.

***Keywords:** Numerical Wave Tank (NWT), Wave-Maker, Volume of Fluid (VOF), Dynamic Mesh, Wave Interactions*

1. INTRODUCTION

The experimental research about waves in sea and ocean is very hard work because of difficulties about environmental effects, and cost of water proof materials or building constructions in water. There is also need of people to work and time to set experimental setup. The numerical wave tank (NWT) can be considered as the engineering research tool about sea waves that requires the least manpower and material resources. NWT can be used to simulate the motion of modeling ocean and sea waves.

There are many researches on the numerical studies about modelling of waves. The models are made for to analyze wave generation theories and different methods [1], also the simulation is made for to see breakwater structure's performance on coasts of ocean and sea [2] [3]. Waves formed on the sea water surface have the potential for source of renewable energy. Wave motions can provides big amounts of kinetic and potential energy that can be converted into electrical power. There also studies on electrical power generation from sea waves [4].

It is seen that the analytic results about harvesting electrical energy from sea waves by using piezoelectric materials. [5-7]. Frequency of pressure change on piezoelectric harvester has a considerable effect on electrical energy generation performance.

2. MATERIAL AND METHODS

In this study, the simulation is made for three different situations: NWT is modelled for validation without any solid body in fluids, vertical and horizontal oriented solids placed in fluid for comparisons of dynamic pressures and their changes at chosen points. The dynamic pressure changes at different points on vertical and horizontal plates which assumed fixed under water surface (near to free surface level) in modeling, only top geometry of fixed body is drawn in 2D NWT. The harvester geometry is assumed fixed to base but the geometry under wave level is not shown to let water movement because of 2D simulation.

2.1 Validation

Momentum source term method can be adopted for wave generation and energy absorption in NWT [2]. Ansys CFD (Computational Fluid Dynamics) program FLUENT module is used to simulate the waves (period, length, height) for monitoring transient wave motion in 2D. There are two phases so VOF (Volume of Fluid Method) mixture method is applied. To get the pressure values at different points accurately, dynamic mesh structure is used while transient calculation. When there is a solid body in water there are turbulence flows in fluid so k-epsilon turbulence model is chosen. UDF (User Defined

¹ Corresponding author: Firat University, Department of Mechatronics Engineering, 23119, Elazığ, Turkey.
halilymc@gmail.com

² Firat University, Department of Mechatronics Engineering, 23119, Elazığ, Turkey.
dr.koca.ahmet@gmail.com

Functions) are programmed in C language to move the wall at left side of tank. The UDF is written under 'DEFINE_CG_MOTION' macro before compiled and added in Fluent Solver. The left side wall is assumed as a piston type wave maker.

The numerical analyze is based on Navier-Stokes Equations these are:

$$\frac{\partial \rho}{\partial t} + \frac{\partial(\rho u)}{\partial x} + \frac{\partial(\rho v)}{\partial y} = 0 \quad (1)$$

$$\frac{\partial(\rho u)}{\partial t} + u \frac{\partial(\rho u)}{\partial x} + v \frac{\partial(\rho v)}{\partial y} = \mu \left(\frac{\partial^2 u}{\partial x^2} + \frac{\partial^2 u}{\partial y^2} \right) - \frac{\partial p}{\partial x} \quad (2)$$

$$\frac{\partial(\rho v)}{\partial t} + u \frac{\partial(\rho v)}{\partial x} + v \frac{\partial(\rho v)}{\partial y} = \mu \left(\frac{\partial^2 v}{\partial x^2} + \frac{\partial^2 v}{\partial y^2} \right) - \frac{\partial p}{\partial y} - \rho g \quad (3)$$

For 2D NWT, x and y position in coordinate system; ρ density of fluid; t time; u horizontal speed component; v vertical speed component; μ turbulent viscosity; g gravitational acceleration.

Figure 1 shows the dimensions of NWT. NWT has a length of 200m, water depth is 16m, and gravitational acceleration is 9.81 m/s^2 . Wave specifications to generate are $L = 53.6 \text{ m}$, $H = 1 \text{ m}$, $T = 6 \text{ s}$. The mesh structure is made as all quadratic and all dimensions of quadric meshes are 0.1 m. The element numbers of mesh is 640000.

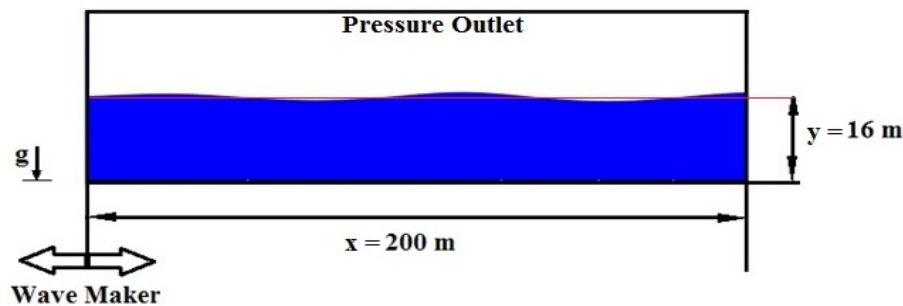


Figure 1. Dimensions and modeling parameters of NWT

Generally, three types of wave-makers can use while wave generation (Flap-type, Piston-type, Hinged-type). In present study the piston type wave maker is modelled as wave-maker. Left side wall of the geometry is moved with UDF code which made by using following equations [8]:

$$\left(\frac{H}{S} \right)_{\text{piston}} = \frac{2(\cosh(k_p h) - 1)}{\sinh(k_p h) + 2k_p h} \quad (4)$$

In the above equation, S ; wave maker's horizontal stroke, H ; wave height, k_p ; wave number, h ; water depth. $k_p = 2\pi / L$, where L is the wavelength. It is possible to determine the equation that controls the movement of the mobile wall with last equation. This motion equation is defined by [9]:

$$X(t) = \frac{S_0}{2} \left(1 - e^{-\frac{t}{T}} \right) \sin(\omega t) \quad (5)$$

In the above equation, S_0 is the maximum displacement of the piston (wave generator), T is the period of the wave and ω is frequency, given by $\omega = 2\pi / T$. In the UDF code the parameter is velocity and it can be calculated from displacement equation that velocity as a derivative function of time [1]:

$$V(t) = \left(\frac{S_0}{2} \right) \left(1 - e^{-\frac{t}{T}} \right) \omega \cos(\omega t) + \frac{S_0}{2T} e^{-\frac{t}{T}} \sin(\omega t) \quad (6)$$

Figure 2 shows the water level changes with time at 20m from left side of the tank; Figure 3 shows the same point and parameters [1] study used for validation. If the figures are compared, our numerical method can be acceptable for this problem.

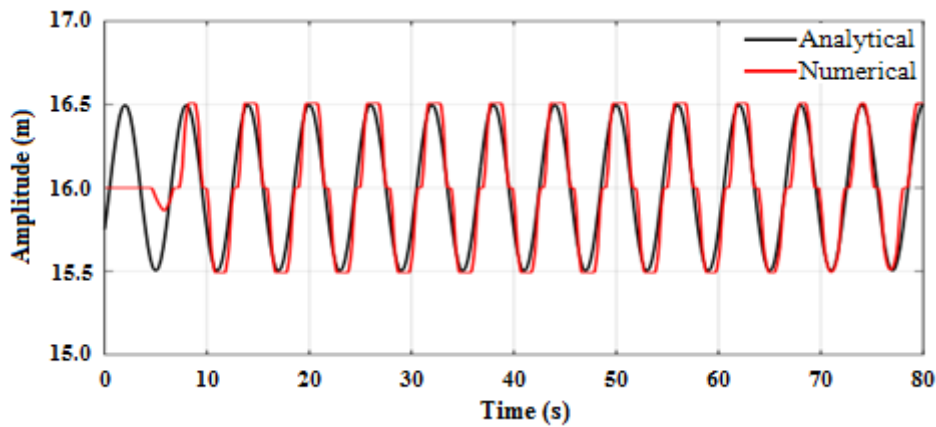


Figure 2. Magnitude of wave for $x=20$ m.

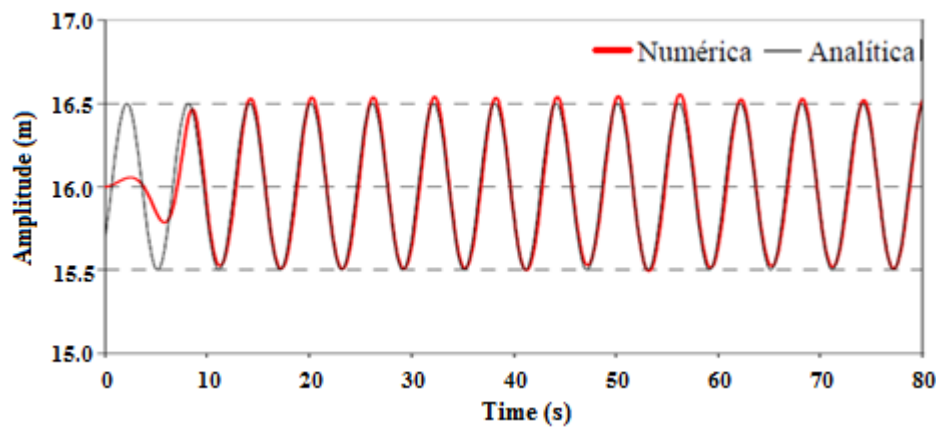


Figure 3. Magnitude of wave for $x=20$ m [1].

VOF method formulation use volume fraction parameter to simulate mixture of two or more phases. In aforementioned simulation there are two phase air and water. Volume fraction value of water is 1 and volume fraction value of air is 0, $0 < \text{volume fraction} < 1$ this situation is used for mixture where occurs between water and air at assumed sea or ocean surface [10]. Figure 4 shows volume fractions of NWT at different chosen times. Red area represents water, blue area represents air. There is a colorful area at free surface water level. The interaction (2.2 and 2.3.) cases are made at the same tank length and water depth.

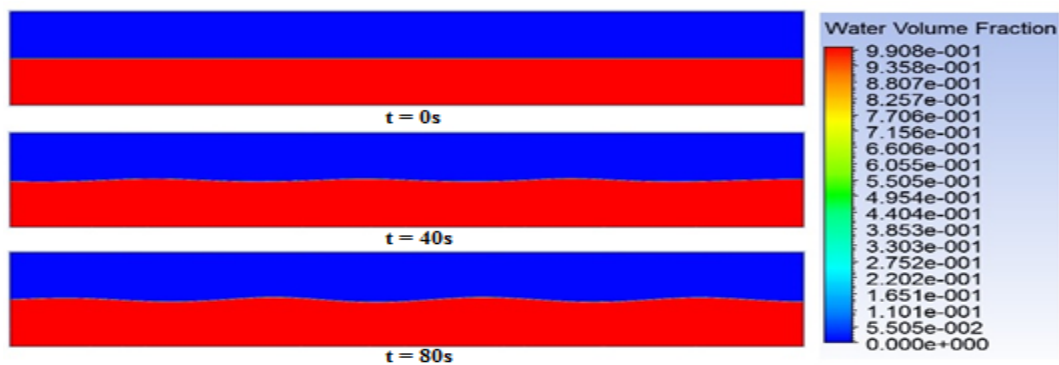


Figure 4. Water volume fraction contours in different times ($t=0s, 40s, 80s$) in NWT

Figure 5 and 6 shows the velocity components contours at $t=80s$.

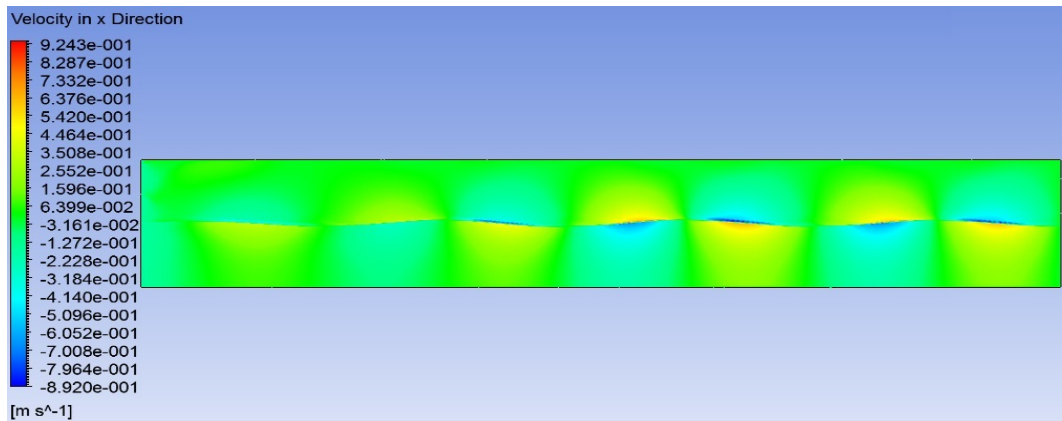


Figure 5. Velocity in x direction as contours in NWT at $t=80s$

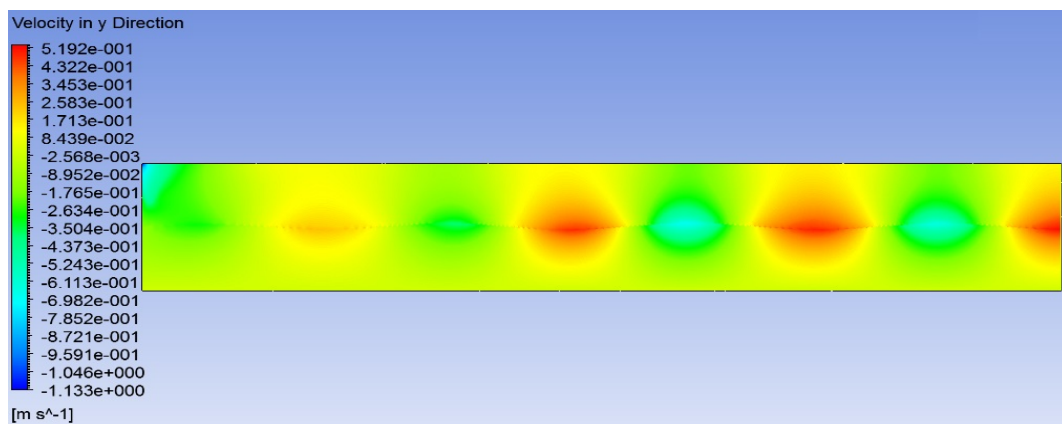


Figure 6. Velocity in y direction as contours in NWT at $t=80s$

2.2 Vertical Plate Case

The place of the solid body in fluid is shown in Figure 7, it is placed 0.2 m under water surface level before wave generation. The left side of solid position in x direction is chosen 20 m from left side of the tank. The length of solid body is 1 m and width is 0.2 m. There are six points on line $x=20$ m and difference from water surface A 0.2 m, B 0.3 m, C 0.5 m, D 0.7 m, E 0.9 m, F 1.1 m. The number of elements in NWT is 638323 while simulation. The orthogonal quality of mesh is 0.999. Simulation is made as transient for 40 seconds.

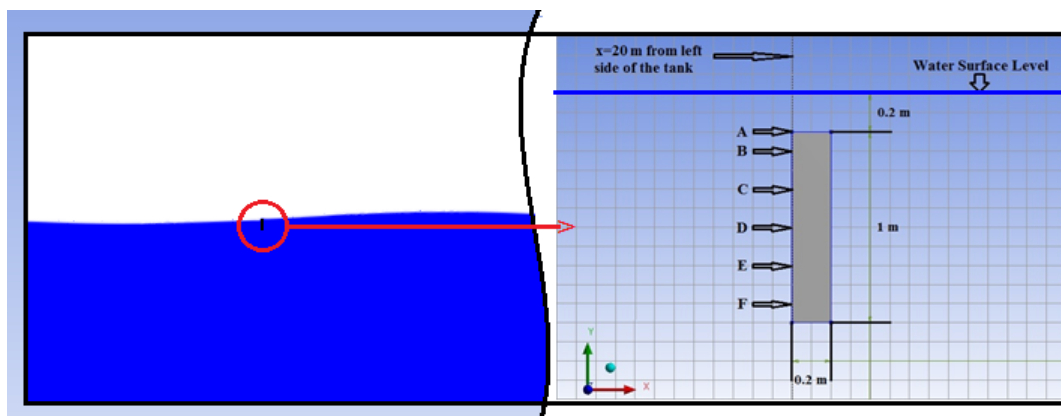


Figure 7. Solid Body positioning in fluid (Vertical)

2.3 Horizontal Plate Case

The place of the solid body in fluid is shown in Figure 8, it is placed 0.2 m under water surface level before wave generation. The left side of solid position is the same as vertical plate case. The geometry of solid body is the same with vertical plate case. The difference of cases is positioning in fluid. 90° plate position change. There are five points on line 0.2 m under water surface if classification is accepted as far from x = 20 m line G 0.1 m, H 0.3 m, I 0.5 m, J 0.7 m, K 0.9 m. The number of elements in NWT is 640039 while simulation. The orthogonal quality of mesh is 0.999. Simulation is made as transient for 40 seconds.

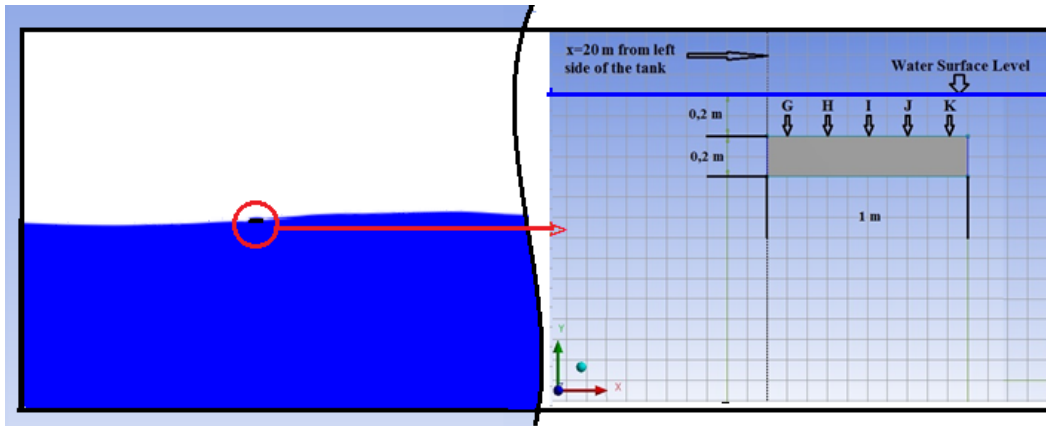
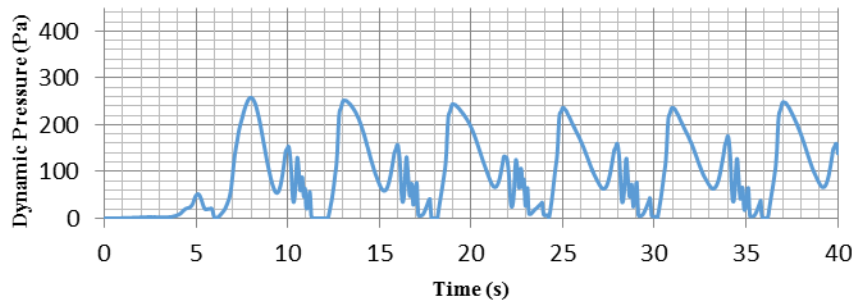


Figure 8. Solid Body positioning in fluid (Horizontal)

3. RESULTS AND DISCUSSION

The dynamic pressure value q are calculated from Ansys Solver by using formulation [10]. There are charts of stated points below. Figure 9-19 show the Dynamic Pressure vs Time values at points. V is velocity magnitude, ρ density of mixture in the cell, ρ_0 is the reference density.

$$q = \frac{\rho - \rho_0}{2} V^2$$



(7)

Figure 9. Dynamic pressure vs time chart at point A

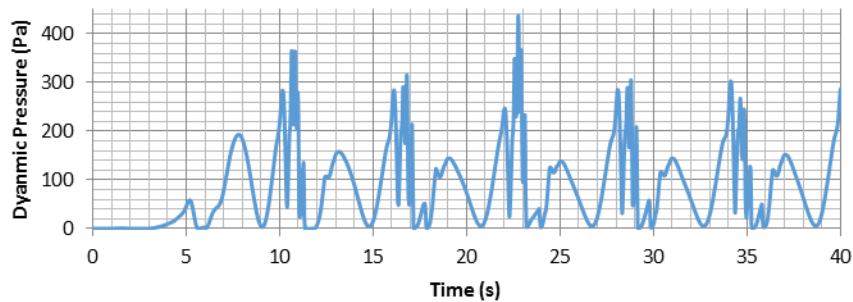


Figure 10. Dynamic pressure vs time chart at point B

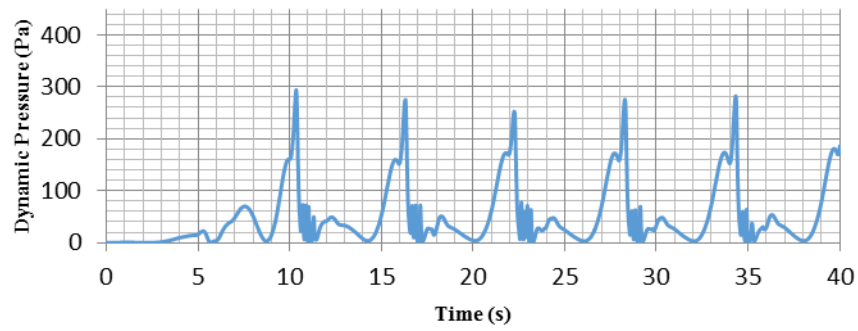


Figure 11. Dynamic pressure vs time chart at point C

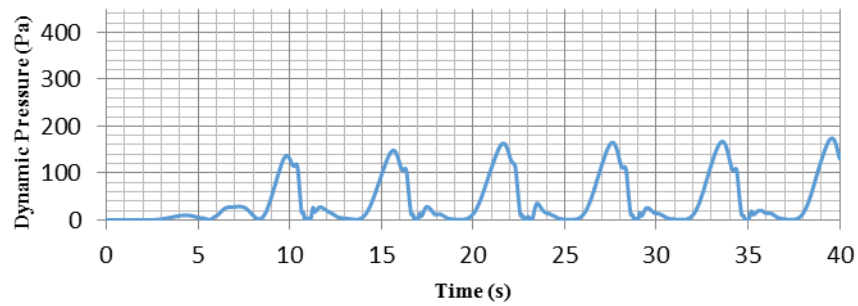


Figure 12. Dynamic pressure vs time chart at point D

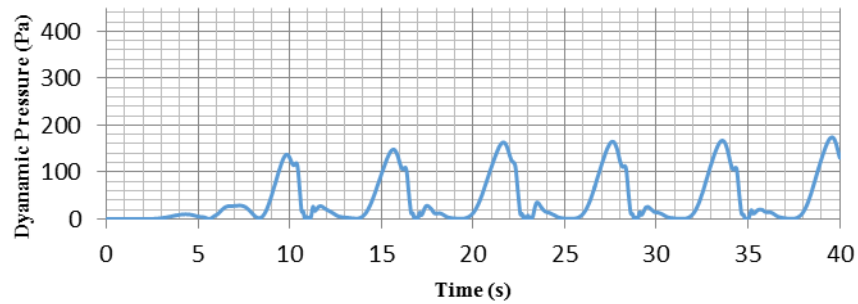


Figure 13. Dynamic pressure vs time chart at point E

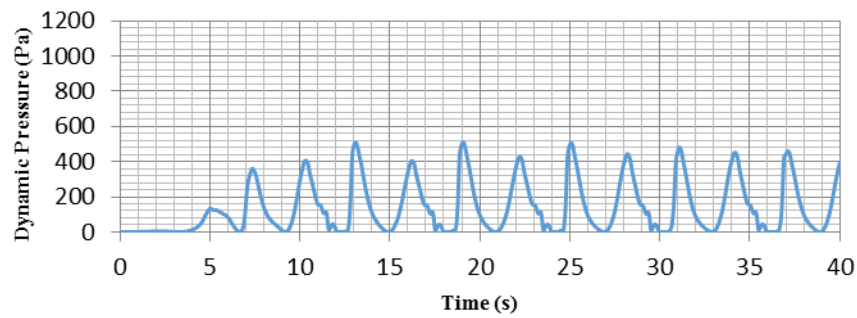


Figure 14. Dynamic pressure vs time chart at point G

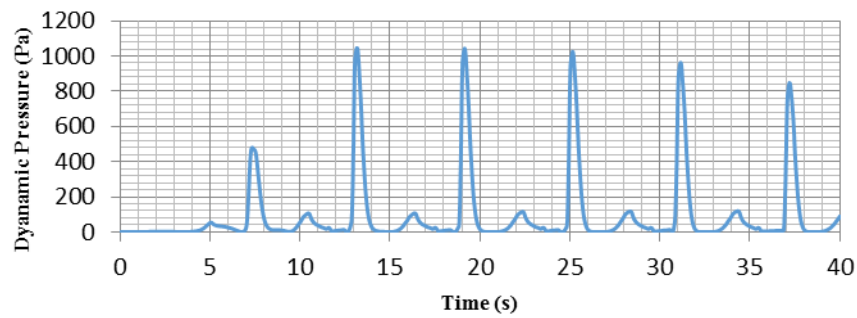


Figure 15. Dynamic pressure vs time chart at point H.

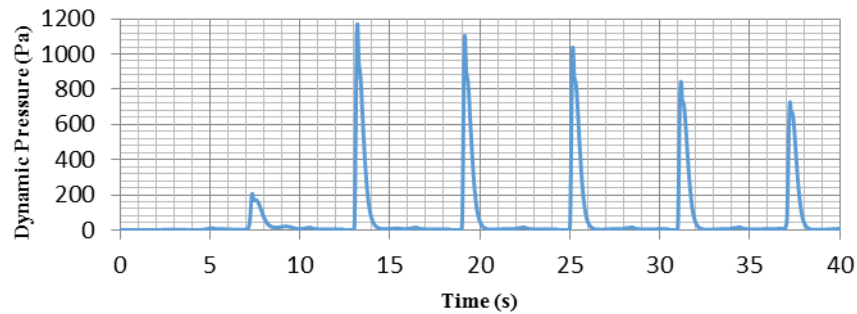


Figure 16. Dynamic pressure vs time chart at point I

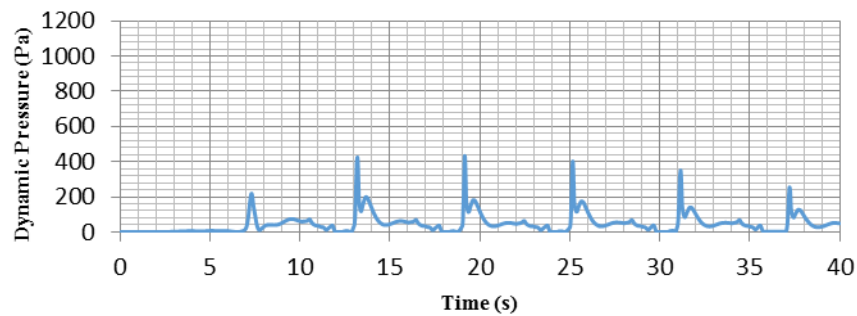


Figure 17. Dynamic pressure vs time chart at point J

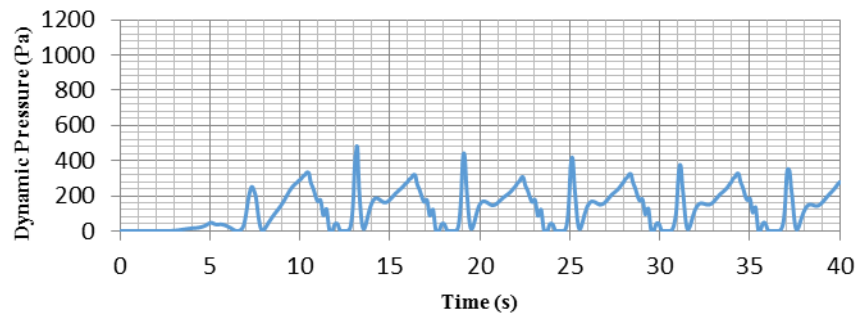


Figure 18. Dynamic pressure vs time chart at point K

Comparison of two different cases shows that horizontal placing has more pique pressures. The pique values in horizontal case reaches the biggest values at points H and I which are at the middle of plate. There is an assumption of rigid fixed body but in reality the two ends of plate move or buckle, if the situation is at real life the similar dynamic pressure values can be get from horizontal solid body's upper surface. Vertical placing shows that points D and E also F have the same behaviour. These points are stay under free surface even it is minimum at y direction. Aforementioned study shows energy harvesters are efficient at place in water where level changes at height of free surface.

CONCLUSIONS

In this study, the dynamic pressures show that wave energy can be converted into electrical power with point energy harvesters. There are some pressure changes and due to these effects the frequency changes with time along wave motion. It means piezoelectric materials can generate electrical power.

As future work, bodies in simulations can be modelled as moving or structures of solid can be deformed by power of waves. The harvesters' specifications can effect on energy generation so these parameters are added and calculated to get accurate value of electrical energy generation.

REFERENCES

- [1] M. N. Gomez, C. R. Olinto, L. A. E. Rocha, J. A. Souza, and L. A. Ísoldi, "Computational modeling of a regular wave tank," *Engenharia Termica (Thermal Engineering)*, vol. 8, pp. 44-50, June 2009.
- [2] Y. Zhu, Y. Li, A. Tao, and J. Zhang, "Numerical modeling of wave interaction with double curtain-wall breakwater," *Proceida Engineering*, vol. 116, pp. 1009-1018, 2015.
- [3] B. Liang, G. Wu, F. Liu, H. Fan, and H. Li, "Numerical study of wave transmission over double submerged breakwaters using non-hydrostatic wave model," *Oceanoglia*, vol. 57, pp. 308-317, July 2015.
- [4] E. B. Agamloh, A. K. Wallace, and A. v. Jouanne, "Application of fluid-structure interaction simulation of an ocean wave energy extraction device," *Renewable Energy*, vol. 33, pp. 748-757, 2008.
- [5] X. D. Xie, Q. Wang, and N. Wu, "Potential of a piezoelectric energy harvester from sea waves," *Journal of Sound and Vibration*, vol. 333, pp. 1421-1429, 2014.
- [6] N. Wu, Q. Wang, and X. D. Xie, "Ocean wave harvesting with a piezoelectric coupled buoy structure," *Applied Ocean Research*, vol. 50, pp. 110-118, 2015.
- [7] X. D. Xie, Q. Wang, and N. Wu, "Energy harvesting from transverse ocean waves by a piezoelectric plate," *International Journal of Engineering Science*, vol. 81, pp. 41-48, 2014.
- [8] R. G. Rean and R. A. Dalrymple, *Water Wave Mechanics for Engineers and Scientist*, P. L-F Liu, Jr, Ed. Singapore, World Scientific, 1991.
- [9] E. Liu, B-S. Hyun, and K-Y Hong, "Application of numerical wave tank to OWC air chamber for wave energy conversion," in *Proc. Eighteenth International Offshore and Polar Engineering Conference*, 2008, p. 305-357.
- [10] ANSYS FLUENT 12.0 Theory Guide, 2009.

BIOGRAPHY

Halil İbrahim Yamaç : He is a Research Assistant in the Department of Mechatronics Engineering at the University of Firat where he has been a faculty member since 2013. His MSc is continuous at Firat University. His research interests lie in the area of mechatronics, renewable energy, computational fluid dynamics.

Landscape Design Principles of University Campuses: A Case Study in Campus of Alaeddin Keykubat, Selcuk University

Ahmet Tugrul Polat¹, Sertac Gungor², Metin Demir³

Abstract

The outside areas on university campuses plays a significant role for the daily campus life and activities. For a comfortable and safe life of the teaching staff, students and other employees, university campuses should be built on the basis of landscape planning and design criteria. This case will also affect the quality of the education system and scientific researches positively. Selcuk University with its 6 institutes, 6 colleges, 22 vocational schools, 1 state conservatory and close to 90,000 students is one of the largest educational institutions in Turkey. Selcuk University Alaeddin Keykubat Campus has been serving nearly 30 years. Due to the process which developed very rapid and unplanned, especially spatial problems emerged. In this study, planning, design, development and sustainability principles for university campus landscapes have been revealed. Also, supporting the regeneration of the Selcuk University campus landscape in terms of aesthetic and functionality was purposed.

***Keywords:** Landscape Design, Landscape Planning, Selcuk University, University Campus*

1. INTRODUCTION

Awareness of environmental issues has been growing within the further and higher education sector during the past decade. University is an institutional organization where young people are oriented for the future. It provides community to have social interaction, cultural, scientific and recreational activity areas for the whole city and its environs. Universities are often the first places to explore new initiatives [1]. Planned development and planned use of the natural resources which is an indispensable requirement of modern life must also be taken into consideration in the foundation of the university campuses [2].

The exterior spaces in the university campuses play an important role in the daily campus life and activities. The construction of the university campuses must be carried out on the basis of landscape planning and design criterion in order to ensure that the members of the teaching staff, students and other employees live comfortably and with security. This situation shall also be reflected positively in the quality of education, teaching and scientific research.

Campus landscape refers to the total complex of physical elements within the campus and evolves as a result of interaction between man, and "nonhuman" nature. It includes not only living plant materials (lawns, trees, shrubs and ground covers) but also all exterior site development such as ground surfaces (paving, concrete) and grading and land forms. Landscape may have a combination of natural surfaces, including ponds, and hard surfaces such as paves, sidewalks or brick patios. Additional to aesthetic and functional aspects of campus landscape design, it has environmental and security aspects that can reduce noise, control dust, divert traffic, secure boundaries, afford privacy and mitigate disaster risks- floods, erosion, snowfalls etc. Every university campus has its own ecological system based on its climate and ecosystem relationship. Differences in climate, sun-shadow patterns, soil, topography and plant selection are fundamental factors that have influence on the size, appearance, and quality of the campus natural environment [3].

The primary objective of campus landscape planning is to make decisions about the use of resources. Campus landscape plans offer land uses and connections between buildings, open spaces, parking and transit, recreational areas, and infrastructure. Campus landscape planning process includes many important activities such as Long Range Development Plans, Campus Master Plans, Campus Landscape Plans, and Environmental Impact Assessments.

Campus Landscape Master Plan provides the overall guidance for landscape projects to assure campus-wide physical and visual coordination. In particular, it defines major landscape principles of the campus design, as well as potential sites for future development. Briefly, a master plan provides a strategy for universities' missions, goals and objectives [1].

¹ Corresponding author: Selcuk University, Faculty of Agriculture, Department of Landscape Architecture, 42075, Kampüs Selçuklu/Konya, Turkey. atpolat@selcuk.edu.tr

² Faculty of Agriculture, Department of Landscape Architecture, 42075, Kampüs Selçuklu/Konya, Turkey.

³ Faculty of Architecture and Design, Department of Landscape Architecture, 25030, Kampüs Erzurum, Turkey.

2. CAMPUS CIRCULATION SYSTEM

A transportation system comprising motor vehicle, bicycle and pedestrian components is made use of in order to ensure the relationships between the various forms of use in the campus as well as their relationships with the city. The circulation system in the campus area must be designed by prioritizing the understanding of the “campus of pedestrians”. A correctly designed circulation system makes it for an individual, who is on-the-move in the campus, to establish communication with the objects around him/her more easily [4].

2.1 Entrances

Besides their general functions, the entrances are important institutional symbols. Aesthetical concerns and cultural forms of expressions are also taken up besides the analysis related to technical specifications in their designs [3]-[5]. The entrance to the campus has a crucial importance as the beginning and dispersion point from the point of view of design. The number of the entrances in a campus area may be more than one depending on the size of the campus. However, as the number of entrances increase security and hierarchical problems begin to appear [6].

2.2 Vehicle roads

Vehicle roads functions as the skeleton in the design of the campus and are the primary component in the configuration of the lay-out. What is first of all important in the transportation through motor vehicles is to ensure more freedom for the pedestrian traffic and let the areas where teaching and research activities are carried out clear of the noise of vehicles. For that reason, transportation by vehicles should meet the needs of the spaces where the academic building are located and areas of public use by passing through their surroundings. On the other hand, when the transportation by vehicles must pass through the academic spaces and areas of public use, attention must be paid to avoid its intersection with the existing pedestrian traffic and to ensure that the pedestrians are not thereby negatively affected [7].

2.3 Pedestrian way

The pedestrian traffic in the campuses is divided into two parts, namely primary and secondary pedestrian connections. The primary pedestrian roads fulfil the function of ensuring transportation at the level of the whole campus. The secondary pedestrian roads on the other hand are the secondary roads connected to the primary roads [7]. The circulation of the pedestrians inside the campus must have an easy access to the interior spaces and other exterior spaces like the squares, reaction areas etc. Pedestrian circulation which must be designed uninterruptedly must be expanded from place to place by means of meeting areas allocated for various activities [8].

2.4 Bicycle track

The use of bicycles is an alternative transportation system that reduces the intensity of vehicle traffic, pollution and problems related to parking lots. It is a recreational activity besides the fact that it provides ease of transportation. Riding bicycle has become a traditional and a well rooted culture in some universities. For example, the universities of Illinois, Minnesota and California [3]. In the campus motor vehicle, pedestrian and bicycle tracks must be designed in an integrated manner.

2.5 Parking lots

Parking lots must be designed either close to the buildings or at the locations that would ensure serving definite groups of buildings depending on the number of vehicles which are planned to be taken into the campus. The parking lots which cover large areas inside the campus must be located on the vehicle roads surrounding the academic buildings and the sites of public use and at the suitable spots of the pedestrian roads that connect those regions and vehicle roads [7]-[9].

3. FUNCTIONAL AREAS INSIDE THE CAMPUS

Universities play an important role in the development of the students not only through educational and teaching programs but also social and cultural activities that they offer. For that reason, areas which would provide the possibility of carrying out different activities must also be taken into consideration together with the settlement of the buildings while designing the campus areas [5].

3.1 Meeting and sitting areas

The design of the university campuses must comprise such units as the sitting areas in which the students may carry out such activities as relaxation outdoors, work, eating and drinking, chat, spending leisure outside the course hours. Sitting areas around the faculty, large green fields, open spaces of cafes and restaurants, shielded sitting units like pergola/camellia and sitting areas which are designed inside the greenery or along the pedestrian roads must be used inside the campus area in order to fulfil those functions [10].

A student needs stop walking maximum after 5 minutes with an average speed of 90 meters /minute. For that reason, facilities like a square, water supply and cafeteria must be available at every 450 meters. Recreation facilities which are provided with such short distances shall ensure the students to be effective in the physical texture of the campus [11].

3.2 Sports areas

Sports areas which are designed for professional or recreational use in the campus are among the areas which are preferred the most by the students. Students and the personnel working in the university evaluate their leisure in these areas and find the opportunity to keep away from routine works in this way [12].

3.3 Squares

The squares which are located in the campuses of the universities are designed around the areas which are used effectively and in which there is an intensive flow of pedestrian traffic all day long. like library, student center, gyms, the vicinity of cafeterias. This makes it possible for the students to use the area more frequently [10].

3.4 Amphitheatre

Outdoor theaters are interesting landscape components from the historical and architectural point of view. In the university campuses amphitheater is used for the purpose of realizing activities such as outdoor activities, graduation ceremonies, theater plays and musical shows, concerts and festivals. It must be located in the sloped parts of the land or in the specially prepared wells taking into consideration its form and features [3]-[5].

3.5 Water element

Water elements are designed for aesthetical purposes in the entrance to the campus, square, sitting areas or in front of the buildings. Besides their visual effects, these water elements have also other effects like refreshing the ambient atmosphere or reducing the level of noise [5]. The water element which is used in the area forms a focus point thanks to its function as an element that complements the space. While the use of water as a moving element creates a dynamic space through its vocal and visual effects while a standing water surface creates a relaxing space [3].

4. MATERIAL USED OUTDOORS IN THE CAMPUS

4.1 Urban furnitures

Campus lighting fulfills such functions as providing the visual perception in the best manner, ensuring the users to feel they are in security, increasing the use of campus at night, protecting the environment, creating light areas, provide guidance to those who are on-the-move and emphasizing the building and other elements in the campus [3].

Waste baskets must be placed near the sitting areas, in the dining areas, on the sites where there is an intense pedestrian traffic in a number that meets the needs of the space in question depending on the intensity of the area used [13].

The use of coordinated marking system in the campus plays an important role not only for ensuring a proper traffic circulation but also for ensuring the visitor and other users of the campus to perceive the space easily. For that reason, the informatory and guidance signboards which are placed in the campus must be in suitable sizes and colours, easily readable and easily visible by the users who come from different angles either as pedestrians or with motor vehicles [3].

4.2 Flooring material

Generally, the flooring material which is used in the pedestrian roads, squares or other sitting areas fulfill functions like accessibility, adding a character to the space, forming a background, establishing a relationship among the elements and providing guidance [14].

The following points of concern regarding the type and specifications of the flooring material come to the fore when the areas which form the campus are evaluated [5]:

Pedestrian ways must be wide enough to enable people to move quickly and ensure the flow of circulation in a short time. For that reason, material like gravel, crushed stone etc. which makes walking difficult must be avoided and the use of the material which can be used for a long time and is not easily affected by external factors must be preferred. Besides it is possible to design more organic roads using different material since there is no intensive flow of pedestrians on the excursion ways which stretches through the green fields in the campus.

On the other hand, flooring material which have different scales, colours and patterns than pedestrian roads must be used in the squares and other sitting areas. These elements must not be slippery, must not bother the eyes and must create a directive effect with its form and patterns.

Material like natural or artificial stone plaques, parquet, brick, asphalt or concrete are used in the vehicle roads. For that reason, factors such as availability, cost, durability, attractiveness, easiness of maintenance, traffic density, security, ability to reflect sound and light must be taken into consideration.

4.3 Sculptures

Artistic objects symbolizing the understanding of culture, development, the characteristic features of the university and the fields of education are used in campus areas. These objects have such functions as forming a focal point, attracting interest and giving a message to the people [5].

Campus Plantation

Either different spaces may be created in the Campus or the non attractive spaces may be concealed by creating horizontal or vertical planes using the plant material of different sorts. Besides, it is possible to use the botanical material in various spaces as a complementary or guiding object or as an object for ensuring unity, emphasizing things or as an object that softens the sharpness of the space caused by its structural forms or as an object for introductory purposes or as a visual element that surrounds the view [14].

The plants add a meaning and identity to the campuses not only with their colours and textures but also by using the same species of plants intensively. Pine trees in Bowdoin College, cactus trees used in the State University of Arizona, palm trees in Miami University and wild apple trees in Colorado Fort Lewis College may be given as examples of the symbolic meaning that the plants grown in a region add to the Campuses [8].

The most obvious vegetation activity within the Campus is the afforestation of roads and paths. The plants which shall be used in the afforestation of the roads must be selected from the species of plants which branches out above, are thorn less and of which fruits don't damage the vehicles, taking into consideration the height of the vehicles [15].

Sustainable And Renewable Forms Of Use Within The Campus

University campuses, as places of science and innovation as well as community grounds, can lead communities by training younger generations via educational programmes and also by being better examples of the implementation of green design principles [1].

Energy consumption produces the most significant environmental impact associated with campus operations. There is a need to operate campus in an energy-efficient manner and to employ conservation measures wherever possible. The energy source used by campus operations and the equipment chosen for campus buildings and landscapes are very important from sustainability stand point [16].

The efforts aiming at reusing the grey water, collection and use of solar energy, renewal of the underground waters and the xeriscape applications that define the form of design that minimizes the use of water are the methods that come to the fore in the design of the sustainable landscape. The energy-effective design of the landscape brings about such benefits like the reduction of CO₂ level, various social benefits, increasing the quality of the public life, reducing and preventing the damage on the ecology-system [17].

A proper settlement which shall be achieved by means of the planning and design of the land shall in most cases be cheaper and much more energy efficient than other solutions for the control of sun rays and protection of energy [18].

One of the components which must be dealt with about water and vegetation is the application of mulch. Mulch is a mixture of organic substances which is used for covering the surface of the soil in order to consummate the missing substances and maintain the desired humidity. Organic and inorganic mulch applications are made in order to form lasting colours and patterns in the landscape. The application of mulch makes a contribution for saving on the use of water by maintaining the balance of humidity of the soil and preventing the drying. The application of mulch reduces water need up to 40 % [19].

Solar powered lighting features, low voltage lights and motion detectors help to conserve energy at campus outdoors. The specially designed solar panels or cells in solar powered lights collect natural sunlight and convert it into electrical power that is stored in highly efficient rechargeable batteries. They have built- in photo sensors so they automatically turn off during the day and turn on at night. Light from solar powered lamps does not require the burning of fossil fuels and the generation of carbon dioxide (CO₂) and pollutants associated with the generation of electricity by a utility. At Cornell University there is a program called "The Solar-Powered Lighting System" which aims to provide a cost-efficient, environmentally friendly alternative to traditional passenger shelter lighting options. In 1996 Solar powered lights were installed in the passenger shelters of the University campus [20].

Management of rain water is one of the hydrological works which come to the foreground in the campuses. Collecting the rain waters through various methods and using it for the irrigation of landscape is one of the methods to which the campuses inside the city recourse especially in order to reduce the use of the urban water network. One of the methods of the collection of rain waters provides an application which creates recreative features in the landscape areas at the same time. In one of the other methods of collection of rain waters, the drainage systems which are set up by making use of the slopes of the land collects the rain water and ensures it to be used effectively [9].

5. SELCUK UNIVERSITY ALAEDDIN KEYKUBAT CAMPUS

5.1 Information about the area

Selcuk University which comprises 21 faculties, 8 institutes, 6 higher education schools, 22 schools of vocational higher education and 1 state conservatory is among the largest educational institutions in Turkey with its more than 70,000 students [21]. Alaeddin Keykubat campus is located on Buzluk site which is within the boundaries of Ardıçlı village on the 20th km of the road to Istanbul [22]. Selcuk University which has been founded in the year 1975 has begun continuing its activities in the campus of Alaeddin Keykubat following the opening of that campus in the year 1989 [23]. The data on Selcuk University and Alaeddin Keykubat Campus are given in the table 1 while its location is shown in figure 1.

Table 4. The data on the Alaeddin Keykubat Campus [22]

Alaeddin Keykubat Kampüsü	
Total campus area	15.400.000 m ²
The campus area currently in use	4.900.000 m ²
The Indoor area	590.000 m ²
The number of students	81.000
The recreation area	225.000 m ²
The parking lots area	120.000 m ²
The number of academic staff	2.120
The number of staff	780

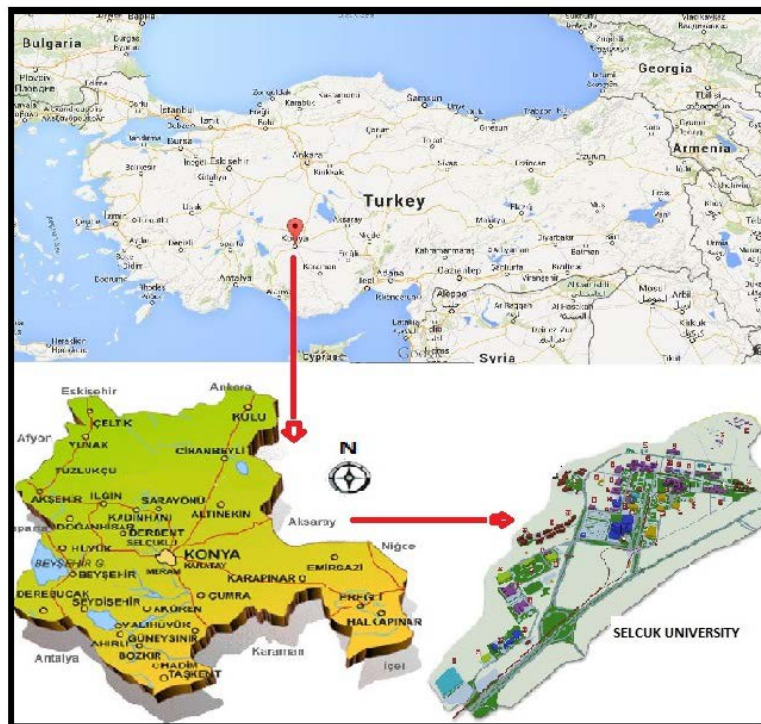


Figure 2. The campus location

5.2 Circulation system

The circulation system of Selcuk University is formed by vehicle roads, tramway and pedestrian ways (Figure 2). The Campus has one main entrance gate and 4 secondary entrance gates. The bicycle road of the city reaches the main entrance of the campus but it ends at a short distance inside the campus. Parking lots have been designed near the architectural structures. The vehicle roads and pedestrian roads frequently intersect in the circulation system inside the Campus and this leads to problems regarding the traffic security. The new vehicle road which has been opened around the Campus has carried the vehicle traffic outside of the Campus center. However, the interconnections from that road to the buildings could not have been established yet. Since the tramway line makes round trip at the center of the Campus it has a negative impact on the vehicle and pedestrian traffic and causes negative images to appear in visual terms.

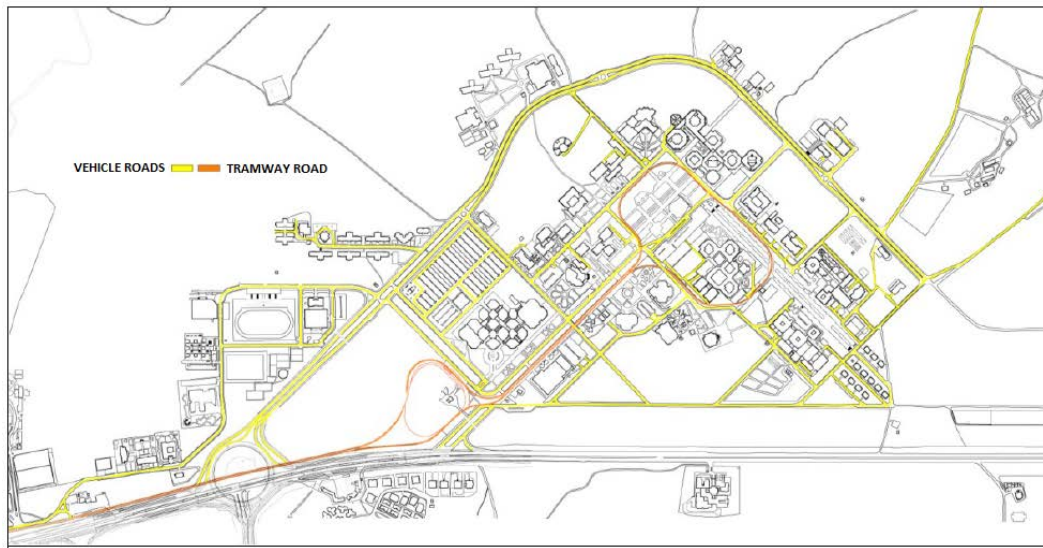


Figure 2. The circulation system of vehicle-tramway [22]

5.3 Functional areas

The number of open areas, in which the students can meet together, are limited (Figure 1). There are no open spaces which can serve the whole of the Campus. Besides smaller sitting areas, which the students can use during the pauses and leisure must be created around the faculty buildings. This need is generally met through the benches which are placed in front of the buildings.

Basketball court, tennis court and football pitch are the sports areas that are available in the Campus (Figure 3). However, their spatial distribution inside the Campus is not functional. These sports areas are located near the Faculty of Physical Training and Sports. There is an amphitheatre on the South of the Campus. There is an amphitheatre south of the campus. However, this structure has not been maintained properly for a long time and consequently is not used at the present time. Types of use containing the water element are very few at the entrance of the Campus. There are ornamental pools at the campus entrance and near some of the faculty buildings. These pools are small-scale and equipped with ejectors and cascades. There are numerous fountains inside the campus.

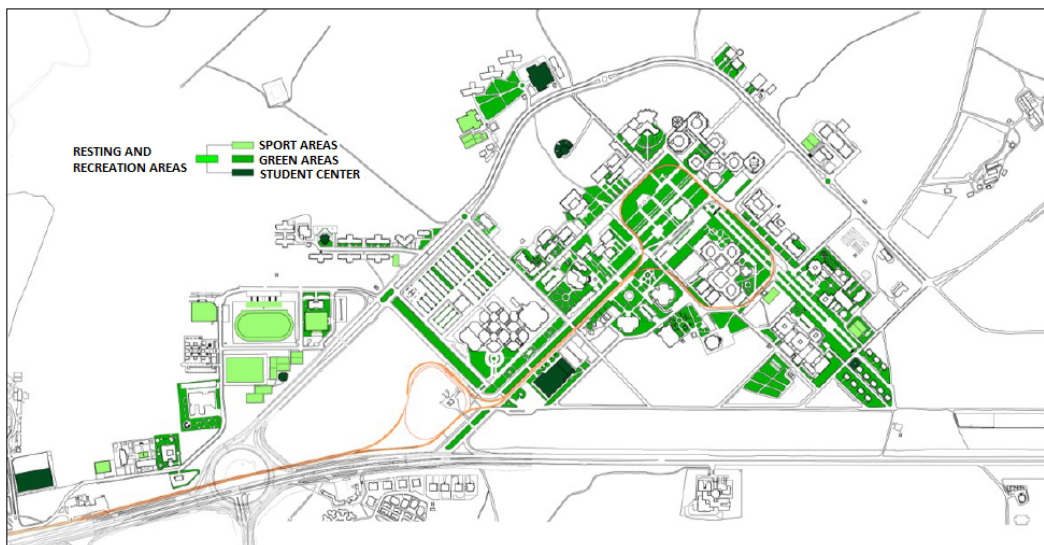


Figure 3. The resting and recreation areas [22]

5.4 Material which is used outdoors

There are outfits like benches, waste basket, lighting fixtures, arbor, pergola, stops, king posts etc. inside the Campus. However, there is a large variety of them and this leads to problems regarding their distribution, use and maintenance in the area. Interlocking paving Stone has been used as the flooring material to a great extent on the vehicle and pedestrian roads of the Campus. Collapses arising from the ground stabilisation have appeared. However, the said flooring material provides

easiness regarding the infrastructural problems since it is renewable and has a drainage function. It is disliked visually. There are sculptures symbolizing the history and culture of the region in the Campus area.

5.5 Plantation

The surrounding of the campus has been vegetated in the form of a belt. Coppice forests containing pine (*Pinus nigra*) and cedar (*Cedrus libani*) trees have been set up. The surrounding of the buildings and parking lots have been afforested. Pedestrian and vehicle roads have been vegetated in the form of a boulevard. Some of the trees that have been used are: white birch (*Acer negundo*), horse chestnut (*Aesculus hippocastanum*), linden (*Tilia tomentosa*), sycamore (*Platanus orientalis*) etc.

5.6 Sustainable forms of use

The sustainable forms of use are almost none inside the Campus. Among a few of them are the lighting fixtures which collect and use solar energy, an equipment that ensures the recycling of the waste plant pieces, which are available in the landscape and afforestation unit, after grinding them and laying coloured gravel as an alternative to grass.

CONCLUSION

The lay-outs and designs of the campus areas must be prepared within the framework of the master plan. These master plans must be prepared by the commissions of which members are the specialists of the disciplines of space design, representatives of the user groups, municipalities, non-governmental organizations, sociologists and educators. Master plans must be revised and renewed in the future depending on the state of development of the Campus and the functions of the producers.

The suggestions for the Alaeddin Keykubat Campus of Selcuk University;

- If the tramway line is designed together with the vehicle road that passes through the surrounding of the campus, the negative conditions related to security and aesthetics may be corrected,
- A large center line must be formed which is pedestrianized beginning from the previous entrance of the campus and stretching towards the North and the circulation of the pedestrians must be distributed from that center line,
- Riding bicycle must be encouraged by forming a circulation of bicycle road inside the campus,
- Visual quality must be increased by concealing the parking lots through plants,
- It must be ensured that the students meet together by forming several main open spaces which are located on or near the general center line and can address to the Campus in general,
- Small meeting areas must be formed around the faculty buildings using the outfits,
- The need for meeting areas must be met by forming open, flat and large grass areas inside the campus,
- The campus must be put into a usable form by renovating the amphitheatre,
- A large water surface must be set up like an artificial lake in the campus and recreational activities must be developed in connection with it,
- Outfit elements and flooring material must be specially designed and must add character and identity to the campus of Selcuk University,
- The means of providing maintenance services for the plants in the Campus area must be increased and the incorrect plantations must be corrected,
- Uses aiming at an energy-effective protection must be rapidly put into operation.

REFERENCES

- [1] G. Tuna, *Assessing Green Design Approach to Develop a Conceptual Model for Landscape Planning in University Campuses*, Istanbul Technical University, Institute of Science and Technology, Department of Urban and Regional Planning (Landscape Planning), M.Sc. Thesis, 2006.
- [2] A. Baytorun, *Açılış Konuşmaları*, II. Ulusal Üniversite Yerleşke Planlaması ve Çevre Düzenlemesi Çalıştayı, 9–10 Haziran 2005, Kahramanmaraş: 2005.
- [3] R.P., *Dober. Campus Landscape Functions, Forms, Features*, John Wiley & Sons, Inc, US. 2000.
- [4] F. Subasıoğlu, *Üniversite Kampuslarının Çevre Tasarımı Açısından İncelenmesi ve Kentsel Donatımları*, Yüksek Lisans Tezi, HÜ, SBE, Ankara:1991.
- [5] G. Ayvacı, *A Research on The Determination of the User Requirements in Open Spaces Design For University Campuses*, ITU, Institute of Science and Technology, Landscape Architecture, M.Sc. Thesis, 2009.
- [6] A.,D. Tetik, *Üniversite Kampüsleri Tasarım Kriterlerinin Türkiye'de 2006 Sonrası Yeni Kurulan Devlet Üniversitelerinde İrdelenmesi*, Gazi Üniversitesi, Fen Bilimleri Enstitüsü, Mimarlık Anabilim Dalı, Yüksek Lisans Tezi, 2013.
- [7] M.N., Türeyan, *Yükseköğretim Yapıları – Kampus*, Tasarım Yayın Grubu, İstanbul. 2002.
- [8] S. Öner, *Kütahya Dumlupınar Üniversitesi Merkez Kampus Alanı Peyzaj Planlaması*, Yüksek Lisans Tezi, AÜ, FBE, Ankara: 1999.

- [9] S.,H. Açııkay, *Explicating Urban University Campuses According To Ecological Landscape Design Principles*, Istanbul Technical University, Institute of Science and Technology, Department of Landscape Architecture, M.Sc. Thesis, 2015.
- [10] C. Marcus, C. Francis, *People places: Design Guidelines for Urban Open Spaces*, Van Nostrand Reinhold, New York: 1990.
- [11] R. Zengel, *Kampüs planlamasında ulaşılabilirlik ölçütü açısından bir yaklaşım*, Yapı Dergisi, 252, 64-67, 2002.
- [12] H. Agan, *Design Criteria of in-campus Sport Facilities with Reference to World University Sports Competitions a Case Study in IZTECH Campus*, Master Thesis, 2000.
- [13] A. Nuhoglu, *Ülkemizde Bazı Üniversite Kampüslerinin Peyzaj Mimarlığı Açısından İrdelenmesi Üzerine Bir Arastırma*, Yüksek Lisans Tezi, AÜ, FBE, Ankara: 1989.
- [14] N.K. Booth, *Basic Element of Landscape Architectural Design*, Waveland Press, Inc., USA. 1990.
- [15] M.B. Tolon, *Üniversite Kampüsleri Dış Mekan Tasarım İlkeleri ve Ankara Üniversitesi Gölbaşı Kampüsü Peyzaj Tasarımı*, Yüksek Lisans Tezi, AÜ, FBE, Ankara: 2006.
- [16] W. Simpson, *Energy Sustainability and the Green Campus, Planning for Higher Education*, 31(3),150-158, 2003.
- [17] L. Seabrook, C.A. M.E. Mcalpine, Bowen, *Restore, repair or reinvent: options for sustainable landscapes in a changing climate. Landscape and Urban Planning*, Sayı 100, Sf. 407-410, 2011.
- [18] E. Sert, *Rain Water in The Energy Efficient Urban Landscape Design*, Istanbul Technical University, Institute of Science and Technology, Department of Landscape Architecture, M.Sc. Thesis, 2013.
- [19] K. Yeang, *Ecodesign, A Manual for Ecological Design*. John Wiley & Sons, Inc., ISBN: 983-2726-40-9. 2006.
- [20] Anonimous^a, Cornell University, *Solar-Powered Lighting, Energy and Climate Change*, 2005.
- [21] Anonimous^b, *Selçuk Üniversitesi Web sayfası* (<http://www.selcuk.edu.tr/>) 2016.
- [22] Z. Kuyrukçu, *Kampüslerde Fiziksel Değişim Üzerine Bir Arastırma: Selçuk Üniversitesi Alaeddin Keykubat Kampüsü Örneği*, Selçuk Üniversitesi, Fen Bilimleri Enstitüsü, Mimarlık Anabilim Dalı, Yüksek Lisans Tezi, 2012.
- [23] H. Gökbel, Y. Semiz, A. Çelik, *Çift Başlı Kartalın Kanatları Altında Selçuk Üniversitesinin 40 Yılı*, Selçuk Üniversitesi Basım Evi, ISBN 978-975-448-207-2 Konya: 2015.

Investigation of SIFT, SURF, and GPU-SURF Algorithm for Feature Detection

*Zafer Guler**¹, *Ahmet Cinar*¹ *Erdal Özbay*¹,

Abstract

Automatic, accurate and robust feature detection is critical task in image matching and processing. This paper compares the three different feature detection algorithms in terms of execution time, feature size and matching size for image matching and processing application. These methods are Scale Invariant Feature Transform (SIFT), Speed up Robust Features (SURF) and Graphics Processing Unit (GPU) based SURF.

We use ETH Zürich object dataset which is being accepted in academic's area for all the experiments of the feature detection methods. At first, for 53 object image SIFT algorithm has found 220 features on average. However, SURF and GPU-SURF algorithms have found only 100 and 82 features respectively. After feature matching we have achieved in average 31 features for SIFT 13 features for SURF and 10 features for GPU-SURF algorithm for 53 objects. Experiments show that, in most situation SIFT algorithm is more stable than other methods. These results show SIFT's stability but it is slow because of computational cost. For execution time, GPU based SURF algorithm 2.5 – 3.5 times faster than SURF algorithm and 8 – 9 times faster than SIFT algorithm. Applications are implemented on a machine equipped with an Intel Core i7-3770 CPU at 8GB RAM and a GeForce GTX 660 Ti GPU which is has 7 streaming multiprocessor (SM) and each SM has 192 CUDA processor. As a future work, the authors are planning to make mentioned three methods on real time or half real time video images.

Keywords: *Feature Detection, GPU-SURF, SIFT, SURF*

1. INTRODUCTION

Feature detection and image matching are used widely in computer vision. Nowadays, feature detection and image matching, are used in many areas such as object tracking, image retrieval and image registration. [1] Despite the many methods available in the literature, there is no universally accepted methods for feature detection and image matching. For example, one method is successful for some situation, but there are also cases that, they are fail. Some of these parameters are given below. [2]

- Scale
- Occlusion
- Orientation
- Cluster
- Illumination

Feature detection first performed in 1998 by Harris and Stephens [3]. This algorithm was later named as Harris Corner Detection. Thanks to the popularity of Harris Corner Detection, lots of corner detection algorithm published in 1990s [4, 5]. In 1997 Fast algorithm has published by Trajkovic and Hedley [6]. The objective of the Fast algorithm is to find corner with less computational cost. In 2004 Scale Invariant Feature Transform (SIFT) has published by Lowe to find distinctive invariant features [7]. But SIFT algorithm works relatively slow. For solving this problem PCA-SIFT algorithm was proposed in 2004 by Ke and Sukthankar [8]. PCA-SIFT speedier then SIFT but, SIFT more distinctive then PCA-SIFT [2]. Speed-Up Robust Feature Detector (SURF) was proposed in 2008 by Bay et. al [9]. The SURF algorithm distinctive as SIFT and fast as PCA-SIFT [2]. With the expansion of GPU technology, GPU version of SIFT and SURF algorithm were developed.

Multiprocessor structures are used in both industrial and academic research. Some of the difficulties and problems can be solved quickly with these structures. Nowadays, many problems can be implemented easily with multiprocessor structures. [10]

Graphics processor unit (GPU) to be used for general purpose applications is not an approach that emerged in recent years, but in 2007, with the development of the CUDA architecture, it is expanded rapidly. The CUDA architecture provides to execute general purpose application without the graphics knowledge. GPU-based applications are used not only in the scientific field, but also in other fields that require high performance such as, image and video processing, fluid dynamics simulation [11]. Therefore detecting and tracking moving object for real time application, parallel architecture must be used. [10]

In this work, we compare performance of SIFT, SURF and GPU based SURF algorithm. For GPU based SURF algorithm we use NVIDIA CUDA Architecture for GPU implementation [10].

¹ *Firat University, Department of Software Engineering, 23119, Elazig, Turkey, zaferguler@firat.edu.tr

The remaining of paper is organized as follow: section 2 provide brief description of SIFT and SURF algorithm. Also provides information on the new generation of GPU and description of GPU-SURF algorithm. Section 3 shows the implementation details and experiment result. The last section is conclusion and further work.

2. OVERVIEW OF METHODS

2.1 SIFT and SURF Algorithm

SIFT algorithm can be adopted successfully many computer vision algorithm such as object detection and tracking and robotic mapping. SIFT algorithm achieves very good results against scaling and rotation invariance. But it requires high computing capacity therefore, sift algorithm cannot be achieved sufficient speed in real-time system [2]. SIFT algorithm basically composes of four stages [7, 12].

Stage-1: Scale space extreme detection: Scale space is formed by applying the Gaussian filter of images in different scales and defined as a function $L(x,y,\sigma)$. This function calculated from the convolution of Gaussian $G(x,y,\sigma)$ and input image $I(x,y)$ [7]. To increase the application speed SIFT uses difference of Gaussian (DOG) instead of Gaussian. Convolved image ($D(x,y,\sigma)$), can be computed with the equation (1). After these operations candidate interest points are selected as the minimum and maximum of DOG [7].

$$D(x,y,\sigma) = (G(x,y,k\sigma) - G(x,y,\sigma)) * I(x,y) \quad (1)$$

where k is a constant factor and $*$ is a convolution operation.

Stage-2: Update location: The location information of each candidate is updated by the color values using the neighboring pixels [13].

Stage-3: Keypoint refinement and filtering: Low contrast Candidates and Candidates along edge are eliminated [13].

Stage-4: Keypoint descriptor calculation: gradient calculated for each of the remaining interesting point [13].

SIFT algorithm detects a greater number of interest points compared to other methods. The reason for this is to calculate the interesting points with different scales and different resolutions. As a result, the SIFT algorithm generates more interesting points and also it is more resident to image deformations [1].

SIFT algorithm can detect interesting point successfully, but for real time application it was comparatively slow. For that reason, SURF algorithm was introduced by Bay, H., Tuytelaars, T. and Van Gool, L. SURF algorithm inspired by SIFT algorithm and can be used for object recognition, classification, registration, etc. [12].

The SURF algorithm has same step as SIFT, but the implementation details in each steps are different. For scale space extreme detection SURF algorithm uses box filter to approximate difference of Gaussian. Box filter can easily compute from integral images, thus algorithm speed increases. SURF uses determinant of the Hessian Matrix to detect interest points. Thus, scale space builds with varies filter size and same image size. Furthermore, SURF uses wavelet response for orientation assignment and feature description. As a conclusion, with SURF algorithm a lot of feature improved. Same studies shows that SURF Algorithm 3 times faster than SIFT Algorithms with a comparative detection performance [1, 2, 9, 12].

2.2 GPGPU Architecture

Graphics processors are rapidly developed and become available for general purpose applications. Thus it has become to use in many areas to improve the speed of application. CUDA architecture developed by NVIDIA company and this architecture allows high increase in computing performance. In fact, this performance difference is due to the fact that, the GPU architecture designed for parallel operations. GPU has a large number of arithmetic logic unit (ALU), but its cache memory is low [10, 11]. GPUs execute a large number of threads on a set of data at the same time. Therefore, it is only appropriate for parallel data. Thus the successful result can be obtained. For example if a program contains many flow control, its calculation speed may be reduce rather than increase [10, 14].

A CUDA C programming language introduces a small number of extensions to C language and allows us to define C function called kernel. With kernel we can define and execute N function in parallel. When kernel calls, unique threadId is available. Thus, with the Id number we can determine which thread is currently running within the kernel. Threads are organized in blocks. In the same as thread, blocks have an identification number. So that which block and which thread actually running, can be easily determined in large data sets. But the number of thread in the block is limited. Current GPUs are supported up to 1024 thread. Threads and blocks can be one, two or three dimensional. Blocks are organized in grids [10, 15].

CUDA architecture supports many memory types. Threads, blocks and type of memory are illustrated in figure 1. Each thread access registers, local memory, shared memory, constant memory and global memory. The CPU part of the application can be access global memory and constant memory [15].

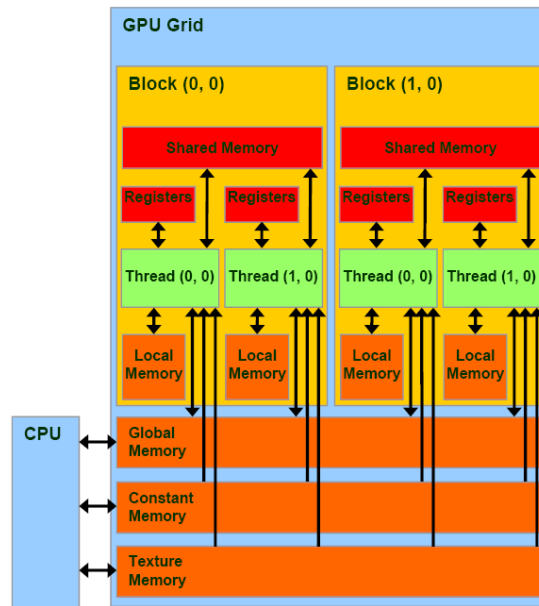


Figure 1. GPU hardware architecture and memory types [11].

The remaining of paper is organized as follow; section 3 provide brief description of SIFT and SURF algorithm. Also provides information on the new generation of GPU and description of GPU-SURF algorithm. Section 4 shows the implementation details, experimental results and discussion. The last section is conclusion and further work.

3 EXPERIMENT RESULTS

In this section we present experimental results obtained by the implemented application. All experiments were performed on a machine equipped with an Intel Core i7-3770 CPU at 8GB RAM and a GeForce GTX 660 Ti GPU. GPU has 7 streaming multiprocessor (SM) and each SM has 192 CUDA processor. This means 1344 computing core per chip. The number of register per multiprocessor is 65536, the total amount of constant memory is 64KB. The amount of shared memory per multiprocessor is 48KB, organized into 32 banks. The 2GB amount of global memory is reached through a GGDR5 interface. The architecture supports the double precision floating point arithmetic.

In this study, we compare standard SIFT, SURF and GPU based SURF algorithm according to performance and number of feature. For this purpose, we use ETHZ Object Dataset [16]. Samples from the dataset are shown in figure 2. The first column of the figure includes main object and the remaining columns include different images of same object.

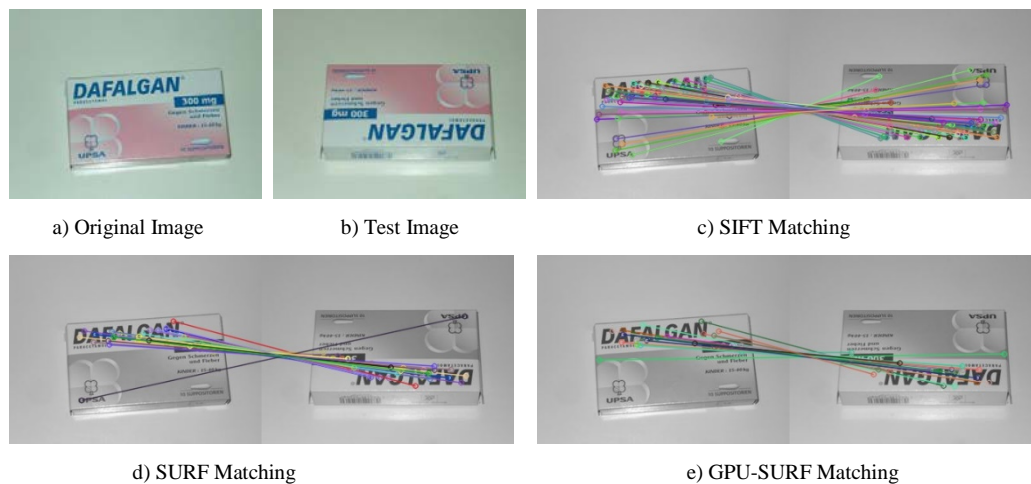


Figure 2: Comparison of SIFT, SURF and GPU-SURF algorithm.

ETHZ Object Dataset consists of 53 different objects and each object has 4 different images. Totally 164 images with 320x240 resolution. The dataset contains a variety of object images with different perspective, so this dataset is suitable for SIFT and SURF algorithms. To test the performance, we selected first image for training. The remaining 4 images have been used for testing. The trained image has been compared with four test images one to one and every matching results have been saved. These steps are done for SIFT, SURF and GPU-SURF algorithm separately. Figure 3 shows an example of matching results using SIFT, SURF and GPU-SURF algorithm. Figure 3 (a) shows original image and figure 3 (b) shows test image.

Figure 3 (c), (d) and (e) shows the matching result using SIFT, SURF and GPU-SURF algorithm respectively. It is observed that SIFT algorithm matches more features than other algorithms. The reason for this SIFT algorithm finds more features on the image. While SIFT algorithm has found 216 features, SURF algorithms has found 86 and GPU-SURF algorithm has found 71 features on original image. For test image, SIFT, SURF and GPU-SURF algorithm has found 228, 99, 77 features respectively. Figure 3 (c) (d) (e) shows matching keypoint for SIFT, SURF and GPU-SURF algorithm. Matching keypoint size for these algorithm is 95 for SIFT 40 for SURF and 23 for GPU-SURF algorithm.

We have evaluated number of keypoint number and matching keypoint number with SIFT, SURF and GPU-SURF algorithm. The 53 object images in dataset have been selected for evaluation. Some of the results have been presented in Figure-4 and Figure-5 shows the results of feature size. SIFT algorithm has found an average of 220 features. However, SURF and GPU-SURF algorithm were able to find only 100 and 82 features on average. So it is observed that SIFT algorithm finds more features than SURF and GPU-SURF algorithm. Also as shown in figure-5, we have obtained same result for feature matching. All results related to the feature size is summarized in table-1.

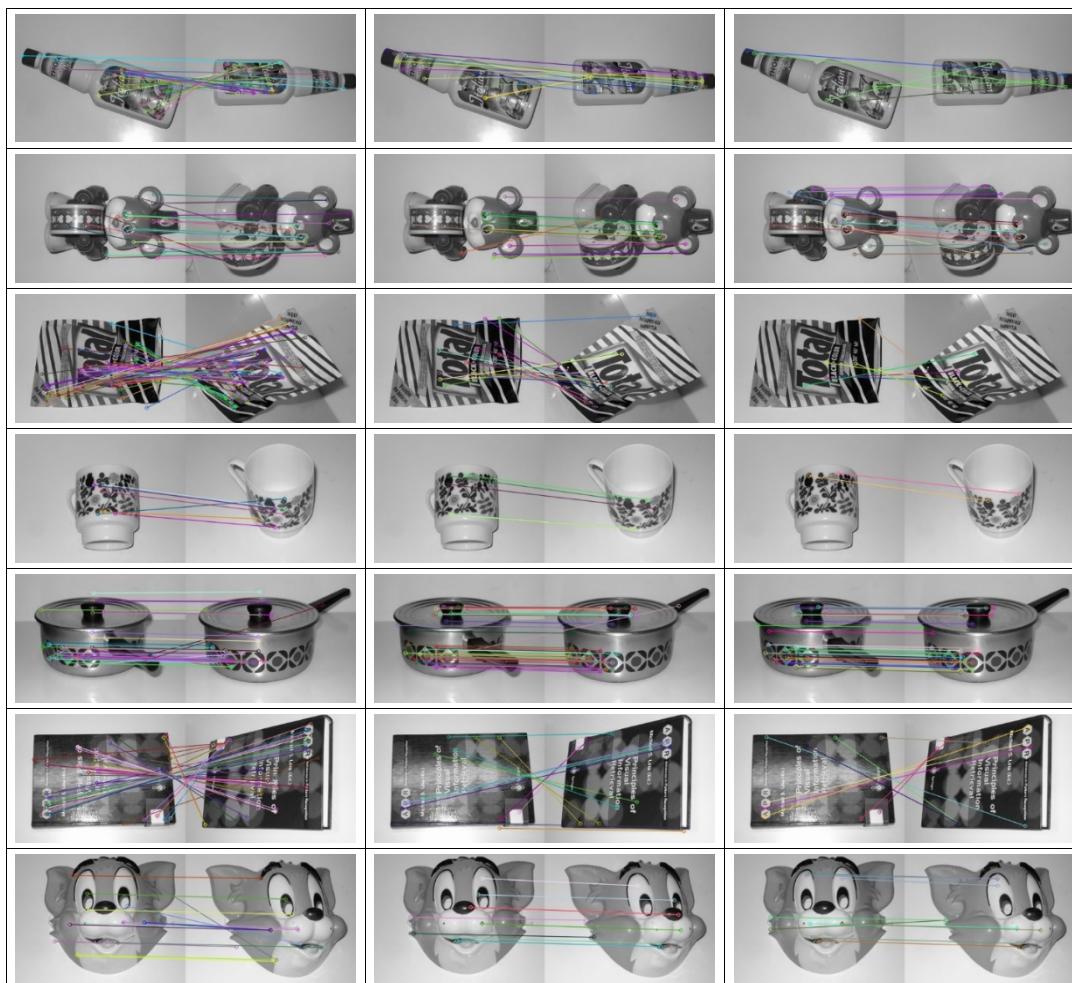


Figure-3: Result of SIFT, SURF and GPU-SURF algorithm.

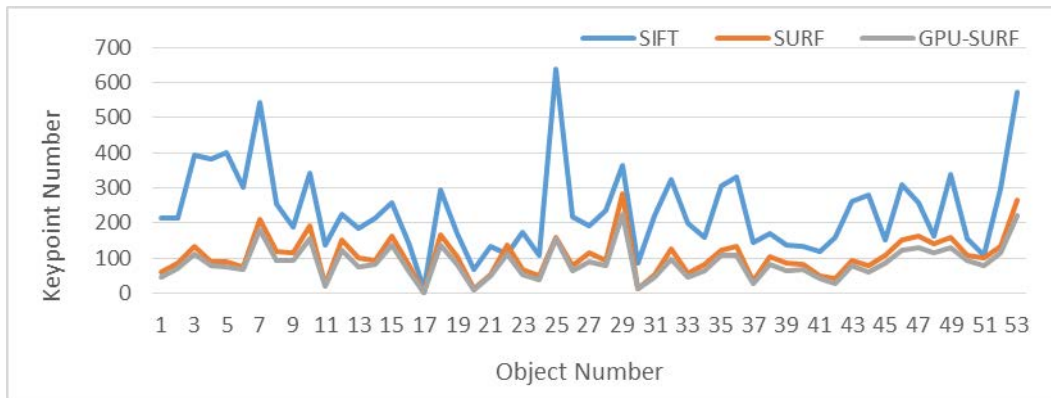


Figure-4: SIFT, SURF and GPU-SURF keypoint number

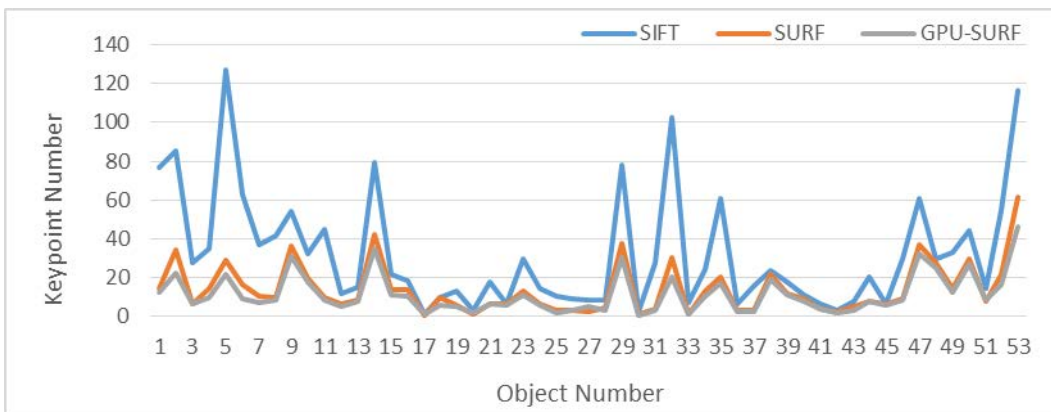


Figure-5: SIFT, SURF and GPU-SURF average matching keypoint number

Table-1: SIFT, SURF and GPU-SURF average feature size and matching size.

	Feature Size	Matching Size
SIFT	222.3	32.1
SURF	101.7	13.7
GPU-SURF	83.3	11.2

Also we have tested execution time for each method separately. To test the execution time, we select every image in dataset with different image sizes. Original image size of the dataset is 320x240 but we converted them to 640x480, 960x720 and 1280x960. Results are presented in figure-6 for 320x240 image size and figure-7 for 640x480 image size. Results show that with a small image size SURF and GPU-SURF algorithms have same execution time. But with the growing size of the image, GPU version works faster. For these reason, GPU version does not make sense to use small sized images. All results related to the execution time is shown in table-2.

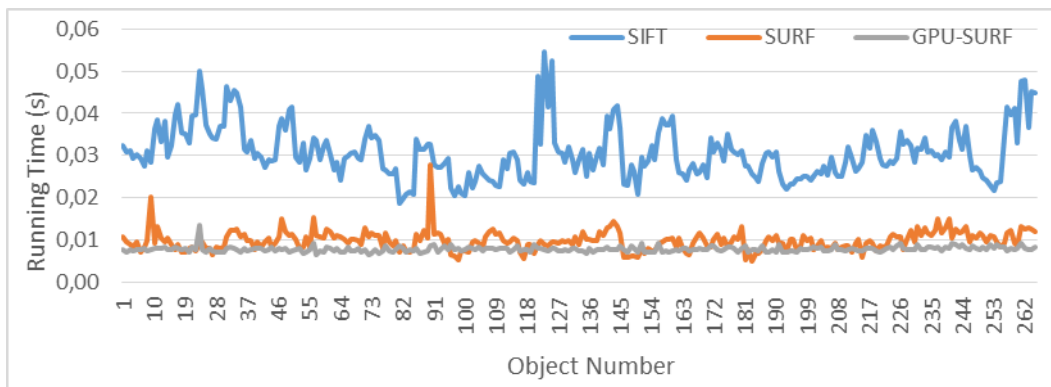


Figure-6: Running time for 320x240 size image.

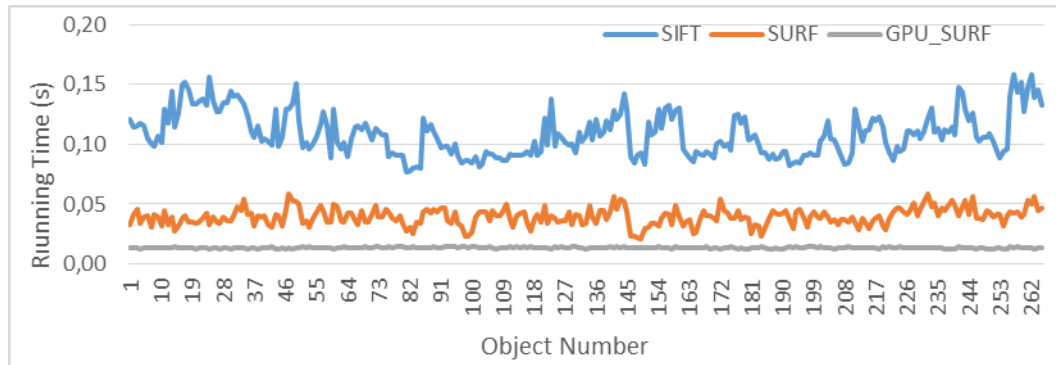


Figure-7: Running time for 640x480 size image.

Table-2: Running time of SIFT, SURF and GPU-SURF algorithm with different image size.

Image Size	SIFT		SURF		GPU-SURF		
	Run. T. (s)	Ratio	Run. T. (s)	Ratio	Run. T. (s)	Ratio (SIFT)	Ratio (SURF)
320x240	0.0308	1	0.00987	3.12	0.00783	3.93	1.26
640x480	0.109	1	0.0396	2.75	0.0135	8.07	2.93
960x720	0.213	1	0.0789	2.7	0.0239	8.9	3.3
1280x960	0.358	1	0.126	2.84	0.0406	8.82	3.1

4 CONCLUSIONS

This paper has evaluated SIFT, SURF and GPU based SURF algorithm for features size and execution time. As a result, SIFT algorithm finds more features than SURF algorithm but SIFT algorithm much more slowly than SURF and GPU-SURF algorithms. According to the results of experiments, GPU based SURF algorithm works 3 times faster than SURF algorithm and 8 times faster than SIFT algorithm. As a future work, the authors are planning to make mentioned three methods on real time or half real time video images.

REFERENCES

- [1] N. Y. Khan, B. McCane ve G. Wyvill, "SIFT and SURF Performance Evaluation Against Various Image Deformations on Benchmark Dataset", *2011 International Conference on Digital Image Computing: Techniques and Applications*, Noosa, QLD, 2011.
- [2] M. G. Peña, "A Comparative Study of Three Image Matching Algorithms: SIFT, SURF, and FAST," Utah State University, Master Thesis, Logan, Utah, 2011.
- [3] C. Harris ve M. Stephens, "A combined corner and edge detector". *In Proc. of Fourth Alvey Vision Conference*, 1988.
- [4] S. M. Smith ve J. M. Brady, "SUSAN—A New Approach to Low Level Image Processing", *International Journal of Computer Vision*, cilt 23, no. 1, pp. 45-78, 1997.
- [5] H. Wang ve M. Brady, "A practical solution to corner detection", *Image Processing, IEEE International Conference*, Austin, TX, 1994.
- [6] M. Trajković ve M. Hedley, "Fast corner detection", *Image and Vision Computing*, cilt 16, no. 2, pp. 75-87, 1998.
- [7] D. G. Lowe, "Distinctive Image Features from Scale-Invariant Keypoints", *International Journal of Computer Vision*, cilt 60, no. 2, pp. 91-110, 2004.
- [8] Y. Ke ve R. Sukthankar, "PCA-SIFT: a more distinctive representation for local image descriptors", *IEEE Computer Society Conference on Computer Vision and Pattern Recognition*, 2004.
- [9] H. Bay, A. Ess, T. Tuytelaars ve L. V. Gool, "Speeded-Up Robust Features (SURF)", *Computer Vision and Image Understanding*, cilt 110, no. 3, pp. 346-359, 2008.
- [10] Z. Güler ve A. Çınar, "GPU-Based Image Segmentation Using Level Set Method With Scaling Approach", *Second International Conference on Advanced Information Technologies and Applications*, 2013.
- [11] J. Sanders ve E. Kandrot, "CUDA By Example: An Introduction to General-Purpose GPU Programming", Addison-Wesley, 2011.
- [12] L. Juan ve O. Gwon, "A Comparison of SIFT, PCA-SIFT and SURF," *International Journal of Image Processing*, cilt 3, no. 4, pp. 143-152, 2009.
- [13] A. Yilmaz, O. Javed ve M. Shah, "Object Tracking: A Survey," *ACM Computing Surveys (CSUR)*, 2006.
- [14] S. Cook, "Cuda Programming: A Developer's Guide to Paralel Computing with GPUs", Elsevier, Morgan Kaufmann., 2012.

- [15] J. Cheng, M. Grossman ve T. McKercher, "Professional CUDA C Programming", Wiley, 2014.
- [16] H. Shao, T. Svoboda, T. Tuytelaars ve L. Van Gool, "HPAT indexing for fast object/scene recognition based on local appearance", *computer lecture notes on Image and video retrieval*, Springers, 2003, pp. 71-80.

BIOGRAPHY

Zafer Güler: He is a Research Assistant in the Department of Software Engineering at the University of Firat where he has been a faculty member since 2012. He completed his MSc at Firat University. His research interests lie in the area of programming languages, computer graphics, image processing, human computer interaction, mesh generation, ranging from theory to design to implementation, with a focus on improving software quality.

Ahmet Çınar: He received the PhD degree in Electric-Electronics Engineering in 2003 from Firat University. He has been working on Firat Univ. Department of Computer Engineering, (Assistant Professor). His research is interested in development and improvement of mesh generation methods, and applications of virtual reality, augmented reality, artificial intelligence and game programming.

Erdal Özbay: He is a Research Assistant in the Department of Computer Engineering at the University of Firat where he has been a faculty member since 2012. He completed his MSc at Firat University. His research interests lie in the area of programming languages, computer graphics, image processing, human computer interaction, mesh generation, ranging from theory to design to implementation, with a focus on improving software quality.

Object-Oriented Program Controlled Biosensing

Emrah Kaplan¹

Abstract

Electroanalytical sensors, as a prominent member of the biosensing family, have the advantage of being able to operate in opaque mediums. The minimal requirements to operate electrochemical sensors are a potentiostat and a PC with a particular software installed. However, the parameters of the applied signal and the results are restricted by the limits of the hardware and the software. The system structure can become more flexible and capable by using a custom circuit design instead of a commercial potentiostat device. However, it will require a signal generator and an oscilloscope to supply the triggering signal and measure the resulting current flow through the sensor. Such a complex system cannot be a practical and cost-effective solution.

In this paper, a system designed to control an ultra-sensitive electroanalytical sensor is explained. The software, programmed in LabVIEW platform, controls the potentiostat circuit and presents the relevant data on the PC screen. The design which has a graphical interface gives the data in a ready to use format thanks to the additional units.

The system, which improved the controllability and usability, made it possible to run more efficient and faster tests on new sensor designs with less cost. Monitoring both input and output data on a single screen enables to perceive the errors during the experiments instantly and eliminates the frequently encountered time losses. In the following stage, the design will be modified to control the surface acoustic wave (SAW) unit which works as an effective sensitivity enhancing unit.

Keywords: Biosensor, electrochemical, Object-Oriented Program

1. INTRODUCTION

The electroanalytical analysis is a scientific branch dealing with the electron flow between an analyte and an electrode. Various info such as reaction rate and concentration can be obtained thanks to the measured data [1]. Electrochemical methods can be used in non-transparent mediums which appear as a distinctive advantage. These devices can be used in miniaturized applications such as lab on a chip since they can be fabricated in smaller dimensions [2].

A basic electrochemical system (Figure 1) consists of four main sections; sensing part, function generator, potentiostat circuit, and a monitoring system. The sensing part generally contains three electrodes which physically contact with the sample solution. The signal generator is used to apply the required signal, between the working and counter electrodes, to run the electroanalytical test. The monitoring system measures the current flow through the working electrode. The potentiostat circuit is used as an interface between the electrodes and other two parts. Moreover, it keeps the applied potential at a constant level by getting a feedback via the reference electrode (RE) [3]. The current flow through the RE is relatively slow thanks to the resistivity supplied by the potentiostat circuitry [4],[5]. The main current flow occurs between the counter electrode and working electrode. The flow is measured via the monitoring system [6]. A typical circuit design of the potentiostat circuit is given in Figure 2.

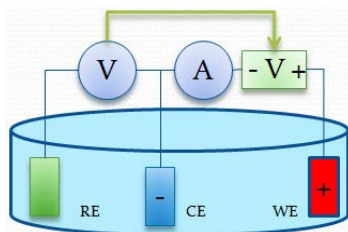


Figure 3. A schematic presenting the working principle of a potentiostat using three electrode sensing system. The system manipulates the applied potential between WE and CE. Secondly, the current flow of the RE is kept very low. Final results were obtained from the amperometer.

Commercial potentiostat devices on the market are generally too large sized to be used with miniaturized sensing systems. This case does not allow to design hand-held analytical devices. Moreover, the adaptation of the potentiostat to very specific

¹ Gümüşhane University, Electrical- Electronics Engineering, 29100 Gümüşhane, Turkey,
ekaplan@gumushane.edu.tr

sensing methods requires a significant amount of work. However, designing a complete new potentiostat can make a big difference by a flexible interface and extra capabilities. Therefore, the system can be automated for faster analysis regardless of the complexity of the sensing mechanism and data measurements. This paper explains the LabVIEW-based solution for the issue explained.

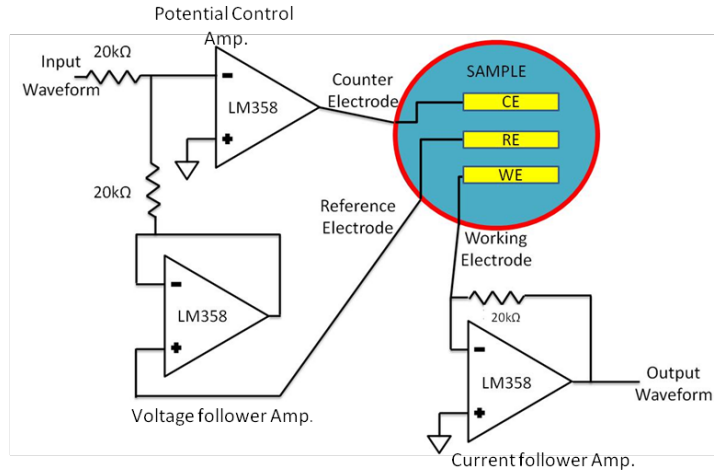


Figure 4. A schematic showing a potentiostat circuit containing three operational amplifiers and a three electrode sensing system immersed into the sample chamber.

2. MATERIALS AND METHODS

Electroanalytical tests were performed on a 10 mM potassium ferrocyanide ($K_4[Fe(CN)_6]$) model solution via the LabVIEW controlled potentiostat system. The liquid system was also containing a 100 mM supporting electrolyte (KCl). The sensing electrodes were fabricated on a glass slide via the photolithography method. The electrodes were made with 100 nm gold on the substrate.

The PVC reaction chambers surrounding the sensing electrodes were filled with 6 μ l of samples. At the next stage, the measurements were performed on a hemoglobin detection system instead of the potassium ferrocyanide solution. The sample was comprised of 2 μ l TMB- H_2O_2 (100 mM KCl) substrate, 2 μ l Hemoglobin (5 mg/ml in PBS buffer) and 2 μ l stopper solution (1 M H_2SO_4). The results presented in Figure 4 was obtained via the new system, however, the noise filtering was done with a separate system.

The LabVIEW based system was capable of receiving the experimental parameters entered by the operator and apply them to the reaction chamber via the electrodes. Top and bottom limits of the agitation signal of the redox system can be entered randomly since the system can differentiate them and proceed between those values. The system stops working if the values are the same. The shape of the reaction triggering signal is defined by the instruction given from outside. The defined output signal and the measured output signals are both presented on the interface screen of the program. The final measurement is presented after the filtering and averaging steps.

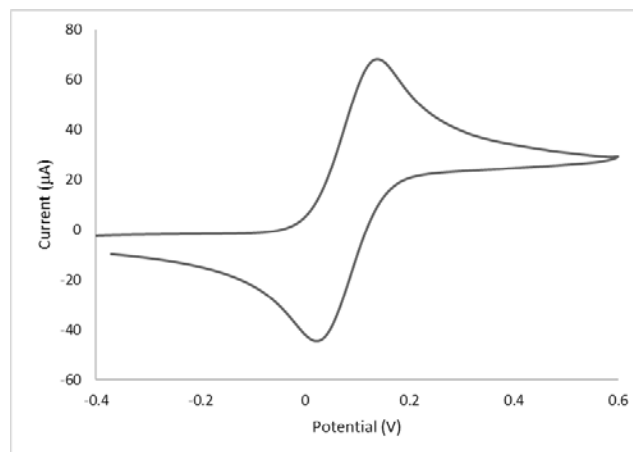


Figure 5. The cyclic voltammogram was obtained from a potassium ferrocyanide solution. The applied triangle input signal was between -0.4 V and 0.6 V with a 0.1 V/s.

3. RESULTS AND DISCUSSION

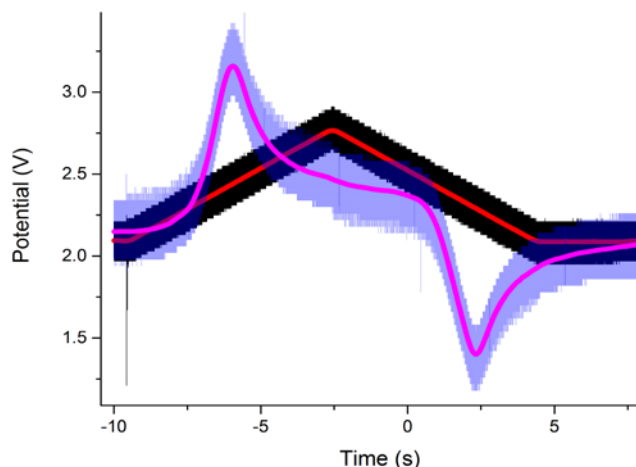


Figure 6. The LabVIEW based system configuration triggers the redox system with a triangle signal (red) and the resulting graphic was obtained (pink). The triangle voltage was varied between 2.2 and 2.8 V with a scan rate of 0.1 V/s. The liquid system was the label-free Hb detection solution instead of the model solution. It was containing 2 μ l TMB- H_2O_2 (100 mM KCl) substrate system, 2 μ l Hemoglobin solution (5 mg/ml in PBS buffer) and 2 μ l of stopping solution (1 M H_2SO_4).

Experiments performed with the new potentiostat system combination gave successive results both with the model solution and the biological analyte. Especially the filtering and averaging enabled the elimination of the noise. Obtained result showed that the new system was capable of giving relevant results according to the amount of redox couple in the sample. The hysteresis shape of the graphical results proved the ability of the new design.

CONCLUSION

The results proved that this new system combination can be integrated on miniaturized diagnostic or other types of analytical test applications. The capability of the system for new arrangements or new hardware attachments makes a significant distinction comparing to commercial devices on the market. This advantage can decrease the experimental time enable faster and more successive tests thanks to the automated design. Moreover, the mistakes and delays caused by the operator can also be eliminated.

As a secondary stage, another control unit will be added in the system combination. It will manipulate the micro-mixing part of the hardware. This enhancement will make the electroanalytical biosensing system more sensitive but still controlled from a single center.

REFERENCES

- [1] F. Ricci, G. Adornetto, and G. Palleschi, "Electrochimica Acta Review article A review of experimental aspects of electrochemical immunosensors," *Electrochim. Acta*, vol. 84, pp. 74–83, 2012.
- [2] J. Wang, "Electrochemical detection for microscale analytical systems: a review," *Talanta*, vol. 56, no. 2, pp. 223–231, Feb. 2002.
- [3] R. J. Flanagan, D. Perrett, and R. Whelpton, *Electrochemical Detection in HPLC: Analysis of Drugs and Poisons*. Royal Society of Chemistry, 2005.
- [4] T. J. Smith and K. J. Stevenson, *Reference Electrodes*. 2007.
- [5] P. Vanýsek, *Impedance in Electrochemistry — From Analytical Applications to Mechanistic Speculation 2, Issue 20*. The Electrochemical Society, 2009.
- [6] A. J. Bard and Faulkner, *Electrochemical methods : fundamentals and applications*, vol. 6. New York ; Chichester ET - 2nd: John Wiley, 2001.

BIOGRAPHY

Emrah Kaplan has a Degree in Electrical & Electronics Engineering (2008).

Studied as an Erasmus Exchange Student in BEng in Computers, Networking and Communications Technology Dep.- Coventry University (2007-2008).

Worked as a QA/QC & Site Engineer in an Expansion Project of a BOTAS Petrol Pipe Line (2008-2009).

Completed his Ph.D. in Biomedical Engineering (2015).

Currently working as Asst. Prof. in Electrical & Electronics Engineering department - Gumushane University/ TURKEY (since 2009)

Internship Experiences (2004-2007):

- ANADOLU CAM SANAYI A.Ş. -Turkey's biggest glass and bottle factory
- MEKOSAN A.Ş. - An automation and control panel producing company
- HES FIBEL A.Ş. - Ranks as Turkey's one of the largest telecom cable provider and exporter
- SEZAL ELEKTRONİK A.Ş. - An Electric motor factory
- MAINTENANCE, REPAIR AND CALIBRATION UNIT in Medical Centre of Fırat University

Acoustic Heating on Droplet-Based Analysis

Emrah Kaplan¹

Abstract

This work is based on the application of travelling acoustic waves to an electrochemical sensing platform. In order to obtain a pure heating system, the acoustic energy was converted to heat and the streaming was blocked. The acoustic transducer and the sensing electrodes were micro-fabricated via photolithography. The substrate used for the transducer was a piezoelectric material (LiNbO₃) while the analytical electrodes were fabricated on another slide. The sensing unit was also including a droplet trap which was surrounding the sensing electrodes. The sample was in a droplet form and pinned on the sensing electrodes. A polydimethylsiloxane (PDMS) layer was sandwiched between the sensing and heating units to bond them to each other. This layer was used to block the dragging force of the leaky sound waves and convert them to the heat energy. The temperature of the sample was gradually increased by varying the power of the RF signal of the SAW transducer. The increment of the temperature changed the physiochemical characteristics of the sample due to the growing number of high energy collisions. Consequently, the reaction rate, therefore, the measured amperometric results were increased. The results obtained from the electroanalytical unit showed that the SAW technology can be used as a fast and highly controllable heating mechanism for numerous micro-analytical devices. Furthermore, the PDMS appeared as a suitable material to eliminate the pressure waves and convert from mechanical into heat energy.

Keywords: *electroanalysis, heater, lab-on-a-chip (LOC), surface acoustic wave (SAW)*

1 INTRODUCTION

New microfluidic technologies enabled to develop advanced lab-on-a-chip (LOC) applications for various areas [1]. Sound based actuation [2],[3], micro-mixing [4], and sensing [5] are some of the common techniques used for such new generation devices. Moreover, surface acoustic wave (SAW) is an emerging technique for heat required applications [2] such as polymerase chain reaction (PCR) which is used to make multiple copies of a segment of a DNA (Deoxyribonucleic acid) [6], [7], [8].

This paper explains the effect of temperature variation on the amperometric measurements performed on a droplet-based design. The temperature variation on samples was provided with a SAW platform. SAWs are capable of inducing an effective fluid streaming effect [5] into microfluidic applications. Furthermore, the travelling mechanical waves produce heat [7]. However, a possible overheating can be destructive for the piezoelectric material on which the SAW transducer is fabricated. Therefore, the generated heat needs to be dissipated with an alternative method [9]. However, in this work, the heat generation was the focus of the experimental process since the SAW IDT was used as a micro-heater. Some modifications were performed on the SAW platform to enhance the conversion of SAW into heat. The measurements were performed via the amperometry method. The target analyte in the liquid sample was potassium ferrocyanide (a redox material).

2 MATERIALS AND METHODS

The main part of the system combination was the SAW platform. The mechanical wave transducer was fabricated on a piezoelectric (LiNbO₃) substrate. The SAW device was a single-phase unidirectional transducer (SPUDT) which generate only single direction SAW propagation [10]. The resonance frequency of the mechanical wave transducer device was measured as 12.2 MHz by a scattering analysis test (S11) performed with a network analyzer. The substrate was coupled to a heat sink with a heat transfer compound for a rapid heat transfer to protect the SAW platform from breaking due to overheating.

SAW devices normally create heat energy due to the molecular friction on the substrate surface. In our design a PDMS layer (2 mm thick) was immobilized in front of the SAW device on the acoustic beam path. This change was increased the SAW to heat conversion ratio even further. This modification converted the SAW platform into a heating platform.

¹ Gümüşhane University, Electrical- Electronics Engineering, 29100 Gümüşhane, Turkey, ekaplan@gumushane.edu.tr

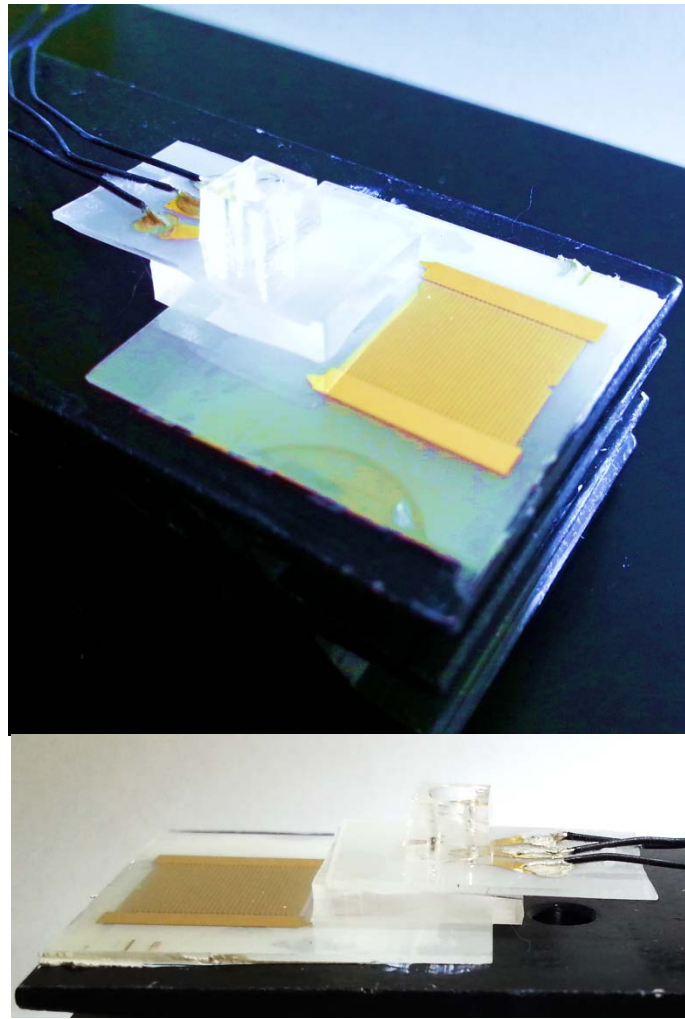


Figure 7. Images of the experimental setup. The entire system is located on a heat sink to control the temperature. A PDMS layer was sandwiched between the three electrode sensing platform and the SAW platform to transform the mechanical energy into heat. The sample was also surrounded by a secondary PDMS layer to block the leaky SAWs.

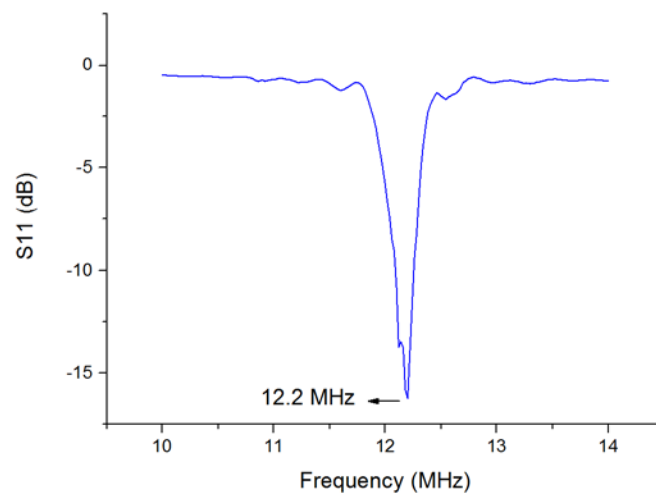


Figure 8. Resonance frequency of the SPUDT was measured as 12.2 MHz by the S11 method.

The electroanalytical sensing system was attached on the PDMS layer by a heat conductive compound. The sensing electrodes were surrounded by a hydrophobic layer with a 2 mm of diameter to obtain a circle shaped hydrophilic area. The purpose of the sample trap was to keep the shape and location of the droplet as constant. Secondly, a PDMS chamber (5mm diameter) was attached on the electrodes. The main purpose of the surrounding chamber was to stop the air stream around droplet to minimize the evaporation. Also, the PDMS chamber was working as a secondary block to stop the leaky mechanical waves on the surface and convert them into heat energy. This addition was a requirement since the SAWs are capable of passing from one layer to another one in a leaky wave form which can still make a dragging and mixing effect in the sample [11].

Electroanalytical tests were performed on a 4 μ l sample droplet pinned on the sample trap. The sample was containing 10 mM potassium ferrocyanide and 100 mM KCl as a supporting electrolyte. The amperometric tests were performed at a constant voltage (0.2 V) applied through the three electrode system for 100 s. for each measurement. The applied SAW power was increased from 0 to 4 W leading to temperature increase on the sample.

3 RESULTS AND DISCUSSION

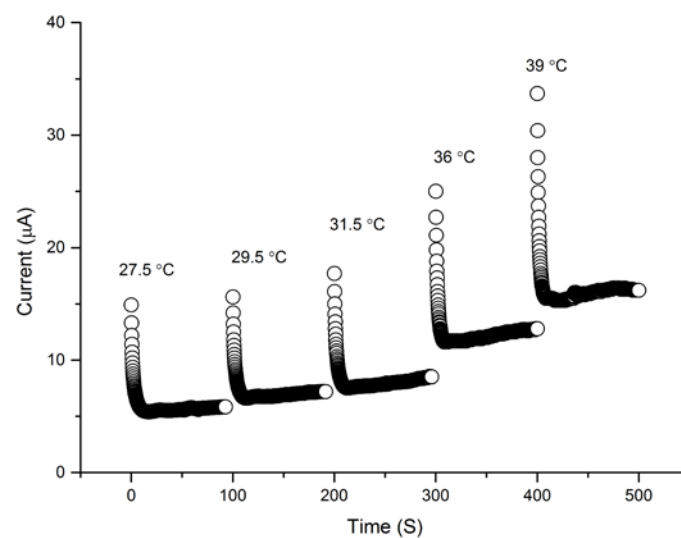


Figure 9. Amperometric measurements at varying SAW powers (0 to 4 W) increased the sample temperature from 27.5 °C to 39 °C. The constant voltage (0.2 V) applied through the three electrode system for 100 s. for each test. The 4 μ l sample was containing 10 mM potassium ferrocyanide and 100 mM KCl.

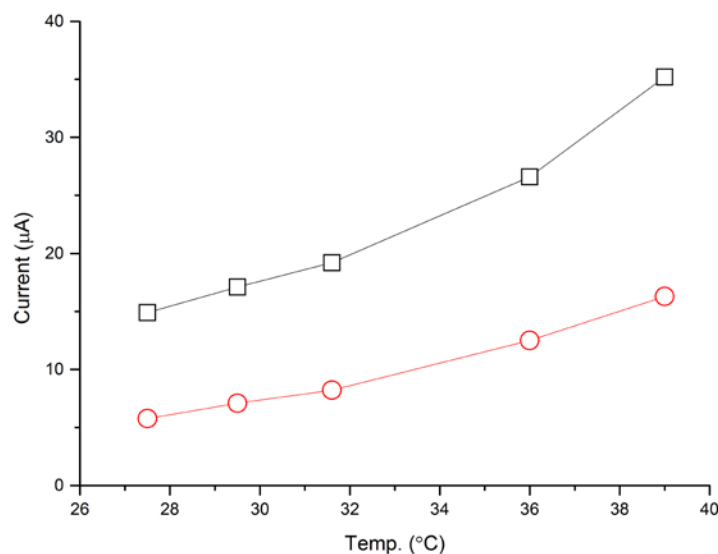


Figure 10. Evaluation graph of the amperometric measurements presented in the previous graph. The peak (square) and steady state (circle) current values of the amperometric results separately presented in the graph. The increasing temperature was also increased the current values measured during the amperometric measurements.

The temperature increment technique relies on heat radiation due to the damping of the vibrations by the PDMS layer sandwiched between the SAW and sensing platforms. Therefore, the amperometric measurements (Figure 3 and Figure 4) gave incremental data as a result of increasing temperature values. The main reason was the increment of the amount of energized molecules due to the temperature increment. This was enabling more molecules to have the minimum energy to react. Therefore, more current was flowing through the sensing electrodes.

4 CONCLUSION

Overall results showed that the new micro heater design is capable of enhancing the temperature of the reaction chambers of analytical devices. Moreover, the temperature variation was presented a significant enhancement during the amperometric measurements of the model solution. This device concept appeared as a new thermodynamic electroanalytical measurement method. The results obtained from the electroanalytical unit showed that the SAW technology can be used as a fast and highly controllable heating mechanism for numerous micro-analytical devices. Furthermore, the PDMS appeared as a suitable material to eliminate the pressure waves and convert from mechanical into heat energy.

REFERENCES

- [1] T. H. Schulte, R. L. Bardell, and B. H. Weigl, "Microfluidic technologies in clinical diagnostics," *Clin. Chim. Acta*, vol. 321, pp. 1 – 10, 2002.
- [2] S. Thalhammer and A. Wixforth, "Surface Acoustic Wave Actuated Lab-on-Chip System for Single Cell Analysis," *Biosens. Bioelectron.*, vol. 4, no. 3, pp. 1–7, 2013.
- [3] M. Kurosawa, T. Watanabe, A. Futami, and T. Higuchi, "Surface acoustic wave atomizer," *Sensors and Actuators A: Physical*, vol. 50, no. 1–2, pp. 69–74, 1995.
- [4] M. Alghane, B. X. Chen, Y. Q. Fu, Y. Li, J. K. Luo, and a J. Walton, "Experimental and numerical investigation of acoustic streaming excited by using a surface acoustic wave device on a 128° YX-LiNbO₃ substrate," *J. Micromechanics Microengineering*, vol. 21, no. 1, p. 015005, Jan. 2011.
- [5] K. Lange, G. Blaess, A. Voigt, R. Götzen, and M. Rapp, "Integration of a surface acoustic wave biosensor in a microfluidic polymer chip," *Biosens. Bioelectron.*, vol. 22, no. 2, pp. 227–232, 2006.
- [6] B. H. Ha, K. S. Lee, G. Destgeer, J. Park, J. H. Jung, and H. Jin, "An Acoustothermal Microheater with Omni-temperature Controllability An acoustothermal microheater with omni-temperature controllability," in *2015 International Congress on Ultrasonics*, 2015, no. MAY.
- [7] A.-L. Zhang, Y.-Q. Wei, and Q.-J. Han, "A Microreactor With Surface Acoustic Wave Micro-Heating System," *Ferroelectrics*, vol. 432, no. 1, pp. 22–31, 2012.
- [8] T. Roux-Marchand, D. Beyssen, F. Sarry, and O. Elmazria, "Rayleigh surface acoustic wave as an efficient heating system for biological reactions: Investigation of microdroplet temperature uniformity," *IEEE Trans. Ultrason. Ferroelectr. Freq. Control*, vol. 62, no. 4, pp. 729–735, 2015.
- [9] A. Renaudin, V. Chabot, E. Grondin, V. Aimez, and P. G. Charette, "Integrated active mixing and biosensing using surface acoustic waves (SAW) and surface plasmon resonance (SPR) on a common substrate.," *Lab Chip*, vol. 10, no. 1, pp. 111–5, Jan. 2010.
- [10] R. Shilton, M. K. Tan, L. Y. Yeo, J. R. Friend, L. Y. Yeo, M. K. Tan, R. Shilton, M. K. Tan, L. Y. Yeo, and J. R. Friend, "Particle concentration and mixing in microdrops driven by focused surface acoustic waves," *J. Appl. Phys.*, vol. 104, no. 1, p. 014910, 2008.
- [11] B. H. Ha, K. S. Lee, G. Destgeer, J. Park, J. S. Choung, J. H. Jung, J. H. Shin, and H. J. Sung, "Acoustothermal heating of polydimethylsiloxane microfluidic system.," *Sci. Rep.*, vol. 5, p. 11851, 2015.

BIOGRAPHY

Emrah Kaplan has a Degree in Electrical & Electronics Engineering (2008). Studied as an Erasmus Exchange Student in BEng in Computers, Networking and Communications Technology Dep.- Coventry University (2007-2008).

Worked as a QA/QC & Site Engineer in an Expansion Project of a BOTAŞ Petrol Pipe Line (2008-2009).

Completed his PhD in Biomedical Engineering (2015).

Currently working as Asst. Prof. in Electrical & Electronics Engineering department - Gumushane University/ TURKEY (since 2009)

Internship Experiences (2004-2007):

- ANADOLU CAM SANAYI A.Ş. -Turkey's biggest glass and bottle factory
- MEKOSAN A.Ş. - An automation and control panel producing company
- HES FIBEL A.Ş. - Ranks as Turkey's one of the largest telecom cable provider and exporter
- SEZAL ELEKTRONİK A.Ş. - An Electric motor factory
- MAINTENANCE, REPAIR AND CALIBRATION UNIT in Medical Centre of Fırat University

A Study on Sustainable Agriculture Practices in Turkey

Hulya Dogan¹, Alihan Cokkizgin², Cuneyt Cesur¹ Selen Alniak Sezer¹

Abstract

In recent years, agricultural sector has mainly been affected by the rapid improvement of technological change, and hence, the use of intensive technology in agriculture raised agricultural productivity. Moreover, agricultural land is decreasing due to industrialization and urbanization. Another problem is soil erosion. This agricultural land is decreasing day by day. There are a total of 13 003 million hectares of land in the world, and 4 911 million hectares agriculture area. On the other hand Turkey has 77 million hectares land area and 38.3 million hectares agriculture area. To avoid the problem of hunger and poor nutrition, agricultural lands should be protected both for the World and Turkey. In this study, the sustainable agriculture is taken in hand the agriculture land on the problems and solutions are discussed for Turkey.

Key words: Sustainable Agriculture, soil pollution, environment

1. INTRODUCTION

Development of the industry provides to people a better living environment. When people realize it, they are damaging to the environment. All people have to leave a liveable world for future generations. The future of life on Earth depends on it. On the other hand to live in a healthy environment is a human right.

Sustainable resource management is one of the most complex concerns today. Society has spent billions on conserving productive and marginal soils in cultivation yet it is unclear whether these efforts buy sustainability. Further study about which soils need conservation merits consideration (e.g. [13]).

Soil sustainability trends differ from region to region. More developed areas of the world, huge increases in yield per unit area over the last century (e.g. [2]–[10]). Similarly, land and water resources management is difficult due to the lack of the same everywhere in Turkey. Soil structure varies according to geographical regions and provinces.

Turkey are the reasons for the deterioration of land resources, such as soil misuse, contamination, deterioration, erosion, degradation of pastures, forest lands disqualifies.

Soil and water resources are absolutely necessary for the continuation of human existence. Water is the basis of life and soil is the source of all nutrients. Soil management, especially in agriculture, is a key issue for research. The purpose of this paper is to provide an overview of the land resource sustainable use in Turkey.

2. CAUSES OF SOIL POLLUTION

2.1. Urbanization

The soil will be polluted as a result of different human activities, Most of these pollutions are caused by vehicle accident which moves contaminants. The other pollutants, which cause soil pollution, include cars, trucks and airplanes that do not move the waste; rather, they carry materials like fuel which can cause soil pollution as a result of pouring and emitting them from the vehicle (e.g. [9]).

2.2. Industrial, radioactive and household wastes

Some of these factors are home, workplace, hospital, industrial, radioactive wastes and pesticides etc. On the other hand dumping of toxic substances like different types of solvents, colored materials and detergents will extend earth and soil pollution.

¹ Corresponding author: Bozok University, Vocational School, Department of Seed Science, 66000, Merkez/Yozgat, Turkey. hulya.dogan99@hotmail.com

² Gaziantep University, Vocational School of Higher Education, 27000, Gaziantep, Turkey. aymececur@hotmail.com

2.3. Soil erosion

Soil erosion is a naturally occurring process involving the mobilisation and deposition of soil particles, mainly by water and air (e.g. [8]). Erosion, creates a serious threat for sustainable agriculture. Each year, about 75 billion tons of soil are eroded from the world's terrestrial ecosystems. Most agricultural land in the world is losing soil at rates ranging from 13 tons/ha/year to 40 tons/ha/year (e.g. [14]). On the other Turkey 500 million tonnes per annum of soil, is losing due to erosion (e.g. [12]).

2.4. Pesticides and fertilizers use

A pesticide is any substance or mixture of substances intended for preventing, destroying, repelling, or mitigating any pest (insects, mites, nematodes, weeds, rats, etc.), including insecticide, herbicide, fungicide, and various other substances used to control pests (e.g. [4]). First use of synthetic pesticides was in 1940 and its consumption is increasing worldwide. The use of active ingredients is 2.26 million ton according to World Health Organization data (e.g. [15]). On the other hand total fertilizer consumption was 141.28 million ton in the world and 1.74 million ton in Turkey (e.g. [5]).

2.5. Other causes

Pollution in underground water, high salinity in soil solution, reduce in vegetation, ecological imbalance etc.

3. EFFECTS OF SOIL POLLUTION

3.1. Agricultural effects

Reduced soil fertility, reduced nitrogen fixation, increased erosion, larger loss of soil and nutrients, deposition of silt in tanks and reservoirs, reduced crop yield and imbalance in soil fauna and flora (e.g. [11]).

3.2. Industrial effects

Dangerous chemicals entering underground water, ecological imbalance, release of pollutant gases, release of radioactive rays causing health problems, increased salinity and reduced vegetation (e.g. [11]).

3.3. Urban effects

Clogging of drains, inundation of areas, public health problems, pollution of drinking water sources, foul smell and release of gases and waste management problems (e.g. [11]).

4. PREVENTION OF SOIL POLLUTION

Location of the industry and house should be avoided on agricultural area. The use of pesticides and artificial fertilizers should be considered. Agricultural areas be covered with vegetation. Household, industrial and radioactive wastes should be destroyed without any damage to the soil.

5. LAND RESOURCES IN TURKEY

Turkey is a country of hills and mountains, the average altitude is 1132 m in the north Black Sea, is surrounded by the southern Mediterranean and the Aegean Sea. Turkey's territorial diversity, climate, topography, vegetation and geological differences affect plant (e.g. [1]). In Turkey, 20.5 million hectares of arable land, pasture and grazing land, 14.6 million hectares of forest, 11.4 million hectares of forest land, permanent products 3 million hectares of fallow land to 4 million hectares, while other areas are 27.2 million hectares. On the other hand, total organic agriculture in Turkey is 615 000 hectares, that 326 000 hectares of organically certified, and 289 000 hectares of land is a transition to organic agriculture (e.g. [6]).

6. SUSTAINABLE AGRICULTURE

Sustainable agriculture is one that produces abundant food without depleting the earth's resources or polluting its environment. It is agriculture that follows the principles of nature to develop systems for raising crops and livestock that are, like nature, self sustaining. Sustainable agriculture is also the agriculture of social values, one whose success is indistinguishable from vibrant rural communities, rich lives for families on the farms, and wholesome food for everyone (e.g. [7]).

7. OVERVIEW OF FUTURE DIRECTIONS

Organic agriculture currently occupies 0.3% of agricultural land, mostly in developed countries. This land is farmed according to rules administered by various organic agriculture regulating associations that, in the case of crops, disallow the use of most inorganic compounds for crop nutrition, synthetic compounds for pest, disease and weed control, and more recently,

genetically modified cultivars. The rules also encourage rotations and intercrops to build soil fertility, improve crop nutrition, and to control or limit production problems associated with pests, diseases, and weeds. These latter aspects of organic agriculture are practiced much more widely outside organic agriculture, but those systems, here referred to as conventional agriculture, vary enormously in range and amount of 'organic agriculture-prohibited' inputs (e.g. [3]). On the other hand conventional agriculture has a lot of problem such as the following soil pollution, water pollution, human health etc. Between organic agriculture and conventional agriculture, which is an application good agricultural practices can be use in agriculture for Turkey and World. This type of agriculture ensures the continuity of the feeding as well as protects the natural balance.

REFERENCES

- [1]. E., Aksoy, P. Panagos, L. Montanarella, A. Jones. Integration of the Soil Database of Turkey into European Soil Database 1:1.000.000. JRC Scientific and Technical Reports, 45p, 2010.
- [2]. J S. Amthor. Perspective on the relative insignificance of increasing atmospheric CO₂ concentration to crop yield. *Field Crops Research* 58: 109-127, 1998.
- [3]. D.J. Connor, Organic agriculture cannot feed the world. *Field Crops Research* 106:187-190, 2008.
- [4]. (2009) EPA. website (Online). Available: What is a Pesticide? <http://www.epa.gov>
- [5]. (2002) FAO. website (Online). Available: Fao Statistical Database <http://www.fao.org>
- [6]. (2011)FAO. website (Online). Available: Fao Statistical Database <http://www.fao.org>
- [7]. R. Earles, P. Williams, Sustainable Agriculture: An Introduction. A Publication of ATTRA, the National Sustainable Agriculture Information Service, 8p, 2005.
- [8]. A. Inman., Soil erosion in England and Wales: causes, consequences and policy options for dealing with the problem. WWF-UK, 30p, 2006.
- [9]. P. P. N. Khakbaz, S. Mahdeloei, A. Heidari. Soil Pollution Control Management Techniques and Methods. *Annals of Biological Research*, 3(7): 3101-3109, 2012.
- [10]. P.A. Matson, W.J. Parton, A.G. Power and M.J. Swift. Agricultural intensification and ecosystem properties. *Science* 277: 504-509,1997.
- [11]. NSDL, Natural Science Digital Library. Soil Pollution, <http://nsdl.niscair.res.in/bitstream/123456789/990/1/>, 2013.
- [12]. T. Oztas, A.K. Ozbek, M. Turan., The cost of soil lost from fields due to removal on harvested sugarbeet: A case study in Turkey. *Soil Use and Management* 18: 236-237, 2002.
- [13]. J. Popp, D. Hoag, J. Ascough., Sustainable Soil Management: A Framework for Analysis In: D.E. Stott, R.H. Mohtar and G.C. Steinhardt (eds). *Sustaining the Global Farm. Selected papers from the 10th International Soil Conservation Organization Meeting.* p.061-067, 2001.
- [14]. D. Pimentel, N. Kounang, Ecology of Soil Erosion in Ecosystems. *Ecosystems*, 1: 416-426,1998.
- [15]. (2008) WHO. website (Online). Available: World Health Organization <http://www.who.int>.

The Effects Of Artificial Pasture Mixture Prepared in Central Anatolia Conditions on Turkey Weights

Ugur Ozkan¹ Nurdan Sahin Demirbag¹, Hulya Dogan², Selen Alniak Sezer¹

Abstract

In recent years, the red meat is expensive in turkey led to the prominence of white meat. Turkey pasture evaluation capacity is higher than the other poultry. In addition to this turkey feed protein and energy to turn meat is more superior than cattle and sheep. In the livestock business, total in put costs constituting 65-70% coming from forage and it is important to meet some parts of forage from the low-cost pasture. To close the rough age deficit, it is important to breeding work to do in pasture and the creation of suitable artificial pasture to graze on the type of animal. In light of this information is to develop a pasture mixture for turkey grazing to accelerate the increase in body weight it is becoming important for this sector. In this study; changes in different measurement periods of weight increase follow a straight line, as expected in both 2015 and 2014 study years, on the last measurements have reached the highest weight. Effect on turkey weights of different mixture ratios, in both years experiments were reached an average weight of turkeys in the first and second mixture is determined that more than a third mixture. As a result of this study, the pasture with effects of turkey weight increase will be established with different hay mixtures.

Key words: Turkey weight, hay, pasture mixture

1. INTRODUCTION

Rapid increase in world population has laid emphasis on the importance of nutrition problem day by day. This situation has brought forth the need of searching new sources and doing research on alternative foodstuffs. Besides, expensiveness of red meat in recent years has brought white meat into the forefront in Turkey. Chicken and especially turkey breeding within the framework of poultry farming, which could be an alternative for animal protein sources and has become an industry in our country, has come into prominence in meeting our protein insufficiency. Regarding people eating food of animal origin today, white meat has become preferable compared to red meat since cholesterol leads to vascular occlusion and various circulatory abnormalities. Turkey is superior to cattle and sheep in converting feed protein and energy into meat. Therewithal, its capacity of utilizing pasture is higher compared to other poultries. In other words, the meat obtained from turkey is produced at cheaper prices. Turkeys can pasture when they are 1,5-2 months old and they can feed on any kind of grass and insect. On the other hand, the amount of meat in breast and thigh that are the best-quality parts of poultry meat is much more in turkeys than other poultries. Turkey meat tastes very good and at the same time, its cholesterol level is very low. Turkey meat will be the best alternative to red meat in the next years due to its quality and product variety. The fact that turkey is more robust and long-lived, has a high carcass yield and nutritional value, is highly consumed in New Year, and its meat is used in fermented sausage and salami by being mixed with veal makes turkey breeding more attractive. In intensive conditions along with the impact of industrialization and mechanization, high productivity is reached in turkey breeding since number of animals per business is high (e.g. [3]). However, this condition has negative effects such as pecking and cannibalism. Pecking and cannibalism are the leading common behavioural problems of poultry. Bleeding wounds due to feather pecking are the main problems triggering and leading to cannibalism (e.g. [7]). According to Huber-eicher and Wechsler, the behaviour of pecking each other's feather is a condition occurring due to lack of soil pecking and activity under poultry-house conditions. However, availability of perching places in open areas and use of wide areas sort this problem out (e.g. [2], [7]). In our country in recent years, production of free-range, pasture-roaming Bronze or black turkey species has been switched to turkey meat of white California origin raised in broiler type closed area. Turkey breeding has drawn the attention of private sector and thus, productions are being maintained under intensive conditions. However, the most important reason of the low production amount in our country is the fact that turkey meat consumption is low. In addition the fact that turkey meat is more expensive than chicken meat and that it cannot be bought wholly since it is large can be listed among the reasons. In our country in 2015, the number of turkeys slaughtered was about 5,4 million and the turkey meat produced was about 52723 tons (e.g. [11]). While consumption of turkey meat per capita in developed countries is around 8-10 kg, it is only 0,4-0,6 kg in our country. It

¹ *Ankara University, Faculty of Agriculture, Department of Field Crops, Diskapi, Ankara, Turkey.
ugur.ozkan@ankara.edu.tr*

² *Bozok University, Vocational School, Department of Seed Science, 66000, Merkez/Yozgat, Turkey.
hulya.dogan@bozok.edu.tr*

has become a necessity to increase the production and consequently, the consumption of turkey meat, which is a valuable nutritional source. Today, it is impossible to ignore the need of natural or sown pasture grazing systems for poultry that prioritize the animal welfare and behaviour and is put forth by scientific studies in harmony with each region's own climatic and ecologic conditions rather than superficial applications. Grass pastures are essential for healthy and cheap breeding of our animals. Within the framework of this study, the objective is to put forth the effects of the pasture to be formed by different grass mixtures on turkeys' performance.

2. MATERIAL AND METHOD

2.1. General Characteristics of Haymana Research and Application Farm Where the Pasture was Formed

The place where the study was carried out and the pasture was formed is Research and Application Farm of Agricultural Faculty of Ankara University located in Haymana, established on 4200-decare area. It has an altitude of 1060 m and receives 250-300 mm of annual precipitation in average for consecutive years.

2.2. Forming Sown Pasture

The size of the area of the sown pasture formed is about 2-decare in total. In the pasture formed, rotational grazing system was applied and 2-decare area was initially divided into 2 main parcels (as main parcels A and B). In the main parcels A and B, turkeys were grazed rotationally for 14-day period. Each main parcel of 1-decare size was divided into 9 sub-parcels in total as so there are 3 different pasture mixtures and each mixture has 3replications. Mixtures were distributed randomly to the sub-parcels. Each sub-parcel size is 100 m² (100 x 9=900 m² for main parcel A; 100 x 9=900 m² for main parcel B). Mixtures are named as **K1, K2, and K3**. The most important criteria in forage plants to be added to sown pasture mixture was to choose rootstalk and fescue plants which would ideally response to irrigation under Central Anatolia conditions, be the best for poultry to graze, and have high resistance to scratching.

K1: % 40 Awnless Bromus (*Bromus inermis*) + %20 Alfalfa (*Medicago sativa* L.) + %40 bird's-foot trefoil (*Lotus corniculatus*)

K2: % 40 Meadow fescue (*Festuca pratensis*) + %20 Alfalfa (*Medicago sativa* L.)+ %40 bird's-foot trefoil (*Lotus corniculatus*)

K3: % 40 Orchard grass (*Dactylis glomerata*) + % 20 Alfalfa (*Medicago sativa* L.) + % 40 bird's-foot trefoil (*Lotus corniculatus*)

As a result of the calculation made by taking competition index of plants to be added to the mixture into account, the ratios were calculated in terms of the percentage values in the mixture as follows, and the amount of seeds to be spread to decare were determined accordingly: Brom as 1,9kg/da, Meadow fescue as 6,0 kg/da, Orchard grass as 3,5 kg/da, alfalfa as 1,5 kg/da, yellow-flowered bird's-foot trefoil as 2,7 kg/da. American Bronze turkey poults were used. After turkey poults were naturalized to the pasture in the 9th and 10th weeks, they were enumerated as of the 11th week and 6 jake turkey poults to each sub-parcel (if turkeys cannot be procured as all-male, it will be distributed as 3 jenny and 3 jake) and 54 poults to 9 sub-parcels were put. Every other day, turkeys were fed with wheat of 150g/grains per turkey. Live weight and live weight increases were determined in 14-day periods throughout the study. By using SPSS 20.0 package program, based on general linear model (ANOVA/MANOVA) and according to 5% and 1% significance levels, variance analysis was applied to the results obtained from the research.

3. RESULTS AND DISCUSSION

3.1. Animal Weights

As a result of variance analysis made over average animal weights obtained on seven different measurement dates (GLM-Repeated Measures), it was detected that different observation dates and different mixture ratios make a statistical difference on the increase of animal weights and this difference is significant at (P<0.05) level. Measurement dates are presented in Table 1. The averages and standard errors in question are shown in Table 2, Table 3, and Table 4.

Table 1. Measurement dates of 2014-2015

Measurement Dates	2014	2015
1 rd	7-31-2014	7-31-15
2 rd	8-14-2014	8-14-2015
3 rd	8-31-2014	8-31-2015
4 rd	9-15-2014	9-16-2015
5 rd	9-29-2014	9-29-2015
6 rd	10-13-2014	10-12-2015
7 rd	10-27-2014	10-26-2015

Table 2. Average Animal Weights and Standard Error in Form Periods

Measurement Dates	2014		2015	
	Turkey Weights	Standart Error	Turkey Weights	Standart Error
1 rd	2441,667 e	32,210	636,667 d*	23,651
2 rd	3216,667 de	41,942	1155,000 cd	29,959
3 rd	4059,028 cd	71,508	1955,000 cd	47,810
4 rd	4845,833 c	87,967	2812,500 bcd	59,047
5 rd	6703,472 b	150,988	3595,833 bc	76,549
6 rd	7537,500 ab	172,155	4848,333 ab	70,619
7 rd	8125,000 a*	160,305	6310,833 a	124,371

** Indicates different groups according to tukey's multiple comparison test statistics.

Table 3. Average Animal Weights and Standard Error in Different Mixture Ratios

Mixtures	2014		2015	
	Turkey Weights	Standart Error	Turkey Weights	Standart Error
K1	5518,452 a	161,148	3216,786 a*	72,561
K2	5318,452 ab	161,148	3130,714 a	72,561
K3	4989,881 b	161,148	2787,143b	72,561

** Indicates different groups according to tukey's multiple comparison test statistics.

Regarding the changes in turkey weight increases in different measurement periods, weight increases were linear in both 2014 and 2015 research years as expected. On the last measurement date, the highest weight was reached. The average turkey weight obtained on the last observation date is noted to be greater in 2015 than it was in 2014. The fact that the initial weights of the test animals at the beginning of the experiment in 2014 were greater and more developed compared to those in 2015 although they were at the same age (in terms of weeks) could have affected their final weights and the rate of gaining weight during the experiment. Regarding the effect of different mixture rates on turkey weights, the average weight turkeys reached under the 1st and 2nd mixture conditions was greater compared to the 3rd mixture in both years of the experiment,. Difference among these statistical group averages are shown in Table 2. It can be inferred that Poaceae Forage Plants mixtures including Awnless Bromus in the 1st mixture and Meadow Fescue in the 2nd mixture have a positive and greater effect on turkey weight increases compared to Orchard Grass mixture. It is known that Festuca Pratensis (Meadow Fescue) is one of the most suitable forage plants for pasture areas that are under continuous heavy grazing. Particularly, one of the most important points to pay

attention in choosing plants for poultry pastures is to choose the species that can recover from and tolerate substantial damages to growth points of poaceae against the pressure caused by the intense pecking, scratching, and grazing of poultries (e.g. [4]–[10]). Also in our study, not only Meadow crested wheatgrass but also awnless Bromus continued their existences in the pasture against grazing, in addition to having a positive effect on animal weights. A substantial part of the meadow fescue sown in Southern and Eastern regions of U.S.A is continuously used as pastures(e.g. [8]). It was determined that in these regions, pasture capacity and live weight increase per animal of the pastures formed with meadow fescue is higher compared to other cooler climate poaceae forage plants (e.g. [5], [9]). Particularly in spring and early summer, the animals grazing in orchard grass pasture consume more forage and gain more live weight compared to the animals grazing in tall fescue pasture. In a study carried out for 3 years, 1-year old calves grazing in orchard grass pasture gained 765 g/day live weight, the ones grazing in reedy fescue pasture gained 527 g/day live weight, and the ones grazing in awnless bromus pasture gained 835 g/day live weight (e.g. [6]). It was determined that weight gain of grazing animals is slower in pasture turkey husbandry in Germany compared to traditional backyard turkey husbandry, however, pasture turkey husbandry is superior with regards to meat aroma, taste, and quality. In traditional backyard turkey husbandry, while turkeys gain weight 400% times more of their own weight in a short time of 4,5-5 months, they face intestinal and joint diseases. As the weight increases, the wounds under animals' feet due to faeces and moisture in the poultry-house cause trouble for the animals. For this reason, analgesics relieving animals' increasing pains are added to their rations. In a study, it was confirmed that turkey per m² is 2,7 and weight per m² is 60 kg in the poultry-house. However, in grazing turkey husbandry, animal's over-walking and engaging in instinctive social activities can eliminate troubles caused by over and rapid weight gain, and strengthens immune system (e.g. [1]).

Table 4. Comparing different groups since interaction of different form periods and different mixture ratios is found statistically significant in variance analysis

Measurement Dates	Mixtures	2014		2015	
		Turkey Weights	Standart Error	Turkey Weights	Standart Error
1 rd	K1	2445,83 f*	303,572	610,00 d*	194,395
	K2	2400,00 f	273,464	675,00 d	197,017
	K3	2479,17 f	239,073	625,00 d	155,174
2 rd	K1	3250,00 ef	406,469	1130,00 cd	236,421
	K2	3204,17 ef	331,635	1265,00 cd	262,127
	K3	3195,83 ef	323,673	1070,00 cd	192,217
3 rd	K1	4075,00 de	674,537	1960,00 bcd	371,908
	K2	4110,42 de	612,191	2080,00 bcd	390,142
	K3	3991,67 de	524,128	1825,00 bcd	347,737
4 rd	K1	4920,83 d	733,057	2752,50 bcd	452,617
	K2	4891,67 d	684,561	3087,50 abcd	449,817
	K3	4725,00 d	815,742	2597,50 bcd	469,455
5 rd	K1	6900,00 bc	1284,354	3625,00 abcd	618,040
	K2	6875,00 bc	1256,029	3727,50 abcd	593,712
	K3	6335,42 c	1302,713	3435,00 abcd	565,941
6 rd	K1	7956,25 ab	1226,723	5190,00 abc	547,626
	K2	7700,00 b	1618,910	4860,00 abcd	481,664
	K3	6956,25 bc	1508,621	4495,00 abcd	604,784
7 rd	K1	9081,25 a	924,052	7250,00 a	1029,307
	K2	8047,92 ab	1523,831	6220,00 ab	1041,684
	K3	7245,83bc	1541,027	5462,50abc	799,815

** Indicates different groups according to tukey's multiple comparison test statistics.

4. CONCLUSION

In recent years, as a result of the growing concerns regarding animal welfare and secure food production, relevant institutions and consumers has headed towards new pursuits. Consequently, organic and free-grazing systems have been developed as an alternative for conventional systems in broiler turkey breeding. Since legislative regulations related to protection of animal welfare has been acquiring critical dimension gradually, it is estimated that this breeding systems will be on the agenda more frequently in the future and the production made by means of these systems will show increase. Therefore, breeding practices by means of alternative system and welfare standards are noteworthy subjects that should be put emphasis on.

REFERENCES

- [1] (2015) Anonymous, Available: <http://www.spiegel.de/wirtschaft/service/huehner-mast-bio-hof-und-konventioneller-betrieb-im-vergleich-a-854356.html>.
- [2] J. Berk, and E. Cottin,.Verhalten, Lauffähigkeit und Tibiale Dyschondroplasia in Abhängigkeit von Besatzdichte und strukturierter Haltungsumwelt bei männlichen Puten.NKTBL-Schrift 441, 156-165, 2005.
- [3] H.J. Blokhuis,. Recent developments in European and international welfare regulations. World's Poultry Science Journal 60, 469-477, 2004.
- [4] A. Cavallero, C. Grignani, and A. Reyneri,. Comparison Between Continuous and Rotational Grazing for two Grass- White Clover Mixtures in North Italian Plain. White Clover in Europe. State of the Art. FAO REUR Technical Series 29, s. 48-51, 1993.
- [5] H.D. Gross, G. Lervel, W.B. Gilbert, and G.L. Ellis,. Beef grazing system in pisdment, North Carolina. Agron.J. 58: 307-10, (1966).
- [6] J.Henning, and N. Risner,. Orchardgrass <https://muextension.missouri.edu/explore/agguides/crops/g04511.htm>
- [7] Huber-eicher, B. ve Wechsler, B (1997). Feather pecking in domestic chicks: its relation to dustbathing and foraging. Animal Behaviour 54 (4), 757-768, 1993.
- [8] RR. Lopez, A.G. Matches, and J.D.Baldrige,.Vegetative development and organic reserves of tall fescue under conditions of accumulated growth. Crop. Sci. 7: 409-12, 1967.
- [9] G.O. Mott, C.J. Kaisser, R.C. Peterson, J.R. Randall Peterson, and C.L. Rykerd,. Supplemental feeding of steers on Festuca arundinacea Schreb. Pastures fertilized at three levels of nitrogen Agronomy Journal, 63: 751-54, 1971.
- [10] H. Schäublin,. Eignung verschiedener Grasmischungen im Weideauslauf von Legehennen. Aktualisierung Geflügelproduktion Schweiz, Aktuelles Weideprojekt, 2011.
- [11] (2015) TUIK, website (Online). Available: <https://biruni.tuik.gov.tr/medas/?kn=80&locale=tr>.

Preparation and Stability Analysis of Water Based Al₂O₃, TiO₂ and ZnO Nanofluids

*Adnan Topuz¹, Tahsin Engin², A. Alper Ozalp³, Beytullah Erdogan*¹
Serdar Yurduseven², Serdar Mert², Ahmet Perut⁴*

Abstract

For nanofluids to be able to use practically, they must not cluster and precipitate. Namely, they have to become stable. The target of this study is to determine the parameters that are effective at preparing stable nanofluid and to obtain stable one.

To follow nanofluid stability, its sedimentation state is determined by photo capturing and controlling continuously. It is verified by SEM images that the nanofluids, which do not precipitate and are determined as stable, are distributed homogeneously and do not constitute considerable agglomerates.

The work fluid is made from Al₂O₃, TiO₂, ZnO nanoparticles and deionized water as base fluid. The solutions are prepared with 0.1%, 0.3%, 0.5%, 0.7% and 1.0% volume concentration. They are mixed 30 minutes by probe type of ultrasonic homogenizer at environment conditions. Sodium Dodecyl Sulfate (SDS) was added to the solutions as surfactant to prevent instability occurred due to agglomeration and sedimentation.

At this study, it is investigated that from where the contradictory data for stability experiments in the literature stems. Moreover, the various stable nanofluid preparation parameters that are not available in the literature are given.

It is observed that Al₂O₃, TiO₂ and ZnO nanofluids have stability up to 5 days, 7 days and 21 days without considerably sedimentation, respectively. It is ascertained that properties of nanoparticle and nanofluid preparation parameters are important to enable stability.

***Keywords:** Al₂O₃, TiO₂, ZnO, Nanofluid, Stability, Surfactant*

1. INTRODUCTION

Heating and cooling demands needed at many sectors like transport, electronic, nuclear, military, space, energy production play a rather important role for appearing new technologies [1], [2].

To meet these demands at present applications, various methods are used. Some of them are increment at surface areas that heat transfer occurs, higher temperature difference for more heat transfer and material usage having durable to high temperature. However, it is already reached to usage limits of these methods due to the causes like dimensional limits, durable limits of material, production costs. Moreover, due to performance limits of available work fluids i.e. antifreeze, engine oil, fluids that have particles with mili-micrometer sized are used as a solution. Yet, instability occurred because of agglomeration and sedimentation at these particles induces clogging in microchannels and desired developments not be able to be obtained [3]. With time, thanks to production technology developed, particles with nanometer sized and nanofluids have obtained. Nanofluid usage has started as work fluid.

Nanofluid is a suspension obtained by dispersing particles with nanometer sized in a fluid. Nanoparticle sizes used in nanofluids are generally between 1 nm and 100 nm [1], [4] - [7]. Nanofluids are prepared by one of the methods called 1-step or 2-step. At 1-step method, nanofluid is prepared by chemical reaction at one-step. As for 2-step method, firstly, particle is produced at nanometer size, and then nanofluid is obtained by mixing them in a base fluid. Nanofluids obtained by 1-step method are more stable than ones obtained by 2-step. However, at 1-step method, particle size cannot be controlled. At 2-step method, nanoparticles needed can be found at desired size and property from many producers [1], [4].

At 2-step method, nanofluids can be prepared by numerous sub methods: Magnetic stirrer, high shear mixer, ball mill, ultrasonic bath, probe type ultrasonic homogenizer, adding surfactant, changing pH, surface modification of particle [1], [4], [6]. In 2-step methods, the most efficient and effective one is determined probe type ultrasonic homogenizer in the literature [6], [8], [9].

Nanofluids are desired the properties like high thermal conductivity, high heat transfer performance, long stability time. However, they are not demanded clogging at microchannels due to agglomeration and sedimentation, and increase at pumping losses due to viscosity increment and pressure drop. These unwanted results are generally related to nanofluid stability.

¹ Corresponding author: Bülent Ecevit University, Engineering Faculty, Department of Mechanical Engineering, Zonguldak, Turkey.
beytullaherdogan@hotmail.com

² Sakarya University, Engineering Faculty, Department of Mechanical Engineering, Sakarya, Turkey.

³ Uludağ University, Engineering Faculty, Department of Mechanical Engineering, Bursa, Turkey.

⁴ Kale Auto Radiator Industry and Trade Inc., Kocaeli, Turkey.

Stability of nanofluids can be examined by various methods: Ultra Violet-Visible Spectrophotometer (UV-Vis), Zeta potential, SEM, TEM, DLS, XRay Diffraction, sedimentation method, 3-omega, centrifugation method, photo capturing [1], [4], [10].

Nanofluid stability is enabled by the methods like using surfactant, pH changing, modification of nanoparticle [1], [4]. To enable nanofluid stability, the researchers who do not want a change at thermal properties of nanofluid did not use surfactant [11] - [13]. However, those who use surfactant desired it to prevent stability problem [12], [14] - [16], [17] Pg.31, [18] Pg.57, [19].

Even after only ultrasonic mixing, attraction forces existed between particles cause them to cluster. Nanoparticle groups at micrometer and bigger sized occurred due to that clustering start to behave like particles at macro sized. For they have bigger density than base fluid, they make instability by collapsing the bottom of base fluid. Surfactants are used to prevent that sedimentation. Surfactant covers surface of nanoparticle and make repelling force between them. So, clustering of particles is prevented considerably. Only surfactant usage is not enough to enable stability. Because, when nanoparticles are dispersed in base fluid for the first time, since they are clustered, surfactant cannot affect among them. These agglomerations can be broken by ultrasonication [3].

In the literature, there are different results for same nanofluids whose stability changes from 1 hour to 1 year [12]. There are limited number of studies that include stable nanofluid preparation parameters and indicate them to be standardized [17] Pg.76. This study works to determine the parameters that are effective at preparing stable nanofluid, to standardize these parameters and to obtain stable nanofluid.

This study consists of four sections: Material and Method, Experiment, Results, Conclusions. Material and Method section includes properties of used materials and how to be prepared nanofluids. Experiment section includes two subsections in the way nanofluid stability parameters and nanofluid SEM/TEM images.

2 MATERIAL AND METHOD

2.1. Properties of nanoparticles

Al₂O₃, TiO₂ and ZnO nanoparticles are used to prepare nanofluid. Average sizes of these particles are 20 nm, 10-25 nm and 18 nm, respectively. Nanoparticles are bought from "Nanografi Ltd. Company". All properties of nanoparticles are given in Table 1, their TEM images supplied by the producer are given in Figure 1.

Sodium Dodecyl Sulfate (SDS) as surfactant was used to prevent sedimentation of nanoparticles by clustering and to make nanofluid stability keep on. SDS was bought from "Merck Inc." The density of this matter is 1.1 g/cm³ and its pH value is between 6 and 9.

2.2. Preparation of nanofluids

All nanofluids at this study were prepared by 2-step method. Probe type ultrasonic homogenizer was used to disperse nanoparticles in a deionized water (Ultrasonic Homogenizer Mark/Model: Optic Ivymen System / CY-500, Power: 500W, Frequency: 20kHz, Probe Diameter/Length: Ø5.6/60mm).

Firstly, mass amounts of nanoparticle, deionized water and SDS were calculated in accordance with desired nanofluid volumetric concentration, nanofluid volume and SDS weight concentration from Table 2. These quantities were weighed by a precision balance (AND GX-600, Max Mass: 610g, Deviation: 0.001g). Then, nanofluids were prepared in a flask by paying regard to many parameters considered to be effective at nanofluid stability. The nanofluid taken from the bottom location of the flask by a pipet was filled in the glass tubes, which have Ø16x160 mm dimensions with screw thread. Stabilities of nanofluids were examined by photo capturing method according to time. The most suitable parameters were determined by these images. According to these parameters, the most stable nanofluids were prepared.

The equations used in Table 2 for nanofluids to be prepared are the following:

Volume concentration of nanofluid,

$$\phi = \frac{V_{np}}{V_{nf}} = \frac{\rho_{nf} - \rho_{bf}}{\rho_{np} - \rho_{bf}} \quad (1)$$

Volume of nanofluid,

$$V_{nf} = V_{np} + V_{bf} \quad (2)$$

Mass of nanofluid,

$$m_{nf} = m_{np} + m_{bf} \quad (3)$$

Density for nanofluid, nanoparticle and deionized water,

$$\rho = \frac{m}{V} \quad (4)$$

Weight concentration of SDS/Nanoparticle,

$$\phi = \frac{m_{SDS}}{m_{np}} \quad (5)$$

During mixing nanofluids by ultrasonic homogenizer, when it was not taken any precaution, too temperature increment was seen in the sample (nanofluid). Such that, this temperature increment reached 60 degrees in 10 minutes. During mixing, increased temperature affects both chemical-thermal properties of nanofluid and causes ultrasonic homogenizer to work unproductively [17] Pg.32. At the experiments done in this study, it was seen that uncontrolled temperature increment decreased vibrations of ultrasonic homogenizer. This was noticed by change of ultrasonic sound and decrease at surge of the top surface of the sample. Therefore, a heat bath was used to hold nanofluid temperature constant (Mark/Model: Cole Parmer / EW-12108-25, Temperature: -20~200oC, Temperature Stability: ±0.01oC, Bath Capacity: 6L, Heating Capacity: 1kW, Cooling Capacity: 200W, Flow Rate: 11~24L/min). The flask included nanofluid was put in the heat bath held at constant temperature as Figure 2. So, 100 mL of nanofluids were prepared. In addition, during ultrasonication, high temperatures were seen at the probe of ultrasonic homogenizer. To compensate it, the probe was cooled by a fan.

Table 5. Properties of nanoparticles

Nano Particle	Type	Density (kg/m ³)	Purity	Average Size	Specific Surface Area m ² /g	Shape
Al ₂ O ₃	Gamma	3890	>%99	20 nm	138	Close to spherical
TiO ₂	Anatase	3900	>%99.5	10-25 nm	200-240	Close to spherical
ZnO	—	5606	%99.95	18 nm	40-70	Close to spherical

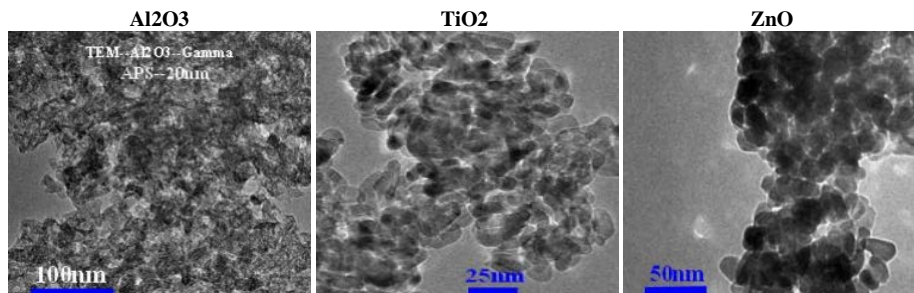


Figure 11. TEM images of nanoparticles

Table 6. Nanofluids according to volumetric concentration at 20oC

Nano Fluid	Volume Concent.	Nanofluid Volume	Base Fluid Density	Particle Density	Particle Volume	Base Fluid Volume	Particle Mass	Base Fluid Mass	SDS-Particle Weight Concent.	SDS Mass
	ϕ (%)	V_{nf} (mL)	ρ_{bf} (kg/m ³)	ρ_{np} (kg/m ³)	V_{np} (mL)	V_{bf} (mL)	m_{np} (g)	m_{bf} (g)	$\phi_{w,SDS}$ (%)	m_{SDS} (g)
Al ₂ O ₃	0,10%	100	998,0	3890	0,10	99,90	0,389	99,700	50,00%	0,195
	0,30%	100	998,0	3890	0,30	99,70	1,167	99,501	25,00%	0,292
	0,50%	100	998,0	3890	0,50	99,50	1,945	99,301	15,00%	0,292
	0,70%	100	998,0	3890	0,70	99,30	2,723	99,101	15,00%	0,408
	1,00%	100	998,0	3890	1,00	99,00	3,890	98,802	15,00%	0,584
TiO ₂	0,10%	100	998,0	3900	0,10	99,90	0,390	99,700	50,00%	0,195
	0,30%	100	998,0	3900	0,30	99,70	1,170	99,501	25,00%	0,293
	0,50%	100	998,0	3900	0,50	99,50	1,950	99,301	15,00%	0,293
	0,70%	100	998,0	3900	0,70	99,30	2,730	99,101	15,00%	0,410
	1,00%	100	998,0	3900	1,00	99,00	3,900	98,802	15,00%	0,585
ZnO	0,10%	100	998,0	5606	0,10	99,90	0,561	99,700	50,00%	0,280
	0,30%	100	998,0	5606	0,30	99,70	1,682	99,501	50,00%	0,841
	0,50%	100	998,0	5606	0,50	99,50	2,803	99,301	25,00%	0,701
	0,70%	100	998,0	5606	0,70	99,30	3,924	99,101	15,00%	0,589
	1,00%	100	998,0	5606	1,00	99,00	5,606	98,802	15,00%	0,841

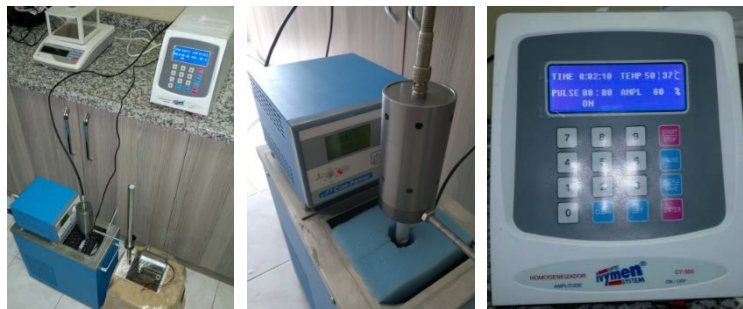


Figure 12. Preparation of nanofluid with temperature control

3 EXPERIMENT

3.1. Nanofluid stability parameters

The parameters that affect stability of nanofluids are classified as follows:

- Adding surfactant
- Ultrasonic power intensity
- Ultrasonic mixing time
- Bath temperature
- Height of ultrasonic probe
- Flask diameter
- Nanoparticle type

The effect of each parameter on nanofluid stability was investigated as subtitles. The information at the top row of the figures that show effect of these parameters includes (Figure 3–Figure 10): 1. Nanofluid volumetric concentration, 2. Nanofluid type, 3. Investigated parameter, 4. Time passed after preparing nanofluid.

Stability was examined by the photos taken daily, according to be transparent from the top surface of the tube and sedimentation at the its bottom.

3.1.1. Adding surfactant

In this section, it was investigated whether surfactant usage is necessary and if it is necessary, what its concentration value must be. For this purpose, the nanofluids included and not included surfactant were prepared (Figure 3). It was seen that the nanofluids not included surfactant were settled by agglomerating in 20 minutes (Figure 3-a,b,c). After that result was obtained, to enable nanofluid stability, SDS was selected as surfactant widely used in the literature [1], [4]. At the nanofluids prepared by using SDS, it was seen that agglomeration was prevented and stability was enabled (Figure 3-d,e,f). As a result, it was decided to use SDS for all nanofluids. In order to determine SDS concentration, the nanofluids included SDS between 1% and 100% in the way SDS/Nanoparticle as mass were prepared (Figure 4). At Figure 4, for the nanofluid with 0.5% volumetric concentration, while stability was enabled for SDS with 15% and higher weight concentration, SDS with same 15% weight concentration was insufficient for the nanofluid with 0.2% volumetric concentration. From here, it was concluded that SDS having different weight concentration is necessary for nanofluids with different volumetric concentration. As general trend, it was seen that the more nanofluid volumetric concentration decreases, the more SDS weight concentration needed increases (Figure 4-d,e,f). By this way, the lower limit of SDS weight concentration was determined in a way to change from 15% to 50% for all nanofluids by some experiments (Table 2). In the literature, SDS weight concentration is generally given as "Surfactant/Nanoparticle" ([12], [14], [20]). Yet, in some studies, this ratio is also given as "SDS/Nanofluid" ([21], [22]). Therefore, it must be paid attention which reference SDS concentration values are given according to.

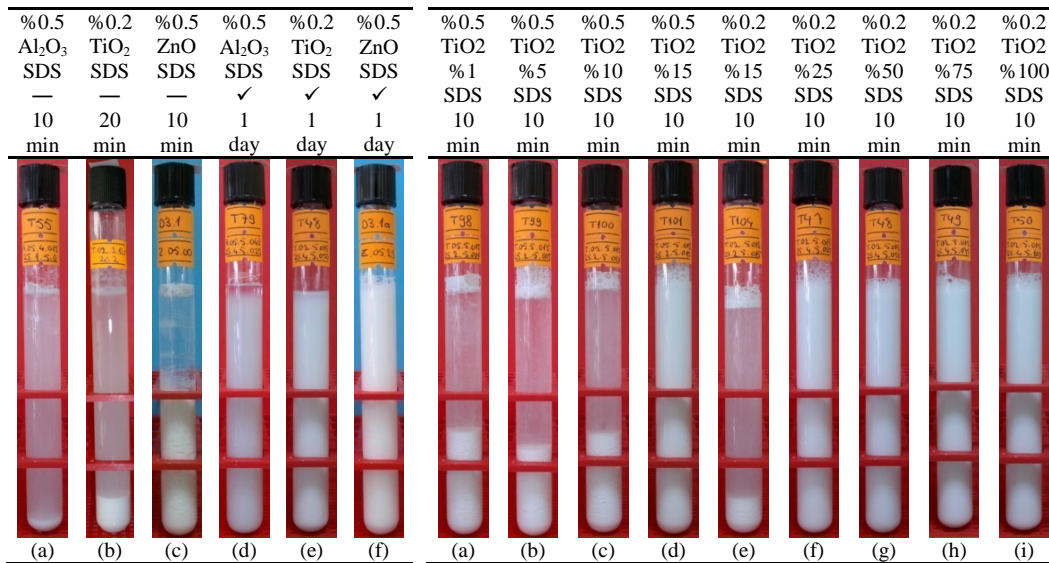


Figure 13. Controlling whether surfactant is necessary or not

Figure 14. Determining SDS weight concentration

It was worked to find a lower limit for using SDS. Because, SDS amount must be used many enough to enable nanofluid stability; it must be used little enough to decrease concretion, not to increase cost and not to affect thermodynamic properties.

3.1.2. Ultrasonic power intensity

Ultrasonic vibration power (W/mL) per nanofluid volume was investigated. For this purpose, three different nanofluids were prepared in a way to be their power intensity 3, 4, 5 W/mL (Figure 5). It was seen that the more bigger ultrasonic power intensity is, the more longer stability time is (Figure 5-d,e,f).

As a result, it was decided that ultrasonic power must be applied to all nanofluids at full power (500 W) and this power must remain as a constant parameter.

3.1.3. Ultrasonic mixing time

It was examined for how much time it is necessary for the nanofluids to expose to ultrasonic vibration. For this, the nanofluids changed from 5 minutes to 240 minutes their mixing time were prepared (Figure 6). It could not be seen that mixing time lasting than 30 minutes had apparent effective on nanofluid stability time (Figure 6-e,f,g). Therefore, it was decided that all nanofluids must be exposed to ultrasonic vibration for 30 minutes. This time is same as numerous studies in the literature ([14], [17] Pg.32, [23]).

3.1.4. Bath temperature

It was investigated at what temperature nanofluid must be during mixing it with ultrasonic homogenizer. For that purpose, during mixing, the nanofluids held their temperature constant at 20, 30, 40 and 50 degrees were prepared (Figure 7). It was not seen that temperature had significant effective on stability (Figure 7-e,f,g,h). Consequently, in order to prevent too temperature increase during mixing, it was seen that the heat bath is necessary to be held constant at any temperature. However, since high temperature causes efficiency of ultrasonic homogenizer to decrease and nanofluid volumetric concentration to change (increase) due to evaporating of water, it was made a decision that the heat bath must be held constant at 20-25°C environment temperature.

3.1.5. Ultrasonic probe height

Ultrasonic power that ultrasonic homogenizer gives fluid is mainly given from the top surface of the probe. Since conical volume that the tip surface of the probe makes and exposed vibrations changes, it was examined at how many height the probe must be from the bottom of the flask. To control that situation, the nanofluids were prepared by being held the probe at 1, 2, 3, 4 and 5 cm height (Figure 8). It was not seen that the probe height is effective on stability. As a conclusion, the probe can be held at any height from the bottom of the flask. Yet, even if it is little, to benefit from ultrasonic vibrations distributed from the side surfaces of the probe and to decrease noise during working, it was decided that the probe must be held at 1-2 cm height from the bottom of the flask.

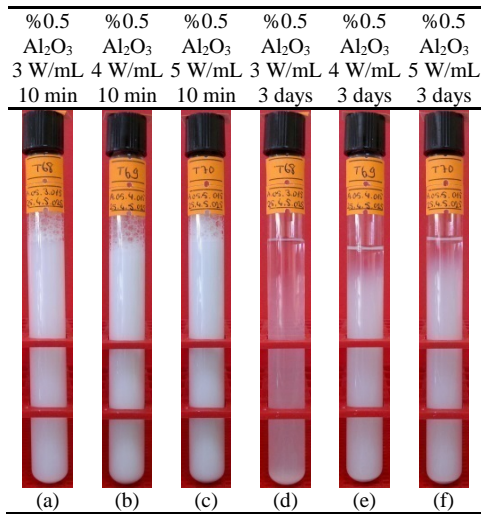


Figure 15. Determining ultrasonic power intensity

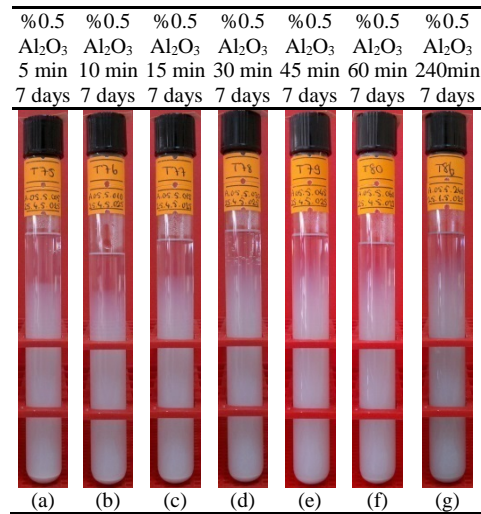


Figure 16. Determining ultrasonic mixing time

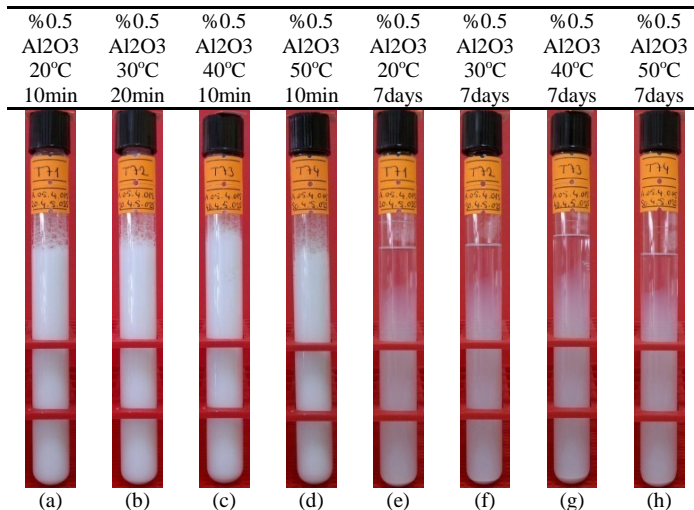


Figure 17. Determining bath temperature

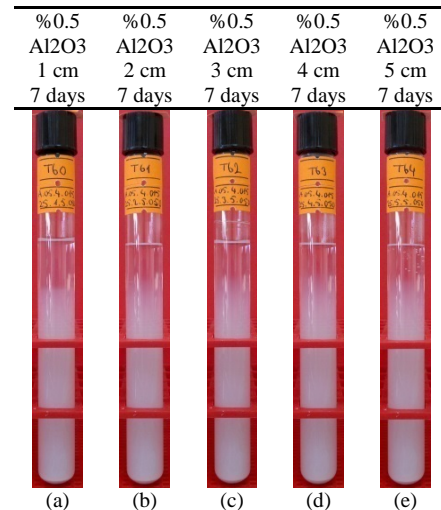


Figure 18. Determining height of ultrasonic probe

3.1.6. Flask diameter

Due to the reasons described at the probe height section, it was examined what flask diameter must be. For this purpose, the nanofluids were prepared by using 5, 7 and 9 cm diameter of the flask (Figure 9). As determined at the probe height, similarly it was not seen that the flask diameter is effective on stability (Figure 9-d,e,f). As a result, a flask with any diameter can be used.

3.1.7. Nanoparticle type

For nanofluids included different nanoparticles have different stability time, nanoparticle type was investigated effect on stability. The aim is to determine the nanofluid that had the longest stability time trend between different nanofluids. Al₂O₃, TiO₂ and ZnO nanoparticles were used to test stability time. The stability times of the nanofluids prepared were determined as ZnO, TiO₂ and Al₂O₃ from the longest stability time to the least, respectively (Figure 10).

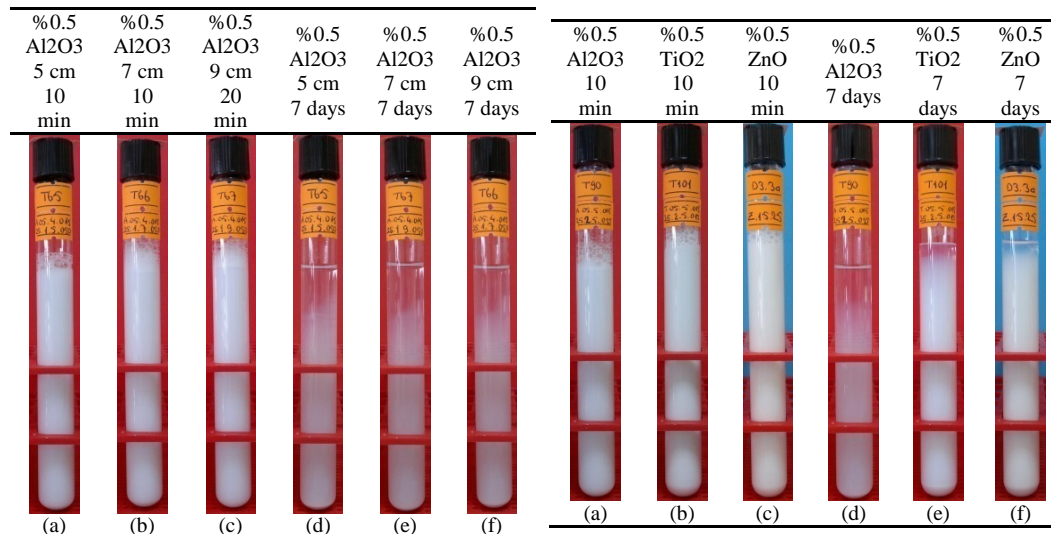


Figure 19. Determining flask diameter

Figure 20. The effect of the nanoparticle type on the stability time

3.2. Stability control of nanofluid

The nanofluids were prepared by considering the optimum values of the parameters that affect nanofluid stability time. The optimum parameters can be summarized as follows:

- Surfactant : SDS (Table 2)
- Ultrasonic power : 500 W
- Mixing time : 30 min
- Bath temperature : 25°C
- Probe height : 1-2 cm
- Nanofluid volume : 100 mL (Table 2)

The nanofluids were prepared according to the values in Table 2 under above conditions. Their images are given in Figure 11 three hours after preparing.

The nanofluids that have the longest stability time at Figure 11 were determined as 0.5%, 0.7% and 1.0% volumetric concentrations for Al₂O₃; 0.3% for TiO₂; all concentrations for ZnO. The stability time without apparently sedimentation for these concentrations was enabled up to 5 days for Al₂O₃, up to 26 days for TiO₂, up to 21 days for ZnO (Figure 12). It changed from some days to 2 weeks for other concentrations. As average, it can be said that the stability time continued up to 5 days for Al₂O₃ nanofluid, 7 days for TiO₂ nanofluid, 21 days for ZnO nanofluid.

SEM images were taken in order to confirm that the stable nanofluids prepared were distributed homogeneously and did not include big clusters according to the original nanoparticle size. Moreover, TEM images were taken in order to verify that they were at the desired size. SEM and TEM images of the Al₂O₃, TiO₂ and ZnO nanofluids with 0.5% volumetric concentration were given in Figure 14 and Figure 15.

For SEM images, SEM device (FEI Quanta FEG 450, STEM Detector, 30 kV) in Bülent Ecevit University, Science and Technology Application and Research Center (ARTMER) was used (Figure 13). As for TEM images, TEM device (FEI Tecnai G² Spirit BioTwin, CTEM, 120 kV) in Middle East Technical University, Central Laboratory, R&D Education and Measurement Center was used.

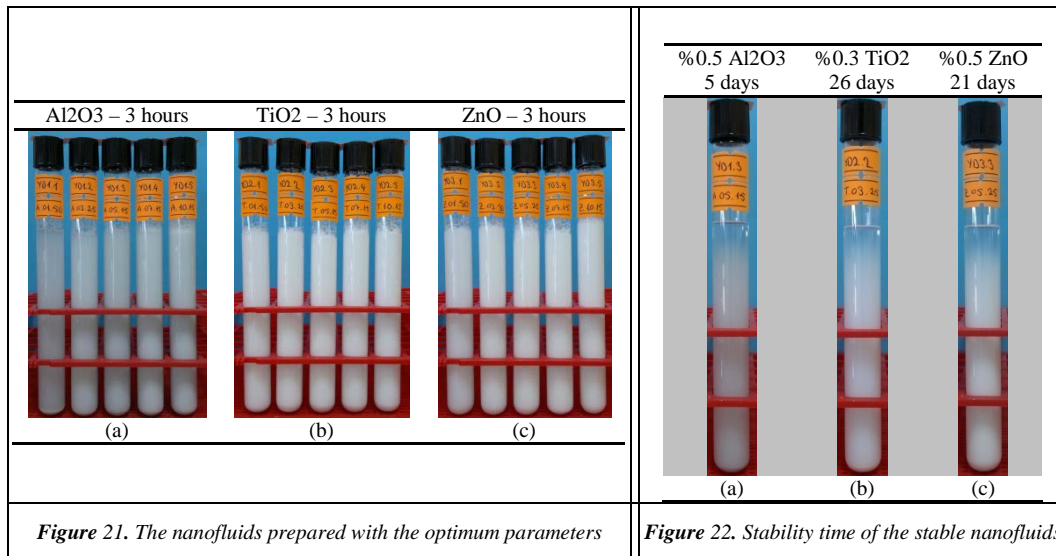


Figure 21. The nanofluids prepared with the optimum parameters

Figure 22. Stability time of the stable nanofluids



Figure 23. STEM device in ARTMER

4 RESULTS

The following results were found by the parameters that were investigated to obtain stable nanofluids:

- To prevent sedimentation of nanofluids by agglomerating, SDS as surfactant is necessary. For this study, SDS weight concentrations are given in Table 2.
- It is required to run the ultrasonic homogenizer at full power. In this study, the device was run at 500 W powers.
- The ultrasonic mixing time was determined as 30 minutes.
- The bath temperature was chosen as 25°C.
- The tip of the ultrasonic probe was held at 1-2 cm height from the bottom of the flask.
- It was seen that Al₂O₃, TiO₂ and ZnO nanofluids prepared with the optimum parameters at 0.1%, 0.3%, 0.5%, 0.7% and 1.0% volumetric concentrations didn't show apparently sedimentation up to 5, 7 and 21 days as average, respectively.
- It was found that the nanofluids prepared with the optimum parameters remained stable max. 5 days for 0.5% Al₂O₃, 26 days for 0.3% TiO₂ and 21 days for ZnO.
- SEM and TEM images were taken for the stable nanofluids. It was found that homogeneous distribution obtained and the nanoparticles were at the specified size from the images.

5 CONCLUSIONS

- To minimize some controversial results (i.e. instability, stability time up to one year, anomalous thermal conductivity increase, too heat transfer increase) seen at different studies, nanoparticle properties used have to be same. Some of these properties are producer, nanoparticle size (20nm, 50nm), nanoparticle shape (spherical, cylindrical, porous), nanoparticle purity (99%) and quality (homogeneous size distribution, specified size and shape).
- At nanofluid stability researches, zeta potential of nanofluid can be compared with images showed it remained stable. By this way, it can be appeared physically whether 30 mV of zeta potential limit value is enough ([1], [2], [4]).
- At SEM/TEM images given for nanofluid stability analyses, not only nanoparticle size images, but images at scale showed suspension distributed homogeneously must be also given.

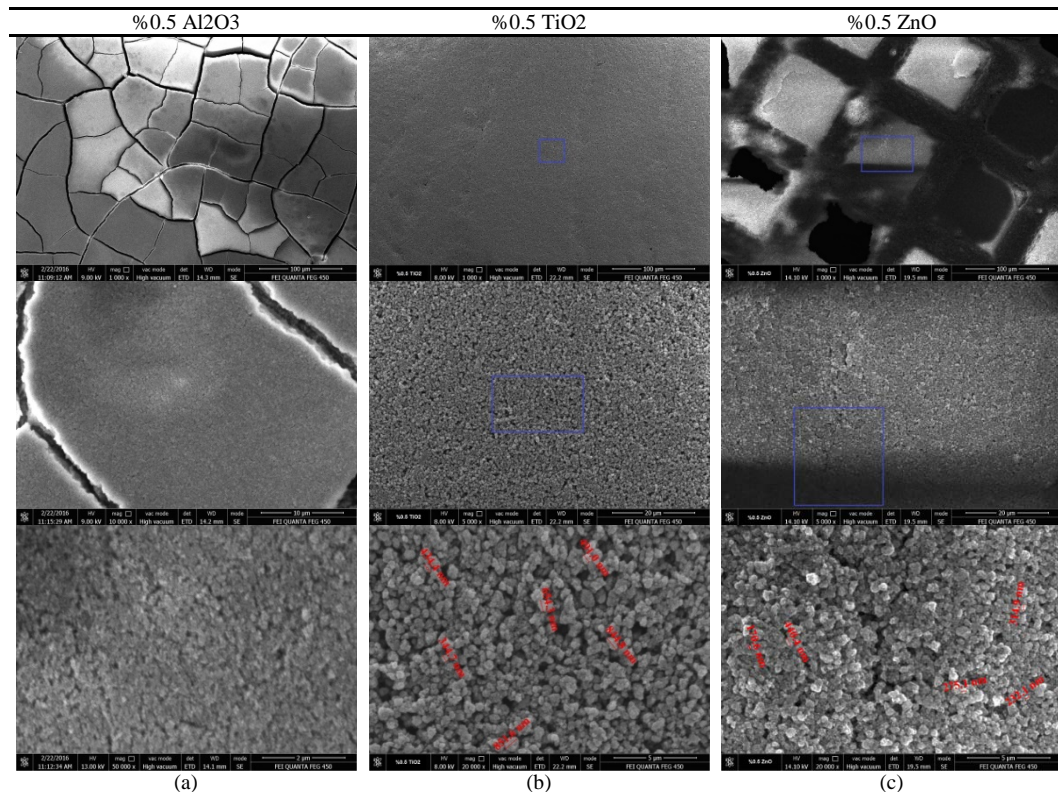


Figure 24. SEM images the nanofluids with 0.5% vol. concentration

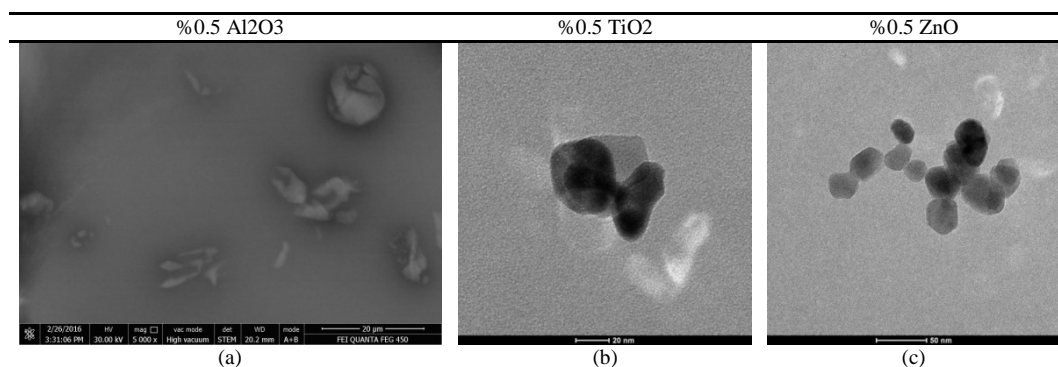


Figure 25. TEM images the nanofluids with 0.5% vol. concentration

ACKNOWLEDGEMENT

This project was supported by "The Scientific and Technological Research Council Of Turkey" (TUBITAK, Project No. 5140013). The authors gratefully acknowledge the financial supports from TUBITAK.

REFERENCES

- [1] A. Ghadimi, R. Saidur, H.S.C. Metselaar, A review of nanofluid stability properties and characterization in stationary conditions, *International Journal of Heat and Mass Transfer* 54 (2011) 4051–4068.
- [2] W. Yu, H. Xie, A Review on Nanofluids: Preparation, Stability Mechanisms, and Applications, *Hindawi Publishing Corporation Journal of Nanomaterials* Volume 2012, Article ID 435873.
- [3] Y. Hwang, J.-K. Lee, J.-K. Lee, Y.-M. Jeong, S. Cheong, Y.-C. Ahn, S. H. Kim, Production and dispersion stability of nanoparticles in nanofluids, *Powder Technology* 186 (2008) 145 – 153.
- [4] S. Mukherjee, S. Paria, Preparation and Stability of Nanofluids - A Review, *IOSR Journal of Mechanical and Civil Engineering (IOSR-JMCE)*, e-ISSN: 2278-1684, p-ISSN: 2320-334X, Volume 9, Issue 2 (Sep. - Oct. 2013), PP 63-69.
- [5] M.F. Zawrah, R.M. Khattab, L.G. Girgis, H. El Daidamony, R. E. A. Aziz, Stability and electrical conductivity of water – base Al₂O₃ nanofluids for different applications, *HBRC Journal* (2015).
- [6] R. Mondragon, J. E. Julia, A. Barba, J. C. Jarque, Characterization of silica–water nanofluids dispersed with an ultrasound probe: A study of their physical properties and stability, *Powder Technology* 224 (2012) 138–146.
- [7] A. Ghadimi, I. H. Metselaar, The influence of surfactant and ultrasonic processing on improvement of stability, thermal conductivity and viscosity of titania nanofluids, *Experimental Thermal and Fluid Science* 51 (2013) 1–9.
- [8] M. J. Pastoriza-Gallego, C. Casanova, R. Páramo, B. Barbés, J. L. Legido, and M. M. Piñeiro, A study on stability and thermophysical properties (density and viscosity) of Al₂O₃ in water nanofluids, *Journal of Applied Physics* 106, 064301 (2009).
- [9] S.J. Chung, J.P. Leonard, I. Nettleship, J.K. Lee, Y. Soong, D.V. Martello, M.K. Chyu, Characterization of ZnO nanoparticle suspension in water: Effectiveness of ultrasonic dispersion, *Powder Technology* 194 (2009) 75–80.
- [10] J. Lee, K. Han, J. Koo, A novel method to evaluate dispersion stability of nanofluids, *International Journal of Heat and Mass Transfer* 70 (2014) 421–429.
- [11] M.M. Heyhat, F. Kowsary, A.M. Rashidi, M.H. Momenpour, A. Amrollahi, Experimental investigation of laminar convective heat transfer and pressure drop of water-based Al₂O₃ nanofluids in fully developed flow regime, *Experimental Thermal and Fluid Science* 44 (2013) 483–489.
- [12] N. A. C. Sidik, H.A. Mohammed, O. A. Alawi, S. Samion, A review on preparation methods and challenges of nanofluids, *International Communications in Heat and Mass Transfer* 54 (2014) 115–125.
- [13] S. Z. Heris, M. N. Esfahany, S.Gh. Etemad, Experimental investigation of convective heat transfer of Al₂O₃/water nanofluid in circular tube, *International Journal of Heat and Fluid Flow* 28 (2007) 203–210.
- [14] B.A. Bhanvase, M.R. Sarode, L.A. Putterwar, Abdullah K.A., M.P. Deosarkar, S.H. Sonawane, Intensification of convective heat transfer in water/ethylene glycol based nanofluids containing TiO₂ nanoparticles, *Chemical Engineering and Processing* 82 (2014) 123–131.
- [15] J. Philip, P.D. Shima, Thermal properties of nanofluids, *Advances in Colloid and Interface Science* 183–184 (2012) 30–45.
- [16] S. Kakaç, A. Pramuanjaroenkij, Review of convective heat transfer enhancement with nanofluids, *International Journal of Heat and Mass Transfer* 52 (2009) 3187–3196.
- [17] A. Turgut, Investigation of Thermophysical Properties of Nanofluids, *Dokuz Eylül University, Graduate School of Natural and Applied Sciences, PhD Thesis*, 2010.
- [18] E.F. Dilek, Nanoakışkanların hazırlanması ve ısı iletkenliklerinin belirlenmesi (Preparation of nanofluids and determination of thermal conductivities of nanofluids), *MS Thesis, Graduate School of Natural and Applied Sciences, Atatürk University*, 2008.
- [19] M. Naraki, S.M. Peyghambarzadeh, S.H. Hashemabadi, Y. Vermahmoudi, Parametric study of overall heat transfer coefficient of CuO/water nanofluids in a car radiator, *International Journal of Thermal Sciences* 66 (2013).
- [20] H. M. Ali, H. Ali, H. Liaquat, H. T. B. Maqsood, M. A. Nadir, Experimental investigation of convective heat transfer augmentation for car radiator using Zn-water nanofluids, *Energy* 84 (2015).
- [21] Wang X.-J., Li H., Li X.-F., Wang Z.-F., Lin F., Stability of TiO₂ and Al₂O₃ Nanofluids, *Chin. Phys. Lett.* Vol. 28, No. 8 (2011) 086601.
- [22] G. Xia, H. Jiang, R. Liu, Y. Zhai, Effects of surfactant on the stability and thermal conductivity of Al₂O₃/de-ionized water nanofluids, *International Journal of Thermal Sciences* 84 (2014) 118-124.
- [23] M. Karimzadehkhoei, S. E. Yalçın, K. Şendur, M. P. Mengüç, A. Koşar, Pressure drop and heat transfer characteristics of nanofluids in horizontal microtubes under thermally developing flow conditions, *Experimental Thermal and Fluid Science* 67 (2015) 37–47.

Thermodynamics Property Measurements of Water Based Al₂O₃, TiO₂, ZnO Nanofluid

*Adnan Topuz¹, Tahsin Engin², A. Alper Ozalp³, Beytullah Erdogan*¹,
Serdar Yurduseven², Serdar Mert², Ahmet Perut⁴*

Abstract

It is necessary for thermophysical properties of nanofluids to be determined in order to evaluate their thermal performances like heat transfer, convection heat transfer coefficient, Nusselt number. The purpose of this study is to obtain thermophysical properties of nanofluids. Al₂O₃, TiO₂ and ZnO metal oxides are used as nanoparticle, while deionized water is used as base fluid. The solutions included nanoparticles in a way to be each with 0.5%, 0.7% and 1.0% volume concentration were prepared. The nanofluids were obtained by mixing those solutions 30 minutes by probe type of ultrasonic homogenizer at environment conditions. Sodium Dodecyl Sulfate (SDS) was added to the solutions as surfactant to prevent instability occurred due to agglomeration and sedimentation. For thermal conductivity measurement, the device that works by transient hot wire method was used between 30-60°C temperatures. In addition, for viscosity measurement, the device that works as based on vibrating plates method was used between 20-50°C temperatures. Density and specific heat values are obtained with help of the well-known equations while thermal conductivity and viscosity are measured. Thanks to this study, it is emphasized how thermophysical properties of nanofluids change according to temperature and volume concentration. Moreover, their curve fitting equations are obtained. All of thermophysical properties are also shown as graphics. It is established that thermal conductivity of nanofluids is proportional to temperature, and viscosity of it is proportional to volume concentrations but inversely with temperature.

Keywords: Al₂O₃, TiO₂, ZnO, Nanofluid, Thermal conductivity, Viscosity.

1 INTRODUCTION

Thermophysical properties of nanofluids are required to determine numerous performance types like heat transfer, pumping losses. These properties of nanofluids take different values depending on concentration, temperature, particle size and shape. For this purpose, information about the studies in the literature is given and nanofluid thermophysical measurements are done. Azmi 2016 has worked on giving a comprehensive review on the research progress and on the enhancement of effective thermal conductivity and effective dynamic viscosity of nanofluids such as Al₂O₃ (Aluminum oxide), Cu (pure Copper), CuO (Copper oxide), Fe₃O₄ (Iron oxide), SiC (Silicon carbide), SiO₂ (Silicon dioxide), TiO₂ (Titanium oxide), ZnO (Zinc oxide) and ZrO₂ (Zirconium dioxide). Heyhat M.M., Kowsary F., Rashidi A.M., Momenpour M.H., Amrollahi A., Şahin B., Gültekin G.G., Manay E., Karagöz S.' studies are related to experimental investigation of laminar convective heat transfer and pressure drop of water-based Al₂O₃ nanofluids in fully developed flow regime. Turgut A., Tavman I., Chirtoc M., Schuchmann H.P., Sauter C., Tavman S., Utomo A.T., Poth H., Robbins P.T., Pacek A.W. focused on thermal conductivity and viscosity measurements of water-based TiO₂ nanofluids. Duangthongsuk W., Wongwises S., worked an experimental study on the heat transfer performance and pressure drop of TiO₂-water nanofluids flowing under a turbulent flow regime. Azmi W.H., Sharma K.V., Sarma P.K., Mamat R., Anuar S., investigated comparison of convective heat transfer coefficient and friction factor of TiO₂ nanofluid flow in a tube with twisted tape inserts. Ferrouillat S., Bontemps A., Poncelet O., Soriano O., Gruss J.A., Nguyen C.T., Desgranges F., Roy G., Galanis N., Mare T., Boucher S., Mintsa H.A., searched temperature and particle-size dependent viscosity data and Influence of nanoparticle shape factor on convective heat transfer and energetic performance of water-based SiO₂ and ZnO nanofluids. Sharma K.V., Sarma P.K., Azmi W.H., Mamat R., Kadirgama K., found out correlations to predict friction and forced convection heat transfer coefficients of water based nanofluids for turbulent flow in a tube.

Generally, it is done on the studies between limited temperature ranges for one type of nanofluid. The difference sides of this study according to the other studies are more nanoparticle types, wide temperature ranges and different volumetric concentration. In this study, water based Al₂O₃, TiO₂ and ZnO nanofluids with 0.5%, 0.7% and 1.0% volume concentration were prepared. Thermophysical properties; thermal conductivity and viscosity of these nanofluids were measured between 20-60°C experimentally. All measurements results are given in graphics.

¹ Corresponding author: Bülent Ecevit University, Engineering Faculty, Department of Mechanical Engineering, Zonguldak, Turkey. beytullaherdogan@hotmail.com

² Sakarya University, Engineering Faculty, Department of Mechanical Engineering, Sakarya, Turkey.

³ Uludağ University, Engineering Faculty, Department of Mechanical Engineering, Bursa, Turkey.

⁴ Kale Auto Radiator Industry and Trade Inc., Kocaeli, Turkey.

Nomenclature		Greek symbols	
d	nanoparticle diameter (nm)	α	thermal diffusivity ($\frac{m^2}{s}$)
c_p	specific heat (J/kgK)	μ	dynamic viscosity (Pa.s)
DW	deionized water	ρ	density ($\frac{kg}{m^3}$)
k	thermal conductivity ($\frac{W}{m.K}$)	ϕ	volume concentration ratio
m	mass (kg)	ϕ_w	weight concentration ratio
n	shape factor, particle number per unit volume (1/m ³)	ψ	sphericity
r	nanoparticle radius (nm)		
h	nanolayer thickness (nm)	Subscripts	
SDS	Sodium Dodecyl Sulfate	bf	base fluid
T	temperature (K, °C)	eq	equivalent
TEM	Transmission Electron Microscopy	nf	nanofluid
V	volume (m ³)	np	nanoparticle
		nl	nanolayer

2 MATERIAL AND METHOD

2.1 Properties of nanoparticles

Al₂O₃, TiO₂ and ZnO nanoparticles are used to prepare nanofluid. Average sizes of Al₂O₃ (Sigma-Aldrich), TiO₂ (Nanografi) and ZnO (Nanografi) nanoparticles are 13 nm, 10-25 nm and 18nm respectively. The detailed properties of the nanoparticles and producer's TEM images are given in

Table 1 and Table 2.

Sodium Dodecyl Sulfate (SDS) as surfactant is used to prevent the nanoparticles to precipitate by agglomerating and keep on the stability of nanofluid. However, SDS is not used in Al₂O₃ nanofluid since the desired stability is obtained even without it. SDS (Merck) density is 1.1 g/cm³, and pH value is between 6 and 9.

Table 7. Properties of nanoparticles

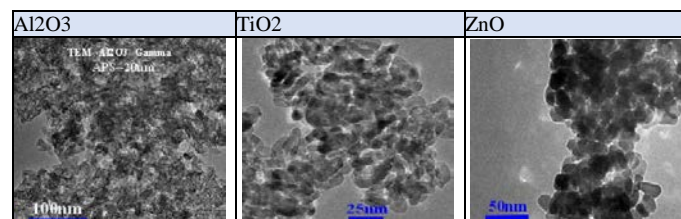
Nano particle	*Purity	*Average Particle Diameter	* Specific Surface Area	* Shape	* Density (kg/m ³)	**Specific Heat (J/kgK)	*** Thermal Conductivity (W/mK)
Al ₂ O ₃	%99.8	13 nm	85-115	Nearly spherical	3890	778	46
TiO ₂	%99.5	10-25 nm	200-240	Nearly spherical	3900	710	10
ZnO	%99.9	18 nm	40-70	Nearly spherical	5606	500	54

*: The data is taken from the producers.

: The specific heat values are taken from the references: **Al₂O₃ [[2], Vol.5, Pg.27, Curve3], **TiO₂** [[2], Vol.5, Pg.249, Curve2] and **ZnO** [[2], Vol.5, Pg.292, Curve1]. The values are given for 300 K temperature.

***: The thermal conductivity values are taken from the references: **Al₂O₃** [[2], Vol.2, Pg.97], **TiO₂** [[2], Vol.2, Pg.208] and **ZnO** [[3], Pg.69]. The values are given for 300 K temperature.

Table 8. TEM images of nanoparticles



2.2 Preparation of Nanofluids

In this study, all nanofluids are prepared by 2-step method. This method is showed in Figure 1 [24], [28]. Namely, at first the nanoparticles are bought the producers. Then the nanoparticles are dispersed in a base fluid with help an ultrasonic

homogenizer. A probe type of ultrasonic homogenizer is used to disperse the nanoparticles in deionized water used as base fluid (Ultrasonic Homogenizer Mark/Model: Optic Ivymen System / CY-500, Power: 500W, Frequency: 20kHz, Probe Diameter/Length: Ø5.6/60mm). All nanofluids are got at three different volume concentrations (0.5%, 0.7%, 1.0%) at certain conditions.

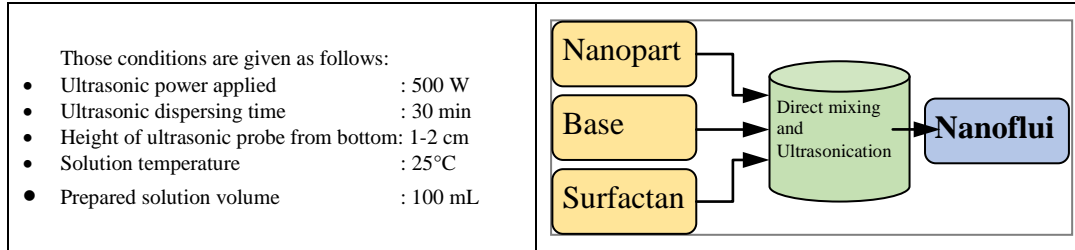


Figure 26. Two-step preparation process of nanofluids

Mass amounts of nanoparticle, deionized water and SDS are calculated by taking into account the desired nanofluid volumetric concentration, volume of nanofluid and mass concentration of SDS. These values are given in Table 3. Mass amount is measured by a precision balance (AND GX-600, Max: 610g, Deviation: 0.001g). The equations used in Table 3 for the nanofluids are the following:

$$\phi = \frac{V_{np}}{V_{nf}} = \frac{\rho_{nf} - \rho_{bf}}{\rho_{np} - \rho_{bf}} \quad (1)$$

and base fluid densities, respectively.

Volume of nanofluid, where ϕ is volume concentration of nanofluid; V_{np} and V_{nf} are nanoparticle and nanofluid volume; ρ_{nf} , ρ_{np} and ρ_{bf} are nanofluid, nanoparticle and base fluid densities, respectively.

$$V_{nf} = V_{np} + V_{bf} \quad (2)$$

where V_{bf} is base fluid volume. Mass for nanoparticle and water,

$$m = \rho V \quad (3)$$

where m is mass of interested matter. Mass concentration of SDS/Nanoparticle,

$$\phi_{w} = \frac{m_{SDS}}{m_{np}} \quad (4)$$

where ϕ_{w} is mass concentration of SDS according to nanoparticle.

Table 9. Calculated mass amounts for definite concentrations and volume of nanofluid at 20°C

Nano Fluid	Volume Concent.	Volume of Nanofluid	Density of Base Fluid	Particle Density	Volume of Particle	Vol. of Base Fluid	Particle Mass	Base Fluid Mass	SDS-Particle Concent.	SDS Mass
	ϕ (%)	V_{nf} (mL)	ρ_{bf} (kg/m ³)	ρ_{np} (kg/m ³)	V_{np} (mL)	V_{bf} (mL)	m_{np} (g)	m_{bf} (g)	$\phi_{w,SDS}$ (%)	m_{SDS} (g)
Al ₂ O ₃	0,50	100	998,0	3890	0,50	99,50	1,945	99,301	It is not used for Al ₂ O ₃ nanofluid	
	0,70	100	998,0	3890	0,70	99,30	2,723	99,101		
	1,00	100	998,0	3890	1,00	99,00	3,890	98,802		
TiO ₂	0,50	100	998,0	3900	0,50	99,50	1,950	99,301	15,00%	0,293
	0,70	100	998,0	3900	0,70	99,30	2,730	99,101	15,00%	0,410
	1,00	100	998,0	3900	1,00	99,00	3,900	98,802	15,00%	0,585
ZnO	0,50	100	998,0	5606	0,50	99,50	2,803	99,301	25,00%	0,701
	0,70	100	998,0	5606	0,70	99,30	3,924	99,101	15,00%	0,589
	1,00	100	998,0	5606	1,00	99,00	5,606	98,802	15,00%	0,841

3 EXPERIMENT

3.1 Density

Densities of nanofluids are determined by simple density equations and precision balance. As expressed in Azmi et al. [20], nanofluid volumetric concentration equation showed by Eq.(5) was used to obtain density of nanofluid. For each nanofluid, the change of density values according to temperature and volumetric concentration is given in Figure 2, Figure 3 and Figure 4.

$$\rho_{nf} = \rho_{np}\phi + \rho_{bf}(1 - \phi) \tag{5}$$

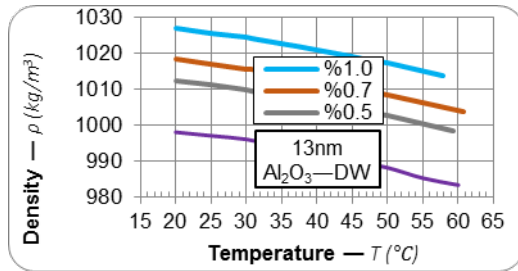


Figure 27. Change of density of Al₂O₃ nanofluid

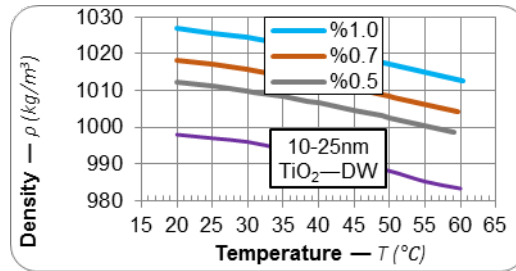


Figure 28. Change of density of TiO₂ nanofluid

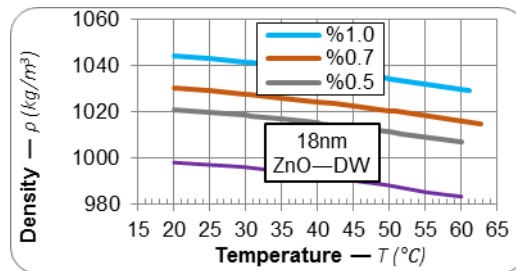


Figure 29. Change of density of ZnO nanofluid.

While the densities of Al₂O₃ and TiO₂ nanofluids are approximately same, the density of ZnO one is bigger than others. Because, the density of ZnO nanoparticles is bigger than that of Al₂O₃ and TiO₂. This can be seen in

Table 1. Although Eq.(5) doesn't have a temperature parameter directly, the density values change with temperature. The reason is that it is available indirectly. It is considered the change of the density of base fluid, which is deionized water here, according to temperature. If the change of density of the base fluid were not taken into account, densities would have become constant along temperature.

3.2 Specific Heat

Specific heats of nanofluids are determined by using specific heat equation expressed as Eq.(6). In the literature, some researchers measured specific heats of nanofluids [25], [27], [29], [30] some calculated it by equations [9], [16], [31], [32]. In addition, some of them explained that the results obtained by Eq. (6) are compatible with ones measured [1], [20], [26], [27]. Therefore, in this study, the results obtained from the equation are used. For each nanofluid, the change of specific heat values according to temperature and volumetric concentration is given in Figure 5, Figure 6 and Figure 7.

$$\rho_{nf}c_{nf} = \rho_{np}c_{np}\phi + \rho_{bf}c_{bf}(1 - \phi) \tag{6}$$

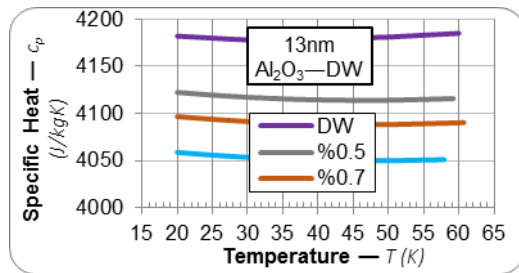


Figure 30. Change of specific heat of Al_2O_3 nanofluid

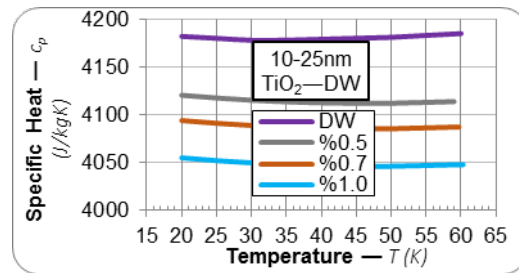


Figure 31. Change of specific heat of TiO_2 nanofluid

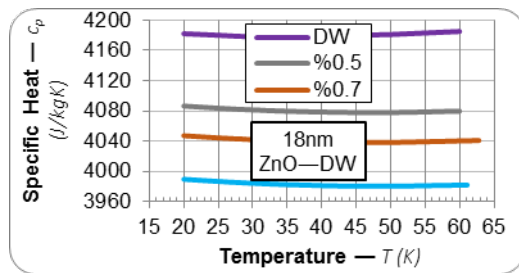


Figure 32. Change of specific heat of ZnO nanofluid

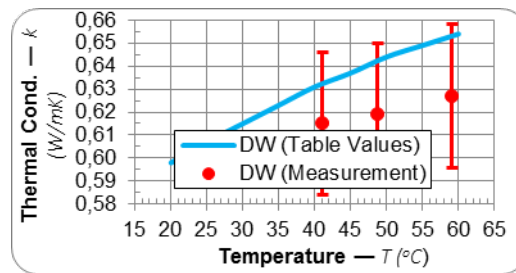


Figure 33. Comparison between deionized water data from measurement and from table [35]

Since it is used similar equation to find specific heat like density, the explanations given for density are valid for specific heat, too.

3.3 Thermal Conductivity

For thermal conductivity measurement of nanofluids, it is used a device that works by transient hot wire method (Mark/Model: Decagon/KD2 Pro, KS-1 Probe Thermal Cond. Measurement Range: 0.02-2 W/mK, KS-1 Probe accuracy: ± 0.01 W/mK between 0.02-0.2 W/mK and $\pm 5\%$ between 0.2-2 W/mK, Temperature Measurement Range: $-50 \sim +150^\circ C$) [37]. Each thermal conductivity measurement takes 90 seconds totally, which consist of 30 seconds thermal balance, 30 seconds heating and 30 seconds waiting.

This method and the device were used to measure thermal conductivity at a lot of works widely [1], [6], [9], [10], [13], [17], [20], [30], [33], [34]. For calibration of KS-1 probe of the device used, the calibration sample (Glycerin, $k=0.285$ W/mK @ $20^\circ C$), which comes with the device, was used. When thermal conductivity of glycerin was measured, it was found as 0.277 W/mK at $22^\circ C$. This means about 3% deviation that is in 5% range. However, since change with temperature on values measured is more important, the measurements were done with deionized water. The calibration results according to temperature for deionized water are given in Figure 8. In addition, $\pm 5\%$ accuracy range on the measurement values is showed at same figure. The table values were taken from the reference [35] Pg.920.

As seen in Figure 8, it is found that the measurement results are in 5% deviation. This is compatible with the deviation indicated in the device specification. Thermal conductivity measurements of nanofluids are done just after they are prepared. Since thermal conductivity is dependent on temperature, it was necessary for measurements to be done at constant temperature. For this purpose, the nanofluid to be measured its thermal conductivity was filled into a 15 mL of plastic tube and the tube was put in a heat bath. The measurement probe (KS-1) of the device was put in the tube by changing and passing from the cap of the tube that was drilled before. The cap was drilled in the way to shrink fit the probe needle with 1.27 mm diameter. This blue cap has screw thread and when it screwed to the tube, it made a constant, no-vibration and stable construction. Temperature value was also measured with same probe. Nanofluid temperature controlled by the heat bath was increased over some degree of the desired temperature. Afterwards, the tube was taken out the heat bath. During measurement, the tube was put in a different, bigger plastic bottle by turning it upside-down in order to prevent heat loss from the tube and minimize its temperature change. This bottle wrapped its surroundings with insulation material was filled water that was taken from the heat bath at nanofluid temperature. Therefore, during measurement, reducing nanofluid temperature change to minimum, both the defective measurement values due to rapid temperature change were decreased and the desired temperatures were approached. The upside-down tube in the bottle was put on polyurethane insulation foam with KS-1 probe on its cap. As a result, during measurements, vibrations that cause natural convection effects and air bubbles around the needle of the probe were prevented, it was enabled all surface of the needle to contact with fluid. In this way, thermal conductivity measurements of nanofluids were conducted (Figure 9).

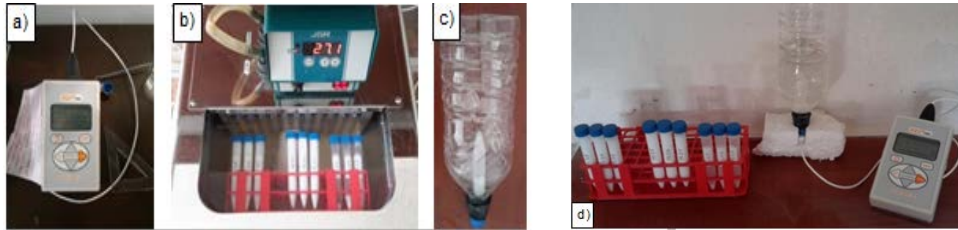


Figure 34. Thermal conductivity measurement a) Device, b) Tubes in heat bath
c) Tube in bottle, d) Tube with probe put on insulation foam

3.4 Viscosity

For viscosity measurement of nanofluids, it is used a device that works by tuning-fork vibration method (Mark/Model: AND/SV-10, Viscosity Measurement Range: 0.3 mPa.s – 10 Pa.s, Accuracy: $\pm 3\%$ between 0.3-1000 mPa.s, Temperature Measurement Range: 0 ~ +160°C) [38] Pg.58. Each viscosity measurement takes about 15 seconds. The device was used with a heat bath (Cole-Parmer, Digital, Heating: 1 kW, Cooling: 200 W) that controls temperature of fluid. For calibration of the device used, pure water was used. The calibration results according to temperature for pure water are given in Figure 10. In addition, $\pm 3\%$ between 20-30°C and $\pm 5\%$ (estimated) for higher than 30°C accuracy range on the measurement values is showed at same figure. The table values were taken from the reference [35] Pg.920.

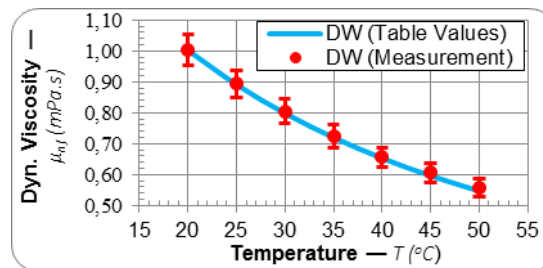


Figure 35. Comparison between pure water data from measurement and from table [35]

As seen in Figure 10, it is found that the measurement results are in 5% deviation (accepted value over 30°C). This is compatible with the deviation indicated in the device specification [38] Pg.58. Dynamic viscosity measurements of nanofluids are done just like thermal conductivity ones similarly. Since viscosity is dependent on temperature, it is necessary to do measurement at constant temperatures. A heat bath was used to increase nanofluid temperature to the desired values. For that purpose, 100 mL of nanofluid to be measured its viscosity was filled in a 250 mL of flask. The flask was set in the heat bath. The measurement unit of the viscosity device was inserted in the flask. Before taking a value, nanofluid temperature was waited to reach the desired temperature in ± 0.1 degree range. In this way, viscosity measurements of nanofluids were done (Figure 11).



Figure 36. Dynamic viscosity measurement

4 RESULTS

4.1 Thermal conductivity of nanofluids

The obtained thermal conductivity values of nanofluids and their ratios are given in Table 4, Table 5 and Table 6. Here, the base fluid is deionized water (DW). Besides, the graphics obtained from these tables are given in between Figure 12 and Figure 15.

All graphics are given as ratio of thermal conductivity of nanofluid to base fluid since the ratio both shows increase according to base fluid and enables to compare with other researchers' results as dimensionless easily. Moreover, to be able to see thermal conductivity trend and make comparison easy, the data points were added trend lines or were combined. Therefore, intermediate values may not always show correct ones.

As seen from Figure 12, Figure 13 and Figure 14, while temperature or volume concentration increases, thermal conductivity ratio also increases generally. However, their increment trends or slopes change according to nanofluid type, volumetric concentration and temperature. The highest thermal conductivity increase of Al_2O_3 , TiO_2 and ZnO nanofluids according to base fluid (DW) are determined approximately 11%, 8% and 9% for 1% vol. concentration respectively.

Table 10. Thermal conductivity results of Al_2O_3 -DW

Vol. Conc.	Temp.	Thermal	Ratio
of nano.			
ϕ	T (°C)	k_{nf}	k_{nf}/k_{bf}
0,5%	30,74	0,609	0,988
	37,73	0,639	1,019
	47,92	0,673	1,050
	59,24	0,700	1,071
0,7%	30,80	0,635	1,030
	38,47	0,642	1,023
	49,18	0,697	1,086
	60,67	0,726	1,109
1,0%	30,83	0,686	1,112
	37,12	0,660	1,055
	46,57	0,710	1,112
	57,93	0,722	1,108

Table 11. Thermal conductivity results of TiO_2 -DW

Vol. Conc.	Temp.	Thermal	Ratio
of nano.			
ϕ	T (°C)	k_{nf}	k_{nf}/k_{bf}
0,5%	30,88	0,633	1,026
	38,48	0,650	1,035
	49,04	0,672	1,048
	59,00	0,677	1,037
0,7%	30,88	0,640	1,038
	39,29	0,658	1,047
	50,55	0,688	1,069
	59,74	0,691	1,057
1,0%	30,89	0,661	1,071
	38,84	0,680	1,082
	47,69	0,675	1,055
	60,28	0,696	1,063

Table 12. Thermal conductivity results of ZnO -DW nanofluid

Vol. Conc.	Temp.	Thermal	Ratio
of nano.			
ϕ	T (°C)	k_{nf}	k_{nf}/k_{bf}
0,5%	30,66	0,623	1,011
	40,39	0,655	1,039
	51,82	0,657	1,019
	60,04	0,696	1,064
0,7%	30,43	0,637	1,034
	42,34	0,661	1,044
	50,99	0,680	1,056
	62,77	0,702	1,069
1,0%	30,45	0,666	1,081
	42,30	0,681	1,076
	49,40	0,682	1,063
	61,15	0,715	1,092

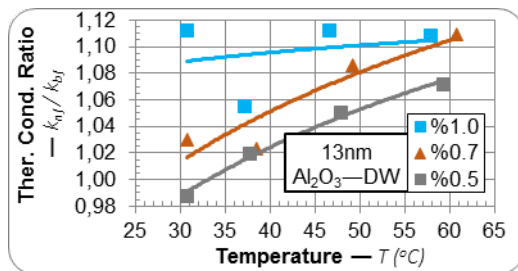


Figure 37. Change of ratio of thermal conductivity of Al_2O_3 nanofluid to base fluid

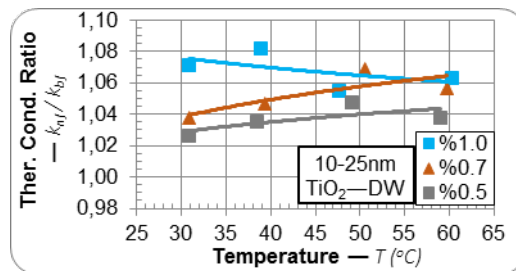


Figure 38. Change of ratio of thermal conductivity of TiO_2 nanofluid to base fluid

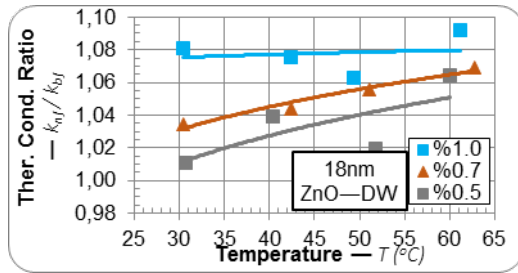


Figure 39. Change of ratio of thermal conductivity of ZnO nanofluid to base fluid

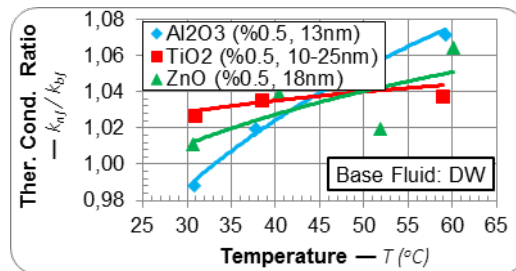


Figure 40. Comparison of ratio of thermal conductivity of nanofluids to base fluid with each other

4.2 Viscosity of nanofluids

The obtained dynamic viscosity values of nanofluids and their ratios are given in Table 7, Table 8 and Table 9. Here, the base fluid is deionized water (DW). Besides, the graphics obtained from these tables are given between Figure 16 and Figure 19.

Table 13. Dynamic viscosity results of Al_2O_3 -DW nanofluid

Vol. Con.	Temperature T (°C)							Temperature T (°C)							
	20	25	30	35	40	45	50	20	25	30	35	40	45	50	
ϕ	20	25	30	35	40	45	50	20	25	30	35	40	45	50	
Dynamic Viscosity of Nanofluid — μ_{nf} (mPa.s)								Dynamic Viscosity Ratio of Nanofluid — μ_{nf} / μ_{bf}							
0,5%	1,014	0,960	0,842	0,780	0,675	0,637	0,605	1,012	1,077	1,056	1,084	1,034	1,069	1,107	
0,7%	1,012	0,961	0,847	0,786	0,708	0,638	0,605	1,010	1,078	1,062	1,092	1,085	1,071	1,106	
1,0%	1,007	0,979	0,853	0,799	0,718	0,645	0,610	1,005	1,098	1,069	1,109	1,100	1,081	1,115	

Table 14. Dynamic viscosity results of TiO_2 -DW nanofluid

Vol. Con.	Temperature T (°C)							Temperature T (°C)							
	20	25	30	35	40	45	50	20	25	30	35	40	45	50	
ϕ	20	25	30	35	40	45	50	20	25	30	35	40	45	50	
Dynamic Viscosity of Nanofluid — μ_{nf} (mPa.s)								Dynamic Viscosity Ratio of Nanofluid — μ_{nf} / μ_{bf}							
0,5%	1,080	0,910	0,849	0,747	0,689	0,621	0,569	1,078	1,021	1,063	1,038	1,055	1,041	1,040	
0,7%	1,090	0,951	0,877	0,779	0,705	0,647	0,592	1,088	1,067	1,098	1,082	1,079	1,085	1,082	
1,0%	1,091	0,946	0,918	0,825	0,780	0,743	0,659	1,089	1,062	1,150	1,146	1,195	1,246	1,205	

Table 15. Dynamic viscosity results of ZnO-DW nanofluid

Vol. Con.	Temperature T (°C)							Temperature T (°C)							
	20	25	30	35	40	45	50	20	25	30	35	40	45	50	
ϕ	20	25	30	35	40	45	50	20	25	30	35	40	45	50	
Dynamic Viscosity of Nanofluid — μ_{nf} (mPa.s)								Dynamic Viscosity Ratio of Nanofluid — μ_{nf} / μ_{bf}							
0,5%	1,016	0,948	0,878	0,777	0,710	0,652	0,577	1,014	1,064	1,100	1,079	1,087	1,093	1,055	
0,7%	1,016	0,949	0,889	0,786	0,713	0,655	0,575	1,014	1,066	1,114	1,092	1,092	1,100	1,051	
1,0%	1,032	0,972	0,906	0,808	0,742	0,679	0,600	1,030	1,091	1,135	1,122	1,136	1,139	1,096	

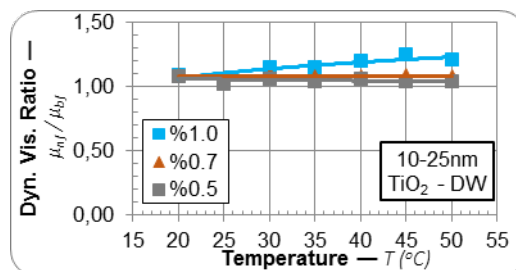
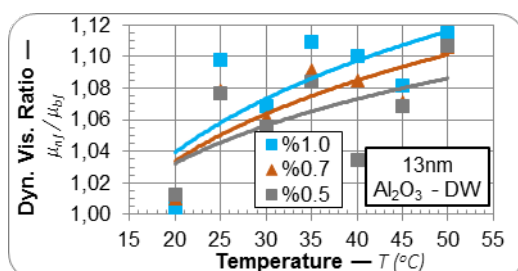


Figure 42. Change of ratio of dynamic viscosity of TiO_2

Figure 41. Change of ratio of dynamic viscosity of Al_2O_3 nanofluid to base fluid

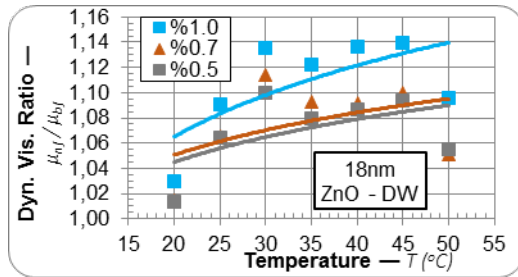


Figure 43. Change of ratio of dynamic viscosity of ZnO nanofluid to base fluid

nanofluid to base fluid

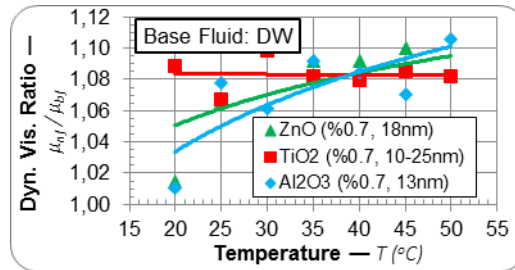


Figure 44. Comparison of ratio of dynamic viscosity of nanofluids to base fluid with each other

As seen from Figure 16, Figure 17 and Figure 18, while temperature or volume concentration increases, thermal conductivity ratio also increases generally. It can be confounding viscosity to increase with temperature. This is due to ratios. Yet, if absolute values are examined in e.g. Table 7, it must be paid attention that viscosity decreases with increasing temperature. The highest viscosity increase of Al_2O_3 , TiO_2 and ZnO nanofluids according to base fluid (DW) are determined approximately 11%, 24% and 14% for 1% vol. concentration respectively.

5 CONCLUSIONS

Thermodynamic properties of nanofluids change with time due to agglomeration and sedimentation. Therefore, it must be denoted how much time measurements are done after nanofluids are prepared.

Devices used for thermal conductivity and viscosity measurement can be affected from sedimentation of nanofluid positively or negatively. Namely, for thermal conductivity measurement, since Decagon KD2-Pro device measures thermal conductivity of nanofluid from bottom of tube/bottle that is turned upside-down, sedimentation can cause unexpected increases at measurement results. As for viscosity measurement, since AND SV-10 device measures viscosity of nanofluid from top surface or medium level of tube/bottle depending on its height, sedimentation can produce too decrease at measurement values. Besides, in case other viscosity devices worked by torque measurement, since viscosities of nanofluids including nanoparticle up to 2-3% volumetric concentration are closed to pure water and they have limited viscosity measurement range, it is seen problems related to obtaining a result at temperatures over 30 degree. Thus, for example, if it is prepared a nanofluid whose stability is one day at least, and a measurement is done just after its preparation, then a more correct and reasonable result will be obtained. During thermal conductivity measurements, when measurement device applies higher heat pulses to fluid or temperature of fluid increase, its viscosity decreases, since convection effects (natural convection) appear, bigger measurement results can occur. For all these descriptions can affect thermal conductivity and nanofluid results considerably and their control is not easy, they can be showed as some of controversial results in the literature.

ACKNOWLEDGEMENT

This project was supported by "The Scientific and Technological Research Council Of Turkey" (TUBITAK, Project No. 5140013). The authors gratefully acknowledge the financial supports from TUBITAK.

REFERENCES

- [1] Heyhat M.M., Kowsary F., Rashidi A.M., Momenpour M.H., Amrollahi A., Experimental investigation of laminar convective heat transfer and pressure drop of water-based Al_2O_3 nanofluids in fully developed flow
- [2] Touloukian Y.S., Powell R.W., Ho C.Y., Klemens P.G., Thermophysical Properties of Matter – TPRC Data Series, 1970.
- [3] Adachi S., Handbook on Physical Properties of Semiconductors, Volume 3, II-VI Compound Semiconductors, Kluwer Academic Publishers, 2004.
- [4] Erkut T.Z., Nanoakışkan kullanarak elektrikli radyatörlerin ısı veriminin iyileştirilmesi (Thermal efficiency enhancement of electrical radiators by using nanofluids), Ondokuz Mayıs University, Institute of Natural Science, MS Thesis, 2012.
- [5] Sankar B.R., Experimental investigations on the performance of Al_2O_3 -Water nanofluid as radiator coolant in an automobile engine, Andhra University, College of Engineering, PhD Thesis, 2012.
- [6] Modak M., Srinivasan S., Garg K., Chougule S.S., Agarwal M.K., Sahu S.K., Experimental investigation of heat transfer characteristics of the hot surface using Al_2O_3 -Water nanofluids, Chemical Engineering and Processing 91 (2015) 104–113.
- [7] Turgut A., Investigation of thermophysical properties of nanofluids, Dokuz Eylül University, Graduate School of Natural and Applied Sciences, PhD Thesis, 2010.
- [8] Akyürek E.F., Nanoakışkanların ve türbülatorlerin iç içe borulu ısı değiştirici ısı performansına etkilerinin incelenmesi (Investigation of nanofluids and tabulators' effects on the thermal performance of concentric heat exchanger), Ataturk University, Graduate School of Natural and Applied Sciences, PhD Thesis, 2014.
- [9] Şahin B., Gültekin G.G., Manay E., Karagöz S., Experimental investigation of heat transfer and pressure drop characteristics of Al_2O_3 -Water nanofluid, Experimental Thermal and Fluid Science 50 (2013) 21–28.

- [10] Chandrasekar M., Suresh S., Bose A.C., Experimental investigations and theoretical determination of thermal Conductivity and viscosity of Al₂O₃/Water nanofluid, *Experimental Thermal and Fluid Science* 34 (2010) 210–216.
- [11] Fedele L., Colla L., Bobbo S., Viscosity and thermal conductivity measurements of Water-Based nanofluids containing titanium oxide nanoparticles, *International Journal of Refrigeration* 35 (2012) 1359–1366.
- [12] Turgut A., Tavman I., Chirtoc M., Schuchmann H.P., Sauter C., Tavman S., Thermal conductivity and viscosity measurements of Water-Based TiO₂ nanofluids, *Int. J. Thermophys.* (2009) 30:1213–1226.
- [13] Hojjat M., Etemad S.Gh., Bagheri R., Thibault J., Thermal conductivity of non-Newtonian nanofluids: Experimental Data and Modeling Using Neural Network, *International Journal of Heat and Mass Transfer* 54 (2011) 1017–1023.
- [14] Longo G.A., Zilio C., Experimental measurement of thermophysical properties of Oxide–Water nano–fluids down to ice–point, *Experimental Thermal and Fluid Science* 35 (2011) 1313–1324.
- [15] Duangthongsuk W., Wongwises S., An experimental study on the heat transfer performance and pressure drop of TiO₂–Water nanofluids flowing under a turbulent flow regime, *International Journal of Heat and Mass Transfer* 53 (2010) 334–344.
- [16] Azmi W.H., Sharma K.V., Sarma P.K., Mamat R., Anuar S., Comparison of convective heat transfer coefficient and friction factor of TiO₂ nanofluid flow in a tube with twisted tape inserts, *International Journal of Thermal Sciences* 81 (2014) 84–93.
- [17] Utomo A.T., Poth H., Robbins P.T., Pacek A.W., Experimental and theoretical studies of thermal conductivity, viscosity and heat transfer coefficient of titania and alumina nanofluids, *International Journal of Heat and Mass Transfer* 55 (2012) 7772–7781.
- [18] Ferrouillat S., Bontemps A., Poncelet O., Soriano O., Gruss J.A., Influence of nanoparticle shape factor on convective heat transfer and energetic performance of water-based SiO₂ and ZnO nanofluids, *Applied Thermal Engineering* 51 (2013) 839–851.
- [19] Raykar V.S., Singh A.K., Thermal and rheological behavior of acetylacetone stabilized ZnO nanofluids, *Thermochimica Acta* 502 (2010) 60–65.
- [20] Azmi W.H., Sharma K.V., Mamat R., Alias A.B.S., Misnon I.L., Correlations for thermal conductivity and viscosity of water based nanofluids, *Materials Science and Engineering* 36 (2012) 012029.
- [21] Pastoriza-Gallego M.J., Casanova C., Paramo R., Barbes B., Legido J.L., Pineiro M.M., A study on stability and thermophysical properties (density and viscosity) of Al₂O₃ in water nanofluid, *Journal of Applied Physics* 106, 064301 (2009).
- [22] Nguyen C.T., Desgranges F., Roy G., Galanis N., Mare T., Boucher S., Mints H.A., Temperature and particle-size dependent viscosity data for water-based nanofluids – Hysteresis phenomenon, *International Journal of Heat and Fluid Flow* 28 (2007) 1492–1506.
- [23] Suganthi K.S., Rajan K.S., Temperature induced changes in ZnO–water nanofluid: Zeta potential, size distribution and viscosity profiles, *International Journal of Heat and Mass Transfer* 55 (2012) 7969–7980.
- [24] Angayarkanni S.A., Philip J., Review on thermal properties of nanofluids: Recent developments, *Advances in Colloid and Interface Science* 225 (2015) 146 – 176.
- [25] Kulkarni D.P., Vajjha R.S., Das D.K., Oliva D., Application of aluminum oxide nanofluids in diesel electric generator as jacket water coolant, *Applied Thermal Engineering* 28 (2008) 1774–1781.
- [26] Shahrul I.M., Mahbulbul I.M., Khaleduzzaman S.S., Saidur R., Sabri M.F.M., A comparative review on the specific heat of nanofluids for energy perspective, *Renewable and Sustainable Energy Reviews* 38 (2014) 88–98.
- [27] Murshed S.M.S., Determination of effective specific heat of nanofluids, *Journal of Experimental Nanoscience* Vol. 6, No. 5, October 2011, 539–546.
- [28] Solangi K.H., Kazi S.N., Luhur M.R., Badarudin A., Amiri A., Sadri R., Zubir M.N.M., Gharekhani S., Teng K.H., A comprehensive review of thermos-physical properties and convective heat transfer to nanofluids, *Energy* 89 (2015) 1065–1086.
- [29] Ghanbarpour M., Haghigi E.B., Khodabandeh R., Thermal properties and rheological behavior of water based Al₂O₃ nanofluid as a heat transfer fluid, *Experimental Thermal and Fluid Science* 53 (2014) 227–235.
- [30] Elias M.M., Mahbulbul I.M., Saidur R., Sohel M.R., Shahrul I.M., Khaleduzzaman S.S., Sadeghipour S., Experimental investigation on the thermo-physical properties of Al₂O₃ nanoparticles suspended in car radiator coolant, *International Communications in Heat and Mass Transfer* 54 (2014) 48–53.
- [31] Hussein A.M., Bakar R.A., Kadrigama K., Sharma K.V., Experimental measurement of nanofluids thermal properties, *International Journal of Automotive and Mechanical Engineering (IJAME)*, Volume 7, pp. 850–863, January-June 2013.
- [32] Karimzadehkhoei M., Yalçın S.E., Şendur K., Mengüç M.P., Koşar A., Pressure drop and heat transfer characteristics of nanofluids in horizontal microtubes under thermally developing flow conditions, *Experimental Thermal and Fluid Science* 67 (2015) 37–47.
- [33] Dilek E.F., Nanoakışkanların hazırlanması ve ısı iletkenliklerinin belirlenmesi (Preparation of nanofluids and determination of thermal conductivities of nanofluids), MS Thesis, Graduate School of Natural and Applied Sciences, Atatürk University, 2008.
- [34] Timofeeva E.V., Gavrilov A.N., McCloskey J.M., Tolmachev Y.V., Thermal conductivity and particle agglomeration in alumina nanofluids: Experiment and theory, *Physical Review E* 76, 061203 2007.
- [35] Çengel Y.A., Ghajar A.J., *Heat and Mass Transfer: Fundamentals & Applications*, McGraw-Hill, New York, 5th Edition, 2015.
- [36] Azmi W.H., Sharma K.V., Mamat R., Najafi G., Mohamad M.S., The enhancement of effective thermal conductivity and effective dynamic viscosity of nanofluids – A review, *Renewable and Sustainable Energy Reviews* 53 (2016) 1046–1058.
- [37] DECAGON KD2-Pro User Guide, October 2014.
- [38] AND SV-10 Instruction Manual, 2008.

Prediction of Performance and Exhaust Emissions of a Diesel Engine Fueled with Biodiesel by using Linear Regression and Artificial Neural Networks

Omer F. Ertugrul^{1}, Sehmus Altun²*

Abstract

In this study, the prediction of the performance and emissions of a diesel engine fueled with biodiesel was performed by using ML methods such as linear regression (LR), which is polynomial characteristic, and artificial neural network (ANN), which is an iteration-based method. The experimental test results were obtained by using conventional diesel, biodiesel and their blends in a direct-injection diesel engine at constant engine speed under different load conditions. The fuel type, engine speed and load are taken as the input parameters, while the values of brake specific fuel consumption and emissions were used as the outputs. Fourth degree LR was applied and the results were calculated by 7-folds cross-validation while generalized regression type ANN was employed. Mean R^2 values were obtained as 0.70 and 0.92 by LR and ANN, respectively. Also, the mean absolute errors (MAE) were about 0.15 for LR and 0.23 for ANN. Although higher R^2 values were obtained by ANN, MAE results showed that LR performed better than ANN in case of using less experimental data. This may be attributed to the ANN characteristic which needs much more samples to obtain better performance.

Keywords: *Linear Regression; Artificial Neural Networks; Diesel Engine; Biodiesel*

1 INTRODUCTION

Biodiesel has received significant attention due to its increasing share among the renewable energies and its technical and environmental benefits making it attractive as an alternative renewable fuel for using in diesel engines. Biodiesel has the capability to reduce the emissions of particulate matter (PM), unburned hydrocarbons (HC) and carbon monoxide (CO) with an increase in nitrogen oxides (NO_x) as reported in the literature [1, 2]. However, the exact change in the performance and emissions in comparison to petroleum diesel may be varied considerably as the biodiesel feedstock, the biodiesel percentage in the fuel, the test engine, and conditions could be different [3, 5]. In this case, it is needed to carry out much more experiments for understanding better the effect of variables mentioned above despite the experimental studies are complex, time-consuming and costly. Alternatively, the performance and emission values of an engine fueled with different fuels can be predicted by using artificial intelligence (AI) methods. For instance, artificial neural networks (ANN) was recommended to predict the engine's performance and emissions instead of having to undertake complex and time-consuming experimental studies in the study of Çanakçı et al. [6], and it has been researched severely during the last decades for analyzing of the diesel engines fueled with petroleum and alternative fuels [7-10].

However, ANNs need much more samples to obtain a good performance since it is an iteration-based method and the diversity and distribution range of a set of samples plays a significant role in its performance. Another disadvantage of ANNs is choosing NN parameters such as hidden neuron and layer numbers, transfer function, method and performance criteria of training etc., and it is still slow and needs high process capacity. ML methods with polynomial characteristic such as linear regression (LR) can show success in the case of a small number of experimental data. On the other hand, no comparison has been found in the literature between the prediction of emissions and performance of diesel engines by using ANN and LR. Therefore, it is not clear whether the method used in the prediction has an effect on the prediction accuracy or not. Finally, to

¹ Dept. Electrical and Electronic Engineering, Batman University, 72100 Batman, Turkey.
omerfarukertugrul@gmail.com

² Dept. Automotive Engineering, Batman University, 72100 Batman, Turkey.

the author's best knowledge, this is the first study on estimating the performance and exhaust emissions from diesel engines fueled with biodiesel and its blends with petroleum diesel by using linear regression and comparing with the results obtained by ANN.

In this study, the applicability of linear regression (LR) for predicting the performance and exhaust emissions of a diesel engine fueled with petroleum diesel and biodiesel fuel was investigated. Then, after showing the applicability of the method, comparison of LR and ANN has been performed. All of the experimental data were used for prediction and the accuracy was calculated by using the predicted curves with regression methods according to the experimental data.

2 EXPERIMENTAL WORK

A conventional ultra-low sulfur diesel fuel (ULSD) was supplied by a local filling station, and used as base-fuel for current work. Biodiesel was obtained from waste cooking oil, which is originated cottonseed oil collected from local patisseries, via transesterification reaction using methanol in the presence of potassium hydroxide (KOH) as base-catalyst. Both fuels and their blends in percentages of 20% (v/v) and 50% (v/v) were tested in a three-cylinder, four-stroke and direct-injection diesel engine to obtain the experimental data set. The experiments were conducted at different loads and an engine speed of 1500 rpm. Fuel consumption was measured by an electronic scale and digital chronometer. Firstly, test engine was investigated by using ULSD in order to obtain references data. Afterwards, alternative fuels were tested under the same conditions. In tests, fuel consumption, NO_x, HC and opacity were measured for each fuel by using related devices. Detailed information about test fuels and engine tests can be found in previous work [11].

3 METHODS

3.1. Linear Regression (LR)

LR is built on finding a relation between the dependent variable and the independent variable or variables [12]. This method depends on the assumption that the relationship of these variables is polynomial as in Equation 1.

$$y_i = \beta_1 x_{i1} + \dots + \beta_p x_{ip} + \varepsilon_i \quad (1)$$

where $i = 1, \dots, n$. Equation 1 can also be shown as a format of Equation 2.

$$y = X\beta + \varepsilon \quad (2)$$

where y is the dependent variable, X is the independent variable, β is the parameter vector and ε is the error term as shown below.

$$y = \begin{bmatrix} y_1 \\ y_2 \\ \vdots \\ y_p \end{bmatrix}, X = \begin{bmatrix} x_{11}^T \\ x_{21}^T \\ \vdots \\ x_{n1}^T \end{bmatrix} = \begin{bmatrix} x_{11} & \dots & x_{1p} \\ \vdots & \ddots & \vdots \\ x_{n1} & \dots & x_{np} \end{bmatrix}, \beta = \begin{bmatrix} \beta_1 \\ \beta_2 \\ \vdots \\ \beta_p \end{bmatrix}, \varepsilon = \begin{bmatrix} \varepsilon_1 \\ \varepsilon_2 \\ \vdots \\ \varepsilon_p \end{bmatrix}$$

3.2. Artificial Neural Networks (ANN)

ANN is based on human nervous system and has been employed successfully in many research areas [12]. The general structure of an ANN is given in Figure 1.

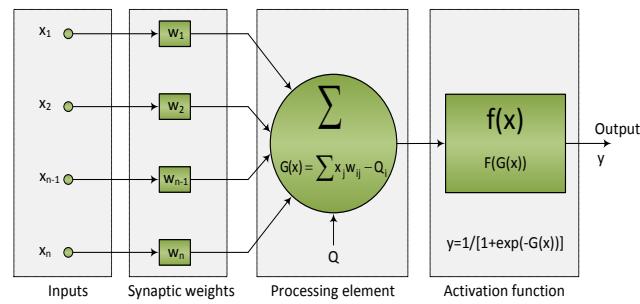


Figure 1 Artificial neuron model.

In the Figure 1, inputs, weights, output, bias, and activation function were represented by symbols x_n , w , y , θ and $G()$ respectively. Then, the output of the ANN can be calculated by:

$$y(t+1) = F\left(\sum_{j=1}^n w_{ij} x_j(t) - \theta_i\right) \quad net_i = \sum_{j=1}^n w_{ij} x_j - \theta_i \quad (3)$$

There are many different types of ANN, which can be classified according to their structure or employed training algorithm [13]. In this study, generalized regression neural network type ANN was employed in experiments.

3.3. Implementation Procedure

The experimental results obtained for diesel fuel and biodiesel in a direct injection diesel engine were used to predict the performance and emission parameters. The fuel type, engine speed, and load were utilized as input parameters and brake specific fuel consumption (BSFC), which is an indicator engine performance and emissions were outputs of ANN. The implementation procedure of this study is shown in Figure 2.



Figure 2. Estimating Algorithm of first regression

The learning procedure was employed based on 7-folds cross-validation scheme and utilized error parameters are Mean Absolute Error (MAE), which is used expressing mean error rate without considering the errors direction and Coefficient of Determination (R^2), which is used for calculating how close are the estimated value to true value, are given in Equation 4 and 5, respectively.

$$MAE = \frac{1}{N} \sum_{i=1}^N |f_i - y_i| \quad (4)$$

$$R^2 = 1 - \frac{\sum_{i=1}^N (f_i - y_i)^2}{\sum_{i=1}^N y_i^2} \quad (5)$$

where f_i is the prediction value and y_i is the true value.

4. RESULTS AND DISCUSSION

LR and ANN methods were employed in predicting the BSFC, NO_x, Smoke and HC parameters of the engine when different types of fuels were used. The parameters of regression methods, which were found in trials, were polynomial degree was 4 and regularization parameter was 1×10^{-9} of LR. Achieved accuracies were summarized in **Table 1**.

Table 1. Achieved accuracies by ANN and LR

Parameter	Biodiesel Type	ANN		LR	
		R ²	MAE	R ²	MAE
BSFC	B0	0.851	0.149	0.995	0.018
	B20	0.850	0.148	0.947	0.042
	B50	0.850	0.149	0.043	0.104
	B100	0.849	0.157	0.860	0.053
HC	B0	0.924	0.211	0.995	0.018
	B20	0.986	0.263	0.700	0.214
	B50	0.994	0.272	0.136	0.160
	B100	0.995	0.254	0.983	0.038
Smoke	B0	0.855	0.279	0.996	0.018
	B20	0.941	0.261	0.173	0.449
	B50	0.846	0.264	0.848	0.083
	B100	0.857	0.359	0.474	0.481
NO _x	B0	0.983	0.231	0.714	0.245
	B20	0.964	0.230	0.676	0.302
	B50	0.949	0.206	0.757	0.190
	B100	0.958	0.187	0.980	0.034

Obtained mean accuracies in estimating each parameter, which is given in **Table 1**, are summarized in **Table 2** in order to make a comparison easier.

Table 2. Summarized mean accuracies by ANN and LR

Parameter	ANN		LR	
	R ²	MAE	R ²	MAE
BSFC	0.850	0.151	0.711	0.054
HC	0.975	0.250	0.704	0.108
Smoke	0.875	0.291	0.623	0.257
NO _x	0.963	0.214	0.782	0.193
Mean	0.916	0.226	0.705	0.153

As seen in **Table 2**, the achieved mean R² values were obtained by LR and ANN are 0.70 and 0.92, respectively. These results show that the estimated parameters by ANN suit better than those by LR. On the other hand, MAE are obtained as 0.153 for LR and 0.226 for ANN, suggesting the estimated values by LR are closer to experimental results than those by ANN. As a summary, obtained results are acceptable based on results reported in the literature [14, 15]. Furthermore, LR performed better

than ANN in the case of using less experimental data. Additionally, to compare ANN and LR over engine's performance and emission parameters of diesel and biodiesel curves are obtained and given in **Figures 3** and **4**, respectively.

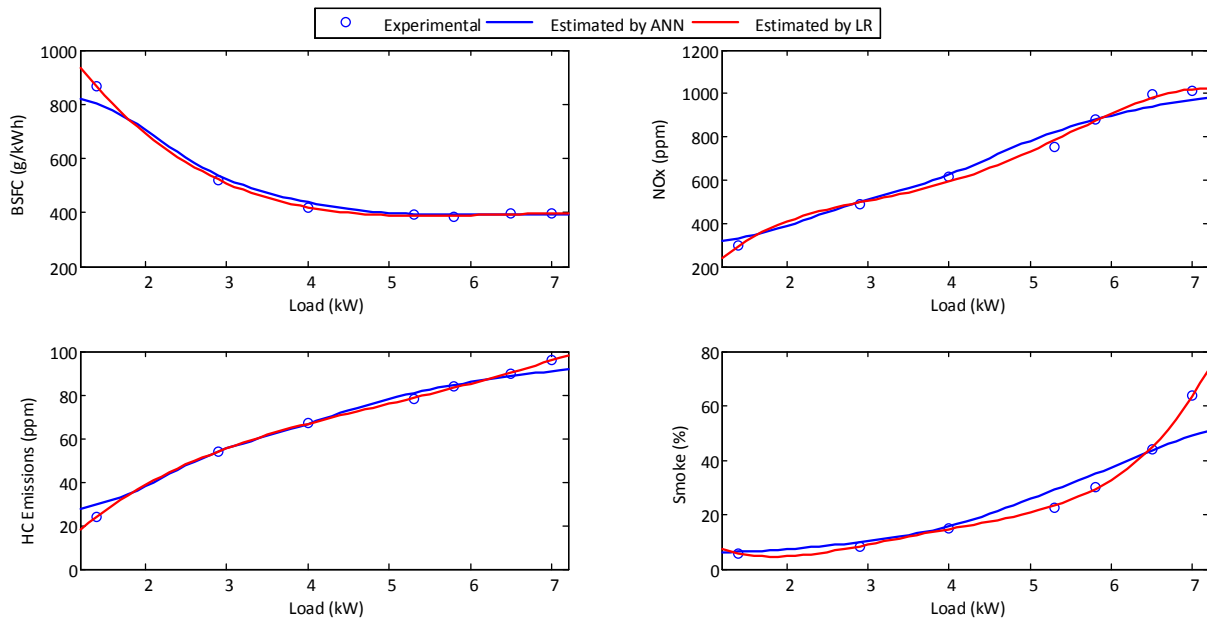


Figure 3. Comparisons of predicted and experimental results for diesel fuel (B0)

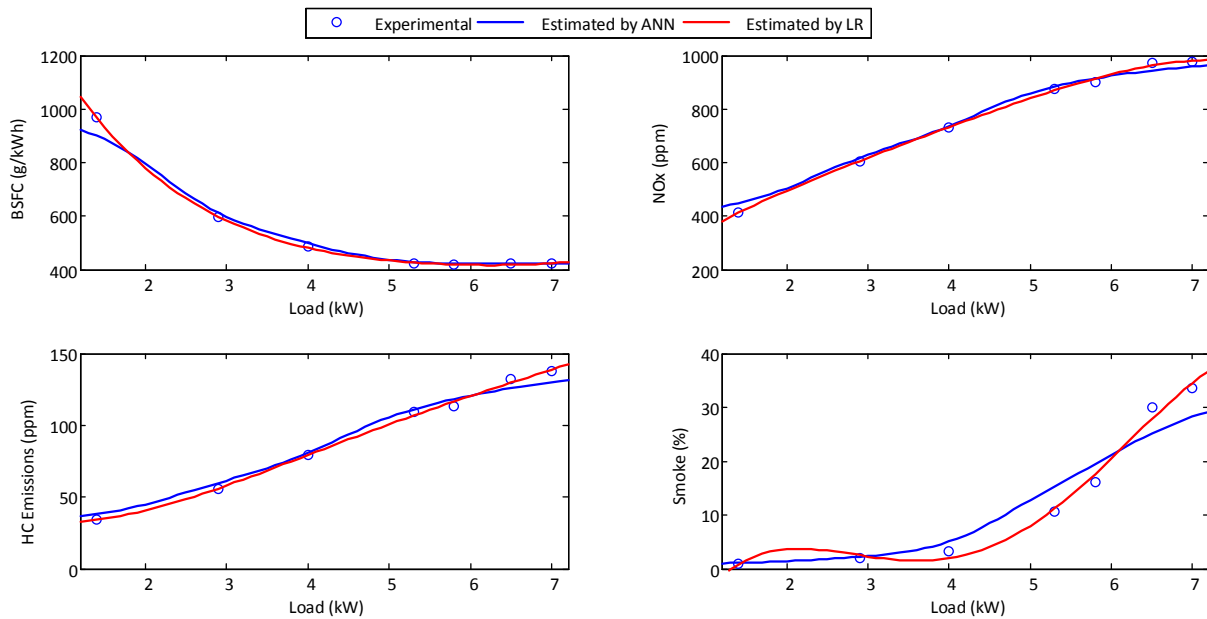


Figure 4. Comparisons of predicted and experimental results for biodiesel (B100)

As seen in **Figure 3** and **4**, the structure of the predicted curves by LR agrees well with experimental results. As seen in these figures, the experimental and the estimated values are very close to each other. The experimental results are on or near the estimated curves which can also be recognized by analyzing errors in **Table 1** and **2**. Addition to accuracy, the process speed

is another major parameter that is related to the computational complexity. Based on this fact, obtained training and testing time by ANN and LR are summarized in **Table 3**.

Table 3. Process Time (sec)

Parameter	ANN		LR	
	Training	Testing	Training	Testing
BSFC	0.778	0.317	0.126	0.055
NO _x	0.063	0.016	0.006	0.004
HC	0.057	0.013	0.006	0.004
Smoke	0.057	0.012	0.005	0.004

As seen in **Table 3**, LR has faster training and testing stages than ANN. The main problem of this study was to have only seven (7) experimental results for each performance and emission parameters of each biodiesel blend of biodiesel-fueled diesel. Therefore, regression methods with kernels or with a polynomial structure show better performance such as LR has the polynomial characteristic. Furthermore, for having more accurate error calculation by minimizing the randomize errors, 7-folds cross-validation scheme was employed in simulations.

5. CONCLUSION

The applicability of ML methods with characteristic polynomial such as linear regression (LR) in estimating the performance and exhaust emissions of a diesel engine fueled with petroleum and biodiesel fuel was investigated. After showing the applicability of LR methods, a comparison of its performance with ANN was performed. All of the experimental data were used for estimations and the accuracy was calculated by using the estimated curves with regression methods according to the experimental data. As result of this study, using LR, which has polynomial characteristic, is highly recommended instead of using ANN with average R^2 values of 0.70 and 0.92 and average MAE of 0.15 and 0.23 by using LR and ANN methods, respectively. However, beginning regions of the figures may not be physically meaningful due to choose regression method's characteristic. On the other hand, it was concluded that using LR is more accurate than using ANNs for these types of problems without having enough number of experimental data when compared with methods with polynomial characteristic. Additionally, LR has faster training and testing stage than ANN.

REFERENCES

- [1] Lapuerta M, Armas O, Rodríguez-Fernández J. Effects of biodiesel fuels on diesel engine emissions. *Prog Energy Combust Sci* 2008;34:198-223.
- [2] Hoekman SK, Robbins C. Review of the effects of biodiesel on NO_x emissions. *Fuel Process. Technol.* 2012;96:237-49.
- [3] Altun Ş, Lapuerta M. Properties and emission indicators of biodiesel fuels obtained from waste oils from the Turkish industry. *Fuel* 2014;128:288-95.
- [4] Giakoumis EG, Rakopoulos CD, Dimaratos AM, Rakopoulos DC. Exhaust emissions of diesel engines operating under transient conditions with biodiesel fuel blends. *Prog Energy Combust Sci* 38 (2012) 691-715.
- [5] Altun Ş., Effect of the degree of unsaturation of biodiesel fuels on the exhaust emissions of a diesel power generator. *Fuel* 117 (2014) 450-457.
- [6] Çanakçı M, Erdil A, Arcaklıoğlu E. Performance and exhaust emissions of a biodiesel engine. *Applied Energy*, 83 (2006) 594-605.

- [7] H. Oğuz, I. Sartaş and H. E. Baydan, Prediction of diesel engine performance using biofuels with artificial neural network. *Expert Systems with Applications*, 37, 6579–86, 2010.
- [8] A. Parlak, Y. Islamoglu, H. Yasar and A. Egrisogut, Application of artificial neural network to predict specific fuel consumption and exhaust temperature for a Diesel Engine, *Applied Thermal Engineering*, 26, 824–828, 2006.
- [9] M. Canakci, A. N. Ozsezen, E. Arcaklioglu and A. Erdil, “Prediction Of Performance And Exhaust Emissions Of A Diesel Engine Fueled With Biodiesel Produced From Waste Frying Palm Oil”, *Expert Systems with Applications*, 36, pp. 9268–9280, 2009.
- [10] J.M. Alonso, F. Alvarruiz, J.M. Desantes, L. Hernandez, V. Hernandez and G. Molto, “Combining Neural Networks and Genetic Algorithms to Predict and Reduce Diesel Engine Emissions”, *IEEE Transactions on Evolutionary Computation*, Vol. 11, No. 1, pp. 46-55, 2007.
- [11] Altun Ş, Yaşar F. A comparison of performance and emissions of a diesel power generator fueled with biodiesels from waste frying oils. In: *Proceedings of EuroTecS-2013*. 2013;1:139-143. Sarajevo, Bosnia and Herzegovina.
- [12] C. Bishop, “*Neural Networks for Pattern Recognition*”, Oxford: University Press, 1995.
- [13] L. Fausett, “*Fundamentals of Neural Networks*”, New York: Prentice Hall, 1994.
- [14] N. K. Togun and S. Baysec, “Prediction of torque and specific fuel consumption of a gasoline engine by using artificial neural networks”, *Applied Energy*, 87, pp. 349–355, 2010.
- [15] J. W. Goodrum and M. A. Eiteman, “Physical Properties of Low Molecular Weight Triglycerides for the Development of Bio-Diesel Fuel Models”, *Bioresource Technology*, 56, pp. 55-60., 1996.

Classification of Point Cloud Images

Erdal Ozbay¹, Ahmet Cinar², Zafer Guler¹

Abstract

Classification of 3D point cloud data is an emerging topic attracting increasing research interest. Especially feature matching has become an increasingly used method for comparing images. In this paper, we address the issues of the efficient detection of real object models by means of 3D point cloud data images. The efficiency of the method is verified according to real 3D point cloud data. The used data sets consist of a large number of point cloud and its images, and it has been acquired with calibration of Kinect sensor camera. We embed our approach in a framework that is a combination of feature extraction of point cloud data and three different types of image feature detection algorithms. These are SIFT, SURF, and GPU based SURF. These methods have been used to compare images to improve the outcome of the classification stage. This paper proposes a novel approach to recognition of the object categories over point cloud images. For this aim, classification of 3D point cloud data allows robust segmentation and feature descriptions into different objects. Selection of 3D classification is generated on extracted partial 3D shapes from the point clouds images and quantizing 3D SURF local descriptors. For execution time, GPU based SURF algorithm 2.5-3.5 times faster than SURF algorithm and 8-9 times faster than SIFT algorithm. Applications are implemented on a machine equipped with an Intel Core i7-3610 QM CPU at 8GB RAM and a GT 650M GPU. In the future, authors are planning to work with complex scene data.

Keywords: *Classification, Feature Detection, GPU-SURF, Point cloud, SIFT, SURF.*

1 INTRODUCTION

Object recognition and classification are the most important problems considering in computer vision. In recent years, computer animation, computer games, virtual and augmented reality, many in the field of computer graphics applications such as human-computer interfaces have begun to use real objects and their digital coordinate information [1].

There has been much research in the past few years in object detection and classification and various methods are proposed [2]. Most of the research is based on images taken by visible-light cameras, which is a natural way to do it just as what human eyes perform. Point Cloud (PC) began to be widely used in reconstruction methods with the creation of 3D models of real objects and feature in the conclusions of these objects, in many applications such as object recognition and object detection. It also allows us to make three-dimensional digital environment on two-dimensional images [3].

3D object scanning technique have been applied widely in various areas, such as industry, cultural heritage, medicine, criminal investigation within this recent decade. Technologies of 3D real word object scanning have been improved much better and they can capture surface information from physical objects quickly and precisely. A structural lighting based scanner is the typical example popular in industry. It can capture huge amount of surface points from a physical object within a few seconds [4].

The RGB camera and low cost sensor cameras have been applied in object identification for many application. However, Kinect has changed this situation. Because of the wide use of three-dimensional (3D) processing, the point cloud library (PCL) now enables people to easily use in a 3D environment. The most important reason to prefer point clouds are shortage in the method of obtaining the 3D object data and the production and extraction of 3D models created through this object. Point cloud objects which obtained by a combination of clusters are made to be significantly associated with combining points on the triangle, the geometrical entities such as lines and surfaces [5].

¹ Corresponding author: Firat University, Department of Computer Engineering, 23119, Elazig, Turkey
erdalozbay@firat.edu.tr,

² Firat University, Department of Software Engineering, 23119, Elazig, Turkey,
zaferguler@firat.edu.tr

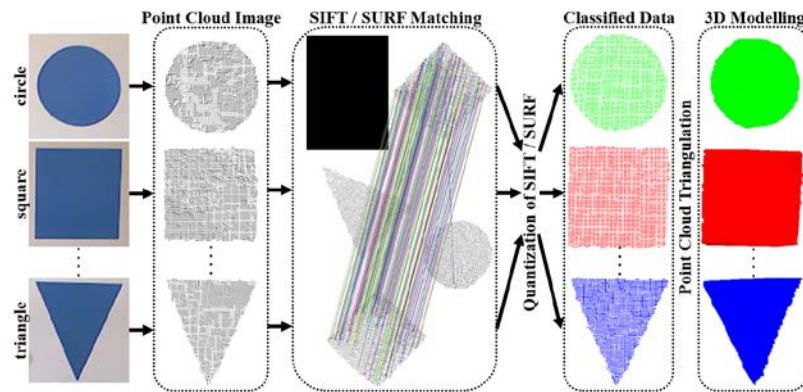


Figure 45. 3D model classification flowchart

Figure 1 is shown that proposed approach using SIFT and SURF matching of 3D geometric object surface on the point cloud images for object recognition. We quantize 3D SIFT and SURF descriptors, extracted from partial 3D shapes computed from single depth (PC) images, into 3D visual words.

In this paper we study how to use the feature descriptors to implement the object detection and its classification for general real geometric surface objects with the Point Cloud Library (PCL). We present a system for general object detection in simple geometric scenes. A point cloud image containing the object to be recognized from a Kinect sensor camera, for general object at will, must be extracted a point cloud model of the object with the Cluster Extraction method, and then we can compute the features matching of the object model, making up the model database after processing many frame images. The database contains only three different simple geometric objects in the scene. Here the general feature we used is SIFT and SURF feature matching from Point Cloud (PC) images [6].

2 RELATED WORK

There are two fundamentally different principles in the field of real object detection; one of them is using RGB images from standard camera and one another is using N dimensional Point Cloud from 3D range scanners like Kinect sensor camera. Depending on the different images, different 2D distinctive local or global features have been developed.

2.1 Point Cloud Image Processing

A point cloud is often used in order to obtain 3D point data. A data set is defined as a collection of multi-dimensional points. In a 3D point cloud, points are often above the sample surface. x , y , and z coordinates are defined geometrically. Point clouds can be obtained by hardware sensors such as stereo cameras, 3D scanners or time-of-flight cameras. PCL supports the Open-NI and it can acquire and process data such as from Microsoft Kinect and Prime Sensor 3D camera devices [7].

Since one single Kinect sensor camera is adopted in the process of obtaining 3D point cloud data, it only sees our scene from a single point of view for simple geometric surface objects. Reasons such as the noise of border area and the shadow of occluding part. These reasons can cause limit data access. In order to eliminate these immortality we set the noise, shadow, and occlusion area projection to the given background of the scene. Three-dimensional point cloud data are obtained using the Point Cloud Library, transformed into the appropriate format is illustrated. At present, there are plenty ways to access to the 3D geometric object surface information and one of them called Kinect Fusion, which is provided by the Kinect SDK [8]. (a) Geometrical object in the scene, (b) its depth images, and the screen shot of the (c) 3D point cloud data are shown in Figure 2. In this paper, we use PCL to programming for acquisition of the 3D geometric object surface information. Point clouds can be obtained by hardware sensors such as stereo cameras, 3D scanners or time-of-flight cameras. PCL supports the Open-NI and it can acquire and process data such as from Kinect and Prime Sensor 3D camera devices [9].



Figure 2. (a) Real geometric objects (b) Depth image (c) Point Cloud images

In this work firstly we capture the current scenes within the real geometric object, and we obtain the point cloud image which contain the object to be recognized. We use the Kinect sensor to capture image based on our experiment condition. Because we are to detect the real geometric object, so no matter whatever the shape or color of the object is, just locate the object with

no occlusion. The remaining of paper is organized as follow; section 3 provide brief description of SIFT and SURF algorithm. Also provides information on the new generation of GPU and description of GPU-SURF algorithm. Section 4 shows the implementation details, experimental results and discussion. The last section is conclusion and further work.

3 OVERVIEW OF THE THREE METHODS

3.1 SIFT Algorithm

SIFT algorithm is one of the successful algorithms in many computer vision algorithm for use in fields such as object detection and recognition and tracking. SIFT algorithm achieves very good results against scaling and rotation invariance. But it requires high computing capacity therefore, sift algorithm cannot be achieved sufficient speed in real-time system. SIFT algorithm is composed of four substantial stages; scale-space extrema detection, update localization, keypoint refinement and filtering and keypoint descriptor calculation. The first stage used difference-of-Gaussian function to identify potential interest points [10], which were invariant to scale and orientation. DOG was used instead of Gaussian to improve the computation speed [11].

- Scale space extreme detection: Scale space is formed by applying the Gaussian filter of images in different scales. These images are used to create difference of Gaussian (DOG). Candidate interest points are selected as the minimum and maximum of DOG.
- Update localization: The location information of each candidate is updated by the color values using the neighboring pixels.
- Keypoint refinement and filtering: Low contrast Candidates and Candidates along edge are eliminated.
- Keypoint descriptor calculation: Gradient calculated for each of the remaining interesting point.

$$D(x, y, \sigma) = (G(x, y, k\sigma) - G(x, y, \sigma)) * I(x, y) = L(x, y, k\sigma) - L(x, y, \sigma) \quad (1)$$

where k is a constant factor and $*$ is a convolution operation.

In equation (1) scale space is formed by applying the Gaussian filter of images in different scales and defined as a function $L(x, y, \sigma)$. This function calculated from the convolution of Gaussian $G(x, y, \sigma)$ and input image $I(x, y)$. To increase the application speed SIFT uses difference of Gaussian (DOG) instead of Gaussian. Convolved image ($D(x, y, \sigma)$), can be computed with the following formula [11].

In the keypoint localization step, they rejected the low contrast points and eliminated the edge response. Hessian matrix was used to compute the principal curvatures and eliminate the keypoints that have a ratio between the principal curvatures greater than the ratio. An orientation histogram was formed from the gradient orientations of sample points within a region around the keypoint in order to get an orientation assignment [11].

SIFT algorithm is determine a larger number of interest points compared with other methods. As a reason for this situation is to calculate the interesting points with different scales and different resolutions. Thus the SIFT algorithm produces more interesting key points and also it is more resident to image deformations. SIFT algorithm can catches a plurality of salient points successfully, but for real time application it was relatively slow. For that reason, SURF algorithm was introduced by Bay, H., Tuytelaars, T. and Van Gool, L. SURF algorithm inspired by SIFT algorithm and can be used for object detection, recognition, classification, registration, etc. [10].

3.2 SURF Algorithm

The SURF algorithm involves the same steps as SIFT algorithm, but the implementation details are slightly different in each of said application step. These algorithms provide slightly different ways of detecting features [12]. As an example, the SURF algorithm uses box filter to approximate difference of Gaussian for scale space extreme detection. Box filter can easily computed from integral images, thus algorithm speed increase. SIFT builds an image pyramids, filtering each layer with Gaussians of increasing sigma values and taking the difference. On the other hand, SURF creates a “stack” without 2:1 down sampling for higher levels in the pyramid resulting in images of the same resolution [10]. Due to the use of integral images, SURF filters the stack using a box filter approximation of second-order Gaussian partial derivatives, since integral images allow the computation of rectangular box filters in near constant time [13].

SURF uses Hessian Matrix to detect interest points. Furthermore, SURF uses wavelet response for orientation assignment and feature description. As a conclusion, with SURF algorithm a lot of feature improved. Same studies shows that SURF Algorithm 3 times faster than SIFT Algorithms with a comparative detection performance.

Nearest Neighbor (NN) is identifies as the keypoint with minimum Euclidean distance for the invariant descriptor vector in the keypoint matching step. Lowe has determined a distance in the low rate operation of the closest neighbor to that second-closest neighbor as 0.5 thus we decided to choose 0.5 as effective measurement distance ratio like Lowe did in SIFT [11].

3.3 GPGPU Architecture

Graphics processors are rapidly developed in the computer graphics field and began to be used for general purpose applications in this area. Thus it has become available to increase the speed performance in many application areas. CUDA architecture developed by NVIDIA company and this architecture allows high increase in computing performance.

In fact, this performance difference is due to the fact that, the GPU architecture designed for parallel operations. GPU has a large number of arithmetic logic unit (ALU), but its cache memory is low [14]. GPUs execute a large number of threads on a set of data at the same time. Therefore it is only appropriate for parallel data. Thus the successful result can be obtained. For example if a program contains many flow control, its calculation speed may be reduce rather than increase [15].

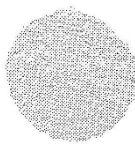
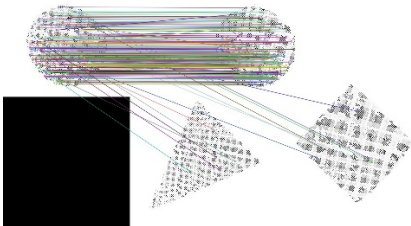
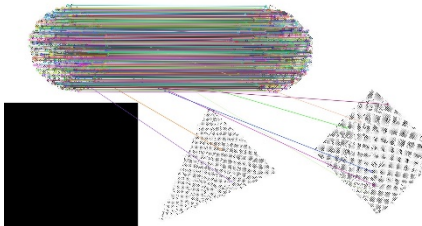
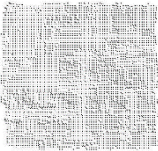
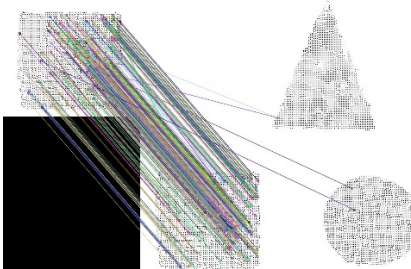
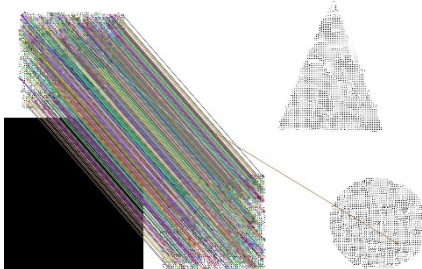
A CUDA C programming language introduces a small number of extensions to C language and allows us to define C function called kernel. With kernel we can define and execute N function in parallel. When kernel calls, unique thread id is available. Thus, with the Id number we can determine which thread is currently running within the kernel. Threads are organized in blocks. In the same as thread, blocks have an identification number. So that which block and which thread actually running, can be easily determined in large data sets. But the number of thread in the block is limited. Current GPUs are supported up to 1024 thread. Threads and blocks can be one, two or three dimensional. Blocks are organized in grids. CUDA architecture supports many memory types. Threads, blocks and type of memory are illustrated. Each thread access registers, local memory, shared memory, constant memory and global memory. The CPU part of the application can be access global memory and constant memory.

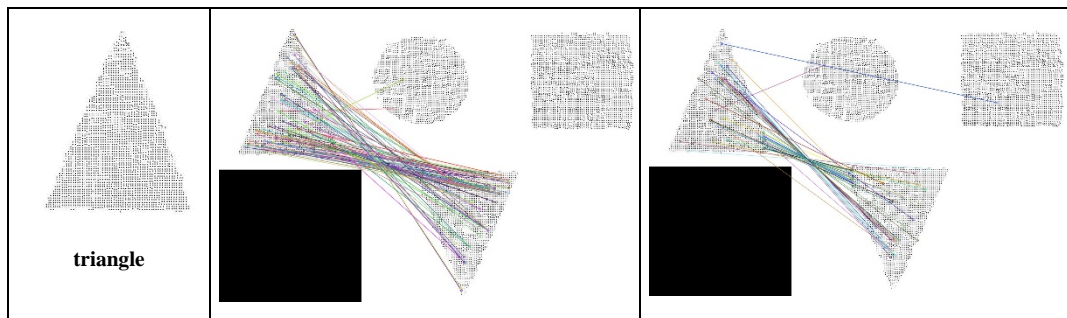
4 RESULTS AND DISCUSSION

We present experimental results obtained by the prepared application with paired images of the cloud point on real geometric objects in this section. All experiments were performed on a machine equipped with an Intel Core i7-3610 QM CPU at 8GB RAM and a GT 650M GPU. The 2GB amount of global memory is reached through a GGDR5 interface. The architecture supports the double precision floating point arithmetic.

This study compared the point cloud images contains multiple objects in the same scene with the single object point cloud images that will be on classification. For this purpose we have used standard SIFT, SURF, and GPU based SURF algorithm by means of performance in this study. The point cloud images are used as a data set with real objects which are three distinct geometric shape. Sample of the matching examples of point cloud images are shown in Table I. The first column of the figure include main object and the remaining columns include matching algorithm results of same object.

Table 1. Results of SIFT, SURF matching algorithm

Test Objects	SIFT Matching	SURF Matching
 circle		
 square		



As seen in Table I. SIFT and SURF matching algorithms evaluation results are given. Accordingly we have applied matching processing for three different geometric objects in the multiple object scene which belong to different location. We have evaluated number of keypoint number and matching keypoint number with SIFT, SURF and GPU-SURF algorithms. The three objects point cloud images have been selected for evaluation. In total, 144 separate matching process was carried for three different geometric objects which are captured from different angles. Implementation of these algorithms the matching of feature keypoints are shown in Table I. SURF algorithm has found an average of 227 features. However SIFT and GPU-SURF algorithm were able to find only 124 and 146 features on average. So it is observed that SURF algorithm finds more features than SIFT and GPU-SURF algorithm. Also as shown in Table II. we have obtained same result for feature matching and its average running times is summarized in Figure 3.

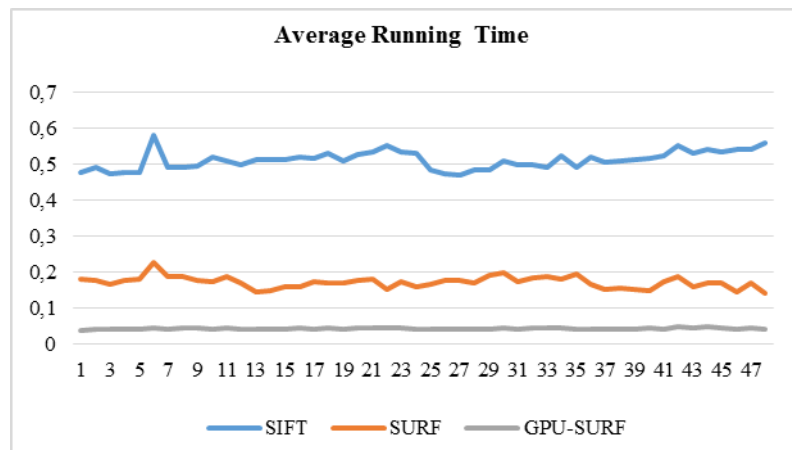


Figure 3. Total average running time results of SIFT, SURF, and GPU-SURF algorithms

Table 2. Results of SIFT, SURF, GPU-SURF matching feature size and running time

	Average Running Time			Average Matching Feature Size
	Test Object	Test Image	Total	
SIFT	0.159	0.353	0.512	124.3
SURF	0.037	0.135	0.172	227.7
GPU-SURF	0.011	0.032	0.043	146

While the point clouds images of the objects are not equal size in the matching process, the average size of the images are 400X300. Results show that with a small image size SIFT and GPU-SURF algorithms have approximately same average matching feature size. But GPU-SURF version works faster than the others. The total average running time is sum of the point clouds obtained from a single object and multiple object scenes of three different image. As a result, you need to make an assessment, produces the highest number of feature matching has been SURF algorithm. The algorithm that performs this process as soon as possible has been GPU-SURF. This algorithm works 4 times faster compared to the SURF algorithm and 12 times faster to the SIFT algorithm.

4.1 Extract Clusters

The first work in the study, matching the images obtained by point cloud images producing from geometric objects to determine which object is classified. Single object test image were matched with multiple objects in the scene. Object provided most matches are determined to be classified within this scene. The second work was to extract clusters from the whole scenes, extracting the point cloud image of the object. This could be done by the class `pcl::EuclideanClusterExtraction` (ECE).

The class `pcl::ECE` is an extracting cluster method based on Euclidean Distance, with a simple idea of distance, just viewing the point cloud that is within the distance threshold as a cluster. If $p_i, q_i \in P$, and P is a point cloud set, then the Euclidean distance dL is as following [6]:

$$dL = \sqrt{\sum_{i=1}^n (p_i - q_i)^2} \quad (2)$$

The basic principle of the classification is as follows. Investigating m data points in m -dimensional space, defined a nature closeness clustering between points, set m data points are n classes, iterations until the distance between any two is greater than a predetermined threshold value or the number of classes is less than the specified number, then we complete segmentation to extract clusters.

In classification algorithm, we'll need to calculate every point of the point cloud to find out which point belongs to which object. Hence, one needs to know the point of this sequential port adjacent to each other. k -NN is used to determine the adjacent points [16]. According to the principle of the closest neighborhood, to determine the closest point to the point of operation, one needs to evaluate the Euclid distance of the neighboring point from the given point numbers. Every point the objects point clouds parameters has been defined as $P(x, y, z)$ respectively. Every Z sized object has a stable, equal distance and because of their point cloud parameters being joint, it has been disabled. After the point parameters has been determined and set, plane with a specified threshold distance (t) are assigned to the point in the remaining planes. In every point cloud, the first reference data is accepted as the threshold value's first divergent points coordinates. To identify if any points remain within the threshold points, $P_i(x_i, y_i)$ and $P_{i+1}(x_{i+1}, y_{i+1})$ one has to calculate the Euclid distance between the points. The threshold value distance (t) to a camera that is pointing at an object from approximately 1.5 meters is set as 6mm.

$$d(P_i, P_{i+1}) = \sqrt{(x_i - x_{i+1})^2 + (y_i - y_{i+1})^2} \leq t \quad (3)$$

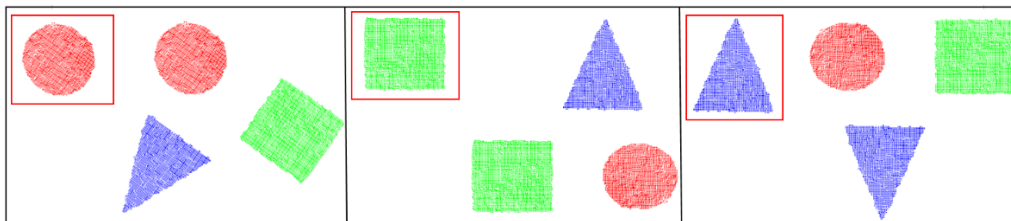


Figure 4. Classified point cloud of geometric objects, from left to right, circle, square, and triangle

The equation (3) is shown with the Euclid distance calculation formula, which does this by calculating every close distance of sequential point with another point inside data set. Clustering algorithm can split the point cloud model of an object that we need, just setting the appropriate clustering threshold parameter values. Then we could extract the objects to be recognized from a complex scene image, to obtain separate clusters shown in Figure 4. The threshold value (t) was adopted 6mm which applied to a calibrated camera from a distance of 1.5 m in the above equation. In the classification result each point of a geometric object in same scene is indicated depending on the different primary color. As a result of the classification of a scene who has 8495 point cloud data numbers, 4024 number of data is red, 2277 number of data is green, 2194 number of data point cloud is colored in blue shown in Figure 4.

4.2 Mesh Generation

In this section we describes a method for generating meshes. The algorithm, based on the Delaunay triangulation, can treat objects of essentially arbitrary complexity. In order to preserve the surface triangulation of solid objects, it is necessary to override the Delaunay property and redefine the triangulation when points are introduced that are close to solid boundaries [17]. After generating the classified point cloud data from the physical geometric object's surface, we used the Delaunay triangulation method to determine the mesh, which is known to combine the coordinate data points with its nodes [18].

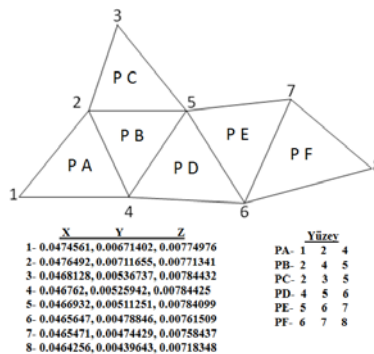


Figure 5. The triangulation of data points

Polygon in a cage, each polygon has three corners, each corner may be part of multiple polygons. A point may represent a corner of the multiple edges. Figure 5. is a polygon mesh consisting of three corners, you can see every surface. For example, PA surface is composed of 1, 2, and 4 corners. At the same time we can see that the corner is a part of most of the multiple surface. For example; corner 5 is part of the PD, PB, PC, and PE surfaces [19]. As shown in the Figure 5. vertices of x, y, z coordinate points combined with the form of polygons are associated with each other. Delaunay triangulation method is used in combination phase of the point cloud data. Then point cloud data modelling visualized in Figure 6. which classified by triangulation [20].

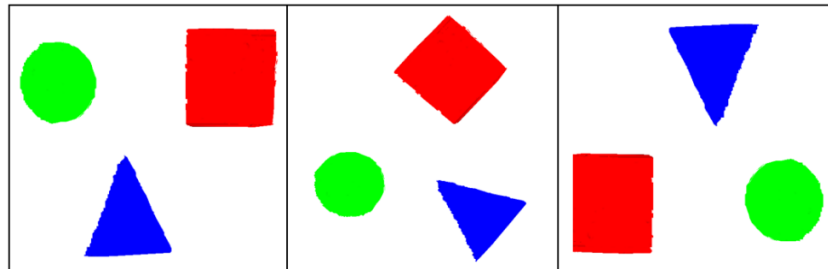


Figure 6. Classified point cloud models from different angles

CONCLUSIONS

In this study has evaluated SIFT, SURF and GPU based SURF algorithms applied on cloud point images of real objects for features size and execution time. Exception of 2D RGB images of objects, these algorithms when applied onto the 3D point cloud images has been shown to give good results according to the evaluation results. In line with these results the scene within the multiple objects images are classified by matching with a single point cloud images. Classified models are visualized with different geometric objects in the same scene applying the mesh generation on the classified version of the real object. As a result of further evaluation algorithms, SURF algorithm finds more features then SIFT and GPU-SURF algorithm. SIFT algorithm is much more slowly than SURF and GPU-SURF algorithms. According to the results of experiments, GPU based SURF algorithm works 4 times faster than SURF algorithm and 12 times faster than SIFT algorithm. Also in further study, the classification process will focus on separation of data from a single object such as classification of the human body and limbs.

REFERENCES

- [1] N. Duarte, O. Postolache, and J. Scharcanski, "KSGphysio-Kinect serious game for physiotherapy," *In Electrical and Power Engineering (EPE), International Conference and Exposition on*, 2014, pp. 606-611.
- [2] L. Xia, C. C. Chen, and J. K. Aggarwal, "Human detection using depth information by Kinect," *In Computer Vision and Pattern Recognition Workshops (CVPRW), IEEE Computer Society Conference on*, 2011, pp. 15-22.
- [3] Y. Guo, M. Bennamoun, F. Sohel, M. Lu, and J. Wan, "An Integrated Framework for 3-D Modeling, Object Detection, and Pose Estimation From Point-Clouds," *Instrumentation and Measurement, IEEE Transactions on.*, vol. 64, pp. 683-693, 2015.
- [4] C. T. Hsieh, "An efficient development of 3D surface registration by Point Cloud Library (PCL)," *In Intelligent Signal Processing and Communications Systems (ISPACS), International Symposium on*, 2012, pp. 729-734.
- [5] R. B. Rusu, and S. Cousins, "3d is here: Point cloud library (pcl)," *In Robotics and Automation (ICRA), IEEE International Conference on*, 2011, pp. 1-4.
- [6] Q. Zhang, L. Kong, and J. Zhao, "Real-time general object recognition for indoor robot based on PCL," *In Robotics and Biomimetics (ROBIO), IEEE International Conference on*, 2013, pp. 651-655.
- [7] E. Ozbay, and A. Cinar, "3D Reconstruction Technique with Kinect and Point Cloud Computing," *Global Journal on Technology, 3rd World Conference on Information Technology on*, 2013, pp. 1748-1754.
- [8] T. Dutta, "Evaluation of the Kinect™ sensor for 3-D kinematic measurement in the workplace," *Applied ergonomics*, vol. 43, pp. 645-649, 2012.
- [9] Z. Y. Huang, J. T. Huang, and C. M. Hsu, "A Case Study of Object Identification Using a Kinect Sensor," *In Systems, Man, and Cybernetics (SMC), IEEE International Conference on*, 2013, pp. 1743-1747.
- [10] L. Juan, and O. Gwun, "A comparison of sift, pca-sift and surf," *International Journal of Image Processing (IJIP)*, vol. 3, pp. 143-152, 2009.
- [11] D. G. Lowe, "Distinctive image features from scale-invariant keypoints," *International journal of computer vision*, vol. 60, pp. 91-110, 2004.
- [12] Z. L. Yang, and B. L. Guo, "Image mosaic based on SIFT," *In Intelligent Information Hiding and Multimedia Signal Processing, IHHMSP'08 International Conference on*, 2008, pp. 1422-1425.
- [13] H. Bay, T. Tuytelaars, and L. Van Gool, "Surf: Speeded up robust features," *In Computer vision—ECCV, Springer Berlin Heidelberg*, 2006, pp. 404-417.
- [14] N. Y. Khan, B. McCane, and G. Wyvill, "SIFT and SURF performance evaluation against various image deformations on benchmark dataset," *In Digital Image Computing Techniques and Applications (DICTA), International Conference on*, 2011, pp. 501-506.
- [15] M. Kass, A. Witkin, and D. Terzopoulos, "Snakes: Active contour models," *International journal of computer vision*, vol. 1, pp. 321-331, 1988.

- [16] F. Rottensteiner, G. Sohn, J. Jung, M. Gerke, C. Baillard, S. Benitez, and U. Breitkopf, "The ISPRS benchmark on urban object classification and 3D building reconstruction," *ISPRS Ann. Photogramm. Remote Sens. Spat. Inf. Sci.*, vol. 1, pp. 293-298, 2012.
- [17] A. Cinar, E. Ozbay, "Üç Boyutlu Derinlik Bilgileri Yardımıyla Modelleme Yöntemlerinin İncelenmesi," *7. Mühendislik ve Teknoloji Sempozyumu, Çankaya Üniversitesi*, 2014, pp. 101-107.
- [18] R. Jonathan, and S. Delaunay, "Refinement Algorithms for Triangular Mesh Generation," *Computational Geometry*, vol. 22, pp. 21-74, 2002.
- [19] B. S. Bischoff, M. Botsch, S. Steinberg, S. Bischoff, L. Kobbelt, and R. Aachen, "OpenMesh—a generic and efficient polygon mesh data structure," *In OpenSG Symposium*, 2002.
- [20] E. Özbay, and A. Çınar, "A novel approach to smoothing on 3d structured adaptive mesh of the kinect-based models," *2th International Conference on Advanced Information Technologies and Applications ICAITA*, 2013, pp. 13-22.

BIOGRAPHY

Erdal Özbay: He is a Research Assistant in the Department of Computer Engineering at the University of Firat where he has been a faculty member since 2012. He completed his MSc at Firat University. His research interests lie in the area of programming languages, computer graphics, image processing, human computer interaction, mesh generation, ranging from theory to design to implementation, with a focus on improving software quality.

Ahmet Çınar: He received the PhD degree in Electric-Electronics Engineering in 2003 from Firat University. He has been working on Firat Univ. Department of Computer Engineering, (Assistant Professor). His research is interested in development and improvement of mesh generation methods, and applications of virtual reality, augmented reality, artificial intelligence and game programming.

Zafer Güler: He is a Research Assistant in the Department of Software Engineering at the University of Firat where he has been a faculty member since 2010. He completed his MSc at Firat University. His research interests lie in the area of programming languages, computer graphics, image processing, cpu programming, ranging from theory to design to implementation, with a focus on improving software quality.

A New Approach to Swarm based Computational Intelligence: Whale Optimization

Feyza Altunbey Ozbay¹, Bilal Alatas²

Abstract

Swarm optimization algorithms are relatively newer subfield of computational intelligence and recently getting strong and becoming more popular. They are inspired from intelligent behaviors resulting from the local interactions of swarm agents between each other and environment. They are adaptable and general purposed solution methods that can be applied to the high-scale combinatorial and non-linear search and optimization problems in case of concurrent different decision variables, objective functions, and constraints and they do not depend on the solution space type, the number of decision variables, and the number of constraint functions. Furthermore, they do not require very well defined mathematical models that are hard to derive. Their computation power is also good and they do not require excessive computation time. Their transformations and adaptations are easy. Due to these advantages, these algorithms are densely being used in many different fields.

Whale Optimization (WO) is the most current swarm based computational intelligence algorithm inspired from the hunting behavior of humpback whales and uses three operators for simulating the search for prey, encircling prey, and bubble-net attacking. This paper explains the main steps of WO and represents its and other current computational intelligence algorithms' comparative results obtained from the benchmark functions. WO is very novel and no optimization has been done in its parameters and its more efficient multi-objective, distributed, and parallel versions for different type of problems should be proposed for future works.

Keywords: Computational Intelligence, Performance, Swarm Optimization, Whale Optimization.

1 INTRODUCTION

Optimization problem is concerned with finding the optimal solutions of a function in scientific fields. Metaheuristic algorithms can be applied to all kinds of these problems and described as a general method to solve various optimization problems. The algorithms provide guidance based on the heuristic to find the search space more effectively. Nature is inspiring researchers to improve efficient and powerful optimization methods for solving optimization problems. Due to general applicability of these algorithms, the methods gain significant interest in science and engineering applications. The common characteristic of whole metaheuristic optimization methods is that they start with an initial population as solutions, iteratively produce new solution with generation rules and finally conclude to obtain best solution to objective function.

Metaheuristic algorithms have become a popular part of modern optimization methods. There are many reasons for this popularity: they are easy to combine with other optimization methods and they provide very effective solutions of dealing with complex problems. These algorithms can be classified in nine different main categories, as shown in Figure 1.

¹ Corresponding author: Firat University, Department of Software Engineering, 23119, Elazig, Turkey. faltunbey@firat.edu.tr

² Firat University, Department of Software Engineering, 23119, Elazig, Turkey. balatas@firat.edu.tr

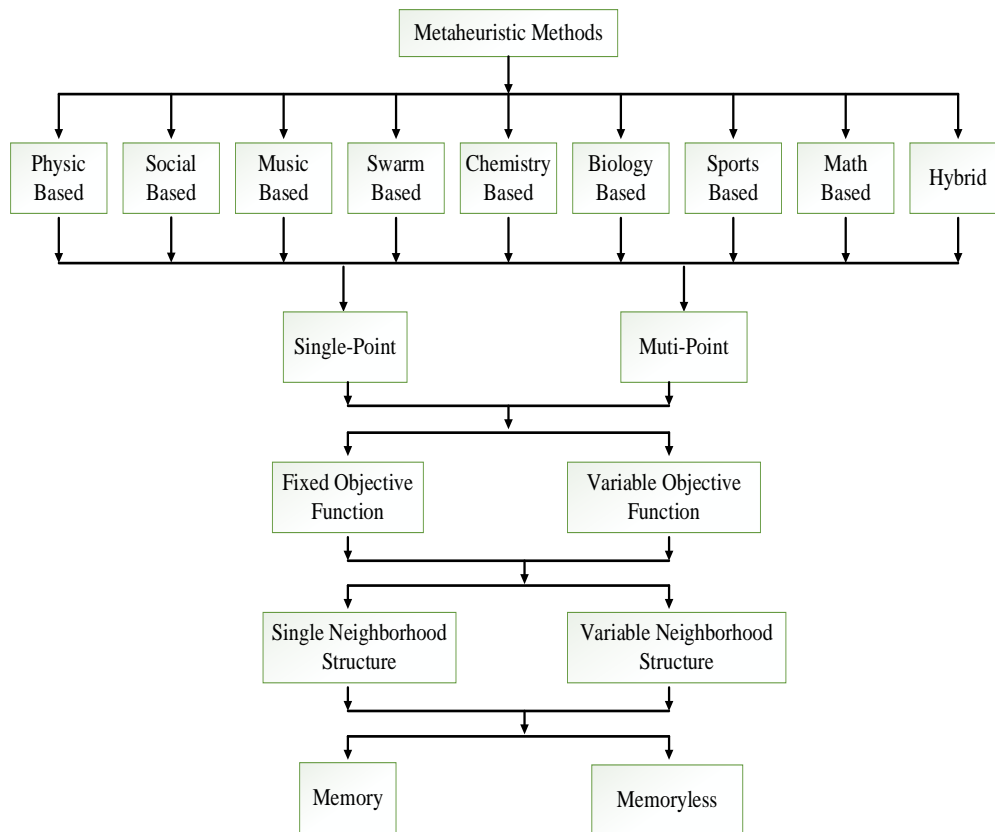


Figure 46. Metaheuristic methods

Physics based metaheuristic optimization methods mimic the physical rules. The most popular physics based methods are Magnetic Optimization Algorithm, Gravitational Search Algorithm, Magnetic Charged System Search, Ions Motion Optimization (IMO), Electromagnetism-like Algorithm, Central Force Optimization Algorithm, Intelligent Water Drops Algorithm, River Formation Dynamics Algorithm, Space Gravitational Algorithm, Particle Collision Algorithm, Big Bang-Big Crunch Algorithm, Galaxy Based Algorithm, Big Crunch Algorithm, Integrated Radiation Algorithm, Charged System Search Algorithm, Artificial Physics Algorithm, and Magnetic Optimization Algorithm [1, 2].

Social based optimization algorithms are inspired from behaviors of people, human learning mechanism, and many features associated with social situation of the people. Social based optimization algorithms can be listed as: Imperialist Competitive Algorithm, Parliamentary Optimization Algorithm, Teaching Learning based Optimization, Social Emotional Optimization Algorithm, Brain Storm Optimization Algorithm, Group Leaders Optimization Algorithm, Hierarchical Social Algorithm, Human Group Formation Algorithm, and Social Based Optimization [3].

Harmony Search, Melody Search, and Musical Composition Algorithm are music based methods [4]. Artificial Chemical Reaction Optimization Algorithm is chemistry based method. Genetic Algorithm, Differential Evolution Algorithm, Ant Colony Algorithm are well known biological based optimization methods.

Sports based optimization algorithms are inspired by the optimization of football systems. These algorithms are Soccer Game Optimization, Soccer League Optimization, Golden Ball Algorithm, Soccer League Competition Algorithm, and Football Optimization Algorithm.

Base optimization and matheuristics are mathematics based metaheuristic methods.

Whale Optimization (WO) is one of the newest swarm based metaheuristic optimization method and mimics the social behaviors of humpback whale [5].

In this paper, WO is introduced and this method has been compared with different swarm based metaheuristic method for benchmark functions. Section 2 illustrates the details of WO. Comparative results obtained from Bird Swarm Algorithm (BSA) [6] and WO for different benchmark functions are presented in Section 3. Finally, some conclusions are given in Section 4.

2 WHALE OPTIMIZATION ALGORITHM

Whale Optimization (WO) is a new swarm-based metaheuristic optimization method that mimics the social behavior of humpback whales. Humpback whale is one of the biggest baleen whales. The most interesting social feature of the humpback whales is their special hunting method called bubble-net feeding method. The algorithm consists of three operators to imitate

encircling prey, spiral bubble-net feeding maneuver, and search for prey. In WO, the first step of optimization process starts with a set of random solutions. Search agents update their positions according to either a randomly selected search agent or the best of obtained solution at each iteration. For updating the position of the search agents, a random search agent is selected when $|A| > 1$, while the best solution is chosen when $|A| < 1$. Finally, if the termination condition is satisfied, the WO algorithm terminates [5]. The pseudo code of WO is given in Figure 2.

```

Initialize the whales population  $X_i (i = 1, 2, \dots, n)$ 
Compute the fitness values of each search agent
 $X^*$  = the best search agent
while ( $t <$  maximum number of iterations)
  for each search agent
    Update  $a, A, C, l$ , and  $p$ 
    if1 ( $p < 0.5$ )
      if2 ( $|A| < 1$ )
        Update the position of the current search agent
      else if2 ( $|A| \geq 1$ )
        Choose a random search agent ( $X_{rand}$ )
        Update the position of the current search agent
      end if2
    else if1 ( $p \geq 0.5$ )
      Update the position of the current search
    end if1
  end for
  Check if any search agent goes beyond the search space and change it
  Compute the fitness values of each search agent
  Update  $X^*$  if there is a better solution
   $t = t + 1$ 
end while
return  $X^*$ 

```

Figure 2. Pseudo code of WO

3 EXPERIMENTAL RESULTS

To evaluate the performance of WO, two benchmark test functions with different characteristics have been used. These benchmark functions are frequently used to evaluate and compare the characteristics of optimization algorithms in terms of convergence, precision, robustness, and general performance. The nature, complexity, and other properties of these benchmark functions can be easily obtained from their definitions and the difficulty levels of these benchmark functions can be adjusted by changing their dimension and interval parameters [7]. The selected benchmark functions and its properties have been demonstrated in Table 1. The dimensions (n) for all benchmark functions have been determined as 30. Sphere is a unimodal function with less complexity and it can be used to evaluate the converging behaviors of algorithms [8]. Rastrigin function is a multi-modal function with many local optima and it can be used to test the global search ability of the optimization algorithms in avoiding premature convergence [9]. Their graphs with two dimensions have been shown in Figure 3 and Figure 4.

Table 1. Benchmark functions

Function No	Function Name	Definition	Interval	Characteristics
1	Sphere	$f_1(x) = \sum_{i=1}^n x_i^2$	$-100 \leq x_i \leq 100$	Unimodal
2	Rastrigin	$f_2(x) = 10n + \sum_{i=1}^n x_i^2 - 10\cos(2\pi x_i)$	$-5.12 \leq x_i \leq 5.12$	Multi-modal

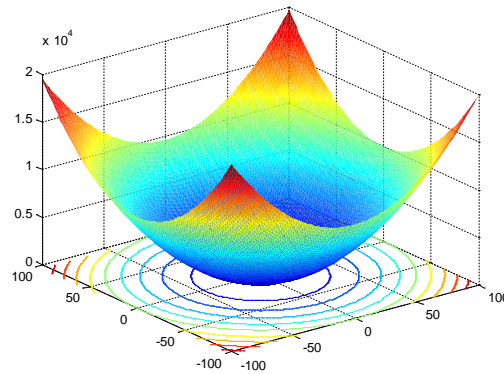


Figure 1. Sphere function with two variables

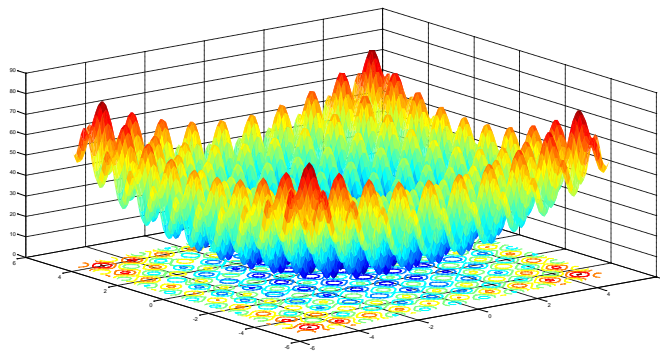


Figure 2. Rastrigin function with two variables

The performance of WO has been tested with Bird Swarm Algorithm (BSA) for Sphere function with 30 dimensions. Initial population size of both algorithm is selected as 30 and they are terminated after 200 iterations. The frequency of birds' flight behaviors (FQ), cognitive accelerating coefficient (c_1), social accelerating coefficient (c_2), indirect and direct effect parameters on the birds' vigilance behaviors (a_1 and a_2) used for BSA have been listed in Table 2.

Table 2. Parameter values of BSA

Parameter	FQ	c_1	c_2	a_1	a_2
Value	10	1.5	1.5	1	1

Both algorithms have been run for 30 times and objective function values obtained from Sphere function have been demonstrated in Table 3. From the experimental results, it can be seen that BSA has better performance than WO in unimodal function. Wilcoxon rank-sum test have also been performed for these experiment results. Table 3 reports the obtained test results for Sphere function. This is used to test the null hypothesis that the means of two populations (obtained from WOA and BSA) are equal with 95% confidence. With a two-tail test (inequality), if $t \text{ Stat} < -t \text{ Critical two-tail}$ or $t \text{ Stat} > t \text{ Critical two-tail}$, we reject the null hypothesis. It can be seen that the observed difference between the sample means is convincing enough to say that success of BSA is significantly better than that of WOA.

Table 3. Obtained results from WOA and BSA for Sphere function

Experiment No.	WOA	BSA
1	3.9671e-26	4.1191e-84
2	3.871e-29	8.6915e-91
3	2.6689e-28	6.8609e-82
4	9.5586e-31	3.3194e-89
5	3.8525e-28	6.0915e-86
6	2.5057e-34	1.8859e-84
7	4.708e-32	1.9371e-83
8	4.0294e-27	1.2695e-81
9	1.2902e-29	7.1079e-89
10	3.6743e-33	4.2864e-82
11	6.2633e-27	9.0407e-84
12	5.2439e-29	9.6429e-86
13	1.0942e-26	8.5036e-93
14	5.4157e-30	1.2066e-86
15	1.3688e-28	1.4124e-77
16	4.6033e-30	8.0177e-81
17	6.4686e-31	1.0633e-83
18	4.6725e-27	2.0229e-85
19	4.3435e-31	5.8456e-81
20	1.7188e-27	7.9718e-79
21	4.6126e-28	9.0930e-88
22	4.9547e-33	4.8172e-86
23	6.0371e-26	1.2766e-87
24	8.8936e-29	4.8393e-85
25	1.4958e-31	1.1833e-92
26	4.1442e-31	1.2867e-83
27	2.0762e-27	3.1480e-89
28	1.6947e-31	5.9188e-76
29	8.9696e-29	2.7977e-87
30	2.8813e-29	1.0435e-85

Table 4. Wilcoxon rank-sum test results obtained from WOA and BSA for Sphere function

	WOA	BSA
Mean	4.38E-27	2.02E-77
Variance	1.67E-52	1.2E-152
Observations	30	30
Hypothesized Mean Difference	0	
df	29	
t Stat	1.854243	
P(T<=t) one-tail	0.03695	
t Critical one-tail	1.699127	
P(T<=t) two-tail	0.0739	
t Critical two-tail	2.04523	

The obtained results from WOA and BSA for multi-modal Rastrigin function with 30 dimensions have been shown in Table 5. Initial population size of both algorithms is selected as 30 and they are terminated after 50 iterations. From the experimental results, it can be seen that BSA has better performance than WO in this multi-modal function. Wilcoxon rank-sum test has also been performed in Table 6 for the results obtained from Rastrigin function. It can be seen that the observed difference between the sample means is convincing enough to say that success of BSA is significantly better than that of WOA.

Table 5. Obtained results from WOA and BSA for Rastrigin function

Experiment No.	WOA	BSA
1	30.1309	0
2	0.01136	1.1369e-13
3	0.0012374	0
4	0.00086272	0
5	0.00013125	1.4984e-10
6	9.7538e-07	0
7	0.00029807	0
8	0.0023691	1.1369e-13
9	1.1837e-06	0
10	1.0737e-05	0
11	1.7224e-05	0
12	0.00074477	2.1978e-09
13	24.0951	0
14	3.4102e-07	0
15	29.793	0
16	0.0052797	0
17	183.341	5.6843e-14
18	0.00064019	0
19	202.6096	0
20	66.1202	0
21	1.5577e-05	0
22	1.3277e-06	0
23	0.00013833	0
24	269.4407	5.6843e-14
25	0.013915	0
26	150.8407	5.6843e-13
27	110.6747	1.1369e-12
28	181.7451	2.3711e-9
29	0.00019012	0
30	0.090213	9.6634e-13

Table 6. Wilcoxon rank-sum test results obtained from WOA and BSA for Rastrigin function

	WOA	BSA
Mean	41.63061	1.57E-10
Variance	5863.816	3.36E-19
Observations	30	30
Hypothesized Mean Difference	0	
df	29	
t Stat	2.977716	
P(T<=t) one-tail	0.002907	
t Critical one-tail	1.699127	
P(T<=t) two-tail	0.005813	
t Critical two-tail	2.04523	

4 CONCLUSIONS

Due to many advantages of metaheuristic algorithms, they are intensely used as search and optimization techniques for different types of complex problems. There is not one algorithm that gives the best results for all types problems. That is why, new algorithms inspired from nature or new versions of current algorithms are proposed. Whale Optimization (WO) is the most current swarm based computational intelligence algorithm inspired from the hunting behavior of humpback whales and uses three operators for simulating the search for prey, encircling prey, and bubble-net attacking. In this paper, working principle of WO has been introduced and its performance have been tested using different types of benchmark functions. Obtained results from WO have been compared with those obtained from Bird Swarm Algorithm (BSA) and it has been shown that BSA is better than WO for the selected functions. It can be concluded that more works should be performed in order to increase the convergence, precision, robustness, and general performance of WO.

REFERENCES

- [1] U. Can and B. Alatas, "Physics Based Metaheuristic Algorithms for Global Optimization," *American Journal of Information Science and Computer Engineering*, vol. 1, pp. 94-106, 2015.
- [2] F. Altunbey and B. Alatas, "Review of Computational Intelligence Method Inspired from Behavior of Water", 1st International Conference on Engineering Technology and Applied Sciences ICETAS, 2016.
- [3] F. Altunbey and B. Alatas, "Review of Social-Based Artificial Intelligence Optimization Algorithms for Social Network Analysis," *International Journal of Pure and Applied Sciences*, vol. 1, pp. 33-52, 2015.
- [4] F. Altunbey and B. Alatas, "Review of Music based Computational Intelligence Methods", 1st International Conference on Engineering Technology and Applied Sciences ICETAS, 2016.
- [5] S. Mirjalili and A. Lewis, "The Whale Optimization Algorithm," *Advances in Engineering Software*, vol. 95, pp. 51-67, 2016.
- [6] X. B. Meng, X. Z. Gao, L. Lu, Y. Liu and H. Zhang, "A new bio-inspired optimisation algorithm: Bird Swarm Algorithm", *Journal of Experimental & Theoretical Artificial Intelligence*, pp. 1-15, 2015.
- [7] B. Alatas, E. Akin, A. B. Ozer, "Chaos Embedded Particle Swarm Optimization Algorithms", *Chaos, Solitons & Fractals*, vol. 40, pp. 1715-1734, 2009.
- [8] (2016) GEATbx: Examples of Objective Functions. [Online]. Available <http://www.pg.gda.pl/~mkwies/dyd/geadocu/fcnfun1.html>
- [9] (2016) GEATbx: Examples of Objective Functions. [Online]. Available <http://www.pg.gda.pl/~mkwies/dyd/geadocu/fcnfun6.html>

BIOGRAPHY

Feyza Altunbey Ozbay: She received her BSc in Computer Engineering from Firat University, Turkey in 2013. She completed her MSc in Software Engineering at Firat University. At present she is pursuing Ph. D. in Software Engineering, Firat University, Turkey. She is a Research Assistant in the Department of Software Engineering at the Firat University. Her research interests include social network analysis, computational intelligence and metaheuristic optimization.

Bilal Alatas: Alatas received his B.S., M.S., and Ph.D. degrees from Firat University. He has been working as Head of Software Engineering Department at Firat University in Elazig, Turkey. His research interests include artificial intelligence, data mining, and metaheuristic computation. Dr. Alatas has published over 50 papers in many well-known international journals and proceedings of refereed conference since 2001. He has been editor of nine international journals and reviewer of twenty international journals

A Simple and Global Physics based Metaheuristic Method: Water Evaporation Optimization

Feyza Altunbey Ozbay¹, Bilal Alatas²

Abstract

Metaheuristic methods are very popular and efficiently used in many complex real world search and optimization problems. Due to the philosophy of continually searching the best and absence of the most efficient metaheuristic method for all types of problems, novel algorithms or new variants of current algorithms are being proposed. Water Evaporation Optimization Algorithm (WEOA) is the most current physics inspired metaheuristic algorithm and based on the evaporation of a tiny amount of water molecules on the solid surfaces with different wetting capabilities. This paper explains the operators of WEOA and represents the comparative results obtained from novel metaheuristic methods for different benchmark functions. Although WEOA is one of the newest algorithm and no optimization has been done for its parameters, obtained results from the experiments are promising. WEOA seems a simple and efficient global optimization algorithm that may be used in many complex search and optimization problems and its variants may be proposed for efficiency in future works.

Keywords: Global Optimization, Metaheuristics, Water Evaporation Optimization.

1 INTRODUCTION

Metaheuristic methods are general purposed solution algorithms and use the information being gathered to guide the search towards the global optimum. They are efficiently used in solving of complex, multimodal, high dimensional and nonlinear search and optimization problems. They are population based methods and start the search within the search space with more than one candidate points and are capable of escaping from a local optima. In recent years, they have been very popular due to their good computation power and easily transformations [1].

General purposed metaheuristic methods are generally classified in different groups like biological based, social based, music based, sports based, chemistry based, and physics based. There are also hybrid methods formed with these methods. Genetic Algorithm, Differential Evolution Algorithm, and Ant Colony Algorithm are biological based; Tabu Search is social based; Artificial Chemical Reaction Optimization Algorithm is chemistry based; Harmony Search Algorithm is musical based algorithms and models. Although there are many effective and successful methods that have been introduced to the literature, it is an important task for the science that there should be always effort to improve and search for the best. Also, there have not been any algorithm that can solve all types of problems effectively, often new algorithms are introduced and also improved versions of the introduced ones are proposed in order to improve their effectiveness. Especially in recent years, researchers have introduced such new metaheuristic methods to the literature and performed successful applications [2].

Although there are many metaheuristic optimization methods that are based on physics, many of them are not known by scientists and there are very limited works about these methods. Physics inspired metaheuristic methods can be listed as: Gravitational Search Algorithm, Electromagnetism-Like Algorithm, Central Force Optimization Algorithm, Space Gravitational Algorithm, Particle Collision Algorithm, Big Bang-Big Crunch Algorithm, Galaxy Based Algorithm, Big Crunch Algorithm, Ions Motion Optimization, Integrated Radiation Algorithm, Charged System Search Algorithm, Artificial Physics Algorithm, Magnetic Optimization Algorithm, Gravitation Field Algorithm, Gravitational Interactions Optimization, Hysteretic Optimization, Light Ray Optimization Algorithm, Ray Optimization, Spiral Optimization Algorithm, Intelligent Water Drops Algorithm, River Formation Dynamics Algorithm, Water Cycle Algorithm, Water Flow Algorithm, Water Flow-like Algorithm, Water Wave Optimization, Circular Water Wave Algorithm, Artificial Showering Algorithm. The last eight algorithm is especially inspired from the events, process, and behavior of water [3]. Water Evaporation Optimization Algorithm (WEOA) is one of the newest physically inspired algorithm and mimics the evaporation of a tiny amount of water molecules on the solid surface with different wettability which can be studied by molecular dynamics simulations [4]. It has been recently proposed and there is only one article introducing the WEOA.

In this paper, the operators of WEOA has been introduced and the comparative results obtained from other novel physics based metaheuristic methods for different benchmark functions have been presented. Section 2 WEOA has been explained. Section 3 defines the benchmark functions used for comparisons. Section 4 presents the experimental results and finally Section 5 concludes the paper along with future research directions.

¹ Corresponding author: Firat University, Department of Software Engineering, 23119, Elazig, Turkey. faltunbey@firat.edu.tr

² Firat University, Department of Software Engineering, 23119, Elazig, Turkey. balatas@firat.edu.tr

2 WATER EVAPORATION OPTIMIZATION ALGORITHM

Water Evaporation Optimization Algorithm (WEOA) is based on the evaporation of a tiny amount of water molecules on the solid surfaces with different wetting capabilities. As the surface changed from hydrophobicity to hydrophilicity, the evaporation speed increases first, and then decreases after reaching a maximum value. When the surface wettability of the substrate is not high enough, the water molecules accumulate into the form of a sessile spherical cap. When the surface wettability of the substrate is high enough, the water molecules spread to a monolayer and the geometric factor no longer affects much and the energy barrier provided by the substrate affects the evaporation speed [3]. Based on these explanations, the analogy between water evaporation phenomena and a population based metaheuristic algorithm can be summarized as shown in Table 1. The flow chart of WEOA is demonstrated in Figure 1 [4].

Table 16. Analogy between water evaporation and metaheuristic optimization

Water Evaporation	Metaheuristic Optimization
Water molecules	Candidate solutions
Solid surface (substrate)	Search space
Decreasing wettability of the surface	Decreasing of objective function
Evaporation flux rate of the water molecules	A measure for deciding local or global search

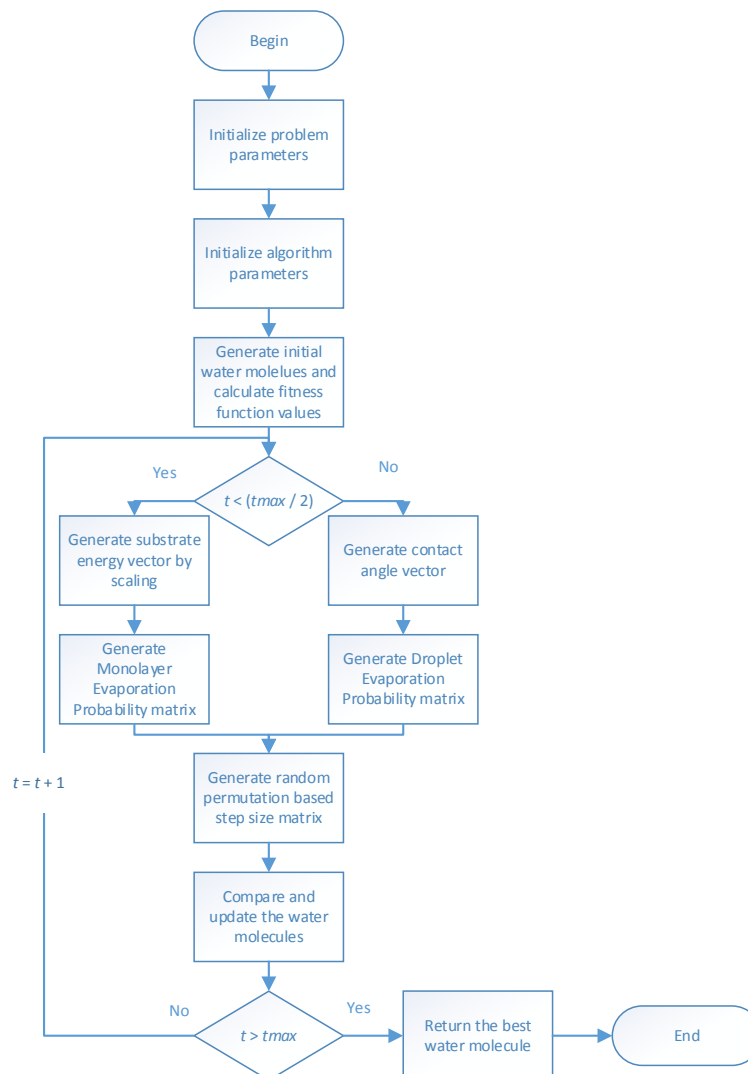


Figure 17. Flow chart of WEOA

3 BENCHMARK FUNCTIONS

Benchmark test functions are used to evaluate and compare the characteristics of optimization algorithms in terms of convergence, precision, robustness, and general performance as a rule. The nature, complexity and other properties of these

benchmark functions can be easily obtained from their definitions. The difficulty levels of most benchmark functions are adjustable by setting their parameters [5]. The selected benchmark functions and its properties have been demonstrated in Table 2. The dimensions for all functions have been determined as 30. Sphere function is unimodal with less complexity and it can be used to evaluate the converging behaviors of algorithms [6]. Schwefel function is multi-modal function with many local optima and it can be used to test the global search ability of the algorithms in avoiding premature convergence [7].

Their graphs with two dimensions have been shown in Figure 2 and Figure 3.

Table 2. Benchmark functions

Function No	Function Name	Definition	Interval
1	Sphere	$f_1(x) = \sum_{i=1}^n x_i^2$	$-100 \leq x_i \leq 100$
2	Schwefel	$f_2(x) = n \times 418.9829 + \sum_{i=1}^n -x_i \sin(\sqrt{ x_i })$	$-500 \leq x_i \leq 500$

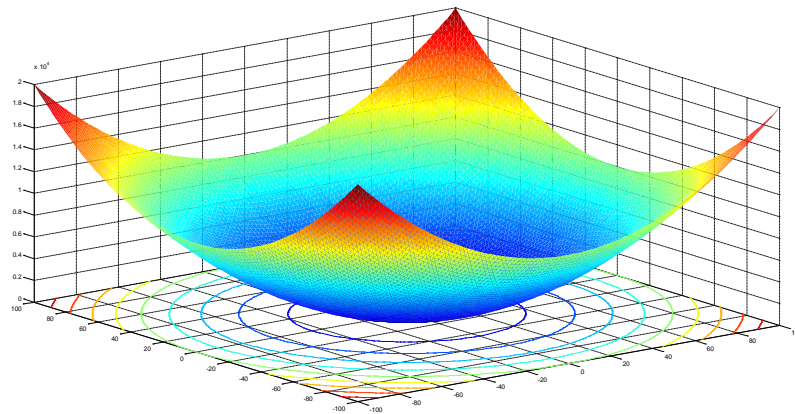


Figure 2. Sphere function with two variables

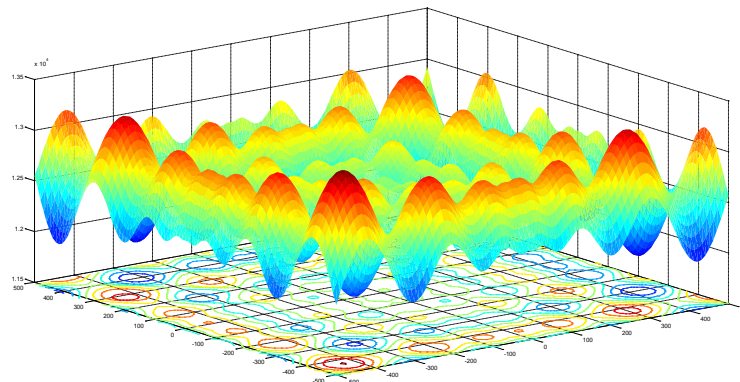


Figure 3. Schwefel function with two variables

4 EXPERIMENTAL RESULTS

Obtained results for Sphere function from WEOA and Gravitational Search Algorithm (GSA) [8, 9], one of the newest physics inspired metaheuristic method, have been demonstrated in Table 3 and Table 4. Both algorithms have run 10 times with different numbers of starting search points (5, 10, 15, 20, 30, 50, and 100). During each run, the maximum number of function evaluations is 2×10^5 . The maximum number of algorithm iterations is equal to the result of dividing the maximum number of function evaluations to the number of starting search points, water molecules in WEOA. Minimum and maximum value of monolayer evaporation probabilities of the algorithm are determined as 0.03 and 0.6 respectively. Minimum and maximum

value of droplet evaporation probabilities are selected as 0.6 and 1 respectively. It can be seen that when the maximum number of iteration is fixed, with low and big population size, performance of WEOA is better than that of GSA. Increasing the number initial search point results in poor performance of the WEOA whereas results in better performance of the GSA.

Table 3. Obtained results for Sphere function from WEOA and GSA with population size 5, 10, 15, and 20

Initial population size	5		10		15		20	
	WEOA	GSA	WEOA	GSA	WEOA	GSA	WEOA	GSA
Mean	989.86	1.9160e-13	7.941e-99	1.5609e-15	3.369e-61	2.9789e-16	9.158e-41	1.0110e-15
Best	94.27	3.0896e-11	5.96e-101	1.3615e-14	6.716e-62	7.1881e-16	1.052e-41	6.4508e-16
Worst	2404.18	4.3105e-12	2.161e-98	3.6971e-15	9.761e-61	4.6119e-16	2.717e-40	1.1258e-15

Table 4. Obtained results for Sphere function from WEOA and GSA with population size 30, 50, and 100

Initial population size	30		50		100	
	WEOA	GSA	WEOA	GSA	WEOA	GSA
Mean	1.082e-22	2.2587e-17	6.386e-11	6.1634e-18	0.0038	2.2672e-18
Best	6.077e-23	4.1430e-17	2.359e-11	1.4860e-17	0.0021	3.7250e-18
Worst	2.453e-22	3.0127e-17	9.162e-11	1.0793e-17	0.0046	3.1977e-18

Obtained results for Schwefel function from WEOA and GSA have been reported in Table 5 and Table 6. Both algorithms have run 10 times with different numbers of starting search points (5, 10, 15, 20, 30, 50, and 100). During each run, the maximum number of function evaluations is 2×10^5 . The same parameter values of the algorithms have been used for this function. From these tables, it can be concluded that performance of WEOA is better than that of GSA in multi-modal Schwefel function.

Table 5. Obtained results for Schwefel function from WEOA and GSA with population size 5, 10, 15, and 20

Initial population size	5		10		15		20	
	WEOA	GSA	WEOA	GSA	WEOA	GSA	WEOA	GSA
Mean	1142.2	7.6596e+3	23.70	9.4366e+3	1.338e-2	9.5591e+3	0.40637	9.4890e+3
Best	473.76	9.6143e+3	1.338e-2	1.0603e+4	1.338e-2	1.0622e+4	1.338e-2	1.0770e+4
Worst	1658.2	8.6784e+3	118.45	1.0004e+4	1.338e-2	1.0234e+4	1.9209	1.0244e+4

Table 6. Obtained results for Schwefel function from WEOA and GSA with population size 30, 50, and 100

Initial population size	30		50		100	
	WEOA	GSA	WEOA	GSA	WEOA	GSA
Mean	135.054	9.7690e+3	439.861	9.5412e+3	1081.773	9.1358e+3
Best	1.822	1.0524e+4	354.563	1.0179e+4	902.645	1.0107e+4
Worst	237.063	1.0085e+4	568.096	9.8156e+3	1188.139	9.4765e+3

5 CONCLUSIONS

Due to the philosophy of continually searching the best and absence of the most efficient metaheuristic method for all types of problems, novel algorithms or new variants of current algorithms are being proposed. Water Evaporation Optimization Algorithm (WEOA) is the most current physics inspired metaheuristic algorithm and based on the evaporation of a tiny amount of water molecules on the solid surfaces with different wetting capabilities. In this paper, WEOA has been briefly described and its performance has been tested with another physics based metaheuristics method, namely Gravitational Search Algorithm (GSA) for different benchmark functions. Although WEOA is one of the newest algorithm and no optimization has been done for its parameters, obtained results from the experiments are promising. WEOA seems a simple and efficient global optimization algorithm that may be alternatively used in many complex search and optimization problems. Its variants containing multi objectivity, dynamic parameter selection, different initial population methods, different termination criterion,

and its hybrids with other metaheuristic or heuristic methods may be proposed for efficient solution future works as WEOA has a high potential to solve various search and optimization problems in different areas.

REFERENCES

- [1] F. Altunbey and B. Alatas, "Review of Social-Based Artificial Intelligence Optimization Algorithms for Social Network Analysis", *International Journal of Pure and Applied Sciences*, vol. 1, pp. 33-52, 2015.
- [2] S. Akyol and B. Alatas, "The Current Swarm Intelligence Optimization Algorithms", *Nevsehir Universitesi Fen Bilimleri Enstitusu Dergisi*, vol. 1, pp. 36-50, 2012.
- [3] U. Can and B. Alatas, "Physics Based Metaheuristic Algorithms for Global Optimization," *American Journal of Information Science and Computer Engineering*, vol. 1, pp. 94-106, 2015.
- [4] A. Kaveh and T. Bakhshpoori, "Water Evaporation Optimization: A Novel Physically Inspired Optimization Algorithm", *Computer Sciences*, vol. 167, pp. 36-50, 2016.
- [5] B. Alatas, E. Akin and A. B. Ozer, "Chaos Embedded Particle Swarm Optimization Algorithms", *Chaos, Solitons & Fractals*, vol. 40, pp. 1715-1734, 2009.
- [6] (2016) GEATbx: Examples of Objective Functions. [Online]. Available <http://www.pg.gda.pl/~mkwies/dyd/geadocu/fcnfun1.html>
- [7] (2016) GEATbx: Examples of Objective Functions. [Online]. Available <http://www.pg.gda.pl/~mkwies/dyd/geadocu/fcnfun7.html>
- [8] E. Rashedi, H. Nezamabadi-pour and S. Saryazdi, "GSA: A Gravitational Search Algorithm," *Information Sciences*, vol. 179, pp. 2232-2248, 2009.
- [9] B. Gu and F. Pan, "Modified Gravitational Search Algorithm with Particle Memory Ability and its Application", *International Journal of Innovative Computing, Information Control*, vol. 9, pp. 4531-4544, 2013.

BIOGRAPHY

Feyza Altunbey Ozbay: She received her BSc in Computer Engineering from Firat University, Turkey in 2013. She is a Research Assistant in the Department of Software Engineering at the Firat University. She completed her MSc in Software Engineering at Firat University. At present she is pursuing Ph. D. in Software Engineering, Firat University, Turkey. Her research interests include social network analysis, computational intelligence and metaheuristic optimization.

Bilal Alatas: Alatas received his B.S., M.S., and Ph.D. degrees from Firat University. He has been working as Head of Software Engineering Department at Firat University in Elazig, Turkey. His research interests include artificial intelligence, data mining, and metaheuristic computation. Dr. Alatas has published over 50 papers in many well-known international journals and proceedings of refereed conference since 2001. He has been editor of nine international journals and reviewer of twenty international journals

Ecology and Turkish Economics

Soner Akin¹, Ugur Yildirim² Cemil Serhat Akin³

Abstract

Turkish ecosystem services, biophysical magnitudes of the changes in ecosystem services which were derived from human actions can be a questionable sphere. Possible full economic valuation of several agricultural landscape management options for Central Anatolia, including managing for water quality, biodiversity, and crop productivity will be discussed in this paper via Ministry of Agriculture and Ministry of Environment and Urbanization datum taken from Turkish Statistics Institutions. In this respect, climate, global biogeochemical cycles, water filtration, soil formation, erosion control, flood protection datum could be seen in a platform on discussing to use Turkish economic potential for agricultural production.

Keywords: Turkish ecology in economics, ecology management, agriculture in economics, ecology for agriculture, Turkey in agriculture

1 INTRODUCTION

Ecology, today, becomes one of the interest areas in human economies and earth's natural ecosystems based improvement or sustainability researches. Ecosystem in traditional outlooks gave a framework for most of the researches by being accepted as the main resource of natural goods. Differently from environmental approaches on economics, ecology based perspectives mainly focus on the protection or high rational using of ecological system benefits or resources. Ecological view or perspectives are highly based on the idea as sustainability. In policy making session, we can witness the inspirations for the rise of green economics as well.

In this study, major ecological indicators are discussed through county samples. Indeed, the economic reflection of ecological variable changes was questioned. As a case study or an interpretation arena, Turkey is to be taken into a comparative platform in order to assess the economic outcome of ecological policies beyond its potential.

2 ECOLOGY AND TIES IN ECONOMICS

Many environmental or salt ecology based items as climate, global biogeochemical cycles, water filtration, soil formation, erosion control, flood protection are directly related with the conditions behind economic production or related activities [1]. In our time, many countries are dealt with ecological footprint studies, in order to know their own destruction and sustainability limits, which are also valid for economic potential using. An independent organization named as Global Ecological Footprint Network is presenting the related data in this sphere and mostly gives global hectares per capita. This group is mostly focused on using and preservation of resources in ecology at first. According to their evaluation, a nation's insufficient ecological resources within its own territory can cause local ecological deficits which makes them ecological debtor country. In the reverse situation, a country an ecological remainder and it is called an ecological creditor country [2]. Looking at ecological items and their evaluation, we can easily witness a solid economic outlook, indeed.

2.1 Turkish Economy in Ecological Limits

In geographic terms, Turkey is settled in two different continents as Asia and Europe. Black Sea ties and its own road path for Siberia, Mediterranean Region and Iran peninsula gives Turkey a high advantage in transportation alternatives, which supports economic outputs' trade facilities. Thinking the diversity of biological species, Turkey can also be seen a rich country, by means of plant and animal diversity. Turkey became final destination of many species which had come from three different continents as Asia, Africa and Europe, which made Turkey's potential fauna and flora nearly equal to Europe [3]. Nine thousand plant and eight thousand animal species are estimated in Turkey's potential. The main environmental threats in Turkey are accepted as the weak conservation of biodiversity, not evaluating drainage, high water pollution from the industrial dumping of chemicals and home cleaning staffs as detergents, high outdoor and indoor air pollution, methane, carbon dioxide and green gases emissions, greenhouse gases, and land degradation with flood.

¹ Corresponding author: Mustafa Kemal University, Teaching Assistant Doctor, Department of Foreign Trade, 31440, Kırıkhan/Hatay, Turkey. sakin@mku.edu.tr

² Kahramanmaraş Sutcu Imam University, Professor Doctor, Public Administration Department, Kahramanmaraş, Turkey, uyildirim@ksu.edu.tr

³ Mustafa Kemal University, Assistant Professor Doctor, Department of Economics, Hatay, Turkey. csakin@mku.edu.tr

2.2 Agricultural Production in Turkey

Turkish Statistic Institute and Ministry of Food, Agriculture and Husbandry datum gave us the dramatic condition of Turkey on weak position benefiting from economic output potential of ecological status. Turkey does not have sufficient water, and this position is not taken into a healing position. Approximately three quarters of water consumed is used for irrigation in agriculture [4]. Turkey had 22 600 000 tones wheat production 2015 [5]. This production volume makes its order in world as 7th to 10th. Similarly in same studies, 38 566 thousand hectares were estimated for total utilized agricultural land in 2015's Turkey, being decreased from the number 40967 hectares of the year as 2001. Value of production in Turkish Liras for crop and animal production is estimated in 119.724.118.432,488 TL which around 42.813.344,5968 US dollars for 2015.

Biochemical cycle for Turkey can be discussed for the using of petroleum products by means of the economic out and reflections in ecology. Turkey has weak on using alternative resources as thermo chemical energies though. The underwater resources for thermal facilities are not rightfully benefited. According to a research project, managed by a private sector group as *Tarakluterma* in 2015, its potential in those terms make her the first in Europe and seventh in world. Coastal erosion is estimated around 6% of GNP for capital loss, thinking the fact that coastal cities cover less than 5% of the total surface area of Turkey, indeed they are settled by 51% of the population and the platforms for 80% of industrial activities and 90% of tourism income resources [6].

2.3 Resources about Data

As the sample for analysis was chosen for this study the ecological footprint researches by Global Footprint Network, the declared list known as "Ecological Footprint Atlas" was used. In this list Turkey's ecological footprint in gha/pers is 2.70. Two higher points are given in an order for Romania as 2.71 and Bosnia and Herzegovina as 2.75. Following this, two lower point are given firstly to Costa Rica as 2.69 and Botswana as 2.68 [7] World Bank datum was used for study by choosing those 5 countries for panel data analysis.

Table 1. Agriculture, value added (% of GDP) for countries

Countries/ Years	2004	2005	2006	2007	2008	2009	2010	2011	2012	2013	2014
Bosnia and Herzegovina	10.7	10.1	10.1	9.7	8.9	8.5	8.3	8.2	7.5	8.3	7.2
Romania	14.0	9.5	8.7	5.5	6.6	6.0	6.3	7.3	5.3	6.2	5.4
Turkey	10.9	10.8	9.4	8.5	8.5	9.1	9.5	9.0	8.8	8.3	8.0
Costa Rica	8.6	9.0	8.9	8.5	7.2	7.4	7.2	6.4	6.1	5.6	5.6
Botswana	2.5	2.0	2.3	2.5	2.9	3.3	2.9	2.8	3.0	2.6	2.4

Resource: World Bank [8]

Table 2. Improved water source, rural (% of rural population with access) for countries

Countries/ Years	2004	2005	2006	2007	2008	2009	2010	2011	2012	2013	2014
Bosnia and Herzegovina	97	98	98	98	98	99	99	99	100	100	100
Romania	81	83	85	87	90	92	94	96	98	100	100
Turkey	89	90	85	87	90	92	94	97	98	99	100
Costa Rica	90	90	90	91	91	91	91	91	92	92	92
Botswana	90	90	91	91	91	91	92	92	92	92	92

Resource: World Bank [8]

Table 3. Forest rent of GDP in countries below

Countries/ Years	2004	2005	2006	2007	2008	2009	2010	2011	2012	2013	2014
Bosnia and Herzegovina	0.9	0.8	0.8	0.7	0.8	0.7	0.8	0.8	0.7	0.8	0.7
Romania	0.6	0.4	0.4	0.3	0.3	0.3	0.3	0.4	0.3	0.3	0.3
Turkey	0.1	0.1	0.1	0.1	0.1	0.1	0.1	0.1	0.1	0.1	0.1
Costa Rica	0.9	0.9	1.2	1.2	1.2	1.1	1.5	1.2	1.2	1.2	1.1
Botswana	0.3	0.3	0.3	0.3	0.4	0.5	0.3	0.3	0.3	0.4	0.5

Resource: World Bank [8]

Table 4. Forest area (sq. km) of sample countries

Countries/ Years	2004	2005	2006	2007	2008	2009	2010	2011	2012	2013	2014
Bosnia and Herzegovina	21850. 0	21850. 0	21850. 0	2185 0.0	2185 0.0	2185 0.0	2185 0.0	2185 0.0	2185 0.0	2185 0.0	2185 0.0
Romania	63860. 0	63910. 0	64158. 0	6440 6.0	6465 4.0	6490 2.0	6515 0.0	6584 2.0	6653 4.0	6722 6.0	6861 0.0
Turkey	105662 .0	106620 .0	107702 .0	1087 84.0	1098 66.0	1109 48.0	1120 30.0	1130 54.0	1140 78.0	1151 02.0	1171 50.0
Costa Rica	24680. 0	24910. 0	25138. 0	2536 6.0	2559 4.0	2582 2.0	2605 0.0	2635 2.0	2665 4.0	2695 6.0	2756 0.0
Botswana	120614 .0	119430 .0	118246 .0	1170 62.0	1158 78.0	1146 94.0	1135 10.0	1124 88.0	1114 66.0	1104 44.0	1084 00.0

Resource: World Bank [8]

2.4 Data and Methodology

Panel data analysis is performed for this study. World Bank panel datum sets were used in the analysis. As an economic dependent variable the agriculture, value added (% of GDP) for countries is coded as LAGGDP in equation. For ecological independent variables, we made a research on finding time series about the years 2004-2014 again. We found the independent ecological variables as forest area values, forest rent of GDP and improved water source values for rural people. LFA is used for forest area (sq. km) of sample countries. Forest rent of GDP in countries below is named as LFR. Finally, improved water source, rural (% of rural population with access) for countries is called as LIWS. Apergis and Payne [9], also used and contributed of the referred equation set below that we use. E-views 8 software was chosen for inputting panel data and making estimations. The letter "L" in front of the symbols of variables shows that logarithmic transformation was done to the related variable series.

$$LAGGDP_{it} = \alpha_i + \beta_1 LFA_{it} + \beta_2 LFR_{it} + \beta_3 LIWS_{it} + v_t + \epsilon_{it} \quad (1)$$

In the models concerning the implementation (Equation 1) index i refers to countries, index t symbolizes time, α_i represents fixed country effects and v_t indicates unobservable time effect, last but not least ϵ_{it} denotes the error term. In the application section, the panel data analysis method which is composed of cross-sectional and time-series data has been preferred. Panel data analysis method has several advantages compared to time series analyses. Panel data analysis provides more informative data through the combination of cross-sectional observation with time series; furthermore, it makes studying meaningful via more efficient model with few multiple linearity of variables (multi collinearity) and more degrees of freedom. In addition, panel data analysis diagnoses and measures the effects which are not observed only in cross-sectional or just in time series [10] In simple panel models defined in Equation 2, α and β coefficients do not include sub-indices with the assumption that coefficients are the same for all different individuals and time.

$$Y_{it} = \alpha_i + \beta X_{it} + u_{it} \quad (2)$$

If a panel data has the same number of observations for each variable, it is called as a balanced panel. Panel data analysis used in the study is balanced. The estimation to be made was performed by preferring one of the three methods which are used in simple linear panel data analyses. These methods are as follows: *Pooled ordinary least square method – POLS* having common fixed principal method, *fixed effect model- FEM* hosting country and time effects and *random effect model- REM* putting country and time difference into the model as random parameters rather than fixed parameters [11]. In the study, the tests used while making choice among the panel data analysis methods are F test (12), LM test [13] and Hausman (1978) [14] tests. Primarily, in order to compare the presence of group specific-fixed effects (SE), common fixed and OLS, H_0 hypothesis ($H_0: \alpha_1 = \alpha_2 = \dots = \alpha_N$) was tested. According to the hypothesis H_0 , the constants belonging to the groups are equal. The method which can be applied in the event of such homogeneity will be OLS method with common fixed. The second basic tool in the choice of model is the Breusch-Pagan (1980) [13] Lagrange Multiplier test. In this test, the null hypothesis is that the random effects variance between the units is zero ($H_0: \sigma_u^2 = 0$). That the rejection of the null hypothesis fails leads to the fact that random effects between units are not significant. In the absence of the effect of random panel, Pooled-OLS estimator will be preferred. Hausman (1978) [14] test is widely used for the choice between these two estimators if unit-specific fixed and random effects are significant in F and LM tests. The main point to be considered in the separation of fixed and random effects methods is whether the elements related to individual and time is correlated with the explanatory variables in the model or not. The correlation of these elements with X_{it} refers to the fixed effects model while the absence of this correlation reveals random effects model. H_0 hypothesis shows that "there is not a correlation between the explanatory variables and unit effects". When H_0 hypothesis is accepted, both estimators will be consistent; nevertheless, as random effects estimator is much more efficient, it will be appropriate to use it.

In case of the rejection of the hypothesis H_0 , as random effects estimator would be deviated, the use of consistent fixed effects estimator would be appropriate. In addition, before using the appropriate estimator, the presence of autocorrelation and the presence of the heteroscedasticity problems should be explored. In order to detect the autocorrelation in practice, Baltag and Li (1995) [15] LM statistic test and to detect variance change, LMh test statistics developed by Greene [16] were used. [17]

2.5 Results and Discussion

In order to determine the estimation method, F, LM, LM-Honda and Hausman tests were performed and the results are presented in Table-5 along with the results related to heteroscedasticity and autocorrelation tests. Fixed effects estimator is significant at 1% for all models compared to the POLS estimator which is pooled according to the probability values of F-test. In this case, H_0 hypothesis related to F test suggesting that fixed effects belonging to the groups are equal is rejected. On the other hand, random effect estimator is significant at the 1% compared to the estimator OLS estimator which is pooled according to the probability values of LM test. That H_0 hypothesis is rejected for LM test results in the fact that the random effects between the units are significant compared to the OLS estimator. When the random effects are examined, while H_0 hypothesis is rejected for the group effect, it cannot be rejected for time effect. According to these results, it is evident that there is random group effect but not time effect. In both tests, pooled OLS estimator is not preferred. Following this stage, a preference is to be made between fixed and random effects. According to the Hausman test probability value, H_0 hypothesis is rejected at 1% significance level. Thus, the model to be used in the study is random effects model (REM). In the analysis, the test results of the autocorrelation and heteroscedasticity (H_0 : hypothesis is rejected in the both tests) shows that the problems mentioned arise for all models [17]. Asymptotic t statistics cannot be used; instead, autocorrelation and heteroscedasticity-resistant [robust] "t" statistics (White period standard errors & covariance) were used [18-19].

Table 5: Panel Model Estimation Results

DEP.VAR: LAGGDP VARIABLES	RE (Group)	RE (Two way)	
LFA	-0.717*** (-4.106)	-0.651*** (-3.546)	
LFR	-0.329** (-2.530)	-0.26** (-1.944)	
LIWS	-2.479*** (-3.314)	-2.422*** (-3.318)	
CONSTANT	20.61*** (5.039)	19.69*** (4.871)	
Observations	55	55	
Num. of count.	5	5	
Fstatistics	9.18	8.31	
Adjusted R-Squarre	0.312	0.288	
Model Choice and Diagnostic Test Results			
F-twoway_fixed	12.97***	Honda-group_random	5.69***
LM-group_random	32.38***	Honda-time_random	0.3580
LM-time_random	0.1280	Honda-twoway_random	4.27***
LM-twoway_random	32.51***	Hausman	66.05***
Heteroscedasticity tests			
LMh_random		17.18***	
Autocorrelation tests for random effects model			
LM-murho		33.05***	
LM-mulrho		23.03***	

The random effects estimation results which are performed for countries are presented in Table 2. With regard to a general evaluation model, the coefficient relevant to the LFA is observed to be negative and significant at 1%. 1% decrease in LFA variables causes 0.717 % increase LAGGDP in mentioned countries. On the other, 1% decrease in LFR variable increase LAGGDP at the rate of 0.329 %. Considering LIWS variable, it was found that there is a statistically significant and negative relationship between this variable and LAGGDP. Compared with the other variables included in the study, it is obvious that LIWS variable effect LAGGDP highest level in a negative way. Accordingly, 1% decrease in LIWS variable leads to 2,479% increase LAGGDP. The analyses performed in two way method results was found similar. 1% decrease in LFA variables causes 0.651 % increase LAGGDP in mentioned countries. On the other, 1% decrease in LFR variable increase LAGGDP at the rate of 0.260 %. 1% decrease in LIWS variable leads to 2,422 % increase LAGGDP.

3 CONCLUSIONS

Economic outputs of rational using of ecological resources in sustainable limits can bring nations demanded benefits in long terms. When Turkey grows economically on the other hand diminishes its natural resources. In this study found that there is a negative relationship between agriculture value added % GDP and natural resources. %1 increase in LAGGDP lead to respectively decrease in 0.717 % LFA, 0.329 %. LFR -2,479% LIWS. In two way method, 1% decrease in LFA variables

causes 0.651 % increase LAGGDP in mentioned countries. On the other, 1% decrease in LFR variable increase LAGGDP at the rate of 0.260 %. 1% decrease in LIWS variable leads to 2,422 % increase LAGGDP. It is noteworthy reduction occurring in natural resources.

Turkey has a great potential on using sustainable alternatives such as using renewable energies in thermal energy sector or benefiting from other sustainable methods. On the other hand some ecological threats have to be taken into consideration as erosion, flood, decrease of species and pollution. Green economics are widely used and preferred perspectives in sustainable choices [20]. In this respect, managing the issues on ecological changes, Turkish policy makers have to take into consideration the issues as long term economic outcomes [21]. Planned and integrated policies are needed for countries. As it is seen our study, forestry market should be in a planned economic agenda within a managed interaction with other economic outcomes. The possible agricultural production outcome, after deforestation, has to be planned. The improving conditions of rural sections have to be reflected in proper inducement towards agricultural production. Finally, ecological market sectors have to be resembled with common policies under a rational policy roof.

REFERENCES

- [1] R. Plummer and D. Armitage, D. "A resilience-based framework for evaluating adaptive co-management: linking ecology, economics and society in a complex world". *Ecological economics*, v.61.1,2007,pp: 62-74.
- [2] A.M. Omer, "Biodiversity, the green ecology, economics and ecosystem engineering." *Agricultural Advances*, v.5.2, 2016, pp:227-250.
- [3] (2016) All about Turkey web site [Online]. Available:<http://www.luxuryistanbul.com/pageDetails.aspx?id=22>
- [4] (2016) Ministry of Food, Agriculture and Husbandry [Online]. Available: www.tarim.gov.tr
- [5] (2016) Turkish Statistical Institution [Online]. Available: www.tuik.gov.tr
- [6] E. P. Albayrakoğlu, "Climate Change and Security: The Case for Turkey" *Gazi Academic View*, vol.5.9, 2011
- [7] (2016) Global Footprint Network Organization. [Online]. Available: <http://www.footprintnetwork.org/>
- [8] (2016) The World Bank web site. [Online]. Available: <http://www.worldbank.org/>
- [9] N. Apergis, and J. E. Payne. "Energy consumption and economic growth in Central America: evidence from a panel cointegration and error correction model." *Energy Economics* vol. 31.2, 2009,pp. 211-216
- [10] D. N. Gujarati, *Temel Ekonometri*, Çev: Ümit Senesen ve Gülay G. Senesen, Literatür Yayıncılık, 2001 İstanbul.
- [11] D. Asteriou, and S. G., Hall, "Applied Econometrics : A Modern Approach Using Eviews And Microfit". 2007, New York: Palgrave Macmillan.
- [12] B. R., Moulton and W. C., Randolph, "Alternative Tests of the Error Components Model". *Econometrica*, 57(3), 1989,pp. 685–693. Doi:10.2307/1911059
- [13] T. S. Breusch,, and A. R Pagan,, "The Lagrange Multiplier Test and its Applications to Model Specification in Econometrics". *The Review of Economic Studies*, v.47(1), 1980, pp.239–253. Doi:10.2307/2297111
- [14] J. A. Hausman, "Specification Tests in Econometrics". *Econometrica*, 1978, 46(6), 1251–1271. Doi:10.2307/1913827
- [15] B.H. Baltagi, and Q. Li, Testing AR(1) against MA(1) disturbances in an error component model. *Journal of Econometrics*, v.68(1) 1995,pp: 133–151.
- [16] W.H Greene., "Econometric Analysis", 6th Ed., 2008, Upper Saddle River, N.J.Prentice Hall
- [17] B.G Aktakas., C.S Akin, and C. Aytun "Escaping From the Burdens of Growth: the Information and Communication", 2015
- [18] H. White" A heteroskedasticity-consistent covariance matrix estimator and a direct test for heteroskedasticity. *Econometrica* v.48(4), 1980,pp: 817–838.
- [19] H. White, Asymptotic Theory for Econometricians. Orlando, FL: Academic Press.Technologies Versus Bureaucracy"*Siyaset, Ekonomi ve Yönetim Araştırmaları Dergisi*, (3) 3, 1984. pp 33-44
- [20] (2016) Ecology and The Society Organization [Online]. Available: www.ecologyandsociety.org
- [21] (2016) Türk Çevre Koruma Vakfı web site [Online]. Available: www.tucev.org

A Vhdl Implementation of Hénon Map Pseudo-Random Sequence Generator

Zeynep Kaya¹, Erol Seke²

Abstract

Chaos theory based random sequences are recently being given particular attention for their properties that can be useful in communication applications that employ cryptography. Given a generator key, fast generation of corresponding sequence is imperative for such a scheme to be successful since the sequences themselves should not be stored. In this paper, we present an FPGA implementation of a discrete-time chaotic signal generator that uses Hénon map algorithm. Designed using VHDL, the generator employs IEEE-754 floating point arithmetic which allows reaching the required precision. ISIM and MatLAB simulation results are provided and numerical results are compared. It is concluded that FPGA implementations of chaotic generators can be effectively used in real-time cryptography applications such as secure communication.

Keywords: Chaos, Chaotic Pseudo-Random Sequence Generator, Cryptography, Fpga, Hénon Map, Vhdl.

1 INTRODUCTION

Chaotic systems were discovered by the mathematician Edward Norton Lorenz in 1963. Lorenz found the first chaotic attractor when he is studying atmospheric convection [1]. It is known that chaotic systems have some advantages in random sequence generation, such as sensitivity to small changes in initial conditions, non-periodicity and unpredictability. In recent years, chaos theory started to play significant roles in many applications including secure data transmission, communication systems [2], simulation, diagnostics, image processing [3], control systems [4] and sequence generation. Increasing importance of secure communication systems stemmed the appearance of many new and low-cost implementations. Many of them involve some chaotic system for secure communication such as chaotic masking, chaos shift keying, and chaotic modulation [5]-[6]. One of the secure communication system applications that use chaotic map algorithms is Pseudo-Random Sequence Generator (PRSG). Using various chaotic mappings, crypto algorithms mathematically secure the data where it is nearly impossible to guess, regenerate the keys and immensely difficult to reverse engineer.

In this paper, we propose a chaotic pseudo-random sequences generator based on Hénon map algorithm. The proposed design is implemented on Xilinx Virtex6 FPGA device using VHDL (Very High-Speed Integrated Circuit Hardware Description Language) and has been designed using the IEEE 754-1985 floating-point format. The following presents a short description of the Hénon map algorithm and MatLAB Simulink model with simulation results. Section 2.2 describes detailed design methodology and implementation issues related to the Xilinx FPGA platform. ISIM simulation results of implementation and measurements are given. We conclude with the resource usage of the proposed design and a brief summary on some features.

2 MATERIALS AND METHODS

2.1 Hénon Map

The Hénon map was proposed by the French astronomer Mihel Hénon (1976) as 2-D iterated map for chaotic solutions.

The Hénon system iterative update equations are

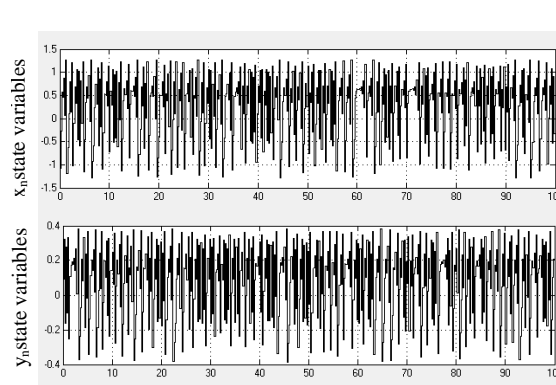
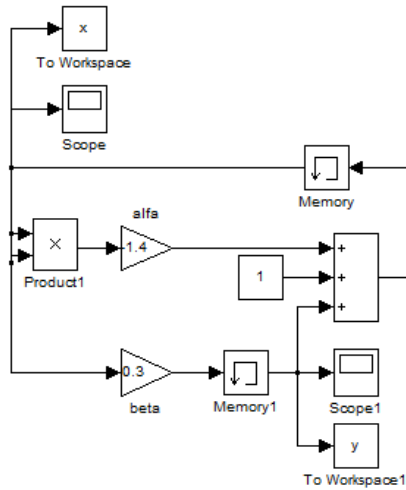
$$x_{n+1} = 1 + y_n - ax_n^2 \tag{1}$$

$$y_{n+1} = 1 + bx_n$$

¹Zeynep KAYA: ¹BilecikSeyhEdebali University, Department of Electrical and Electronics Engineering, 11230, Bilecik, Turkey. zeynep.kaya@bilecik.edu.tr

²Erol SEKE: Eskisehir Osmangazi University, Department of Electrical and Electronics Engineering, 26480, Eskisehir, Turkey. erol.seke@ogu.edu.tr

where a and b are constants and $a = 1.4$, $b = 0.3$. Depending on the initial values (x_0, y_0) , the sequence generated by iteration never converges to a particular mapping. Hénon chaotic generator is verified by MatLAB Simulink model given in Fig. 1a. Figure 1b shows the values of the state variables x_n and y_n .



(a) (b)
Figure 47. Hénon chaotic generator Simulink model and simulation results

The Hénon map does not control the nonlinearity

and dissipation for all coefficient and initial values. Except for the standard parameters of $a = 1.4$ and $b = 0.3$, it does not have a strange attractor. Only for these values does the generator show the chaotic behaviour. Corresponding Hénon trajectory (attractor), whose initial

values (x_0, y_0) are zero, is shown in Fig. 2 as a MatLAB plot.

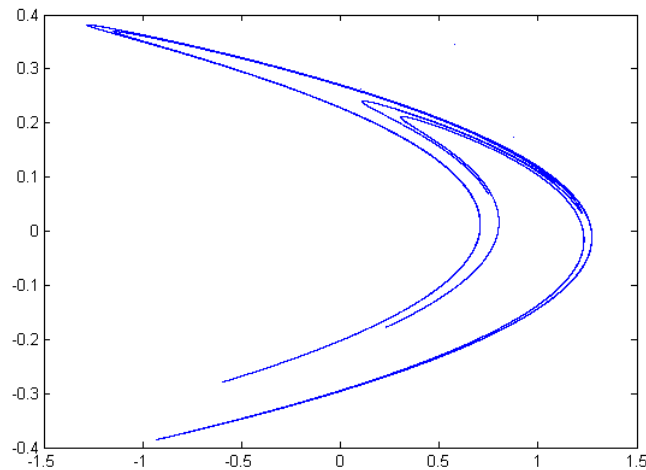


Figure 2. Hénon attractor

2.2 Proposed Hénon Map Pseudo-Random Sequence Generator

Hénon map pseudo-random sequence generator is implemented in VHDL for Virtex6 XC6VLX75T FPGA chip of Xilinx. Chaotic generator was constructed with a fixed-point representation of 48 bit data precision of which 43 are reserved for the fraction part, leaving 5 bits for the integer part including the sign bit. The fixed-point representation allows a useful and attractive accommodation to high speed and low area cost. Following the VHDL implementation of the chaotic system for the named chip, effectiveness of the proposed generator is verified by using ISIM simulation tool and viewing the resulting sequence. Part of the sequence is shown in Fig. 3, where x_k and y_k are chaotic Hénon sequence data obtained using the coefficients and initial values given in previous section.

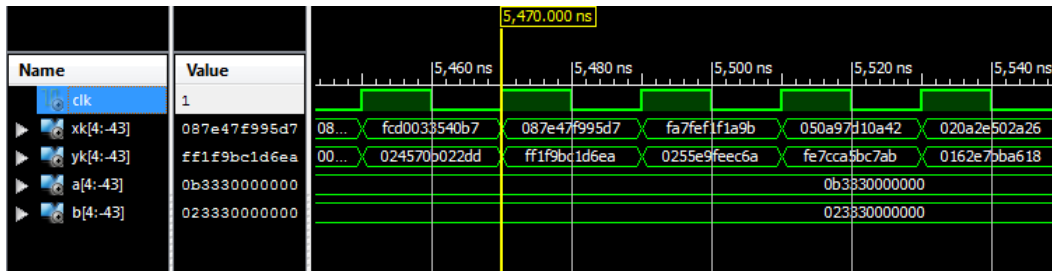


Figure 3. ISIM simulation results

Implementation specific parameters are obtained using the Xilinx ISE software. Interestingly, the design had a maximum operating frequency of 37.801 MHz. It seems that combinatorial path is longer than expected; a phenomenon that needs further investigation. Logic source usage in terms of slices and multipliers and performance analysis of the architecture were detailed. Design summary results and advanced HDL synthesis report are presented in Tables 1 and 2. IOB figures are irrelevant since they are not actually used but the signals are ported so that the optimizer would not trim them. On the other hand, the number of DSP slices show that arithmetic operations performed in 48 bits fixed-point representation requires high number of slices since the integer and fractional parts are handled separately. This also requires further attention and tuning.

Table 18. Design summary results of FPGA implementation

Logic Utilization	Used	Available	Utilization
Number of Slice Registers	96	93120	0%
Number of Slice LUTs	1025	46560	2%
Number of fully used LUT-FF pairs	96	1025	9%
Number of bonded IOBs	97	240	40%
Number of BUFG/BUFGCTRLs	1	32	3%
Number of DSP48E1s	32	288	11%

Table 2. Advanced HDL synthesis report

Logic Source	Number of usage	
Multipliers	48x43-bit multiplier	1
	48x45-bit multiplier	1
	48x48-bit multiplier	1
Adders/Subtractors	49-bit adder	4
	50-bit subtractor	1
Registers	Flip-Flops	96
Multiplexers	1-bit 2-to-1 multiplexer	9
	48-bit 2-to-1 multiplexer	21
Xors	1-bit xor2	3

3 CONCLUSION

In this work, we first verified the Hénon chaotic system model by MatLAB/ Simulink. Further, we have shown that Hénon chaotic system model can be implemented using fixed-point arithmetic for FPGA's. It is shown that a pseudo-random sequence generator that uses Hénon map can be effectively implemented in VHDL for FPGA architecture. Although the resource usage was somewhat higher than expected and requires further investigation, it is still allowable. The maximum operating frequency of the digital design can be improved by employing pipelining techniques. However, since the generator is recursive, this would probably require doubling the multipliers/adders; keeping two copies of the design in parallel.

Since the coefficients cannot be changed, different initial values are to be used for the generation of different sequences. This leaves us 2×48 bits to control the sequence and 2^{96} possible different sequences. Chaotic systems, by definition, can generate enormously different sequences with a small change on the initial values. This is a desired property of such sequences when used in cryptology and secure communication.

REFERENCES

- [1] C. Sparrow, "The Lorenz Equations: Bifurcations Chaos and Strange Attractors", Springer, New York, vol.21, pp. 106-110, 1982.
- [2] G. Heidari-Bateni, C. McGillem, "A chaotic direct-sequence spread-spectrum communication system." Communications, IEEE Transactions on 42.234 (1994): 1524-1527.
- [3] W. Klonowski, "Signal and image analysis using chaos theory and fractal geometry." Machine Graphics and Vision 9.1/2 (2000): 403-432.
- [4] Pence, B. L., Fathy, H. K., Stein, J. L., "Recursive Estimation for Reduced-Order State-Space Models Using Polynomial Chaos Theory Applied to Vehicle Mass Estimation", Control Systems Technology, IEEE Transactions on, Vol. 22, no.1, pp.224-229, 2014.
- [5] T. Chien, T. Liao, " Design of secure digital communication systems using chaotic modulation, cryptography and chaotic synchronization" Chaos, Solitons and Fractals vol. 24 pp.241–255, July 2005.
- [6] T. Yang, "A Survey of Chaotic Secure Communication", International Journal of Computational Cognition Vol. 2, Num.2, pp. 81–130, June 2004.

The Health Politics of Environment in Turkey, EU Candidate Country

Soner Akin¹, Ugur Yildirim²

Abstract

This study is about the role of the political process in preventing environmental health risks. In this respect, the factors for the lack of immediate steps in public health sector in Turkey, comparative perspectives on environmental concerns, comprehensive policy alternatives for protection against environmental threats will be discussed within national strategies across European member countries and Turkish case. In this study, a panel data analysis was performed for environmental health policy makers. A randomly chosen country groups were discussed via time series declared by World Bank, in which years European Union Environmental Action Plan was on agenda, and then it is found that non applicant countries needs to gain an action to set out health policy based developing outcomes.

Keywords: EU environmental health, public health for environment, ecosystem management, environment risks in Turkey, integrated policies

1 INTRODUCTION

Health issue and the positive outcomes for healthy life has become a common aim in most of political practices. Today environment and health finally became an integrated topic, and a new terminology as environmental health is arrived. Environmental Health area is related with many of environmental issues and occupational medicine and related studies even in toxicology, climate change issues, chemicals, pollution, radioactivity and epidemiology [1]. The better health issue being an environmental policy outcome is also accepted by scientists and practitioners in all areas of environmental science where human health and well-being are naturally perceived, both directly and indirectly. Environmental Health is now a public health subtitle in some institutions of European Union, serving the public health for related community, society and scientists who are related and relevant on matters of environment interest as well. In this study, the condition of Turkey will be taken in a general outlook about European Union member countries which have a solid experience on gaining health policy positive results in their environmental agenda via an action plan called as EHAP [2]. Turkey has not been a part of this plan, and has a weak condition on gaining an integrated outlook for environment and health. Hence, the condition of applicatory countries and the other samples are tried to be analyzed in this paper in order to involve Turkey in a balanced perspective of comparison base, where the econometric outcomes can be seen.

2 HEALTH AS AN ENVIRONMENTAL OUTPUT

As a separated branch, health policy in public sphere is mostly planned and contributed by different organizations or policy strategies. On the other hand, many environmental or reformist steps can be improved by legal regulation or action plans today. Specifically, developing countries usually choose the road on gaining economic success on being one of regional leaders or maybe improving the infrastructure based conditions in many spheres on environment. In this type of case, the policies which are not integrated to each other can present surprising positive improvements to each other. At first outlook, this could be seen a positive condition, though it can be interpreted by the expertise as a lack of condition on improving environmental conditions or even not experiencing environmental health policy practices at all [2].

2.2 Environmental Health

Throughout modern history, the environmental health based initiatives mostly addresses all the molecular, physical, chemical, and biological threats being external to an individuals. Policy steps are mainly related with assessment and control of those environmental effects that can potentially affect health. Environmental health branch is about disappearing diseases and creating or improving healthy conditions in environments. Today, environmental health is seen a modern version of anthropocentric outlook for environment, which was mostly popular until 1980s.

2.3 Institutional Supplements behind Environmental Health Policy in Europe

European Commission can be seen the main intuitional platform on supporting for revival of a perspective about the integration of health and environment polices [2]. In 2003, a draft was accepted by EU and named as communication on a

¹ Corresponding author: Mustafa Kemal University, Teaching Assistant Doctor, Department of Foreign Trade, 31440, Kırıkhan/Hatay, Turkey. sakin@mku.edu.tr

² Kahramanmaraş Sutcu Imam University, Professor Doctor, Public Administration Department, Kahramanmaraş, Turkey, uyildirim@ksu.edu.tr

European Environment and Health Strategy in order to foster effective policy making regarding environment and health issues. After this development, Directorate General for Health and Consumers, General Directorate of Environment and European Environmental Agency became the main executor of this strategy [3].

2.4 Environmental Health in Some Progenitor Countries of EU

Indoor quality improving, electromagnetic fields, training experts on environmental health were the main and relatively new themes in the action plan known as EHAP [4]. Five countries among 28 different members are clearly active on integrating environment and health practices, and finally gained experience about it. In Europe, France, Luxemburg, Netherlands, Belgium and United Kingdom can be seen the very first applicants. United Kingdom has national institutions on environmental health, before the action plan was taken into agenda for the years 2004-2010. One of it can be exemplified with the Charter Institute of Environmental Health in United Kingdom. France is the draft communication paper creator for European Commission, and has the French agency for Food, Environmental and Occupational Health Safety. Netherlands has a specifically named independent organization as the Netherlands National Institute for Public Health and the Environment. Belgium is the only country which created a national Environmental Health Action Plan which was inspired from the same model of EHAP, and the strongest nongovernmental organization is settled in this country, known as HEAL. Finally Luxemburg can be seen as a country in which the activities and policy practices about European environmental health are executed. Country's national institute on science and technology as LIST has its own environmental health research group. LIST had great contribution on parallel researches about environmental health in the continent, for example another legal action plan REACH for chemicals can be recalled herein [2].

2.5 Health as an Environmental Policy Output in Turkey

Turkey is a candidate country for European Union membership. However, it has no specific institution or agency on environmental health. In Turkey there is a differentiated structure on environmental health responsibilities. Turkish Public Health Institution has a general directorate on this subject, which is tied on Ministry of Health. This institution is not an independent research or policy making organ. Hence, every step on separately in Turkey about environmental improvement can filled the spaces as symbols of needs also in environment [5]. A mature mechanism for environmental policy is not sustained yet in the country, after the environmental action plans are clearly defined and applied. Turkey has no solid environmental health action plan which is aimed on developing indoor quality, consciousness about environmental health threats, radioactivity, electromagnetic threats, chemicals etc[1]. In other words, most of the environmental huge policy reforms can ironically show its positive reflection on many health related position or variables in the country, as the list of the hot blooded issues in environment continue to exist.

2.6 Resources about Data

World Bank databases were used on gaining some part of data. Specifically life expectancy at birth datum were taken from this data base. Indeed, this datum was used as the dependent variable across the countries to question whether the health policy solid outcomes are also the results of environmental policies. In this respect the relatively superior position of environmental health policy applicant countries are compared with the other countries, among which Turkey exists. Life expectancy at birth is taken as the dependent variable, indicating the possible output of traditional or environmental health revised policies. In this respect, carbon dioxide emissions, methane emissions and green gases emissions are taken as the environment themed independent variables for our panel data analysis. Our environmental health applicant countries profiles are ordered as Luxemburg, France, Belgium, United Kingdom and Netherlands. Turkey as a candidate country is taken into another set of evaluation, called in a name of non applicant of environmental health approaches, at least in terms of European Union style. Neighbor or near-geography countries as Russia, Egypt, Georgia and Azerbaijan are randomly taken as the countries which are far way from European Union legacy and practices about environmental health, as those countries are not member or tied with EU legacy. The years are chosen as 2006-2007-2008-2009-2010, as those years are the relevant years in which EU EHAP plan is applied. The parallel evaluation for non applicant countries was also done by using related panel data [6] about those same years as well.

Table 1. Life expectancy at birth in environmental health applicant countries(years)

Countries/Years	2006	2007	2008	2009	2010
Luxemburg	79	79	81	81	81
France	81	81	81	81	82
United Kingdom	79	79	80	80	80
Netherlands	80	80	80	81	81
Belgium	79	80	80	80	80

Resource: World Bank [7]

Table 2. Life expectancy at birth for years in environmental health applicant countries(years)

Countries/Years	2006	2007	2008	2009	2010
Turkey	73	73	74	74	74
Russia	67	67	68	69	69
Georgia	73	73	74	74	74
Azerbaijan	69	70	70	70	70
Egypt	70	70	70	70	70

Resource: World Bank [7]

Table 3. CO2 emissions (kt) in environmental health applicant countries

Countries/Years	2006	2007	2008	2009	2010
Luxemburg	11,349	11,023	10,939	10,392	10,968
France	381,467	374,914	371,735	356,627	357,437
United Kingdom	541,374	528,323	521,513	473,237	492,192
Netherlands	167,109	171,491	173,163	169,364	181,927
Belgium	106,776	103,215	103,882	104,022	109,093

Resource: World Bank [7]

Table 4. CO2 emissions (kt) in environmental health non- applicant countries(kt)

Countries/Years	2006	2007	2008	2009	2010
Turkey	261,615	284,658	285,274	277,845	298,002
Russia	1,669,618	1,667,598	1,715,639	1,574,368	1,742,540
Georgia	6,150	6,421	6,417	6,271	6,531
Azerbaijan	39,167	30,509	35,504	31,903	30,678
Egypt	178,616	193,343	196,797	198,069	204,677

Resource: World Bank [7]

Table 5. Methane emissions in environmental health applicant countries (kt of CO2 equivalent)

Countries/Years	2006	2007	2008	2009	2010
Luxemburg	1,070	1,116	1,146	1,280	1,236
France	83,232	83,078	82,893	83,639	83,757
United Kingdom	63,014	61,771	61,176	60,727	61,177
Netherland	20,876	20,543	20,590	20,156	20,288
Belgium	9,584	9,547	9,538	9,586	9,632

Resource: World Bank [7]

Table 6. Methane emissions in environmental health non-applicant countries(kt of CO2 equivalent)

Countries/Years	2006	2007	2008	2009	2010
Turkey	67,180	70,618	75,649	76,301	77,307
Russia	495,215	504,013	511,550	507,742	533,546
Georgia	4,528	4,653	4,708	4,821	4,863
Azerbaijan	13,077	14,807	16,946	17,922	18,401
Egypt	49,735	50,232	52,003	50,896	50,958

Resource: World Bank [7]

Table 7. Green gases emissions in environmental health applicant countries (thousand metric tons of CO2 equivalent)

Countries/Years	2006	2007	2008	2009	2010
Luxemburg	113	123	134	141	146
France	16,519	17,934	19,365	20,118	21,845
United Kingdom	11,161	12,256	12,910	13,368	14,312
Netherland	3,981	4,203	4,500	4,670	4,912
Belgium	2,218	2,412	2,607	2,684	2,779

Resource: World Bank [7]

Table 8. Green gases emissions in environmental health nonapplicant countries(thousand metric tons of CO2 equivalent)

Countries/Years	2006	2007	2008	2009	2010
Turkey	6,238	6,594	6,981	8,696	8,335
Russia	495,215	504,013	511,550	507,742	533,546
Georgia	4,528	4,653	4,708	4,821	4,863
Azerbaijan	1,185	552	526	406	1,142
Egypt	3,412	3,587	3,677	3,828	3,965

Resource: World Bank [7]

2.7 Material and Methods

Panel data analysis is performed for this study. 5 European Union environmental health applicant countries were chosen in this analysis. And Turkey and some other countries within near geography of Turkey were chosen as non applicant of environmental health policies. Our time limitation was designed for a specific period in which European Union Environment-Health Action Plan was on application. As is early mentioned, this action plan was lasted 2004-2010. A five year section in this program's most active years after beginning session and final stages as, 2006, 2007, 2008, 2009, 2010 were handled as the proper years for analysis in order to make a comparison between European Union policy practices effective and own reflection to health policy outcomes and the status of other countries. Among all European countries, Luxemburg, France, United Kingdom, Belgium and Netherlands can be seen the progenitor countries, being model for European Union policy practices by means of intuitional structures, policy initiatives, founding specific agencies, starting an integrated policy agenda and supporting citizen consciousness. LEAB abbreviation is used for "life expectancy at birth". CO2 emissions (kt) are entitled in the equation and analysis as CO2. Methane emission is coded as ME. This is mostly coming from industrial or wrong agricultural production methods in terms of environmental health. Other greenhouse gas emissions, HFC, PFC and SF6 were evaluated. This green gas emissions item is named as SGE in the equation of our study. Apergis and Payne [6],also used and contributed of the referred equation set below that we use. Eviews 7.1 software was chosen for inputting panel data and making estimations.

$$LEAB_{it} = \alpha_i + \beta_1 CO2_{it} + \beta_2 ME_{it} + \beta_3 SGE_{it} + \epsilon_{it} \quad (1)$$

2.8 Results and Discussion

Those datum which were presented in resources and data section above, are being input into Eviews 7.1 software and "pooled least squares" method was used. In this respect we have estimated cross-sectioned analysis result patterns, total pooled balanced observations, r-squared results, adjusted r-squared results, regression analysis and its standard errors or deviations, sum squared residuals, logarithmic likelihood, mean dependent variable, standard deviation of dependent variable, akaike info criterion value, schwarz criterion value and durbin watson statistics. The results and related probability values of independent variables can be seen below table.

Table 9. Analysis results to find cross-section random effects

Variable	Coefficient	Std. Error	t-Statistic	Prob.
C	80.25345	0.224691	357.1720	0.0000
ME	-2.58E-05	3.54E-05	-0.728623	0.4743
CE	-4.29E-06	1.81E-06	-2.367539	0.0276
GGE	0.000243	0.000134	1.812299	0.0843

Effects Specification

	S.D.	Rho
Cross-section random	0.083314	0.0161
Idiosyncratic random	0.650910	0.9839
Weighted Statistics		
R-squared	0.504592	Mean dependent var 77.14259
Adjusted R-squared	0.433819	S.D. dependent var 0.815794
S.E. of regression	0.613844	Sum squared resid 7.912887
F-statistic	7.129766	Durbin-Watson stat 1.120227
Prob(F-statistic)	0.001755	
Unweighted Statistics		
R-squared	0.519329	Mean dependent var 80.24000
Sum squared resid	7.959904	Durbin-Watson stat 1.113610

Among the variables, only the carbon dioxide emission is randomly affecting the life expectancy at birth time series. European Union has relatively long and more systematic challenging pattern compared with other sectors related with environmental health. Moreover, the fixed effects testing can be performed via Hausman test. The test results can be seen below on the table.

Table 10. Hausman test performed to find possible fixed effects

Correlated Random Effects - Hausman Test

Equation: Untitled

Test cross-section random effects

Test Summary	Chi-Sq. Statistic	Chi-Sq. d.f.	Prob.
Cross-section random	0.676379	3	0.8787

Cross-section random effects test comparisons:

Variable	Fixed	Random	Var(Diff.)	Prob.
CE	0.000003	-0.000004	0.000000	0.6648
GGE	0.000254	0.000243	0.000000	0.9239
ME	-0.000220	-0.000026	0.000000	0.6210

Cross-section random effects test equation:

Dependent Variable: LEAB

Method: Panel Least Squares

Date: 04/30/16 Time: 20:42

Sample: 2006 2010

Periods included: 5

Cross-sections included: 5

Total panel (balanced) observations: 25

Variable	Coefficient	Std. Error	t-Statistic	Prob.
C	85.37623	12.28658	6.948736	0.0000
CE	2.69E-06	1.62E-05	0.166135	0.8700
GGE	0.000254	0.000178	1.429197	0.1711
ME	-0.000220	0.000394	-0.557770	0.5843
Effects Specification				
Cross-section fixed (dummy variables)				
R-squared	0.565058	Mean dependent var		80.24000
Adjusted R-squared	0.385965	S.D. dependent var		0.830662
S.E. of regression	0.650910	Akaike info criterion		2.233448
Sum squared resid	7.202631	Schwarz criterion		2.623488
Log likelihood	-19.91810	Hannan-Quinn criter.		2.341628
F-statistic	3.155102	Durbin-Watson stat		1.196389
Prob(F-statistic)	0.025015			

According to test results, we see that 0.8787 probability ration is bigger than 0.05, so the existence of null hypothesis on the availability of random effect can be accepted. It was mainly because the early stages of precaution about the sector in environmental health. On the other hand the product of European policies can be observed in carbon dioxide emissions' random effects. When we look at the table -9 again, we find that CO2 probability value is 0.0276, which is smaller than 0.05. The coefficient value for this independent variable can be observed as -4.29, hence it means that the decrease of carbon dioxide emissions can be randomly related with the positive increase of life expectancy through years in Europe. In long term life expectancy being dependent on solving environmental issues becomes less explanatory for variation in environmental health policy countries. Among the independent variables, CO2 emissions issue continues to be hot topic in political agenda [7]. For the case of non applicant profile for environmental policy, the countries' profile has to be seen more dependent on separate reforms [8]. Traditional and separate policies on health issues or environmental issue are mainly designed for the terms about battling problematic issues, such as communicable diseases, industrial pollution. Turkey, Russia, Georgia, Egypt and Azerbaijan were paid attention in the same outlook used above.

Table 11. Cross section random effects analysis for non applicant countries about environmental health

Dependent Variable: LEAB

Method: Panel EGLS (Cross-section random effects)

Date: 04/30/16 Time: 21:32

Sample: 2006 2010

Periods included: 5

Cross-sections included: 5

Total panel (balanced) observations: 25

Swamy and Arora estimator of component variances

Variable	Coefficient	Std. Error	t-Statistic	Prob.
C	71.75145	0.298883	240.0651	0.0000
CE	-3.46E-06	2.09E-06	-1.654869	0.1128
ME	1.36E-05	6.79E-06	2.003278	0.0582
GGE	-9.34E-06	6.01E-06	-1.553772	0.1352
Effects Specification				
			S.D.	Rho
Cross-section random			0.381852	0.4592
Idiosyncratic random			0.414415	0.5408
Weighted Statistics				
R-squared	0.342103	Mean dependent var		31.00136
Adjusted R-squared	0.248118	S.D. dependent var		1.136397
S.E. of regression	0.985383	Sum squared resid		20.39056
F-statistic	3.639969	Durbin-Watson stat		0.302248
Prob(F-statistic)	0.029412			
Unweighted Statistics				
R-squared	0.389248	Mean dependent var		71.00000
Sum squared resid	80.61921	Durbin-Watson stat		0.076446

The Hausman test is performed after the random cross section effects test is performed. Indeed, it is seen that the probability ration is seen below 0.05. Then it can be easily talked about the direct effects of explanatory independent variables on a health related output. It means that health issue based problematic are in opposition to be supplemented by environment based reforms. It signs a clear need in political sphere.

Table 12. Hausman test results for non applicant countries about environmental policy

Correlated Random Effects - Hausman Test			
Equation: Untitled			
Test cross-section random effects			
Test Summary	Chi-Sq. Statistic	Chi-Sq. d.f.	Prob.
Cross-section random	100.729636	3	0.0000

Cross-section random effects test comparisons:

Variable	Fixed	Random	Var(Diff.)	Prob.
CE	-0.000011	-0.000003	0.000000	0.0176
ME	0.000015	0.000014	0.000000	0.3165
GGE	0.000064	-0.000009	0.000000	0.0000

Cross-section random effects test equation:

Dependent Variable: LEAB

Method: Panel Least Squares

Date: 04/30/16 Time: 21:33

Sample: 2006 2010

Periods included: 5

Cross-sections included: 5

Total panel (balanced) observations: 25

Variable	Coefficient	Std. Error	t-Statistic	Prob.
C	67.08650	1.659592	40.42349	0.0000
CE	-1.09E-05	3.77E-06	-2.892563	0.0101
ME	1.53E-05	7.00E-06	2.188446	0.0429
GGE	6.37E-05	1.82E-05	3.498902	0.0028

Effects Specification

Cross-section fixed (dummy variables)

R-squared	0.977882	Mean dependent var	71.00000
Adjusted R-squared	0.968775	S.D. dependent var	2.345208
S.E. of regression	0.414415	Akaike info criterion	1.330438
Sum squared resid	2.919570	Schwarz criterion	1.720478
Log likelihood	-8.630469	Hannan-Quinn criter.	1.438618
F-statistic	107.3723	Durbin-Watson stat	1.964796
Prob(F-statistic)	0.000000		

After Hausman test cross section fixed effects panel analysis was estimated. The results are now presented on below table. As is seen, all independent variables show probability values below 0.05. Looking at the coefficients, carbon dioxide showed a reverse correlation. When carbon dioxide emission rates are increased, the life expectancy at birth is generally decreased. On the other hand, thinking the issue on battling with nutrition needs, the rates of growing methane values or the industrial

development based needs which are solved with economic activities that caused green gases emissions are observed and, indeed they are positively correlated variables in many countries, out of EU and its environmental health legacy[7] today.

Table 13. Fixed effects analysis for non applicant environmental health policy countries

Dependent Variable: LEAB				
Method: Panel Least Squares				
Date: 04/30/16 Time: 22:08				
Sample: 2006 2010				
Periods included: 5				
Cross-sections included: 5				
Total panel (balanced) observations: 25				
Variable	Coefficient	Std. Error	t-Statistic	Prob.
C	67.08650	1.659592	40.42349	0.0000
CE	-1.09E-05	3.77E-06	-2.892563	0.0101
ME	1.53E-05	7.00E-06	2.188446	0.0429
GGE	6.37E-05	1.82E-05	3.498902	0.0028
Effects Specification				
Cross-section fixed (dummy variables)				
R-squared	0.977882	Mean dependent var	71.00000	
Adjusted R-squared	0.968775	S.D. dependent var	2.345208	
S.E. of regression	0.414415	Akaike info criterion	1.330438	
Sum squared resid	2.919570	Schwarz criterion	1.720478	
Log likelihood	-8.630469	Hannan-Quinn criter.	1.438618	
F-statistic	107.3723	Durbin-Watson stat	1.964796	
Prob(F-statistic)	0.000000			

3 CONCLUSIONS

Environmental health has become a hot topic because of the opportunities created by the integrated policies. As a global leader on environmental policies and preservation based precaution steps, witnessed on creating protocols and a legal mechanism on CO₂, European Union can be seen one of the architects in this issue. Many countries are in an age of mature position about environmental health today[7]. On the other hand, some countries in the world, among Turkey, need the basic steps on founding institutions, agencies, research groups, applying action plans [9] and improving consciousness on environmental health. Only in such circumstances, those countries separate policies about health and environment will also reflect the positive development on their paths, and only then some basic indicators as life expectancy or etc could be guaranteed in high levels without meeting with threatening environmental obstacles for people's lives.

REFERENCES

- [1] S.Cairncross and R.Feachem *Environmental health engineering in the tropics: an introductory text* , 2nd ed., John Wiley & Sons Ltd..UK, 1993.
- [2] (2016) European Union website [Online]. Available: <http://ec.europa.eu/health/>
- [3] (2016) European Environmental Agency Website [Online]. Available: www.eea.europa.eu
- [4] M. J. Nieuwenhuijsen, *Exposure Assessment in Environmental Epidemiology*. Oxford University Press, USA. 2015.
- [5] M.Soykenar, Y, Uzuntarla, and Ş. Varol, Ş. "Çok uluslu görevlerde kaliteli çevre sağlığı hizmetinin uygulanması". *Health Care*, vol. 3(1),2016, p.1.
- [6] N. Apergis, and J. E. Payne. "Energy consumption and economic growth in Central America: evidence from a panel cointegration and error correction model." *Energy Economics* vol. 31.2, 2009,pp. 211-216
- [7] (2016) The World Bank web site. [Online]. Available: <http://www.worldbank.org/>
- [8] (2016) Environmental Health News Organization web site. [Online]. Available: www.environmentalhealthnews.org/
- [9] (2016) Türk Çevre Koruma Vakfı web site [Online]. Available: www.tucev.org

Multi Project Scheduling Problems and Their Solution

Aynur Kazaz¹, Murat Cevikbas², Cenk Ocal³

Abstract

A project is a temporary endeavor to create a unique product by means of scarce resources such as material, equipment, cost and labor. Indisputably, these resources constitute biggest part of a project in terms of management efforts. In this study, Development of Muscat International Airport (DMIA) Project is examined and results reveal that considering more than one project interrelated with each other such as projects under programme and Portfolio, resource management becomes more sophisticated compared to a single project. Because external dependencies contain negative risks and play crucial roles in the resource dependent projects in terms of prioritizing the resources considering the objective of project, programme and portfolio individually. Therefore, in this study, methods to improve resource allocation process in terms of productivity and efficiency are suggested to implement. Firstly, importance of establishing heuristic method through software related to scheduling is emphasized in order to control and optimize resources among interrelated projects. Additionally, using the same software and similar Work Breakdown Structure (WBS) and Resource Breakdown Structure (RBS) in different projects under the programme and Portfolio also enable the organization to get a consolidated report which has the whole project controlled and monitored simultaneously. Moreover, priority of project and availability of resources should be decided at the outset of the project. Positive contribution of programme and portfolio committee over the resource distribution between the project is undeniable. Furthermore, easing of decision making process to utilize the scarce resources efficiently is dependent the type of organization. Hence strong matrix organization and projectized organization are proposed.

Keywords: *Multi project scheduling, resource allocation, external dependency, Heuristic Method, Strong Matrix Organization, Projectized Organization*

¹Corresponding Author: Akdeniz University, Engineering Faculty, Department of Civil Engineering, Antalya, Turkey, akazaz@akdeniz.edu.tr

² Süleyman Demirel University, Faculty of Technology, Department of Civil Engineering, Isparta, Turkey, muratcevikbas@sdu.edu.tr

³ Süleyman Demirel University, Faculty of Technology, Department of Civil Engineering, Isparta, Turkey, cenkocal@sdu.edu.tr

1 INTRODUCTION

Programme is a structure for combining the projects in order to achieve common goal and maximum benefits through focusing on all projects' activities [1], [2] while Portfolio is a collection of projects, program and sub portfolio having not necessarily common goal but organizational objectives. Therefore, portfolio components should be quantifiable and ranked [3] to determine their importance within the organization and sequencing of resource allocation respectively. Interest to maximize organization profit under the pressure of competition among the firms, over the last decades, companies tend to conduct numerous projects simultaneously, and organizations involve these projects under a programme or a portfolio. Projects in both programme and portfolio, resource allocation becomes biggest concern in terms of maintaining and enhancing both projects and organization objectives. For instance, productivity and efficiency of common resources should be maximize through optimizing the resource allocation between projects. It can be done through allowing the resources to work continuously. However, work order of these resources should be determined according to importance and sequence of projects. If the project activities requiring same resources in the different projects start and finish one after another, scheduling process is easy. However, if these resources require to inject to more than one project at the same time, decision making process can be exhausting and lead to collision due to conflict of interest among the project managers [4]. In this case, senior management and other stakeholders' requirements should be involved to the projects without interrupting the process of each project management through proper programme and portfolio management. Hence, communication is very important asset for the programme and portfolio management, and efficiency of communication can be fostered by project management software and correct organizational structure. Therefore, in this study, Development of Muscat International Airport Project (DMIA) constructed by TAV Construction Company/Consolidated Construction Company (CCC) in Oman has been elaborated to dedicate problems and to figure out the methods used to tackle with these problems. There are three major issues determined to handle with the resource allocation in project or between the projects, namely, using the heuristic technique (Rule of thumb approaches) through same project management software in an organization, using the same Work Breakdown Structure (WBS) and Resource Breakdown Structure (RBS) in an organization, establishing organizational structure, such as Strong Matrix and Projectized Organization, providing more authority to the Project Managers (PM) in order to expedite decision making process.

2 MATERIALS AND METHODS

This research intends to highlight the problems resulted from resource allocation between the projects and to propose solutions in many work situations. With respect to determine the problems, DMIA project is reviewed. The reasons behind the choosing the DMIA project are that this project can be considered as a mega projects due to having budget over US\$1 billion, it has more than 10 km² total project area and it is considered under a portfolio. Many major resource problems effecting the project success and solutions to these problems were derived from this project as a lessons learned. Firstly, importance of implementing heuristic method through project management software and implementation methods to the projects and portfolio have been understood from the DMIA project. Secondly, it is observed that there is a strong relation between resource leveling and resource efficiency. Lastly, issue of conflict between the managers was dedicated as a main problem in the DMIA project. Hence, academic papers are reviewed as per the title of "programme management", "portfolio management", "multi project schedule", "resource allocation", "heuristic method", through the database of "International Journal of Project Management" and "European Journal of Operational Research". Relevant papers to our determined problems are reviewed in order to eliminate duplicate papers to find the most relevant papers to gather supportive information in order to compose mosaic of strategies to accommodate resources in the most efficient manner.

3 RESULTS AND DISCUSSION

3.1 Project Background

3.1.1. Development of Muscat International Airport Project (DMIA)

Project was awarded on 17th June 2009 and planned to complete on 2nd April 2012. Project contains two phases. First phase is building new international airport, second phase is refurbishment of existing airport to convert it domestic airport. Contract type was International Federation of Consulting Engineers (FIDIC) and design issues belonged to client, namely Ministry of Transport and Communications of Sultanate of Oman. At the outset of the project, WBS was defined according to Bill of Quantity (BOQ) and totally 17,459 activities listed to make a schedule. All these activities require equipment and manpower. As seen in the Figure 1. machinery usage was achieved to 1.010 as a peak in August 2010. The list of machinery as per their type is illustrated in the below Table 1.

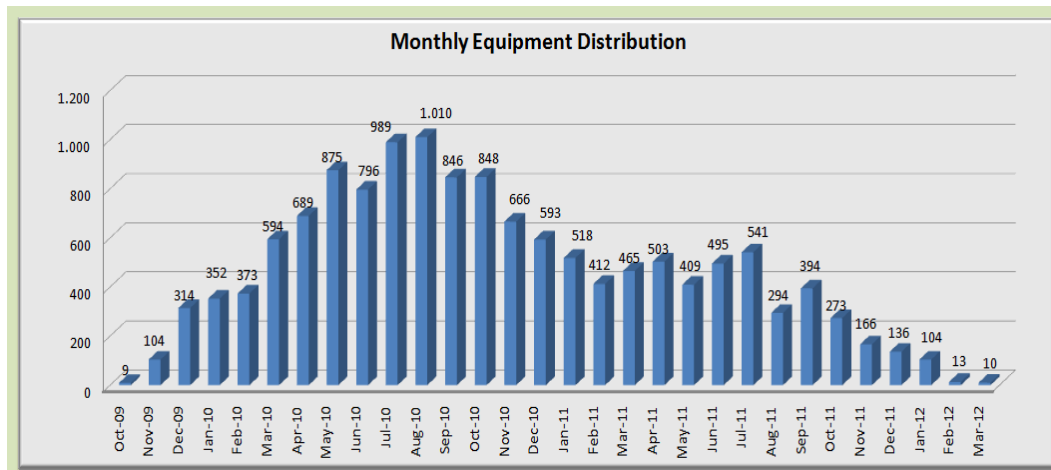


Figure 1. DMIA Project - Planned Number of Monthly Equipment

Table 1. DMIA Project - Type of Equipment at the Peak Month of August

Date	Manpower Summary	Equipment Summary											
31-Aug-10	6.449	1.010											
CCC/TAV JV Equipment	Excavator	Dozer	Loader	Pavers & Grader	APC Paver	Roller	Transmixer	Trailer	Tankers	Concrete Pumps	Welding Machine	Drilling Machine	
	990	17	14	46	4	137	17	29	85	571	43	0	27
Subcontractor's Equipment	Stone Columns Rig	Piling Rig	Telescopic Handler	Crane	Cable Pulling Machine	Trailer							
	20	0	4	13	0	3	0						

2010

In this project resource planning was embedded to the overall schedule and resources were levelled as per sequence of work (hard and soft logic) and importance of works according to contract requirements and company objectives. Therefore, decision about activity and resource sequence were mapped according to top down requirement list. Top of the requirement is 9 contractual milestones referring the each project zones, and their dates were depicted in the project contract as illustrated in the Table 2. below. Secondly, logic is applied to the activities considering hard logic resulted from resource allocation and soft logic resulted from independent/ slightly dependent works. As a conclusion, approximately 45.000 relationship were established between the activities to create Baseline Schedule. It is very complicated process itself. Additionally, this project schedule was updated Bi Weekly basis during the project life cycle. In the each update, methods to expedite resource efficiency on the Critical Path and Subcritical Paths were developed. Scheduling in this project itself is very sophisticated. Therefore, it requires project management software to automate all these calculation.

Table 2. DMIA Project - Type of Equipment at the Peak Month of August 2010

Key Dates	Contract Milestone Date
MS1: Phase 1 - Provide Permanent Power & Utilities supplies to MC2 and MC 4(NDA).	02-Dec-10
MS2: Phase 1 - Provide Permanent Power Supply to SNC 9 & 10 works at Northern Runway, Taxiways and Aprons	02-Dec-10
MS3: Phase 1 - Provide Permanent Power Supply and Utilities supplies to MC2 works at ATC Tower	02-Feb-11
MS4: Phase 1 - Provide Permanent Power Supply and Utilities supplies to MC3 works at Passenger Terminal Building	02-Feb-11
MS5:Phase 1 - Complete Northern Runway, Taxiways, utilities, ancillary buildings and control systems.	03-Apr-11
MS6: Phase 2 - Complete Northern Development Area Landside Road System, ready for Sectional Taking Over by the Employer.	03-Apr-11
MS7: Phase 2 - Complete remaining Landside Road System ready for Sectional Taking Over by the Employer.	01-Jan-12
MS8: Phase 2 - Complete Aprons & Fuel Hydrant System ready for Sectional Taking Over by the Employer.	01-Jan-12
MS9: Phase 2 - Complete all remaining works ready for Taking Over by the Employer.	02-Apr-12

3.2 Using Heuristic Method to Find Optimum Solution

In the DMIA project, heuristic technique based on experience is preferred during planning stage. Heuristic method is more different than the precise method, and the conditions for choosing the heuristic techniques rather than the exact methods are demonstrated below [5].

- When there is no problem solving method
- When available software and hardware does not allow to use existing exact method
- When the heuristic technique is more flexible compared to exact method

In order to have good heuristic in hand, there should be a solution after some attempts according to high possibility of optimal solution and low possibility of far from optimal solution. Since early work with respect to scheduling under a resource constraints was released by Kalley [9] in 1963, since then, many heuristic methods have been studied considering time, cost and resources. In real life, project is confined by limited resources and require resource leveling (minimum deviation of resource usage) in order to minimize the slack between resources and overall project duration respectively. After establishing leveling, Time Cost Tradeoff (TCT) should be evaluated to optimize duration and cost within a project. Hence, in the DMIA Project, as a Heuristic Method, Critical Path Method (CPM) is used to tackle with resources to optimize. Concerning the CPM, it is for unlimited resources. Therefore, limited resources should be leveled according to sequencing of activities and their free and total float. This can be obtained as per distributing the resources considered early dates and late dates. Early or late start are determined via forward pass, and early or late finish are determined via backward pass for an activity [5-7]. These calculation can be done up to small number of activities by hand. However, all these calculation methods become more sophisticated considering the resource allocation in project having big number of activities and resources such as a project of DMIA. At the present time, most of the planning software allow the user to level the scarce resources according to CPM such as Primavera and MS Project Software. In the DMIA Project, as a project management software, Primavera 6.0 was used which was also obligated by the Main Contract. At the end of the project, it is observed that CPM method has advantages to

resolve the scheduling leveling problems. If project management software was not used in this project, project couldn't be achieved to its objectives considering these resources and their interrelation. Additionally, to establish better planning, control and monitoring, Linear Scheduling Method (LSM) could have been used in addition to CPM in the project. LSM's advantages over the CPM is maintaining the resources continuously at a project. LSM was developed from Line of Balance Technique (LOB) invented by U.S. Army in the early 1950s. This method is suitable for repetitive resource dependent works contained in projects such as roads, railways, pipe line etc.

3.3 Improving Productivity and Efficiency of Resources

Planning is one of the project process group and should consider in all interdependent resources and project constraints in order to prioritize activities along with their resources. In multi projects, resource allocation becomes more sophisticated where the resources are utilized in more than one project. With respect to using equipment in a multiple project, specific machinery schedule should be prepared at the outset in order to use them effectively among the projects without having time lost. For instance, there is a gap between two excavations as seen in the chart below. During this gap, excavator should be utilized in the other area within the project or in different projects to maintain continuity as simply illustrated in Figure 2. This resource allocation can be simulate in planning software easily. Linking activities between two projects require using the same software in the concerned projects. Using the same project management software for the each project under the same programme and portfolio is essential to control resources between projects. However, in the construction project, project manager mostly take all the responsibility of project and has full authority on project with other senior management staff. It is observed that project managers tend to use project management software recognized by them. Using different project management software within organization complicates to gather consolidated report. Thus, execution cannot be properly controlled and monitored and put the maintaining overall organization objective at risk.

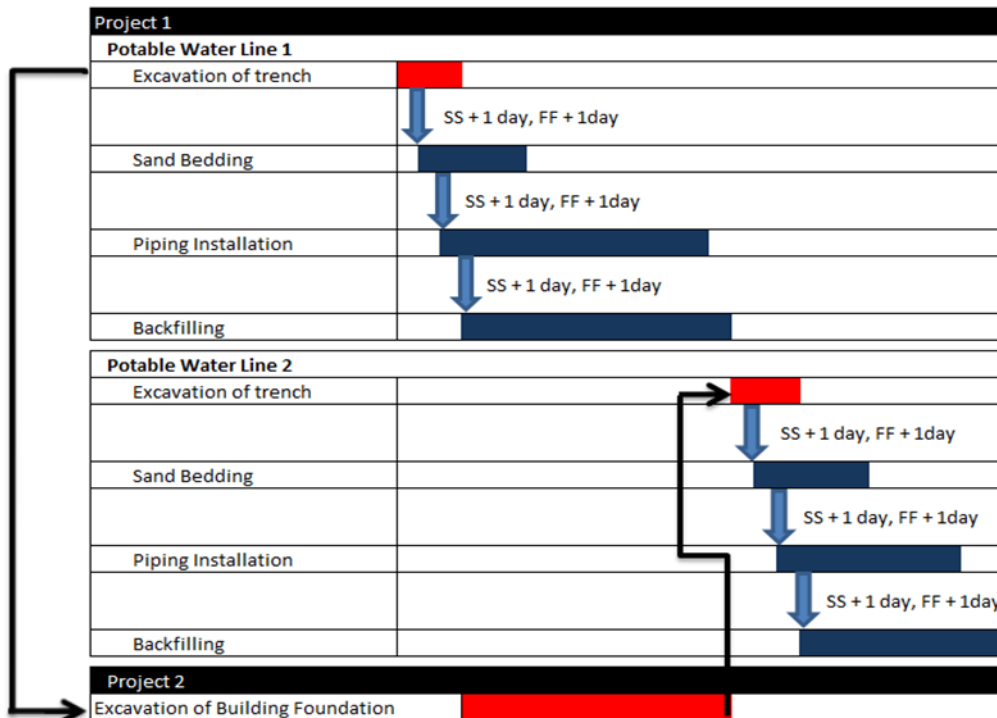


Figure 2. Example of resource allocation between projects

DMIA project was a Joint Venture (JV) Project containing the companies of TAV and CCC. CCC was in charge of the providing the machinery resources. CCC has many projects in the Africa Continent and planned to transfer their machineries between the projects. During the period of DMIA project, CCC had 8 projects in Oman, 14 projects in United Arab Emirates, 9 projects in Qatar, 3 projects in Saudi Arabia, 5 projects in Kuwait. They planned their resources according to their portfolio requirements. Therefore, they want to use same software in the project used in their other project. Additionally, during the planning stages, in the projects CCC has, WBS and RBS should be similar to each other in order to link the activities between projects. Using the Primavera software and establishing same WBS and RBS to CCC's projects under their portfolio enable us the control resources efficiently. Thus this study recommends that to monitor, control and optimize resource allocation as per project and organization objectives and to ease the communication between each stakeholder, common project management software along with common WBS and RBS should be established for each project under the same organization.

3.4 Resolving the Conflict between Managers to Increase Efficiency

Projects are conducted by different project managers. Project is more valuable for its project manager and sometimes there can be a conflict between them due to determining the resource order between projects. Therefore, there should be an agreement between them on the allocation of resources at the outset of the project. Therefore, senior managers or program / portfolio managers should interfere the concerned resource related project in order to balance project resources through identifying the resource distribution according to importance of projects (considering programme/ portfolio objectives) and availability of resources. Also Yang et al. [8], tabulated the decision making flow for the balancing the resources of multi projects in the Figure 3. below. Using the same scheduling software showing the resource allocation provides better information to program / portfolio managers to distinguish and prioritize resource dependent activities in the projects.

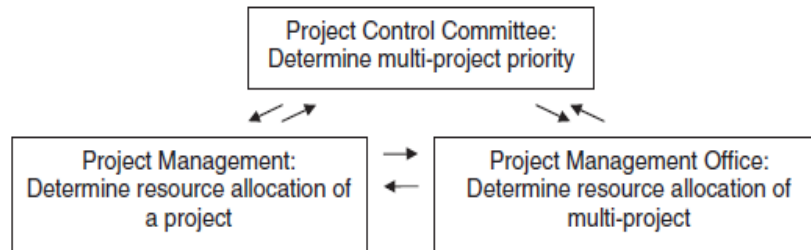


Figure 3. Organization responsibility and interrelationship of resources-based constrained scheduling

Second step is to control resources within a project without having any debate within project. Thereby, instead of functional organizational structure, using strong Matrix organization structure or Projectized Organizational Structure are proposed to tackle with the conflict between managers [4], [6]. Because PM has more authority in these organizational types comparing to Weak Matrix, Balanced Matrix and Functional Organization. Hence, decision making process in a project can be more quick and rigid through these kinds of organization providing more authorities comparing to other organizational type. In the DMIA project, projectized organization was chosen in order to give full authority to the PM to accelerate decision making process. Additionally, CCC had Regional Manager who was acting a senior manager to decide resource allocation order between their projects. It was observed as a lessons learned that establishing projectized organization and having a senior manager to discuss the resource problem resolved the many issue quickly during the life cycle of the project.

4 CONCLUSION

This work only reveals common resource allocation problems among the projects and solution to these problems. Technique of LSM and CPM have the potential of providing all of the analytical features to maintain resources with an efficient way. Shifting the resources within projects on time can be ensured through proper controlling and monitoring through using the same software, WBS and RBS in the projects under the same programme an/or portfolio. However, due to conflict of interest among the project manager, process of sequencing the works can be exhausting and time consuming. Therefore, Project Control Committee of programme and portfolio should determine multi project priority for the each resource. Additionally, project manager should be given adequate authority by means of strong matrix organization or projectized organization to accelerate the decision making process.

REFERENCES

- [1] D.C. Ferns, "Developments in programme management", .International Journal of Project Management, vol.9(3), 1991.
- [2] S. Pellegrinelli, "Programme management: organizing project-based change" .International Journal of Project Management, vol. 15(3), pp. 141-149 1997.
- [3] Project Management Institute *The standard for portfolio management*. 3rd ed. Newtown Square, 2013.
- [4] Z. Laslo, and A.I. Goldberg, "Resource allocation under uncertainty & in a multi-project matrix environment: is organizational conflict inevitable?" International Journal of Project Management, vol. 26 (8), pp.773-788, 2008.
- [5] R. Martí, and G. Reinelt, "The linear ordering problem: exact and heuristic methods in combinatorial optimization." Berlin: Springer-Verlag. 2011.
- [6] J.H Gordon, "Heuristic methods in resource allocation" *International Journal of Project Management*, vol. 1(3), pp. 163-168, 2013.
- [7] A. Lova, C. Maroto and P. Tormos "A multicriteria heuristic method to improve resource allocation in multi project scheduling" *European Journal of Operational Research*, vol. 127, pp.408-424, 2000.
- [8] S. Yang, and L. Fu, "Critical chain and evidence reasoning applied & to multi-project resource schedule in automobile R&D process." International Journal of Project Management, vol. 32 (1), pp.166-177, 2012
- [9] J.E. Kelley, 'The critical path method - resources planning and scheduling' Industrial scheduling, Muth & Thompson 1963.

A Novel Dual-Band FSS Reflector for RCS Reduction

Sibel Unaldi¹, Hande Bodur², Sibel Cimen², Gonca Cakir³

Abstract

In this study, dual band Frequency Selective Surface (FSS) design with Radar Cross Section (RCS) reduction for planar reflectarray antenna is presented. A 9 x 9 elements reflectarray is used for verify RCS reduction. Simulation results of the reflectarray antenna backed on metallic ground and reflectarray antenna grounded with designed FSS are compared. The simulation results demonstrate that RCS reduction of reflectarray antenna was achieved using FSS backed.

Keywords: dual-band stop FSS, RCS reduction

1 INTRODUCTION

A microstrip reflectarray antenna is a structure, composed of finite number of periodic resonant units on a dielectric substrate. The units providing radiation by adjusting the phase delay of each units in order to getting equal phase surface in a specific direction [1]. Recently, microstrip reflectarray antennas are widely preferred instead of the parabolic reflector antennas when the high gain antenna applications are required. Parabolic reflector antennas are bulky and main beam directivity is obtained by mechanical movements. However microstrip reflectarray antennas have some advantages as low cost, low profile with the beam scanning ability.

Antennas importantly increase the level of radar cross section (RCS) and in this case constitutes a negative impact on stealth technologies. There are several methods to overcome this problem For example the application of radar absorbing material (RAM) [2], passive or active cancellations [3], ferrite substrate [4] and using frequency selective surfaces (FSS)[5]. The coating of RAM has disadvantage with its bulky structure. These methods for RCS reduction minimize the radar signature while make the system more complicated or increase the cost. But RCS reduction with using FSS as a ground plane of the reflectarray antenna is investigated in this study.

The aim of this work is reduce the RCS level of the reflect array antenna backed on designed FSS instead of metallic ground plane. A 9 x 9 elements reflect array antenna grounded on FSS structure are designed and simulated. FSS consists of 9 x 9 unitcells which has the same size with the reflectarray antenna. Simulation results show that the FSS grounded reflectarray antenna reduce the RCS level significantly compared with the ground plane in the equal dimensions. This paper organized as follows. Design parameters and designed structure of the unit cell of FSS and reflect array antenna are take place in Section II. In Section III Monostatic RCS analyses result of reflectarray antenna backed on ground plane and grounded with designed FSS are compared.

2 DESIGN

2.1 Design of FSS

In order to reduce of the RCS level of the used reflect array antenna, a band- stop frequency selective surface designed as a ground plane. In Figure 1 unit cell of the designed FSS structure and design parameters are shown. The elements of the unit cell are periodic in x and y dimensions.

¹ Corresponding author: Bilecik Şeyh Edebalı University, Department of Electric-Electronic Engineering, 11230, Merkez/Bilecik, Turkey.
sibel.unaldi@bilecik.edu.tr

² Sakarya University, Institute of Natural Sciences, 54187, Serdivan/Sakarya, Turkey.

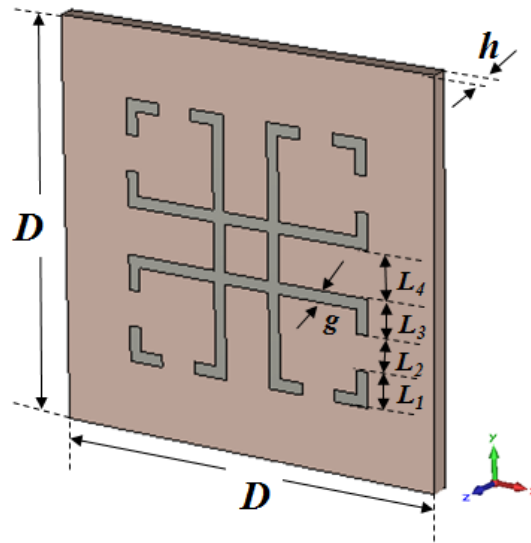


Figure 1. Unit cell of the designed FSS.

The unit cell is designed on a substrate named Arlon Di 880 with a thickness $h = 0.762$ mm, a relative permittivity $\epsilon_r = 2.2$ and a loss tangent $\tan \delta = 0.0009$. Considering x and y directions, lengths of the unit cell are 17 mm x 17 mm. Lengths of the unit cell of the designed FSS and reflectarray antenna are equal. Parameters of designed unit cell are shown in Table 1. g is the width of the metallic elements.

Table 19. dimension of the presented FSS

D	L ₁	L ₂	L ₃	L ₄	h	g
17 mm	1.5 mm	1.5 mm	1.5 mm	2.0 mm	0.762 mm	0.50 mm

Figure 2 shows transmission and reflection coefficient of the FSS. In this study we present a dual band FSS has band-stop frequency characteristic which operating at X band. The designed FSS working at 9 GHz and 11.75 GHz. Also reflectarray antenna which used for validated this study, has Ultra Wide Band (UWB) reflection characteristic.

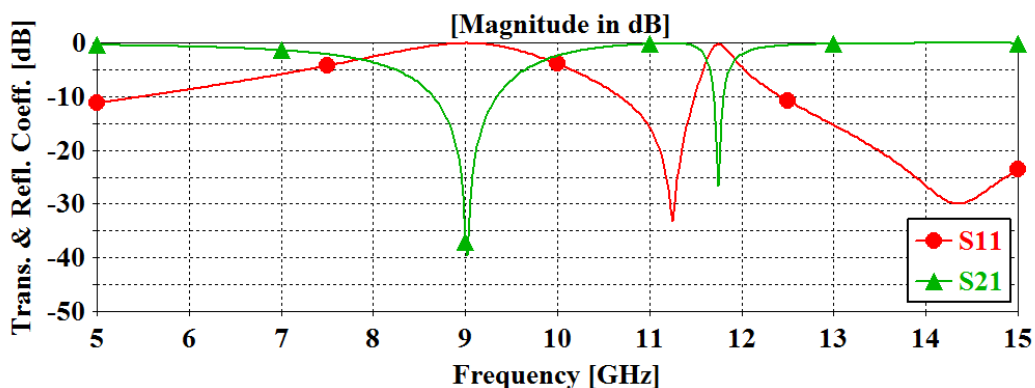


Figure 2. Reflection and transmission coefficient of the FSS.

2.2 Reflectarray Antenna Structure

The reflectarray used for RCS reduction consists of 9 x 9 elements and each element's overall dimensions 17 x 17 mm in xy plane. In Figure 3 (a) and (b) are demonstrate the unit cell of the reflect array antenna. Table 2 shows the reflectarray antenna design parameters. There is 5mm thick air layer between substrate and ground plane shown in Figure 3 (b). Also while making

a RCS analysis with FSS grounded reflectarray antenna, 5mm thick air layer between reflectarray antenna and FSS ground plane is preserved.

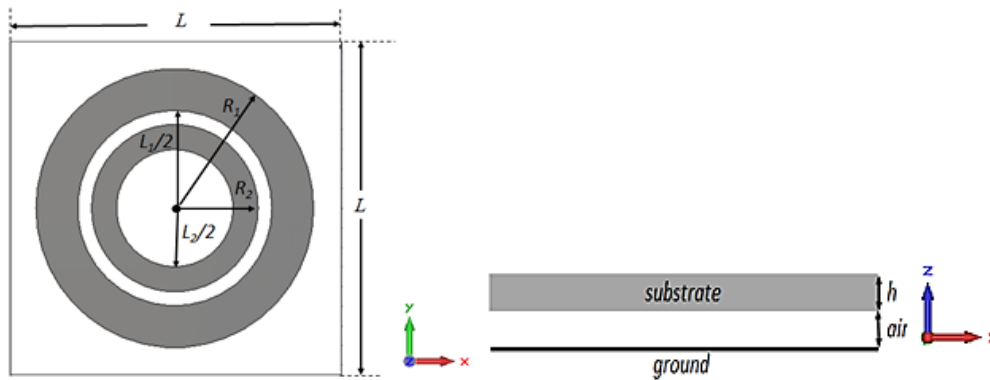


Figure 48. (a) Front view of the reflect array unit cell. (b) Bottom view of the reflect array unit cell.

Reflectarray unit cell is designed on a dielectric slab Arlon AR 600 ($\epsilon_r=6$) with thickness $h=0.508$ mm Design parameters is given in Table 2.

Table 2. dimension of the used Reflectarray antenna

L	L ₁	L ₂	R ₁	R ₂	h
17 mm	3.99 mm	2.395 mm	5.7 mm	3.42 mm	0.508 mm

3 RESULTS AND CONCLUSION

3.1 Simulation Result

In Figure 4 the comparison of the reflection of reflectarray antenna with metallic ground plane and FSS ground plane is illustrated.

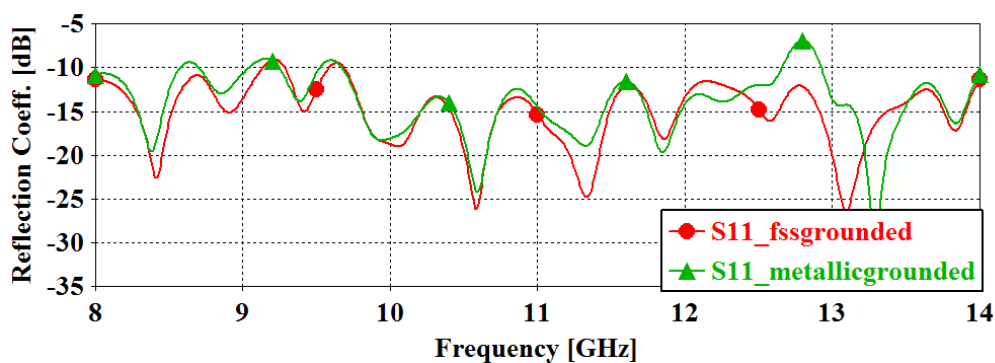


Figure 4. S_{11} parameter of reflectarray antenna with metallic ground plane and FSS ground plane.

The comparison of the radiation patterns of the antenna with metallic ground and FSS ground for the first resonating frequency and the second resonating frequency of the FSS is given in Figure 5 and Figure 6 respectively.

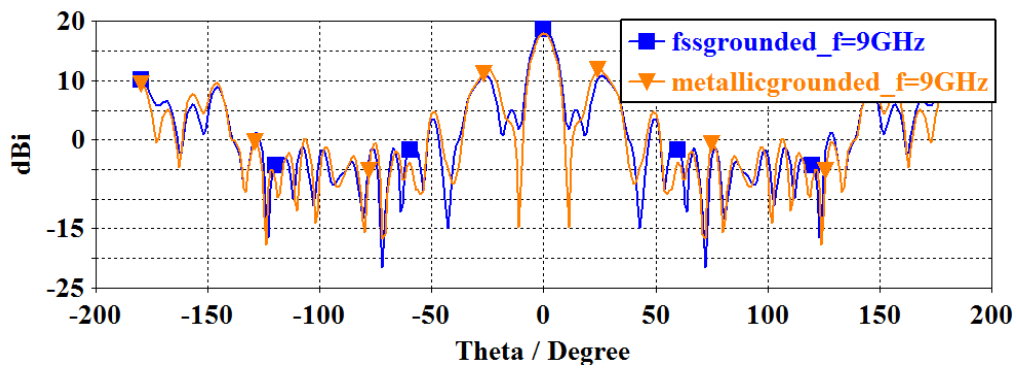


Figure 5. Radiation pattern at 9 GHz in the $\phi = 90^\circ$ for metallic grounded and FSS grounded reflectarray antenna.

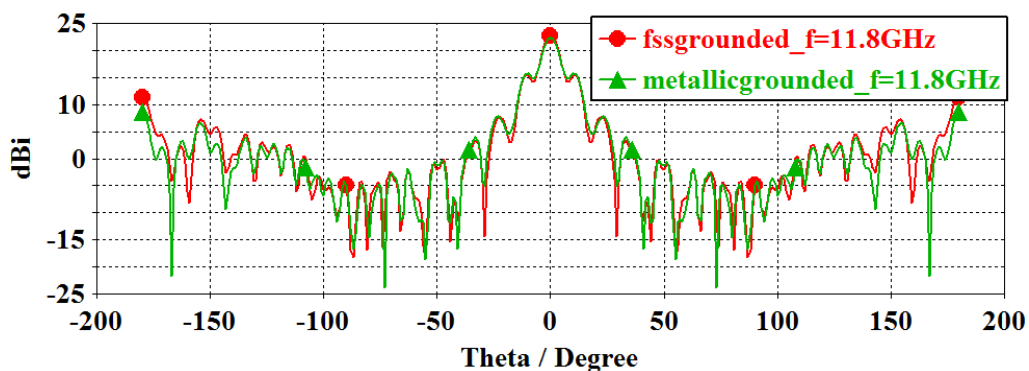


Figure 6. Radiation pattern at 11.8 GHz in the $\phi = 90^\circ$ for metallic grounded and FSS grounded reflectarray antenna.

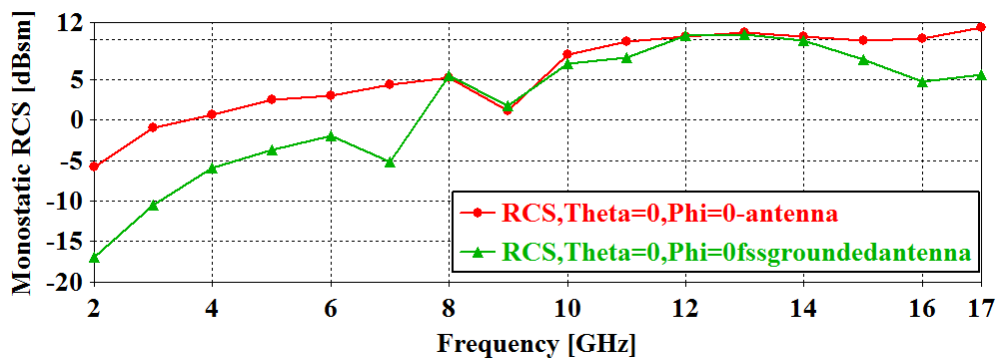


Figure 7. Simulation of monostatic RCS of the reflectarray antenna with metallic ground and proposed FSS.

In Figure 7 simulation results of the monostatic RCS of the reflectarray antenna grounded with metallic plane and proposed FSS is illustrated. Through the Figure 4 RCS level for the two different scenario is obviously observed. RCS level of the reflectarray antenna is reduced by using proposed FSS ground.

Main goal of this work is reduction of the RCS value of the reflect array. Also it is necessary not to change the operating characteristics of the antenna. Therefore the effects of the proposed FSS, used for reduction of the RCS of the reflectarray antenna are investigated on performance of the reflectarray. For this purpose reflection coefficient and radiation pattern curves are compared in each case. Obtained reflection coefficient curves given in Figure 4 show that reflection characteristics of the reflectarray antenna in each case are not different from each other. Directivity of the reflectarray antenna has been stable in resonating frequencies as seen in Figure 5 and Figure 6.

3.2 Conclusion

Dual band-stop FSS design that using as a ground of a microstrip reflectarray antenna with the intend of RCS reduction is presented. FSS structure and FSS backed reflectarray antenna integration are designed and tested by using CST Microwave

Solver. Simulation result shows that FSS ground decrease the 'out of band' RCS level substantially compared with the metallic ground plane reflectarray antenna in equal dimension.

ACKNOWLEDGMENT

The authors wish to acknowledge the assistance and support of The Scientific and Technological Research Council of Turkey (TUBITAK) for supporting this work (Project No: 114E500).

REFERENCES

- [1] Y. Chen, I. Chen, H. Wang, X. T. Gu and X. W. Shi, "Dual-band crossed-dipole reflectarray with dual-band frequency selective surface," IEEE Antennas and Wireless Propagation Letters, Vol. 12, pp. 1157 – 1160, Sept. 2013.
- [2] G. G. Peixoto, A. L. de Paula, L. A. Andrade, C. M. A. Lopes and M. C. Rezende, "Radar absorbing material (RAM) and shaping on radar cross section reduction of dihedral comers," SBMO/IEEE MTT-S International Conference on Microwave and Optoelectronics, 2005.
- [3] E. F. Knott, J. F. Shaeffer, and M. T. Tuley, "Radar Cross Section", Raleigh, NC, USA: SciTech, 2004
- [4] D. M. Pozar, "Radiation and scattering characteristics of microstrip antennas on normally biased ferrite substrates," EEE Trans. Antennas Propag., vol. 40, pp. 1084–1092, 1992.
- [5] S. Genovesi, F. Costa, and A. Monorchio, "Low-profile arraywith reduced radar cross section by using hybrid frequency selective surfaces," IEEE Trans. Antennas Propag., vol. 60, no. 5, pp. 2327–2335, May 2012.

Examination of Partial Resistance Against to Leaf Rust on Some Bread Wheat Genotypes

Husnu Aktas¹

Abstract

Leaf rust, caused by *Puccinia recondita* Roberge. Ex. *desmazii* f. sp. *tritici* is the one of most serious disease of wheat globally including southeastern Anatolia of Turkey. Twelve spring wheat genotypes were artificially inoculated and protected in GAP International Agricultural Research Institute, Diyarbakir during 2011-12 season, to investigate yield losses and yield components. Artificial inoculation was with a collection of mixed inoculum of urediniospores from different locations of southeast Turkey. Inoculation was started at Zadoks-29, tillering stage and disease severity and infection type were recorded four times every 9 days. Genotypes were evaluated for adult plant stage by two partial resistance parameters: final disease severity and area under disease curve. The area under disease progress curve (AUDPC) ranged from 80 to 1400. Yield losses ranged from 18% to 40.1% , while TKW loss ranged from 0.69 to 22.5 % . Genotypes G5, G7 and G10 had lowest yield loss; G2, G8, G11 and G12 showed moderate yield loss; and the higher yield loss were given by G1, G3, G4, G6 and G9. According to regression analysis, yield loss and AUDPC had a positive significant relationship. Three major clusters, based on AUDPC, final disease severity, and yield loss percentage, formed for 12 wheat genotypes. Partially resistant genotypes lost less grain yield and seemed appropriate against severe leaf rust pressures.

Key words : *Leaf rust, AUDPC, Yield Loss, TKW*

1 INTRODUCTION

Leaf rust caused by *Puccinia triticina* Eriks., is one of the main diseases of wheat (*Triticum aestivum* L.) in Turkey, causing up to 50% of yield losses. Genetic resistance is the most economic and effective means of reducing yield losses caused by the disease. However, breeding genotypes for disease resistance is a continuous process and plant breeders need to add new effective sources to their breeding materials.

Leaf rust attacks the leaf blades of wheat, although it can also infect glumes in highly sensitive wheat genotypes [11]. Number of seed per spike and thousand kernel weight reduction occurred in wheat genotypes infected by leaf rust (e.g. [17], [13]). Yield loss caused by rust diseases depend on level of sensitivity, disease development rate and duration, also environmental conditions for rust diseases. Early infection of leaf rust on wheat generally can cause higher yield losses; 60–70% infection on the flag leaf at spike emergence may account for a yield loss of more than 30% [12]. Yield loss caused by leaf rust is lower compare to stripe rust in Southeast Region of Turkey, because the vegetation time is short for developing leaf rust spores. Specially in longer vegetation season and irrigated conditions leaf rust causes more yield loss in Southeast of Turkey. It was reported that stripe rust epidemics in Cukurova Region, Turkey decreased yield %50 in 1995-1996 [8]. Similarly several authors reported that losses in kernel weight of wheat varieties due to leaf rust infection ranged between 2.0% and 41% according to the level of resistance or susceptibility and yield loss due to leaf rust reached up more than 50% in susceptible cultivars, those improving and using resistance cultivar is very important issue for food security (e.g. [4], [2], [22]). This study were conducted to estimate of yield loss because of leaf rust using genotypes that have different resistance level.

2 MATERIALS AND METHODS

The study was conducted at experimental area of GAP International Agricultural Research and Training Center in 2011-12 season with protected and inoculated experiments. Twelve winter bread wheat genotypes obtained from International Winter Wheat Improvement Program (IWWIP) were used as a plant material in this study (Table 1). The experiments were in four replication randomized complete-block design. Both infected and protected experiments were planted into 1.2 × 5 m plots with sowing machine. Each plot had 20 cm away 6 rows. The seedling rate was 400 seed/m². Optimum nutrient (160 N: 80 P: 0 K) was applied.

Protected (experiment- 2) plots in both locations were protected by the fungicide Opera® (with 12.5% active ingredients pyraclostrobin and epoxiconazole; Nufarm Ltd, Laverton North, Vic.). The concentration and rate was according to the manufacturer's recommendations. The fungicide applied in protected experiment on 25th March and 15nd April resulted in a complete protection. Infected (experiment-1) plots were artificially inoculated with equal doses of the mix inoculum of urediniospores that collected from different locations in Southeast Turkey, possessing virulence for leaf rust resistance genes against *Lr19*, *Lr22a*, *Lr23*, *Lr25*, *Lr28* and *Lr35*. To provide and maintain the rust inoculum pressure inoculated experiment

¹ *Mardin Artuklu University, Vocational School of Kiziltepe, 4700, Mardin*

was inoculated by dusting method twice in a week during growing season, also inoculated experiment was surrounded by sowing highly susceptible cultivar Morocco to spread the inoculum.

The first leaf rust severity were recorded when the susceptible genotype Morocco reach up 50%. The leaf severity data was recorded on 2th, 11th, 20th and 29th of April at an interval of 9 days by following the modified Cobb's scale [16].

The area under the disease progress curve (AUDPC) was calculated using computer program developed at CIMMYT [5].

The yield losses due to yellow rust were calculated based on Area under the Disease Progress Curve (AUDPC). The AUDPC was calculated by the trapezoidal integration of the disease severity in time, considering the whole period evaluated, as follows:

$$AUDPC = \sum_{i=1}^{n-1} \left(\frac{X_i + X_{i+1}}{2} \right) (t_{i+1} - t_i)$$

Where X is the disease severity (percentage of plants diseased), n the number of evaluations, and $(t_{i+1} - t_i)$ the time interval (days) between two consecutive evaluations [7].

The relative losses in yield, thousand kernel weight (TKW), and test weight (TW) were determined as a percentage of the protected plots of the respective genotypes. Yield losses were for each genotype, as:

$$RL (\%) = \frac{(Y1 - Y2)}{Y1} \times 100$$

The variance analysis for yield per ha (kg/ha), thousand kernel weight (TKW), were performed [9] using SAS (1999) version 8.2 [19]. Regression analysis was performed using by Excel to determine relationships among disease and yield parameters.

Table 1. Wheat Genotypes with their pedigrees and Origin

Genotypes	Pedigrees	Origin
G1	FRTL//AGRI/NAC	IWWIP
G2	MOTAH/BOUHOUTH6	IWWIP
G3	BACANORA /3/2163/2174//AGSECO 7853 (OK01224)	IWWIP
G4	BESKOPRU	Turkey
G5	SERI.1B*2/3//KAUZ*2//BOW//KAUZ/4//BAGCI2002	IWWIP
G6	KK8514.1.1//TAM200//KAUZ	IWWIP
G7	J15418/MARAS//SHARK/F4105W2.1/3//SHARK/F4105W2.1	IWWIP
G8	TAM200//KAUZ//BECUNA-6	IWWIP
G9	KAMBARA1//KALYOZ-17	IWWIP
G10	Lr64/Iz1813//093-44/3//No57/4//Sut66/5//Sabalan/6//Bez//Bez/Tvr/3//Kremena/Lov29/4//Katya 1	IWWIP
G11	SERI.1B*2/3//KAUZ*2//BOW//KAUZ/4//BAGCI2002	IWWIP
G12	KONYA	Turkey

3 RESULTS AND DISCUSSION

Data related of examined traits were given in Table 2. Grain yield in protected experiment ranged from 4.20 to 6.99 ton ha⁻¹, and thousand kernel weight ranged from 29.1 to 41.4 gr, while mean of grain yield and thousand kernel weight were 5.13 ton ha⁻¹ and 32.7 gr. Grain yield of genotypes in infected experiment were between 2.82 and 5.60 ton ha⁻¹ and thousand kernel weight ranged from 20.6 to 37.2 gr.

Genotypes gave different reaction to leaf rust in infected experiments while they were almost free from the leaf rust at the protected experiment. (Table 2). Disease severity ranged from 5 to 80% in infected experiment. Genotypes G10, G6, and G7 had the lowest rust severity (with 5 MR, 10 MR and 10 MR respectively), followed by G8, and G12 (with 20MS). The disease severity of the rest genotypes ranged from 30 to 80%. Genotypes with high disease severity had high yield loss. Previously study indicated that small FDS value for durum lines exhibiting slow rusting, a kind of partial resistance, and they had less grain yield loss compared to susceptible checks [21].

Area under progress curve (AUDPC) changed from 80 to 1400, and genotypes with the highest AUDPC lost the highest yield losses, while the genotypes with the lowest AUDPC lost less (Table 2). G1, G2, G3, G4 and G5 that could be evaluated as lowest partial resistance had highest AUDPC values (620; 1080; 1240; 1400 and 900 respectively). Moderate partial resistance genotypes G9 and G11 had moderate high AUDPC values (240 and 420) while genotypes G6, G7, G8, G10 and G12 were the high partial resistance and had lowest AUDPC values (120; 200; 160; 20 and 200). Several researcher found that high AUDPC values caused great significant loss in yield and yield components such as TKW and number kernel per spike (e.g. [3], [14], [21]). Similarly the other also concluded that genotypes with small AUDPC and FDS had the least yield or yield components' reduction (e.g. [10], [11], [1]).

Table 2. Data of examined traits in infected and protected experiment

	Grain Yield (t ha ⁻¹)			Thousand Kernel Weight (g)			Data of disease in the infected experiment	
	Protect	Infected	Yield Loss (%)	Protect	Infected	Yield Loss (%)	FDS value in infected experiment	AUDPC value in infected experiment
G1	4.20 e	2.82 ef	33	37.2	30.5	18.0	50S	540
G2	5.95 bc	4.25 c	29	33.2	27.5	17.2	80S	1080
G3	6.39 ab	3.85 cd	40	41.4	32.1	22.5	60S	1240
G4	6.99 a	4.19 c	40	36.4	31.1	6.9	70S	1400
G5	2.83 f	2.30 f	19	25.7	20.6	9.3	80S	380
G6	6.06 bc	4.10 c	32	28.9	26.5	8.3	10MR	320
G7	6.89 a	5.60 a	19	33.6	30.4	9.5	10MR	180
G8	5.85 bc	4.49 bc	23	32.9	29.9	9.1	20MS	160
G9	5.01 d	3.11 de	38	28.1	21.8	22.4	30S	360
G10	6.39 ab	5.24 ab	18	39	37.2	4.6	5MR	80
G11	5.48 cd	4.11 c	25	33.2	29	12.7	40S	420
G12	5.44 cd	3.89 c	28	29.1	28.9	0.7	20MS	200
Mean	5.62 A	3.99 B	29	33.3 A	28.8 B			
CV (%)	8.5	12.8						

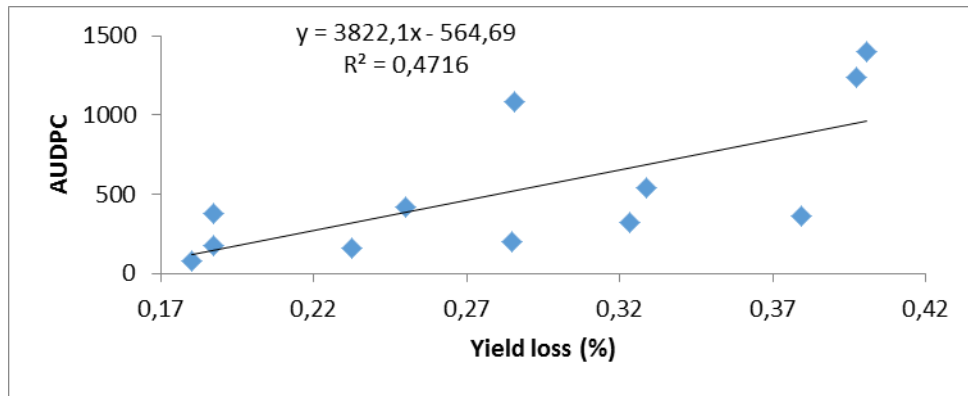


Figure 1. Regression analysis showing relation between yield loss and AUDPC

Loss percent in grain yield and TKW were displayed in Table 2. The grain yield loss (%) ranged from 18 to 40.1%. G5, G7 and G10 had lowest yield loss (with 18,7%; 18,7% and 18%); G2, G8, G11 and G12 showed moderate yield loss (with 28,7%; 23,2% and 28,5%); the higher yield loss were given by G1, G3, G4, G6 and G9 with 32,9%, 39,7%; 40,1 and 37,9%.

TKW losses ranged from 0.7 % to 22.5 %. G4, G10 and G12 had lowest TKW loss which ranged from 0.7- 6.9 %; moderate TKW loss showed by G5, G6, G7, G8 and G11 and ranged from 8.3 – 12.7 %. G1, G2, G3, and G9 had highest TKW loss and ranged from 17.2 to 22.5. It was reported that yield loss under artificial inoculation ranged from 11.2 to 73.6 for grain yield and reached up 20% for TKW [2]. Similar results of report indicated that yield gain in protected plots ranged from 7.8 % to 18.3 % depends on resistance level of the genotypes in study conducted in Turkey conditions [15].

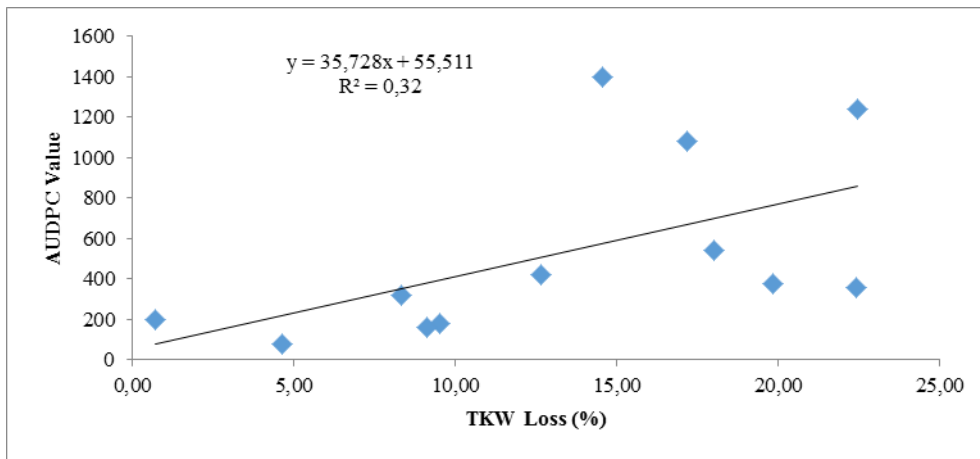


Figure 2. Regression analysis showing relation between TKWL loss (%) and AUDPC

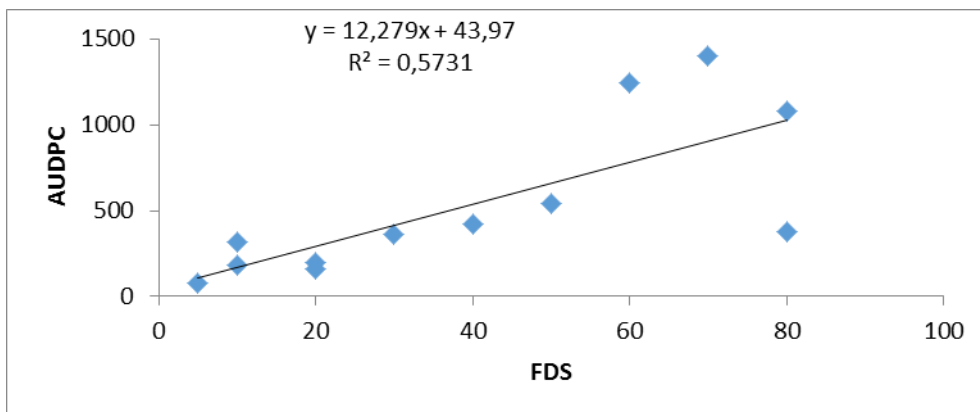


Figure 3. Regression analysis showing relation between FDS and AUDPC

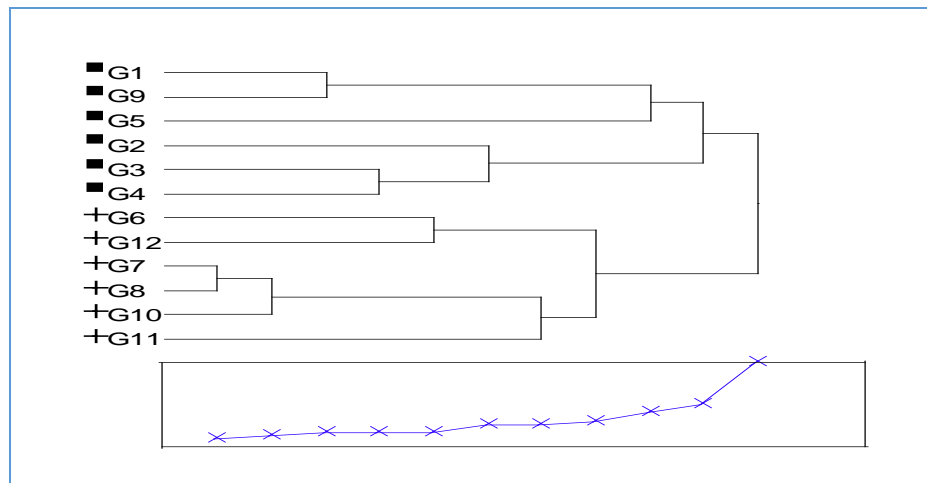


Figure 4. Cluster analysis based on yield loss, TKW loss, final disease score(FDS) and AUDPC values

Regression analysis that indicated relationship AUDPC with loss percent in grain yield, 1000 kernel weight and final disease severity (FDS) showed in Fig 1 - Fig3. A positive and significant relation were determined between AUDPC and grain yield loss ($R^2 = 0.47^*$) which means that high AUDPC value caused more yield loss and also positive but non-significant were determined for TKW loss ($R^2 = 0.32$). Relation between AUDPC and FDS was high and significant according to regression analysis ($R^2 = 0.57^*$). Safavi (2015) found that highest correlation between AUDPC and yield loss ($r=0.95$) and TKW loss ($r = 0.78$). In previous study reported that genotypes with small AUDPC identified with slow rusting characteristics should be improved further by accumulating 4-5 minor genes to achieve near-immunity prior to deployment as control measure for management of leaf and yellow rust diseases [20].

Cluster analysis based on yield loss, TKW loss, final disease score (FDS) and AUDPC values displayed in Fig 4. According to cluster analysis, genotypes separated into high (G7, G8, G10 and G11), moderate (G6 and G6) and low (G1, G2, G3, G4, G5 and G9) partial resistance groups. Similar results obtained in study that performed to assessment of quantitative resistance to yellow rust for ranking of wheat breeding lines, according to the resistance level based on disease severity (DS) along with other slow rusting parameters, it was found that resistance levels ranged from very low (in Taichung 23) to very high (in Parula) among the tested wheat breeding lines [6].

4 CONCLUSION

The present study concluded that the genotypes were having enough diversity regarding partial resistance, ranging from low to partial resistant lines. Genotypes with high partial resistance displayed better performance under high disease pressure comparing to susceptible genotypes. These genotypes were supposed to be having genes for varying degrees of slow leaf rusting and enough diversity was observed to be used for further genetic manipulations. In addition, testing for stability over years and locations for leaf rust along with other desirable characters must be made before approval.

REFERENCES

- [1]S. Ahmad, M. Afzal, I.R. Noorka, Z. Iqbal, N. Akhtar, Y. Iftkhar, and M. Kamran., "Prediction of yield losses in wheat (*Triticum aestivum* L.) caused by yellow rust in relation to Epidemiological factors in Faisalabad". Pakistan Journal Botany 42: 401-407, 2010.
- [2]B. Akın, S. Yüce, R. Singh, H.J. Braun, N. Zencirci, and A. Morgunov., "Leaf rust (*Puccinia triticina*) resistance in winter-facultativa wheat (*Triticum aestivum* L.) cultivar from different countries". Open science Repository Agriculture. Online/open-access), e23040506. Doi: 10.7392/openaccess.23040506., 2013
- [3]S. Ali, S.J.A. Shah, M. Ibrahim., "Assessment of wheat breeding lines for slow yellow rusting (*Puccinia striiformis* west. tritici)". Pak J Biol Sci 10, 3440-3444., 2007
- [4]M.A. Bajwa, K.A. Aqil, and N.I. Khan., "Effect of leaf rust on yield and kernel weight of spring wheat". RACHIS 5: 25-28., 1986
- [5]M.E. Bjarko, and R.F. Line., "Quantitative determination of the gene action of leaf rust resistance in four cultivars of wheat". *Triticum aestivum*. Phytopathology 78: 451-456., 1998
- [6]L.H.M. Broers, X.C. Subias, and R.M.L. Atilano., "Field assessment of quantitative resistance to yellow rust in ten spring bread wheat cultivars". Euphytica 90, 9-16., 1996
- [7]C.L. Campbell, and L.V. Madden., "Introduction to Plant Disease Epidemiology, John Wiley & Sons, New York., 1990
- [8]F. Düşünceli, L. Cetin, S. Albustan, and S.P.S. Beniwal., "Occurrence and impact of wheat stripe rust (*Puccinia striiformis*) In Turkey in 1994/95 crop season". 9th European and Mediterranean Cereal Rusts and Powdery Mildews Conference. Netherlands. 309.,1996
- [9]K.A. Gomez, and A.A. Gomez., "Statistics for Agric. Res. (2nd Ed.)". John Willey & Sons, New York., 1984
- [10]D. Hailu, and C. Fininsa., "Relationship between stripe rust (*Puccinia striiformis*) and grain quality of bread wheat (*Triticum aestivum*) in the highlands of Bale, southeastern Ethiopia". International Journal of Food, Agriculture and Environment 5: 24-30., 2007

- [11] S.A. Herrera-Foessel, R.P. Singh, J. Huerta-Espino, E.J. Crossa, E.A. Djurle, and J. Yuen, J. 2007 "Evaluation of slow rusting resistance components to leaf rust in CIMMYT durum wheats". *Euphytica* 155: 361–369; Doi: 10.1007/s10681-006-9337-7., 2007
- [12] J.A. Kolmer, "Genetics of resistance to wheat leaf rust. *Annual Review of Phytopathology*". September 1996, vol. 34, p. 435-455., 2004
- [13] C.N. Marasas, M. Smale, R.P. Singh., "The Economic Impact in Developing Countries of Leaf Rust Resistance Breeding in CIMMYT-related Spring Bread Wheat. *International Maize and Wheat Improvement Center, Mexico, DF*"., 2004
- [14] J.I. Mirza, R.P. Singh, I. Ahmed, "Resistance to leaf rust in Pakistani wheat lines". *Pak. J. Biol Sci* 3, 1056-1061., 2000
- [15] A. Morgounov, B. Akin, L. Demir, M. Keser, A. Kokhmetova, S. Martynov, S. Orhan, F. Özdemir, I. Özseven, Z. Sapakhova, and M. Yessimbekova., "Yield gain due to fungicide application in varieties of winter wheat (*Triticum aestivum*) resistant and susceptible to leaf rust". *Crop & Pasture Science* <http://dx.doi.org/10.1071/CP14158>, 2015
- [16] R.F. Peterson, A.B. Campbell, and A.E. Hannah., 1948. "A diagrammatic scale for estimating rust intensity on leaves and stems of cereals". *Canadian J. Res.* 26: 496-500., 1948
- [17] A.P. Roelfs, R.P. Singh, and E.E. Saari., "Rust Diseases of Wheat: Concepts and Methods of Disease Management. CIMMYT, Mexico., 1992. Available at www.cimmyt.org.
- [18] S.A. Safavi, "Effects of yellow rust on yield of race-specific and slow rusting resistant wheat genotypes". *Journal. Crop Protection* 4: 395-408., 2015
- [19] SAS., "SAS/STAT User's Guide, Version 8.2, 1st printing". Vol. 2. SAS Institute Inc, SAS Campus Drive, Cary, North Carolina., 1999
- [20] R.P. Singh, A. Mujeeb-Kazi, J. Huerta Espino., "Lr46: A gene conferring slow-rusting resistance to leaf rust in wheat". *Phytopath* 88: 890-894., 1998
- [21] R.P. Singh, J. Huerta-Espino, and S. Rajaram., "Achieving near-immunity to leaf and stripe rusts in wheat by combining slow rusting resistance genes". *Acta Phytopat et Entomol Hungarica* 35, 133–139., 2000
- [22] M. Yaqoob., "Study on rusts and tolerance in wheat cultivars in greed lines in Pakistan". M.Sc. Thesis, Department of Plant Pathology, University of Agriculture, Faisalabad, pp. 98., 1991

Comparison of the Apparent Porosity and Porosity Values on Different Rock Types (Gümüşhane-Türkiye)

Serhat Dag¹

Abstract

This study aimed to indirect estimation of porosity value considering the apparent porosity value. For this purpose, 200 cylindrical test samples, equally obtained from 5 different rock units outcropping in Gümüşhane (NE, Türkiye) province, which have characteristics of granite, andesite, limestone, sandstone and andesitic tuff, were prepared. The apparent porosity values were obtained by considering their saturated and dry weight values. Next, the porosities were determined by using dry unit weights and grain unit weights of the test samples. To determine if there is a relationship between the apparent porosity and porosity values, simple regression analyses were performed. A total of 150 samples, 30 from each rock group, were used in the analysis. When all rock samples considered together, very strong positive correlation ($r = 0.99$) was obtained among the samples. Then, each sample was analyzed in its own rock group. In this case, correlation coefficients between apparent porosity and porosity values were determined as $r = 0.94$ in granites, 0.97 in andesite and 0.99 in andesitic tuffs, limestone and sandstone samples, and there is a very strong positive relationship here. The significance of correlation coefficients obtained from these analyses was tested by both using t-test and comparing it with the critical r values of Pearson correlation coefficient. In addition, 50 data randomly selected in the beginning among the samples of each rock group were excluded from analyses to be used to test the interoperability of equation derived from regression analysis. As a result of this analysis, it was determined that the data released a very strong positive relationship. In conclusion, the studied rock types showed no significant difference between porosity and apparent porosity values. Besides, using the specified equations in a healthy way, it is expected that the porosity values can be estimated indirectly benefiting from the apparent porosity values.

Keywords: Apparent porosity, porosity, simple regression analyses, correlation coefficient

1 INTRODUCTION

Rock mediums are heterogeneous and anisotropy. Characteristics of rocks such as their structural features and mineralogical compound; dimension, shape and arrangement of grains, type of cement in sedimentary rocks, crystallization degree and weathering in magmatic rocks influence treatment of rocks.

The relationships between physical and mechanical properties of rocks have been a subject-matter for many studies having been conducted up to now in the literature [1]-[11]. One of the general objectives of these studies is to indirectly determine time-consuming, more costly and more difficultly assigned mechanical properties by means of more easily determined physical ones. [1] identifies the relationships between the engineering properties and petrographic features of granites having been collected from different regions. They propounded that the increasing quartz content of granite has significant effects on total porosity and dry unit weight. For them, when Quartz / feldspar ratio increases, the dry unit weight value increases, but the value of the total porosity reduces. [2] identifies negative exponential relationships between porosity and the uniaxial compressive strengths through the experimental studies he carried out on the marl and limestone samples from different areas. [7], by using ultrasonic velocity and porosity data, developed equations to estimate the uniaxial compressive strength of carbonate rocks such as limestone, travertine and onyx. In basalts with different weathering degrees, [8] investigated the relationships between united alteration index (UAI) and physical properties such as unit weight, water absorption, porosity and P wave velocity, mechanical properties like the uniaxial compressive strength and different chemical alteration indexes by regression analyses. [9], using axial and diametric point load strength tests and apparent porosity values on different rock types, have identified statistical equations to estimate the uniaxial compressive strength of rocks. [11] investigated if there is a significant relation between the porosity and point load strength index and tensile strength in rocks. As a result of the assessments, significant equations are suggested in indirectly estimating the point load strength index and tensile strength values by using the porosity values for different rock groups.

Having a significant impact on water conductivity of rocks, porosity also causes adverse effects on mechanical behaviours and engineering performances of rocks. Therefore, determining porosity in a healthy way in any engineering work to be carried out in rock environment is of great importance. The value of apparent porosity is widely used, since it can be achieved more easily in practical applications. However, this may lead us to erroneous assessments, for it does not take unrelated pores in the

¹ Corresponding author: Gümüşhane University, Department of Geological Engineering, 29000, Gümüşhane, Türkiye.
serhatdag@gumushane.edu.tr

rock into account. Therefore, this study aimed to investigate this situation and indirect estimation of porosity value considering the apparent porosity value. In this study, 200 cylindrical test samples, equally obtained from 5 different rock units outcropping in Gümüşhane (NE, Türkiye) province, which have characteristics of granite, andesite, limestone, sandstone and andesitic tuff, were used.

2 GEOLOGY OF THE STUDY AREA

Different rocks used in the study were from lithological units outcropping in Gümüşhane province and its vicinity (Figure 1). This area is located in South Zone of Pontide Tectonic Union [12] from Anatolian Tectonic Zones. In the study area, from Paleozoic to Eocene, units with different ages and litologies are observed (Figure 2).

Lithological characteristics of rocks used in experimental studies are presented briefly in the following paragraphs from older to younger.

Early-Late Carboniferous-aged granites are easily distinguished from surrounding rocks with regard to color tone and lithological variations. They are typical with pink colors in their fresh surfaces and whitish as a result of argillisations in their weathered surfaces along the cracks and generally with their coarse orthoses. The crystal size is approximately 5 mm and shows granular texture. As the main components of granites consist of quartz, alkali feldspar, amphibole, plagioclase and biotite, they contain chlorite and sericite as decomposition product. Late Jurassic-Early Cretaceous-aged Berdiga Formation begins with cherty limestone and gray-white colored, medium-thick, massive bedded limestones at the base [13]. Sandstones are exposed in Late Cretaceous-aged Kermutdere Formation. This formation is a volcano-sedimentary series. It begins, at the base, with green-brown colored, medium bedded, fine-medium grained sandstones and green colored, thin-medium layered marl, and both their colors and layer thicknesses often change. Formation ends with coarse-grained sandstones [14]. Tuffs located in Kermutdere Formation are andesitic character. This unit begins with base conglomerate and contains sandy limestones that include *Nummulites* fossils and limestones at its base level. The main body of Eocene aged Alibaba Formation is composed of andesite, basalt and their pyroclastics [15].

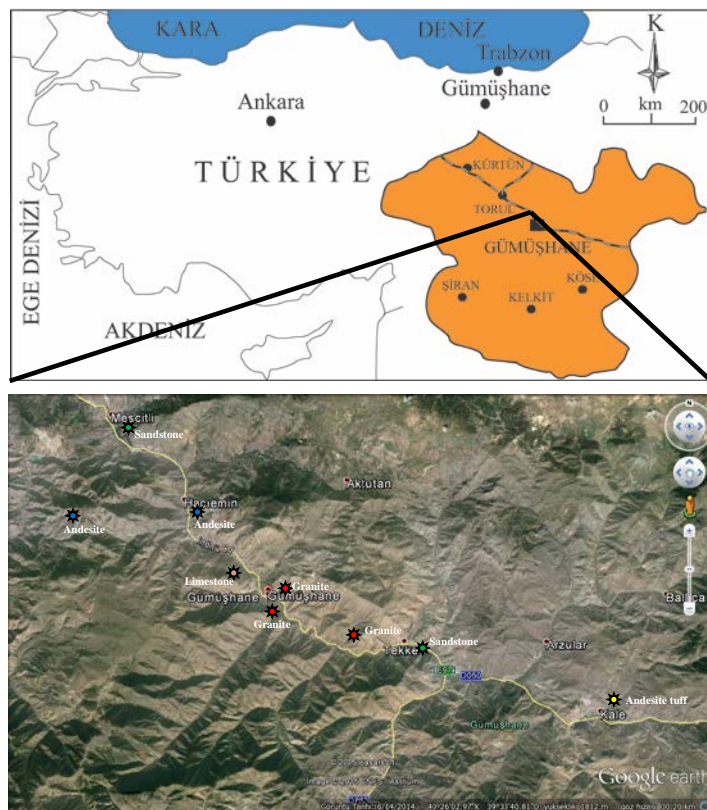


Figure 1. Location map of the study area

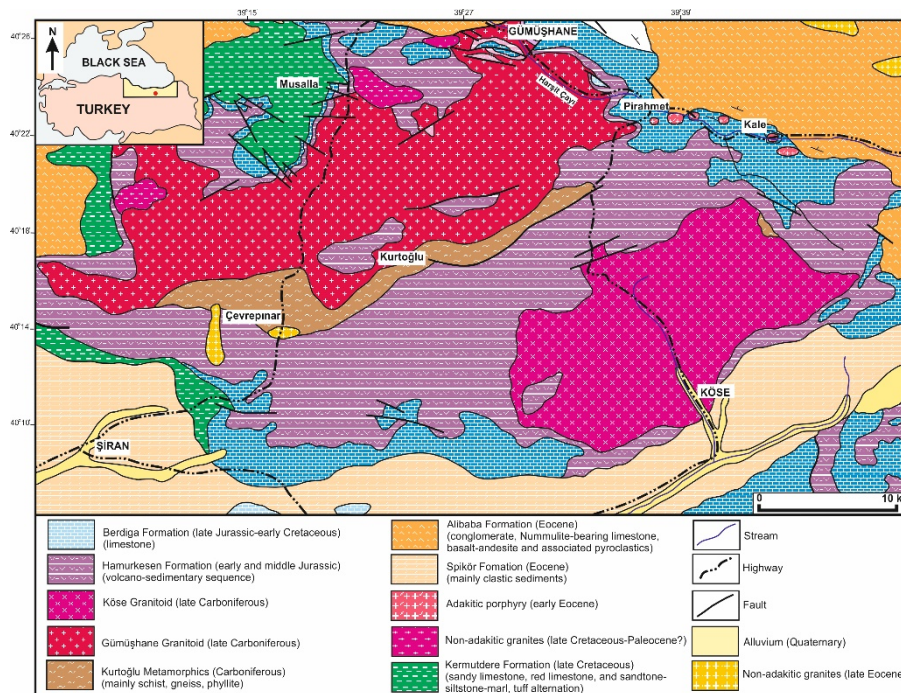


Figure 2. Geological map of Gümüşhane province and its surroundings [16]

3 LABORATORY STUDIES

To determine the physical and mechanical properties of the rocks which have different lithological characteristics outcropping in Gümüşhane province and its vicinity, field studies were carried out and block samples with approximate sizes of 20x30x40cm were taken. Later, considering the suggested method from ISRM [17], 200 cylindrical test samples are prepared in the laboratory out of these blocks. In this study, using experiment methods suggested by ISRM, physical features of rocks such as specific gravity, dry unit weight, saturated unit weight, water absorption weight, apparent porosity (water absorption in volume), porosity, void ratio, saturation degree were determined.

Firstly, these samples were saturated for 48 hours under laboratory conditions and then dried in the oven at 105 °C for 24 hours to remove the water in their pores. In this way, the apparent porosity values (n_{ap}) were obtained by considering their saturated and dry weight values. To determine the apparent porosity of samples, the following equations (1, 2) were used.

$$Vv = \frac{W_s - W_d}{g_w} \quad (1)$$

In this equation; Vv; void volume, Ws; saturated weight, Wd; dried weight, gw; density of water

Thus, void volume was calculated and then apparent porosity (n_{ap}) values were determined as following equation.

$$\%n_{ap} = \frac{Vv}{V} \times 100 \quad (2)$$

In this equation; n_{ap} ; apparent porosity, V; volume of sample

Besides, in this study, the specific gravity of each sample was determined after grinding. Next, the total porosities were determined by using dry densities and specific gravities of the test samples. The results related to physical properties of rocks are given in Table 1.

Table 1. Some physical properties of the studied rocks

Rock Type	Physical Properties	γ_{dry} (kN/m ³)	γ_{sat} (kN/m ³)	G_s	n (%)	n_{ap} (%)	e (%)	Sr (%)	Aw (%)
	N. Sample	40	40	40	40	40	40	40	40
Andesite	Maximum	26.4	26.7	2.73	6.93	6.75	7.44	68.10	2.68
	Minimum	24.9	25.5	2.64	2.53	2.48	2.60	5.96	0.88

	Average	25.8	26.2	2.69	4.40	4.31	4.63	43.71	1.68
	Std. D.	0.4	0.3	0.03	1.33	1.48	1.46	13.55	0.59
Granite	N. Sample	40	40	40	40	40	40	40	40
	Maximum	26.5	26.7	2.72	4.08	3.93	4.25	58.14	1.63
	Minimum	24.2	24.6	2.50	0.96	0.47	0.97	21.62	0.18
	Average	25.8	26.0	2.63	1.82	1.46	1.86	40.60	0.57
	Std. D.	0.5	0.5	0.04	0.81	0.76	0.85	9.46	0.31
Limestone	N. Sample	40	40	40	40	40	40	40	40
	Maximum	27.4	27.4	2.8	9.42	9.10	10.40	43.44	3.64
	Minimum	24.9	25.9	2.7	0.87	0.49	0.87	0.70	0.18
	Average	26.4	26.8	2.75	4.14	3.92	4.36	5.85	1.50
	Std. D.	0.6	0.4	0.02	1.95	2.00	2.16	10.64	0.80
Sandstone	N. Sample	40	40	40	40	40	40	40	40
	Maximum	26.5	26.8	2.73	9.85	9.80	10.93	66.48	4.1
	Minimum	23.5	24.3	2.54	2.04	1.77	2.08	40.58	0.68
	Average	25.1	25.6	2.65	5.41	5.15	5.79	50.99	2.09
	Std. D.	0.9	0.7	0.04	2.47	2.51	2.75	7.78	1.07
Andesitic tuff	N. Sample	40	40	40	40	40	40	40	40
	Maximum	22.1	23.0	2.53	15.96	15.85	19.00	65.31	7.51
	Minimum	19.6	21.0	2.28	9.04	8.71	8.71	39.49	4.01
	Average	20.6	21.8	2.36	12.64	12.49	14.52	51.42	6.09
	Std. D.	0.6	0.5	0.05	1.88	1.81	2.46	7.86	1.02

4 STATISTICAL ANALYSIS

Simple correlation investigates the degree, size and direction of the relation between two variables. As to simple regression, it is a statistical analysis which is utilized to calculate the value of one variable with the help of the other [18]. After determining the correlation coefficient, it should be tested to learn if it is significant or not. Two methods are used for this. In one of them, the correlation coefficient is tested in a certain level of significance and at n-2 degrees of freedom through the equation no (3) by using t test.

$$t = r \sqrt{\frac{n-2}{1-r^2}} \quad (3)$$

In this equation; t; t-test, n; number of sample and r; correlation coefficient.

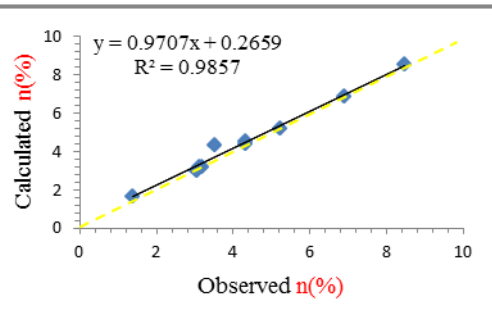
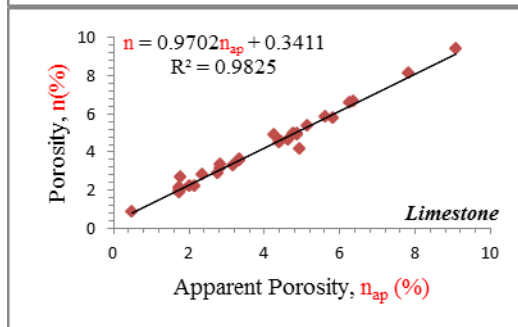
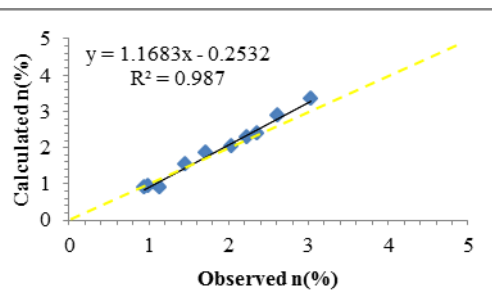
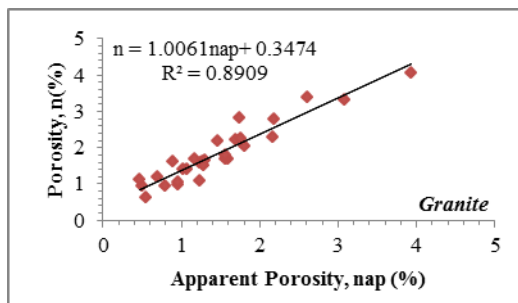
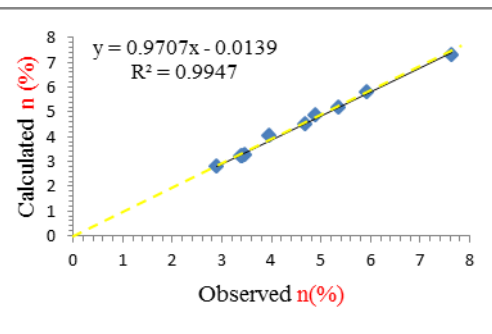
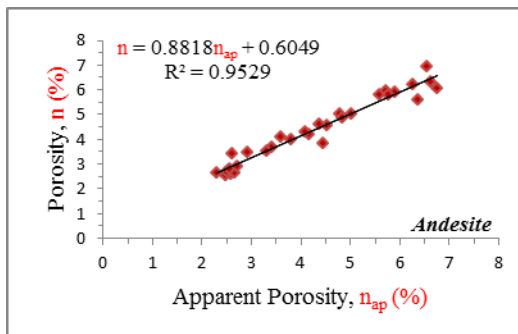
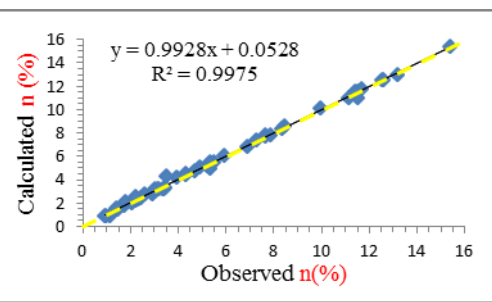
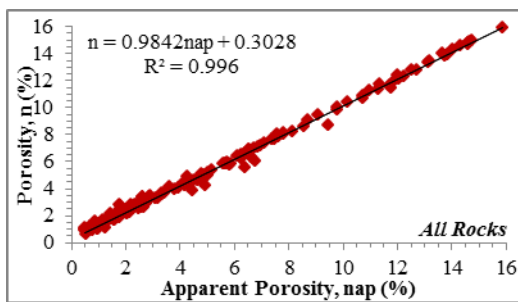
If the value obtained from the formula is larger than the value of t table, correlation coefficient is significant.

Another method is to compare correlation coefficient value (r) and critical r value of Pearson correlation coefficient. In this case, if the relation is significant, correlation coefficient having been determined for variables has to be greater than the critical r value [8,18].

In this study, simple regression analyses were performed to determine if there is a relationship between the apparent porosity (n_{ap}) and porosity (n) values of different rock types. A total of 150 samples, 30 from each group, were used in analyses and the results are given in Table 2.

Table 2. Result of simple regression analysis

Rock Type	Sample	Equation	R ²	r	Pearson Critical r	t Calculate	t Table
All Rock	150	$n = 0.9842n_{ap} + 0.3028$	0.996	0.998	0.196	55.94	1.98
Andesite	30	$n = 0.8818n_{ap} + 0.6049$	0.9529	0.976	0.361	23.82	2.04
Granite	30	$n = 1.0061n_{ap} + 0.3474$	0.8909	0.943	0.361	15.12	2.04
Limestone	30	$n = 0.9702n_{ap} + 0.3411$	0.9825	0.991	0.361	50.58	2.04
Sandstone	30	$n = 0.9797n_{ap} + 0.3673$	0.9974	0.999	0.361	110.83	2.04
Andesitic Tuff	30	$n = 1.0306n_{ap} - 0.2376$	0.9864	0.993	0.361	67.72	2.04



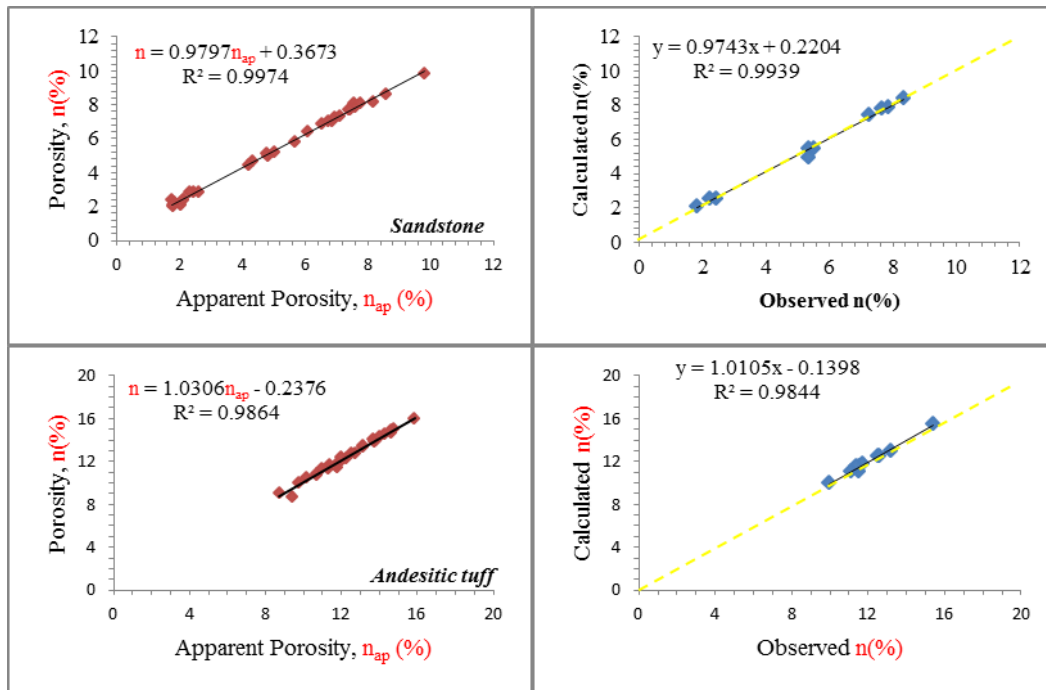


Figure 3. Statistical analysis about samples

5 CONCLUSIONS

Porosity causes adverse effects on mechanical behaviours and engineering performances of rocks. Therefore, determining porosity in a healthy way in any engineering work to be carried out in rock environment is of great importance.

The significance of correlation coefficients obtained from these analyses was tested by both using t-test and comparing it with the critical r values of Pearson correlation coefficient. For all determined coefficients, the value obtained from the formula was larger than the value of t table ($t_r > t_{table}$). Furthermore, all determined correlation coefficients were bigger than critical Pearson correlation coefficient value. This shows that correlation coefficients are significant.

In addition, 50 data randomly selected in the beginning among the samples of each rock group were excluded from analyses to be used to test the interoperability of equation derived from regression analysis. In doing this, porosity values obtained from test results and porosity values estimated from apparent porosity values were analysed as observed and calculated data. As a result of this analysis, it was determined that the data released a very strong positive relationship. In conclusion, the studied rock types showed no significant difference between porosity and apparent porosity values. Besides, using the specified equations in a healthy way, it is expected that the porosity values can be estimated indirectly benefiting from the apparent porosity values.

ACKNOWLEDGMENTS

Authors express their sincere thanks to the undergraduate students for their contributions during laboratory studies in the scope of this research.

REFERENCES

- [1] A. Tuğrul and I.H. Zarif, "Correlation of Mineralogical and Textural Characteristics with Engineering Properties of Selected Granitic Rocks From Turkey", *Engineering Geology*, vol. 51, pp. 303-317, 1999.
- [2] H. Yenice, "Bazı Kayaların Tek Eksenli Basınç Dayanımları ile Diğer Malzeme Özellikleri Arasındaki İlişkiler", *DEÜ Mühendislik Fakültesi Fen ve Mühendislik Dergisi*, Cilt 4, Sayı 2, s: 65-71, 2002.
- [3] H. Başarı, M. Kumral, and A. Özsan, "Kayaların Tek Eksenli Basınç Dayanımının Basit Deney Yöntemleriyle Tahmini", *KAYAMEK'2004-VII. Bölgesel Kaya Mekaniği Sempozyumu*, 2004, Sivas, Türkiye.
- [4] A. Teymen, "Bazı Kayaların Petrografik, Fiziksel ve Mekanik Özellikleri Arasındaki İlişkilerin İncelenmesi" Y.L. Tezi, Çukurova Üniversitesi, Fen Bilimleri Enstitüsü, Adana, Türkiye, 2005.
- [5] T.N. Singh and P.K. Sharma, "A Correlation Between P-wave Velocity, Impact Strength Index, Slake Durability Index and Uniaxial Compressive Strength". *Bulletin of Engineering Geology and the Environment*, vol.67, 1, pp. 17-22. 2008.
- [6] H. Ersoy, A. Özdemir, B. Yalçınalp, "Geology and Geotechnical Properties of Kalecik (Gümüşhane) Travertines". *Proceedings of the 21st International Mining Congress and Exhibition of Turkey, Antalya*, 2009, p. 639-648.

- [7] D. Kanık, “Karbonat Kayaların Tek Eksenli Basınç Dayanımlarının Basit İndeks Deneyle Kullanılarak Tahmini” Y.L. Tezi, KTÜ., Fen Bilimleri Enstitüsü, Trabzon, Türkiye, 2010.
- [8] S. Alemdağ ve Z. Gürocak “Üst Kretase Yaşlı Bazaltlarda (Trabzon/Türkiye) Birleşik Ayrışma İndeksi (UAI) İle Fiziksel, Mekanik ve Kimyasal Özellikler Arasındaki İlişkiler”, FU Mühendislik Bilimleri Dergisi , Cilt 23, Sayı 1, s:1-10, 2011.
- [9] K. Karaman ve A. Kesimal, “Kayaların Tek Eksenli Basınç Dayanımı Tahmininde Nokta Yüğü Deneyle Yöntemleri ve Porozitenin Değerlendirilmesi” Madencilik, Cilt 51, Sayı 4, s:3-14, 2012.
- [10] Z. Gürocak, P. Solanki, S. Alemdağ, M. Zaman, New Considerations for Empirical Estimation of Tensile Strength of Rocks” Engineering Geology, 145-146, pp. 1-8, 2012.
- [11] S. Dağ, S. Alemdağ, F. Alkan, “Kayalarda Gözeneklilik ile Dayanım Özellikleri Arasında Görgül İlişkilerin Araştırılması”, MÜHJEO’2015 Ulusal Mühendislik Jeolojisi Sempozyumu, Bildiriler Kitabı, s. 286-293, Trabzon, Türkiye, 2015.
- [12] İ. Ketin, “Türkiye’nin Tektonik Birlikleri”. MTA Dergisi, Cilt, 66, s:20-34, Ankara, 1966.
- [13] S. Pelin, “Alucra (Giresun) Güneydoğu Yöresinin Petrol Olanakları Bakımından Jeolojik İncelenmesi” KTÜ Yayını, No:87, Trabzon, 1977.
- [14] Ç. Saydam, “Doğu Pontidler’de Geç Kretase Yaşlı Kıvrımlı Çökellerin Sedimenter, Petrografik ve Organik Jeokimyasal Özellikleri”, Doktora Tezi, KTÜ, Fen Bilimleri Enstitüsü, Trabzon, Türkiye, 2002.
- [15] S. Tokel, “Stratigraphical and Volcanic History of the Gümüşhane Region, N.E. Turkey”, University College, London. 1972.
- [16] Y. Eyuboglu, M. Santosh, O.F. Dudas, E. Akaryalı, S. Chung, K. Akdağ, O. Bektaş, “The Nature of Transition From Adakitic to Non-Adakitic Magmatism in a Slab Window Setting: A Synthesis From The Eastern Pontides, NE Turkey”, Geoscience Frontiers, vol. 4,4 page: 353-375, 2013.
- [17] ISRM, *The Complete ISRM Suggested Methods for Rock Characterization, Testing and Monitoring: 1974-2006*. R. Ulusay and J.A. Hudson (eds.), *Suggested Methods Prepared by the Commission on Testing Methods, International Society for Rock Mechanics, Compilation Arranged by the ISRM Turkish National Group*, Kozan Ofset, Ankara, Turkey, 628 p. 2007.
- [18] N. Tüysüz, G. Yaylalı, G. Jeostatistik Kavramlar ve Bilgisayarlı Uygulamalar, 1. Baskı, K.T.Ü., Trabzon. 2005.

Bearing Capacity Determination of Soil/Foundation System for a School Building Based on a Detailed Site and Laboratory Investigation

Tufan Cakir¹, Serhat Dag²

Abstract

The topic of bearing capacity calculation has spawned extensive research and numerous methods of analysis. The factors affecting the bearing capacity of foundations generally incorporate the soil properties, foundation type, footing geometry/dimensions and the interaction between them. Furthermore, subsurface exploration is necessary in both selecting the type and depth of foundation suitable for a structure and evaluating the load-bearing capacity of the foundation. In this study, it is aimed to compute the bearing capacity of soil for construction of a six-story school building having a base area of 406 m². In line with this purpose, firstly, three boreholes were drilled to a total depth of 57 m in the field. Then, laboratory studies such as sieve analysis, liquid and plastic limit tests, direct shear tests were fulfilled on the soil samples taken from the boreholes. The soils were classified as GW-GC (well-graded gravel with clay and sand), GM-GC (silty, clayey gravel with sand), SM-SC (silty, clayey sand with gravel), SP (poorly graded sand with gravel), and SW (well-graded sand) by using Unified Soil Classification System. Internal friction angle and cohesion of soils vary between 26° and 34°, and between 2.1 kPa and 7.9 kPa, respectively. The liquid limit values of soils range from 20% to 30%, and the values of plastic limit range from 15% to 22%. Finally, depending on the variation of foundation type, footing dimensions, and embedment depth, bearing capacity of soils were computed by using Terzaghi and Vesic theories. The results obtained from the parametric analyses indicate that the bearing capacity can change remarkably due to the foundation type, footing dimensions and embedment depth.

Keywords: Bearing capacity, embedment depth, foundation type, subsurface exploration, Terzaghi and Vesic theories

1 INTRODUCTION

The soil/foundation must be capable of carrying the structural loads transmitted by any structure placed upon it without a shear failure and with the resulting settlements being tolerable for that structure. The structural loading and settlement of the foundation must be within the allowable limits for a safe foundation design. The most fundamental parameter that defines the interface between a shallow foundation and the soil that supports it is the *bearing pressure*. Shallow foundations transmit the applied structural loads to the near-surface soils. In the process of doing so, they induce both compressive and shear stresses in these soils. The magnitudes of these stresses depend largely on the bearing pressure and the size of the footing. If the bearing pressure is large enough, or the footing is small enough, the shear stresses may exceed the shear strength of the soil or rock, resulting in a bearing capacity failure [1]. Although the integral of the bearing pressure across the base area of a shallow foundation must be equal to the force acting between the foundation and the soil, this pressure is not necessarily distributed evenly. Analytical studies and field measurements indicate that the actual distribution depends on several factors, including eccentricity, magnitude of the applied moment, structural rigidity of the foundation, stress-strain properties of the soil and roughness of the bottom of the foundation [2],[3]. One must understand the relationship between bearing capacity, structural load, footing dimensions, foundation depth, and physical and mechanical soil properties in order to analyze foundations for bearing capacity failures and design them in a way to avoid such failures. To study these relationships, there are a variety of techniques, including a) evaluation of the performance of real foundations, incorporating full-scale load tests, b) load tests on model footings, c) limit equilibrium analyses, d) detailed stress analyses, such as finite element method (FEM) analyses in the literature. Limit equilibrium analyses are the dominant way to assess bearing capacity of shallow foundations. These analyses define the shape of the failure surface, and then evaluate the stresses and strength along this surface. Furthermore, they usually include empirical factors developed from model tests [1]. In this study, only limit equilibrium methods of bearing capacity analyses are taken into consideration, since these methods are used on the overwhelming majority of projects. Over the years, a number of limit equilibrium equations were proposed by researchers for determination bearing capacity of soils. One of the early sets of bearing capacity equations was proposed by Terzaghi [4]. Terzaghi's equations were produced from a slightly modified bearing capacity theory of Prandtl from using the theory of plasticity to analyze the punching of a rigid base into a softer (soil) material [5].

¹ Gümüşhane University, Department of Civil Engineering, 29100, Bağlarbaşı/Gümüşhane, Turkey. cakirtufan@hotmail.com

² Corresponding author: Gümüşhane University, Department of Geological Engineering, 29100, Bağlarbaşı/Gümüşhane, Turkey. serhatdag@gumushane.edu.tr

The topic of bearing capacity has spawned extensive research and numerous methods of analysis. Skempton [6], Meyerhof [7]-[8], Hansen [9]-[10], Debeer and Ladanyi [11], Vesic [12]-[13], and many others have contributed to this area. The Terzaghi equations, being the first proposed, have been very widely used. Because of their greater ease of use, they are still used—probably more than they should be. They are only suitable for a concentrically loaded footing on horizontal ground. They are not applicable for footings carrying a horizontal shear and/or a moment or for tilted bases [5]. Both the Meyerhof and Hansen methods are widely used. Moreover, the formula developed by Vesic is based on theoretical and experimental findings, and is an excellent alternative to Terzaghi. It produces more accurate bearing values and it applies to a much broader range of loading and geometry conditions. The primary disadvantage is its added complexity [1]. It is worth-emphasizing here that it is good practice to use at least two methods and compare the computed values of bearing capacity.

2 FIELD AND LABORATORY STUDIES

Subsurface exploration is necessary in both selecting the type and depth of foundation suitable for a structure and evaluating the load-bearing capacity of the foundation. The subsurface exploration comprises several steps, including the collection of preliminary information, reconnaissance and site investigation. The site investigation phase of the exploration program consists of planning, making test boreholes, and collecting soil samples at desired intervals for subsequent observation and laboratory tests [14]. In light of this information, three boreholes were drilled to a total depth of 57 m in the field. Then, soil samples obtained from the field were brought to laboratory for further classification and testing. Index tests, classification, shear strength tests (direct shear tests) were fulfilled on the soil samples taken from the boreholes to obtain physical and mechanical properties of soils. It was determined that from the ground surface to a depth of 12 ~ 13 m, the soil medium generally consist of gravelly sand with small amounts of fine-grained soil in the area of investigation. After a depth of 13 m, the medium is made of granite bedrock. The moist unit weight of soil was calculated between 17.9 kN/m³ and 20.1 kN/m³, the saturated unit weight of soil was computed between 20.3 kN/m³ and 21.3 kN/m³. The water content of soil was estimated between 8.1% and 11%. The liquid limit values of soils range from 20% to 30%, and the values of plastic limit range from 15% to 22% (see Table 1). The soils were classified as GW-GC (well-graded gravel with clay and sand), GM-GC (silty, clayey gravel with sand), SM-SC (silty, clayey sand with gravel), SP (poorly graded sand with gravel), and SW (well-graded sand) by using Unified Soil Classification System (see Table 1). As shown in Table 2, internal friction angle and cohesion of soils vary between 26° and 34°, and between 2.1 kPa and 7.9 kPa, respectively. It is prudent to design for the worst-case conditions, so nearly always the saturated strength is used when performing bearing capacity analyses, even if the soil is not currently saturated in the field [1]. For footings on saturated sands and gravels, any excess pore water pressures are very small and dissipate very rapidly. Therefore, effective cohesion and effective friction angle were determined in the direct shear tests. Furthermore, the position and movements of the groundwater table are of critical importance in foundation design. The presence of a water table near a foundation significantly affects the foundation's load bearing capacity and settlement, among other things. Therefore, subsurface investigations must include an evaluation of groundwater conditions. The design level should represent the worst groundwater level that is likely to occur during the design life of the project. It was observed in the investigation area that the groundwater level ranges from 8 m to 9.5 m.

Table 1. Laboratory test results

Boring information		Sieve analysis		Atterberg Limits			Classification by Unified Soil Classification System (USCS)
Borehole No	Depth (m)	Retained on No. 4 sieve (%)	Percent passing No. 200 sieve (%)	LL (%)	PL (%)	PI (%)	
BH-1	1.50-1.95	38.52	13.97	24	17	7	SM-SC
BH-1	3.00-3.45	22.45	23.29	27	22	5	SM
BH-1	4.50-4.95	47.23	11.05	30	21	9	GW-GC
BH-2	1.50-2.00	11.52	4.61	-	-	-	SW
BH-2	2.60-3.00	47.33	14.44	24	17	7	GM-GC
BH-2	3.00-3.45	25.47	17.47	20	15	5	SM-SC
BH-2	5.50-6.00	13.24	14.81	22	15	7	SM-SC
BH-2	6.50-7.00	46.91	4.48	-	-	-	SP
BH-3	1.50-1.95	27.91	20.26	24	17	7	SM-SC
BH-3	3.00-3.45	35.93	4.92	-	-	-	SP

Table 2. Calculated shear strength parameters along the depth from direct shear tests

Borehole No	Depth (m)	Cohesion (c) (kN/m ²)	Internal friction angle (ϕ) (degree)
BH-1	3-3.45	7.4	29
BH-1	4.5-4.95	4.2	34
BH-2	2.6-3	7.2	31
BH-2	3-3.45	7.9	28
BH-2	5.5-6	2.4	26
BH-2	6.5-7	2.1	30
BH-3	3-3.45	2.5	32

3 RESULTS AND DISCUSSIONS

In this section, bearing capacity evaluations are made with variation of the foundation type, foundation width, foundation depth and bearing capacity theories. In the analyses, Terzaghi and Vesic formulas were used for determination of bearing capacity of soils, and the results obtained were compared with each other. The theoretical bases and backgrounds of these formulas are well known and summarized in various studies, and need not be repeated herein. Table 3 and Table 4 report the values of allowable bearing capacity for strip foundations, by using Terzaghi and Vesic formulas, respectively. Terzaghi formula is valid only in case the depth of the foundation is less than or equal to its width. Therefore, as shown in Table 3, allowable bearing capacity values were not calculated in case the depth of foundation is larger than its width. The allowable bearing capacity is determined by dividing the ultimate bearing capacity by a factor of safety. The factor of safety was taken into consideration as 3 in the analyses. The bearing capacity was evaluated using the lowest values of unit weight and internal friction angle in case of the cohesionless soil conditions since the soil medium generally consists of gravelly sand. Furthermore, in order to remove the apparent cohesion effects and simulate to worst case condition, the bearing capacity was calculated in cohesionless soil conditions.

Table 3. Allowable bearing capacity values calculated by using Terzaghi formula for strip foundation

Foundation width (B) (m)	Foundation depth (D _i) (m)	Allowable bearing capacity (q _a) (kN/m ²)
1.00	1	67
	2	-
	3	-
	4	-
	5	-
	6	-
1.50	1	76
	2	-
	3	-
	4	-
	5	-
	6	-
2.00	1	85
	2	134
	3	-
	4	-
	5	-
	6	-
2.50	1	95

	2	143
	3	-
	4	-
	5	-
	6	-
3.00	1	104
	2	153
	3	201
	4	-
	5	-
	6	-
3.50	1	113
	2	162
	3	211
	4	-
	5	-
	6	-

Table 4. Allowable bearing capacity values calculated by using Vesic formula for strip foundation

Foundation width (B) (m)	Foundation depth (D _f) (m)	Allowable bearing capacity (q _a) (kN/m ²)
1.00	1	75
	2	131
	3	191
	4	251
	5	311
	6	371
1.50	1	81
	2	137
	3	196
	4	256
	5	316
	6	376
2.00	1	90
	2	149
	3	202
	4	261
	5	321
	6	381
2.50	1	100
	2	155
	3	209
	4	267
	5	327

	6	386
	1	109
	2	163
3.00	3	224
	4	274
	5	333
	6	392
	1	120
	2	171
3.50	3	230
	4	281
	5	339
	6	398

Tables 3 and 4 clearly indicate the effects of foundation width and depth on allowable bearing capacity. It is observed from these tables that as the foundation width and depth increases, the bearing capacity value tends to increase for all conditions. For example, according to the Terzaghi formula, while the allowable bearing capacity is estimated as 67 kN/m² for B = 1 m and D_f = 1 m, the same quantity is calculated as 113 kN/m² for B = 3.5 m and D_f = 1 m. It can be highlighted that foundation width affects the quantity so that the increment in the value is almost at a level of 69%. Similarly, according to the Vesic formula, while the allowable bearing capacity is estimated as 90 kN/m² for B = 2 m and D_f = 1 m, the same quantity is computed as 381 kN/m² for B = 2 m and D_f = 6 m. This reflects an increment of about 323% in bearing capacity value due to the variation of the foundation depth. If similar comparisons are made for the other conditions from Tables 3 and 4, a similar trend of an increase in the allowable bearing capacity value can be clearly seen. The most important point arising from these comparisons is that the variation of the foundation depth and width notably affects the bearing capacity of the soil/foundation system. This implies that amplification or reduction pattern is highly dependent on the values of foundation depth and width.

Similar evaluations can be done for mat foundation. Table 5 and Table 6 summarize the values of allowable bearing capacity for mat foundations, by using Terzaghi and Vesic formulas, respectively. Effects of the foundation depth on the allowable bearing capacity can also be clearly observed from these tables. For example, according to the Terzaghi formula, the value of bearing capacity is 321 kN/m² for B = 17.5 m and D_f = 1 m, whereas the same value is estimated as 565 kN/m² for B = 17.5 m and D_f = 6 m. It is obvious that increase in the foundation depth value leads to the increment in bearing capacity value. Similar comparisons can be performed from Table 6.

Table 5. Allowable bearing capacity values calculated by using Terzaghi formula for mat foundation

Foundation width (B) (m)	Foundation depth (D _f) (m)	Allowable bearing capacity (q _a) (kN/m ²)
	1	321
	2	370
17.50	3	419
	4	468
	5	517
	6	565

Table 6. Allowable bearing capacity values calculated by using Vesic formula for mat foundation

Foundation width (B) (m)	Foundation depth (D _f) (m)	Allowable bearing capacity (q _a) (kN/m ²)
17.50	1	320
	2	378
	3	439
	4	501
	5	566
	6	632

4 CONCLUSIONS

In this study, it was aimed to conduct a series of bearing capacity analyses for construction of a six-story school building having a base area of 406 m². (17.50 m x 23.20 m). The subsurface exploration was carried out to determine the locations and thicknesses of the soil strata, to select the type and depth of foundation suitable for a given structure, to determine the location of the groundwater table as well as any other groundwater-related characteristics, and to define potential foundation problems. Three boreholes were drilled to a total depth of 57 m in the field. Several routine tests including water content, unit weight, Atterberg limits, grain-size distribution, and shear strength were fulfilled on many of the samples taken from the boreholes along the depth to ascertain the general characteristics of the soil profile.

Limit equilibrium analyses are the dominant way to assess bearing capacity of shallow foundations. In this connection, depending on the variation of foundation type, foundation width and foundation depth, a series of bearing capacity analyses were conducted by using the Terzaghi and Vesic bearing capacity equations. It was concluded that the bearing capacity of foundation/soil system is quite sensitive the soil properties underlying the foundation, location of the groundwater table, footing dimensions, foundation type, and foundation depth. Therefore, the wrong determination of the parameters above-stated may cause underestimation or overestimation of the bearing capacity, and this, in turn, may lead to unsafe or uneconomical design of foundations. These evaluations should be considered as an alert that especially both the soil properties and foundation characteristics are of paramount importance, and thus should be measured with utmost care.

It is good practice to use at least two methods and compare the computed values of allowable bearing capacity. However, there are several advantages and disadvantages of the bearing capacity theories to each other. It is recommended that more numerical examples should be analyzed by using the other bearing capacity equations before generalization could be made.

REFERENCES

- [1] D.P. Coduto, *Foundation Design: Principles and Practices*, 2nd. ed., Prentice Hall, Upper Saddle River, New Jersey, 2001.
- [2] E. Schultze, "Distribution of stress beneath a rigid foundation," in *Proc.*, 5th International Conference on Soil Mechanics and Foundation Engineering, 1961, pp. 807-813, Paris.
- [3] J.P. Dempsey and H. Li, "A rigid rectangular footing on an elastic layer," *Geotechnique*, vol. 39(1), pp. 147-152, 1989.
- [4] K. Terzaghi, *Theoretical Soil Mechanics*, John Wiley, New York, 1943.
- [5] J.E. Bowles, *Foundation Analysis and Design*, 5th ed., McGraw-Hill, New York, 1996.
- [6] A.W. Skempton, "The bearing capacity of clays," in *Proc.*, Building Research Congress, 1951, vol. 1, pp. 180-189, London.
- [7] G.G. Meyerhof, "The ultimate bearing capacity of foundations", *Geotechnique*, vol. 1(1), pp. 301-331, 1951.
- [8] G.G. Meyerhof, "Some recent research on the bearing capacity of foundations," *Canadian Geotechnical Journal*, vol. 1(1), pp. 16-26, 1963.
- [9] J.B. Hansen, "A general formula for bearing capacity," Bulletin No.11, Danish Geotechnical Institute, Copenhagen, 1961.
- [10] J.B. Hansen, "A revised and extended formula for bearing capacity," Bulletin No.28, Danish Geotechnical Institute, Copenhagen, 1970.
- [11] E.E. DeBeer and B. Ladanyi, "Experimental study of the bearing capacity of sand under circular foundations resting on the surface," in *Proc.*, 5th International Conference on Soil Mechanics and Foundation Engineering, 1961, vol. 1, pp. 577-585, Paris.
- [12] A.S. Vesic, "Analysis of ultimate loads of shallow foundations," *ASCE Journal of the Soil Mechanics and Foundations Division*, vol. 99(SM1), pp. 45-73, 1973.
- [13] A.S. Vesic, *Bearing Capacity of Shallow Foundations*, First edition, Foundation Engineering Handbook, Newyork, pp. 121-147, 1975.
- [14] B.M. Das, *Principles of Foundation Engineering*, 7th edition, Cengage Learning, USA, 2011.

Developing a QFD Methodology to Increase Customer Satisfaction in Public Transport Companies

Muhammet Deveci¹, Fatih Canitez², Nihan Cetin Demirel³

Abstract

As understanding people's expectations from public transport services and providing a people-centered mobility become more and more indispensable for liveable cities; the need for passenger-oriented service improvement methods also becomes necessary for public transport sector. With the implementation of Quality Function Deployment (QFD) methodology, IETT, the public bus operator and authority of Istanbul, is currently able to translate passenger expectations into service quality characteristics for every category of process development. Both the strategic plan which gives direction to IETT about strategies and policies and Integrated Management System (IMS) necessitate the implementation of such a customer-oriented approach for continuous service improvement. Since effectively and immediately responding to passenger demands is the guiding principle of IETT, QFD methodology is the most efficient way to enable that the expectations of passengers are rightly taken into consideration when providing public transport services. QFD methodology provides a priority list of passenger demands and technical requirements so that the necessary actions are taken according to this list, ensuring minimum cost while providing what the passengers exactly need.

Keywords: Quality function deployment (QFD), Public transport, Customer satisfaction.

1 INTRODUCTION

Quality Function Deployment (QFD) was developed in Kobe Shipyard of Mitsubishi in 1972. The method was used firstly in the USA by Ford and Xerox companies in 1986 [1]. QFD is a quality system assuring the customers' satisfaction within the scope of total quality management [2]. Basically, Quality Function Deployment aims better products with more relevant cost. Also, the number of the complaints arising from engineering changes, design process, start-up costs and product are decreased on a large scale with the help of this method [3, 4]. Quality House is a matrix consisting of six sections. Sections in this matrix are like this [5]: (1) Voice of customer, (2) Technical Characteristics, (3) Planning matrix, (4) Relation matrix, (5) Correlation matrix, (6) Technical Priorities, Sorting, Comparisons and Targets.

2 APPLICATION OF QFD IN PUBLIC TRANSPORT SERVICES

2.1 The Aim of the Study

Maintaining a customer oriented service concept is one of the most basic elements for IETT to achieve the principles specified within the scope of integrated management system which the corporation put into practice and the strategic goals specified in strategic plans. Customer orientation becomes possible by improving the current service quality continuously. With the project of Quality Function Deployment (QFD), it is determined how much improvement needs to be made in which topics in order to specify the expectations of people of Istanbul, as known as "voice of customer" according to QFD, turn them into service design features for IETT by using Quality House approach and meet these expectations. With this study, we will have the opportunity to determine in which fields we need more urgent improvements quantitatively to meet the customers' demands and expectations more effectively. Target of the study is specified as follows:

¹*Yildiz Technical University, Department of Industrial Engineering, 34349, Besiktas/Istanbul, Turkey.*

muhammetdeveci@gmail.com

²*Corresponding author: IETT, Public Transport Company in Istanbul, Manager of Business Intelligence and Project Management Department, Istanbul, Turkey,*

fatihcanitez40@gmail.com

³*Yildiz Technical University, Department of Industrial Engineering, 34349, Besiktas/Istanbul, Turkey.*

nihan@yildiz.edu.tr

- (1) To organize the public transport services while satisfying the mobility needs by including the customers' expectations «before they become demands» in corporate processes
- (2) To present a fast, impeccable, customer expectation-and-demands-oriented service deployment process
- (3) To reduce the expenditures spent on inefficient fields, because most of the sources will be spent to carry out the expectations which the customers attach more importance.

2.2 General Information About The Company

IETT is a public enterprise that provides urban public transport services. Because IETT has 24 % of all of the passenger transportation and 57 % of public transport, it is integrated with the daily life of people of İstanbul and has a corporate culture with its more-than-130-year history. Road network of IETT is up to 1250 km and total route length is up to 6100 km. Its fleet containing more than 2500 buses covers more than about 420.000 km every day [6].

Primary duty of IETT is to provide a reliable, comfortable and accessible public transport service for people of İstanbul. Therefore, it is very important to observe the customers' expectations continuously and improve the service quality with it. Customer orientation is to shape the attempts from the design of the service to the delivery of service and marketing in line with the customers' demands, needs and choices.

2.3 Study Methodology and Data Acquisition

The mission of IETT is specified as "Organising the public transport services to satisfy the mobility needs". Stages of QFD practice that is one of the innovator practices performed to fulfill this mission are designed to reach this ultimate goal. The steps performed and the method used within the scope of the practice can be specified as follows:

- (1) Customers' expectations were specified with the help of Passenger Satisfaction Survey.
- (2) Passenger Satisfaction Levels were analysed.
- (3) Related technical specifications were specified to satisfy the passengers' expectations.
- (4) Relationship levels between passengers' expectations and technical specifications were specified.
- (5) Absolute and relative significance values of the technical specifications were calculated.
- (6) Relationships between technical specifications were specified and correlation matrix was made.
- (7) The most critical technical specifications were specified. Improvement fields were determined and related units were enabled to take action.

Data needed in the practise was acquired in two different ways. Firstly, 2015 "Customer Satisfaction Survey" results were used to determine what the passenger expects from the public transport management or forecast it. Customer significance level of each demand and expectation on 10-scale by using the rate part where the passengers expect from IETT were determined. So, the expectations were collected by many passengers under 8 titles: (1) Availability, (2) Accessibility, (3) Informing, (4) Timing, (5) Staff, (6) Environment, (7) Comfort and (8) Safety.

Technical values needed to be determined to acquire the data that are essential to the study in the second step. To do this, data were requested from related units in IETT and it was added to the study in order to determine the value in the quality matrix.

2.4 Application

After making the analyses of the data to be used in the study, we continued to carry out the project according to QFD steps mentioned at the previous section.

2.4.1 Determination of Customers' Expectations

2015 Customer Satisfaction Survey of IETT was used to specify the customers' expectations. We sorted and categorised all of the customers' expectations in the voice of customer part of the quality house.

Table 1. Significance level of the customers in the quality house

Type	Voice of Customer	CUSTOMER SIGNIFICANCE LEVEL	RELATIVE WEIGHT %
Availability/5	Transitions at transfer points should be easy.	1	0.6
	Transport fees should be cheap.	8	6
Accessibility/ 4	Vehicles should be expedient to disabled citizens.	7	6.8
	Stops should be expedient to disabled citizens.	7	6.3
	Access distance to buses and stops should be short.	4	2.6
	Istanbul card should be provided easily.	2	1.3
	Istanbul card/akbil should be loaded easily.	2	1.2
Informing / 2	Website informing should be clear, understandable and updated.	2	1.2
	Informing in the stops should be clear, updated and informative.	3	2
	In and out-vehicle informing should be clear, understandable and informative.	3	2.1
	Responses to demands and complaints should be fast and problems should be solved.	2	1.8
	Call center should be quickly accessible and responds should be fast.	2	1.3
Timing / 7	Vehicles should come to stops at the right time.	8	6.8
	Vehicles should leave the stops at the right time.	8	6.2
	Waiting time at the stops should be short.	10	9
	Vehicles should go to the places at the right time.	1	0.7
Staff / 6	Drivers and officers should be informed and interested.	5	3.9
	Drivers and officers should be polite to the passengers.	6	4.7
	Drivers should drive the vehicle carefully without disturbing the passengers.	6	4.7
Environment / 1	Gas emission of the vehicles should be low.	1	0.8
	Noise of the vehicles should be low.	1	0.7
Comfort / 5	Vehicles should not be crowded.	9	8.7
	In-vehicle equipment should be durable and practicable.	1	0.7
	Sitting areas should be enough in the vehicles.	5	3.8
	Ventilation systems in the vehicles should be running.	5	4.1
	Interior of the vehicles should be clean.	4	2.8
	Outer of the vehicles should be clean.	4	2.8
Safety / 3	Lost properties should be found easily.	1	0.7
	Vehicles should be safe.	4	2.8
	Stops should be safe.	4	2.9

We specified the customer significance level belonging to each expectation by considering how many passengers demand each expectation to be met. Thus, a part of Quality House was created.

2.4.2 Customer Satisfaction Levels Analysis

The values belonging to the following titles were specified in part B of the quality house:

- a. Current Service Success: It was calculated by considering the customer satisfaction rates in Customer Satisfaction Survey and valued between 1 and 10.
- b. Targeted Service Success: Its values were specified by considering how open to improvement every expectation is.
- c. Improvement Rate: It was calculated with this formula, $(\text{Targeted Service Success} - \text{Current Service Success}) * 0.1 + 1$. Improvement Rate for every customers' expectation was between 1 and 1.5.
- d. Effect on Customer Satisfaction: It was valued between 1 and 1.5 in order to show that unit improvement for every expectation has how much effect on customer satisfaction.
- e. Total Weight : It is the total weight measure of every expectation calculated with this formula, $(\text{Customer Significance Level} * \text{Improvement Rate} * \text{Effect on Customer Satisfaction})$
- f. Total Percentage: It is the measure of calculated total weights in percentage.

Received results belonging to these values are given in the following Table 2.

Table 2. Customer satisfaction levels

Current Service Success	Targeted Service Success	Improvement Rate	Effect on Customer Satisfaction	Absolute Weight
6	7	1.1	1	1.139
3	3	1	1.4	11.143
2	5	1.3	1.4	12.675
2	4	1.2	1.4	11.7
7	8	1.1	1.1	4.871
7	9	1.2	1	2.486
8	9	1.1	1	2.2
8	9	1.1	1	2.2
5	6	1.1	1.1	3.771
6	8	1.2	1.1	3.986
2	6	1.4	1.2	3.4
4	5	1.1	1.1	2.514
5	7	1.2	1.3	12.686
5	6	1.1	1.3	11.629
5	7	1.2	1.4	16.714
5	7	1.2	1.1	1.286
5	7	1.2	1.2	7.286
6	8	1.2	1.2	8.743
6	8	1.2	1.2	8.743
3	6	1.3	1.1	1.486
3	5	1.2	1.1	1.371
1	3	1.2	1.5	16.2
3	4	1.1	1.1	1.257
3	4	1.1	1.3	7.071

3	5	1.2	1.3	7.714
5	6	1.1	1.2	5.186
5	6	1.1	1.2	5.186
3	4	1.1	1.1	1.257
5	6	1.1	1.2	5.186
4	5	1.1	1.2	5.343

2.4.3 Determination of Technical Specifications

Part C of Quality House means that opinions of the customer is turned into technical needs. The point to take into consideration while specifying the technical needs should not be to find direct solutions to determined customer requests. The goal is to turn every opinion into one or more technical needs. For this purpose, technical specifications we specified for IETT were sorted in the following: (1) Stop, (2) Accessibility, (3) Informing, (4) Equipment / Cleaning, (5) Planning, (6) Environment, (7) Istanbul Card and Akbil and (8) Other.

Subtitles of the technical specifications we specified are categorised as in Table 3:

Table 3. Categorisation of technical specifications

Stop	Accessibility		Informing	
D i s t a n c e B e t w e e n S t o p s S m a r t S t o p S t o p R a t e A V L - S t o p T i m e C o n t r o l 	L o w F l o o r e d V e h i c l e R a t e 	M o t h e r C h i l d H a n d i c a p A r e a S t e p l e s S e a t 	I n - V e h i c l e I n f o r m a t i o n S c r e e n A u d i b l e A f f i r m a t i o n S y s t e m C u r r e n c e o f I n f o r m a t i o n I n f o r m a t i o n S o f t w a r e C l i c k 	C R M W e b s i t e N u m b e r o f C o m p l a i n t s W e b s i t e T o t a l C l i c k R e q u e s t / C o m p l a i n t C e n t r e R e q u e s t / C o m p l a i n t R o u t e S i g n s C o m p l a i n t E - M a i l
Equipment/ Cleaning	Planning	Environment	Istanbul Card and Akbil	Other

Air Circuits / Fairs	Distance Between Seats	Cleaning Interval of the Vehicles	AVL Time of Arrival System Break down Points	Compliance with Euro Standards	Travel Card Application Centers	Instant Card Top-Up Center	Fare Properly / Lost Property	Driver Staff Training Hours
----------------------------	------------------------------	--	---	---	--	-------------------------------------	--	--------------------------------------

2.4.4 Specification of Relationships and Correlation Matrix

While specifying the relationship between customers' demands and technical specifications, this transaction is started by asking the question that every cell of the matrix affects "what" and "how". We valued 9 for strong relationships, 3 for normal relationships and 1 for weak relationships. Thus, we filled part D of Quality House.

2.4.5 Calculation of Absolute and Percentage Significance Values of Technical Specifications

We found it by multiplying relationship values in the technical specification column by customers' expectations for each technical specification. Technical needs with higher absolute significance level are dwelled on more. Technical specifications are sorted according to their relative significance levels in Table 4.

Table 4. Absolute and relative significance values of technical specifications

Calculation of Absolute and Relative Values of Technical Specifications	ABSOLUTE SIGNIFICANCE LEVEL	RELATIVE SIGNIFICANCE LEVEL (%)
---	-----------------------------------	---------------------------------------

Stop	Smart Stop	345.07	12.55
Planning	Scheduling	321.69	11.7
Other	Driver Staff Training Hours	222.943	8.11
Informing	In-Vehicle Informing Screen	153.72	5.59
Informing	Audible Announce System	149.95	5.45
Stop	Stop Time Control	121.37	4.41
Planning	AVL Fleet Command System	114.17	4.15
Accessibility	Low Floored Vehicle Rate	114.08	4.15
Accessibility	In-Vehicle Handicap Area	114.08	4.15
Accessibility	Mother Child Handicap Area	114.08	4.15
Accessibility	Stepless Seat	114.08	4.15
Other	Fares	100.29	3.65
Equipment/Cleaning	Cleaning Interval of the Vehicles	93.34	3.39
Equipment/Cleaning	Air Conditioner/Radiator	80.74	2.94
Equipment/Cleaning	Distance Between Seats	63.64	2.31
Planning	AVL-Estimated Time of Arrival At Breaking Points	61.71	2.24
Equipment/Cleaning	Camera	57.99	2.11
Stop	Distance Between Stops	54.1	1.97
Informing	Call Center Request/Complaint	53.23	1.94
Stop	Covered Stop Rate	48.09	1.75
Informing	SMS Informing	35.87	1.3
Informing	Currency of the Information	31.76	1.15
Informing	Request/Complaint via E-Mail	30.6	1.11
Istanbul Card and Akbil	Card Distribution Channels	22.37	0.81
Istanbul Card and Akbil	Travel Card Application Centers	22.37	0.81
Informing	Website Total Click	19.8	0.72
Istanbul Card and Akbil	AVM	19.8	0.72
Istanbul Card and Akbil	Istanbul Card Top-Up Center	19.8	0.72
Environment	Compliance with Euro Standard	13.37	0.49
Environment	Compliance with 2007/34 Standard	12.34	0.45
Informing	Route Signs	11.96	0.43
Other	Found Property/Lost Property	11.31	0.41

2.4.6 Determination of Relationship Between Technical Specifications and Correlations

Part E of the quality house is the part where relationships between technical specifications are determined. We marked the relationship with (+) if an improvement of any technical specification causes another technical specification to improve and marked it with (-) if it causes it to decrease.

Table 5. Relationships between Technical Specifications and Correlation

Relationships Between Technical Specifications and Correlation		Current Technical Values
Stop	Distance Between Stops	535 m.
	Smart Stop	757
	Covered Stop Rate	4057
	AVL-Stop Time Control	31 secs.
Accessibility	Low Floored Vehicle Rate	1478
	In-Vehicle Handicap Area	Except IKARUS (901 vehicles) avg. 7 seats
	Mother Child Handicap Area	Except IKARUS (901 vehicles) avg. 7 seats
	Stepless Seat	At least 6 seats
Informing	In-Vehicle Informing Screen	Vehicles except IKARUS and MAN (1477 vehicles)
	Audible Announce System	Vehicles except IKARUS and MAN (1477 vehicles)
	Currency of the Information	Daily Update
	SMS Informing	Monthly 58.115
	Website Total Click	71002
	Call Center Request/Complaint	Monthly Avg. 27.969
	Request/Complaint via E-Mail	Monthly Avg. 8.880
Equipment/ Cleaning	Air Conditioner/Radiator	Vehicles except IKARUS and MAN (1477 vehicles)
	Camera	CAPACITY (250 vehicles) and CITARO (100 vehicles)
	Distance Between Seats	-
	Cleaning Interval of the Vehicles	Once a day
Planning	AVL-Estimated Time of Arrival at Breaking Points	Different for every route and not all of the route data.
	AVL Fleet Command System	Movement Description Rate= %88
	Scheduling	-
Environment	Compliance with Euro Standard	124 vehicles
	Compliance with 2007/34 Standard	124 vehicles
Istanbul Card and Akbil	Card Distribution Channels	3
	Travel Card Application Centers	12
	AVM	190
	Istanbul Card Top-Up Center	1500 Active Centers
Other	Fares	Adult 1.75 TL, Student 1.00 TL, Teacher 1.10 TL
	Found Property/Lost Property	%7.11
	Driver Staff Training Hours	11 Hours per Year for Each Driver Staff

2.4.7 Determination of Target Values

Part F of the Quality House is the part where current technical values and targeted technical values are determined. After filling all of the other parts of the Quality House, the goal is set by considering significance level of every technical

specification, relationships between technical specifications and technical specification values of rival companies if there are any. Since there are not any rival companies in our position, we decided it by considering technical specification target values, significance level of the technical specifications and relationship between them.

3 STUDY ANALYSIS AND RESULTS

As a result of the study, 3 most critical customers' expectations are as follows. These three passengers' expectations constitute 32,3% relative significance level of total expectations.

(1) Waiting time at the stops should be short, (2) Vehicles should not be crowded, and (3) Vehicles should come to the stops at the right time.

3 critical technical specifications that are directly related with 3 most critical passengers' expectations are as follows: (1) Smart Stop, (2) Scheduling, and (3) Driver Staff Training

As a result of the studies carried out, 3 actions to be taken in response to 3 most critical technical specifications are as follows: (1) 757 current smart stops (6.9%) should be increased up to 10% as soon as possible, (2) Scheduling should be adjusted by reducing the waiting times to minimum, and (3) Driver staff training hours (11 hours per year/driver staff) should be increased or current training should become more effective. These actions have been found out to be connected with timing, informing and main staff criteria. In the following table, actions which every unit in the corporation needs to take are listed and categorised according to their significance levels. At this stage, the negations specified with QFD study need to be removed by working with in-house administrative units coordinately.

4 CONCLUSIONS AND SUGGESTIONS

In public transportation, it is necessary to select the optimal transit fare increase for both the passengers and the institution providing the public transportation service. In an attempt to realize this, not only the passenger satisfaction about the transit fare must be ensured, but also the costs of this service for the provider must be met. On the other hand, while providing a fair distribution between different transit fare categories, the rate of increase of the inflation rate, fuel prices and labor/driver costs must not be exceeded. It is possible to carry out this optimal transit fare selection process defined by all of these criteria through the AHP method. With the applied AHP method the second proposal was accepted, and was implemented after Transportation Coordination Committee's approval, which is responsible for fare setting in Istanbul. With this study, a more rational decision making method to determine the transit fare increase rate in public transportation has been revealed. Having a standard method to determine transit fares changes peoples' perception about transit fare setting in a positive way. Communicating this methodology with people also leads them to think that transit fares are not determined in an ad hoc and random way, but in a rigorous and sound method.

With QFD study, opinions of the passengers were added to corporate processes of IETT. Thus, passengers' requests and needs are given primacy in the design of public transport service. A customer oriented, fast and impeccable development process can be produced in the service design. Convergent technical specifications and needs were determined at pre-servicing stages. An important step was taken about carrying out service delivery and satisfying the passengers' expectations in a shorter period of time.

Since we know to which technical specifications we need to give priority, we will be able to take action about both reducing the costs and getting maximum performance in service delivery and process design. Because we spend our resources to satisfy the expectations our passengers care most, we will reduce the cost spent to unnecessary fields. In the study done, the expectations about timing and vehicle density like "Waiting time at the stops should be short", "Vehicles should come to the stops at the right time" and "Vehicles should not be crowded" are the expectations with the highest priority. Technical specifications developed to satisfy these and other expectations like "Smart Stop", "Scheduling" and "Driver Staff Training" are the technical specifications with the highest priority level and are needed to be improved primarily.

About timing, smart stop project that shows how long the passengers have to wait at the stop is needed to be put into practice at all stops right away. In addition to this, an optimum scheduling to be done according to passenger density is critical in order to satisfy the timing expectation of the passenger. Another prominent technical specification is to increase the hours of training for the drivers. Passengers' expectations that the drivers are well-informed and polite and driving the vehicle carefully increased the importance and priority of this technical specification. Organizing the training of drivers to satisfy the passengers' expectations and increasing the training hours are the primary actions to be taken to this end.

REFERENCES

- [1] E. Doğu and B. Özgürel, A study about analysing of technique characteristics of insurance companies which market individual pension systems with QFD. *Dokuz Eylül Üniversitesi İşletme Fakültesi Dergisi*, 9(1), 2008.
- [2] R. E. Zultner, "TQM for Technical Teams", *CACM* 10 (October):79-91, 1993.

- [3] Y. Taptık and Ö. Keles, Kalite Savas Araçları, Kal-Der Yayınları No:23-Istanbul, 1998.
- [4] G.H. Mazur, Voice of the Customer (Define): QFD to Define Value. Proceedings of the 57th American Quality Congress. Kansas City: 1-7, 2003.
- [5] L. Cohen, Quality Function Deployment How to Make QFD Work for You. Addison Wesley Longman, 1995.
- [6] <http://ibb.gov.tr/>

Setting the Optimal Transit Fare in Public Transportation by Using Analytical Hierarchy Process (AHP): The Case of IETT, Istanbul

Muhammet Deveci¹, Fatih Canitez², Nihan Cetin Demirel³

Abstract

Setting the optimal fare in public transportation is an important issue not just for passengers but also for public transport providers. The objective should be ensuring both the user satisfaction and sustaining the financial balance of the public transit agencies at the same time. This paper examines the process of specifying the optimal fare by utilizing Analytical Hierarchy Process (AHP) methodology in IETT, the public transport authority and operator of Istanbul. AHP is used to provide a through and robust framework for this decision problem by determining and quantifying the elements of this problem and connecting them with the overall objective of an optimal fare selection. In other words, this technique is used to structure the decision hierarchy and quantifying the effect of decision factors on optimal fare. A public transport authority takes into account a number of criteria when deciding on the transit fares. While these criteria are mainly the passenger satisfaction and financial balance of the transit provider, the constraints primarily include inflation rate, labor costs (drivers, administrative staff, maintenance staff etc.) and fuel costs. In this paper, how to implement AHP methodology step by step in deciding on optimal transit fare in public transportation is analyzed and supported with a case example.

Keywords: Public transportation, Optimal transit fares, Analytical hierarchy process (AHP), Decision making.

1 INTRODUCTION

Public transportation provides significant opportunities such as providing mobility in the city and making city life easier as well as reducing the level of environmental pollution as a result of private car use. Therefore, achieving these benefits expected from the public transportation services first and foremost relies on providing these kind of services in an efficient manner. Determining the transit fare for public transportation is one of the most important parameters of these services.

The approach employed for setting transit fares in public transit services is an important factor that ultimately affects urban sustainability in economic, social and environmental aspects. The goals sought to be realized by the implemented pricing policy is of vital importance. These objectives can be divided into 5 groups as follows [1]:

1. To increase the level of public transportation use
2. To increase the journey income of the public transit company
3. To minimize the reaction that will be formed against the new fares
4. To create a fair, affordable transit fare for users
5. To meet the costs of public transportation

When determining transit fare, some of the goals set above stands out more from the others. For example, in the study conducted by Beasley and Grimsey on public transit companies, it is seen that while economic goals such as making profits and reducing costs stand out, social goals such as reducing environmental pollution and traffic jams remain in the background [2]. Just like the many other cities in the world, public transportation is financed through local budget revenues in Istanbul. Positive externalities, such as providing mobility in the city, facilitating access to opportunities about employment and education and developing sustainable urban structure, have a significant effect in financing public transportation services this way [3].

There is a need for a solid methodology for determining transit fares on public transportation in an optimal way. This methodology should include certain criteria when choosing the most appropriate transit fare and their relative significance and the selection of the most appropriate alternative transit fare proposal accordingly. The most notable criteria for public

¹*Yildiz Technical University, Department of Industrial Engineering, 34349, Besiktas/Istanbul, Turkey.*

muhammetdeveci@gmail.com

²*Corresponding author: IETT, Public Transport Company in Istanbul, Manager of Business Intelligence and Project Management Department, Istanbul, Turkey,*

fatihcanitez40@gmail.com

³*Yildiz Technical University, Department of Industrial Engineering, 34349, Besiktas/Istanbul, Turkey.*

nihan@yildiz.edu.tr

transportation are passenger satisfaction, revenue growth and fair/balanced transit fare. Along with these criteria, there are also some constraints that need to be taken into account. To the extent possible, the transit fare increase should not exceed the rate of increase of inflation rate, fuel prices and labor/driver costs. The goal here for determining the transit fare increase is not to maximize the profits but doing so with an approach of meeting the costs. This is the result of the IETT operating in a service-oriented approach instead of a market-oriented one as a public institution in public transportation sector just like in many cities around the world.

In a decision making process described as above utilization of Analytical Hierarchy Process approach would be vastly helpful in determining the optimal transit fare. In such a selection process where criteria and alternatives are concerned, the AHP which quantifies the relationships between these alternatives and criteria, as well as in themselves and as a result determines the best alternative among the alternative transit fare proposals that meets the criteria is suggested. Because the AHP is an approach that determines the best result for all of the criteria and provides numerical proof unlike the other methods that determine transit fare, it is believed that the results obtained from it will shed light on the approaches in setting transit fare.

2 LITERATURE REVIEW

When the studies and the research on the methods of setting transit fares in public transportation and AHP applications are examined, it is seen that mostly the advantages and disadvantages of the single fare or distance dependent fare models are discussed rather than which methodologies to use when increasing the transit fare. Other than these, there are many application studies in the literature performed with the AHP technique. However, the information in the literature is inadequate on how to approach to decision-making problems such as transit fare increase in a sector with public service feature like public transportation. Therefore, it is hoped that this work will fill an important gap in this area. In recent years, there are some papers on fare policies have been published [4-6].

3 METHODOLOGY

AHP is a multi-criteria decision-making technique developed by Thomas L. Saaty in the 1977 [7]. AHP is a mathematical method used in decision making which considers the group or individual priorities, evaluates the qualitative and quantitative variables together and is used for measurement and decision-making [8]. It is not only a system that is easy to understand and implement by the business executives, but also a method that can help improve the decision-making process [9]. This method is intended for helping decision makers for more effective decision-making.

AHP generally consists of four stages; (1) identifying the criteria and its sub criteria according to the goals of the decision maker and developing the hierarchical system, (2) identifying the purpose and setting out the criteria influencing the selection according to this purpose, (3) identifying potential alternatives in consideration with the criteria, (4) and finally creating a hierarchical system for the decision [10]. In the second step, after the creation of this system, alternatives for each criteria must be compared. The importance scale defined in the Table 1 is used for the purposes of this comparison [7]. Even numbers not shown on this table can be used if the decision maker is in conflict. The third step is performing the normalization of the relationship matrix. This process is accomplished by dividing the sum of each column of a matrix to the values of all the column elements. Values of each line is collected by using normalized matrix, and percentage importance intensity for each criterion is resolved by dividing to the size of the matrix.

The examination of whether the comparison between the criteria is consistent is an important factor affecting the accuracy of the result. Therefore, it is necessary to examine the consistency of the obtained relation matrix. Consistency is determined by calculating the consistency rate (CR) developed by Saaty [7]. Consistency rate is calculated through the formula below:

CI: Consistency index and RI: Random Index

$$CR = CI/RI$$

$$CI = (\tau_{max} - n) / (n - 1)$$

Table 1. The importance intensity scale

Intensity of importance	Definition
1	Equal importance
3	Moderate importance of one over another
5	Essential or strong importance
7	Very strong importance
9	Extreme importance

The last step of the AHP process is finding the priority values for each alternatives by multiplying the importance intensity of criteria and alternatives. The alternative with the highest value is the best alternative for the decision problem.

4 APPLICATION

In this part, IETT's the optimal transit fare selection process between the available proposals using the AHP method for a fare rate increase will be explained. The current transit fares for the IETT before the fare rate increase are shown in the table below:

Table 2. Current transit fares before increase

		Current Transit Fare
Adult Card Akbil		1.75
Discount Card Akbil		
	Student	1.00
	Teacher +	1.20
	Senior Citizen	1.20
Adult Transfer		
	1st Transfer	1.00
	2nd Transfer	0.95
	3rd Transfer	0.90
	4th Transfer	0.85
	5th Transfer	0.80
Student Transfer		
	1st Transfer	0.40
	2nd Transfer	0.35
	3rd Transfer	0.35
	4th Transfer	0.35
	5th Transfer	0.30
Teacher + Senior Citizen Transfer		
	1st Transfer	0.60
	2nd Transfer	0.55
	3rd Transfer	0.50
	4th Transfer	0.45
	5th Transfer	0.40
Monthly Card		
	Adult	140
	Student	70
	Teacher/Senior	80

Three proposals/alternatives prepared for the transit fare change are as follows:

Table 3. Alternative transit fares

	Proposal - 1	Proposal - 2	Proposal - 3
Adult Card	1.85	1.95	1.90
Student Card			
Student	1.10	1.10	1.10
Teacher	1.35	1.35	1.30
Senior Citizen	1.35	1.35	1.30
Adult Transfer			
1st Transfer	1.25	1.25	1.20
2nd Transfer	1.00	1.00	1.10
3rd Transfer	0.90	0.75	0.90
4th Transfer	0.80	0.75	0.80
5th Transfer	0.70	0.75	0.70
Student Transfer			
1st Transfer	0.45	0.40	0.45
2nd Transfer	0.40	0.35	0.40
3rd Transfer	0.35	0.35	0.35
4th Transfer	0.30	0.35	0.30
5th Transfer	0.25	0.35	0.25
Teacher + Senior Citizen Transfer			
1st Transfer	0.75	0.75	0.75
2nd Transfer	0.60	0.60	0.60
3rd Transfer	0.50	0.40	0.50
4th Transfer	0.40	0.40	0.40
5th Transfer	0.30	0.40	0.30
Monthly Card			
Adult	150	155	160
Student	75	75	75
Teacher/Senior	85	90	95

Aside from these, as explained above, the transit fare increase rates must not exceed the following increase rates (Growth rates of the last one year are given in parentheses):

- 1- Inflation rate (9.48%)
- 2- Fuel Growth Rate (15.53%)
- 3- Workers / Driver Cost Growth Rate (10%)

The transit fare increase cannot exceed the minimum (9.48, 15.53, 10) = 9.48%. Total increase rates for each proposal is as follows:

- Proposal 1: 7.85%
- Proposal 2: 9.35%
- Proposal 3: 9.02%

According to this, as the proposed transit fare increase rates do not exceed 9.48%, constraints set forth are met. In the next step, the AHP method will be applied to the alternative transit fares in accordance with the defined evaluation criteria.

The purpose of the AHP application is to select the optimal transit fare proposal. The criteria to be considered when selecting it are:

- 1- Passenger satisfaction: The transit fare increase that is closest to the passengers' expectations is the most appropriate fare.
- 2- Meeting constraints: Indicates the situation that best meets the constraints given above; inflation rate, fuel growth rate and workers/driver cost growth rate.
- 3- Fair transit fare: The transit fare that ensures the optimum distribution between the categories (adult, student, teacher etc.) is most appropriate transit fare.

It is possible to create the importance intensity matrix of the criteria as below by using the importance intensity scale from the Table-1:

Criteria:

Table 4. The importance intensity matrix of the criteria

	Passenger satisfaction	Meeting constraints	Fair transit fare	Weights
Passenger satisfaction	1	2	3	0.54
Meeting constraints	1/2	1	2	0.30
Fair transit fare	1/3	1/2	1	0.16

Consistency Analysis:

$$\begin{vmatrix} 1 & 2 & 3 \\ 0.5 & 1 & 2 \\ 0.33 & 0.5 & 1 \end{vmatrix} \begin{vmatrix} 0.54 \\ 0.30 \\ 0.16 \end{vmatrix} = \begin{vmatrix} 1.62 \\ 0.89 \\ 0.49 \end{vmatrix} = \tau_{max} \begin{vmatrix} 0.54 \\ 0.30 \\ 0.16 \end{vmatrix}$$

$$\tau_{max} = \text{average}(1.62/0.54, 0.89/0.30, 0.49/0.16) = 3.01$$

Consistency Index (CI) is calculated as follows:

$$CI = (\tau_{max} - n) / (n - 1) = (3.01 - 3) / (3 - 1) = 0.005$$

In Saaty's book, there is a Random Index (RI) indicating the number of the top row. The consistency of the above matrix is analyzed by taking the value from this table.

Table 5. Consistency table

1	2	3	4	5	6	7	8	9	10	11	12	13	14	15
0.00	0.00	0.58	0.90	1.12	1.24	1.32	1.41	1.45	1.49	1.51	1.48	1.56	1.57	1.59

A value lower than 10% is an acceptable value. If it is higher than 10%, it means that the matrix is inconsistent and needs to be reconfigured.

According to this, the consistency rate CR is calculated as follows:

$$CR = CI / RI = 0.005 / 0.58 = 0.0086$$

Evaluations are correct because $0.0086 < 0.1$

After this step, alternative priority vectors are calculated for each and every criterion.

We can start with the passenger satisfaction first:

Passenger Satisfaction:

Table 6. Priority vector for passenger satisfaction

	Proposal -1	Proposal -2	Proposal -3	Priority Vector
Proposal-1	1	2	3	0.54
Proposal -2	1/2	1	2	0.30
Proposal -3	1/3	1/2	1	0.16

Meeting Constraints:

Table 7. Priority vector for meeting constraints

	Proposal -1	Proposal -2	Proposal -3	Priority Vector
Proposal -1	1	1/4	1/3	0.12
Proposal -2	4	1	2	0.56
Proposal -3	3	1/2	1	0.22

Fair Transit Fare:

Table 8. Priority vector for fair Transit fare

	Proposal -1	Proposal -2	Proposal -3	Priority Vector
Proposal -1	1	1/3	1/2	0.16
Proposal -2	3	1	2	0.54
Proposal -3	2	1/2	1	0.30

It is possible to illustrate this situation as below:

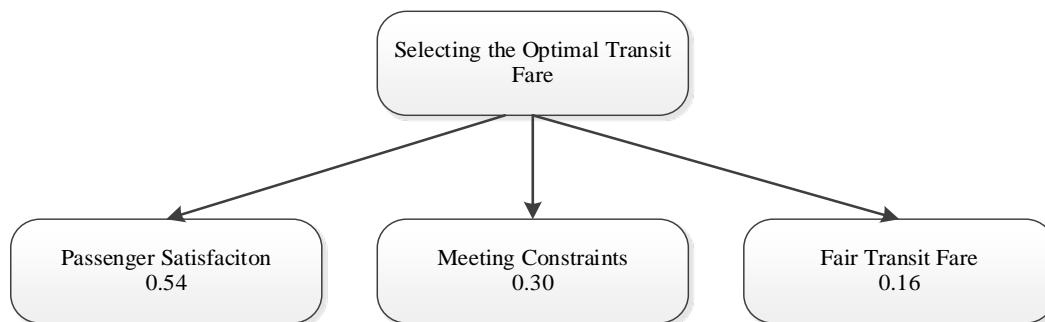


Figure 1. Selecting the optimal transit fare

Proposal- 1	0.54	Proposal -1	0.12	Proposal -1	0.16
Proposal -2	0.30	Proposal -2	0.56	Proposal -2	0.54
Proposal -3	0.16	Proposal -3	0.22	Proposal -3	0.30

Following results are obtained when the priority matrix and the criteria weights are multiplied.

	Passenger Satisfaction	Meeting Constraints	Fair Transit Fare	*	0.54	0.30	0.16	=	0.35	0.42	0.23
Proposal-1	0.54	0.12	0.16								
Proposal-2	0.30	0.56	0.54								
Proposal-3	0.16	0.22	0.30								

According to the result matrix above, Proposal-2 is selected as the new transit fare. With the decision of the Transportation Coordination Center (UKOME) under the Istanbul Metropolitan Municipality, the second proposal has been implemented between 2012 and 2014.

5 RESULTS

In public transportation, it is necessary to select the optimal transit fare increase for both the passengers and the institution providing the public transportation service. In an attempt to realize this, not only the passenger satisfaction about the transit fare must be ensured, but also the costs of this service for the provider must be met. On the other hand, while providing a fair distribution between different transit fare categories, the rate of increase of the inflation rate, fuel prices and labor/driver costs must not be exceeded. It is possible to carry out this optimal transit fare selection process defined by all of these criteria through the AHP method. With the applied AHP method the second proposal was accepted, and was implemented after Transportation Coordination Committee's approval, which is responsible for fare setting in Istanbul. With this study, a more rational decision making method to determine the transit fare increase rate in public transportation has been revealed. Having a standard method to determine transit fares changes peoples' perception about transit fare setting in a positive way. Communicating this methodology with people also leads them to think that transit fares are not determined in an ad hoc and random way, but in a rigorous and sound method.

REFERENCES

- [1] S. Richard, "Urban Public Transport Pricing Schemes The Context and Options", The Second Seminar of the IMPRINT-EUROPE Thematic Network: "Implementing Reform on Transport Pricing: Identifying Mode-Specific Issues", Brussels, 14th/15th May 2002.
- [2] J. C. G. Beasley, "Fares Policy: The Public Interest Report", 49th International Congress Stockholm, 1991.
- [3] S. Benk and T. Akdemir, "Toplu Taşıma Hizmetlerinde Fiyatlama Stratejileri: Teorik Bir Değerlendirme", *Ekonomi Bilimleri Dergisi* Cilt 2, Sayı 1, 2010.
- [4] M. Streeeting and C. Phil, "Developments in Transit Fare Policy Reform", 29th Australian Transport Research Forum <http://espace.library.uq.edu.au/eserv/UQ:7732/nl28.pdf>, 2006.
- [5] L. Spock, "Fare Policy Regarding Regular and/or Inflation-related ("Programmed") Price Increases", NYU Wagner Rudin Center for Transportation Policy&Management, November 2007.
- [6] TCRP (Transit Cooperative Research Program). Fare Policies, Structures and Technologies Report, No:10, Transportation Research Board, Washington, 1996.
- [7] T. L. Saaty, *Fundamentals of Decision Maing and Priority Theory*, 2.Edition, RWS Publications, Pittshburg, 2000.
- [8] M. Dağdeviren, D., Akay and M. Kurt, "İş Değerlendirme Sürecinde Analitik Hiyerarşi Prosesi ve Uygulaması", *Gazi Üniversitesi Mühendislik-Mimarlık Fakültesi Dergisi* 19 (2), 131-138, 2004.
- [9] M. Dağdeviren and T., Eren, "Tedarikçi firma seçiminde analitik hiyerarşi prosesi ve 0-1 hedef programlama yöntemlerinin kullanılması", *Gazi Üniversitesi Mühendislik-Mimarlık Fakültesi Dergisi*, 16(1), 2001.
- [10] T. Murat, "Analitik Hiyerarşi Prosesi Yaklaşımı Kullanılarak Mobilya Sektörü İçin Ege Bölgesi'nde Hedef Pazarın Belirlenmesi". *Yönetim ve Ekonomi Dergisi*, 14(1), 171-180, 2007.

Performance of dual axis solar tracking system using fuzzy logic control: A case study in Pinarhisar, Turkey

Hayrettin Toylan¹

Abstract

Generating electrical via solar energy is one of the most popular renewable energy source. Modular structured solar panels that work according to photovoltaic principles convert solar radiation into electrical energy. There are some ways of increasing the power produced by the photovoltaic panels. One of the most effective ways is to minimize the angel of rays from sun to panel surface by taking the right position according to the angle of the sun. This paper proposes an intelligent control method for solar tracking. This method uses a fuzzy logic controller applied to the DC motors in solar tracking system (STS). STS is designed and developed as dual axis. Fuzzy logic algorithm used in STS was applied separately in order to control DC motors which determine the azimuth and zenith angels of the system. Position error which is obtained by the help of encoders tied to the motors and error variation were taken as input of fuzzy logic algorithm, applied voltage to the motor was taken as output of fuzzy logic algorithm. Finally, results of the photovoltaic panel on the STS controlled by fuzzy logic are compared to those obtained by the photovoltaic panel system without STS according to instantaneous power performance throughout the day in Pinarhisar, Turkey. Experimental results show that the STS which uses fuzzy logic controller increases the efficiency of energy production from PV.

Keywords: Renewable energy; Solar tracking system; Fuzzy logic; Photovoltaic panel

1 INTRODUCTION

Energy is an important factor in industrialization, urbanization and financial growth and social life quality of a country [1]. That is why energy demand worldwide is increasing and this condition is most likely to continue in the future [2, 3]. This demand increase lead people towards renewable energy sources such as wind, geothermal, and solar energy sources since fossil fuels are exhaustible. In Turkey, according to final data in 2014, when distribution of renewable sources in total of 69519.8 MW established power is analyzed, shares of wind, geothermal and solar energy are seen to be respectively 3629.7 MW, 404.9 MW and 40.2 MW [4]. In Turkey, %5.86 of the electricity produced is gained from wind, geothermal and solar energy (Figure 1). Nevertheless, with the use of renewable energy sources, share of electricity production shows an increasing trend in an annual basis.

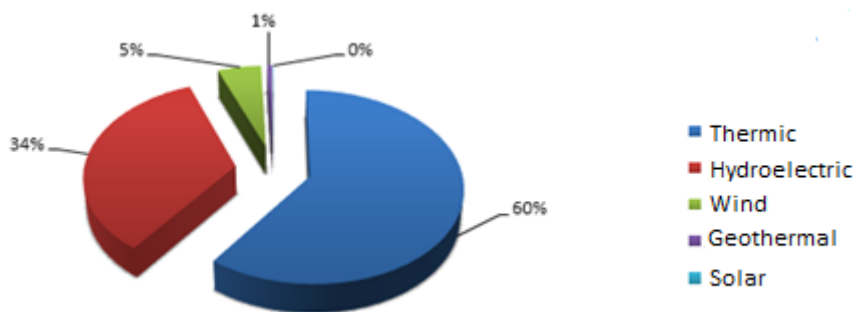


Figure 1. Distribution according to installed power capacity of energy types in Turkey [4]

One of the most important renewable energy sources is surely solar energy. Even though electricity energy produced out of it is lower when compared to other energy sources, thanks to advancements in solar energy industry, with decrease in the initial investment costs and increase in the efficiency, there is no doubt that its contribution rate will be increasing every year. Owing to the geographical position of our country, it can be said that it is in a lucky position in terms of receiving sun when compared to many other countries. Therefore, benefiting from infinite and free solar energy in maximum level will support the interests of our country which is dependent on foreign countries for energy.

Photovoltaic systems enable solar power to turn into electricity energy. Power that these systems produce depend on a variety of factors including the amount of energy they receive from sun rays. In order to increase the efficiency of photovoltaic systems, scientists and engineers have made many researches. In general, there are three ways to increase the efficiency of photovoltaic systems. First method is to increase power production efficiency of solar cells [5, 6]. Second one is related to increasing the effectiveness of control algorithm for energy conversion systems that include maximum power point tracking [7, 8]. Third approach is to use solar tracking system in order to make maximum use of solar energy [9].

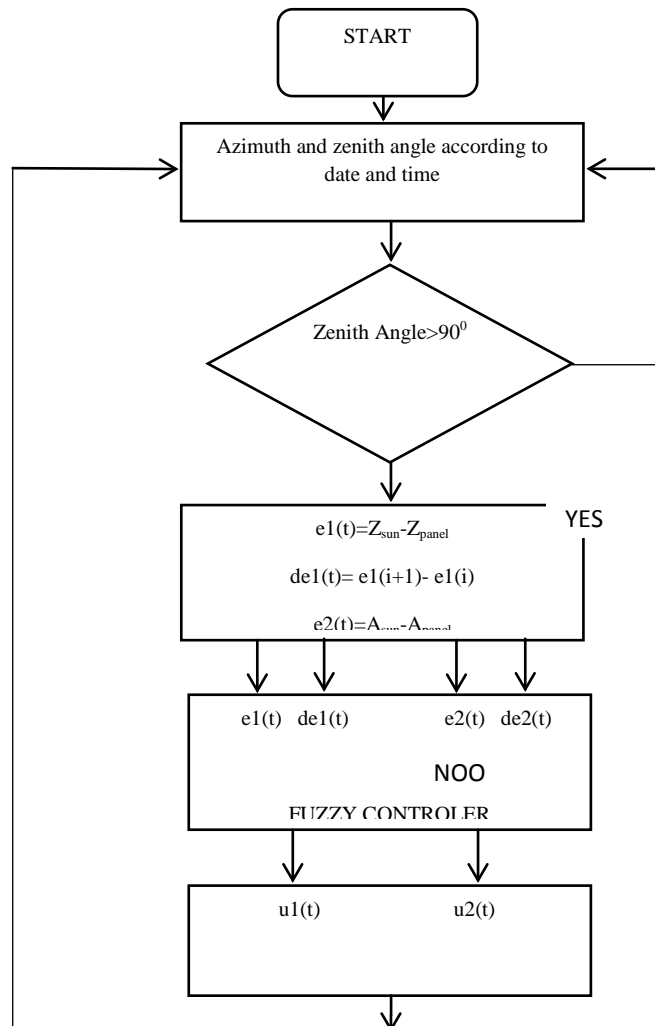
There are a number of works proposed by many researchers to solar tracking. In their work, Sefa et al. have done the design and application of PC-based one axis solar tracking system. The reason why they have used one axis is that they thought system's total weight of 3500 kg would make double axis tracking harder [10]. M.J. Clifford and D. Eastwood have designed a one axis solar tracker that is, in other words, appropriate for use only in Ecuador regions [11]. Tiberiu and Liviu have used one-axis solar tracker and opted to manually adjust the other axis throughout the year with regular intervals [12]. Wafa Batayneh et al. designed dual-axis solar trackers which are driven by a DC motor for each axis of tracking. They presented a fuzzy logic based controller for controlling the DC motors. They used four small PV cells as sensors to find solar position. [13]. While choosing the mechanical system of solar tracking systems, its cost analysis should be made. Cost of the tools to be used in the system and power consumption should be taken into consideration.

In this study, the effect of solar tracking system, which is controlled with fuzzy logic at Kırklareli University Pınarhisar Vocational School, upon the performance of solar panels have been put under the scope. A comparison is made between the daily energy productions of fixed positioned PV panels and PV panels that are positioned on solar tracking system.

2 MATERIALS AND METHODS

2.1 Sun tracking system design and control

In the electro-mechanical system of solar tracking system, there are 2 DC motors, 2 reducers, 2 encoders, 1 double channel motor driver, daq card and a computer. In the mechanical structure of STS, PV panels have the motion ability with two double axis, and are positioned with direct current (DC) motors. By providing the revolution of panels in Azimuth and Zenith angles, sun can be tracked in a way that enables sunrays to fall onto panels with vertical angle.



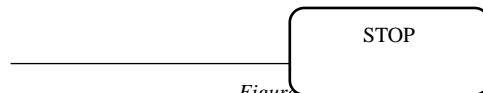


Figure 2. Terminal state of the fuzzy controller

As shown in Figure 2, Azimuth and Zenith angle of Sun is calculated according to time/date and geographical information. If the Zenith angle is more than 90 degrees, sun is set. Running solar tracking system is needless. In the other condition, pulse signals coming from the encoder bound to motors, and consequently the errors and rate of changes of errors are calculated. For each motor, error (e) and change of error (de) are applied to Fuzzy Controller as input. The output of the fuzzy controller will be the motor's speed needed to move the panel.

2.2 STS using Fuzzy Logic

Fuzzy logic controller, which was first created in 1965 by Zadeh [14], is a system defined via fuzzy rules and created by the professional experience. It is a system that includes the linguistic variables instead of the mathematical model of a dynamic system. It has four main parts: (i) Fuzzification (ii) Rule base, (iii) Inference (iv) Defuzzification interface. The proposed system for two DC motors in this study consist of two input variables: error (e) and change of error (de), and one out variable: duty ratio (u), as shown in Figure. 3

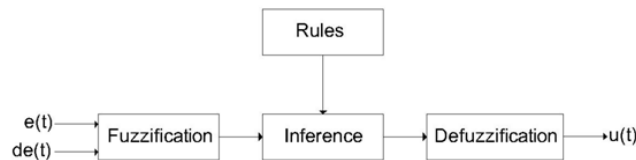


Figure 3. General diagram of a fuzzy controller

Fuzzification

In the fuzzification process, membership function values are assigned to the linguistic variables. In order to carry out this process, the input variable range is transformed to the convenient universal cluster and by this way the input values are transformed to the convenient verbal values. In this study have five fuzzy subsets: NB (negative big), NS (negative small), ZE (zero), PS (positive small), and PB (positive big). In the fuzzification process various membership functions are used. In this study, triangle function is used as the membership function (Figure 4 and Figure 5).

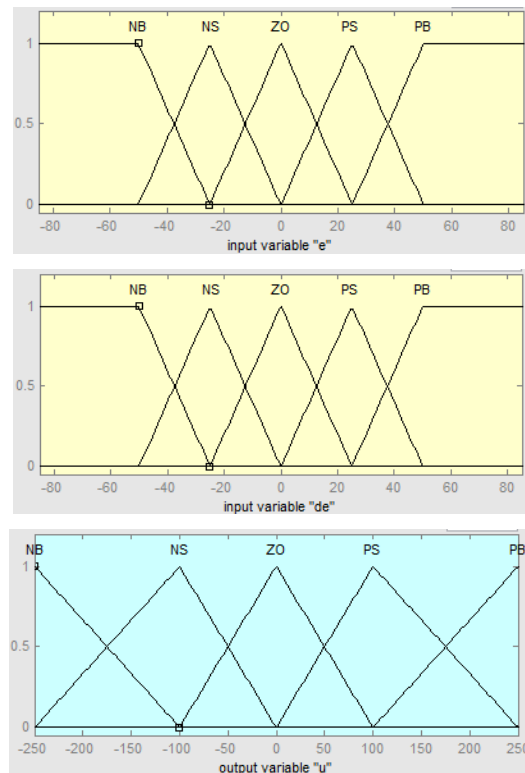


Figure 4. Fuzzy logic membership functions for inputs and output variable of zenith angle.

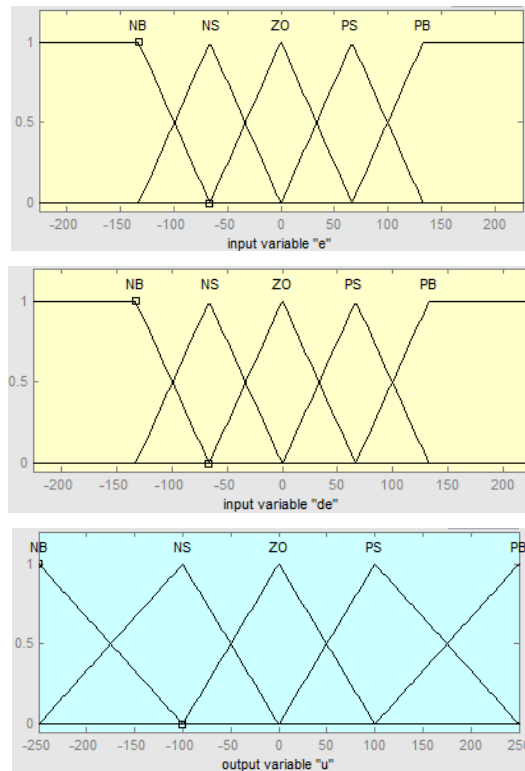


Figure 5. Fuzzy logic membership functions for inputs and output variable of azimuth angle.

Rule base

Rule base, holds the knowledge in the form of a set of rules, of how best to control the system. In this study, 25 number “if-in that case” rules have been created. The result of rules and motor PWM values are determined. In Table 1, a part of rule table which is created for the input variables takes place.

Table 20. Fuzzy controller rules

e/de	NB	NS	ZE	PS	PB
NB	NB	NB	NB	NS	ZE
NS	NB	NB	NS	ZE	PS
ZE	NB	NS	ZE	PS	PB
PS	NS	ZE	PS	PB	PB
PB	ZE	PS	PB	PB	PB

Inference

The data coming to system in the blurring rule base are processed by the inferring mechanism after they are ready to be processed. In this study, Mamdani method, which is one of the inferring method, has been used. While the threshold values of rules are measured in Mamdani inferring method, firstly “and (intersection)” then “or (combination)” processors are used.

Defuzzification

In the defuzzification process, the process of transforming the fuzzy set obtained in the fuzzy inferring motor to a definite value is carried out. In order that the obtained fuzzy set is to be applied the real life, there must be a numerical value. In this study, center of gravity method has been used. The center of gravity of the inferred cluster, which has been created via this method, is found and the value coming to this center as a definite value is assigned.

3 RESULTS AND DISCUSSION

In this study, a dual axis solar tracking system based on fuzzy logic controller, which simultaneously carries four number of 120 W panels, has been designed. According to the researches, before deciding to use solar following systems, the first thing that must be done is to take into account the initial investment cost and energy waste. In order to decrease the initial investment cost, two number of DC motor instead of servo motor have been used in order to move panels in azimuth and zenith angles. Angle position information of panels has been found with pulse signals read with the help of reed sensor instead of industrial encoder. Again in order to decrease the cost, Arduino Mega 2560 model has been chosen instead of industrial daq card.

We use fuzzy logic to control the speeds of the two motors based on date/time aiming at increasing the efficiency of the solar panels. Two different fuzzy logic algorithms have been applied to two motors that control Azimuth and Zenith angles (Figure 6). In both algorithms, the number of rules was 5 and fuzzy logic membership function parameters were determined with the help of experiences.

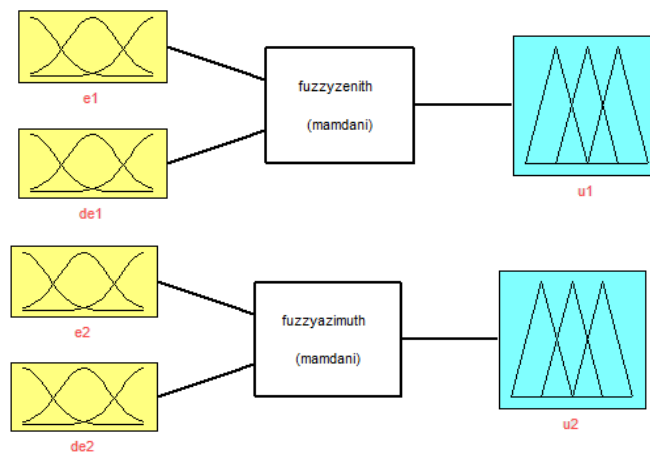


Figure 6. Fuzzy logic controller.

The dual axis solar tracking system presented here is tested experimentally. The experimental study is realized at Pinarhisar Vocational High School in Kırklareli, Turkey. STS has the capacity of carrying four panels, but measurements have been made over a 120 W panel. For performance evaluation, a comparison has been made between all-day productions of fixed panel and the panel positioned on STS. Installation angle of fixed panels have been determined as 38 degree south by considering the latitude angle of Kırklareli University Pinarhisar Vocational School taking into account that they will be used in summer and winter conditions.

Performance analysis of STS located at Kırklareli University Pinarhisar Vocational High school and fixed panel was made on the 17.09.2015.

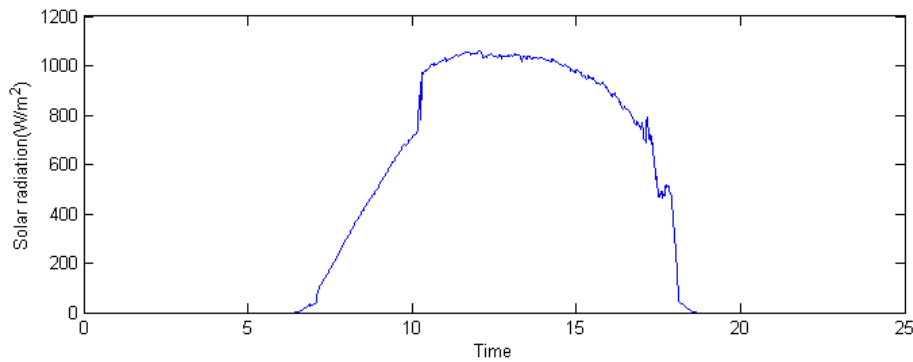


Figure 7. The results solar radiation amount on the 17th of September 2015.

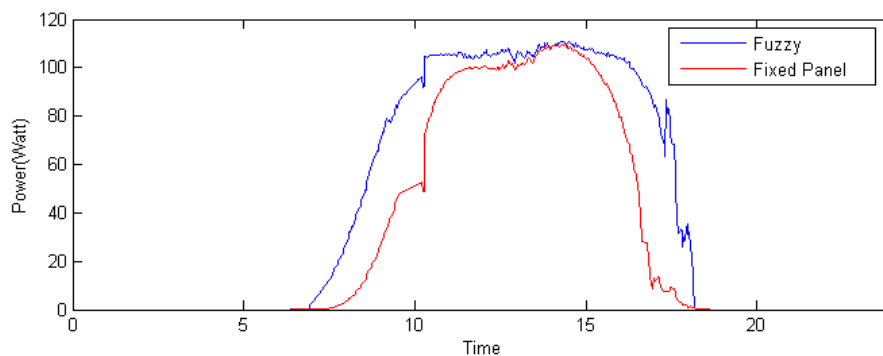


Figure 8. Power output values seems of the fixed panel and the PV panel using STS in Pinarhisar, Turkey. The results presented are on the 17th of September 2015.

It can be seen that throughout the whole day (Figure 8)), the PV panel on STS has the highest power output due to highest solar irradiance exposure. The fixed PV panel has a lower output power compared to the panel on STS due to low solar irradiance. In Pinarhisar on the specified date it was found that the daily output power of the STS used with Fuzzy logic was 35.6% higher than the fixed PV panel

4 CONCLUSIONS

In this paper the speed of DC motors in dual axes solar tracking system is controlled using fuzzy logic controller. Results of the photovoltaic panel on the STS controlled by fuzzy logic are compared to those obtained by the photovoltaic panel system without STS according to instantaneous power performance throughout the day in Pinarhisar, Turkey. Experimental results show that the STS which uses fuzzy logic controller increases the efficiency of energy production from PV.

ACKNOWLEDGMENT

This work was supported by Kırklareli University Scientific Research Projects under project no: KUBAP-018

REFERENCES

- [1] V. Khare, S.Nema, and P.Baredar, "Status of solar wind renewable energy in India," *Renewable and Sustainable Energy Reviews*, vol. 27, pp. 1–10, Nov.2013
- [2] V. Subramanian, "Renewable energy in India: status and future prospects," Ministry of New and Renewable Energy, 2007
- [3] S. K. Sahoo, "Renewable and sustainable energy reviews solar photovoltaic energy progress in India: A review," *Renewable and Sustainable Energy Reviews*, vol. 59, pp. 927–939, June.2016
- [4] (2016) The teias website. [Online]. Available: [http:// www.teias.gov.tr/yukdagitim/kuruluguc](http://www.teias.gov.tr/yukdagitim/kuruluguc)
- [5] S. Sun, J. Brooks, T. Nguyen, A. Harding, D. Wang, and T. David, "Novel Organic and Polymeric Materials for Solar Energy," *Energy Procedia*, vol.57, pp.79 – 88, 2014.
- [6] P. Oelhafen and A. Schuler, "Nanostructured materials for solar energy conversion," *Solar Energy*, vol.79, pp.110–121, August. 2005.
- [7] R. Pradhan and B. Subudhi, "Design and real-time implementation of a new auto-tuned adaptive MPPT control for a photovoltaic system," *Electrical Power and Energy Systems*, vol. 64, pp.792–80, 2015.

- [8] S. Daraban, D. Petreus, and C. Morel, "A novel MPPT (maximum power point tracking) algorithm based on a modified genetic algorithm specialized on tracking the global maximum power point in photovoltaic systems affected by partial shading," *Energy*, vol.74, pp.374-388, Sep.2014.
- [9] I. Stamatescu, I. Făgărășan, G. Stamatescu, N. Arghira, and S.S. Iliescu, "Design and Implementation of a Solar-Tracking Algorithm," *Procedia Engineering*, vol.9, pp. 500-507, 2014.
- [10] İ. Sefa, M. Demirtas, and İ. Çolak, "Application of one-axis sun tracking system, *Energy Conversion and Management*, vol. 50, pp. 2709–2718 Nov. 2009.
- [11] M.J. Clifford and D. Eastwood, "Design of a novel passive solar tracker", *Solar Energy*, vol. 77, pp. 269–280, Sep.2004.
- [12] T. Tudorache, L. Kreindler, "Design of a Solar Tracker System for PV Power Plants," *Acta Polytechnica Hungarica*, vol. 7, no. 1, 2010.
- [13] W. Batayneh, A. Owais, and M. Nairoukh, "An intelligent fuzzy based tracking controller for a dual-axis solar PV system," *Automation in Construction*, vol. 29, pp.100–106, 2013.
- [14] LA Zadeh, "Fuzzy sets," *Information and Control*, vol.8, pp.338-353, Jun.1965.

Potential Use of Nanotechnology in Conservation Applications of Historical Buildings

Semih Yilmaz¹, Nilhan Vural²

Abstract

Main purpose in protection of historical buildings is to protect their structural integrity and allow them to pass on to the future. In order to achieve this goal, being able to sustain the material protection is important. In historical buildings, materials which can be easily distinguished from natural environment have been used mostly. With the improvement of protection awareness, different protective methods and materials have been developed, however; partial inadequacy of such methods, increasing environmental problems worldwide and the requirement for effective use of energy raises the efforts and expectations towards the use of new generation building materials. Developments which may respond to such expectations corresponds with nanotechnology science. Nanotechnology is the fastest developing technology of our age. The importance of nanotechnology arises from its enabling to obtain products with developed or new physical, chemical and mechanical properties by studying at atom/molecule level. It has a wide area of use and shows its most concrete impact in materials science in architectural practices. Nanotechnology enables to develop more solid, more quality, more long-lived, lighter and more functional building materials compared to materials produced by traditional methods. In this study, it was aimed to analyze protection problems which occur in historical buildings through the materials included in external wall construction and examine the nanomaterial usage potential for the solution of identified problems. In this context, six historical buildings which located in Ortamahalle, Akçaabat, Trabzon examined within the work. As a result of negotiations made by the users of selected buildings, building information cards that include foundation information of buildings and basic problems encountered in building protection applications shall be prepared and analyzed. Analyses shall be addresses under three different topics which are internal surface, cross section and external surface on the external wall construction. At the end of the study, nanomaterial application suggestions in protection practices shall be presented and the acquirements to be obtained by the use of nanomaterials in surface elements of historical buildings shall be explained. With these practices, the effective role of nanomaterials in protection of historical buildings compared to traditional methods and materials shall be revealed.

Keywords: Historical buildings, nanomaterials and nanotechnology

1 INTRODUCTION

Historical buildings are among the major heritages for societies and they might be damaged throughout the time due to climate, natural disasters (earthquake, flood etc.), utilization and application faults. The preservation of these historical buildings and to carry them into the future is a necessity.

The understanding of preserving the historical buildings has started in the end of 19th century in Turkey, and in the last two decades it has reached to an important point due to increasing consciousness and the experiences; but all the problems are not solved yet. Problems caused by physical, chemical and mechanical inefficacy of traditional materials are among those. The effort to find solutions for these problems has generated the idea and necessity to use new generation of materials[1].

A field study was conducted in Trabzon province, Akcaabat district, Ortamahalle neighborhood in order to implement this research prepared for the examination of basic problems faced during the implementations related with the preservation of historical buildings and to reveal the utilization of new generation of materials. Damage analysis study was conducted in 6 traditional buildings within the scope of this study and it has been observed that the problems faced were intensified on the construction of exterior walls. These problems were scrutinized depending on the characteristics and utilization possibilities of nano materials as part of these new materials. As a result of the study, description of utilizing nano materials for the preservation of historical buildings and establishing an awareness on this issue is aimed.

¹ Corresponding author: Karadeniz Technical University, Department of Architecture, 61080, Ortahisar/Trabzon, Turkey.
semihyilmaz@ktu.edu.tr

² Karadeniz Technical University, Department of Architecture, 61080, Ortahisar/Trabzon, Turkey.
nvural@ktu.edu.tr

2 APPLICATIONS OF PRESERVATION AND BASIC PROBLEMS

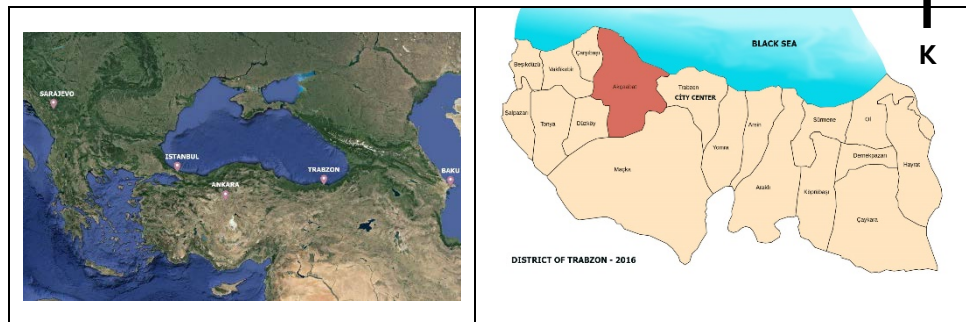
Each cultural asset is destined to fall into ruins by time. In order to keep the history alive, the repair and preservation of historical buildings as witnesses of history must be ensured. According to this necessity, any compulsory interventions implemented in order to carry a historically important building into the future without causing any harm on its uniqueness can be named as applications of preservation. Some problems might appear during these applications[2].

This study has scrutinized the problem of material, which is the most important title among the problems faced in applications of preservation, according to the results of field study conducted and the existing situation was examined in relation with nano-technology and nano-materials.

2.1 Field Study

The concept of preservation had different meanings throughout the time, and today its content has expanded significantly; containing the preservation of historical and cultural assets, collective preservation of areas where historical and cultural assets are located collectively within the urban life and the preservation of natural values within and around the city. Therefore, Ortamahalle within the borders of Akcaabat district of Trabzon province was chosen as the study field due to its characteristics of being one of the oldest habitations of the district and the various cultural assets it contains[3].

Table 1. Satellite image of Turkey and its close surround - District of Trabzon and Akçaabat districts' boundaries.

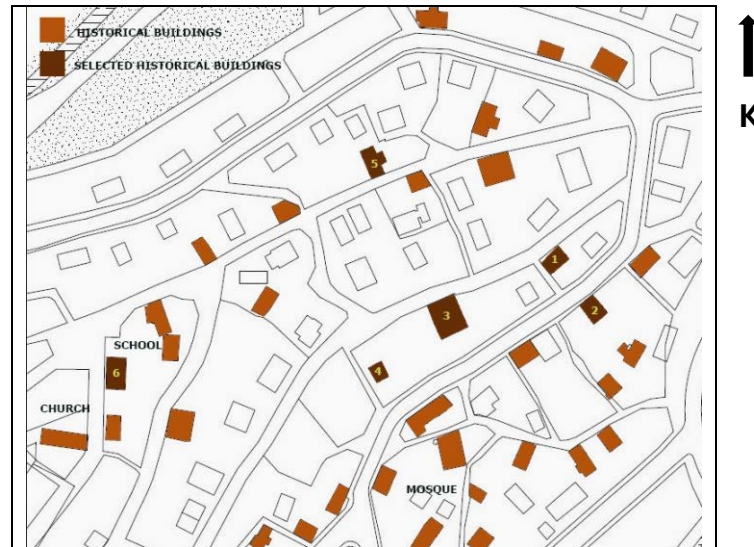


Black Sea Region's traditional housing architecture can be seen in the neighborhood and there are approximately 50 houses in it of which most are still being used and it is a part that can be easily accessed due to its topography. Houses have fronts to east and south and they are located inside a garden next to the streets. They are highly compatible with the nature.

These houses have maximum three floors and they are under the category of "karniyarik" with an internal anteroom. Wide anterooms are in the east and with an open view. Down floors have living spaces, cellar, storage, service areas; and the upper floor has bedrooms with doors towards anteroom. The plans of the houses are similar with each other and there is an outbuilding at the upstairs anteroom, which covers the entrance below[4].

Within the scope of field study, 6 traditional buildings from Ortamahalle were selected, they were marked on the map below and the building information sheets were prepared for these structures. The goal is to introduce the buildings, to determine their structural characteristics and to analyze the problems faced while preserving these buildings.

Table 2. Historical buildings on Ortamahalle and selected historical buildings.



This study was conducted as a pre-study of a comprehensive review. Therefore, only 6 buildings were included into the scope of this study.

Table 3. Pictures of selected historical buildings



2.2 Preparation of Building Information Sheets

Building information sheets were prepared by using interviews with building owners, observations and oral/written information obtained from related institutions and sources. Table 4 displays the building information sheet for Building-4.

Table 4. Building information card – 4.

I · G E N E R A	Building owner	: Ahmet KAZANCI	
	Built time	: 1880-90	
	Original function	: Dwelling	
	Current function	: Dwelling	
	Restoration time	: 1999	

L I N F O R M A T I O N	Address : Timurcu Street		
2 · S T R U C T U R A L F E A T U R E S	<p>This building has about 150 years history. Building can be entered from wide courtyard surrounded with garden walls has a internal plan type. 2-storey building has 1 room, 1 kitchen and 1 wc on first floor, 4 room, 1 wc and 1 bath on second floor.</p> <p>First floor external wall structure of buildings built with stone base materials and second floor external wall structure of buildings built with wood base materials.</p>		
3. DETERMINATION and ANALYSIS of PROBLEMS			
1.	Corruption in wooden materials		
2.	Paint pouring		
3.	Thermal insulation problem		
4.	Plaster pouring		
5.	Pollution		

2.3 Determination of the Problem and Analysis

It has been seen that the detected problems in accordance with the building information sheets for 6 sample buildings in the field of study were intensified on the exterior wall construction. Therefore, Table 5 provides the general information on 6 sample buildings and the detected problems on the exterior walls of these buildings were analyzed.

Table 5. General information about all selected buildings.

GENERAL INFORMATION										
	STRUCTURAL FEATURES				MATERIALS				USAGE	
	Built time	Restoration time	Plan type	Total floor	Structure system	Floor	Door/Window	Roof construction	Current function	Original function
B-1	1866	2010	Interior H.	3	Stone/wood	Wood	Wood	Tile	Dwelling	Dwelling
B-2	1876	2005	Interior H.	2	Stone/wood	Wood	Wood	Tile	Dwelling	Dwelling
B-3	1860	2000	Interior H.	3	Stone/wood	Wood	Wood	Tile	Dwelling	Dwelling

B-4	1860	2010	Interior H.	2	Stone/wood	Wood	Wood	Sheet	Dwelling	Dwelling
B-5	1874	2013	Interior H.	2	Stone/wood	Wood	Wood	Tile	Restaurant	Dwelling
B-6	1867	1997	Interior H.	2	Stone/wood	Wood	Wood	Tile	School	Dwelling

Table 6. Protection problems in selected houses outer wall constructions.

PROTECTION PROBLEMS IN OUTER WALL CONSTRUCTIONS												
OUTER WALL SECTION												
	Material loss	Insulation problem	Paint pouring	Plaster pouring	Hydration	Pollution	Material loss	Insulation problem	Paint pouring	Plaster pouring	Hydration	Pollution
B-1												
B-2												
B-3												
B-4												
B-5												
B-6												

3 NEW GENERATION MATERIAL APPROACHES IN APPLICATIONS OF PRESERVATION

Traditional materials are being used for applications of preservation in historical buildings. But, some negative aspects such as the low endurance of historical materials and the short-term preservation they provide has generated the idea and necessity to utilize new generation materials. In the applications of preservation of historical buildings, maximum efficiency with minimum intervention is considered important. Nano-materials are a new approach and they provide long-term endurance; they resist to external factors such as sunlight and rain, and they provide insulation with small sections; all of which make them suitable for utilizing in historical buildings. Enhancement by using this methodology is conducted with the least intervention to the historic fabric.

4 NANOTECHNOLOGY AND NANOMATERIALS

Nanotechnology controls the materials in nano-scale (one billionth of a meter), it works at atom and molecule levels and provides the chance to generate buildings with completely new physical, chemical and mechanical characteristics[5]. The nano-materials with the potential of solving the problems detected as a result of this field study are examined under the titles of nano-coating and nano heat insulation materials.

4.1 Nano-coatings

Nano-coating is the coating of material surfaces with a layer generated by nano-particle added painting or thin films. In some cases, nano-particles are directly added into the mixtures of traditional materials and the surface characteristics can be improved as required. Some chemical and physical changes, which are not observed at macro dimensions, are witnessed at nano dimension and quality coatings can be obtained by applying the nano-sized particles to the surface properly.

Nano coatings can be applied on all types of surfaces such as glass, metal, ceramic, concrete and plastics [6]- [7]. Nano coatings are applied on the material surface by using various methods (dipping, spray etc.) and they may be classified as self-cleaning, easily cleaned, air cleaning, antibacterial, UV proof, non-scratching and resistant to abrasion[8]-[9].

- **Self-Cleaning Nano Coatings:** They are grouped into two, namely as self-cleaning nano coatings with Lotus effect and self-cleaning nano coatings with photo-catalytic effect. In both applications, dirt and other impurities are removed from the surface by aqua movements. Nano coatings with photo catalytic impact also have the feature of disintegrating the absorbed dirt whenever exposed to sunlight [10]-[11]. They can used at the sides; on wood, stone, ceramic and metal surfaces.
- **Easy-Cleaned Nano Coatings:** The rugged structure that consists of invisible cavities and/or gaps on the material surface cause the sticking of dirt, bacteria and similar unwanted bacteria on the surfaces of material. On such materials; nano coatings with nano size, non-water structure, smooth and with low surface energy can be applied and easy cleaning feature can be acquired [6]. Smoothness and low level of surface energy can significantly prevent the sticking of dirt, bacteria and similar harmful organic components on the surface of material [6]-[9]. These nano coatings can be used at sides, interior and wet areas widely.
- **Air Cleaning Nano Coatings:** Air cleaning with nano-technology is prevalently implemented through disintegrating the unwanted odors and dirt into harmless components by photo catalytic reactions. With the utilization of paints, plasters, concrete, curtain and carpet and similar materials on which photo-catalytic nano coating is applied or which contain nano particles with that effect; unwanted odors and dirt are disintegrated into their harmless components through photo catalytic reactions.
- **Antibacterial Nano coatings:** Nanotechnology makes it possible to produce nano coatings with antibacterial characteristics by using antibacterial nano particles. High quality antibacterial nano coatings acquired by nano sized silver particles can be applied on buildings, ceilings, floors, furnitures and similar surfaces in the form of a thin film[6]-[9].
- **Nano coatings preserving from UV Rays:** The most effective climate condition that plays an important role on the aging and wearing of buildings and building materials is the sun radiation. UV rays particularly defect the molecular structure of organic building materials and causes impacts such as fading of color, changing of color and superficial capillary cracks. These capillary cracks deepen by time and cause the reduction of mechanical characteristics of the material. Traditional UV protective coatings also get affected from UV rays and lose their function by time due to their organic structures. Because of this structural disadvantage, organic structured UV protective coatings cannot provide long-term preservation. Inorganic structured UV protective coatings were produced in order to remove these negative effects. Utilization of nano sized titanium dioxide (TiO₂) and zinc oxide (ZnO) is suitable for the nano coating applications with an effect of preservation from UV rays. UV protective nano materials have a wide range of utilization on wood, stone, metal, ceramic and similar material surfaces; and they are also widely used in the external and internal environment without any weakening in their appearance and endurance[9]-[12].
- **Non-scratching and wear-resistant nano coatings:** Material surfaces are exposed to different rates of abrasive and wearing impact depending on place and type of utilization. These impacts cause physical negations such as scratching and wearing on the surfaces of materials. In order to prevent the occurrence of these physical events that cause negations such as shortening the life of materials and reducing their visual quality; traditional coatings are being used but these materials do not bring the required endurance and opaqueness on the material surfaces. Nano coatings with resistance to scratching and abrasion can provide high endurance and opaqueness with their nano sized structures. With these nano coatings, materials can obtain high level of resistance against scratching and abrasion without any change on their surface displays. Thin films, paints and varnishes produced for this purpose have a wide potential of usage in buildings[6]-[9].

4.2 Nano Thermal Insulation Materials

Nano materials of which the high physical characteristics are discovered with the development of nanotechnology and produced in order to use in heat insulation applications; do not allow the movement of air molecules due to nano sized (20 nm-100 nm) pores in their structure, thereby blocking the heat transfer on the material surface. As they have high surface-volume rate, they can function as heat insulators, which is their most obvious characteristic. When compared with traditional heat insulation materials; nano materials have 6-7 times more performance, and decrease the heating costs in buildings by providing more energy preservation; and they can be applied at side, wall, roof and floor. Aerogel heat insulation covers and vacuum heat insulation panels can be considered as examples of nano heat insulation materials applied for the preservation of historical buildings.

Aerogel heat insulation covers are nano pore and flexible composite materials produced by using silica aerogel and fiber additives. Besides the flexibility; aerogel heat insulation covers have various high characteristics such as low heat transfer

index, high pressure endurance, breathing and hydrophobic surface and their fire endurance classes can be different according to the fiber additive material preferred in their manufacturing.

Vacuumed heat insulation panels (VYP) are materials generally produced by placing an open pore structure internal filling material (vacuumed as such) into an outer cover by using a gas remover/dryer depending on the characteristic of material through vacuuming and closing on atmosphere. Vacuumed heat insulation panels have thinner material thickness when compared with traditional heat insulation materials and they have more effective heat insulation values. In other words, they provide maximum heat insulation value with minimum material thickness[9]-[13].

5 FINDINGS AND DISCUSSIONS

This study has examined the possibility of utilizing the nano materials developed in parallel with the developments in nanotechnology field with high physical, chemical and mechanical characteristics applied for the preservation of historical buildings; and a field study was conducted in Ortamahalle, the main problems faced during preservation applications were tried to be detected. The findings obtained from literature review and observations are indicated on Table 7. Table 7 includes the preservation problems detected on the exterior wall construction of analyzed buildings and the solutions for these problems by nano technologies.

Table 7. Protection problems in outer wall constructions.

PROTECTION PROBLEMS IN OUTER WALL CONSTRUCTIONS														
OUTER WALL SECTION														
NANOMATERIALS	PROBLEM	Material loss	Paint pouring	Plaster pouring	Hydration	Pollution	Vegetation	Discoloration	Material loss	Insulation problem	Paint pouring	Plaster pouring	Hydration	Pollution
Self-cleaning														
Easy to clean														
Anti-bacterial														
Air purifier														
UV protection														
Abrasion-strach res														
Aerojel thermal insulation blanket														

- [6] M.F. Ashby, P.J. Ferreira and D.L. Schodek, *Nanomaterials, Nanotechnologies and Design: An Introduction for Engineers and Architects*, 2nd ed., China: Elsevier, 2009.
- [7] G., G. Avcı, "İşlevsel nanokaplamalar," *Bilim ve Teknik Dergisi*, vol. -, pp. 48-49, Apr. 2009.
- [8] G. Elvin. (2014) Nanotechnology for green building. [Online]. Available: <http://esonn.fr/esonn2010/lectures/maangematin/Nano.Green.Building55ex>
- [9] S. Leydecker, *Nano Materials in Architecture: Interior Architecture and Design*, Germany: Birkhauser Verlag AG, 2008.
- [10] B., O. Küçükıldırım, "Karbon Nanotüpler, Sentezleme Yöntemleri ve Kullanım Alanları," *Mühendis ve Makina*, vol. 53, pp. 34-44, Jul. 2012.
- [11] M., S., E. Naschie, "Nanotechnology for the Developing World," *Chaos Solitons & Fractals*, vol. 30, pp. 769-773, Apr. 2006.
- [12] Hattat, "Doğal Taş Malzeme Koruyucuların Performans Ölçümünde Deneysel Metot Araştırması," Phd. thesis, M.S.G.Ü. Institute of Science, İstanbul, Türkiye, Jun. 2002.
- [13] E. Deniz, "Vakumlu Yalıtım Malzemelerinin Karakteristik Özelliklerinin Deneysel ve Teorik Olarak incelenmesi," Marmara University Institute of Science, Phd. Thesis, İstanbul, Türkiye, Jun. 2009.